

UNIVERSIDAD COMPLUTENSE DE MADRID

FACULTAD DE FARMACIA



TESIS DOCTORAL

**Natural product-related multitarget-directed ligands
for the potential treatment of neurodegenerative diseases**

**Ligandos multidiana relacionados con productos naturales
para el tratamiento potencial de enfermedades neurodegenerativas**

MEMORIA PARA OPTAR AL GRADO DE DOCTOR

PRESENTADA POR

Ángel Cores Esperón

Directores

**José Carlos Menéndez Ramos
Mercedes Villacampa Sanz**

Madrid

UNIVERSIDAD COMPLUTENSE DE MADRID
FACULTAD DE FARMACIA
Unidad Docente de Química Orgánica y Farmacéutica,
Departamento de Química en Ciencias Farmacéuticas



TESIS DOCTORAL

**Natural product-related multitarget-directed ligands for
the potential treatment of neurodegenerative diseases**

**Ligandos multidiana relacionados con productos naturales para
el tratamiento potencial de enfermedades neurodegenerativas**

Ángel Cores Esperón

Directores:

José Carlos Menéndez Ramos
Mercedes Villacampa Sanz

Madrid, 2019



UNIVERSIDAD
COMPLUTENSE
MADRID

DECLARACIÓN DE AUTORÍA Y ORIGINALIDAD DE LA TESIS PRESENTADA PARA OBTENER EL TÍTULO DE DOCTOR

D./Dña. Ángel Cores Esperón,
estudiante en el Programa de Doctorado en Química Médica,
de la Facultad de Farmacia de la Universidad Complutense de
Madrid, como autor/a de la tesis presentada para la obtención del título de Doctor y
titulada:

NATURAL PRODUCT-RELATED MULTI-TARGET-DIRECTED LIGANDS FOR THE POTENTIAL TREATMENT OF NEURODEGENERATIVE DISEASES/
LIGANDOS MULTIDIANA RELACIONADOS CON PRODUCTOS NATURALES PARA EL TRATAMIENTO POTENCIAL DE ENFERMEDADES NEURODEGENERATIVAS

y dirigida por: José Carlos Menéndez Ramos y Mercedes Villacampa Sanz

DECLARO QUE:

La tesis es una obra original que no infringe los derechos de propiedad intelectual ni los derechos de propiedad industrial u otros, de acuerdo con el ordenamiento jurídico vigente, en particular, la Ley de Propiedad Intelectual (R.D. legislativo 1/1996, de 12 de abril, por el que se aprueba el texto refundido de la Ley de Propiedad Intelectual, modificado por la Ley 2/2019, de 1 de marzo, regularizando, aclarando y armonizando las disposiciones legales vigentes sobre la materia), en particular, las disposiciones referidas al derecho de cita.

Del mismo modo, asumo frente a la Universidad cualquier responsabilidad que pudiera derivarse de la autoría o falta de originalidad del contenido de la tesis presentada de conformidad con el ordenamiento jurídico vigente.

En Madrid, a 3 de septiembre de 2019

**CORES
ESPERON
ANGEL -
Fdo.: 77420923W**

Firmado digitalmente
por CORES
ESPERON ANGEL -
77420923W
Fecha: 2019.09.04
02:06:05 +02'00'

TABLE OF CONTENTS

Abbreviations.....	i
Summary of the thesis “Natural product-related multitarget-directed ligands for the potential treatment of neurodegenerative diseases”	iii
Resumen de la tesis “Ligandos multidiana relacionados con productos naturales para el tratamiento potencial de enfermedades neurodegenerativas”	vii
Chapter 1. Introduction	1
1.1. General comments on dementia	3
1.2. Neurodegeneration, oxidative stress and reactive oxygen species	5
1.2.1. General aspects of oxidative stress.....	5
1.2.2. ROS generation	6
1.2.3. Consequences of oxidative stress	7
1.3. Protein misfolding, proteostasis and neurodegeneration.....	8
1.3.1. Protein misfolding and neurodegenerative disease: General aspects	8
1.3.2. Chaperones	10
1.3.3. Autophagy and proteasome activity.....	10
1.3.4. Ageing and altered proteostasis	10
1.3.5. Protein misfolding propagation and toxicity	11
1.4. Neuroinflammation.....	11
1.5. Neuronal calcium signalling and neurodegeneration.....	14
1.5.1. An overview of the neuronal roles of calcium	14
1.5.2. Ageing-associated mitochondrial dysfunction and impaired neuronal calcium homeostasis	15
1.6. Tracking pathologic processes in NDD and feedback loops between NDD hallmarks	16
1.7. Multitarget drug discovery	19
Chapter 2. Objectives	23
Chapter 3. Neuroprotective compounds related to cinnamic esters and curcumin	31
3.1. Oxidative stress and neurodegeneration: A closer look.....	33
3.2. The Keap1-Nrf2-ARE pathway	33
3.2.1. The phase II antioxidant response	33
3.2.2. Nrf2 activation as a useful approach to neurodegenerative disease therapy.....	35
3.2.3. Non-electrophilic Nrf2 activation	36
3.2.4. Electrophilic Nrf2 activation	36
3.2.5. Natural products targeting the Keap1-Nrf2-ARE pathway	38
3.3. Design of cyclic analogues of cinnamic esters and curcumin	39
3.4. Multicomponent synthesis of the pyrrolin-5-one core	41
3.4.1. Multicomponent reactions: A brief introduction.....	41
3.4.2. Literature precedent for the synthesis of 2-pyrrolin-5-ones	43
3.4.3. Hantzsch-like, multicomponent approach to 2-pyrrolin-ones.....	44

3.5. Pyrrolones with embedded cinnamic acid structural fragments.....	48
3.5.1. Synthesis of compounds 3	48
3.5.2. Pharmacological evaluation of compounds 3	50
3.6. Curcumin analogues with a pyrrolinone core	58
3.6.1. Synthesis of compounds 4	58
3.6.2. Pharmacological evaluation of compounds 4	59
3.7. Experimental section	64
3.7.1. General procedure for the synthesis of 2-pyrrolin-5-one derivatives 1	64
3.7.2. Synthesis of 4-benzyloxy-3-methoxybenzaldehydes 2	70
3.7.3. General synthesis of 4-arylmethylen-2-pyrrolin-5-ones 3	71
3.7.4. Curcumin analogues 4	77
Chapter 4. Neuroprotective compounds related to spirooxindole alkaloids.....	81
4.1. Neuroprotective spirooxindole alkaloids.....	83
4.2. Compound design	86
4.3. Synthesis of dispirooxindoles 5 and 6 <i>via</i> a multicomponent [3+2] dipolar cycloaddition	86
4.4. Pharmacological study of dispirooxindoles 5 and 6	90
4.4.1. SHSY5Y cytotoxicity.....	90
4.4.2. Radical scavenging	90
4.4.3. Nrf2 induction in the AREc32 cell line.....	91
4.4.4. Acetylcholinesterase inhibition.....	91
4.4.5. Neuroprotection in a rotenone/oligomycin A oxidative stress model	91
4.4.6. Neuroprotection against tau hyperphosphorylation induced by okadaic acid.....	93
4.5. Experimental section	94
4.5.1. General procedure for the synthesis of dispirooxindoles 5 and 6	95
Chapter 5. Melatonin/2,5,8-quinolinetriene hybrids.....	103
5.1. Biological importance of quinones	105
5.2. Design of quinone-melatonin based multitarget ligands	106
5.3. Synthesis of tryptamine-quinolinetriene hybrids	108
5.3.1 Synthesis of 3-alkyl- and 3-formyl-5,8-dimethoxyquinolin-2-ones.....	108
5.3.2. Synthesis of 5,8-dimethoxyquinolin-2-ones bearing electron-withdrawing groups at C-3 ..	110
5.3.3. Synthesis of 2,5,8-quinolinetrienes	111
5.3.4. Coupling of tryptamines and 2,5,8-quinolinetrienes	111
5.4. Experimental section	114
5.4.1. Synthesis of N-(2,5-dimethoxyphenyl)anilides 7	114
5.4.2. Synthesis of 2-chloro-5,8-dimethoxyquinolines 8	115
5.4.3. Synthesis of 5,8-dimethoxy-2(1 <i>H</i>)-quinolinones 9	116
5.4.4. Preparation of 3,6-dimethoxy-2-nitrobenzaldehyde 10	117
5.4.5. Preparation of 2-amino-3,6-dimethoxybenzaldehyde 11	117
5.4.6. Friedländer synthesis of 5,8-dimethoxyquinolin-2(1 <i>H</i>)-one derivatives 12	118

5.4.7. Synthesis of 2,5,8(1 <i>H</i>)-quinolinetriones 13	118
5.4.8. Synthesis of tryptamine-quinone hybrids 14	119
5.4.9. Synthesis of 5,8-dimethoxy-3-(((2-(5-methoxy-1 <i>H</i> -indol-3-yl)ethyl)amino)-methyl]quinolin-2(1 <i>H</i>)-one (15).....	122
Chapter 6. Aza-CGP-37157/Lipoic acid hybrids.....	123
6.1. Calcium homeostasis and neurodegenerative diseases.....	124
6.1.1. Plasma membrane Ca ²⁺ flow in neuronal physiology.....	124
6.1.2. Endoplasmic reticulum as a calcium store.....	126
6.1.3. Mitochondria and calcium homeostasis.....	127
6.1.4. Calcium deregulation in neurodegenerative disease.....	129
6.2. mNCX blockers.....	130
6.2.1. First mNCX antagonists.....	130
6.2.2. CGP-37157, a mNCH inhibitor, as a lead for drug discovery.....	131
6.3. Enantioselective sulfoxide synthesis and attempted kinetic resolution of the CGP-37157 enantiomers.....	133
6.3.1. Enantioselective synthesis of sulfoxides: Literature precedent.....	133
6.3.2. Studies towards the synthesis of both enantiomers of CGP-37157.....	135
6.4. Preliminary pharmacological characterization of CGP-37157-derived sulfoxides and sulfones.....	141
6.4.1. Cytotoxicity.....	141
6.4.2. Nrf2 induction.....	141
6.5. Design, synthesis and characterization of a multitarget mitochondrial stabilizer for stroke.....	143
6.6. Synthesis of an aza-CGP-37157-lipoic acid hybrid.....	146
6.7. Preliminary pharmacological studies.....	152
6.7.1. Cytotoxicity.....	152
6.8. Experimental section.....	155
6.8.1. Synthesis of CGP-37157.....	155
6.8.2. Asymmetric oxidation of CGP-37157.....	157
6.8.3. Diastereoselective synthesis of CGP-37157 aza-analogue.....	158
6.8.4. Synthesis of 2-(7-chloro-5-(2-chlorophenyl)-2-oxo-2,3,4,5-tetrahydro-1 <i>H</i> -benzo[e][1,4]diazepin-4-yl)ethyl 5-(1,2-dithiolan-3-yl)pentanoate (20).....	165
Chapter 7. Carbohydrate heterocyclic hybrids as galectin modulators.....	167
7.1. Galectins: structure, function and location.....	169
7.1.1. Introduction to galectins.....	169
7.1.2. Role of Gal-3 in neuroinflammation.....	171
7.1.3. Galectin-3 modulators.....	172
7.2. Design of selective galectin-3 modulators.....	173
7.3. Synthesis of heterocyclic-OMe-Lac derivatives as galectin ligands.....	174
7.4. Experimental section.....	177
7.4.1. Synthesis of fragment 38	177

7.4.2. Synthesis of fragment 43	181
7.4.3. Synthesis of fragment 45	183
7.4.4. Synthesis of fragment 48	183
Chapter 8. Conclusions	185
Representative spectra.....	189

ABBREVIATIONS

A β	Amyloid β
AChE	Acetylcholinesterase
AD	Alzheimer's disease
Akt	Protein kinase B
ALS	Amyotrophic lateral sclerosis
AMPA	α -Amino-3-hydroxy-5-methylisoxazole-4-propionate acid
APOE	Apolipoprotein E
ARE	Antioxidant response element
BACE-1	β -Secretase
CAN	Ce(IV) ammonium nitrate
CGNs	Cerebellar granule neurons
CMA	Chaperone-mediated autophagy
CNS	Central nervous system
CRD	Carbohydrate recognition domain
CoQ10	Coenzyme Q10
CSF	Cerebrospinal fluid
DAMPs	Damage-associated molecular patterns
DCF	Dichlorofluorescein
DFCA	2,7-Dichlorofluorescein acetate
DFCH	2,7-dichlorofluorescein
DMF	Dimethyl fumarate
EMRE	Essential MCU regulator
ER	Endoplasmic reticulum
FDG	Fluorodeoxyglucose
GCL	Glutamate cysteine ligase
GFR	Growth factor receptor
GR	Glutathione reductase
GSH	Glutathione
GSK-3 β	Glycogen synthase kinase 3
HD	Huntington's disease
HMGB1	High-mobility group box 1
HNE	4-Hydroxy-2,3-nonenal
IL	Interleukin
IMM	Inner mitochondrial membrane
InsP3Rs	Inositol-1,4,5-tris-phosphate receptors
Keap1	Kelch-like ECH-associated protein 1
LPS	Lipopolysaccharide
MCRs	Multicomponent reactions
MCU	Mitochondrial calcium uniporter
MCUR	MCU regulator
MEF2D	Transcription factor myocyte enhancer
mHtt	Mutant huntingtin
MMF	Monomethyl fumarate
mNCX	Mitochondrial Na ⁺ /Ca ²⁺ exchanger
mPTP	Mitochondrial permeability transition pore

MTDL	Multitarget directed ligands
MS	Multiple sclerosis
MTT	3-(4,5-dimethylthiazol-2-yl)-2,5-diphenyltetrazolium bromide
NDD	Neurodegenerative diseases
NF-κB	Nuclear factor κB
NLRs	NOD-like receptors
NMDA	N-Methyl-D-aspartate
NQO1	NAD(P)H/quinone oxidoreductase 1
Nrf2	Nuclear factor erythroid 2-related factor 2
NOS	Reactive nitrogen species
O	Oligomycin
PAMCA	Plasma membrane Ca ²⁺ ATPase
PAMPs	Pathogen-associated molecular patterns
PET	Positron emission tomography
PI3K	Phosphoinositide 3-kinase
PKCδ	Protein kinase Cδ
PPI	Protein-protein interaction inhibitors
PRRs	Pattern-recognition receptors
PD	Parkinson's disease
R	Rotenone
ROCC	Receptor-operated calcium channels
ROS	Reactive oxygen species
RyRs	Ryanodine receptors
SAR	Structure activity relationship
SERCA	Sarcoendoplasmic reticulum calcium transport ATPase
SOCC	Store-operated calcium channels
SOD1	Superoxide dismutase 1
SOI	Secondary orbital interaction
TDP-43	TAR DNA binding protein-43
TF-fMRI	Task-free functional MRI
TLRs	Toll-like receptors
TNF-α	Tumoral necrosis factor alpha
TREM2	Triggering receptor expressed on myeloid cells 2
VDCC	Voltage-dependent Ca ²⁺ channels
VGCC	Voltage-gated calcium channels

SUMMARY OF THE THESIS “NATURAL PRODUCT-RELATED MULTITARGET-DIRECTED LIGANDS FOR THE POTENTIAL TREATMENT OF NEURODEGENERATIVE DISEASES”

Introduction

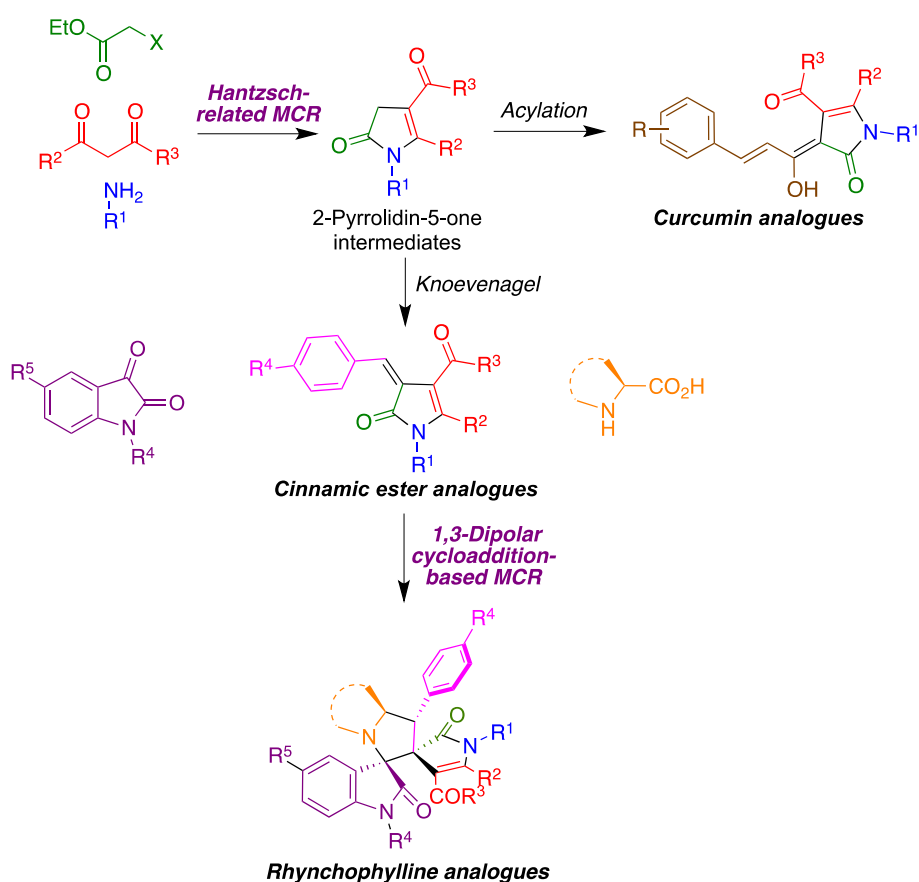
Neurodegenerative diseases are characterized by the loss of neurons in the brain and/or spinal cord and constitute one of the most important health problems worldwide. Although these diseases have different etiologies and clinical manifestations, they share many mechanistic pathways, including: protein misfolding, neuroinflammation, impaired mitochondrial function, increase in oxidative stress, mitochondrial dysfunction, alterations in calcium homeostasis, etc.

Objectives

1. Design, synthesis and characterization of libraries of cyclic analogues of cinnamic esters and curcumin in order to study their antioxidant activity and neuroprotective profiles. The molecular architecture of these compounds was organized around a central 2-pyrrolin-5-one core, which was expected to increase their stability while also providing synthetic handles for the preparation of multitarget-directed ligands.
2. Design, synthesis and characterization of a library of oxindole-derived dispiro compounds as analogues of the neuroprotective alkaloid rhynchophylline.
3. Design, synthesis and characterization of a library of compounds derived from the 2,5,8-quinolinetrione skeleton and containing an indolyethyl side chain. These compounds can be considered vinylogs of the natural antioxidant and neuroprotectant melatonin, and are expected to show also a multitarget neuroprotective profile associated to their heterocyclic quinone moiety.
4. Design, synthesis and characterization of hybrid compounds designed to combine in a single molecule the frameworks of CGP-37157, a well-known inhibitor of the mitochondrial mNCX transporter with neuroprotective activity, and lipoic acid, a natural antioxidant.
5. As part of a collaborative effort, our goal was the synthesis of the heterocyclic fragments of a series of heterocyclic carbohydrate hybrids, designed using a fragment-based approach and potentially active against neuroinflammation.

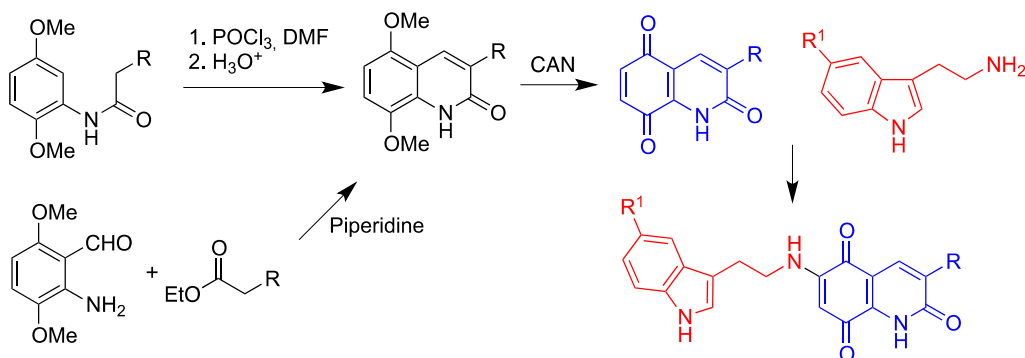
Results and discussion

Objectives 1 and 2 required the development of new synthetic methodology for the preparation of the core 2-pyrrolidin-5-one nucleus, and this was achieved by a modification of the classical Hantzsch three-component pyrrole synthesis. Straightforward Knoevenagel condensation and acylation reactions furnished the target cinnamic ester and curcumin analogues, respectively. A three-component 1,3-dipolar cycloaddition reaction between the Knoevenagel adducts, isatin derivatives and α -amino acids afforded the dispiro compounds designed as rhynchophylline analogues.



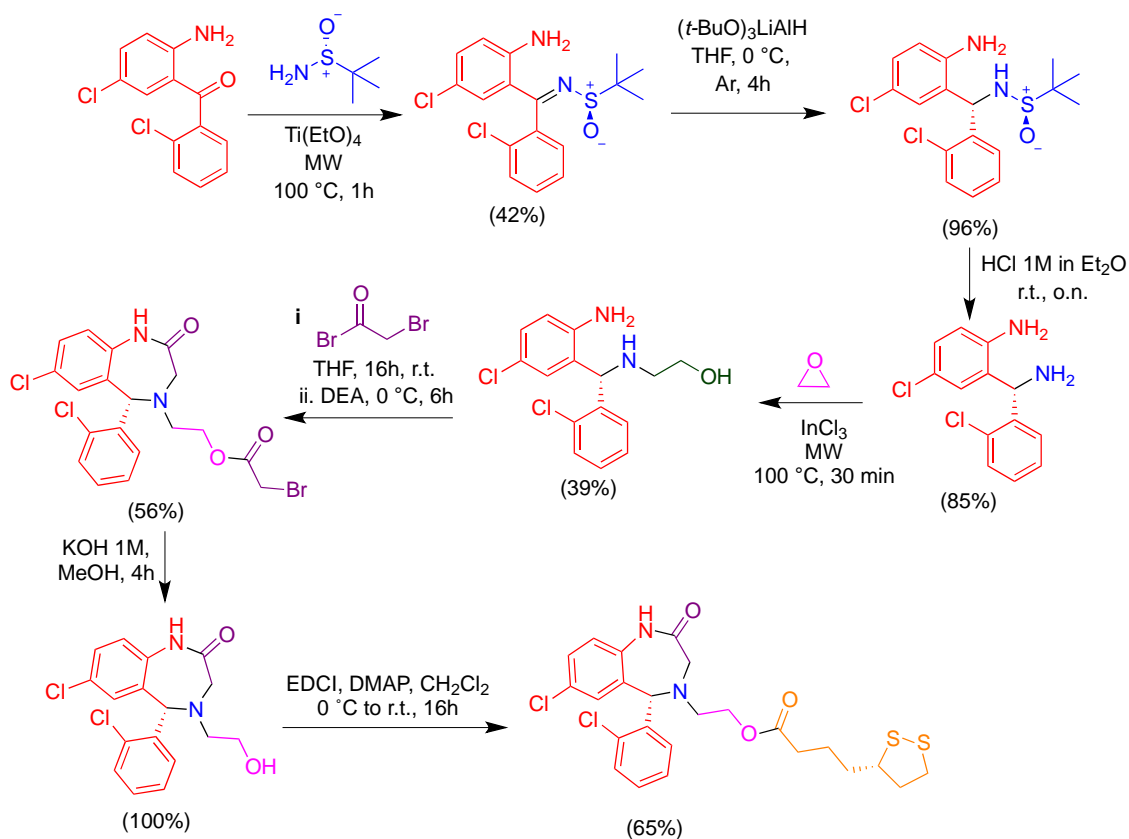
These libraries were pharmacologically assayed through collaborations with the groups led by Dr. Rafael León (Hospital de La Princesa and Instituto Teófilo Hernando, Universidad Autónoma de Madrid) and Drs. Sagrario Martín-Aragón and Paloma Bermejo (Universidad Complutense). These studies revealed interesting multitarget profiles and led to the selection of several compounds as suitable hits for future development.

The melatonin-quinolinetrione hybrids were synthesized in two stages. First, the suitable 2,5,8-quinolinetrione precursors were obtained by routes using as key stages the Meth-Cohn or Friedländer quinoline syntheses. Then, the target hybrid compounds were obtained by regioselective addition of tryptamine derivatives to the quinone C-6 position followed by *in situ* oxidation.



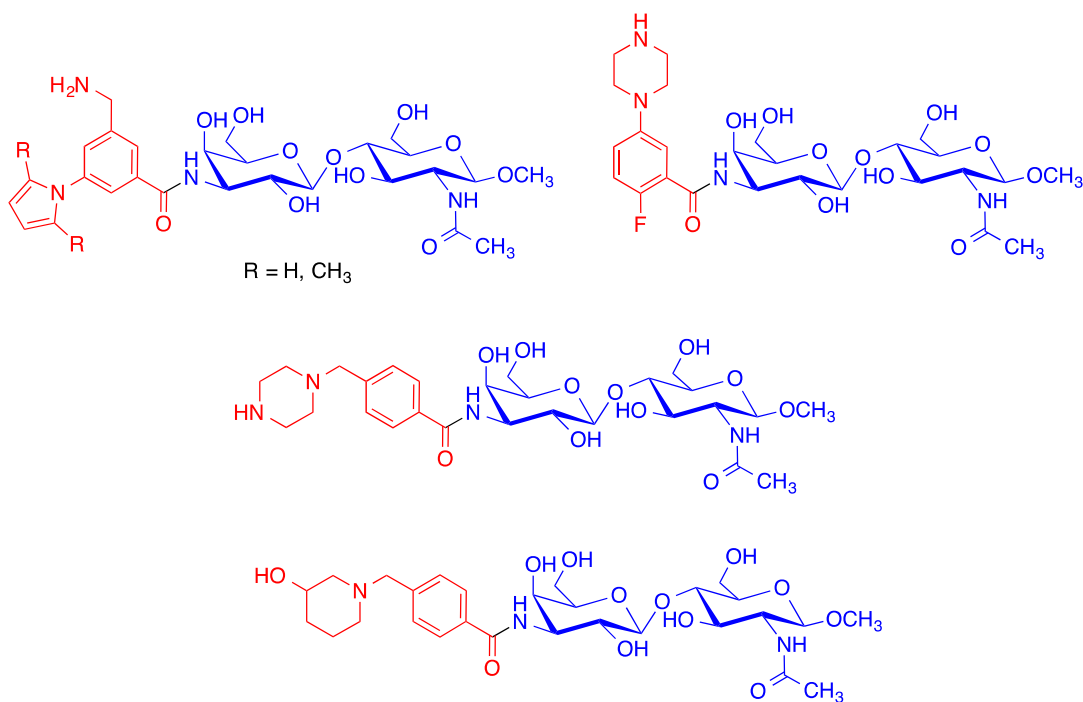
These hybrids are under pharmacological assay through a collaboration with the group led by Dr. Pilar Gómez-Serranillos (Universidad Complutense) and so far have shown very potent antioxidant activities.

A seven-step route, based on the use of Ellman's sulfonamide as a chiral auxiliary,



allowed the preparation of all four enantiomers of our target aza CGP-37157 lipoic acid hybrid structure, as exemplified for one of them. Their pharmacological study was carried out through our collaboration with Dr. Rafael León and showed interesting neuroprotective profiles.

Finally, the heterocyclic moieties of four structurally complex carbohydrate hybrid structures designed as galectin ligands were obtained by multistep routes.



Conclusions

The work performed in this thesis shows that the multitarget approach is promising towards the discovery of molecules that can be used as hits in the development of new drugs for the treatment of neurodegenerative diseases.

RESUMEN DE LA TESIS “LIGANDOS MULTIDIANA RELACIONADOS CON PRODUCTOS NATURALES PARA EL TRATAMIENTO POTENCIAL DE ENFERMEDADES NEURODEGENERATIVAS”

Introducción

Las enfermedades neurodegenerativas se caracterizan por la pérdida de neuronas en el cerebro y/o en la medula espinal y constituyen uno de los más importantes problemas de salud a nivel mundial. A pesar de que estas enfermedades tienen diferentes etiologías y manifestaciones clínicas, comparten diversos mecanismos, incluyendo: incorrecto plegamiento de proteínas, neuroinflamación, función mitocondrial dañada, aumento en el estrés oxidativo, disfunción mitocondrial, alteraciones en la homeostasis del calcio, etc.

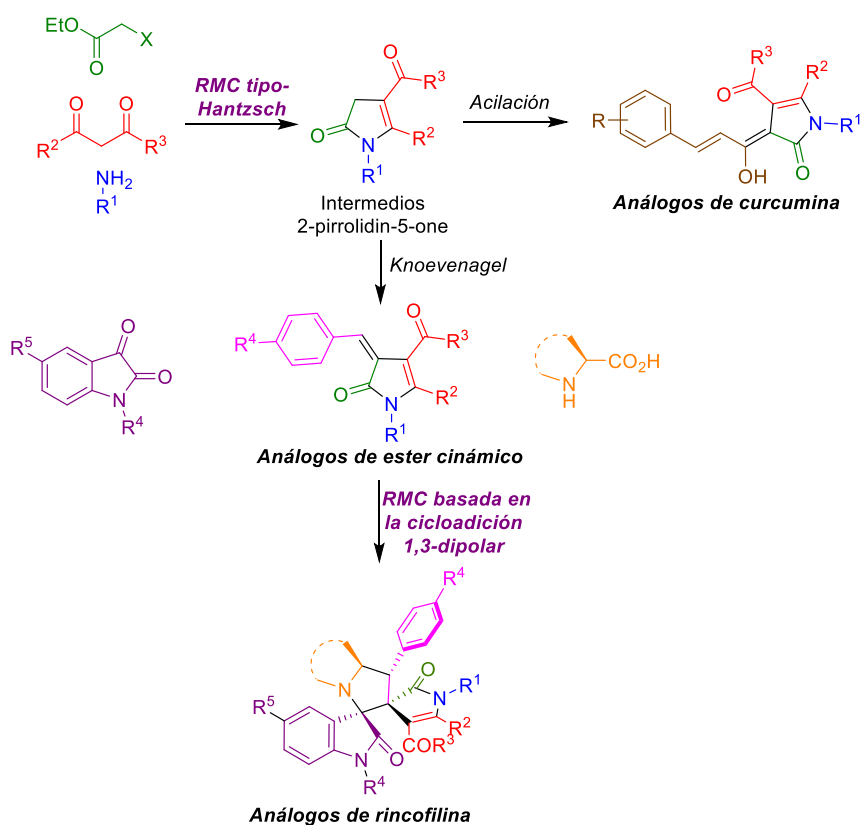
Objetivos

1. Diseño, síntesis y caracterización de librerías de análogos cíclicos de ésteres cinámicos y curcumina para el estudio de su actividad antioxidante y su perfil neuroprotector. La arquitectura molecular de estos compuestos está organizada alrededor de un núcleo central de 2-pirrolin-5-ona, del que se espera que incremente su estabilidad a la vez que proporciona accesibilidad sintética para la preparación de ligandos multidiana.
2. Diseño, síntesis y caracterización de una quimiotecas de compuestos diespirooxindol como análogos del alcaloide neuroprotector ricofilina.
3. Diseño, síntesis y caracterización de una quimiotecas de compuestos derivados del esqueleto de 2,5,8-quinolinatriona y conteniendo grupos indoliletilo como cadenas laterales. Estos compuestos pueden ser considerados vinólogos de la melatonina, un antioxidante natural y neuroprotector, y se espera que muestren además un perfil neuroprotector multidiana asociado a la estructura heterocíclica de quinona.
4. Diseño, síntesis y caracterización de compuestos híbridos que combinan en una sola molécula fragmentos clave de CGP-37157, un inhibidor del transportador mNCX con actividad neuroprotectora, y el ácido lipoico, un antioxidante natural.

5. Síntesis de los fragmentos heterocíclicos de una serie de híbridos de heterociclos con carbohidratos, diseñados como moduladores de las galectinas, con potencial actividad contra la neuroinflamación

Resultados y discusión

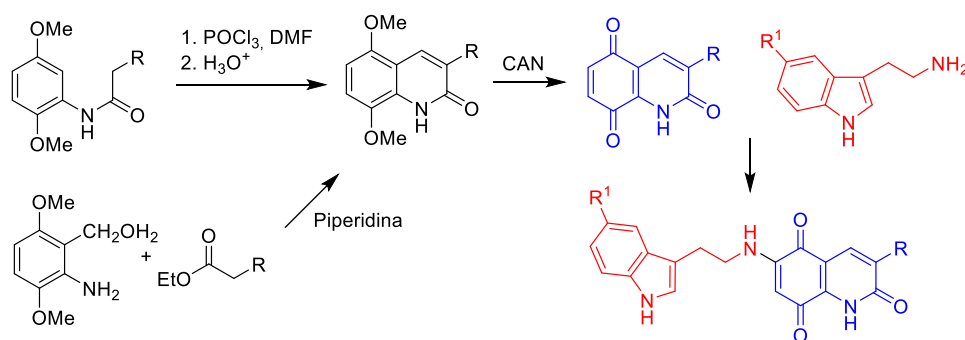
Los objetivos 1 y 2 requieren el desarrollo de nuevas metodologías para la preparación del núcleo de 2-pirrolin-5-ona, y esto se ha logrado por la modificación de la síntesis multicomponente de Hantzsch de pirroles. Empleando reacciones sencillas como la condensación de Knoevenagel o reacciones de acilación se obtuvieron los análogos de éster cinámico y curcumina, respectivamente. Una cicloadición 1,3-dipolar de tres componentes entre el aducto de Knoevenagel, derivados de isatina y α -aminoácidos generó los compuestos de tipo biespiro diseñados como análogos de la rincofilina.



Estas quimiotecas han sido ensayadas farmacológicamente en colaboración con los grupos liderados por el Dr. Rafael León (Hospital de La Princesa e Instituto Teófilo Hernando, Universidad Autónoma de Madrid) y las Dras. Sagrario Martín-Aragón y Paloma Bermejo (Universidad Complutense). Estos estudios revelan interesantes

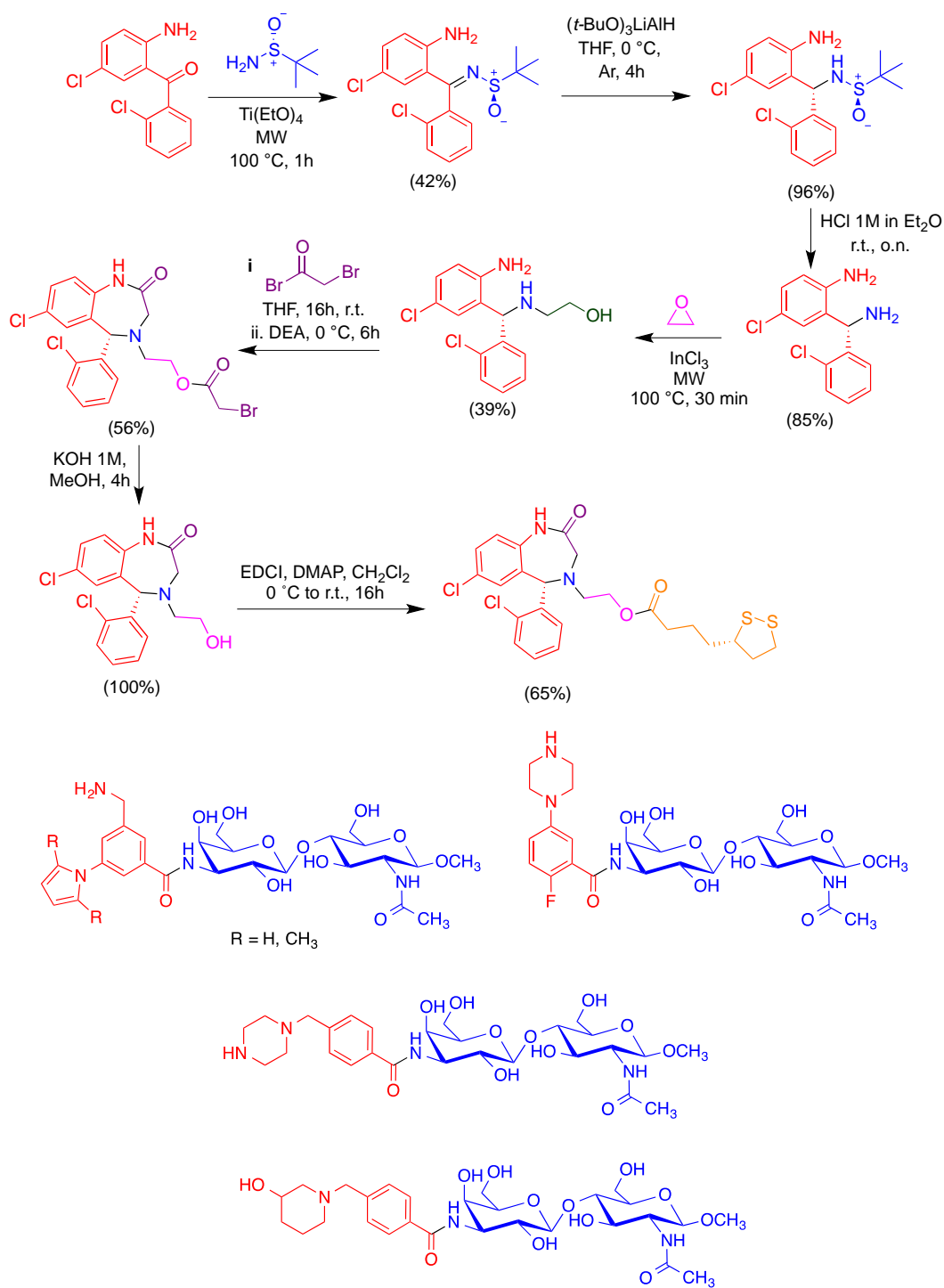
perfiles multidiana y han llevado a la selección de diferentes compuestos como candidatos adecuados para su futuro desarrollo.

Los híbridos de melatonina-quinolinatriona han sido sintetizados en dos fases. En la primera, la 2,5,8-quinolinatriona precursora se obtuvo empleando las síntesis de quinolinas de Meth-Cohn o Friedländer como pasos clave. A continuación, los compuestos híbridos objetivo fueron obtenidos por la adición regioselectiva de derivados de triptamina sobre la posición C-6 de la quinona, seguida por una oxidación *in situ*. Estos híbridos se encuentran bajo su estudio farmacológico a través de una colaboración con el grupo liderado por la Dra. Pilar Gómez-Serranillos (Universidad Complutense) y han mostrado una potente actividad antioxidante.



Una ruta de siete pasos, basada en el uso de la sulfonamida de Ellman como auxiliar quiral, ha permitido la obtención de los cuatro enantiómeros del híbrido aza-CGP-37157-ácido lipóico, como se indica a continuación para uno de ellos. Los estudios farmacológicos están siendo llevados a cabo con la colaboración del Dr. Rafael León y han mostrado perfiles neuroprotectores interesantes.

Por último, los fragmentos heterocíclicos correspondientes a cuatro estructuras híbridas con carbohidratos relacionadas con galectinas han sido obtenidos en rutas de varios pasos que generalmente tienen como etapa clave un acoplamiento catalizado por paladio.



Conclusiones

El trabajo llevado a cabo en esta tesis muestra que la aproximación multidiana es una estrategia prometedora en el descubrimiento de nuevas moléculas que pueden ser empleadas como candidatas en el desarrollo de nuevos fármacos para el tratamiento de enfermedades neurodegenerativas.

CHAPTER 1. INTRODUCTION

1.1. General comments on dementia

Dementia is a general term used to describe a decline in intellectual skills that reduces the ability of the patient to perform routine daily activities. There are about 50 million dementia patients worldwide, and every year 7.7 million new cases are diagnosed. It is estimated that the number of cases will reach 65.7 million in 2030 and 115.4 million in 2050, with nearly 60% patients living in low- and middle-income countries (Figure 1.1). The improvement in life expectancy is the main cause for this growth in incidence, since advanced age is the main risk factor in the development of dementia.

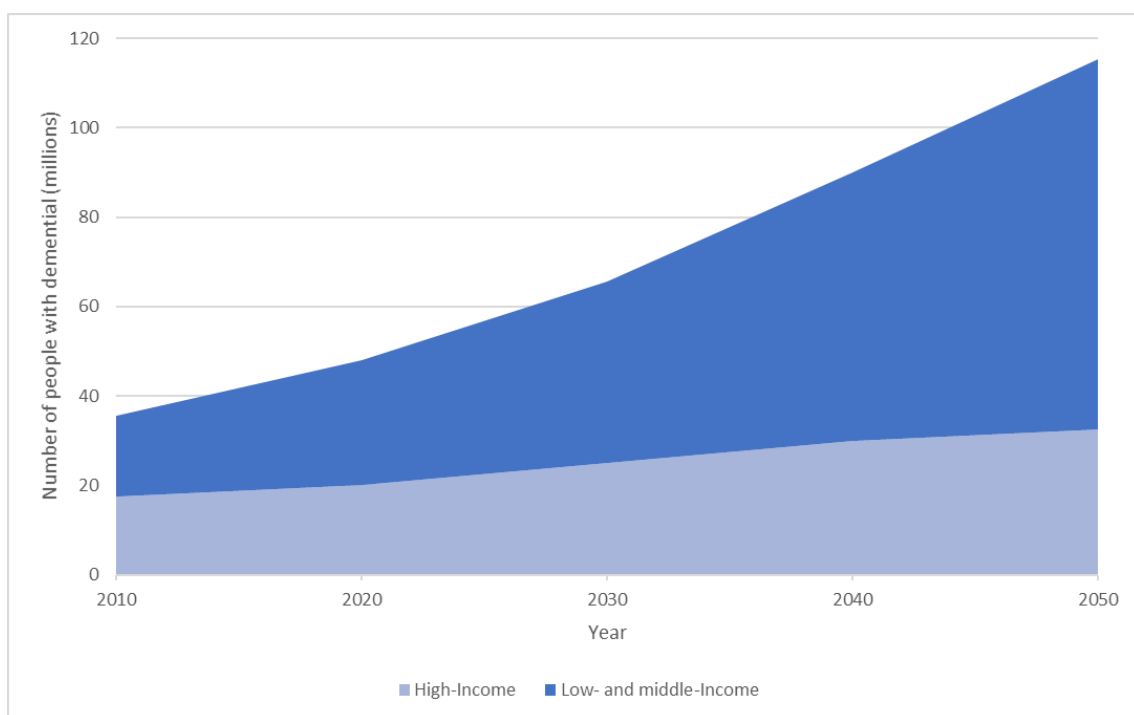


Figure 1.1. Projected growth in the incidence of dementia in high-income and low and middle-income countries. Elaborated from data in reference ¹

The most common forms of dementia are, in order of importance, Alzheimer's disease, vascular dementia, dementia with Lewy bodies and frontotemporal dementia. However, mixed pathologies seem to be more widespread than the pure ones. Thus, the retrospective clinico-pathological study of 1050 elderly patients of dementia showed that in 86% of cases it was Alzheimer's disease-related. However, only 43% of patients had pure Alzheimer's disease, while for the other 67% it was combined with

¹ Dementia: a public health priority. World Health Organization. *World Health Organization* 2012.

Chapter 1. Introduction

other neurodegenerative diseases: cerebrovascular (26%), Parkinson's disease (10%) and others (Figure 1.2).²

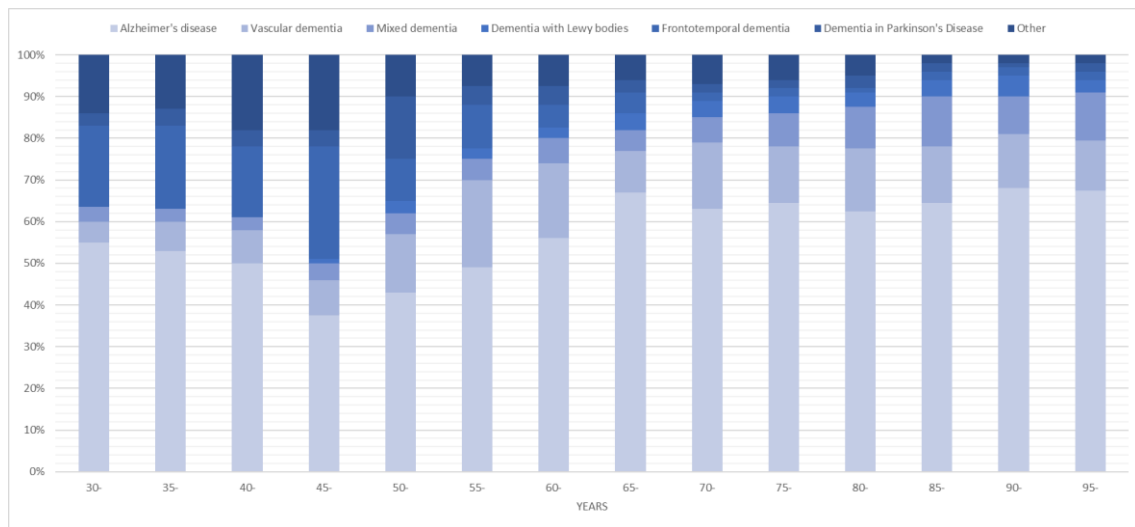


Figure 1.2. Proportion of the different subtypes of dementia in UK female patients

Neurodegenerative diseases are characterized by the loss of neurons in the brain and/or spinal cord. For each particular disease, this loss affects a specific set of neurons in particular, driving in a heterogeneous clinical symptomatology and finally resulting in the different neurodegenerative diseases. These diseases are multi-factorial pathologies with different etiologies, molecular mechanisms and clinical manifestations. Nevertheless, they share many biochemical pathways, including: protein misfolding, neuroinflammation, impaired mitochondrial function, increase in oxidative stress, mitochondrial dysfunction, loss of neuronal plasticity, etc. For instance, Alzheimer's disease (AD) has several pathogenic mechanisms including amyloid β ($A\beta$) aggregation to form plaques, tau hyperphosphorylation-driven formation of neurofibrillary tangles, calcium imbalance, increase in ROS and NOS-associated stress, Ca^{2+} ion dehomeostasis, apoptosis dysfunction, and deterioration of synaptic transmission, particularly at cholinergic neurons. Hundreds of compounds addressed at these individual targets have been investigated, including inhibitors of β and γ secretase, vaccines or antibodies that clear $A\beta$, metal chelators or molecular chaperones to prevent $A\beta$ aggregation, glycogen synthase kinase 3β inhibitors, ROS and NOS scavengers, modulators of calcium channels such as voltage-dependent

² Jellinger, K. A. J. *Alzheimer's Dis.* **2006**, 9, 61-70.

calcium channels blockers, N-methyl-D-aspartate receptor inhibitors, or enhancers of cholinergic neurotransmission such as inhibitors of acetylcholinesterase or butyrylcholinesterase.

1.2. Neurodegeneration, oxidative stress and reactive oxygen species

1.2.1. General aspects of oxidative stress

Reactive oxygen species (ROS) is a general term that describes the chemical species produced in the incomplete reduction of the oxygen molecule.³ These species are, among others, the hydroxyl radical ($\cdot\text{OH}$), the superoxide anion ($\text{O}_2^{\cdot-}$) and hydrogen peroxide (H_2O_2).

ROS are intracellular signalling molecules and is has been reported in the literature.³ Both $\text{O}_2^{\cdot-}$ and $\cdot\text{OH}$ are poor signalling molecules due to their instability, inability to cross the membranes and the short diffusion distances.⁴ In contrast, H_2O_2 can mediate signalling pathways due to its high diffusivity, ability to cross membranes and stability. Cys residues are the main target for H_2O_2 -dependent downstream signalling, which regulates several biochemical pathways such circadian rhythms. An example is the 24 h redox cycles of the peroxiredoxin protein that exists in the red blood cells (Figure 1.3).⁵

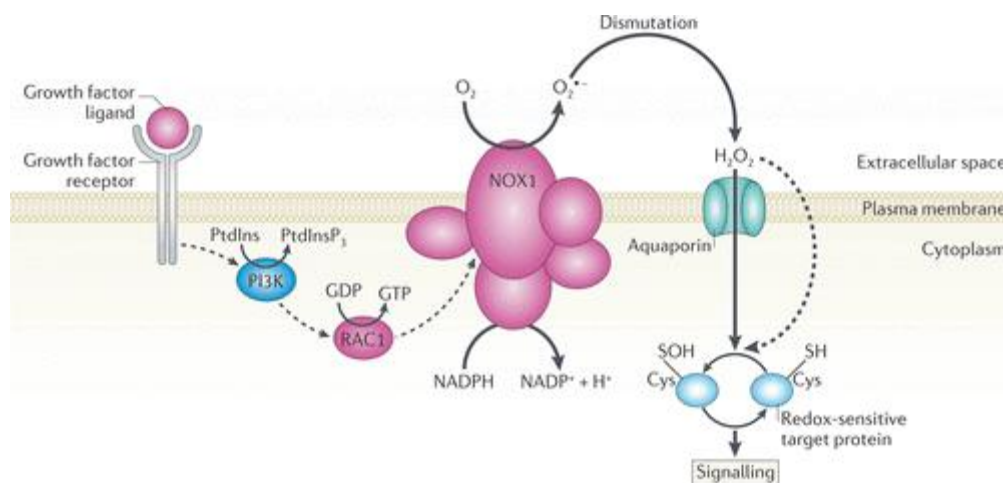


Figure 1.3. Reproduced with permission from reference ⁴

³ D'Autr aux, B.; Toledano, M. B. *Nat. Rev. Mol. Cell Biol.* **2007**, *8*, 813-825.

⁴ Yang, B.; Chen, Y.; Shi, J. *Chem. Rev.* **2019**, *119*, 4881-4985.

⁵ O'Neill, J. S.; Reddy, A. B. *Nature* **2011**, *469*, 498-503.

Chapter 1. Introduction

While ROS have physiological roles as second messengers in moderate concentrations, excessive ROS activity leads to oxidative stress. This increase in ROS concentration was observed in human fibroblasts and induced a senescence-like state.⁶ The imbalance in ROS concentration and senescence were found to be correlated in several pathological processes. Furthermore, oxidative stress is a common hallmark in neurodegenerative diseases, as the result of the hyperproduction of ROS combined with the relatively low antioxidant levels and low regenerative capacity. This imbalance causes brain tissue damage and, as a consequence, neuronal death and neurodegeneration.^{7, 8}

1.2.2. ROS generation

The quantum level of ground state O₂ molecules is a triplet spin state and consequently its interactions with organic compounds are energetically disfavoured. Live organisms have developed metal-containing enzymes to convert O₂ into ROS, that are able to react with organic compounds.

ROS are generated by two major pathways:

- Direct interaction between redox-active metals like copper and iron and oxygen species *via* the Fenton and Haber-Weiss reactions. These metal ions exist in multiple valence states and this multiple valence occupancy is the reason for the presence of these cations in the metalloenzymes responsible for the activation of molecular oxygen. The deregulation of the redox-active metals may lead to an overproduction of ROS. Several NDD-related proteins including A β in AD, SOD1 in ALS and α -synuclein in PD, contain Cu²⁺ or Fe³⁺ contributing to ROS formation. Protein ligation to metal ions rises in the brain with increased age.
- Indirect activation of calcium dependent metalloenzymes such as phospholipases, nitric oxide synthase or xanthine dehydrogenase. NDDs are characterized by an intracellular calcium overload, as described previously. This calcium homeostasis disruption may trigger several cellular process. The interplay between calcium signalling and ROS production is regulated by a feedback signalling process, and it is often difficult to differentiate between

⁶ Serrano, M.; Lin, A. W.; McCurrach, M. E.; Beach, D.; Lowe, S. W. *Cell* **1997**, *88*, 593-602.

⁷ Lotharius, J.; Brundin, P. *Nat. Rev. Neurosci.* **2002**, *3*, 932-942.

⁸ Barnham, K. J.; Masters, C. L.; Bush, A. I. *Nat. Rev. Drug Discov.* **2004**, *3*, 205-214.

cause and effect. An increase in intracellular calcium induces ROS production,⁹ but subtoxic ROS levels act as messengers to rise the intracellular calcium concentration. As a consequence, the precise role of calcium overload in the production of ROS remains controversial.

1.2.3. Consequences of oxidative stress

Lipid peroxidation is a sensitive and selective marker of oxidative stress through oxidative modifications and peroxidations. The radicals previously formed from O₂ attack the double bonds contained in the unsaturated fatty acids such as linoleic acid and arachidonic acid. These highly reactive peroxy radicals initiate a chain reaction of attacks on adjacent fatty acid molecules. The chain reaction affords several products that are characteristic of specific NDDs like 4-hydroxy-2,3-nonenal (HNE) in AD and PD,^{10,11} acrolein and F₂-isoprostanes in AD¹² and malondialdehyde in PD. DNA bases are also susceptible to oxidative damage involving carbonylation, nitration and hydroxylation reactions. Increased levels of 8-hydroxyguanine and 8-hydroxy-2-deoxyguanosine were observed in PD brains.¹³

These oxidative stress evidences are closely related to the molecular mechanism that initiates the neuronal death and neurodegeneration. Acrolein and HNE induce toxicity by crosslinking to cysteine, lysine and histidine residues through Michael additions. The formation of these adducts causes the impairment of enzymes, receptors and DNA mutations leading to malfunction of a variety of biochemical pathways.

Additionally, ROS imbalance causes intracellular calcium overload, widely described in NDDs and associated to an aberrant apoptotic cascade activation.^{14,15,16} The ROS-induced calcium influx exerts an excitotoxic response,¹⁷ driven by the activation of glutamate receptors that trigger the apoptotic cascade. The excitotoxic response takes

⁹ Lewen, A.; Matz, P.; Chan, P. H. *J. Neurotrauma* **2000**, *17*, 871-890.

¹⁰ Selley, M. L.; Close, D. R.; Stern, S. E. *Neurobiol. Aging* **2002**, *23*, 383-388.

¹¹ Dexter, D. T.; Carter, C. J.; Wells, F. R.; Javoy-Agid, F.; Agid, Y.; Lees, A.; Marsden, C. D. *J. Neurochem.* **1989**, *52*, 381-389.

¹² Arlt, S.; Beisiegel, U.; Kontush, A. *Curr. Opin. Lipidol.* **2002**, *13*, 289-294.

¹³ Alam, Z. I.; Jenner, A.; Daniel, S. E.; Lees, A. J.; Cairns, N.; Marsden, C. D.; Jenner, P.; Halliwell, B. *J. Neurochem.* **1997**, *69*, 1196-1203.

¹⁴ LaFerla, F. M. *Nat. Rev. Neurosci.* **2002**, *3*, 862-872.

¹⁵ Gibson, G. E. *Free Radic. Biol. Med.* **2002**, *32*, 1061-1070.

¹⁶ Mattson, M. P.; Chan, S. L. *Cell Calcium* **2003**, *34*, 385-397.

¹⁷ Yamamoto, K.; Ishikawa, T.; Sakabe, T.; Taguchi, T.; Kawai, S.; Marsala, M. *Neuroreport.* **1998**, *9*, 1655-1659.

place in different neurological disorders including stroke, as well as in NDDs such as AD, PD and amyotrophic lateral sclerosis (ALS).¹⁸

A summary of the main processes related to ROS production and their biological consequences can be found in Figure 1.4.

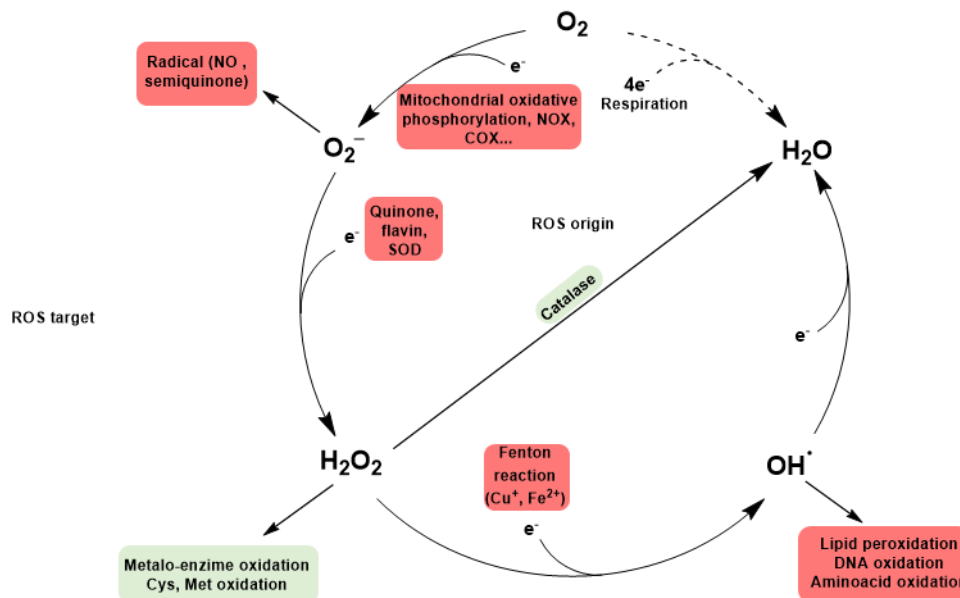


Figure 1.4.

1.3. Protein misfolding, proteostasis and neurodegeneration

1.3.1. Protein misfolding and neurodegenerative disease: General aspects

The misfolding of specific proteins and the consequent protein aggregation in toxic form is the most common feature of NDDs (Table 1.1).¹⁹ The misfolded proteins arise from cell stress, mutations or protein production mistakes. The integrated cellular machinery that regulates the synthesis, proper folding, degradation and clearance of proteins is known as proteostasis. The proteostatic system is regulated by two main components, the chaperones that refold proteins into a stable conformation and two proteolytic pathways, namely the proteasome and the lysosome-autophagy system (Figure 1.5). During the ageing process, the proteostatic system collapses due to accumulation of misfolded proteins. The imbalance between the wrong folding and the

¹⁸ Mattson, M. P. *Neuromolecular Med.* **2003**, 3, 65-94.

¹⁹ Sweeney, P.; Park, H.; Baumann, M.; Dunlop, J.; Frydman, J.; Kopito, R.; Hodgson, R. *Transl. Neurodegener.* **2017**, 6, 6.

protein degradation pathways leads to the accumulation of ubiquitinated inclusion bodies (IBs), which have been observed in several neurodegenerative diseases.²⁰

Table 1.1. Neurodegenerative disease associated with misfolded proteins

Misfolded protein	Neurodegenerative disease
Amyloid β ; Tau; TDP-43	Alzheimer's disease
α -Synuclein; Tau	Parkinson's disease
Huntingtin with tandem glutamine repeats	Huntington's disease
Superoxide dismutase 1; TDP-43	Amyotrophic lateral sclerosis
Prion protein	Spongiform encephalopathies

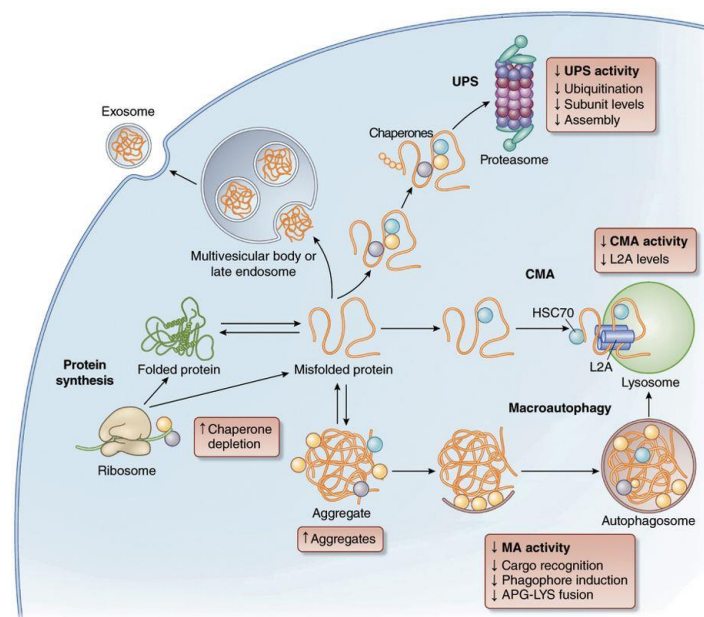


Figure 1.5. The proteostatic system. Reproduced with permission from reference ²¹

The precise neurotoxic mechanisms caused by misfolded proteins are not still completely understood, and differ on the protein species involved. Some examples are amyloid-beta, tau, and alpha-synuclein, all of which interfere with synaptic signalling,^{22, 23, 24} mutant tau impairs microtubule function and neuronal transport mechanisms ²⁴ and alpha-synuclein causes mitochondrial dysfunction.²⁴ Furthermore, larger aggregates of these misfolded proteins may cause toxic effects by binding to and

²⁰ Hipp, M. S.; Park, S. H.; Hartl, F. U. *Trends Cell Biol.* **2014**, *24*, 506-514.

²¹ Kaushik, S.; Cuervo, A. M. *Nat. Med.* **2015**, *21*, 1406-1415.

²² Shankar, G. M.; Li, S.; Mehta, T. H.; Garcia-Muñoz, A.; Shepardson, N. E.; Smith, I.; Brett, F. M.; Farrell, M. A.; Rowan, M. J.; Lemere, C. A.; Regan, C. M.; Walsh, D. M.; Sabatini, B. L.; Selkoe, D. J. *Nat. Med.* **2008**, *14*, 837-842.

²³ Kopeikina, K. J.; Hyman, B. T.; Spire-Jones, T. L. *Transl. Neurosci.* **2012**, *3*, 223-233.

²⁴ Ingelsson, M. *Front. Neurosci.* **2016**, *10*, 408.

sequestering other cytosolic proteins. An example is TAR DNA binding protein-43 (TDP-43) that has been shown to disrupt nucleocytoplasmic transport of both proteins and RNA.²⁵

1.3.2. Chaperones

Chaperones interact with proteins in several processes that include folding, assembly, transport through membranes and targeting for degradation.²⁶ In some cases, the chaperones can refold the protein to its proper conformation and, if the refold is not feasible, direct the protein to the proteolytic pathway that each misfolded protein should follow.

1.3.3. Autophagy and proteasome activity

The proteasome is the most abundant protease in the cytosol and is responsible for the rapid degradation of misfolded proteins. The proteasome target are proteins labelled with the small protein ubiquitin.²⁷

Proteins can be hydrolysed through an alternative process known as autophagy. Several modalities of autophagic protein degradation have been described, including chaperone-mediated autophagy (CMA), micro- and macroautophagy, among others. The choice of the degradation pathway depends on the intrinsic protein properties and how this protein is recognized by the cell and delivered to lysosomes. For example, a single non-aggregated protein could be refolded properly or degraded by any protease pathway, although multiple misfolded proteins are aggregated or form oligomeric complexes that can only be degraded by macroautophagy.²⁸

1.3.4. Ageing and altered proteostasis

The cellular ageing process can be associated with impaired chaperoning activities. Some of the key factors in this regard are poor cellular energetics, caused by mitochondrial dysfunction, deregulation in lipid and glucose metabolism, etc. The lower availability of ATP can explain the repression of ATP-dependent chaperones,

²⁵ Woerner, A. C.; Frottin, F.; Hornburg, D.; Feng, L. R.; Meissner, F.; Patra, M.; Tatzelt, J.; Mann, M.; Winklhofer, K. F.; Hartl, F. U.; Hipp, M. S. *Science* **2016**, *351*, 173-176.

²⁶ Feldman, D. E.; Frydman, J. *Curr. Opin. Struct. Biol.* **2000**, *10*, 26-33.

²⁷ Navon, A.; Ciechanover, A. *J. Biol. Chem.* **2009**, *284*, 33713-33718.

²⁸ Lamark, T.; Johansen, T. *Int. J. Biochem. Cell Biol.* **2012**, *2012*, 736905.

leading to an increase in protein misfolding and a reduction in the cargo recognition and as consequence a proteostasis imbalance.

Age-dependending changes are not restricted to chaperone function or expression. Degradation mechanisms including autophagy and proteasomal activity are both diminished with ageing. Conversely, an overexpression of proteasome subunits or essential autophagy genes increases lifespan and confers stress resistance.²⁸ Also, calory restriction, rapamycin, resveratrol and spermidine extend lifespan and have been proven to improve autophagy through several mechanism.²⁹

1.3.5. Protein misfolding propagation and toxicity

NDDs are characterized by the accumulation of misfolded proteins, which proteins have the ability to recruiting normally folded proteins and induce the wrong-folded, pathogenic conformation *via* a prion-like mechanism. This pathogenic misfolding propagation acts in a interneuronal way or between neuron and glial cells, involving activity-dependent secretion by exosomes³⁰ and chaperone-mediated pathways.^{31,32}

1.4. Neuroinflammation

The central nervous system is protected against external harmful situations (infections, traumas, xenobiotics, etc.) by different physical barriers (blood-brain barrier and cerebrospinal fluid); this anatomic compartmentalization provides CNS with a privileged environment. Furthermore, CNS is endowed with its own immune system, formed by microglia and astrocytes, although in some cases the peripheral immune cells can provide additional protection to the CNS.

The inflammation process plays a fundamental role in the protection process against tumours, infections and is important for the reparation of tissues; however, chronic inflammation can be detrimental. When inflammation happens in the CNS it is called neuroinflammation, and several studies have found strong evidences that the

²⁹ Madeo, F.; Zimmermann, A.; Maiuri, M. C.; Kroemer, G. *J. Clin. Investig.* **2015**, *125*, 85-93.

³⁰ Wu, J. W.; Hussaini, S. A.; Bastille, I. M.; Rodriguez, G. A.; Mrejeru, A.; Rilett, K.; Sanders, D. W.; Cook, C.; Fu, H.; Boonen, R. A.; Herman, M.; Nahmani, E.; Emrani, S.; Figueroa, Y. H.; Diamond, M. I.; Clelland, C. L.; Wray, S.; Duff, K. E. *Nat. Neurosci.* **2016**, *19*, 1085-1092.

³¹ Fontaine, S. N.; Zheng, D.; Sabbagh, J. J.; Martin, M. D.; Chaput, D.; Darling, A.; Trotter, J. H.; Stothert, A. R.; Nordhues, B. A.; Lussier, A.; Baker, J.; Shelton, L.; Kahn, M.; Blair, L. J.; Stevens, S. M. Jr.; Dickey, C. A. *EMBO J.* **2016**, *35*, 1537-1549.

³² Lee, J. G.; Takahama, S.; Zhang, G.; Tomarev, S. I.; Ye, Y. *Nat. Cell Biol.* **2016**, *18*, 765-776.

Chapter 1. Introduction

neuroinflammation is a key process in neurodegeneration and is a common hallmark in NDDs.

Neuroinflammation processes are mediated by microglial cells, which are the macrophages in the CNS but differ from other macrophages in several features such as the ramifications that are present in the cell surface. These ramifications can be used to communicate the microglial cell with surrounding neurons and glial cells.³³

Microglia cells can switch from a resting state (M_0) to two different activate states (M_1 or M_2) by a classical or alternative activation. Bacteria or toxic by-products of cellular metabolism and proinflammatory cytokines promote a classical activation of microglia and lead to the M_1 phenotype. This phenotype is proinflammatory, predominates in the damaged site and releases proinflammatory cytokines such as IL-1 β , IL-6, TNF- α and ROS. An alternative activation route promotes the M_2 state, which is characterized by the production of anti-inflammatory cytokines (IL-4, IL-10 and IL-13) to antagonize the proinflammatory ones. The M_2 phenotype is neuroprotective, immunosuppressive and anti-inflammatory and is involved in the tissue regeneration process.³⁴ Imbalances in M_1/M_2 phenotypes are being extensively studied to understand the complex role of microglia as a neuroprotector or neurodegenerative factor.³⁵

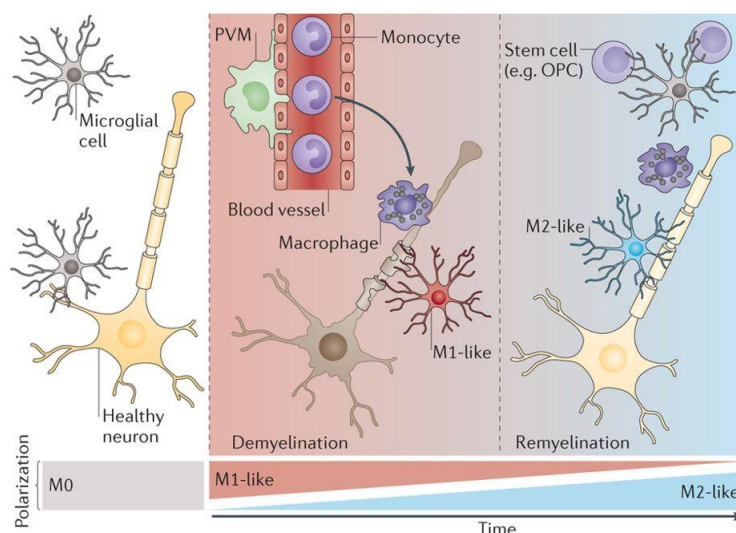


Figure 1.6. Reproduced with permission from reference ³⁶

³³ González, H.; Elgueta, D.; Montoya, A.; Pacheco, R. *J. Neuroimmunol.* **2014**, *274*, 1-13.

³⁴ Orihuela, R.; McPherson, C. A.; Harry, G. J. *Br. J. Pharmacol.* **2016**, *173*, 649-665.

³⁵ Tang, Y.; Le, W. *Mol. Neurobiol.* **2016**, *53*, 1181-1194.

³⁶ Prinz, M.; Priller, J. *Nat. Rev. Neurosci.* **2014**, *15*, 300-312.

The classical activation and M₁ phenotypic differentiation is accomplished by the activation of several surface receptors that are responsible for the recognition of pathogen-associated molecular patterns (PAMPs). These pattern-recognition receptors (PRRs) include toll-like receptors (TLRs), NOD-like receptors (NLRs) and C-type lectin receptors. Microglia expresses all TLRs and they act as the primary PAMP sensors in the CNS, a representative example being the recognition of lipopolysaccharide (LPS) by TLR4. However, the TLR function is not limited to their role as PAMPs receptor. TLRs also recognize damage-associated molecular patterns (DAMPs), such as metabolic products produced by stressed cells or by dead cells like high-mobility group box 1 (HMGB1) and nucleotides.

Prolonged activation of TLRs on microglia by danger signals may have important roles in pathological forms of inflammation and non-apoptotic activation³⁷ that contribute to neurodegenerative diseases.

TLR4 triggering by LPS was shown to sequentially activate caspase 8, followed by caspase 3 and caspase 7. This caspase activation cascade does not induce microglial cell apoptosis but rather contributes to the downstream signalling of TLR4 in microglia. Activated caspase 3 cleaves protein kinase C δ (PKC δ), and cleaved PKC δ modulates the activation of nuclear factor κ B (NF- κ B) and the production of neurotoxic pro-inflammatory mediators such as IL-1 β , tumour necrosis factor (TNF- α) and nitric oxide.³⁷ The inhibition of this caspase was shown to protect neurons in animal models of Alzheimer's and Parkinson's diseases.

The neuron-autonomous toxicity of amyloid β and oligomerized or aggregated pathological forms of amyloid β is associated to the activation of microglia through many receptors, including toll-like receptors (TLRs). Following the recognition of amyloid β , cells induce the production of pro-inflammatory mediators, which are known to be neurotoxic.³⁸

³⁷ Burguillos, M. A.; Deierborg, T.; Kavanagh, E.; Persson, A.; Hajji, N.; García-Quintanilla, A.; Cano, J.; Brundin, P.; Englund, E.; Venero, J. L.; Joseph, B. *Nature* **2011**, *472*, 319-324.

³⁸ Saijo, K.; Glass, C. K. *Nat. Rev. Immunol.* **2011**, *11*, 775-787.

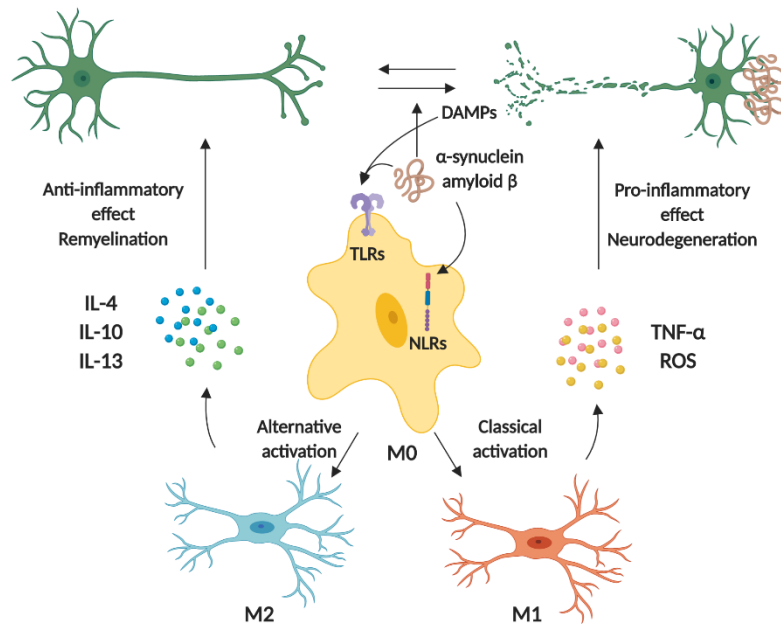


Figure 1.7

1.5. Neuronal calcium signalling and neurodegeneration

1.5.1. An overview of the neuronal roles of calcium

Calcium is a universal second messenger in eukaryotic cells that regulates several common functions like the control of metabolism, phosphorylation, motility, gene transcription and programmed cell death, among others. However, calcium signalling has a particularly important function in neurons that involves the release of neurotransmitters, learning and the formation and consolidation of memory.³⁹ These processes are the result of the direct coupling between plasma membrane depolarization and the increase of intracellular calcium through voltage-dependent and ligand-gated calcium channels.^{40,41,42}

Glutamate, the major excitatory neurotransmitter in the central nervous system, induces an increase in the concentration of cytoplasmic Ca^{2+} by directly activating α -amino-3-hydroxy-5-methylisoxazole-4-propionate acid (AMPA) and N-methyl-D-aspartate (NMDA) receptor channels and by indirectly activating voltage-dependent

³⁹ Brini, M.; Cali, T.; Ottolini, D.; Carafoli, E. *Cell. Mol. Life Sci.* **2014**, *71*, 2787-2814.

⁴⁰ Yuste, R.; Majewska, A.; Holthoff, K. *Nat. Neurosci.* **2000**, *3*, 653-659.

⁴¹ Burnashev, N.; Rozov, A. *Cell Calcium* **2005**, *37*, 489-495.

⁴² Hartmann, J.; Konnerth, A. *Cell Calcium* **2005**, *37*, 459-466.

Ca²⁺ channels (VDCC). Accordingly, antagonists of AMPA and NMDA receptors, or VDCC, have been reported as effective in protecting CNS neurons against glutamate-mediated neuronal death (excitotoxicity).^{43, 44}

1.5.2. Ageing-associated mitochondrial dysfunction and impaired neuronal calcium homeostasis

Under physiological conditions, neurons increase their intracellular Ca²⁺ levels only transiently and this has no damaging effect in neurons. However, ageing compromises the ability to recover the physiological Ca²⁺ concentration, leading to cell impairment.

Mitochondria play a central role in the production of metabolic energy, ROS generation and intracellular calcium storage. Alterations in this organelle such as membrane depolarization, Ca²⁺ overload and release of apoptotic mediators, have a high contribution in the development of NDDs.⁴⁵

The normal ageing process is related with the impairment in the cellular energetic metabolism and an increase in oxidative stress caused, among other factors, by a mitochondrial dysfunction.^{46, 47} Some studies in brain cells of animals of different ages have demonstrated increased levels of oxidative modifications of proteins, lipids and DNA, and reduced energetic mitochondrial production during ageing.⁴⁷

ROS can cause alterations in proteins such as the VDCC and NMDA receptors, as well as oxidative damage to mitochondrial DNA, contributing to intracellular calcium overload and excitotoxicity.⁴⁸

Mitochondrial ATP biosynthesis decreases upon ageing. Also, the neuronal ionic gradient is an ATP-dependent process, which requires that cells spend large amounts of energy in its maintenance. As a consequence of prolonged membrane depolarization and the lack of ionic gradient regeneration, neuronal ATP is depleted, leading to other hallmarks of neurodegenerative disease such as proteostasis dysfunction and increased ROS formation.⁴⁹

⁴³ Mattson, M. P. *Neuromolecular Med.* **2003**, *3*, 65-94.

⁴⁴ Weiss, J. H.; Hartley, D. M.; Koh, J.; Choi, D. W. *Science* **1990**, *247*, 1474-1477.

⁴⁵ Mattson, M. P. *Nature* **2004**, *430*, 631-639.

⁴⁶ Drew, B.; Leeuwenburgh, C. *Acta Physiol. Scand.* **2004**, *182*, 333-341.

⁴⁷ Floyd, R. A.; Hensley, K. *Neurobiol. Aging* **2002**, *23*, 795-807.

⁴⁸ Lee, H. M.; Wang, C.; Hu, Z.; Greeley, G. H.; Makalowski, W.; Hellmich, H. L.; Englander, E. W.; *J. Neurochem.* **2002**, *80*, 928-937.

⁴⁹ Mattson, M, P.; Kroemer, G. *Trends Mol. Med.* **2003**, *9*, 196-205.

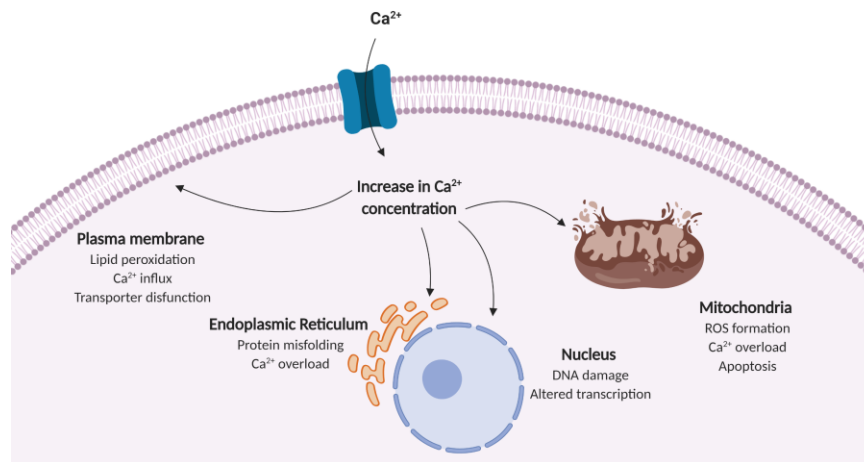


Figure 1.8

1.6. Tracking pathologic processes in NDD and feedback loops between NDD hallmarks

The multifactorial nature of NDD hinders the temporal evolution in the order of appearance of NDD hallmarks. Tracking these events is fundamental in the design of new drugs and to establish proper clinical trials to maximize the probability of success. However, this has not been possible so far for NDDs, which could be due to the lack of suitable biomarkers. A model was proposed for AD based on five well-established biomarkers related to different pathologic characteristics of the disease: A β deposition measured in cerebrospinal fluid (CSF), A β ₄₂ and PET amyloid imaging, increased concentrations of tau and phosphorylated tau (p-tau) in cerebrospinal fluid (CSF), hypometabolism measured by a decreased uptake of fluorodeoxyglucose (FDG) and PET imaging and atrophy on structural MRI.⁵⁰

Several studies show the existence of temporal stages in AD. In a first stage, 5-10 years before dementia diagnosis, A β ₄₂ becomes drastically abnormal, while CSF tau increases more progressively.⁵¹ Changes in CSF A β ₄₂ are an early event that precedes

⁵⁰ Jack Jr, C. R.; Knopman, D. S.; Jagust, W. J.; Petersen, R. C.; Weiner, M. W.; Aisen, P. S.; Shaw L. M.; Vemuri, P.; Wiste, H. J.; Weigand, S. D.; Lesnick, T. G.; Pankratz, V. S.; Donohue, M. C.; Trojanowski, J. Q. *Lancet Neurol.* **2013**, *12*, 207-216.

⁵¹ Buchhave, P.; Minthon, L.; Zetterberg, H.; Wallin, Å. K.; Blennow, K.; Hansson, O. *JAMA Psychiatry* **2012**, *69*, 98-106.

hippocampal atrophy and hypometabolism.⁵² After that, the amyloid PET shows little change in the $A\beta_{42}$ deposition, which becomes static, whereas FDG PET displays an expansion in hypometabolism.⁵³

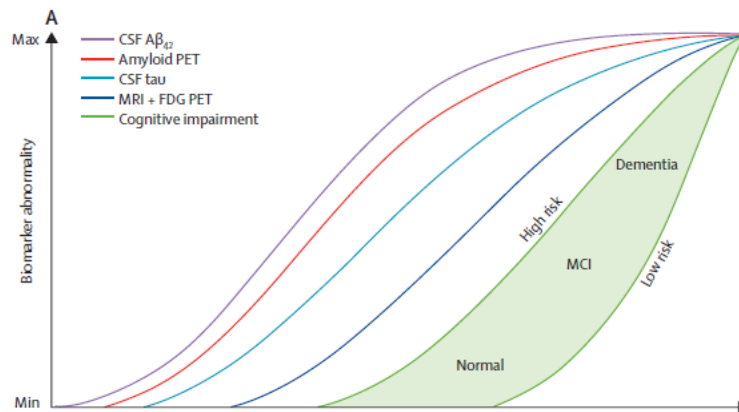


Figure 1.9

In summary, $A\beta_{42}$ and tau become abnormal first, followed by a hypometabolic state and finally neurodegeneration, atrophy and clinical symptoms. However, in some cases the order of appearance of these temporal events may change. For instance, in young adult and middle-aged apolipoprotein E (APOE) $\epsilon 4$ carriers, hypometabolism precedes $A\beta$ aggregation.^{54, 55}

New functional MRI techniques such as task-free functional MRI (TF-fMRI) are being employed to measure the connectivity and network dynamics. TF-fMRI disturbances were described in AD and mild cognitive impairment,⁵⁶ in elderly APOE $\epsilon 4$ carriers who have normal amyloid PET scans⁵⁷ and in cognitively normal people who are amyloid-positive.⁵⁸

⁵² Lo, R. Y.; Hubbard, A. E.; Shaw, L. M.; Trojanowski, J. Q.; Petersen, R. C.; Aisen, P. S.; Weiner, M. W.; Jagust, W. J. *Arch. Neurol.* **2011**, *68*, 1257-1266.

⁵³ Förster, S.; Grimmer, T.; Miederer, I.; Henriksen, G.; Yousefi, B. H.; Graner, P.; Wester, H.-J.; Förstl, H.; Kurz, A.; Dickerson, B. C.; Bartenstein, P.; Drzezga, A. *Biol. Psychiatry* **2012**, *71*, 792-797.

⁵⁴ Morris, J. C.; Roe, C. M.; Xiong, C.; Fagan, A. M.; Goate, A. M.; Holtzman, D. M.; Mintun, M. A. *Ann. Neurol.* **2010**, *67*, 122-131.

⁵⁵ Vemuri, P.; Wiste, H. J.; Weigand, S. D.; Knopman, D. S.; Shaw, L. M.; Trojanowski, J. Q.; Aisen, P. S.; Weiner, M.; Petersen, R. C.; Jack, C. R. *Ann. Neurol.* **2010**, *67*, 308-316.

⁵⁶ Seeley, W. W.; Crawford, R. K.; Zhou, J.; Miller, B. L.; Greicius, M. D. *Neuron* **2009**, *62*, 42-52.

⁵⁷ Sheline, Y. I.; Morris, J. C.; Snyder, A. Z.; Price, J. L.; Yan, Z.; D'Angelo, G.; Liu, C.; Dixit, S.; Benzinger, T.; Fagan, A.; Goate, A. *J. Neurosci.* **2010**, *30*, 17035-17040.

⁵⁸ Sperling, R. A.; LaViolette, P. S.; O'Keefe, K.; O'Brien, J.; Rentz, D. M.; Pihlajamaki, M.; Marshall, G.; Hyman, B. T.; Selkoe, D. J.; Hedden, T.; Buckner, R. L.; Becker, J. A.; Keith, A.; Johnson, K. A. *Neuron* **2009**, *63*, 178-188.

Chapter 1. Introduction

TF-fMRI studies show a reduced functional connectivity in young transgenic AD mice in the same locations where amyloid deposits appear later in life.⁵⁹ These findings suggest that TF-fMRI might locate abnormalities before amyloid biomarkers become abnormal and establish a cause-and-effect relation: a higher synaptic activity generally leads to a higher amyloid deposition.⁶⁰ However, this relationship is subject to inter-individual variability.

The temporal sequence of appearance of events is unclear for all NDDs and more research about this issue is needed to improve efficiency in drug design. On the other hand, there is a great deal of evidence about feedback loops between the hallmarks of NDDs and neurodegeneration.

- Oxidative stress feedback: Oxidative stress may cause modifications of proteins, lipids and DNA, and reduced energetic mitochondrial production during ageing.⁶¹ ROS induce alterations in proteins that lead to their misfolding and aggregation. They also cause malfunction of receptors such as VDCC and NMDA, contributing to intracellular calcium overload and excitotoxicity.⁴⁸ Furthermore, oxidative stress activates redox-sensitive pathways, leading to sustained M₁ microglial activation.⁶²
- Protein aggregation and proteostasis impairment: The accumulation of misfolded proteins may cause calcium signalling abnormalities, mitochondrial dysfunction, oxidative stress, and neuroinflammation. However, the relationship between misfolded proteins and other signs of cellular distress is bidirectional, and they are believed to be a cause as well as a consequence of neurodegeneration. For example, amyloid- β , α -synuclein, and mHtt all cause acute oxidative stress in neurons and/or astrocytes, neuroinflammation and disrupt the anti-oxidant astroglia defences.^{63, 64} Conversely, oxidative stress promotes the aggregation of

⁵⁹ Bero, A. W.; Yan, P.; Roh, J. H.; Cirrito, J. R.; Stewart, F. R.; Raichle, M. E.; Lee, J. M.; Holtzman, D. M. *Nat. Neurosci.* **2011**, *14*, 750-756.

⁶⁰ Jagust, W. J.; Mormino, E. C. *Trends Cogn. Sci.* **2011**, *15*, 520-526.

⁶¹ Floyd, R. A.; Hensley, K. *Neurobiol. Aging* **2002**, *23*, 795-807.

⁶² Rojo, A. I.; McBean, G.; Cindric, M.; Egea, J.; López, M. G.; Rada, P.; Zarkovic, N.; Cuadrado, A. *Antioxid. Redox Signal.* **2014**, *21*, 1766-1801.

⁶³ Jiang, T.; Sun, Q.; Chen, S. *Prog. Neurobiol.* **2016**, *147*, 1-19.

⁶⁴ Angelova, P. R.; Abramov, A. Y. *Biochem. Biophys. Res. Commun.* **2017**, *483*, 1110-1115.

disease proteins, and contributes to age- and disease-related proteostatic collapse.⁶⁵

- Calcium overload feedback: The increase in intracellular calcium concentrations may promote conformational changes in some calcium sensitive proteins, leading to a misfolded structure and protein aggregation. Also, the maintenance of calcium gradient under this continued calcium influx may cause ATP depletion and the subsequent energetic deficiency causes ROS formation and proteasome dysfunction.
- Microglial inflammation feedback: The sustained activation of M₁ microglia contributes to a high oxidative stress status in the cells, mediated by proinflammatory cytokines. There is also some evidence that some cytokines possess the ability to block autophagy in microglia, promoting protein misfolding and aggregation. Also, long-term cytokine activation causes neuronal death.

All these hallmarks are interconnected and thus acting selectively in single one is likely to be an unsuccessful strategy, since the interrelated feedback loops can elude the blocked target by an alternative pathway ultimately leading to neurodegeneration. For this reason, the polypharmacology approach has attracted much interest in NDDs and other multifactorial diseases, since acting in several pathways may exert a more efficient neuroprotective effect.

1.7. Multitarget drug discovery

The “one target, one drug” approach to drug discovery currently dominates research in the pharmaceutical industry. However, there is a current trend towards a paradigm shift caused by the lack of success in drug development in the area of multifactorial diseases. As summarized above, these diseases are characterized by multiple genetic and environmental alterations leading to a pathological state, and hence targeting several diseases checkpoints could lead to a better system regulation.⁶⁶ Multitarget kinase inhibitors exemplify the success of this approach in the therapy of a multifactorial disease, namely cancer.⁶⁷

⁶⁵ Höhn, A.; Weber, D.; Jung, T.; Ott, C.; Hugo, M.; Kochlik, B.; Kehm, R.; König, J.; Grune, T.; Castro, J. P. *Redox Biol.* **2016**, *11*, 482-501.

⁶⁶ Bolognesi, M. L. *Curr. Med. Chem.* **2013**, *20*, 1639-1645.

⁶⁷ Morphy, R.; Rankovic, Z. *Curr. Pharm. Des.* **2009**, *15*, 587-600.

Chapter 1. Introduction

This challenging approach to modify multiple targets simultaneously (polypharmacology) can be achieved by three strategies.⁶⁸

1. Drug cocktails.
2. Combination of several drugs in the same formulation.
3. Multitarget Directed Ligands (MTDL): in this strategy, a single chemical entity possess the ability to modify multiple targets.



Figure 1.10

MTDLs have a profoundly different risk-benefit profile compared with coformulated drugs or drug cocktails. In the first stages of the drug discovery process, it is significantly more difficult to adjust the ratio of activities at the different targets. However, this increased complexity in this initial, less expensive stage, is more than compensated, in terms of the risks and costs involved, at the clinical development phase, which is in principle not different from the development of any other single entity, in comparison with the very complex development required for drug combinations. Another advantage is a lower risk of drug-drug interactions compared to cocktails or multicomponent drugs,⁶⁹ and the avoidance of poor patient compliance issues, one of the drawbacks of drug cocktails.

MTDLs can be classified into three groups according to the design strategy used. “Conjugates” or “hybrids” are MTDLs that contain pharmacophores for each target bound by a linker. Usually these conjugates contain a metabolically stable linker, but it also could be cleavable to release both active fragments *in vivo* (mutual prodrugs). In this strategy, the molecular weight is usually high, which could be a limitation. The

⁶⁸ Morphy, R.; Rankovic, Z. *J. Med. Chem.* **2005**, *48*, 6523-6543.

⁶⁹ Edwards, I. R.; Aronson, J. K. *Lancet* **2000**, *356*, 1255-1259.

“fused” MTDLs arise from the same logical design, but the linker between the active frameworks is removed. The most attractive and complex approach is the “merged” MTDL that combines multiple activities in a single framework formed by combining structural fragments key for the two sought activities without requiring the presence of complete molecules addressed at each target.

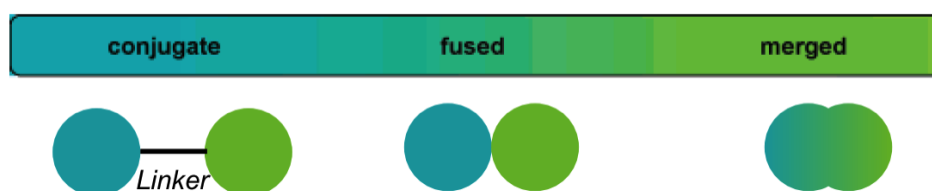


Figure 1.11

CHAPTER 2. OBJECTIVES

Objective 1

Some natural products that contain carbonyl groups or β -dicarbonyl fragments conjugated to one or two styryl chains (ferulic and caffeic acid esters, dehydrozingerone, curcumin) have shown promising neuroprotective activities associated to multiple mechanisms. In this context, our first goal was to design and synthesize libraries of cyclic analogues of cinnamic esters and curcumin in order to study their antioxidant activity and neuroprotective profiles. The molecular architecture of these compounds was organized around a central 2-pyrrolin-5-one core, which was expected to increase their stability while also providing synthetic handles for the preparation of multitarget-directed ligands (Figure 2.1).

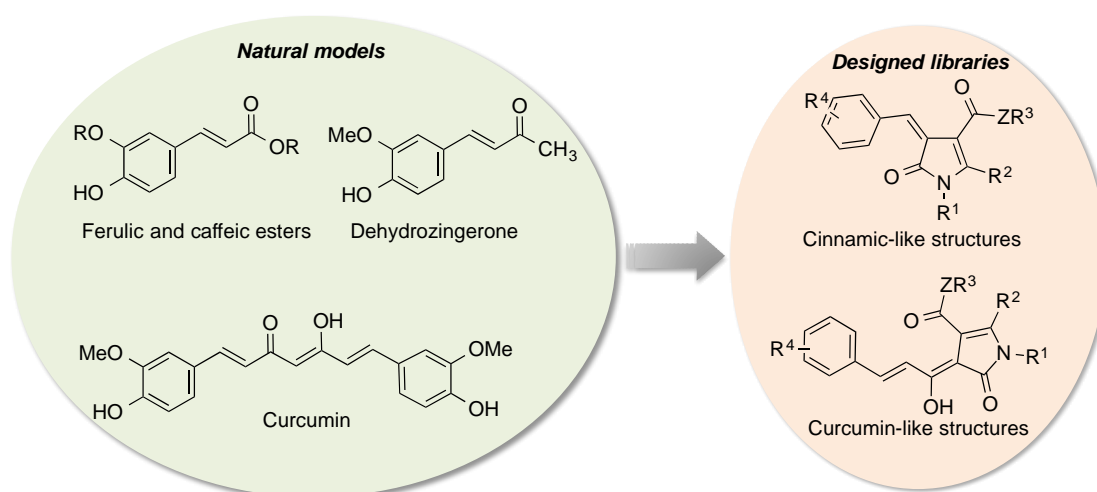


Figure 2.1

This objective can be divided into the following tasks:

- 1.1. Development of a suitable synthetic method for the preparation of the 2-pyrrolin-5-one core. In view of the current importance of multicomponent reactions as a fast and flexible route to molecular diversity, we planned a three-component reaction from primary amines, β -dicarbonyl compounds and α -haloesters, related to the Hantzsch pyrrole synthesis.
- 1.2. Development of suitable conditions for the Knoevenagel reaction of the C-4 position of the pyrrolinone derivatives with aromatic aldehydes, to obtain the cyclic cinnamic-like compounds.

Chapter 2. Objectives

1.3. Development of suitable conditions for the acylation of the pyrrolinone C-4 position with cinnamyl chlorides, to obtain the curcumin analogues.

1.4. Pharmacological study of the libraries thus generated, establishment of structure-activity relationships and selection of candidate compounds for further studies.

Objective 2

The spiro oxindole family of alkaloids provides another interesting natural model in the search for neuroprotective agents. Rhynchophylline, in particular, activates the PI3K/Akt/mTOR signalling pathway and has shown neuroprotection in a variety of neurodegenerative disease models. We have designed a library of oxindole-derived dispiro compounds as rhynchophylline analogues (Figure 2.2).

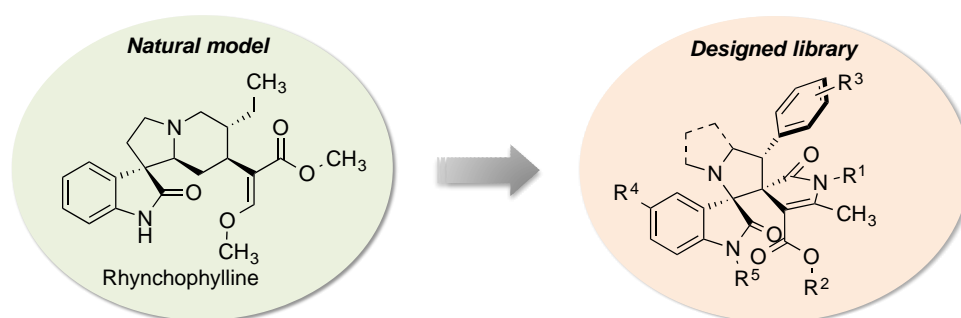


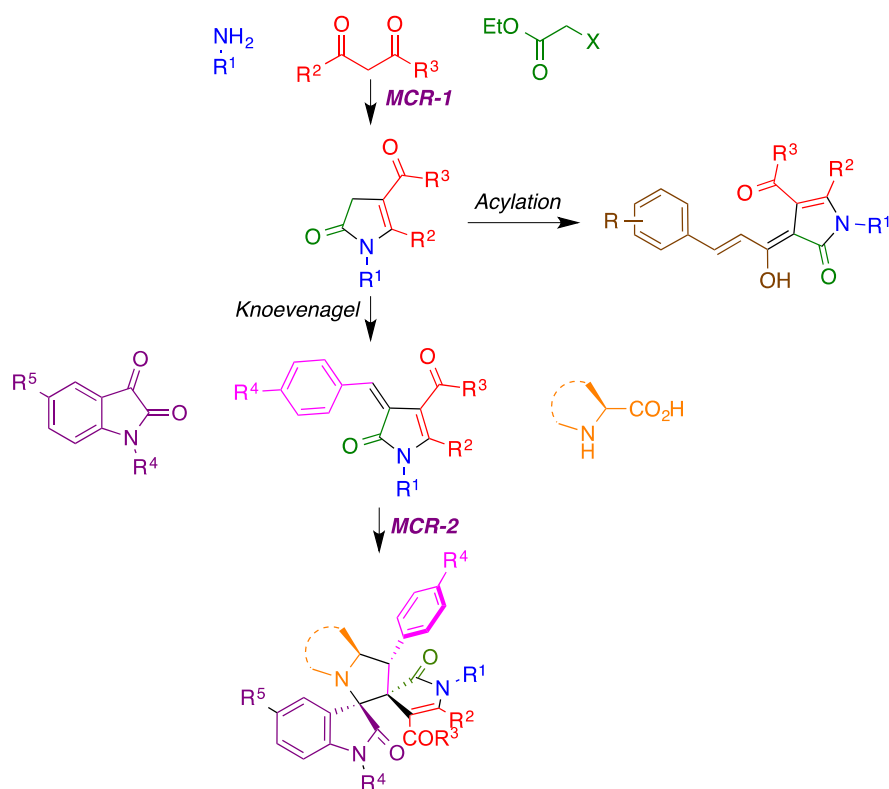
Figure 2.2

This objective can be divided into the following tasks:

2.1. Development of a suitable synthetic method for the preparation of the dispirooxindoles, based on a 1,3-dipolar cycloaddition reaction.

2.2. Pharmacological study of the dispirooxindoles library, including SAR correlations and the selection of compounds for further study.

The synthetic aspects of objectives 1 and 2 are summarized in Scheme 2.1.



Scheme 2.1

Objective 3

Quinone moieties are present in several natural and unnatural compounds with neuroprotective activity. We have designed a library of compounds derived from the 2,5,8-quinolinetriene skeleton and containing an indolyethyl side chain. These compounds can be considered vinyllogs of the natural antioxidant and neuroprotectant melatonin and are expected to show the multitarget profile summarized in Figure 2.3.

Objective 4

The dysregulation of calcium homeostasis plays a central role in neurodegenerative diseases. Neuronal calcium levels depend on the activity of a large number of proteins (the “calcium signalling toolkit”) in membranes of the cell, the endoplasmic reticulum and the mitochondria. The hybrid compound shown in Figure 2.4 was designed to combine in a single molecule the frameworks of CGP-37157, a well-known inhibitor of the mitochondrial mNCX transporter with neuroprotective activity, and lipoic acid, a natural antioxidant. Both structural fragments of the target hybrid bear stereogenic centres, but only lipoic acid is commercially available in both enantiomeric forms.

Chapter 2. Objectives

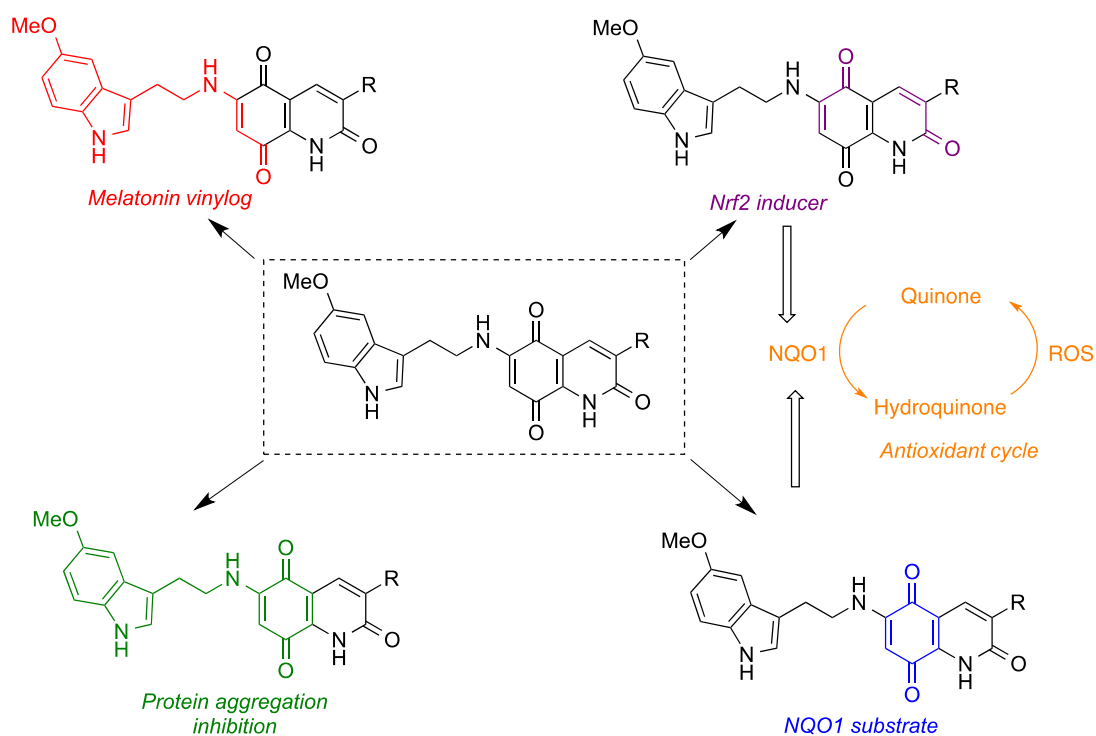


Figure 2.3

This objective can be divided into the following tasks:

- 2.1. Development of suitable synthetic methods for the preparation of CGP-37157 and its aza analogue in enantiomerically pure form to allow the coupling of either enantiomer with both (*R*) and (*S*) lipoic acid.
- 2.2. Pharmacological study of each of the four enantiomers of the target hybrid compound.

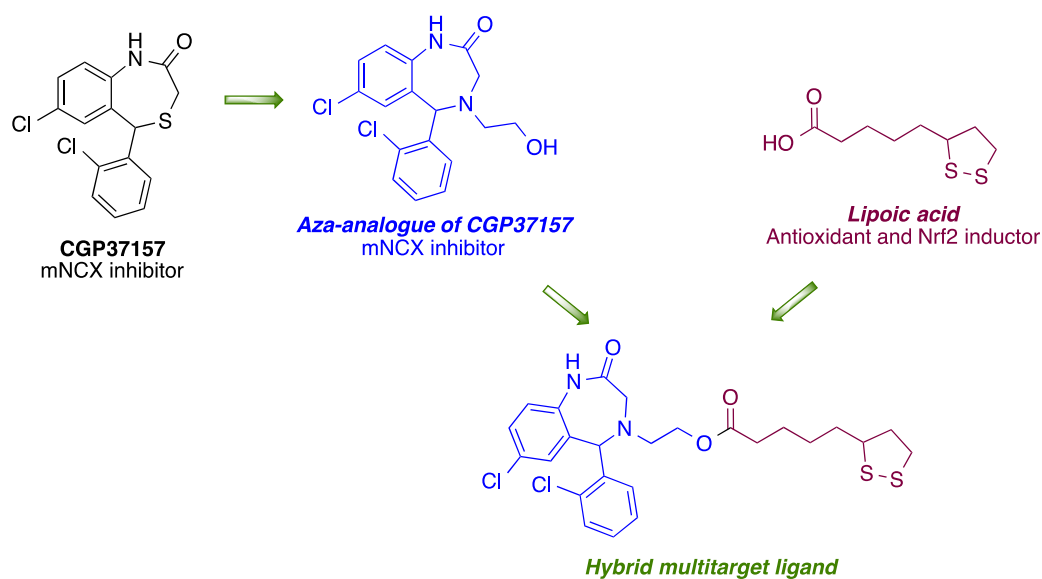


Figure 2.4

Objective 5

Galectins are carbohydrate-binding molecules present in the cell surface that have key roles in a variety of physiological processes, including neuroinflammation. Our goal in this area was the synthesis of the heterocyclic fragments of the hybrid carbohydrate derivatives shown in Figure 2.5.

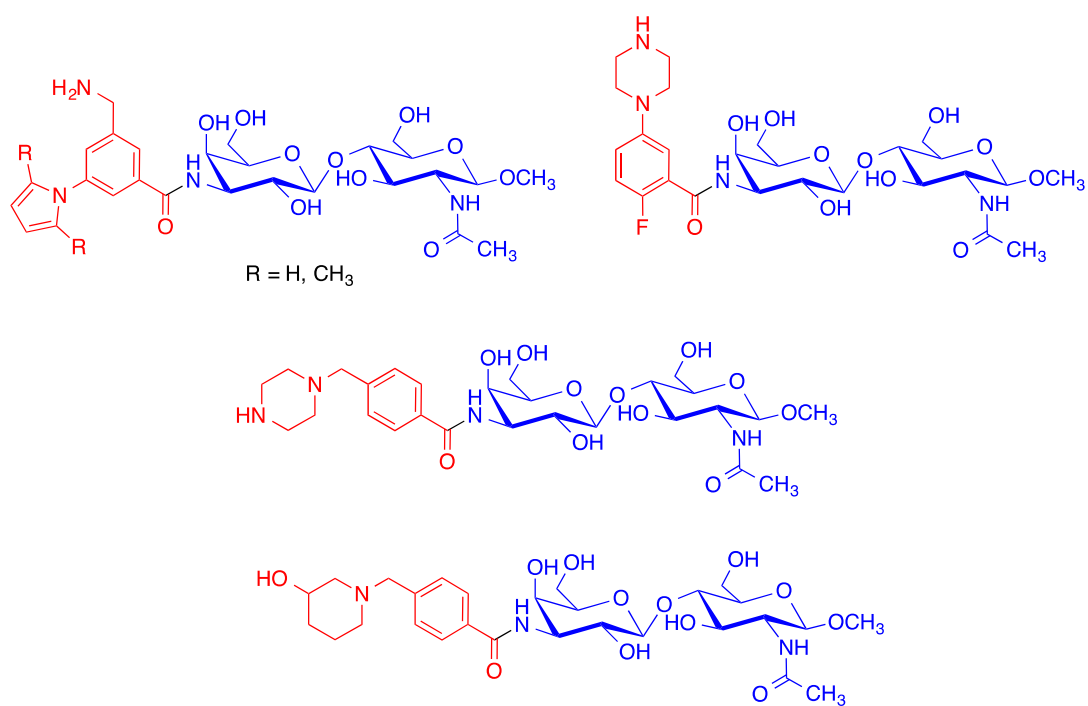


Figure 2.5

**CHAPTER 3. NEUROPROTECTIVE COMPOUNDS
RELATED TO CINNAMIC ESTERS AND CURCUMIN**

3.1. Oxidative stress and neurodegeneration: A closer look

The imbalance in ROS production leads to oxidative stress, as was discussed previously in Chapter 1. While ROS have physiological roles as second messengers in moderate concentrations, the over-production of ROS and senescence were found to be correlated in several pathological processes. Oxidative stress is thus a major hallmark in neurodegeneration, as the result of the hyperproduction of ROS combined with the impairment of antioxidant defences. This imbalance between ROS production and quenching causes brain tissue damage and, as a consequence, neuronal death and neurodegeneration.^{70, 71}

Cells have developed a number of adaptive defences to reduce ROS, while keeping cellular redox homeostasis. These antioxidant systems act through a series of antioxidant molecules and detoxifying enzymes that can provide control over these reactive species either by quickly removing or detoxifying them.

Several antioxidant systems are involved in redox homeostasis, and some of them are mediated by transcription factors. The nuclear factor erythroid 2-related factor 2 (Nrf2) is a master regulator in cellular redox homeostasis and the activation of this pathway an effective mechanism against oxidative or electrophilic stress.⁷²

3.2. The Keap1-Nrf2-ARE pathway

3.2.1. The phase II antioxidant response

Electrophilic or oxidative stimuli induce the biosynthesis of a battery of cytoprotective genes by the Nrf2 transcription factor. Nrf2 is bound to Keap1 in the cytosol under physiological conditions. Keap1 acts as a negative regulatory system, maintaining Nrf2 in the cytoplasm by an interaction with the cytoskeleton and binds to the E3 ligase, leading to ubiquitination Nrf2 and thus promoting its proteasomal degradation.⁷³ In summary, Nrf2 is constitutively synthesized and rapidly degraded by the proteasome

⁷⁰ Lotharius, J.; Brundin, P. *Nat. Rev. Neurosci.* **2002**, 3,932-942.

⁷¹ Barnham, K. J.; Masters, C. L.; Bush, A. I. *Nat. Rev. Drug Discov.* **2004**, 3, 205-214.

⁷² Kumar, H.; Koppula, S.; Kim, I. S.; More, S. V.; Kim B. W.; Choi, D. K. *CNS Neurol. Disord.: Drug Targets* **2012**, 11, 1015-1029.

⁷³ Cullinan, S. B.; Gordan, J. D.; Jin, J.; Harper, J. W.; Diehl, J. A. *Mol. Cell. Biol.* **2004**, 24, 8477-8486.

under unstressed conditions. However, in response to oxidative stress, Nrf2 is released from Keap1 following a conformational change of the latter associated to the oxidation to cystine of two cysteine residues in the “sensor” region of the protein (Figure 3.1). Alternatively, the sensor region of Keap1 may also be activated by reaction of the cysteine residues in the sensor region with electrophiles. Once liberated from Keap1, Nrf2 is translocated into the nucleus, where it promotes the transcription of cytoprotective genes by binding to the ARE sequence of DNA (antioxidant response element),⁷³ with participation of several coactivator proteins.

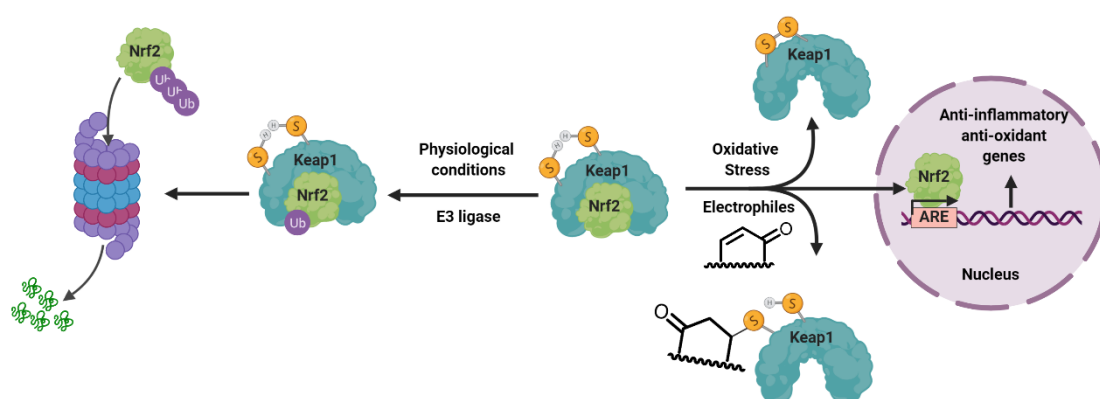


Figure 3.1

The classical Nrf2 target genes encode enzymes distributed in several organelles and subcellular compartments. These enzymes participate in metabolic reactions that that scavenges ROS and neutralizes electrophiles, such as superoxide dismutase (SOD), glutathione peroxidase, catalase, glutathione reductase (GR), glutamate cysteine ligase (GCL), NAD(P)H/quinone oxidoreductase 1 (NQO1).⁷⁴ Nrf2 also plays a critical role in the induction of genes involved in drug metabolism and distribution, including multiple genes encoding non-cytochrome P450 phase-I and phase-II drug metabolism enzymes⁷⁵ Some enzymes are involved in the generation of antioxidant molecules such as glutathione synthase, which is needed for the biosynthesis of glutathione (GSH), the most abundant small-molecule antioxidant, that also takes part in the neutralization of electrophiles.

⁷⁴ Cuadrado, A.; Rojo, A. I.; Wells, G.; Hayes, J. D.; Cousin, S. P.; Rumsey, W. L.; Attucks, O. C.; Franklin, S.; Levonen, A. - L.; Kensler, T. W.; Dinkova-Kostova, A. T. *Nat. Rev. Drug Discov.* **2019**, *18*, 295–317 and references therein.

⁷⁵ Wu K. C.; Cui J. Y.; Klaassen C. D.; *PLOS One* **2012**, *7*, e39006.

3.2.2. Nrf2 activation as a useful approach to neurodegenerative disease therapy

Due to its key role in the management of oxidative stress, the Nrf2/ARE pathway has emerged as a promising target for neurodegenerative diseases, including Alzheimer's disease (AD), Parkinson's disease (PD), Huntington's disease (HD), multiple sclerosis (MS) and amyotrophic lateral sclerosis (ALS).^{76, 77} Furthermore, Nrf2 deficiency has been found in several neurodegenerative diseases and thus AD patients show a dramatic decrease in nuclear Nrf2 in hippocampal neurons,⁷⁸ experimental animal models in a Nrf2-knockout mice of PD shows a specific loss of dopaminergic neurons^{79, 80} and post-mortem studies of patients with ALS show an increased Keap1 mRNA in the motor cortex,⁸¹ leading to a decline in Nrf2 activity.

In this context, it is not surprising that Nrf2 activation has been demonstrated to extend survival in AD,⁸² PD⁸³ and ALS⁸⁴ animal models. Therefore, small-molecule modulators of the Keap1-Nrf2-ARE pathway should be potential preventive and therapeutic agents. Nrf2 activation can in principle be achieved by three mechanisms:

- Activation of the sensor region of Keap1 with electrophilic compounds that have a suitable safety profile.
- Interference with the Keap1-Nrf2 interaction with non-electrophilic compounds that behave as protein-protein interaction inhibitors (PPI).
- Indirect mechanisms based on the activation of certain signalling pathways.

⁷⁶ Kumar, H.; Koppula, S.; Kim, I. S.; More, S. V.; Kim B. W.; Choi, D. K. *CNS Neurol. Disord.: Drug Targets* **2012**, *11*, 1015-1029.

⁷⁷ Zhang, M.; An, C.; Gao, Y.; Leak, R. K.; Chen J.; Zhang, F. *Prog. Neurobiol.* **2013**, *100*, 30-47.

⁷⁸ Ramsey, C. P.; Glass, C. A.; Montgomery, M. B.; Lindl, K. A.; Ritson, G. P.; Chia, L. A.; Hamilton, R. L.; Chu C. T.; Jordan-Sciutto, K. L. *J. Neuropathol. Exp. Neurol.* **2007**, *66*, 75-85.

⁷⁹ Burton, N. C.; Kensler T. W.; Guilarte, T. R. *Neurotoxicology* **2006**, *27*, 1094-1100.

⁸⁰ Chen, P. C.; Vargas, M. R.; Pani, A. K.; Smeyne, R. J.; Johnson, D. A.; Kan Y. W.; Johnson, J. A. *Proc. Natl. Acad. Sci. U. S. A.* **2009**, *106*, 2933-2938.

⁸¹ Sarlette, A.; Kramp, K.; Grothe, C.; Neuhoff, N.; Dengler R.; Petri, S. *J. Neuropathol. Exp. Neurol.* **2008**, *67*, 1055-1062.

⁸² Dumont, M.; Wille, E.; Calingasan, N. Y.; Tampellini, D.; Williams, C.; Gouras, G. K.; Liby, K.; Sporn, M.; Nathan, C.; Flint Beal M.; Lin, M. T. *J. Neurochem.* **2009**, *109*, 502-512.

⁸³ Kaidery, N. A.; Banerjee, R.; Yang, L.; Smirnova, N. A.; Hushpalian, D. M.; Liby, K. T.; Williams, C. R.; Yamamoto, M.; Kensler, T. W.; Ratan, R. R.; Sporn, M. B.; Beal, M. F.; Gazaryan I. G.; Thomas, B. *Antioxid. Redox Signaling* **2013**, *18*, 139-157.

⁸⁴ Neymotin, A.; Calingasan, N. Y.; Wille, E.; Naseri, N.; Petri, S.; Damiano, M.; Liby, K. T.; Risingsong, R.; Sporn, M.; Beal M. F.; Kiaei, M. *Free Radical Biol. Med.* **2011**, *51*, 88-96.

3.2.3. Non-electrophilic Nrf2 activation

The first group of Nrf2 activators act by non-electrophilic, non-covalent direct interference with the protein–protein interaction between Keap1 and Nrf2. Bis-sulphonamide compounds, obtained from a high-throughput screening campaign, are the most efficient inhibitors of the Nrf2–Keap1 interaction.⁸⁵ The availability of the Keap1 crystal structure (pdb 4XMB) has enabled the rational design and optimization of new PPI inhibitors and afforded new lead compounds such as CPUY192018.⁸⁶

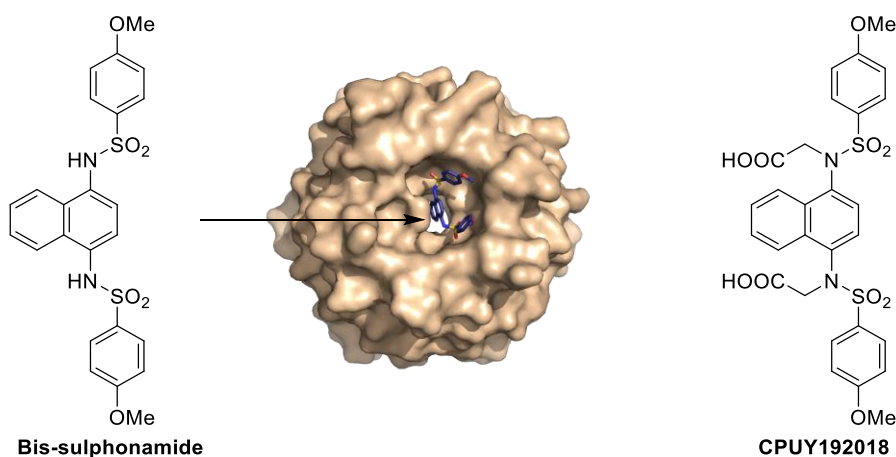


Figure 3.2

3.2.4. Electrophilic Nrf2 activation

As mentioned above, electrophilic compounds bind to cysteine residues present in Keap1 and induce a conformational change that releases Nrf2. Electrophiles have an advantage over scavenger antioxidant molecules because their action is more sustained and amplified by transcription-mediated signalling pathways.⁸⁷

Electrophilic compounds, leading to covalent drug-target interactions, often have a reputation for high toxicity, but nevertheless there is a recent surge in interest in rationally designed covalent inhibitors.⁸⁸ Electrophilic compounds can have both protective and toxic effects on cells in a dose-dependent manner (Figure 3.3). Low-

⁸⁵ Marcotte, D.; Zeng, W.; , Hus J.-C.; McKenzie, A.; Hession, C.; Ji, P.; Bergeron, C.; Lugovskoy, A.; Enyedy, I.; Cuervo, H.; , Wang, D.; Atmanene, C.; Roecklin, D.; Vecchi, M.; Vivat, V.; Kraemer, J.; Winkle, D.; Hong, V.; Chao, J.; , Lukashev, M.; Silvian, L. *Bioorg. Med. Chem.* **2013**, *21*, 4011-4019.

⁸⁶ Jiang, Z. Y.; Lu, M. C.; Xu, L. L.; Yang, T. T.; Xi, M. Y.; Xu, X. L.; Sun, H. P. *J. Med. Chem.* **2014**, *57*, 2736-2745.

⁸⁷ Taguchi, K.; Motohashi, H.; Yamamoto, M. *Genes Cells* **2011**, *16*, 123-140.

⁸⁸ For selected reviews of covalent drugs, see: (a) Singh, J.; Petter, R. C.; Baillie, T. A.; Whitty, A. *Nat. Rev. Drug Discov.* **2011**, *10*, 307-317. (b) Baillie, T. A. *Angew. Chem. Int. Ed.* **2016**, *55*, 13408-13421. (c) De Cesco, S.; Kurian, J.; Dufresne, C.; Mittermaier, A. K.; Moitessier, N. *Eur. J. Med. Chem.* **2017**, *138*, 96-114.

dose stimulation most likely represents an adaptive biological response leading an increase in neuroprotection and longevity.^{89,90} However, high-dose stimulation promotes indiscriminate reaction with thiol groups, resulting in a harmful effect.⁹¹

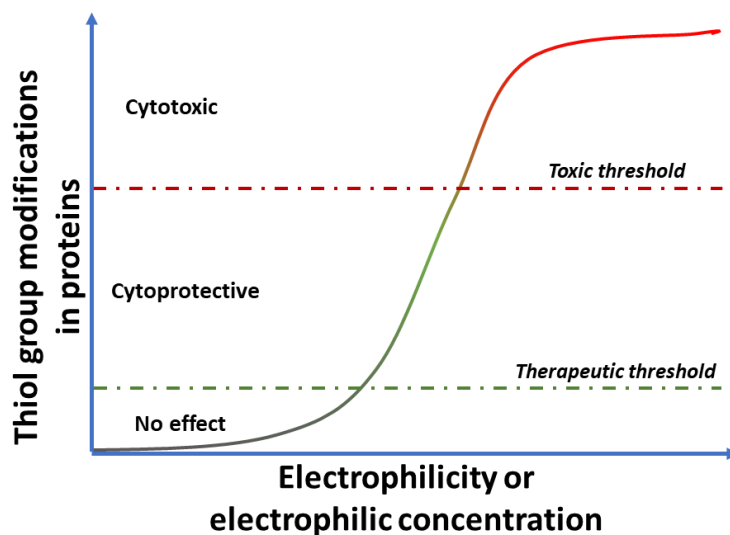


Figure 3.3

A successful example for electrophilic Nrf2 activation against an oxidative stress-connected disease is dimethyl fumarate (DMF, Tecfidera®), which was approved by the FDA in 2014 for the treatment of multiple sclerosis and has a good safety profile.⁹² Dimethyl fumarate acts as a prodrug that, after its *in vivo* hydrolysis, generates monomethyl fumarate (MMF), which reacts with the Cys-151 residue in Keap1 releasing Nrf2.⁹³ Based on this metabolic conversion, several biopharmaceutical companies are now developing new formulations for the slow and sustained release of MMF.

⁸⁹ Birringer, M. *Pharm. Res.* **2011**, *28*, 2680-2694.

⁹⁰ Satoh, T.; Rezaie, T.; Seki, M.; Sunico, C. R.; Tabuchi, T.; Kitagawa, T.; Yanagitai, M.; Senzaki, M.; Kosegawa, C.; Taira, H.; McKercher, S. R.; Hoffman, J. K.; Roth, G. P.; Lipton, S. A. *J. Neurochem.* **2011**, *119*, 569-578.

⁹¹ Groeger, A. L.; Freeman, B. A. *Mol. Interv.* **2010**, *10*, 39-50.

⁹² Dodson, M.; De La Vega, M. R.; Cholanians, A. B.; Schmidlin, C. J.; Chapman, E.; Zhang, D. D. *Annu. Rev. Pharmacol. Toxicol.* **2019**, *59*, 555-575.

⁹³ Linker, R. A.; Lee D. H.; Ryan, S.; van Dam A. M.; Conrad, R.; Bista, P.; Zeng, W.; Hronowsky, X.; Buko, A.; Chollate, S.; Ellrichmann, G.; Brück, W.; Dawson, K.; Goelz, S.; Wiese, S.; Scannevin, R. H.; Lukashev, M.; Gold, R. *Brain* **2011**, *134*, 678-692.

3.2.5. Natural products targeting the Keap1-Nrf2-ARE pathway

Natural products can also inspire the development of analogues with improved bioavailability. Curcumin, a yellow pigment from turmeric (*Curcuma longa*), is a well-known antioxidant due to the presence of two phenolic functional groups responsible for the direct scavenging of ROS.⁹⁴ Curcumin contains two electrophilic positions that can react readily with cysteine residues of Keap1 and promotes the Nrf2 translocation to nucleus increasing the cytoprotective proteins biosynthesis.⁹⁵ Curcumin has also shown to indirectly activate the ARE system by stimulating upstream kinase pathways,⁹⁶ and is also an epigenetic Nrf2 modulator.⁹⁷ Finally, curcumin has been shown to possess a number of additional relevant therapeutic properties including anti-inflammatory, metal chelation and protein aggregation inhibition properties.⁹⁸

Dehydrozingerone is a known metabolic product of curcumin with a simpler structure that has a better pharmacokinetics than its parent compound.⁹⁹ Dehydrozingerone and curcumin both bear styryl ketone moieties with similar substitutions on the phenyl ring.¹⁰⁰

Another family of natural products structurally very close to dehydrozingerone are the cinnamic acid esters, such as caffeic acid phenethyl ester and ferulic acid ethyl ester. These α,β -unsaturated esters were shown to induce the ARE system with comparable potency to curcumin.¹⁰¹ Caffeic acid ester shows antiinflammatory and immunomodulatory properties.¹⁰² Ferulic acid and its derivatives are found in many

⁹⁴ Ak, T.; Gülçin, I. *Chem. Biol. Interact.* **2008**, *174*, 27–37.

⁹⁵ Scapagnini, G.; Colombrita, C.; Amadio, M.; D'Agata, V.; Arcelli, E.; Sapienza, M.; Quattrone, A.; Calabrese, V. *Antioxid. Redox. Signal* **2006**, *8*, 395–403.

⁹⁶ Thangapazham, R. L.; Sharma, A.; Maheshwari, R. K. *AAPS J.* **2006**, *8*, 443–449.

⁹⁷ Khor, T. O.; Huang, Y.; Wu, T.-Y.; Shu, L.; Lee, J.; Kong, A.-N.T. *Biochem. Pharmacol.* **2011**, *82*, 1073–1078.

⁹⁸ Lee, W. H.; Loo, C. Y.; Bebawy, M.; Luk, F.; Mason, R. S.; Rohanizadeh, R. *Curr. Neuropharmacol.* **2013**, *11*, 338–378.

⁹⁹ Priyadarsini, K. I.; Devasagayam, T. P.; Rao, M. N.; Guha, S. N. *Radiat. Phys. Chem.* **1999**, *54*, 551–558.

¹⁰⁰ Rajakumar, D. V.; Rao, M. N. *Mol. Cell. Biochem.* **1994**, *140*, 73–79.

¹⁰¹ Balogun, E.; Hoque, M.; Gong, P.; Killeen, E.; Green, C. J.; Foresti, R.; Alam, J.; Motterlini, R. *Biochem J* **2003**, *371*, 887–895.

¹⁰² Michaluart, P.; Masferrer, J. L.; Carothers, A. M.; Subbaramaiah, K.; Zweifel, B. S.; Koboldt, C.; Mestre, J. R.; Grunberger, D.; Sacks P. G.; Tanabe, T.; Dannenberg, A. J. *Cancer Res.* **1999**, *59*, 2347–2352.

fruits and vegetables and are known to confer a strong protection against oxidation of proteins and lipids.¹⁰³

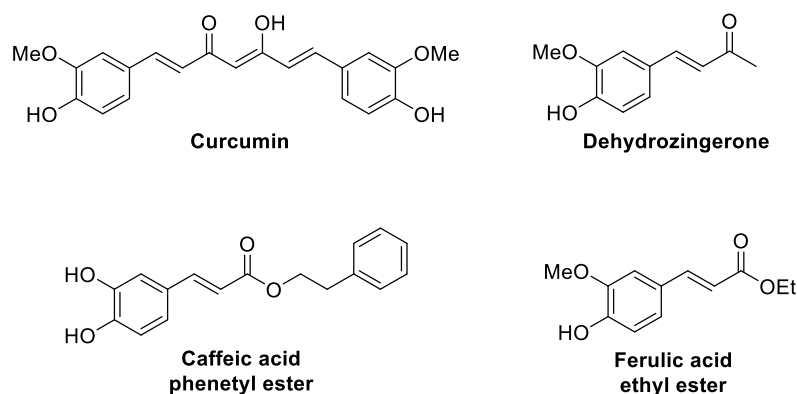


Figure 3.4

3.3. Design of cyclic analogues of cinnamic esters and curcumin

Despite the interesting pharmacological profile and versatile potential applications of curcumin, its weak bioavailability and high degradation suffered upon oral administration hampers its use as a successful therapeutic agent.¹⁰⁴ This unsuitable pharmacokinetic profile of curcumin is due its rapid metabolism,¹⁰⁵ which mainly comprises: (a) successive reductions of the C=C and C=O double bonds; (b) the enzymatic cleavage of the β -diketone moiety,¹⁰⁶ mediated *in vivo* by several aldo-keto reductases;¹⁰⁷ (c) conjugation with glutathione *via* Michael addition; (d) conjugation of the phenolic hydroxyls or the secondary alcohols arising from the reduction reactions with glucuronic acid. Curcumin also suffers from *in vitro* chemical instability at neutral and basic pH.¹⁰⁸

Some strategies to increase the bioavailability of curcumin have been described (Figure 3.5). Its methylation at the 2 and 6 positions decreases the reductive metabolism of curcumin.¹⁰⁹ Also, the bioisosteric replacement of the diketone by a pyrazole (CNB-

¹⁰³ Scapagnini, G.; Butterfield, D. A.; Colombrita, C.; Sultana, R.; Pascale, A.; Calabrese, V. *Antioxid. Redox. Signal* **2004**, *6*, 811-818.

¹⁰⁴ Anand, P.; Kunnumakkara, A. B.; Newman, R. A.; Aggarwal, B. B. *Mol. Pharm.* **2007**, *4*, 807-818.

¹⁰⁵ Metzler, M.; Pfeiffer, E.; Schulz, S. I.; Dempe, J. S. *Biofactors* **2013**, *39*, 14-20.

¹⁰⁶ Nagpure, B. A. L.; Gupta, R. K. *Indian J. Chem., Sect. B Org. Med. Chem.* **2011**, *50*, 1119.

¹⁰⁷ Rosemond, M. J. C.; St. John-Williams, L.; Yamaguchi, T.; Fujishita, T.; Walsh, J. S. *Chem. Biol. Interact.* **2004**, *147*, 129-139.

¹⁰⁸ Tomren, M. A.; Másson, M.; Loftsson, T.; Tønnesen, H. H. *Int. J. Pharm.* **2007**, *338*, 27-34.

¹⁰⁹ Koo, H. J.; Shin, S.; Choi, J. Y.; Lee, K. H.; Kim, B. T.; Choe, Y. S. *Sci. Rep.* **2015**, *5*, 14205.

001) improves the pharmacokinetics of curcumin and maintains or improves some activities such as amyloid β aggregation inhibition.¹¹⁰

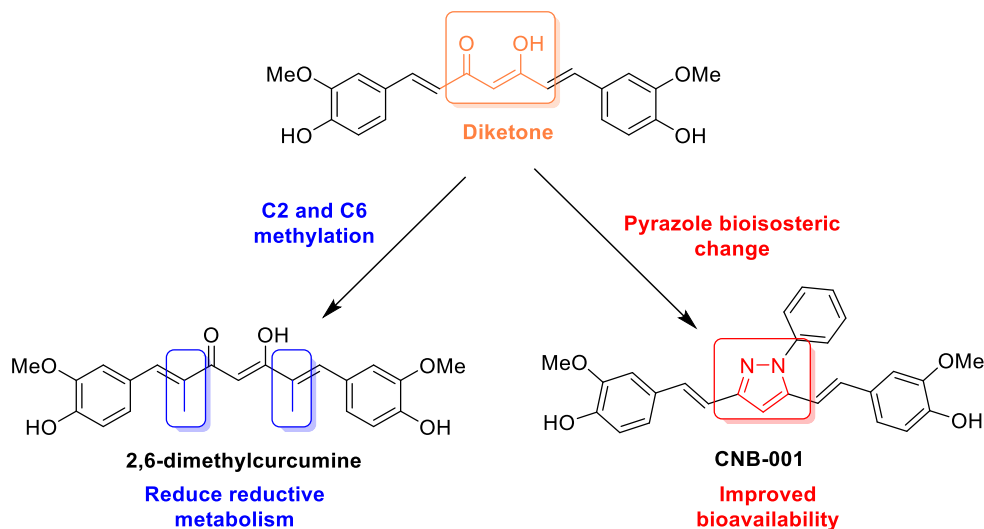


Figure 3.5

Against this backdrop, we envisioned that cinnamic ester and curcumin analogues with a structure restricted by a heterocyclic core in order to reduce their metabolic degradation and improve their bioavailability (Figure 3.6). Also, this methodology introduces additional points of diversity in the structure that in principle allow to generate new multi-target directed ligands against neurodegenerative diseases. Once access to the pyrrolinone core **1** is achieved, compounds **3**, containing a cinnamic acid amide embedded into the pyrrolone fragment, should be accessible by a simple Knoevenagel condensation. A similar approach, with an acylation reaction as the final step, would be employed to obtain compounds **4**, containing a curcumin structural fragment. Our goal was to achieve the preparation of the starting materials **1** by application of a multicomponent strategy based on the classical Hantzsch pyrrole synthesis (see below).

¹¹⁰ Joseph, A. I.; Edwards, R. L.; Luis, P. B.; Presley, S. H.; Porter, N. A.; Schneider, C. *Org. Biomol. Chem.* **2018**, *16*, 3273-3281.

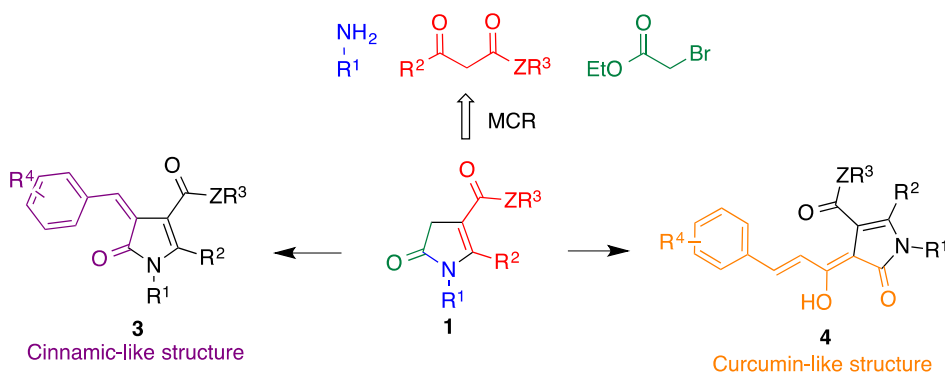


Figure 3.6

3.4. Multicomponent synthesis of the pyrrolin-5-one core

3.4.1. Multicomponent reactions: A brief introduction

Multicomponent reactions (MCRs) are defined as chemical processes where three or more reagents are combined, leading to a final compound containing significant fragments from all starting materials.¹¹¹ Ideally, all the reagents are combined by simultaneous addition, but very often, in order to avoid side reactions, the addition of reagents in a certain order may be necessary to improve the regio- and chemoselectivity, and such transformations are known as sequential multicomponent reactions.

MCRs have emerged as powerful synthetic strategies because of their efficiency, atom economy, high selectivity and potential to allow the convenient construction of multiple new bonds; these characteristics are part of the requirements for the ideal synthesis concept.¹¹² Furthermore, multicomponent reactions are an effective and agile synthetic methodology to introduce diversity in bioactive molecules. From the point of view of the generation of molecular diversity, the development of MCRs with a broad range of functional group tolerance is crucial. In this context, ideal MCRs should be compatible with complexity-generating post-MCR transformations, such as cyclizations, giving rapid access to combinatorial libraries of complex organic molecules for efficient lead structure identification and optimization in drug discovery.^{113, 114}

¹¹¹ For monographs on multicomponent reactions, see: (a) Zhu, J.; Bienaymé, H. (eds.), *Multicomponent Reactions*. Wiley-VCH, **2005**; (b) Zhu, J.; Wang, Q.; Wang, M. (eds.), *Multicomponent Reactions in Organic Synthesis*. Wiley-VCH, **2014**

¹¹² Wender, P. A.; Miller, B. L. *Nature* **2009**, *460*, 197-201.

¹¹³ Sunderhaus J. D.; Martin, S. F. *Chem. Eur. J.* **2009**, *15*, 1300-1308.

¹¹⁴ Sahn, J. J.; Granger B. A.; Martin S. F. *Org. Biomol. Chem.* **2014**, *12*, 7659-7672.

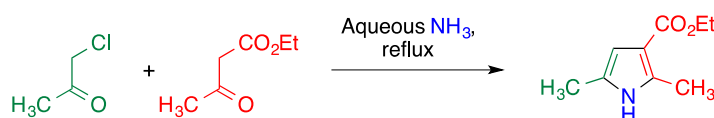
Thus, the renaissance of MCRs and their application in the context of diversity-oriented synthesis can be viewed as one of the changes that have taken place in pharmaceutical industry, at the same level as combinatorial chemistry, high-throughput screening and omics.

Many of the best-known MCRs, including the classical Strecker,¹¹⁵ Biginelli¹¹⁶, Mannich reactions and the Hantzsch dihydropyridine¹¹⁷ syntheses were described during the second half of the XIX century and the beginning of the XX century. These classical MCRs have been developed and drastically improved, and new MCRs have been discovered in the last decades. Representative examples are the isonitrile-based multicomponent reactions, including the Passerini and Ugi reactions,¹¹⁸ and MCRs having a [3+2] dipolar cycloaddition as the key step.

The earliest example of the preparation of a pyrrole derivative *via* a multicomponent strategy^{119, 120} was the Hantzsch pyrrole synthesis, which in its initial version involved the reaction of acetyl acetoacetate, 2-chloroacetoacetate and ammonia to give a derivative of 2,5-dimethylpyrrole (Scheme 3.1).¹²¹ In spite of its status as a classical name reaction, this transformation has received relatively little attention until very recently.¹²²



Arthur Rudolf Hantzsch



Scheme 3.1

¹¹⁵ Strecker, A. *Liebigs Ann.* **1850**, *75*, 27-45.

¹¹⁶ Biginelli, P. *Chem. Ber.* **1891**, *24*, 1317-1319.

¹¹⁷ Hantzsch, A. *Chem. Ber.* **1881**, *14*, 1637-1638.

¹¹⁸ (a) Dömling, A.; Ugi, I. *Angew. Chem., Int. Ed.* **2000**, *39*, 3168-3210; (b) Ugi, A. *Pure Appl. Chem.* **2001**, *73*, 187-191.

¹¹⁹ For reviews of the use of multicomponent reactions for the synthesis of pyrroles, see: (a) Estévez, V.; Villacampa, M.; Menéndez, J. C. *Chem. Soc. Rev.* **2010**, *39*, 4402-4421. (b) Estévez, V.; Villacampa, M.; Menéndez, J. C. *Chem. Soc. Rev.* **2014**, *43*, 4633-4657.

¹²⁰ For general reviews of the synthesis of pyrroles, see: (a) Ferreira, V. F.; de Souza, M. C. B. V.; Cunha, A. C.; Pereira, L. O. R.; Ferreira, M. L. G. *Org. Prep. Prod. Int.* **2001**, *33*, 411-454. (b) Joshi, S. D.; More, U. A.; Kulkarni, V. H.; Aminabhavi, T. M. *Curr. Org. Chem.* **2013**, *17*, 2279-2304. (c) Gulevich, A. V.; Dudnik, A. S.; Chernyak, N.; Gevorgyan, V. *Chem. Rev.* **2013**, *113*, 3084-3213.

¹²¹ Hantzsch, A. *Ber. Dtsch. Chem. Ges.* **1890**, *23*, 1474-1476.

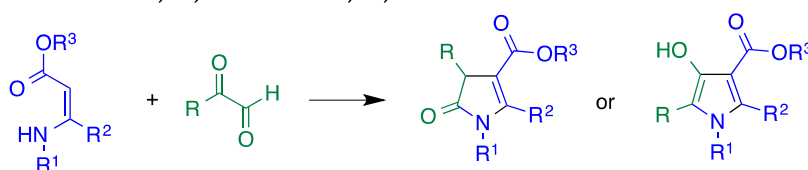
¹²² For a review of the Hantzsch pyrrole synthesis, see: Leonardini, M.; Estévez, V.; Villacampa, M.; Menéndez, J. C. *Synthesis* **2019**, *51*, 816-828.

3.4.2. Literature precedent for the synthesis of 2-pyrrolin-5-ones

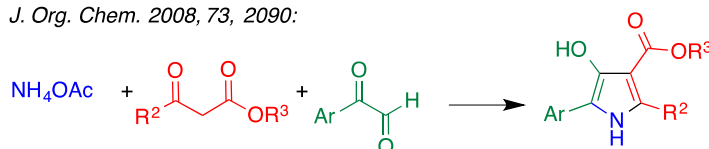
In spite of much recent progress, some pharmacologically promising pyrrole-derived simple frameworks have received very little attention because of their poor synthetic accessibility. This is the case of the 2-pyrrolin-5-one system, which has been reported only a few times, and has normally been accessed by complex multistep routes in very modest yields.¹²³

Encouraged by the experience of our group in the Hantzsch pyrrole synthesis,¹²⁴ we envisioned that it should be possible to adapt this classical reaction for our purpose. This would involve developing the three-component reaction between primary amines, α -haloesters and β -dicarbonyl compounds to furnish compounds **1**. As shown in Scheme 3.2, a two-component process somewhat related to ours and involving the reaction of β -enamino esters with α -ketoaldehydes afforded either of the two possible 4-oxo- or 5-oxo regioisomers (for ketoaldehydes and glyoxal, respectively), while N-hydroxyethyl or N-hydroxypropyl enamino esters gave the 5-oxo derivative,

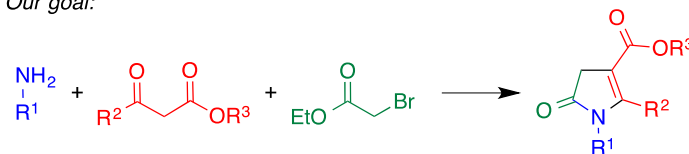
Tetrahedron 1989, 45, 6553 and 1994, 50, 7849:



J. Org. Chem. 2008, 73, 2090:



Our goal:



Scheme 3.2

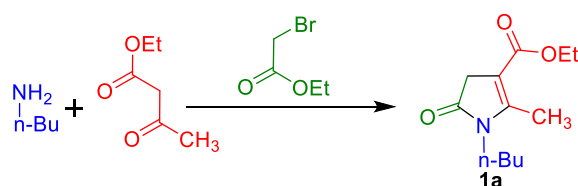
¹²³ (a) Wasserman, H. H.; Liberles, A. *J. Am. Chem. Soc.* **1960**, 82, 2086-2086. (b) Takamizawa, A.; Harada, H.; Makino, I. *Chem. Pharm. Bull.* **1978**, 26, 722-735. (c) Gelin, S.; Gelin, R. *J. Org. Chem.* **1979**, 44, 808-810. (d) Eiden, F.; Grusdt, U. *Arch. Pharm.* **1987**, 320, 1020-1031.

¹²⁴ For a generalization of the Hantzsch pyrrole synthesis under mechanochemical conditions, see: (a) Estévez, V.; Villacampa M.; Menéndez, J. C. *Chem. Commun.* **2014**, 43, 4633-4657. (b) Estévez, V.; Sridharan, V.; Sabaté, S.; Villacampa, M.; Menéndez, J. C. *Asian J. Org. Chem.* **2016**, 2016, 5, 652-662. (c) Leonardi, M.; Villacampa M.; Menéndez, J. C. *Beilstein J. Org. Chem.* **2017**, 13, 1957-1962. (d) Leonardi, M.; Villacampa M.; Menéndez, J. C. *J. Org. Chem.* **2017**, 82, 52570-2578. (e) Leonardi, M.; Villacampa M.; Menéndez, J. C. *Adv. Synth. Catal.* **2019**, 361, 2054-2074.

presumably because of its stabilization by intramolecular hydrogen bonding.^{125, 126} A three-component variation of this reaction, starting from primary amines, α -ketoaldehydes and β -dicarbonyl compounds gives exclusively 4-hydroxypyrroles.¹²⁷

3.4.3. Hantzsch-like, multicomponent approach to 2-pyrrolin-ones

We started our optimization study by examining the model preparation of compound **1a** from butylamine, ethyl bromoacetate and ethyl acetoacetate (Scheme 3.3 and Table 3.1). In our first experiments, these starting materials were combined in ethanol in the presence of 5% Ce(IV) ammonium nitrate (CAN) as a Lewis acid,¹²⁸ initially at room temperature and then under reflux conditions, but no reaction was observed (entries 1 and 2). The use of focused microwave irradiation was also unsuccessful (entries 3 and 4). However, when the reaction was performed under solvent-free conditions, compound **1a** was obtained in 53% yield (entry 5), with no improvement being observed upon increase of the catalyst load (entry 6). Lanthanide triflates, represented by yttrium and ytterbium triflates, were also assayed, again with no improvement (entries 7 and 8). Boron trifluoride etherate failed to catalyze the reaction (entry 9), and aluminium trichloride gave only modest yields, even with 10% catalyst load (entries 10 and 11). Finally, indium trichloride was found to improve the results obtained with CAN, giving a 60% yield of **1a** with a 5% loading (entry 12) and almost the same result with 10% of the catalyst (entry 13). One final attempt was made using Montmorillonite K10, a clay with acidic properties that is compatible with microwave irradiation,¹²⁹ but it failed to promote our reaction (entry 14).



Scheme 3.3

¹²⁵ San Feliciano, A.; Caballero, E.; Pereira, J. A. P.; Puebla, P. *Tetrahedron* **1989**, *45*, 6553-6562.

¹²⁶ Caballero, E.; Puebla, P.; Domercq, M.; Medarde, M.; López, J. L.; San Feliciano, A. *Tetrahedron* **1994**, *50*, 7849-7856.

¹²⁷ Khalili, B.; Jajarmi, P.; Eftekhari-Sis, B.; Hashemi, M. M. *J. Org. Chem.* **2008**, *73*, 2090-2095.

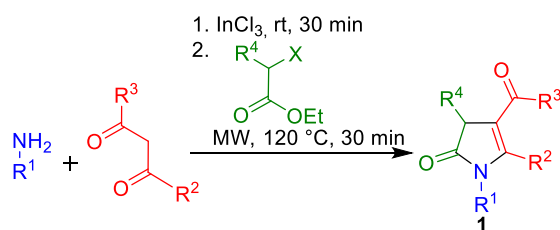
¹²⁸ For a review of the use of CAN as a catalyst in organic synthesis, see: Sridharan, V.; Menéndez, J. C. *Chem. Rev.* **2010**, *110*, 3805-3849.

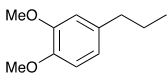
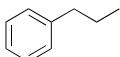
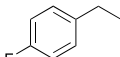
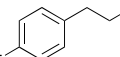
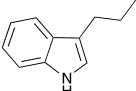
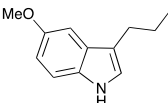
¹²⁹ For a recent example from our group, see: Rocchi, D.; González, J. F.; Menéndez, J. C. *Molecules* **2014**, *19*, 7317-7326.

Table 3.1. Optimization of the synthesis of compound **1a**

Entry	Catalyst (%)	Temp (°C)	Time (h)	Solvent	Yield (%)
1	CAN (5)	r.t.	20	EtOH	0 ^a
2	CAN (5)	80	14	EtOH	0
3	CAN (5)	80 (MW)	0.5	EtOH	0
4	CAN (5)	120 (MW)	0.5	EtOH	0
5	CAN (5)	120 (MW)	0.5	--	53
6	CAN (10)	120 (MW)	0.5	--	52
7	Y(OTf) ₃ (5)	120 (MW)	0.5	--	50
8	Yb(OTf) ₃ (10)	120 (MW)	0.5	--	26
9	BF ₃ .Et ₂ O (10)	120 (MW)	0.5	--	Traces
10	AlCl ₃ (5)	120 (MW)	0.5	--	19
11	AlCl ₃ (10)	120 (MW)	0.5	--	29
12	InCl ₃ (5)	120 (MW)	0.5	--	60
13	InCl ₃ (10)	120 (MW)	0.5	--	58
14	Montmorillonite K10	120 (MW)	0.5	--	Traces

These optimal conditions (5% InCl₃, solvent-free microwave irradiation, 120 °C) were applied to obtain a library of diversely substituted pyrrolinones in a 40-76% range of yields (Scheme 3.4 and Table 3.2), employing simple and commercially available starting materials. The scope of the R¹ substituent on nitrogen included a variety of groups such as alkyl (entries 1-4, 7-9 and 13), arylalkyl (entries 5, 6, 12 and 18-22), allyl (entry 10) and functionalized alkyl (entry 11). The R² chain was chosen among several primary alkyl chains, including methyl, ethyl (entry 7) and propyl (entries 4 and 9). The reaction was compatible with the presence of ester or ketone functions at C-3. While most compounds **1** were unsubstituted at C-4 because our planned subsequent application involved a condensation at this position, we also demonstrated the possibility to prepare a C4-phenyl derivative (entry 13). In this case, the α -haloester component was an iodide, and aluminium trichloride proved to be more efficient in promoting the reaction than indium trichloride. Finally, we also examined several reactions starting from ethyl β -aminocrotonate. Thus, its reaction with ethyl 2-bromoacetate gave the N-unsubstituted pyrrolinone **1n** in 55% yield (entry 14). This is a significant result because a previous preparation of this compound by reaction of the same aminocrotonate with glyoxal required a 7 h reflux in ethanol and afforded **1n** in only 29% yield.¹²⁵ Three additional examples of N-unsubstituted pyrrolinones were obtained by the same

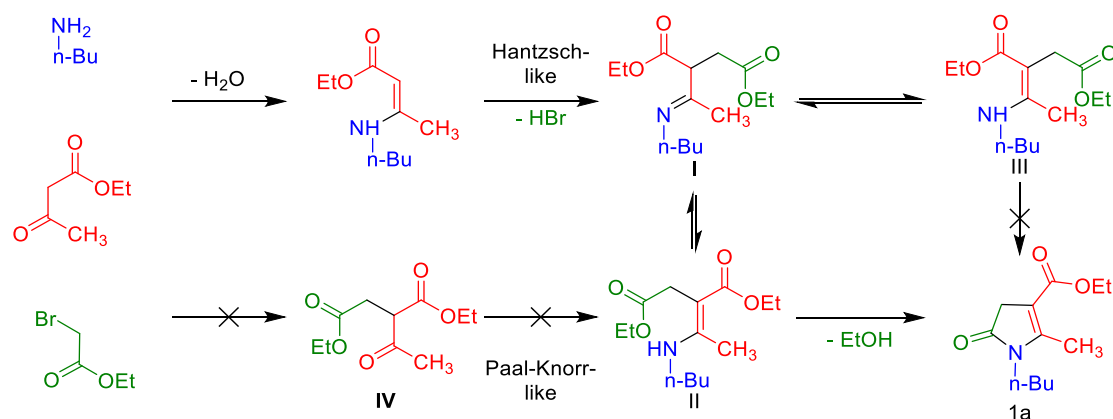
Scheme 3.4. Sequential multicomponent synthesis of 2-pyrrolin-5-ones **1**Table 3.2. Results of the synthesis of compounds **1**

Entry	Cmpd	R ¹	R ²	R ³	R ⁴	Yield (%)
1	1a	<i>n</i> -Bu	Me	OEt	H	60
2	1b	<i>n</i> -Bu	Me	OMe	H	50
3	1c	<i>n</i> -Bu	Me	Me	H	42
4	1d	<i>n</i> -Bu	<i>n</i> -Pr	OEt	H	52
5	1e	Bn	Me	OEt	H	52
6	1f	Bn	Me	OMe	H	55
7	1g	<i>n</i> -Bu	Et	OEt	H	59
8	1h	Me	Me	OEt	H	76
9	1i	<i>n</i> -Hex	<i>n</i> -Pr	OEt	H	72
10	1j	Allyl	Me	OMe	H	50
11	1k	2-Hydroxyethyl	Me	OMe	H	43
12	1l		Me	OMe	H	52
13	1m	<i>n</i> -Bu	Me	OEt	Ph	58 ^b
14	1n	H	Me	OEt	H	55 ^c
15	1o	H	Me	OEt	Me	43 ^c
16	1p	H	Me	OEt	Et	40 ^c
17	1q	H	Me	OEt	Ph	41 ^c
18	1r		Me	OMe	H	54
19	1s		Me	OMe	H	49
20	1t		Me	OMe	H	56
21	1u		Me	OMe	H	36
22	1v		Me	OMe	H	41

^a The X leaving group was Br in all cases except for entry 13, where X = I. ^b In this case the catalyst was aluminium trichloride (10%). ^c From ethyl β -aminocrotonate and the suitable α -bromoester.

method (entries 15-17). Interestingly, we did not observe the isomerization of 2-pyrrolin-5-ones to their regioisomeric 4-hydroxypyrroles noticed by previous authors.¹²⁶ Mechanistically, our three-component process was expected to proceed via a Hantzsch-type mechanism that is depicted in Scheme 3.5 for the reaction leading to compound **1a**. Thus, the reaction would start with the InCl_3 -catalyzed formation of a β -enamino ester,¹³⁰ which would then react with the α -haloester to give intermediate **I**, which can tautomerize to species **II** or **III**. However, only the *E* isomer **II** can undergo cyclization, thus driving these equilibria to the final product.

An alternative Paal-Knorr-like mechanism would involve the formation of a 1,4-dicarbonyl species **IV** that would then react with the primary amine to give the previous intermediate **II**. However, we verified that ethyl acetoacetate and ethyl bromoacetate did not react at all in the presence of InCl_3 under our conditions. Furthermore, we found that treatment of the known¹³¹ ethyl acetosuccinate **IV** with *n*-butylamine failed to give the 2-pyrrolin-5-one **1a** under our conditions. On the contrary, the isolated β -enamino ester arising from *n*-butylamine and ethyl acetoacetate¹³² furnished compound **1a** when treated with ethyl bromoacetate in the presence of InCl_3 under our usual conditions.



Scheme 3.5

¹³⁰ The *Z* configuration of the intermediate β -enamino esters was established by the NH chemical shift and NOE studies, and is probably stabilized by an intramolecular hydrogen bond. See: (a) Zhuo, J.-C.; Schenk, K. *Helv. Chim. Acta* **1997**, *80*, 2137-2147. (b) Vohra, R. K.; Renaud, J.-L.; Bruneau, C. *Synthesis* **2007**, 2007, 731-738. (c) Thorwith, R.; Stolle, A. *Synlett* **2011**, 2011, 2200-2202.

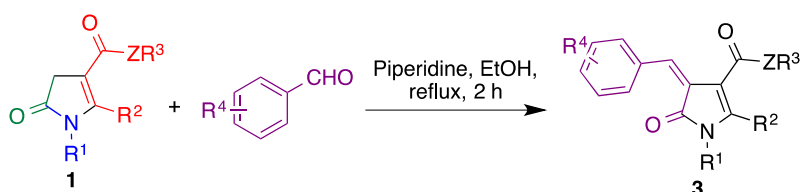
¹³¹ Kádas, I.; Morvai, V.; Árvai, G.; Tóke, L.; Szöllösy, Á.; Tóth G.; Bihari, M. *Monatsch. Chem.* **1995**, *126*, 107.

¹³² Sridharan, V.; Avendaño C.; Menéndez, J. C. *Synlett* **2007**, 2007, 881-884.

3.5. Pyrrolones with embedded cinnamic acid structural fragments

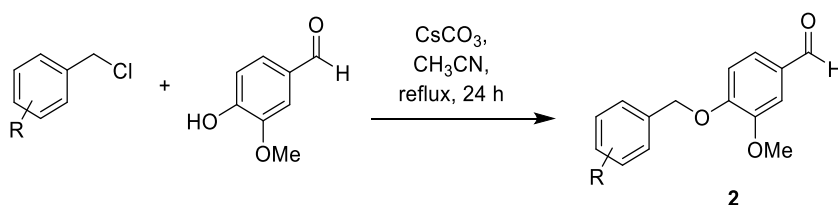
3.5.1. Synthesis of compounds 3

Pyrrolin-5-ones **1**, obtained *via* the multicomponent procedure described above, were reacted with the appropriate aromatic aldehydes **2** by a piperidine-catalyzed Knoevenagel condensation to afford the target 4-arylmethylene-2-pyrrolyn-5-ones **3** (Scheme 3.6).



Scheme 3.6

The selection of the side chains was based on commercial availability of the corresponding aldehydes or by their presence in molecules of interest as neuroprotectants connected with tau protein aggregation.¹³³ Most of the required aromatic aldehydes were commercially available, but some of them (**2a-d**) had to be synthesized by a Williamson reaction, as shown in Scheme 3.7.



Scheme 3.7

The structures and yields of compounds **3** are summarized in Figure 3.7.

¹³³ Gandini, A.; Bartolini, M.; Tedesco, D.; Martínez-González, L.; Roca, C.; Campillo, N. E.; Zaldívar-Díez, J.; Pérez, C.; Zuccheri, G.; Miti, A.; Feoli, A.; Castellano, S.; Petralla, S.; Monti, M.; Rossi, M.; Moda, F.; Legname, G.; Martínez, A.; Bolognesi, M. L. *J. Med. Chem.* **2018**, *61*, 7640-7656.

Chapter 3. Neuroprotective compounds related to cinnamic esters and curcumin

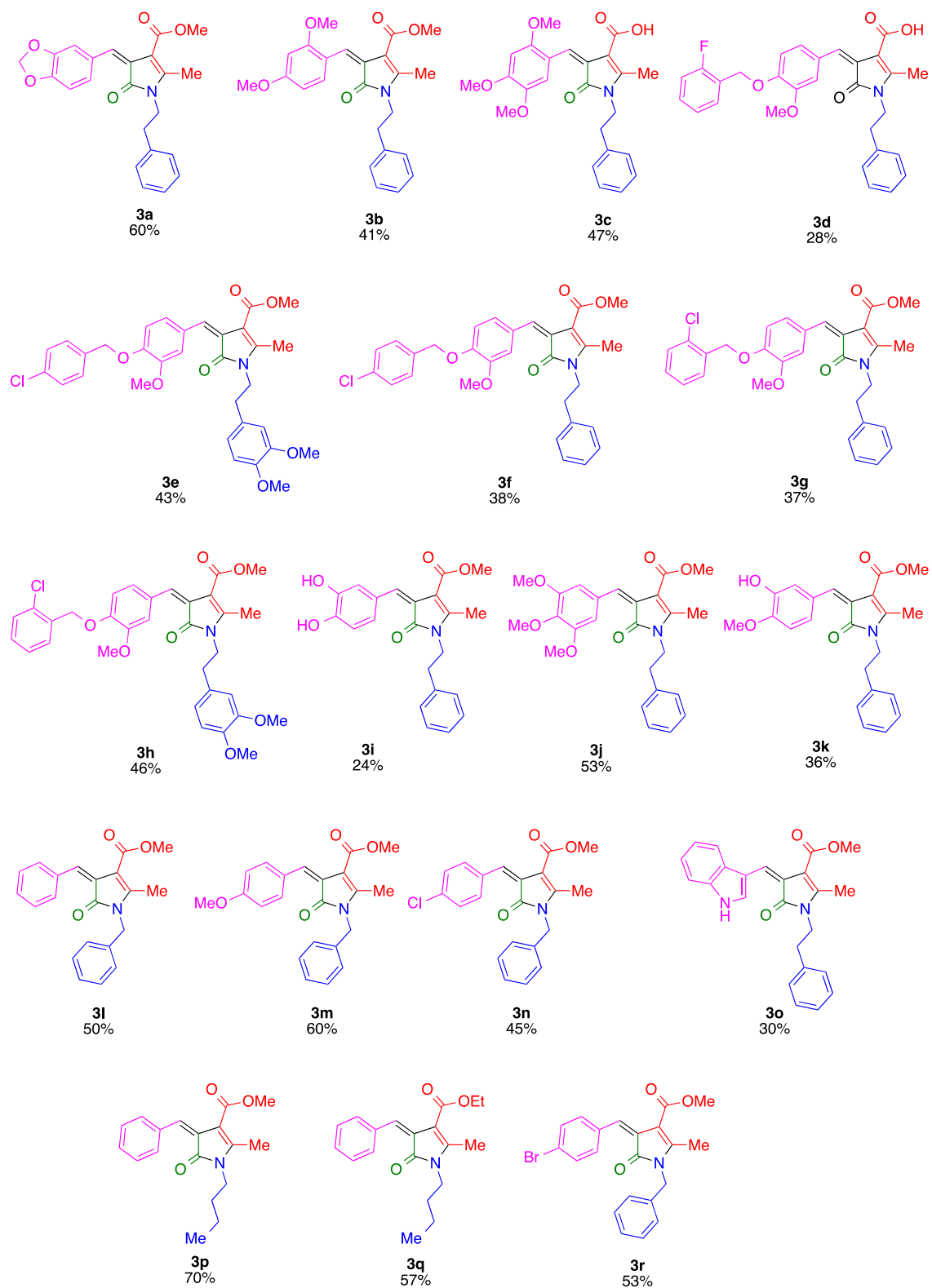


Figure 3.7

3.5.2. Pharmacological evaluation of compounds 3

The pharmacological study of compounds **3** was carried out by Sheila Abril at the group of Dr. Rafael León (Hospital Universitario de la Princesa and Instituto Teófilo Hernando, Universidad Autónoma de Madrid).

(a) SHSY5Y cytotoxicity

An exacerbated Nrf2 induction results in harmful effects for cells, and neurons are particularly susceptible to toxicity. Therefore, the evaluation of a potential neurotoxicity for these compounds, by this or by alternative mechanisms, was necessary prior to the pharmacological study. The cell viability for all compounds was studied in the neuroblastoma SHSY5Y cell line and measured as MTT reduction, and most compounds showed a good safety profile with a LD₅₀ above 100 μM. Compound **3i**, showing LD₅₀ = 92.8 ± 4.6 μM, can also be considered to have a suitable toxicity profile, but **3l** and **3n** were regarded as too toxic (Table 3.3).

Table 3.3

Entry	Compound	LD ₅₀ (μM)
1	3a	> 100
2	3b	> 100
3	3c	> 100
4	3d	> 100
5	3e	> 100
6	3f	> 100
7	3g	> 100
8	3h	> 100
9	3i	92.8 ± 4.6
10	3j	>100
11	3k	>100
12	3l	63.7 ± 12.8
13	3m	>100
14	3n	75.4 ± 15.6
15	3o	>100

(b) Nrf2 induction in the AREc32 cell line

Nrf2 induction was evaluated in the AREc32 cell line, an MCF7 stable clone transfected with 8 x luciferase reporter after the ARE sequence.¹³⁴ Nrf2 activation promotes the transcription of the ARE-dependent phase II genes, expressing luciferase to the same extent. Thus, the increase in luciferase, measured by a luminescence assay, and Nrf2 induction potency are directly correlated. AREc32 cells were incubated during 24 h with increasing concentrations of compounds **3a-3o** (0.3, 3, 10, 30 and 60 μ M) and luminescence was recorded to obtain CD values for each compound. These CD values represent the concentration of compound necessary to double the luciferase activity compared to its basal expression. As shown by the results collected in Table 3.4, all compounds are good Nrf2 inducers, with **3b**, **3d**, **3g** and **3i** showing excellent activities around 10 μ M CD. Compound **3j** was the most potent of the library, with a CD value of 3.18. As a reference for comparison, the CD value for caffeic acid is comprised between 6.5 and 11.75 μ M, and that of curcumin between 3.5 and 6.5 μ M.¹³⁵

Table 3.4

Entry	Compound	CD (μ M)
1	Caffeic acid	6.5 - 11.75
2	Curcumin	3.5 - 6.5
3	3a	17.86 \pm 8.58
4	3b	10.38 \pm 0.80
5	3c	31.06 \pm 6.21
6	3d	11.91 \pm 2.83
7	3e	14.26 \pm 3.89
8	3f	13.97 \pm 4.45
9	3g	7.58 \pm 4.35
10	3h	21.41 \pm 5.72
11	3i	7.51 \pm 3.45
12	3j	3.18 \pm 1.16
13	3k	36.07 \pm 418

¹³⁴ Wang, X. J.; Hayes, J. D.; Wolf, C. R. *Cancer Res.* **2006**, *66*, 10983-10994.

¹³⁵ Wu, K.; McDonald, P.; Liu, J.; Klaassen, C. *Planta Medica* **2013**, *80*, 97-104.

Table 3.5

Entry	Compound	% Scavenging at 0.1 mM	% Scavenging at 1 mM	IC ₅₀ μ M
1	Trolox			11.4 \pm 1.0 (9)
2	Ascorbic acid			16.2 \pm 0.7 (9)
3	Melatonin			1988 \pm 1397 (2)
4	3a	40.5 \pm 5.0	41.6 \pm 4.1	-
5	3b	6.33 \pm 4.2	27.0 \pm 2.6	-
6	3c	9.7 \pm 0.6	9.7 \pm 2.2	-
7	3d	4.3 \pm 2.1	31.3 \pm 3.3	-
8	3e	22.8 \pm 0.2	85.5 \pm 2.7	334.3 \pm 22.9 (3)
9	3f	11.3 \pm 2.6	63.5 \pm 2.2	712.2 \pm 5.4 (3)
10	3g	7.3 \pm 1.4	27.3 \pm 1.0	-
11	3h	12.7 \pm 3.5	73.6 \pm 0.7	552.1 \pm 17.4 (3)
12	3i	90.9 \pm 0.5	-	7.5 \pm 0.4 (3)
13	3j	8.1 \pm 4.7	46.5 \pm 2.3	-
14	3k	89.0 \pm 0.4	-	26.3 \pm 2.1 (3)
15	3l	9.7 \pm 3.8	47.5 \pm 4.9	-
16	3m	6.5 \pm 4.5	27.2 \pm 6.4	-
17	3n	3.7 \pm 3.8	36.6 \pm 3.4	-
18	3o	12.7 \pm 1.9	49.9 \pm 3.4	-

As part of the characterization of the compounds as potential multitarget-directed ligands, they were also investigated as inhibitors of acetylcholinesterase, an interesting target in Alzheimer's disease. Initially, the whole library was studied at a single concentration (10 μ M), and IC₅₀ was also determined for the most active compounds (Table 3.6). Only three of the compounds showed significant activity in this assay and therefore this aspect of the characterization of our compounds was not pursued further.

Table 3.6

Entry	Compound	% Inhibition of EeAChE at 10 μ M	IC ₅₀ (μ M)
1	3a	25.21	
2	3b	24.32	
3	3c	29.29	
4	3d	15.96	
5	3e	17.59	
6	3f	26.20	
7	3g	40.09	22.4 \pm 3.2
8	3h	31.77	
9	3i	27.21	
10	3j	11.62	
11	3k	24.25	
12	3l	27.36	
13	3m	36.27	29.7 \pm 3.0
14	3n	33.47	
15	3o	39.84	12.5 \pm 1.4

(d) Neuroprotection in a rotenone/oligomycin A oxidative stress model

The good Nrf2 induction found for the whole library and the radical scavenging properties of derivatives **3i** and **3k** encouraged us to study their potential neuroprotective role against oxidative stress. An intracellular model of oxidative stress was generated by a combination of rotenone and oligomycin A (R/O) (30/10 μ M) in the neuroblastoma SH-SY5Y cell line. Rotenone and oligomycin A inhibit complexes I and V of the mitochondrial electron transport chain, respectively, disrupting ATP synthesis. Their combination (R/O) constitutes a good model of oxidative stress and neurodegeneration with a mitochondrial origin and has been widely used to evaluate potential protective drugs for neurodegenerative diseases.^{136, 137} Moreover, exposure of laboratory animals to rotenone is well-known to reproduce features of Parkinson's

¹³⁶ Buendia, I.; Navarro, E.; Michalska, P.; Gameiro, I.; Egea, J.; Abril, S.; López, A.; González-Lafuente, L.; López, M. G.; León, R. *Future Med. Chem.* **2015**, *7*, 1961-1969.

¹³⁷ Tenti, G.; Parada, E.; León, R.; Egea, J.; Martínez-Revelles, S.; Briones, A. M.; Martínez-Revelles, S.; Briones, A. M.; Sridharan, V.; López, M. G.; Ramos, M. T.; Menéndez, J. C. *J. Med. Chem.* **2014**, *57*, 4313-4323.

disease,¹³⁸ including selective nigrostriatal dopaminergic degeneration and the appearance of α -synuclein cytoplasmic inclusions. These effects were determined to be associated to oxidative damage.¹³⁹

Compounds **3a-o** demonstrated neuroprotective properties against the rotenone-oligomycin oxidative insult in a concentration-dependent manner (Table 3.7 and Figure 3.8). Compounds **3i**, **3n** and **3o**, in particular, showed a very good neuroprotective profile, with a significantly higher activity than melatonin, a well-known

Table 3.7^a

Entry	Compound	% Survival \pm SEM at 1 μ M	% Neuroprotection \pm SEM at 1 μ M	Statistical significance
1	Basal	100	100	
2	R/O (30/10 μ M)	43.27 \pm 1.97		###
3	Melatonin	78.14 \pm 5.70	61.41 \pm 8.75	***
4	3a	70.65 \pm 5.68	49.79 \pm 9.46	**
5	3b	71.99 \pm 9.21	50.32 \pm 16.34	**
6	3c	72.44 \pm 9.48	50.99 \pm 16.93	**
7	3d	72.53 \pm 8.79	51.19 \pm 15.49	**
8	3e	81.95 \pm 13.82	69.40 \pm 23.95	**
9	3f	76.12 \pm 14.94	79.76 \pm 8.28	*
10	3g	77.20 \pm 12.25	60.26 \pm 20.86	**
11	3h	67.00 \pm 10.26	41.18 \pm 18.85	*
12	3i	94.27 \pm 18.81	90.40 \pm 32.38	**
13	3j	72.01 \pm 15.76	74.47 \pm 7.19	*
14	3k	69.39 \pm 11.13	46.23 \pm 18.89	**
15	3l	68.51 \pm 7.81	44.33 \pm 13.57	**
16	3m	82.05 \pm 18.09	68.05 \pm 31.51	*
17	3n	96.24 \pm 13.30	94.91 \pm 24.25	***
18	3o	94.16 \pm 4.99	90.12 \pm 8.80	***

^a Data are expressed as mean \pm SEM of three experiments by triplicate. One way ANOVA Newman Keuls post test ### p < 0.001; compared to basal. * p < 0.05, ** p < 0.01; *** p < 0.001; compared to toxic.

¹³⁸ For a review of rotenone models of Parkinson's disease, see: Johnson, M. E.; Bobrovskaya, L. *Neurotoxicology* **2015**, *46*, 101-116.

¹³⁹ (a) Sherer, T. B.; Betarbet, R.; Testa, C. M.; Seo, B. B.; Richardson, J. R.; Kim, J. H.; Miller, G. W.; Yagi, T.; Matsuno-Yagi, A.; Greenamyre, T. J. *J. Neurosci.* **2003**, *23*, 10756-10764. (b) Xiong, N.; Xiong, J.; Jia, M.; Liu, L.; Zhang, X.; Chen, Z.; Huang, J.; Zhang, Z.; Hou, L.; Luo, Z.; Ghoorah, D.; Li, Z.; Wang, T. *Behav. Brain Funct.* **2013**, *9*, 13.

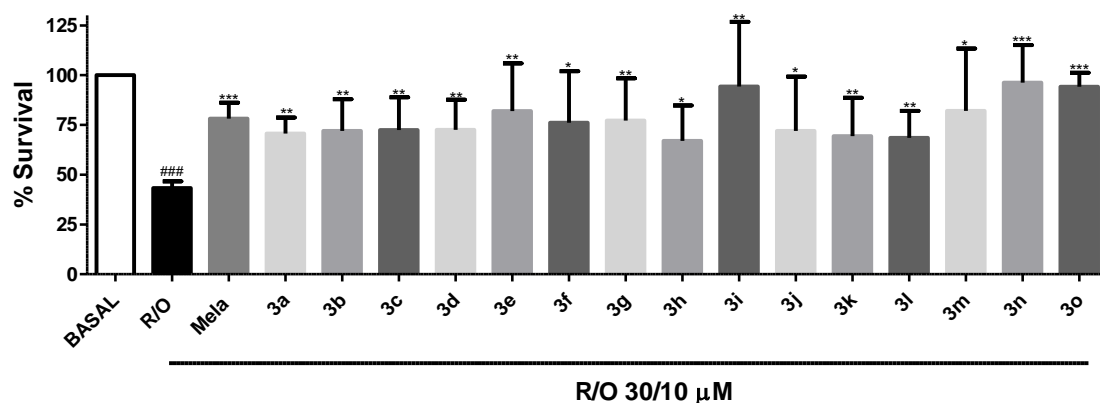


Figure 3.8 Neuroprotective effect of compounds **3a-3o** (1 μ M) against toxicity elicited by the combination of rotenone (30 μ M) and oligomycin A (10 μ M) in SH-SY5Y cells.

neuroprotective agent with an excellent antioxidant profile,¹⁴⁰ at the same concentration.

(e) Neuroprotection against tau hyperphosphorylation induced by okadaic acid

Okadaic acid induces tau hyperphosphorylation by inhibition of protein phosphatase 2A (PP2A), and can be used as a model of neurodegenerative disease-associated tau hyperphosphorylation. Although tau hyperphosphorylation is best known as a feature of Alzheimer's disease, other NDDs, collectively known as tauopathies, are characterized by pathological tau aggregation in neurofibrillary tangles. Recently, increasing evidence of the involvement of tau pathology in Parkinson's disease is accumulating, including the abnormal hyperphosphorylation of tau protein, the formation in about 50% of PD brains of tau aggregates, which seem to be transported from neuron to neuron, and the interaction between tau and α -synuclein.¹⁴¹

Compounds **3a-o** were tested on SH-SY5Y cells treated with okadaic acid, and some of them (**3b**, **3e**, **3i**, **3j**, **3l**) gave a similar neuroprotection to melatonin. The best results were obtained with the phenolic compound **3k**, which showed an excellent neuroprotection against the okadaic acid-induced insult (Table 3.8 and Figure 3.9).

¹⁴⁰ For a review of the neuroprotective role of melatonin in neurological disorders, see: Almgandi, B. S. *J. Neurosci. Res.* **2018**, 96, 1136–1149.

¹⁴¹ Zhang, X.; Gao, F.; Wang, D.; Li, C.; Fu, Y.; He, W.; Zhang, J. *Front. Neurol.* **2018**, 9, 809.

Table 3.8^a

Entry	Compound	% survival \pm SEM at 1 μ M	% Neuroprotection \pm SEM at 1 μ M	Statistical significance
1	Basal	100		
2	OA (20 nM)	60.32 \pm 5.48		###
3	Melatonin	85.48 \pm 7.77	67.70 \pm 13.95	**
4	3a	77.83 \pm 7.38	52.71 \pm 17.20	*
5	3b	85.14 \pm 5.02	62.77 \pm 8.00	**
6	3c	81.19 \pm 4.61	48.30 \pm 10.99	**
7	3d	73.16 \pm 8.91	31.82 \pm 15.21	
8	3e	84.28 \pm 8.18	61.39 \pm 15.75	**
9	3f	82.09 \pm 7.51	51.07 \pm 18.36	**
10	3g	82.40 \pm 11.06	57.14 \pm 22.31	*
11	3h	76.41 \pm 6.63	40.72 \pm 9.85	*
12	3i	85.25 \pm 8.33	60.87 \pm 23.33	**
13	3j	87.70 \pm 9.95	65.73 \pm 29.07	**
14	3k	91.94 \pm 11.82	81.86 \pm 28.54	*
15	3l	84.94 \pm 9.03	68.05 \pm 22.01	*
16	3m	82.20 \pm 4.65	54.15 \pm 14.26	**
17	3n	80.30 \pm 6.20	52.77 \pm 9.96	**
18	3o	76.75 \pm 8.63	46.27 \pm 13.57	*

^a Data are expressed as mean \pm SEM of three experiments by triplicate. One way ANOVA Newman Keuls post test ### p < 0.001; compared to basal. * p < 0.05, ** p < 0.01; *** p < 0.001; compared to toxic.

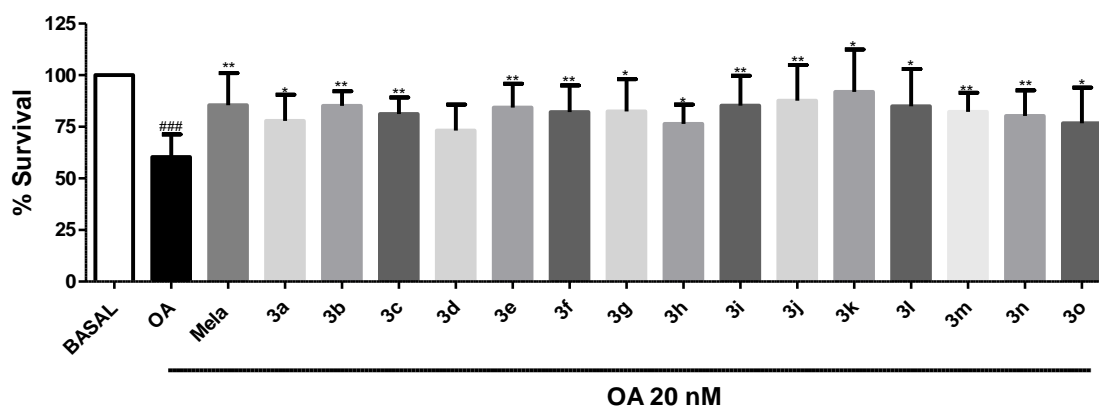


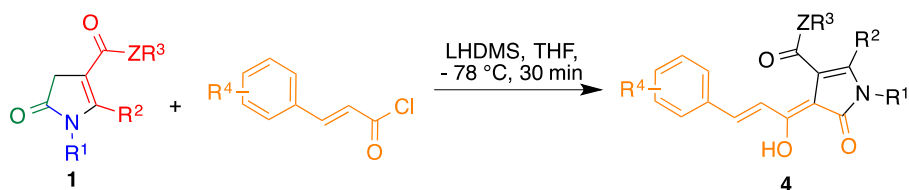
Figure 3.9 Neuroprotective effect of compounds **3a-3o** (1 μ M) against toxicity elicited by the okadaic acid (20 nM) in SH-SY5Y cells.

In summary, our 4-(arylmethylene)-2-pyrrolin-5-one derivatives have an interesting profile as neuroprotective agents. Most of them lack cytotoxicity and are good inducers of the Nrf2-initiated phase II antioxidant response. Some compounds have also shown good neuroprotective properties against toxicity induced by treatment with rotenone/oligomycin or okadaic acid. Compound **3i**, in particular, has a well-balanced multitarget profile and can be considered a good candidate for further development against neurodegenerative diseases.

3.6. Curcumin analogues with a pyrrolinone core

3.6.1. Synthesis of compounds **4**

The curcumin analogues **4e-f** were obtained by acylation of pyrrolinones **1** with the suitable cinnamyl chloride derivative, using LiHMDS as base (Scheme 3.9).



Scheme 3.9

The synthesis of the required cinnamyl chloride derivatives required some experimentation. Several attempts to use thionyl chloride were unsuccessful, but the reaction could be finally performed with a mixture of oxalyl chloride and hexane, where the generated oxalyl chloride was transferred to the apolar phase. Thus, despite the simplicity of the acylation reaction, its scope and yield is limited because of the requirement for hexane solubility of the required cinnamoyl chlorides. The structures and yields of the compounds obtained are summarized in Figure 3.10.

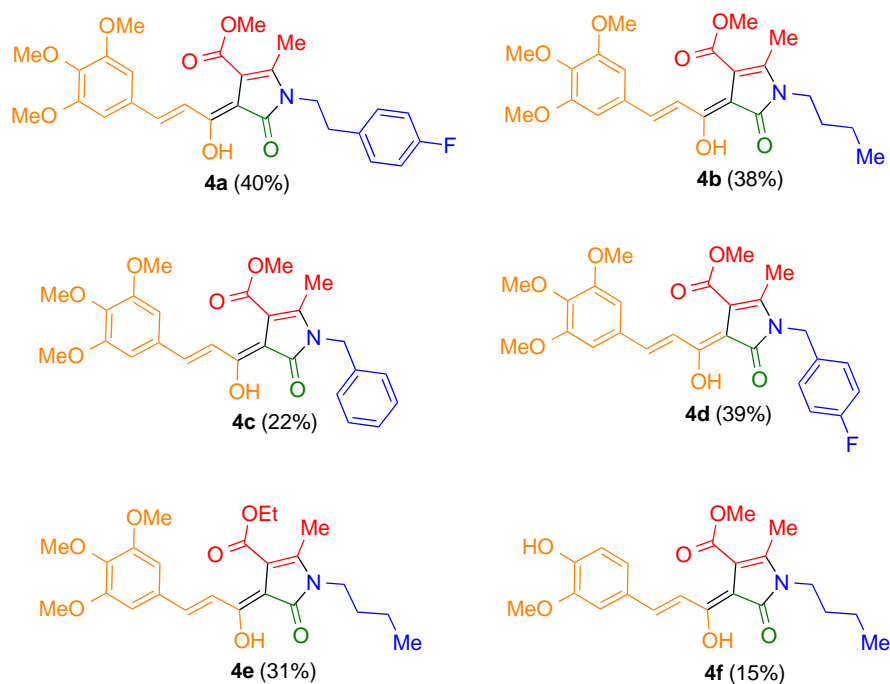


Figure 3.10

3.6.2. Pharmacological evaluation of compounds 4

The initial pharmacological evaluation of compounds **4a-f** was carried out by Drs. Paloma Bermejo and Sagrario Martín-Aragón, at the Departamento de Farmacología, Facultad de Farmacia, Universidad Complutense. The HEK293-Tau3R cell line was kindly supplied by Dr. Jesús Ávila, Centro de Biología Molecular Severo Ochoa, Madrid. Further characterization of the pharmacological profile of these compounds is in progress.

(a) Cellular viability in Hek-Tau cell line (MTT)

Firstly, neurotoxicity for compounds **4a-f** was determined by MTT assay in Hek-Tau cells, which are characterized by the overexpression of tau protein. Compounds **4a-f** were tested at 10 and 5 μM concentrations for 24 h and then cellular viability was determined. No toxicity was detected at 5 μM . Compounds **4e** and **4f** show some neurotoxicity at 10 μM , although lower than that of curcumin (Figure 3.11).

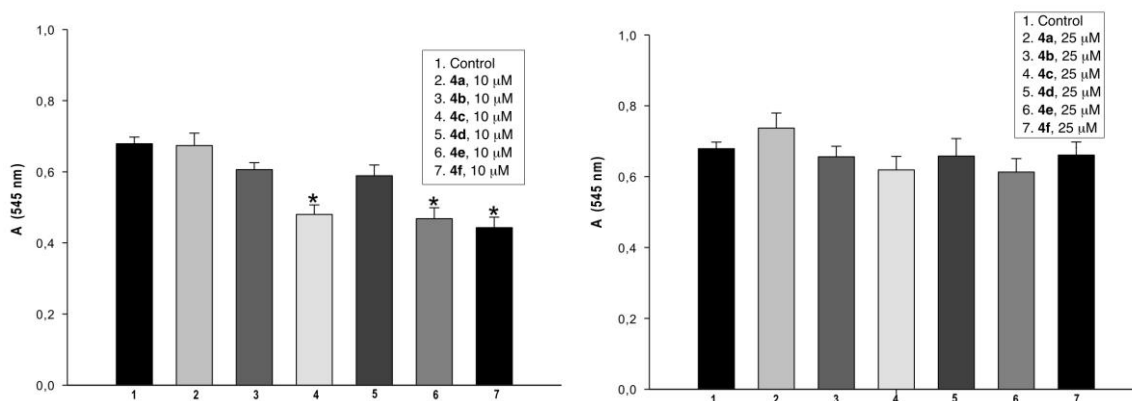
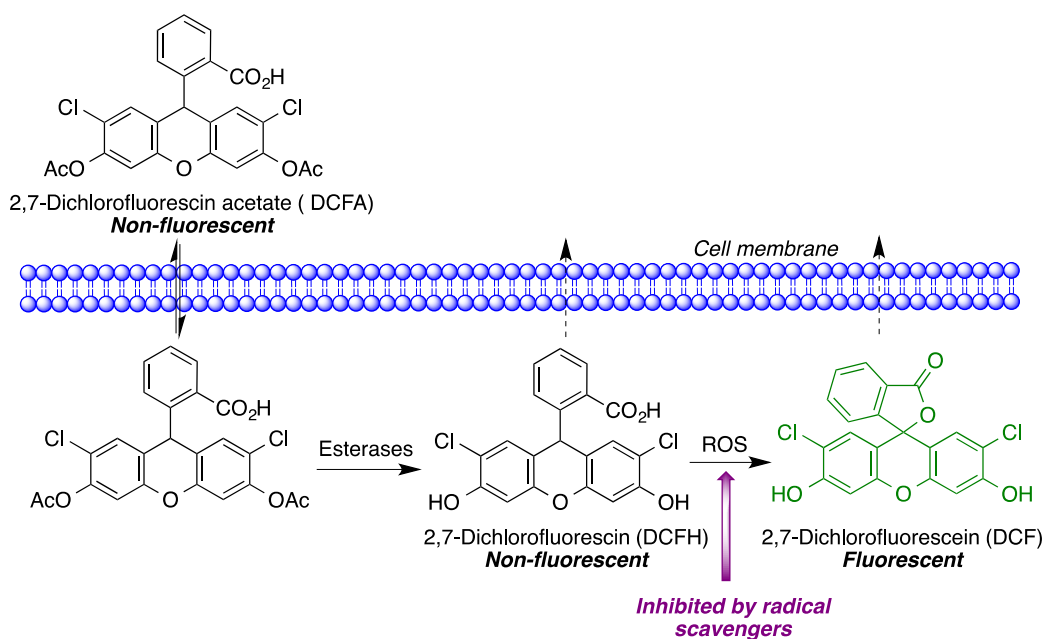


Figure 3.11. Cell viability assay of compounds **4**; $p < 0.05$ indicates statistically significant differences with the control, using the Newman-Keuls test

(b) Free radical scavenging in the Hek-Tau cell line (DCFA-DA)

Radical oxygen scavenging was tested in HEK293-Tau3R using a cellular antioxidant activity assay. The cells were exposed to hydrogen peroxide (200 μM) and treated with the non-fluorescent compound 2,7-dichlorofluorescein acetate (DFCA), a probe that is trapped within cells following its hydrolysis by cellular esterases. The resulting 2,7-dichlorofluorescein (DFCH) is still non-fluorescent, but upon oxidation by ROS becomes the more rigid, highly fluorescent dichlorofluorescein (DCF). Thus, the fluorescence observed in the assay is in an inverse relationship with the scavenging ability of the compounds under assay (Scheme 3.10).



Scheme 3.10

Chapter 3. Neuroprotective compounds related to cinnamic esters and curcumin

Using this assay, variations in the fluorescence signal after addition of the compounds **4a-f** in different concentrations (0.1 to 10 μM) were measured. In these experiments, all compounds showed similar or higher antioxidant activities than curcumin. Particularly interesting results were obtained for compounds **4b**, **4c** and **4d**, which showed a highly increased antioxidant activity compared with the curcumin reference (Figure 3.12).

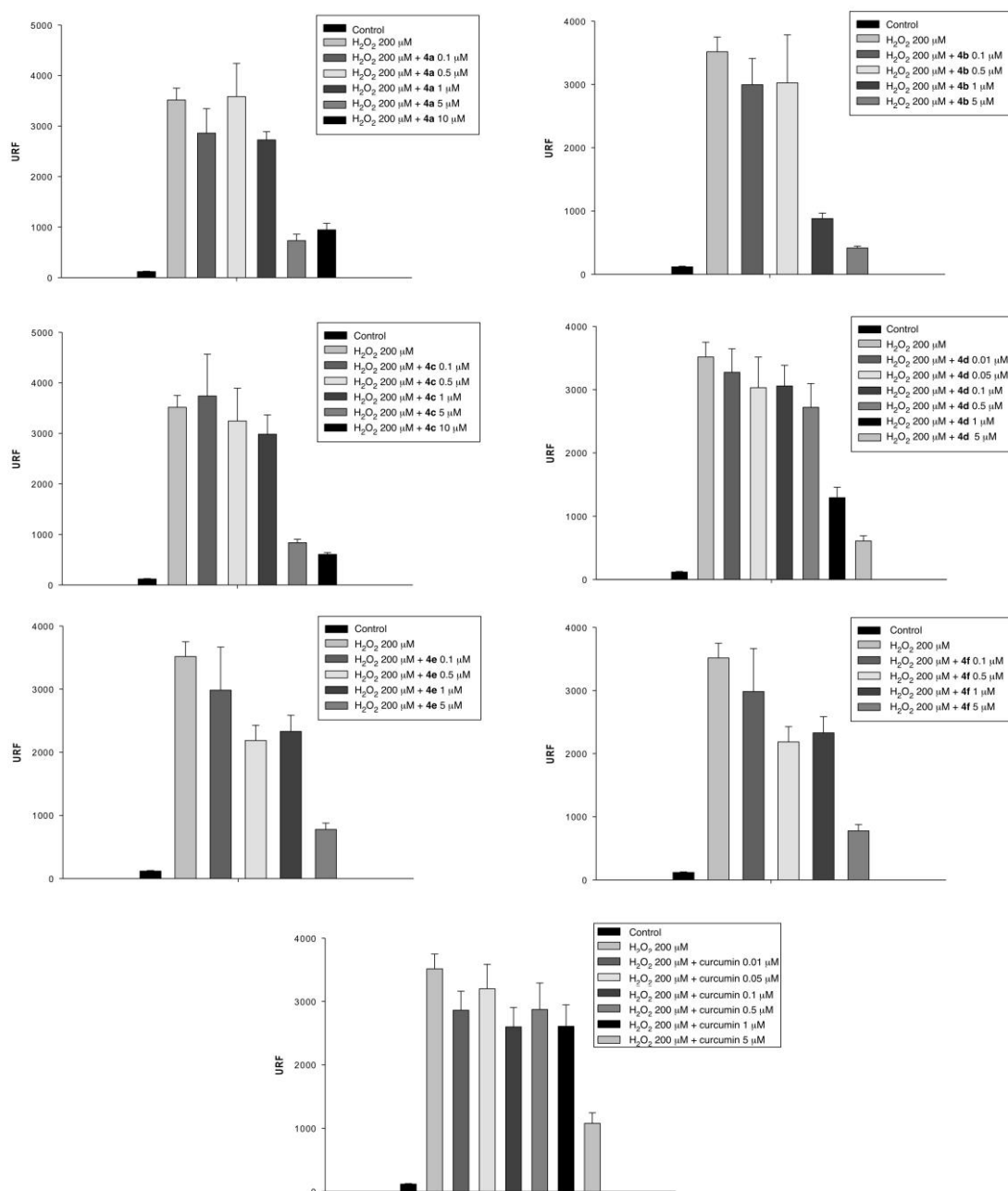


Figure 3.12

(c) Tau aggregation inhibition

The N-acetylated and C-amidated hexapeptide AcPHF6 (MeCOVQIVYK-NH₂), derived from the native tau-hexapeptide sequence ³⁰⁶VQIVYK³¹¹, is involved in the aggregation processes in fibrils with β -sheet conformation and represents a suitable model to study tau protein aggregation inhibition.¹⁴²

Our curcumin analogues (**4a-f**) were shown to reduce the aggregation of the AcPHF6 peptide (Figure 3.13 for the behaviour of individual compounds towards the aggregation of the AcPHF6 peptide and Figure 3.14 for a summary). Compounds **4a**, **4b** and **4d** show a similar antiaggregating activity compared with the parent compound curcumin. On the other hand, the curcumin-related phenolic compound **4f** showed the least potent aggregation inhibition.

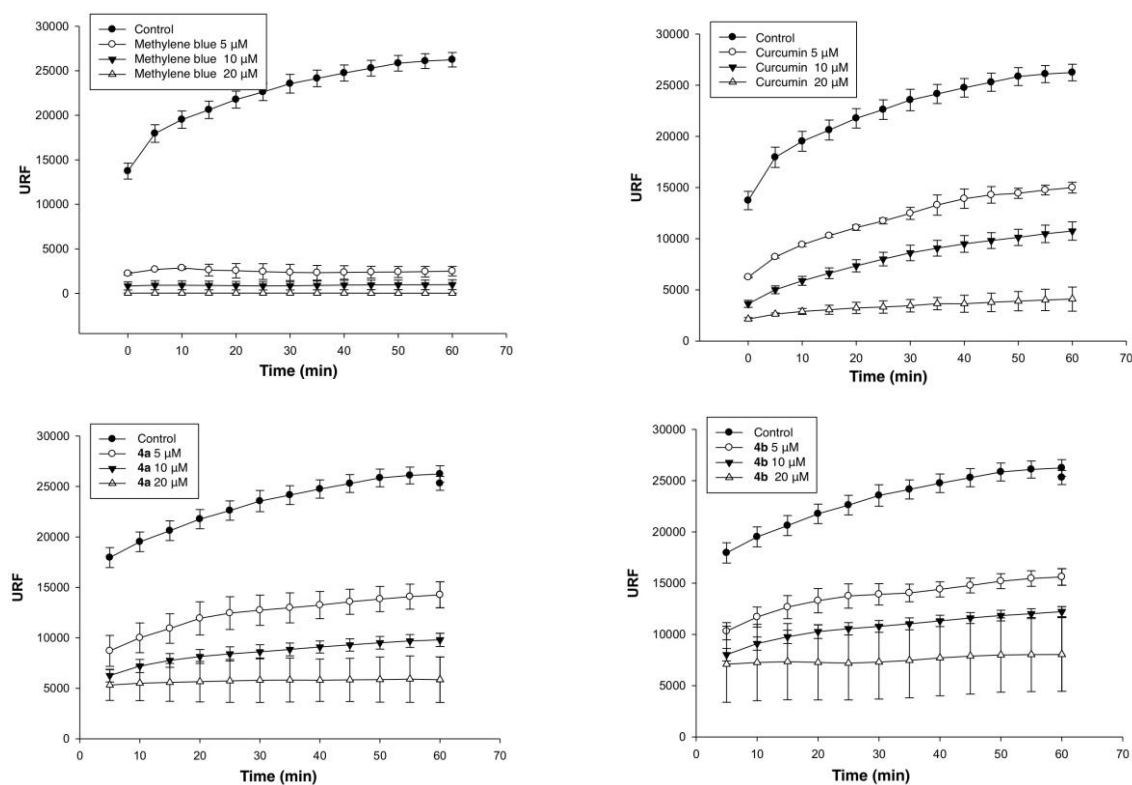


Figure 3.13

¹⁴² See, for instance: Mohamed, T.; Hoang, T.; Jelokhani-Niaraki, M.; Rao, P. P. N. *ACS Chem. Neurosci.* **2013**, *4*, 1559–1570.

Chapter 3. Neuroprotective compounds related to cinnamic esters and curcumin

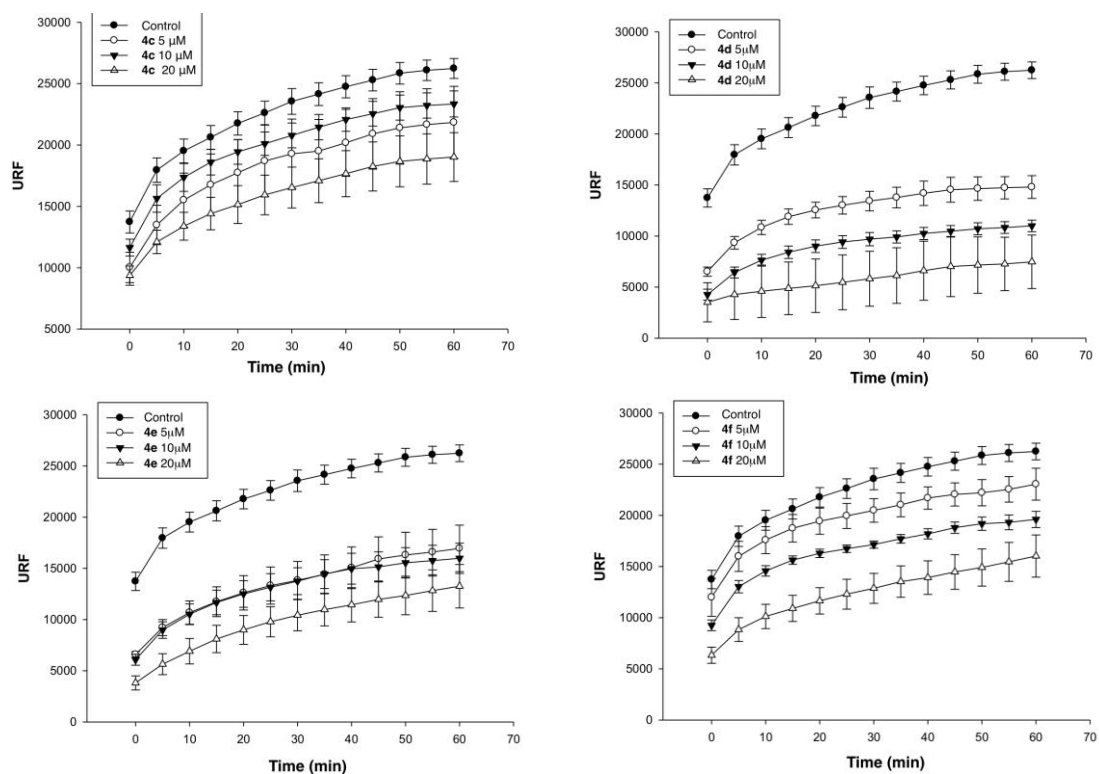


Figure 3.13 (continued)

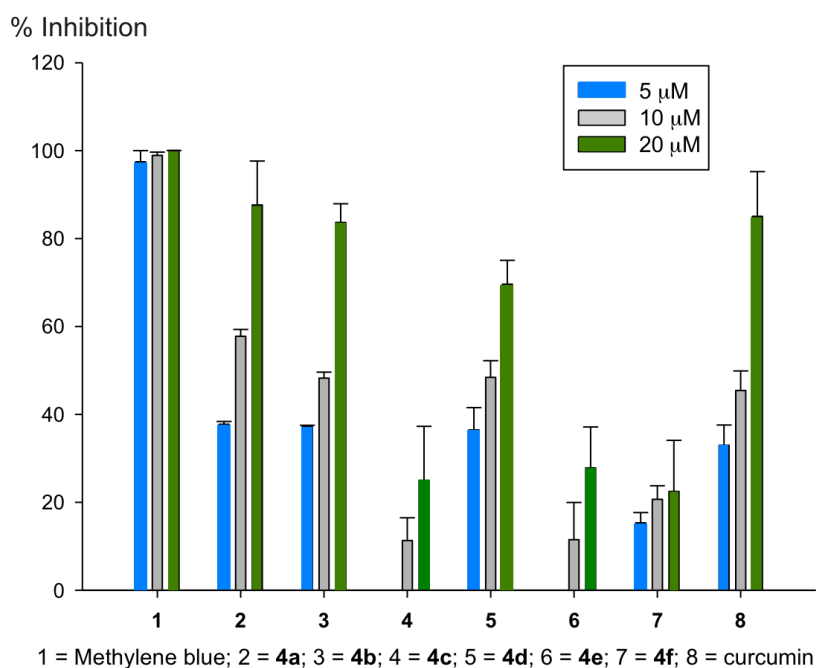


Figure 3.14

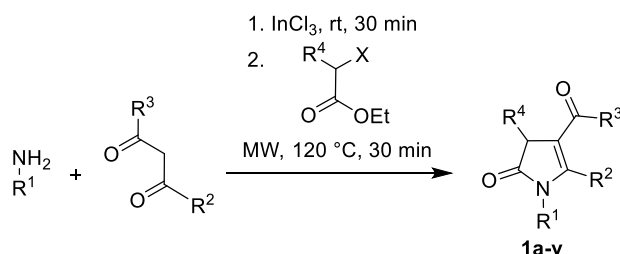
In summary, compounds **4b** and **4d** are attractive multitarget directed ligands against oxidative stress and act as tau protein aggregation inhibitors, with a safe toxicity profile.

3.7. Experimental section

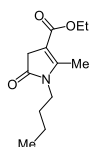
General experimental details

All reagents and solvents were of commercial quality and were used as received. Reactions were monitored by thin layer chromatography on aluminium plates coated with silica gel and fluorescent indicator. Microwave-assisted reactions were performed on a CEM Discover focused microwave reactor. Separations by flash chromatography were performed using a Combiflash Teledyne automated flash chromatograph or on conventional silica gel columns. Melting points were measured with a Kofler-type heating platine microscope from Reichert, 723 model, and are uncorrected. Infrared spectra were recorded with an Agilent Cary630 FTIR spectrophotometer with a diamond ATR accessory for solid and liquid samples, requiring no sample preparation; wavenumbers are given in cm^{-1} . NMR spectroscopic data were obtained using spectrometers maintained by the CAI de Resonancia Magnética, UCM, operating at 250, 300, 400 and 700 MHz for ^1H NMR and, 63, 100 and 176 MHz for ^{13}C NMR; chemical shifts are given in (δ) parts per million and coupling constants (J) in hertz. Elemental analyses were determined by the CAI de Microanálisis, Universidad Complutense, using a Leco CHNS-932 combustion microanalyzer. The enantiomeric excess analysis has been conducted in a HPLC Agilent 1220 Infinity LC with a chiral column ULTRON ES.

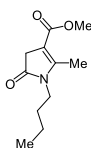
3.7.1. General procedure for the synthesis of 2-pyrrolin-5-one derivatives 1



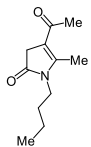
To a suspension of indium trichloride (5% mmol) in the corresponding β -dicarbonyl compound (1 eq.), placed in a microwave reaction vial, was added the suitable amine (1-1.2 eq.). The mixture was stirred at room temperature for 30 minutes and monitored by TLC. After the reaction completion, the excess of amine was evaporated under reduced pressure. Then, the non-isolated enamino ester and the appropriate α -haloester (1 eq.) were exposed to focused microwave irradiation at $120\text{ }^\circ\text{C}$ for 30 minutes. Once the reaction was completed, the mixture was diluted with CHCl_3 (20 mL) and washed with water (2 x 5 mL). The organic phase was dried over anhydrous sodium sulphate and then evaporated under reduced pressure. The mixture was chromatographed on silica gel eluting with a gradient from hexane to 4:1 hexane-ethyl acetate.

Ethyl 1-butyl-2-methyl-5-oxo-4,5-dihydro-1H-pyrrole-3-carboxylate (1a)

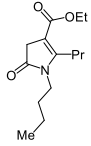
Prepared from ethyl acetoacetate (1 mmol), butylamine (1.2 mmol) and ethyl bromoacetate (1 mmol); orange solid (135 mg, 60%); mp 62-68 °C; $^1\text{H-NMR}$ (250 MHz, CDCl_3) δ 4.21 (q, $J = 7.2$ Hz, 2H), 3.55-3.49 (m, 2H), 3.27 (q, $J = 2.4$ Hz, 2H), 2.47 (t, $J = 2.4$ Hz, 3H), 1.61-1.49 (m, 2H), 1.43-1.24 (m, 2H), 1.31 (t, $J = 7.2$ Hz, 3H), 0.96 (t, $J = 7.2$ Hz, 3H); $^{13}\text{C-NMR}$ (63 MHz, CDCl_3) δ 176.4, 163.9, 159.8, 103.3, 59.6, 37.0, 36.6, 31.5, 20.1, 14.4, 13.7, 12.9; IR (neat, cm^{-1}): 1725, 1691, 1226; elemental analysis (%) calcd. for $\text{C}_{12}\text{H}_{19}\text{NO}_3$: C 63.98, H 8.50, N 6.22; found: C 63.66, H 8.33, N 5.97.

Methyl 1-butyl-2-methyl-5-oxo-4,5-dihydro-1H-pyrrole-3-carboxylate (1b)

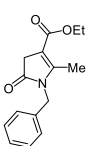
Prepared from methyl acetoacetate (1 mmol), butylamine (1.2 mmol) and ethyl bromoacetate (1 mmol); yellow oil (111 mg, 50%); $^1\text{H NMR}$ (250 MHz, CDCl_3) δ 3.72 (s, 3H), 3.50 (t, $J = 7.2$ Hz, 2H), 3.24 (q, $J = 2.3$ Hz, 2H), 2.44 (t, $J = 2.3$ Hz, 3H), 1.59-1.45 (m, 2H), 1.43-1.23 (m, 2H), 0.93 (t, $J = 7.2$ Hz, 3H); $^{13}\text{C NMR}$ (63 MHz, CDCl_3) δ 176.4, 165.1, 155.0, 103.4, 51.4, 40.4, 37.0, 31.8, 20.5, 14.1, 12.7; IR (neat, cm^{-1}): 1723, 1690, 1223; elemental analysis (%) calcd. for $\text{C}_{11}\text{H}_{17}\text{NO}_3$: C 62.54, H 8.11, N 6.63; found: C 62.43, H 7.89, N 6.19.

4-Acetyl-1-butyl-5-methyl-1,3-dihydro-2H-pyrrole-2-one (1c)

Prepared from acetylacetone (1 mmol), butylamine (1.2 mmol) and ethyl bromoacetate (1 mmol); yellow oil (82 mg, 42%); $^1\text{H-NMR}$ (250 MHz, CDCl_3) δ 3.57-3.51 (m, 2H), 3.34 (q, $J = 2.3$ Hz, 2H), 2.50 (t, $J = 2.3$ Hz, 3H), 2.22 (s, 3H), 1.58 -1.49 (m, 2H), 1.44-1.29 (m, 2H), 0.96 (t, $J = 7.0$ Hz, 3H); $^{13}\text{C-NMR}$ (63 MHz, CDCl_3) δ 192.8, 175.4, 154.0, 111.8, 39.8, 37.1, 31.2, 29.5, 20.0, 13.6, 12.8; IR (neat, cm^{-1}): 1721, 1659; elemental analysis (%) calcd. for $\text{C}_{11}\text{H}_{17}\text{NO}_2$: C 67.66, H 8.78, N 7.17; found: C 67.32, H 8.44, N 6.81.

Ethyl 1-butyl-5-oxo-2-propyl-4,5-dihydro-1H-pyrrole-3-carboxylate (1d)

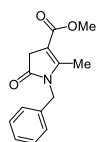
Prepared from ethyl 3-oxohexanoate (1 mmol), butylamine (1.2 mmol) and ethyl bromoacetate (1 mmol); range oil (132 mg, 52%); $^1\text{H-NMR}$: (250 MHz, CDCl_3) δ 4.18 (q, $J = 7.1$ Hz, 2H), 3.50-3.44 (m, 2H), 3.24 (s, 2H), 2.82-2.76 (m, 2H), 1.64-1.48 (m, 4H), 1.40-1.23 (m, 2H), 1.28 (t, $J = 7.1$ Hz, 3H), 1.03 (t, $J = 7.3$ Hz, 3H), 0.93 (t, $J = 7.2$ Hz, 3H); $^{13}\text{C-NMR}$: (63 MHz, CDCl_3) δ 176.3, 163.9, 158.3, 102.9, 59.6, 40.0, 36.6, 31.3, 27.6, 22.0, 20.0, 14.3, 14.0, 13.6; IR (neat, cm^{-1}): 1728, 1694, 1218; elemental analysis (%) calcd. for $\text{C}_{14}\text{H}_{23}\text{NO}_3$: C 66.37, H 9.15, N 5.53; found: C 65.33, H 9.00, N 5.36.

Ethyl 1-benzyl-2-methyl-5-oxo-4,5-dihydro-1H-pyrrole-3-carboxylate (1e)

Prepared from ethyl acetoacetate (1 mmol), benzylamine (1 mmol) and ethyl bromoacetate (1 mmol); yellow oil (135 mg, 52%); $^1\text{H-NMR}$: (250

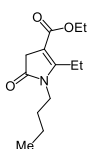
MHz, CDCl₃) δ 7.39-7.30 (m, 3H), 7.22 (dd, $J = 8.0$ Hz, $J = 1.8$ Hz, 2H), 4.79 (s, 2H), 4.22 (q, $J = 7.1$ Hz, 2H), 3.41 (q, $J = 2.4$ Hz, 2H), 2.37 (t, $J = 2.4$ Hz, 3H), 1.32 (t, $J = 7.1$ Hz, 3H); **¹³C-NMR: (63 MHz, CDCl₃)** δ 176.0, 164.2, 154.0, 136.5, 128.9 (2C), 127.7, 126.8 (2C), 103.7, 59.8, 43.4, 36.6, 14.4, 12.6; **IR (neat, cm⁻¹):** 1726, 1693, 1227; **elemental analysis (%) calcd. for C₁₅H₁₇NO₃:** C 69.48, H 6.61, N 5.40; found: C 69.16, H 6.89, N 5.31.

Methyl 1-benzyl-2-methyl-5-oxo-4,5-dihydro-1H-pyrrole-3-carboxylate (1f)



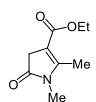
Prepared from methyl acetoacetate (1 mmol), benzylamine (1 mmol) and ethyl bromoacetate (1 mmol); pale brown solid (135 mg, 55%); **mp** 82-84 °C; **¹H NMR (250 MHz, CDCl₃)** δ 7.42-7.15 (m, 5H), 4.79 (s, 2H), 3.75 (s, 3H), 3.40 (q, $J = 2.4$ Hz, 2H), 2.37 (t, $J = 2.4$ Hz, 3H); **¹³C NMR (63 MHz, CDCl₃)** δ 176.4, 154.8, 136.9, 129.3 (2C), 128.2, 127.3 (2C), 103.8, 51.5, 43.9, 37.0, 13.0; **IR (neat, cm⁻¹):** 1727, 1685, 1250; **elemental analysis (%) calcd. for C₁₄H₁₅NO₃:** C 68.56, H 6.16, N 5.71; found: C 68.53, H 6.08, N 5.78.

Ethyl 1-butyl-2-ethyl-5-oxo-4,5-dihydro-1H-pyrrole-3-carboxylate (1g)



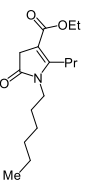
Prepared from ethyl propionylacetate (1 mmol), butylamine (1.2 mmol) and ethyl bromoacetate (1 mmol); yellow oil (142 mg, 59%); **¹H-NMR: (250 MHz, CDCl₃)** δ 4.22 (q, $J = 7.1$ Hz, 2H), 3.55-3.48 (m, 2H), 3.27 (s, 2H), 2.90-2.83 (m, 2H), 1.65-1.40 (m, 4H), 1.39-1.23 (m, 6H), 0.93 (t, $J = 7.2$ Hz, 3H); **¹³C-NMR: (63 MHz, CDCl₃)** δ 176.4, 163.9, 159.8, 102.9, 59.6, 40.0, 36.6, 31.5, 20.1, 19.2, 14.4, 13.7, 12.9; **IR (neat, cm⁻¹):** 1726, 1693, 1228; **elemental analysis (%) calcd. for C₁₃H₂₁NO₃:** C 65.25, H 8.84, N 5.85; found: C 65.16, H 8.89, N 5.79.

Ethyl 1,2-dimethyl-5-oxo-4,5-dihydro-1H-pyrrole-3-carboxylate (1h)



Prepared from ethyl acetoacetate (1 mmol), methylamine (1.2 mmol) and ethyl bromoacetate (1 mmol); yellow oil (140 mg, 76%); **¹H-NMR: (250 MHz, CDCl₃)** δ 4.17 (q, $J = 7.1$ Hz, 2H), 3.05 (s, 3H), 3.23 (q, $J = 2.4$ Hz, 2H), 2.42 (t, $J = 7.1$ Hz, 3H), 1.27 (t, 3H, $J = 2.4$ Hz); **¹³C-NMR: (63 MHz, CDCl₃)** δ 176.0, 164.2, 154.1, 103.2, 59.7, 36.5, 26.3, 14.3, 12.4; **IR (neat, cm⁻¹):** 1725, 1692, 1228; **elemental analysis (%) calcd. for C₉H₁₃NO₃:** C 59.00, H 7.15, N 7.65; found: C 59.22, H 7.30, N 7.52.

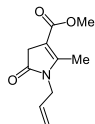
Ethyl 1-hexyl-5-oxo-2-propyl-4,5-dihydro-1H-pyrrole-3-carboxylate (1i)



Prepared from ethyl 3-oxohexanoate (1 mmol), hexylamine (1 mmol) and ethyl bromoacetate (1 mmol); orange oil (203 mg, 72%); **¹H-NMR: (250 MHz, CDCl₃)** δ 4.20 (q, $J = 7.1$ Hz, 2H), 3.57-3.48 (m, 2H), 3.27 (s, 2H), 2.82-2.76 (m, 2H), 1.63-1.57 (m, 4H), 1.34-1.26 (m, 6H), 1.29 (t, $J = 7.1$ Hz, 3H), 1.05 (t, $J = 7.5$ Hz, 3H), 0.91 (t, $J = 7.0$ Hz, 3H); **¹³C-NMR: (63 MHz, CDCl₃)** δ 176.4, 163.9, 158.3, 102.9, 59.6, 40.3, 36.6, 31.3, 29.3, 27.7, 26.5, 22.5, 22.0, 14.4, 14.1, 14.0; **IR (neat, cm⁻¹):** 1726, 1702, 1227; **elemental**

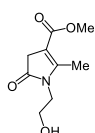
analysis (%) calcd. for C₁₆H₂₇NO₃: C 68.29, H 9.67, N 4.98; found: C 68.22, H 9.30, N 4.82.

Methyl 1-allyl-2-methyl-5-oxo-4,5-dihydro-1H-pyrrole-3-carboxylate (1j)



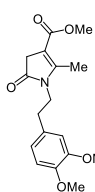
Prepared from ethyl acetoacetate (1 mmol), allylamine (1. mmol) and ethyl bromoacetate (1 mmol); yellow oil (98 mg, 50%); **¹H NMR (250 MHz, CDCl₃)** δ 5.84-5.62 (m, 1H), 5.16-4.96 (m, 2H), 4.11 (dt, *J* = 5.0, 1.7 Hz, 2H), 3.67 (s, 3H), 3.24 (q, *J* = 2.4 Hz, 2H), 2.36 (t, *J* = 2.4 Hz, 3H); **¹³C NMR (63 MHz, CDCl₃)** δ 174.6, 163.6, 153.5, 131.3, 115.8, 102.1, 50.1, 41.0, 35.5, 11.2; **IR (neat, cm⁻¹):** 1720, 1685, 1228; **elemental analysis (%) calcd. for C₁₀H₁₃NO₃:** C 61.53, H 6.71, N 7.18; found: C 61.19, H 6.65, N 6.98.

Methyl 1-(2-hydroxyethyl)-2-methyl-5-oxo-4,5-dihydro-1H-pyrrole-3-carboxylate (1k)



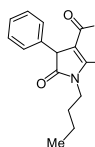
Prepared from methyl acetoacetate (1 mmol), hydroxyethylamine (1 mmol) and ethyl bromoacetate (1 mmol); pale red solid (86 mg, 43%); **mp** 111-114 °C; NMR data are identical to those found in the literature.¹⁴³ **IR (neat, cm⁻¹):** 3482, 2940, 1715, 1669, 1616, 1231; **elemental analysis (%) calcd. for C₉H₁₃NO:** C 54.26, H, 6.58, N, 7.03; found: C 54.14, H 6.39, N 6.79.

Methyl 1-(3,4-dimethoxyphenethyl)-2-methyl-5-oxo-4,5-dihydro-1H-pyrrole-3-carboxylate (1l)



Prepared from methyl acetoacetate (1 mmol), 3,4-dimethoxyphenethylamine (1 mmol) and ethyl bromoacetate (1 mmol); beige solid (166 mg, 52%); **mp** 99-103 °C; **¹H NMR (250 MHz, CDCl₃)** δ 6.73 (d, *J* = 8.0 Hz, 1H), 6.65 (d, *J* = 1.9 Hz, 1H), 6.60-6.59 (m, 1H), 3.79 (s, 3H), 3.78 (s, 3H), 3.68-3.59 (m, 5H), 3.19 (q, *J* = 2.3 Hz, 2H), 2.75 (t, *J* = 7.3 Hz, 2H), 2.13 (t, *J* = 2.4 Hz, 3H); **¹³C NMR (63 MHz, CDCl₃)** δ 175.0, 163.6, 153.5, 148.0, 146.9, 129.4, 119.8, 110.9, 110.3, 101.8, 88.8, 54.9, 50.0, 41.1, 35.5, 33.7, 11.0; **IR (neat, cm⁻¹):** 1717, 1685, 1220; **elemental analysis (%) calcd. for C₁₇H₂₁NO₅:** C 63.94, H 6.63, N 4.39; found: C 63.77, H 6.47, N 4.29.

Ethyl 1-butyl-2-methyl-5-oxo-4-phenyl-4,5-dihydro-1H-pyrrole-3-carboxylate (1m)



Prepared from ethyl acetoacetate (1 mmol), butylamine (1.2 mmol) and methyl α-bromophenylacetate (1 mmol); orange oil (175 mg, 58%); **¹H NMR (250 MHz, CDCl₃)** δ 7.35-7.15 (m, 5H), 4.36 (q, *J* = 2.0 Hz, 1H), 4.13-3.97 (m, 2H), 3.58 (m, 2H), 2.48 (d, *J* = 2.0 Hz, 3H), 1.65-1.53 (m, 2H), 1.41-1.28 (m, 2H), 1.06 (t, *J* = 7.2 Hz, 3H), 0.95 (t, *J* = 7.0 Hz, 3H);

¹⁴³ Caballero, E.; Puebla, P.; Domercq, M.; Medarde, M.; López J. L.; San Feliciano, A. *Tetrahedron* **1994**, *50*, 7849-7856.

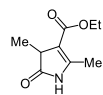
¹³C NMR (63 MHz, CDCl₃) δ 177.8, 164.5, 155.0, 137.0, 129.0 (2C), 128.3 (2C), 127.6, 108.9, 60.0, 53.2, 40.4, 31.8, 20.4, 14.5, 14.1, 12.7; **IR (neat, cm⁻¹):** 1721, 1696, 1218.; **elemental analysis (%) calcd. for C₁₈H₂₃NO₃:** C 71.73, H 7.69, N, 4.65; found: C 71.65, H 7.64, N 4.69.

Ethyl 2-methyl-5-oxo-4,5-dihydro-1H-pyrrole-3-carboxylate (1n)



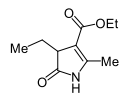
Prepared from ethyl 3-aminocrotonate (1 mmol) and ethyl bromoacetate (1 mmol); beige solid (93 mg, 55%); **mp** 119-123 °C; **¹H NMR (250 MHz, CDCl₃)** δ 8.72 (br s, 1H), 4.22 (q, *J* = 7.1 Hz, 2H), 3.32 (q, *J* = 2.3 Hz, 2H), 2.39 (t, *J* = 2.3 Hz, 3H), 1.32 (t, *J* = 7.1 Hz, 3H); **¹³C NMR (63 MHz, CDCl₃)** δ 178.7, 164.6, 152.0, 104.9, 60.3, 38.0, 14.8, 13.9; **IR (neat, cm⁻¹):** 3165, 1702, 1682, 1251; **elemental analysis (%) calcd. for C₈H₁₁NO₃:** C 56.80, H 6.55, N 8.28; found: C 56.42, H 6.36, N 7.90.

Ethyl 2,4-dimethyl-5-oxo-4,5-dihydro-1H-pyrrole-3-carboxylate (1o)



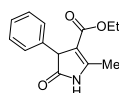
Prepared from ethyl 3-aminocrotonate (1 mmol) and methyl α-bromomethylacetate (1 mmol); yellow oil (79 mg, 43%); **¹H NMR (250 MHz, CDCl₃)** δ 8.11 (br s, 1H), 4.42-4.09 (m, 2H), 3.29 (qq, *J* = 7.6, 2.1 Hz, 1H), 2.40 (d, *J* = 2.1 Hz, 3H), 1.44 (d, *J* = 7.6 Hz, 3H), 1.33 (t, *J* = 7.1 Hz, 3H); **¹³C NMR (63 MHz, CDCl₃)** δ 182.1, 164.7, 150.9, 110.7, 60.1, 43.5, 15.6, 14.8, 14.0; **IR (neat, cm⁻¹):** 3186, 1721, 1686, 1249; **elemental analysis (%) calcd. for C₉H₁₃NO₃:** C 59.00, H 7.15, N 7.65; found: C 58.79, H 6.95, N 7.73.

Ethyl 4-ethyl-2-methyl-5-oxo-4,5-dihydro-1H-pyrrole-3-carboxylate (1p)



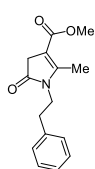
Prepared from ethyl 3-aminocrotonate (1 mmol) and methyl α-bromoethylacetate (1 mmol); yellow oil (79 mg, 40%); **¹H NMR (250 MHz, CDCl₃)** δ 8.22 (br s, 1H), 4.34-4.14 (m, 2H), 3.43-3.29 (m, 1H), 2.41 (d, *J* = 2.2 Hz, 3H), 2.18-1.88 (m, 2H), 1.33 (t, *J* = 7.1 Hz, 3H), 0.83 (t, *J* = 7.5 Hz, 3H); **¹³C NMR (63 MHz, CDCl₃)** δ 181.5, 164.7, 151.8, 108.1, 60.1, 48.9, 22.7, 14.8, 14.1, 9.4; **IR (neat, cm⁻¹):** 3257, 1715, 1689, 1223; **elemental analysis (%) calcd. for C₁₀H₁₅NO₃:** C 60.90, H 7.67, N 7.10; found: C 60.88, H 7.48, N 7.13.

Ethyl 2-methyl-5-oxo-4-phenyl-4,5-dihydro-1H-pyrrole-3-carboxylate (1q)



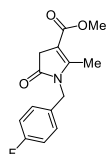
Prepared from ethyl 3-aminocrotonate (1 mmol) and methyl α-bromophenylacetate (1 mmol); yellow oil (101 mg, 41%); **¹H NMR (250 MHz, CDCl₃)** δ 8.21 (br s, 1H), 7.44-7.15 (m, 5H), 4.42 (app. d, *J* = 2.2 Hz, 1H), 4.18-3.93 (m, 2H), 2.47 (d, *J* = 2.2 Hz, 3H), 1.09 (t, *J* = 7.1 Hz, 3H); **¹³C NMR (63 MHz, CDCl₃)** δ 179.4, 164.3, 152.9, 136.4, 129.1 (2C), 128.3 (2C), 127.9, 109.8, 60.1, 54.2, 14.5, 14.0; **IR (neat, cm⁻¹):** 3238, 1719, 1687, 1223; **elemental analysis (%) calcd. for C₁₄H₁₅NO₃:** C 68.56, H 6.16, N 5.71; found: C 68.41, H 6.16, N 5.57.

Methyl 2-methyl-5-oxo-1-phenethyl-4,5-dihydro-1H-pyrrole-3-carboxylate (1r)



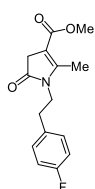
Prepared from methyl acetoacetate (1 mmol), phenethylamine (1 mmol) and ethyl bromoacetate; light brown solid (140 mg, 54%); **mp** 99-103 °C; **¹H NMR (250 MHz, CDCl₃)** δ 7.20-6.91 (m, 5H), 3.56 (t, *J* = 7.3 Hz, 2H), 3.53 (s, 3H), 3.08 (q, *J* = 2.2 Hz, 2H), 2.69 (t, *J* = 7.3 Hz, 2H), 2.00 (t, *J* = 2.2 Hz, 3H); **¹³C NMR (63 MHz, CDCl₃)** δ 175.0, 163.6, 153.5, 137.0, 127.8 (2C), 127.7 (2C), 125.9, 101.9, 50.0, 41.0, 35.5, 34.2, 11.0; **IR (neat, cm⁻¹):** 1703, 1669, 1230; **elemental analysis (%) calcd. for C₁₅H₁₇NO₃:** C 69.48, H 6.61, N 5.40; found: C 69.19, H 6.50, N 5.15.

Methyl 1-(4-fluorobenzyl)-2-methyl-5-oxo-4,5-dihydro-1H-pyrrole-3-carboxylate (1s)



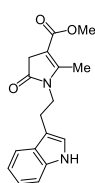
Prepared from methyl acetoacetate (1 mmol), 4-fluorobenzylamine (1 mmol) and ethyl bromoacetate (1 mmol); brown solid (129mg, 49%); **mp** 61-62°C; **¹H NMR (250 MHz, CDCl₃)** δ 7.21 – 7.11 (m, 2H), 7.07 – 6.95 (m, 3H), 4.72 (s, 2H), 3.72 (s, 3H), 3.36 (q, *J* = 2.4 Hz, 2H), 2.34 (t, *J* = 2.4 Hz, 3H); **¹³C NMR (63 MHz, CDCl₃)** δ 176.1, 164.7, 162.4 (d, *J* = 246.8 Hz), 154.2, 132.4 (d, *J* = 3.3 Hz), 128.8 (d, *J* = 8.2 Hz, 2C), 116.0 (d, *J* = 21.7 Hz, 2C), 103.7, 51.3, 43.0, 36.7, 12.8; **IR (neat, cm⁻¹):** 1690, 1630, 1219; **elemental analysis (%) calcd. for C₁₄H₁₄FNO₃:** C 63.87, H 5.36, N 5.32; found: C 62.53, H 5.18, N 5.34.

Methyl 2-methyl-5-oxo-1-(4-fluorophenethyl)-4,5-dihydro-1H-pyrrole-3-carboxylate (1t)

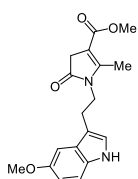


Prepared from methyl acetoacetate (1 mmol), 4-fluorophenethylamine (1 mmol) and ethyl bromoacetate; brown solid (156mg, 56%); **mp** 74-75 °C; **¹H NMR (250 MHz, CDCl₃)** δ 7.15 – 7.07 (m, 2H), 7.02 – 6.94 (m, 2H), 3.75 – 3.64 (m, 5H), 3.25 (q, *J* = 2.3 Hz, 2H), 2.84 (t, *J* = 7.3 Hz, 2H), 2.20 (t, *J* = 2.3 Hz, 3H); **¹³C NMR (63 MHz, CDCl₃)** δ 176.1, 161.9 (d, *J* = 245.8 Hz), 156.0, 154.3, 133.7 (d, *J* = 3.2 Hz), 130.4 (d, *J* = 8.0 Hz, 2C), 115.8 (d, *J* = 21.4 Hz, 2C), 103.1, 51.2, 42.1 (d, *J* = 1.2 Hz), 36.6, 34.5, 12.2; **IR (neat, cm⁻¹):** 1687, 1622, 1213; **elemental analysis (%) calcd. for C₁₅H₁₆FNO₃:** C 64.97, H 5.82, N 5.05; found: C 64.74, H 5.55, N 5.01.

Methyl 1-(2-(1H-indol-3-yl)ethyl)-2-methyl-5-oxo-4,5-dihydro-1H-pyrrole-3-carboxylate (1u)



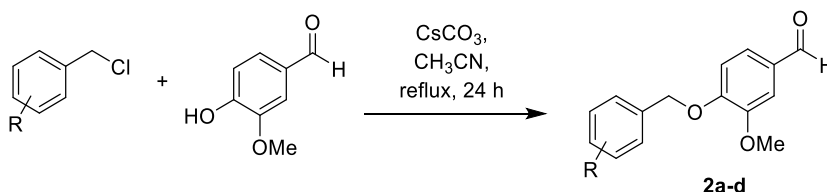
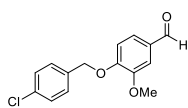
Prepared from methyl acetoacetate (1 mmol), tryptamine (1 mmol) and ethyl bromoacetate; light brown solid (107mg, 36%); **mp** 157 °C; **¹H NMR (250 MHz, CDCl₃)** δ 8.29 (s, 1H), 7.60 (d, *J* = 7.6 Hz, 1H), 7.38 – 7.32 (m, 1H), 7.24 – 7.16 (m, 1H), 7.16 – 7.07 (m, 1H), 6.98 (d, *J* = 2.3 Hz, 1H), 3.82-3.76 (m, 2H), 3.71 (s, 3H), 3.27 (q, *J* = 2.3 Hz, 2H), 3.08 – 2.97 (m, 2H), 2.18 (t, *J* = 2.3 Hz, 3H); **¹³C NMR (63 MHz, CDCl₃)** δ 176.2, 164.8, 154.9, 136.3, 127.2, 122.4, 122.3, 119.7, 118.4, 112.1, 111.5, 102.8, 51.1, 41.2, 36.7, 24.9, 12.2; **IR (neat, cm⁻¹):** 3356, 1691, 1622, 1231; **elemental analysis (%) calcd. for C₁₇H₁₈N₂O₃:** C 68.44, H 6.08, N 9.39; found: C 68.52, H 5.97, N 9.23.

Methyl 1-(2-(5-methoxy-1H-indol-3-yl)ethyl)-2-methyl-5-oxo-4,5-dihydro-1H-pyrrole-3-carboxylate (1v)

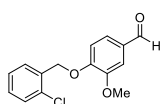
Prepared from methyl acetoacetate (1 mmol), 5-methoxytryptamine (1 mmol) and ethyl bromoacetate; light brown solid (135 mg, 41%); **mp** 155-156 °C; $^1\text{H NMR}$ (250 MHz, CDCl_3) δ 8.13 (br s, 1H), 7.24 (d, $J = 8.7$ Hz, 1H), 7.05 (d, $J = 2.4$ Hz, 1H), 6.95 (d, $J = 2.3$ Hz, 1H), 6.86 (dd, $J = 8.7, 2.4$ Hz, 1H), 3.86 (s, 3H), 3.78 (t, $J = 7.3$ Hz, 2H), 3.70 (s, 3H), 3.26 (q, $J = 2.3$ Hz, 2H), 2.99 (t, $J = 7.3$ Hz, 2H), 2.18 (t, $J = 2.3$ Hz, 3H); $^{13}\text{C NMR}$ (63 MHz, CDCl_3) δ 176.3, 164.8, 155.0, 154.2, 131.4, 127.6, 123.1, 112.5, 112.2, 111.8, 102.8, 100.2, 56.0, 51.2, 41.1, 36.7, 25.0, 12.2; **IR** (neat, cm^{-1}): 3393, 3322, 1692, 1672, 1628, 1222; **elemental analysis (%) calcd. for $\text{C}_{18}\text{H}_{20}\text{N}_2\text{O}_4$** : C 65.84, H 6.14, N 8.53; found: C 65.62, H 6.09, N 8.73.

3.7.2. Synthesis of 4-benzyloxy-3-methoxybenzaldehydes 2

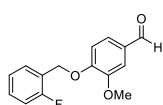
To a solution of vanillin and the suitable benzyl chloride in acetonitrile (10 mL) were added K_2CO_3 and IK and the mixture was stirred at reflux for 3 h. The reaction was cooled to room temperature, diluted with ethyl acetate (20 mL) and washed with brine (2 x 20 mL). The organic layer was dried over sodium sulphate, filtered and the solvent was removed under reduced pressure. The solid residue was pulverized and washed twice with hexane (3 x 10 mL) to afford the desired aldehydes.

**4-[(4-Chlorobenzyl)oxy]-3-methoxybenzaldehyde (2a)**

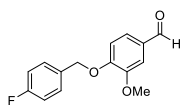
Prepared from vanillin (1.41 mmol) and 4-chlorobenzyl chloride (1.55 mmol); yellow solid (370 mg, 95%); **mp**: 82 °C; $^1\text{H NMR}$ (250 MHz, CDCl_3) δ 9.87 (s, 1H), 7.46 (d, $J = 1.8$ Hz, 1H), 7.45 – 7.38 (m, 5H), 6.99 (d, $J = 8.1$ Hz, 1H), 5.23 (s, 2H), 3.98 (s, 3H); $^{13}\text{C NMR}$ (63 MHz, CDCl_3) δ 191.1, 153.4, 150.2, 134.6, 134.2, 130.6, 129.1 (2C), 128.7 (2C), 126.7, 112.5, 109.5, 70.2, 56.2; **IR** (neat, cm^{-1}): 1668.3, 1580.4, 1504.2, 1258.3, 1227.2; **elemental analysis (%) calcd. for $\text{C}_{15}\text{H}_{13}\text{ClO}_3$** : C 65.11, H 4.74; found: C 65.22, H 4.68.

4-[(2-Chlorobenzyl)oxy]-3-methoxybenzaldehyde (2b)

Prepared from vanillin (3.16 mmol) and 2-chlorobenzyl chloride (3.48 mmol); yellow solid (813 mg, 93%); **mp**: 48 °C; $^1\text{H NMR}$ (250 MHz, CDCl_3) δ 9.85 (s, 1H), 7.58 – 7.49 (m, 1H), 7.47 – 7.35 (m, 3H), 7.32 – 7.23 (m, 2H), 6.97 (d, $J = 8.1$ Hz, 1H), 5.34 (s, 2H), 3.97 (s, 3H); $^{13}\text{C NMR}$ (63 MHz, CDCl_3) δ 191.1, 153.3, 150.2, 133.8, 132.4, 130.6, 129.6, 129.4, 128.6, 127.3, 126.8, 112.5, 109.5, 68.0, 56.2; **IR** (neat, cm^{-1}): 1681.4, 1587.5, 1507.6, 1265.2; **elemental analysis (%) calcd. for $\text{C}_{15}\text{H}_{13}\text{ClO}_3$** : C 65.11, H 4.74; found: C 65.27, H 4.61.

4-[(2-Fluorobenzyl)oxy]-3-methoxybenzaldehyde (2c)

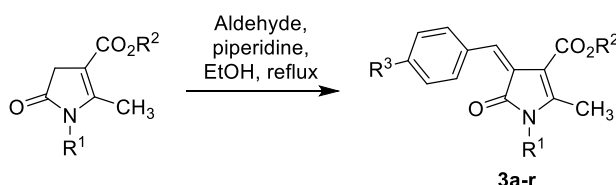
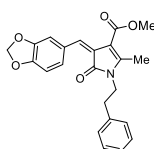
Prepared from vanillin (3 mmol) and 2-fluorobenzyl chloride (3.3 mmol); yellow solid (757 mg, 97%); **mp**: 62-63 °C; **¹H NMR (250 MHz, CDCl₃)** δ 9.67 (s, 1H), 7.34 (td, *J* = 7.5, 1.7 Hz, 1H), 7.27 – 7.21 (m, 2H), 7.13 (ddd, *J* = 7.4, 5.5, 2.0 Hz, 1H), 7.05 – 6.93 (m, 1H), 6.93 – 6.87 (m, 1H), 6.86 (d, *J* = 8.2 Hz, 1H), 5.13 (s, 2H), 3.77 (s, 3H); **¹³C NMR (63 MHz, CDCl₃)** δ 191.1, 160.4 (d, *J* = 246.9 Hz), 153.4, 150.2, 130.6, 130.1 (d, *J* = 8.2 Hz), 129.6 (d, *J* = 3.8 Hz), 126.8, 124.6 (d, *J* = 3.6 Hz), 123.3 (d, *J* = 14.1 Hz), 115.6 (d, *J* = 21.1 Hz), 112.3, 109.5, 64.6 (d, *J* = 4.6 Hz), 56.2; **IR** (neat, cm⁻¹): 1693.9, 1582.9, 1499.6, 1260.5, 1228.9; **elemental analysis (%) calcd. for C₁₅H₁₃FO₃**: C 69.22, H 5.03; found: C 68.99, H 4.89.

4-[(4-Fluorobenzyl)oxy]-3-methoxybenzaldehyde (2d)

Prepared from vanillin (2.3 mmol) and 4-fluorobenzyl chloride (2.5 mmol); yellow solid (573 mg, 88%); **mp**: 74-75 °C; **¹H NMR (250 MHz, CDCl₃)** δ 9.84 (s, 1H), 7.49 – 7.33 (m, 4H), 7.14 – 7.02 (m, 2H), 6.98 (d, *J* = 8.0 Hz, 1H), 5.19 (s, 2H), 3.94 (s, 3H); **¹³C NMR (63 MHz, CDCl₃)** δ 191.1, 162.8 (d, *J* = 246.8 Hz), 153.5, 150.2, 131.9 (d, *J* = 3.2 Hz), 130.6, 129.3 (d, *J* = 8.3 Hz, 2C), 126.7, 115.8 (d, *J* = 21.6 Hz, 2C), 112.5, 109.5, 70.4, 56.2; **IR** (neat, cm⁻¹): 1678.9, 1584.5, 1508.1, 1263.7, 1222.9; **elemental analysis (%) calcd. for C₁₅H₁₃FO₃**: C 69.22, H 5.03; found: C 69.05, H 4.95.

3.7.3. General synthesis of 4-arylmethylen-2-pyrrolin-5-ones 3

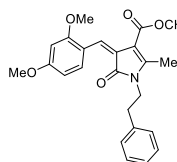
In a round bottom flask the suitable 2-pyrrolin-5-one (0.25 mmol, 1 eq) was suspended in ethanol (10 mL). Then, the corresponding aldehyde (0.28 mmol, 1.1 eq) and piperidine (0.5 mmol, 2 eq) were added. The mixture was refluxed and monitored by TLC. Once the 2-pyrrolin-5-one was no longer detected, the reaction was cooled to room temperature, diluted with ethyl acetate (20 mL) and washed with water (2 x 10 mL). The organic phase was dried over anhydrous sodium sulphate and then the solvent was removed under reduced pressure. The residue was purified by column chromatography on silica gel eluting with a gradient from hexane to 1:1 hexane-ethyl acetate.

**Methyl (Z)-4-benzylidene-2-methyl-5-oxo-1-phenethyl-4,5-dihydro-1H-pyrrole-3-carboxylate (3a)**

Prepared from pyrrolinone **1r** (1 mmol) and piperonal (1.1 mmol); yellow solid (235 mg, 60%); **mp**: 179 °C; **¹H NMR (250 MHz, CDCl₃)** δ 8.17 (d, *J* = 1.6 Hz, 1H), 8.13 (s, 1H), 7.56 (dd, *J* = 8.2, 1.6 Hz, 1H), 7.38 – 7.11 (m, 5H),

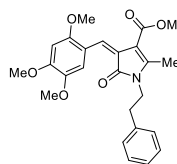
6.88 (d, $J = 8.2$ Hz, 1H), 6.05 (s, 2H), 3.87 (t, $J = 7.3$ Hz, 2H), 3.85 (s, 3H), 2.93 (t, $J = 7.3$ Hz, 2H), 2.25 (s, 3H); ^{13}C NMR (63 MHz, CDCl_3) δ 166.1, 165.3, 151.9, 149.9, 147.8, 141.9, 138.6, 129.6, 129.3 (2C), 129.1 (2C), 127.2, 125.1, 111.7, 108.3, 103.9, 101.9, 51.3, 42.5, 35.8, 13.4; IR (neat, cm^{-1}): 1672.7, 1264.8; elemental analysis (%) calcd. for $\text{C}_{23}\text{H}_{11}\text{NO}_5$: C 70.58, H 5.41, N 3.58; found: C 70.38, H 5.32, N 3.36.

Methyl (Z)-4-(2,4-dimethoxybenzylidene)-2-methyl-5-oxo-1-phenethyl-4,5-dihydro-1H-pyrrole-3-carboxylate (3b)



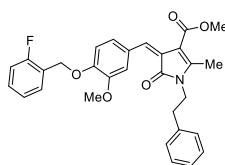
Prepared from pyrrolinone **1r** (0.25 mmol) and 2,4-dimethoxybenzaldehyde (0.28 mmol); yellow solid (42 mg, 41%); mp: 126 °C; ^1H NMR (250 MHz, CDCl_3) δ 8.48 (d, $J = 8.8$ Hz, 1H), 8.41 (s, 1H), 7.35 – 7.07 (m, 5H), 6.55 (dd, $J = 8.8, 2.4$ Hz, 1H), 6.44 (d, $J = 2.4$ Hz, 1H), 3.87 (s, 3H), 3.86 (s, 3H), 3.85 – 3.77 (m, 5H), 2.91 – 2.82 (m, 2H), 2.22 (s, 3H); ^{13}C NMR (63 MHz, CDCl_3) δ 166.1, 165.2, 163.2, 160.2, 151.3, 138.5, 136.6, 133.3, 129.1 (2C), 128.9 (2C), 126.9, 124.2, 116.8, 104.1, 97.9, 55.9, 55.6, 51.0, 42.2, 35.6, 13.0; IR (neat, cm^{-1}): 1680.6, 1594.6, 1268.6, 1205.0; elemental analysis (%) calcd. for $\text{C}_{24}\text{H}_{25}\text{NO}_5$: C 70.75, H 6.18, N 3.44; found: C 70.93, H 6.09, N 3.20.

Methyl (Z)-2-methyl-5-oxo-1-phenethyl-4-(2,4,5-trimethoxybenzylidene)-4,5-dihydro-1H-pyrrole-3-carboxylate (3c)

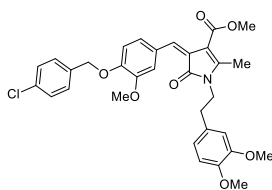


Prepared from pyrrolinone **1r** (0.25 mmol) and 2,4,5-trimethoxybenzaldehyde (0.28 mmol); yellow solid (51 mg, 47%); mp: 141 °C; ^1H NMR (250 MHz, CDCl_3) δ 8.55 (s, 2H), 7.33 – 7.12 (m, 5H), 6.49 (s, 1H), 3.95 (m, 6H), 3.90 (s, 3H), 3.85 – 3.79 (m, 5H), 2.89 (t, $J = 7.3$ Hz, 2H), 2.20 (s, 3H); ^{13}C NMR (63 MHz, CDCl_3) δ 166.0, 165.2, 155.0, 152.5, 150.9, 142.2, 138.6, 135.8, 129.1 (2C), 128.8 (2C), 126.9, 123.7, 115.9, 114.8, 104.2, 95.9, 56.8, 56.6, 56.1, 51.0, 42.1, 35.6, 13.0; IR (neat, cm^{-1}): 1675.3, 1587.8, 1278.9, 1205.3; elemental analysis (%) calcd. for $\text{C}_{25}\text{H}_{27}\text{NO}_6$: C 68.64, H 6.22, N 3.20; found: C 68.45, H 6.19, N 3.31.

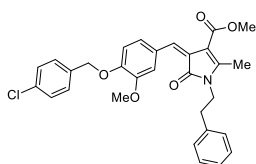
Methyl (Z)-4-[4-[(2-fluorobenzyl)oxy]-3-methoxybenzylidene]-2-methyl-5-oxo-1-phenethyl-4,5-dihydro-1H-pyrrole-3-carboxylate (3d)



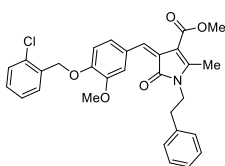
Prepared from pyrrolinone **1r** (0.25 mmol) and aldehyde **2c** (0.28 mmol); yellow solid (35 mg, 28%); mp: 94–95°C; ^1H NMR (250 MHz, CDCl_3) δ 8.29 (d, $J = 2.0$ Hz, 1H), 8.14 (s, 1H), 7.63 (dd, $J = 8.7, 1.8$ Hz, 1H), 7.52 (td, $J = 7.5, 1.7$ Hz, 1H), 7.35 – 7.26 (m, 3H), 7.15 (m, 4H), 6.93 (d, $J = 8.5$ Hz, 1H), 6.86 (d, $J = 11.2$ Hz, 1H), 5.30 (s, 2H), 3.99 (s, 3H), 3.89 – 3.81 (m, 5H), 2.90 (t, $J = 7.2$ Hz, 2H), 2.21 (s, 3H); ^{13}C NMR (63 MHz, CDCl_3) δ 166.0, 165.1, 160.4 (d, $J = 246.1$ Hz), 151.5, 149.9, 148.8, 141.8, 138.4, 129.8 (d, $J = 8.14$ Hz), 129.6 (d, $J = 3.9$ Hz), 129.1 (2C), 128.8 (2C), 128.7, 127.2, 126.9, 124.8, 124.5 (d, $J = 3.6$ Hz), 124.0 (d, $J = 14.2$ Hz), 115.4 (d, $J = 21.1$ Hz), 115.2, 112.5, 103.7, 64.4 (d, $J = 4.6$ Hz), 56.3, 51.0, 42.2, 35.5, 13.2; IR (neat, cm^{-1}): 1675.5, 1586.8, 1267.7, 1140.2; elemental analysis (%) calcd. for $\text{C}_{30}\text{H}_{28}\text{FNO}_5$: C 71.84, H 5.63, N 2.79; found: C 71.64, H 5.62, N 2.81.

Methyl (Z)-4-[4-[(4-chlorobenzyl)oxy]-3-methoxybenzylidene]-1-(3,4-dimethoxyphenethyl)-2-methyl-5-oxo-4,5-dihydro-1H-pyrrole-3-carboxylate (3e)

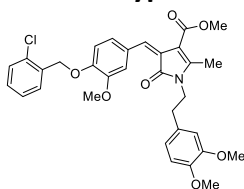
Prepared from pyrrolinone **1l** (0.25 mmol) and aldehyde **2a** (0.28 mmol); yellow solid (62 mg, 43%); **mp**: 70 °C; **¹H NMR (250 MHz, CDCl₃)** δ 8.06 (d, *J* = 2.0 Hz, 1H), 7.94 (s, 1H), 7.41 (dd, *J* = 8.6, 1.8 Hz, 1H), 7.21 – 7.09 (m, 5H), 7.04 (s, 1H), 6.70 – 6.40 (m, 6H), 4.97 (s, 2H), 3.78 (s, 3H), 3.68 – 3.55 (m, 11H), 2.65 (t, *J* = 6.7 Hz, 2H), 1.98 (s, 3H); **¹³C NMR (63 MHz, CDCl₃)** δ 166.0, 165.0, 151.6, 149.9, 149.1, 148.8, 145.0, 141.7, 135.3, 133.9, 131.0, 128.9, 128.8, 128.7, 127.0, 124.9, 121.0, 115.2, 112.7, 112.2, 111.5, 103.6, 70.1, 56.2, 56.0, 56.0, 51.0, 42.3, 35.0, 13.3; **IR (neat, cm⁻¹)**: 1685.9, 1590.4, 1259.1, 1248.0; **elemental analysis (%) calcd. for C₃₂H₃₂ClNO₇**: C 66.49, H 5.58, N 2.42; found: C 66.74, H 5.41, N 2.41.

Methyl (Z)-4-[4-[(4-chlorobenzyl)oxy]-3-methoxybenzylidene]-2-methyl-5-oxo-1-phenethyl-4,5-dihydro-1H-pyrrole-3-carboxylate (3f)

Prepared from pyrrolinone **1r** (0.25 mmol) and aldehyde **2a** (0.28 mmol); yellow solid (49 mg, 38%); **mp**: 68-70 °C; **¹H NMR (250 MHz, CDCl₃)** δ 8.21 (d, *J* = 2.0 Hz, 1H), 8.06 (s, 1H), 7.54 (dd, *J* = 8.7, 1.9 Hz, 1H), 7.37 – 7.05 (m, 9H), 6.78 (d, *J* = 8.5 Hz, 1H), 5.10 (s, 2H), 3.91 (s, 3H), 3.81 – 3.72 (m, 5H), 2.82 (t, *J* = 7.3 Hz, 2H), 2.13 (s, 3H); **¹³C NMR (63 MHz, CDCl₃)** δ 165.9, 165.1, 151.5, 149.9, 148.8, 141.7, 138.4, 135.3, 133.8, 129.1, 128.9, 128.8, 128.7, 127.0, 126.9, 124.8, 115.2, 112.6, 103.7, 70.0, 56.2, 51.0, 42.1, 35.5, 13.2; **IR (neat, cm⁻¹)**: 1686.2, 1592.8, 1260.3; **elemental analysis (%) calcd. for C₃₀H₂₈ClNO₅**: C 69.56, H 5.45, N 2.70; found: C 69.22, H 5.27, N 2.68.

Methyl (Z)-4-[4-[(2-chlorobenzyl)oxy]-3-methoxybenzylidene]-2-methyl-5-oxo-1-phenethyl-4,5-dihydro-1H-pyrrole-3-carboxylate (3g)

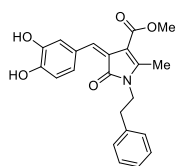
Prepared from pyrrolinone **1r** (0.25 mmol) and aldehyde **2b** (0.28 mmol); yellow solid (47 mg, 37%); **mp**: 112-113 °C; **¹H NMR (250 MHz, CDCl₃)** δ 8.31 (d, *J* = 2.0 Hz, 1H), 8.14 (s, 1H), 7.65 – 7.51 (m, 2H), 7.43 – 7.36 (m, 1H), 7.33 – 7.13 (m, 7H), 6.86 (d, *J* = 8.5 Hz, 1H), 5.34 (s, 2H), 4.01 (s, 3H), 3.90 – 3.76 (m, 5H), 2.90 (t, *J* = 7.3 Hz, 2H), 2.21 (s, 3H); **¹³C NMR (63 MHz, CDCl₃)** δ 166.0, 165.1, 151.5, 149.9, 148.8, 141.8, 138.4, 134.5, 132.3, 129.5, 129.1, 129.1 (2C), 128.9 (2C), 128.7, 128.6, 127.2 (2C), 126.9, 124.8, 115.2, 112.6, 103.7, 67.8, 56.3, 51.0, 42.2, 35.5, 13.2; **IR (neat, cm⁻¹)**: 1674.3, 1586.3, 1274.1; **elemental analysis (%) calcd. for C₃₀H₂₈ClNO₅**: C 66.49, H 5.58, N 2.42; found: C 66.65, H 5.38, N 2.60.

Methyl (Z)-4-[4-[(2-chlorobenzyl)oxy]-3-methoxybenzylidene]-1-(3,4-dimethoxyphenethyl)-2-methyl-5-oxo-4,5-dihydro-1H-pyrrole-3-carboxylate (3h)

Prepared from pyrrolinone **1l** (0.25 mmol) and aldehyde **2b** (0.28 mmol); yellow solid (67 mg, 46%); **mp** 100-101 °C **¹H NMR (250 MHz, CDCl₃)** δ 8.23 (d, *J* = 2.0 Hz, 1H), 8.08 (s, 1H), 7.55 (dd, *J* =

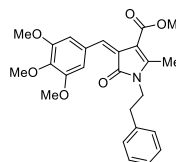
8.7, 1.8 Hz, 1H), 7.51 – 7.43 (m, 1H), 7.35 – 7.29 (m, 1H), 7.22 – 7.15 (m, 2H), 6.79 (d, $J = 8.5$ Hz, 1H), 6.72 (d, $J = 8.2$ Hz, 1H), 6.64 (dd, $J = 8.1, 1.9$ Hz, 1H), 6.56 (d, $J = 1.9$ Hz, 1H), 5.26 (s, 2H), 3.94 (s, 3H), 3.81 – 3.71 (m, 11H), 2.78 (t, $J = 7.1$ Hz, 2H), 2.12 (s, 3H); ^{13}C NMR (63 MHz, CDCl_3) δ 166.0, 165.0, 151.5, 149.9, 149.1, 148.8, 147.9, 141.8, 134.5, 132.3, 131.0, 129.4, 129.0, 128.7, 128.6, 127.2 (2C), 124.8, 121.0, 115.2, 112.6, 112.2, 111.4, 103.6, 67.8, 56.3, 56.0, 56.0, 51.0, 42.3, 35.0, 13.3; IR (neat, cm^{-1}): 1685.9, 1590.2, 1260.3, 1232.4; elemental analysis (%) calcd. for $\text{C}_{32}\text{H}_{32}\text{ClNO}_7$: C 66.49, H 5.58, N 2.42; found: C 66.65, H 5.38, N 2.60.

Methyl (Z)-4-(3,4-dihydroxybenzylidene)-2-methyl-5-oxo-1-phenethyl-4,5-dihydro-1H-pyrrole-3-carboxylate (3i)



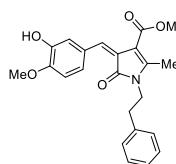
Prepared from pyrrolinone **1r** (0.25 mmol) and 3,4-dihydroxybenzaldehyde (0.28 mmol); yellow solid (23 mg, 24 %); mp: 159-160 °C; ^1H NMR (250 MHz, CDCl_3) δ 8.23 (d, $J = 1.8$ Hz, 1H), 8.15 (s, 1H), 7.45 (dd, $J = 8.3, 1.7$ Hz, 1H), 7.32 – 7.19 (m, 3H), 7.17 – 7.09 (m, 2H), 6.92 (d, $J = 8.3$ Hz, 1H), 3.98 – 3.75 (m, $J = 9.3$ Hz, 5H), 2.87 (t, $J = 7.4$ Hz, 2H), 2.24 (s, 3H); ^{13}C NMR (63 MHz, CDCl_3) δ 166.2, 165.1, 150.7, 147.5, 143.6, 142.9, 138.2, 129.0 (2C), 128.9 (2C), 127.9, 127.6, 127.0, 124.1, 118.4, 115.0, 104.3, 51.2, 42.3, 35.5, 13.1; IR (neat, cm^{-1}): 1689.9, 1650.4, 1595.7, 1289.7, 1169.6; elemental analysis (%) calcd. for $\text{C}_{22}\text{H}_{21}\text{NO}_5$: C 69.65, H 5.58, N 3.69; found: C 69.31, H 5.31, N 3.49.

Methyl (Z)-2-methyl-5-oxo-1-phenethyl-4-(3,4,5-trimethoxybenzylidene)-4,5-dihydro-1H-pyrrole-3-carboxylate (3j)



Prepared from pyrrolinone **1r** (0.25 mmol) and 2,4,5-trimethoxybenzaldehyde (0.28 mmol); yellow solid (58 mg, 53%); mp: 170 °C; ^1H NMR (250 MHz, CDCl_3) δ 8.15 (s, 1H), 7.64 (s, 2H), 7.35 – 7.12 (m, 5H), 3.93 (s, 6H), 3.91 (s, 3H), 3.88 – 3.82 (m, 5H), 2.90 (t, $J = 7.2$ Hz, 2H), 2.20 (s, 3H); ^{13}C NMR (63 MHz, CDCl_3) δ 165.8, 165.0, 152.6 (2C), 152.1, 141.7, 140.1, 138.4, 130.3, 129.1 (2C), 128.8 (2C), 126.9 (2C), 125.9, 109.8, 103.5, 61.1, 56.4 (2C), 51.1, 42.1, 35.5, 13.3; IR (neat, cm^{-1}): 3255.4, 1688.5, 1651.8, 1593.2, 1386.6, 1365.7, 1226.7; elemental analysis (%) calcd. for $\text{C}_{25}\text{H}_{27}\text{NO}_6$: C 74.59, H 5.74, N 7.25; found: C 73.45, H 5.66, N 7.22.

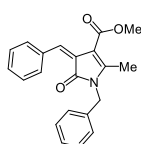
Methyl (Z)-4-(3-hydroxy-4-methoxybenzylidene)-2-methyl-5-oxo-1-phenethyl-4,5-dihydro-1H-pyrrole-3-carboxylate (3k)



Prepared from pyrrolinone **1r** (0.25 mmol) and 3-hydroxy-4-methoxybenzaldehyde (0.28 mmol); yellow solid (35 mg, 36%); mp: 192 °C; ^1H NMR (250 MHz, CDCl_3) δ 9.72 (br s, 1H), 8.35 (s, 1H), 7.38 (d, $J = 8.8$ Hz, 1H), 7.35 – 7.22 (m, 3H), 7.20 – 7.11 (m, 2H), 6.67 (d, $J = 2.6$ Hz, 1H), 6.60 (dd, $J = 8.8, 2.6$ Hz, 1H), 4.00 – 3.89 (m, 2H), 3.85 (s, 3H), 3.83 (s, 3H), 2.93 (t, $J = 7.3$ Hz, 2H), 2.27 (s, 3H); ^{13}C NMR (63 MHz, CDCl_3) δ 168.1, 164.9, 164.3, 161.1, 148.9, 141.4, 138.0, 137.9, 129.0 (2C), 128.9 (2C), 127.01, 121.7,

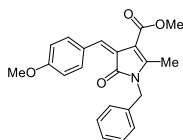
118.8, 109.5, 105.4, 105.4, 55.7, 51.2, 42.7, 35.4, 12.8.; IR (neat, cm^{-1}): 1651.1, 1588.5, 1286.1, 1195.3; elemental analysis (%) calcd. for $\text{C}_{23}\text{H}_{23}\text{NO}_5$: C

Methyl (Z)-1-benzyl-4-benzylidene-2-methyl-5-oxo-4,5-dihydro-1H-pyrrole-3-carboxylate (3l)



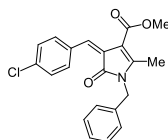
Prepared from pyrrolinone **1f** (1 mmol) and benzaldehyde (1.1 mmol); yellow solid (167 mg, 50%); mp: 83-86 °C; $^1\text{H NMR}$ (250 MHz, CDCl_3) δ 8.28 (s, 1H), 8.22-8.11 (m, 2H), 7.54-7.14 (m, 8H), 4.90 (s, 2H), 3.87 (s, 3H), 2.45 (s, 3H); $^{13}\text{C NMR}$ (63 MHz, CDCl_3) δ 166.2, 165.2, 153.4, 142.2, 137.1, 135.0, 132.1 (2C), 130.5, 129.3 (2C), 128.4 (2C), 128.0, 127.2 (2C), 126.8, 104.3, 51.4, 43.8, 14.2; IR (neat, cm^{-1}): 1684, 1599, 1193; elemental analysis (%) calcd. for $\text{C}_{21}\text{H}_{19}\text{NO}_3$: C 75.66, H 5.74, N 4.20; found: C 75.55, H 5.68, N 4.18.

Methyl (Z)-1-benzyl-4-(4-methoxybenzylidene)-2-methyl-5-oxo-4,5-dihydro-1H-pyrrole-3-carboxylate (3m)



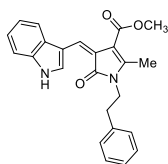
Prepared from pyrrolinone **1f** (1 mmol) and 4-methoxybenzaldehyde (1.1 mmol); yellow solid (218 mg, 60%); mp: 121-124 °C; $^1\text{H NMR}$ (250 MHz, CDCl_3) δ 8.39-8.08 (m, 3H), 7.47-7.10 (m, 5H), 7.03-6.83 (m, 2H), 4.93 (s, 2H), 3.89 (s, 3H), 3.86 (s, 3H), 2.44 (s, 3H); $^{13}\text{C NMR}$ (63 MHz, CDCl_3) δ 166.1, 165.1, 161.5, 151.3, 142.1, 137.0, 134.5 (2C), 132.4, 129.0 (2C), 127.7, 126.9 (2C), 124.3, 113.6 (2C), 104.2, 55.5, 51.0, 43.5, 13.8; IR (neat, cm^{-1}): 1679.0, 1589.4, 1254.4; elemental analysis (%) calcd. for $\text{C}_{22}\text{H}_{21}\text{NO}_4$: C 72.71, H 5.82, N 3.85; found: C 72.46, H 5.84, N 3.92.

Methyl (Z)-1-benzyl-4-(4-chlorobenzylidene)-2-methyl-5-oxo-4,5-dihydro-1H-pyrrole-3-carboxylate (3n)



Prepared from pyrrolinone **1f** (1 mmol) and 4-chlorobenzaldehyde (1.1 mmol); yellow solid (166 mg, 45%); mp: 97-100 °C; $^1\text{H NMR}$ (250 MHz, CDCl_3) δ 8.09 (s, 1H), 8.00 (d, $J = 8.4$ Hz, 2H), 7.35-7.20 (m, 5H), 7.16-7.06 (m, 2H), 4.81 (s, 2H), 3.76 (s, 3H), 2.36 (d, $J = 0.6$ Hz, 3H); $^{13}\text{C NMR}$ (63 MHz, CDCl_3) δ 166.2, 165.1, 153.6, 140.6, 136.9, 136.3, 133.4 (2C), 129.4, 129.3 (2C), 128.7 (2C), 128.1, 127.3, 127.1 (2C), 104.2, 51.4, 43.8, 14.2; IR (neat, cm^{-1}): 1691, 1677, 1602, 1196; elemental analysis (%) calcd. for $\text{C}_{21}\text{H}_{18}\text{ClNO}_3$: C 68.57, H 4.93, N 3.81; found: C 68.20, H 4.88, N 3.81.

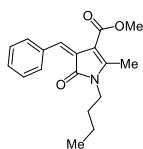
Methyl (Z)-4-[(1H-indol-3-yl)methylene]-2-methyl-5-oxo-1-phenethyl-4,5-dihydro-1H-pyrrole-3-carboxylate (3o)



Prepared from pyrrolinone **1r** (0.25 mmol) and indol-3-carboxaldehyde (0.28 mmol); yellow solid (28 mg, 30%); mp: 223-224°C; $^1\text{H NMR}$ (250 MHz, d_6 -DMSO) δ 12.08 (br s, 1H), 9.42 (d, $J = 2.8$ Hz, 1H), 8.56 (s, 1H), 7.83 – 7.71 (m, 1H), 7.58 – 7.48 (m, 1H), 7.38 – 7.12 (m, 7H), 3.89 (t, $J = 7.3$ Hz, 2H), 3.81 (s, 3H), 2.87 (t, $J = 7.3$ Hz, 2H), 2.32 (s, 3H); $^{13}\text{C NMR}$ (63 MHz, d_6 -DMSO) δ 165.3, 164.5, 148.8, 138.6, 136.0, 133.2, 129.5, 128.9 (2C), 128.5

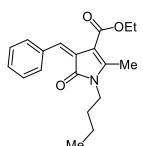
(2C), 128.4, 126.5, 122.6, 121.0, 119.3, 117.4, 112.5, 111.7, 102.1, 50.8, 41.3, 34.7, 12.6; ; IR (neat, cm^{-1}): 1702.4, 1583.3, 1326.7, 1230.4; **elemental analysis (%) calcd. for $\text{C}_{24}\text{H}_{22}\text{N}_2\text{O}_3$** : C 68.64, H 6.22, N 3.20; found: C 68.49, H 6.02, N 3.32.

Methyl (Z)-4-benzylidene-1-butyl-2-methyl-5-oxo-4,5-dihydro-1H-pyrrole-3-carboxylate (3p)



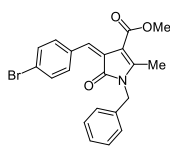
Prepared from pyrrolinone **1b** (1 mmol) and benzaldehyde (1.1 mmol); yellow solid (210 mg, 70%), **mp**: 84-87 °C; $^1\text{H NMR}$ (250 MHz, CDCl_3) δ 8.14 (s, 1H), 8.11-7.99 (m, 2H), 7.45-7.30 (m, 3H), 3.84 (s, 3H), 3.68-3.52 (m, 2H), 2.53 (d, $J = 0.5$ Hz, 3H), 1.67-1.47 (m, 2H), 1.44-1.22 (m, 2H), 0.93 (t, $J = 7.2$ Hz, 3H); $^{13}\text{C NMR}$ (63 MHz, CDCl_3) δ 166.1, 165.3, 155.9, 153.5, 141.6, 135.1, 131.9 (2C), 130.3, 128.3 (2C), 127.1, 51.3, 40.4, 31.9, 20.6, 14.2, 13.8; IR (neat, cm^{-1}): 1699, 1689, 1601, 1213; **elemental analysis (%) calcd. for $\text{C}_{18}\text{H}_{21}\text{NO}_3$** : C 72.22, H 7.07, N 4.68; found: C 72.17, H 6.94, N 4.59.

Ethyl (Z)-4-benzylidene-1-butyl-2-methyl-5-oxo-4,5-dihydro-1H-pyrrole-3-carboxylate (3q)



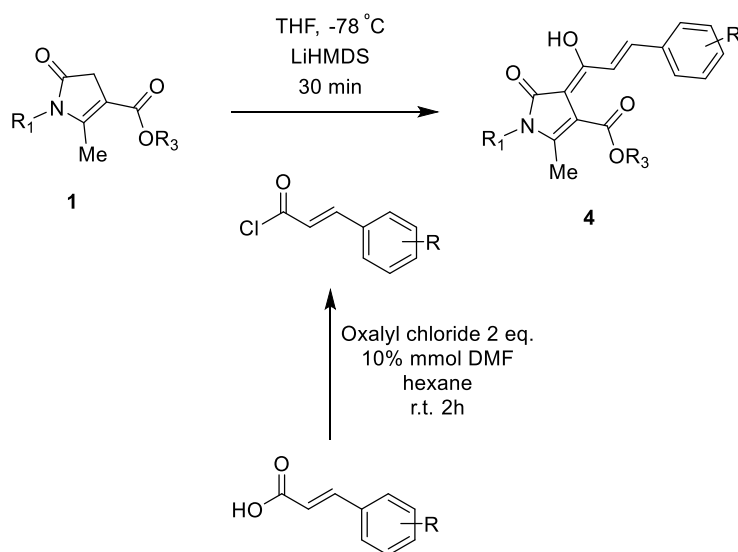
Prepared from pyrrolinone **1a** (1 mmol) and benzaldehyde (1.1 mmol); yellow solid (179 mg, 57%); **mp**: 161-163 °C; $^1\text{H NMR}$ (250 MHz, CDCl_3) δ 8.20 (s, 1H), 7.41 (dd, $J = 4.8, 2.5$ Hz, 2H), 7.43-7.29 (m, 3H), 4.35 (q, $J = 7.1$ Hz, 2H), 3.64 (t, $J = 7.6$ Hz, 2H), 2.56 (s, 3H), 1.66-1.51 (m, 2H), 1.42 (t, $J = 7.1$ Hz, 3H), 1.42-1.30 (m, 2H), 0.96 (t, $J = 7.2$ Hz, 3H); $^{13}\text{C NMR}$ (63 MHz, CDCl_3) δ 166.2, 164.8, 153.3, 141.6, 135.1, 131.9 (2C), 130.3, 128.4 (2C), 127.2, 103.9, 60.2, 40.3, 31.9, 20.6, 14.9, 14.2, 13.8; IR (neat, cm^{-1}): 1672, 1158; **elemental analysis (%) calcd. for $\text{C}_{19}\text{H}_{23}\text{NO}_3$** : C 72.82, H 7.40, N 4.47; found: C 72.85, H 7.34, N 4.51.

Methyl (Z)-1-benzyl-4-(4-bromobenzylidene)-2-methyl-5-oxo-4,5-dihydro-1H-pyrrole-3-carboxylate (3r)



Prepared from pyrrolinone **1f** (1 mmol) and 4-bromobenzaldehyde (1.1 mmol); yellow solid (219 mg, 53%); **mp**: 136 °C; $^1\text{H NMR}$ (250 MHz, CDCl_3) δ 8.16 (s, 1H), 8.02 (d, $J = 8.5$ Hz, 2H), 7.55 (d, $J = 8.5$, 2H), 7.48-7.14 (m, 5H), 4.90 (s, 2H), 3.86 (s, 3H), 2.45 (s, 3H); $^{13}\text{C NMR}$ (63 MHz, CDCl_3) δ 166.2, 165.1, 153.7, 140.6, 136.9, 133.8, 133.6 (2C), 131.6 (2C), 129.3 (2C), 128.1, 127.3, 127.2 (2C), 124.9, 104.2, 51.4, 43.8, 14.2; IR (neat, cm^{-1}): 1691.8, 1674.4, 1602.0, 1196.6; **elemental analysis (%) calcd. for $\text{C}_{21}\text{H}_{18}\text{BrNO}_3$** : C 61.18, H 4.40, N 3.40; found: C 60.99, H 4.38, N 3.26.

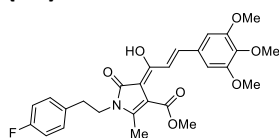
3.7.4. Curcumin analogues 4

**a) Preparation of the cinnamoyl chloride derivatives¹⁴⁴**

The suitable cinnamic acid derivative (1 mmol) was suspended in hexane (3.0 mL) and anhydrous DMF (0.008 mL, 0.1 mmol) and oxalyl chloride (0.17 mL, 2 mmol) were added. The reaction mixture was stirred at rt for 2 h. The hexane was removed under vacuum to provide the crude cinnamoyl chloride derivative, which was immediately used in the next step without further purification.

b) Synthesis of curcumin analogues 4

A solution of the corresponding pyrrolinone derivative **1** (0.5 mmol) in THF (5 mL) was cooled to $-78\text{ }^\circ\text{C}$ and a 1.0 M solution of lithium hexamethyldisilazide (1.5 mL, 1.5 mmol) in THF was added. After 30 min, a solution of the adequate cinnamoyl chloride derivative (1 mmol) in THF (2 mL) was cannulated into the reaction, and the mixture was stirred for 30 min. Then, saturated aqueous NH_4Cl solution was added, and the reaction was warmed to room temperature. The mixture was acidified (HCl 1M) and extracted with ethyl ether (3 x 20 mL). The combined organic layers were dried over anhydrous sodium sulphate, the solvent was removed *in vacuo*, and the residue was purified by column chromatography on silica gel eluting with a gradient from hexane to 1:1 hexane-ethyl acetate.¹⁴⁵

Methyl**(Z)-1-(4-fluorophenethyl)-4-((E)-1-hydroxy-3-(3,4,5-trimethoxyphenyl)allylidene)-2-methyl-5-oxo-4,5-dihydro-1H-pyrrole-3-carboxylate (4a)**

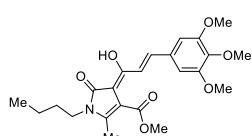
Prepared from pyrrolinone **1t** (0.5 mmol) and 3,4,5-trimethoxycinnamoyl chloride (1 mmol); orange solid (100 mg, 40%); mp: 143-144 $^\circ\text{C}$; $^1\text{H NMR}$ (250 MHz, CDCl_3) δ 14.00 (d, $J =$

¹⁴⁴ Kourra, C.; Klotter, F.; Sladojevich, F.; Dixon, D. J. *Org. Lett.* **2012**, *14*, 1016-1019.

¹⁴⁵ Riggs, R. L.; Morton, C. J.; Slawin, A. M.; Smith, D. M.; Westwood, N. J.; Austen, W. S.; Stuart, K. E. *Tetrahedron* **2005**, *61*, 11230-11243.

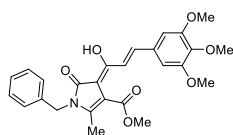
1.5 Hz, 1H), 8.62 (dd, $J = 15.8, 1.5$ Hz, 1H), 7.64 (d, $J = 15.8$ Hz, 1H), 7.20 – 7.09 (m, 2H), 7.01 (t, $J = 8.6$ Hz, 2H), 6.91 (s, 2H), 3.95 (s, 6H), 3.93 – 3.89 (m, 8H), 2.92 (t, $J = 7.1$ Hz, 2H), 2.16 (s, 3H); ^{13}C NMR (63 MHz, CDCl_3) δ 170.1, 167.7, 164.7, 162.2 (d, $J = 245.4$ Hz) 153.8 (2C), 148.8, 139.8, 139.7, 134.4 (d, $J = 3.3$ Hz), 132.4, 130.8 (d, $J = 3.3$ Hz, 2C), 120.7, 116.2 (d, $J = 21.3$ Hz, 2C), 105.7 (2C), 103.4, 102.3, 61.4, 56.6 (2C), 53.0, 42.6 (d, $J = 1.2$ Hz), 34.9, 13.9; IR (neat, cm^{-1}): 1673.4, 1620.6, 1581.8, 1440.6, 1315.6; elemental analysis (%) calcd. for $\text{C}_{27}\text{H}_{28}\text{FNO}_7$: C 65.18, H 5.67, N 2.82; found: C 64.87, H 5.69, N 2.88.

Methyl (Z)-1-butyl-4-((E)-1-hydroxy-3-(3,4,5-trimethoxyphenyl)allylidene)-2-methyl-5-oxo-4,5-dihydro-1H-pyrrole-3-carboxylate (4b)



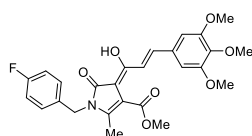
Prepared from pyrrolinone **1b** (0.5 mmol) and 3,4,5-trimethoxycinnamoyl chloride (1 mmol); orange solid (83 mg, 38%); mp: 128-129 °C; ^1H NMR (250 MHz, CDCl_3) δ 13.97 (d, $J = 1.5$ Hz, 1H), 8.60 (dd, $J = 15.8, 1.5$ Hz, 1H), 7.61 (d, $J = 15.8$ Hz, 1H), 6.90 (s, 2H), 3.99 – 3.87 (m, 12H), 3.76 – 3.66 (m, 2H), 2.52 (s, 3H), 1.66 – 1.52 (m, 2H), 1.46 – 1.34 (m, 2H), 0.98 (t, $J = 7.2$ Hz, 3H); ^{13}C NMR (63 MHz, CDCl_3) δ 170.1, 167.8, 164.4, 153.7 (2C), 149.0, 139.7, 139.4, 132.8, 120.6, 105.6 (2C), 103.6, 102.3, 61.4, 56.6 (2C), 53.0, 40.6, 32.0, 20.6, 14.3, 14.2; IR (neat, cm^{-1}): 1671.4, 1620.9, 1579.2, 1500.7, 1314.8, 1120.5; elemental analysis (%) calcd. for $\text{C}_{23}\text{H}_{29}\text{NO}_7$: C 64.02, H 6.77, N 3.25; found: C 63.97, H 6.59, N 3.27.

Methyl (Z)-1-benzyl-4-((E)-1-hydroxy-3-(3,4,5-trimethoxyphenyl)allylidene)-2-methyl-5-oxo-4,5-dihydro-1H-pyrrole-3-carboxylate (4c)



Prepared from pyrrolinone **1f** (0.5 mmol) and 3,4,5-trimethoxycinnamoyl chloride (1 mmol); orange solid (72 mg, 31%); mp: 205 °C; ^1H NMR (250 MHz, CDCl_3) δ 14.02 (br s, 1H), 8.67 (d, $J = 15.7$ Hz, 1H), 7.65 (d, $J = 15.7$ Hz, 1H), 7.40 – 7.26 (m, 3H), 7.18 (d, $J = 6.8$ Hz, 2H), 6.91 (s, 2H), 5.00 (s, 2H), 3.94 (s, 6H), 3.92 (s, 3H), 3.91 (s, 3H), 2.40 (s, 3H); ^{13}C NMR (63 MHz, CDCl_3) δ 170.2, 167.8, 164.8, 153.7 (2C), 149.1, 139.7, 139.7, 137.1, 132.4, 129.3 (2C), 127.9, 126.9 (2C), 120.6, 105.6 (2C), 103.4, 102.8, 61.4, 56.6 (2C), 53.0, 43.8, 14.6; IR (neat, cm^{-1}): 1674.1, 1631.1, 1583.3, 1447.2, 1416.5, 1314.9, 1117.2; elemental analysis (%) calcd. for $\text{C}_{26}\text{H}_{27}\text{FNO}_7$: C 67.01, H 5.85, N 3.01; found: C 66.84, H 5.68, N 3.29.

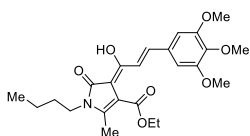
Methyl (Z)-1-(4-fluorobenzyl)-4-((E)-1-hydroxy-3-(3,4,5-trimethoxyphenyl)allylidene)-2-methyl-5-oxo-4,5-dihydro-1H-pyrrole-3-carboxylate (4d)



Prepared from pyrrolinone **1s** (0.5 mmol) and 3,4,5-trimethoxycinnamoyl chloride (1 mmol); orange solid (50 mg, 22%); mp: 169-170 °C; ^1H NMR (250 MHz, CDCl_3) δ 14.02 (d, $J = 1.6$ Hz, 1H), 8.65 (dd, $J = 15.8, 1.6$ Hz, 1H), 7.66 (d, $J = 15.8$ Hz, 1H), 7.24 – 7.12 (m, 2H), 7.12 – 6.97 (m, 2H), 6.91 (s, 2H), 4.96 (s, 2H), 3.97 – 3.92 (m, 9H), 3.91 (s, 3H), 2.41 (s, 3H); ^{13}C NMR (63 MHz, CDCl_3) δ 170.1, 167.8, 165.1, 162.6, (d, $J = 246.3$ Hz) 153.7 (2C), 148.5, 139.9, 139.8, 132.9 (d, $J = 3.2$

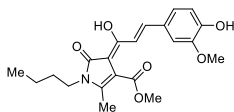
Hz), 132.3, 128.7 (2C, d, $J = 8.2$ Hz), 120.5, 116.2 (2C, d, $J = 21.5$ Hz), 105.7 (2C), 103.2, 103.0, 61.4, 56.6 (2C), 53.1, 43.2, 14.6; **IR** (neat, cm^{-1}): 1673.4, 1630.4, 1582.9, 1501.3, 1444.2, 1315.9, 1220.1, 1117.3; **elemental analysis (%) calcd. for $\text{C}_{26}\text{H}_{26}\text{FNO}_7$** : C 64.54, H 5.42, N 2.90; found: C 64.48, H 5.22, N 2.97.

Ethyl (Z)-1-butyl-4-((E)-1-hydroxy-3-(3,4,5-trimethoxyphenyl)allylidene)-2-methyl-5-oxo-4,5-dihydro-1H-pyrrole-3-carboxylate (4e)



Prepared from pyrrolinone **1a** (0.5 mmol) and 3,4,5-trimethoxycinnamoyl chloride (1 mmol); orange solid (87 mg, 39%); **mp**: 131-132 °C; **$^1\text{H NMR}$ (250 MHz, CDCl_3)** δ 14.08 (d, $J = 1.5$ Hz, 1H), 8.60 (dd, $J = 15.7, 1.5$ Hz, 1H), 7.60 (d, $J = 15.7$ Hz, 1H), 6.89 (s, 2H), 4.39 (q, $J = 7.0$ Hz, 2H), 3.93 (s, 6H), 3.89 (s, 3H), 3.71 (t, $J = 7.3$ Hz, 2H), 2.52 (s, 3H), 1.66 – 1.52 (m, 2H), 1.46 – 1.34 (m, 5H), 0.97 (t, $J = 7.0$ Hz, 3H); **$^{13}\text{C NMR}$ (63 MHz, CDCl_3)** δ 169.7, 167.8, 164.4, 153.7 (2C), 148.9, 139.6, 139.3, 132.5, 120.7, 105.6 (2C), 103.7, 102.5, 62.3, 61.4, 56.6 (2C), 40.5, 32.0, 20.6, 14.8, 14.3, 14.2; **IR** (neat, cm^{-1}): 1664.8, 1620.5, 1598.6, 1579.7, 1414.8, 1316.5, 1121.8; **elemental analysis (%) calcd. for $\text{C}_{24}\text{H}_{31}\text{NO}_7$** : C 64.70, H 7.01, N 3.14; found: C 64.50, H 6.84, N 3.43.

Methyl (Z)-1-butyl-4-((E)-1-hydroxy-3-(4-hydroxy-3-methoxyphenyl)allylidene)-2-methyl-5-oxo-4,5-dihydro-1H-pyrrole-3-carboxylate (4f)



Prepared from pyrrolinone **1b** (0.5 mmol) and feruloyl chloride (1 mmol); orange solid (30 mg, 15%); **mp**: 156-157 °C; **$^1\text{H NMR}$ (250 MHz, CDCl_3)** δ 13.93 (d, $J = 1.6$ Hz, 1H), 8.55 (dd, $J = 15.8, 1.6$ Hz, 1H), 7.60 (d, $J = 15.8$ Hz, 1H), 7.21 – 7.14 (m, 2H), 6.89 (d, $J = 8.7$ Hz, 1H), 5.92 (br s, 1H), 3.94 (s, 3H), 3.91 (s, 3H), 3.73 – 3.63 (m, 2H), 2.48 (s, 3H), 1.61 – 1.47 (m, 2H), 1.43 – 1.30 (m, 2H), 0.94 (t, $J = 7.2$ Hz, 3H); **$^{13}\text{C NMR}$ (63 MHz, CDCl_3)** δ 169.8, 167.4, 164.7, 148.2, 147.3, 146.8, 139.4, 129.2, 123.2, 118.6, 114.7, 109.7, 102.8, 102.0, 56.2, 52.6, 40.3, 31.7, 20.3, 13.9 (2C); **IR** (neat, cm^{-1}): 2955.8, 2630.3, 2870.6, 1698.1, 1647.8, 1619.9, 1587.0, 1571.6, 1322.31284.7, 1117.3, 978.3, 748.8; **elemental analysis (%) calcd. for $\text{C}_{21}\text{H}_{25}\text{NO}_6$** : C 65.10, H 6.50, N 3.62; found: C 64.93, H 6.38, N 3.93.

**CHAPTER 4. NEUROPROTECTIVE COMPOUNDS
RELATED TO SPIROOXINDOLE ALKALOIDS**

4.1. Neuroprotective spirooxindole alkaloids

Spirocyclic frameworks are present in many natural products and are increasingly recognized as interesting scaffolds in drug discovery programs.¹⁴⁶ Spiropyrrolidines, in particular, have shown interesting pharmacological activities including antiproliferative¹⁴⁷ and antitubercular¹⁴⁸ properties, as well as acetylcholinesterase inhibition,¹⁴⁹ among others. Spiropyrrolidine cores are present in numerous natural products, such as (-)-horsfiline, spirotryprostatin A and the *Uncaria rhynchophylla* alkaloids.

The dried stem and hook of *Uncaria rhynchophylla*, also known as cat's claw, have a variety of uses in traditional herbal medicine including the treatment of convulsions, hypertension, headache and dizziness.^{150, 151, 152} *Uncaria rhynchophylla* contains a broad spectra of spirooxindole alkaloids (Figure 4.1), most notably the one that is named after the plant (rhynchophylline). Evidence is accumulating that shows that the pharmacological activities of *Uncaria rhynchophylla* are associated with the presence of rhynchophylline and this has encouraged the investigation of this alkaloid as a drug candidate for neurodegenerative disorders.^{151, 153} Recent studies have highlighted the ability of rhynchophylline to penetrate the blood-brain barrier.¹⁵⁴ This alkaloid exerted neuroprotection in CNS disease models, and was proposed to act *via* a non-competitive antagonism of NMDA receptors.¹⁵⁵ In addition, rhynchophylline improves

¹⁴⁶ For a review of the use of spirocyclic scaffolds in drug discovery, see: Zheng, Y.; Tice, C. M.; Singh, S. B. *Bioorg. Med. Chem. Lett.* **2014**, *24*, 3673-3682.

¹⁴⁷ Almansour, A. I.; Suresh Kumar, R.; Beevi, F.; Shirazi, A. N.; Osman, H.; Ismail, R.; Choon, T. S.; Sullivan, B.; McCaffrey, K.; Nahhas, A.; Parang, K.; Ashraf Ali, M. *Molecules* **2014**, *19*, 10033-10055.

¹⁴⁸ (a) Ranjith Kumar, R.; Perumal, S.; Senthilkumar, P.; Yogeewari, P.; Sriram, D. *J. Med. Chem.* **2008**, *51*, 5731-5735. (b) Kumar, R.; Perumal, S.; Senthilkumar, P.; Yogeewari, P.; Sriram, D. *Eur. J. Med. Chem.* **2009**, *44*, 3821-3829. (c) Suresh Kumar, R.; Rajesh, S. M.; Perumal, S.; Banerjee, D.; Yogeewari, P.; Sriram, D. *Eur. J. Med. Chem.* **2010**, *45*, 411-422. (d) Rajesh, S. M.; Perumal, S.; Menéndez, J. C.; Yogeewari, P.; Sriram, D. *Med. Chem. Commun.* **2011**, *2*, 626-630.

¹⁴⁹ (a) Kia, Y.; Osman, H.; Suresh Kumar, R.; Murugaiyah, V.; Basiri, A.; Perumal, S.; Wahab, H. A.; Bing, C. S. *Bioorg. Med. Chem.* **2013**, *21*, 1696-1707. (b) Kia, Y.; Osman, H.; Suresh Kumar, R.; Basiri, A.; Murugaiyah, V. *Bioorg. Med. Chem.* **2014**, *22*, 1318-1328.

¹⁵⁰ Zhou, J.; Zhou, S. J. *Ethnopharmacol.* **2010**, *132*, 15-27.

¹⁵¹ Ng, Y. P.; Or, T. C.; Ip, N. Y. *Neurochem. Int.* **2015**, *89*, 260-270.

¹⁵² Shao, H.; Yang, Y.; Mi, Z.; Zhu, G. X.; Qi, A. P.; Ji, W. G.; Zhu, Z. R. *Neuroscience* **2016**, *337*, 355-369.

¹⁵³ Hu, S.; Mak, S.; Zuo, X.; Li, H.; Wang, Y.; Han, Y. *Front. Pharmacol.* **2018**, *9*, 768.

¹⁵⁴ Lee, C. J.; Hsueh, T. Y.; Lin, L. C.; Tsai, T. H. *Biomed. Chromatogr.* **2014**, *28*, 901-906.

¹⁵⁵ Kang, T. H.; Murakami, Y.; Matsumoto, K.; Takayama, H.; Kitajima, M.; Aimi, N.; Watanabe, H. *Eur. J. Pharmacol.* **2002**, *455*, 27-34.

Chapter 4. Neuroprotective compounds related to spirooxindole alkaloids

hippocampal synaptic function in Alzheimer mouse models through the blockade of EphA4 signalling.¹⁵⁶

Some recent findings also support the potential beneficial effect of rhynchophylline in Parkinson's disease treatment, as it improves the survival of primary CGNs neurons following cellular toxicity caused by 1-methyl-4 phenylpyridium (MPPC).

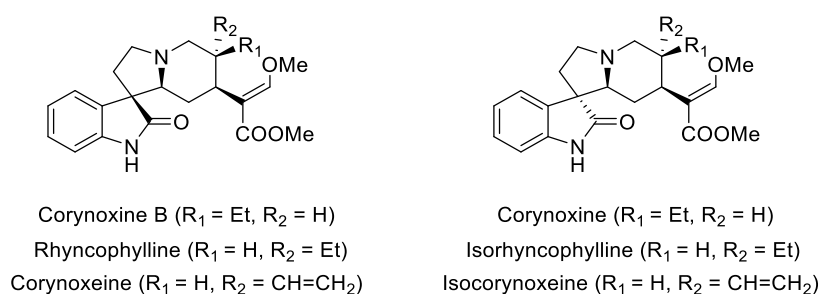


Figure 4.1

Besides NMDA antagonism, rhynchophylline activates the PI3K/Akt/mTOR signalling pathway. PI3K activation leads to Akt phosphorylation, and phosphorylated Akt causes the inactivation of GSK-3 β (Figure 4.2). GSK-3 β inhibition has been proved to have a neuroprotective effect in several neurodegenerative diseases. Among other effects, GSK-3 β promotes Nrf2 cytosolic distribution through two different mechanisms of control: (a) preventing the translocation of Nrf2 to the nucleus, by phosphorylating Nrf2 and promoting its degradation by the proteasome;¹⁵⁷ (b) enhancing Nrf2 exclusion from the nucleus mediated by the tyrosine kinase Fyn that is, in turn, activated by GSK-3 β .^{158, 159} Therefore, GSK-3 β inhibition promotes the nuclear accumulation of Nrf2 and the activation of the ARE transcription.^{160, 161}

On the other hand, GSK-3 β inhibition potentiates the activity of myocyte enhancer transcription factor (MEF2D). Extensive evidence has accumulated showing a link

¹⁵⁶ Fu, A. K.; Hung, K. W.; Huang, H.; Gu, S.; Shen, Y.; Cheng, E. Y.; Ip, F. C.; Huang, X.; Fu, W. Y.; Ip, N. Y. *Proc. Natl. Acad. Sci. U.S.A.* **2014**, *111*, 9959-9964.

¹⁵⁷ Chowdhry, S.; Zhang, Y.; McMahon, M.; Sutherland, C.; Cuadrado, A.; Hayes, J. D. *Oncogene* **2013**, *32*, 3765-3781.

¹⁵⁸ Jain, A. K.; Jaiswal, A. K. *J. Biol. Chem.* **2006**, *281*, 12132-12142

¹⁵⁹ Jain, A. K.; Jaiswal, A. K. *J. Biol. Chem.* **2007**, *282*, 16502-16510.

¹⁶⁰ Rojo, A. I.; de Sagarra, M. R.; Cuadrado, A. *J. Neurochem.* **2008**, *105*, 192-202.

¹⁶¹ Rojo, A. I.; Rada, P.; Egea, J.; Rosa, A. O.; López, M. G.; Cuadrado, A. *Mol. Cell. Neurosci.* **2008**, *39*, 125-132.

between MEF2D and PD,¹⁶² and that MEF2D levels were robustly decreased in the post-mortem brain of Parkinson's patients.¹⁶³ Furthermore, various animal and cellular models highlighted the importance of MEF2D in neuronal survival.^{164, 165}

The PI3K/Akt/mTOR signalling pathway is also involved in autophagy. The *Rhynchophylla* extracts are known to induce autophagy,¹⁶⁶ and in particular corynoxine has been shown to induce autophagy in an mTOR-dependent manner and promote α -synuclein clearance.¹⁶⁷ Consequently, activation of PI3K/Akt/mTOR signalling pathway is a significant mechanism in attenuating neurotoxicity such as damage to dopaminergic cells observed after exposure to PD-related toxins.

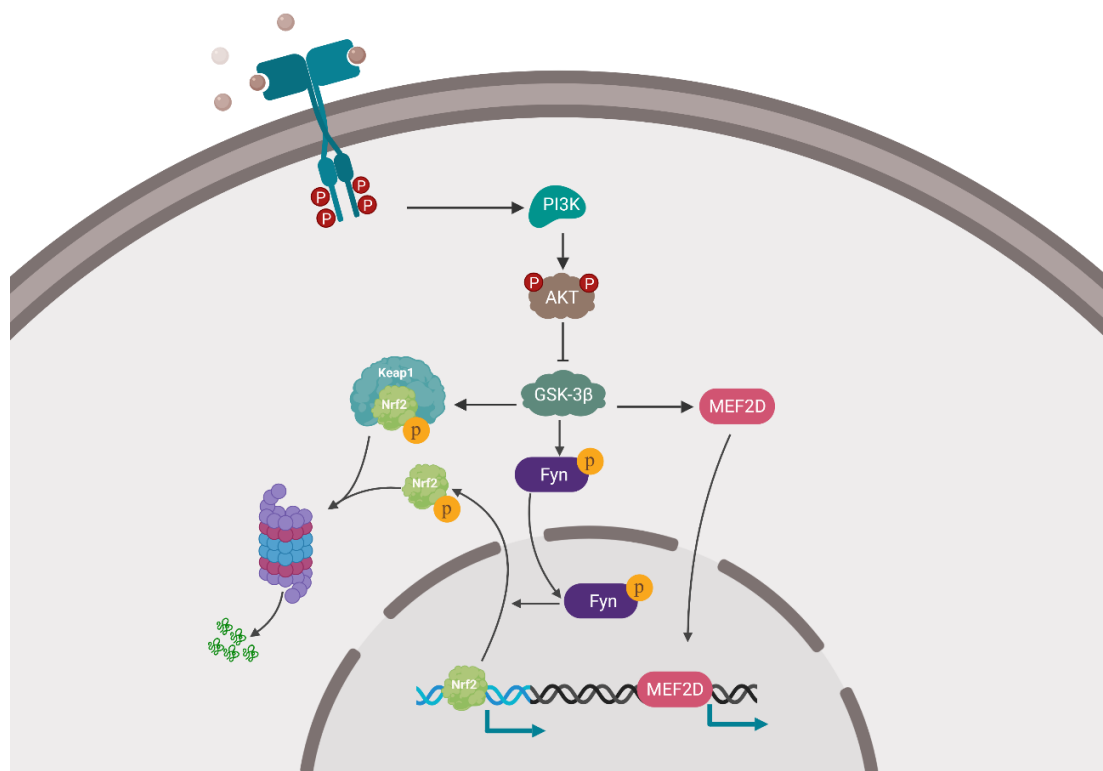


Figure 4.2

¹⁶² Yang, Q.; She, H.; Gearing, M.; Colla, E.; Lee, M.; Shacka, J. J.; Mao, Z. *Science* **2009**, *323*, 124-127.

¹⁶³ She, H.; Yang, Q.; Shepherd, K.; Smith, Y.; Miller, G.; Testa, C.; Mao, Z. *J. Clin. Invest.* **2011**, *121*, 930-940.

¹⁶⁴ Mount, M. P.; Zhang, Y.; Amini, M.; Callaghan, S.; Kulczycki, J.; Mao, Z.; Slack, R. S.; Anisman, H.; Park, D. S. *J. Biol. Chem.* **2013**, *288*, 14362-14371.

¹⁶⁵ Guo, B.; Hu, S.; Zheng, C.; Wang, H.; Luo, F.; Li, H.; Cui, W.; Yang, X.; Cui, G.; Mak, S.; Choi, T. C.; Ma, E. D.; Wang, Y.; Lee, S. M. Y.; Zhang, Z.; Han, Y. *Neuropharmacology* **2017**, *126*, 12-24.

¹⁶⁶ Li, C.; Jiang, F.; Li, Y. L.; Jiang, Y. H.; Yang, W. Q.; Sheng, J.; Xu, W. J.; Zhu, Q. J. *Acta Pharmacol. Sin.* **2018**, *39*, 345-356.

¹⁶⁷ Chen, L. L.; Song, J. X.; Lu, J. H.; Yuan, Z. W.; Liu, L. F.; Durairajan, S. S. K.; Li, M. *J. Neuroimmune Pharmacol.* **2014**, *9*, 380-387.

4.2. Compound design

In this context, we have designed and synthesized two families of related dispiro compounds **5** and **6** that show a closely similarity to rynchophylline in terms of three-dimensional structure, placing the most characteristic moieties in the same spatial region. As shown in Figure 4.3, the oxindole (green) and pyrrolidine (red) rings are completely overlapped in both structures. Hydrophobic moieties (blue) such as the phenyl group of compound **3a** and ethyl from rynchophylline are placed in the same region. The polar ester functions from both structures are also paired in a closely similar spatial arrangement (purple).

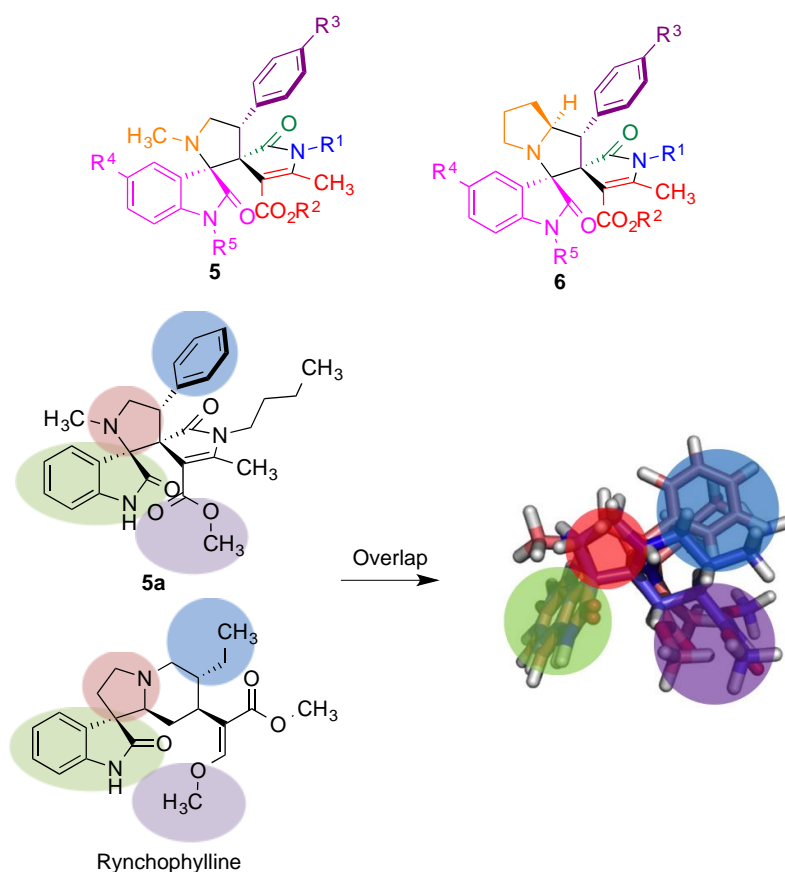


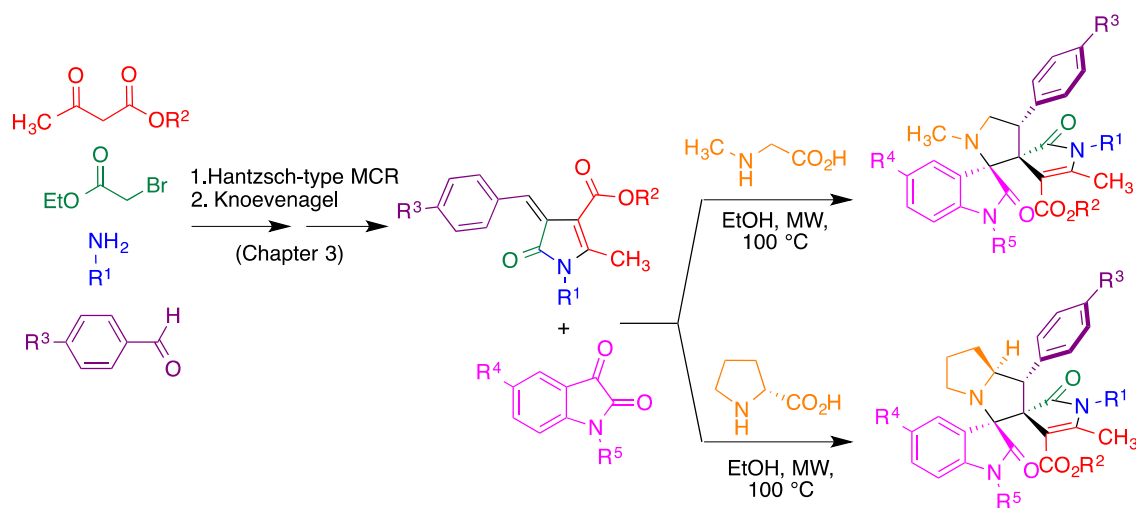
Figure 4.3

4.3. Synthesis of dispirooxindoles **5** and **6** *via* a multicomponent [3+2] dipolar cycloaddition

We envisaged the possibility to prepare dispiro frameworks **5** and **6** by combining our initial Hantzsch-like MCR leading to pyrrolinones with a second one, namely a three-component reaction involving as the key step a [3+2] dipolar cycloaddition of non-

stabilized azomethine ylides with activated olefins,¹⁶⁸ with the previously described Knoevenagel condensation acting as the link between both MCRs. The combination of two multicomponent reactions is an excellent approach to the generation of molecular diversity, although it has not been widely exploited.^{169, 170}

The azomethine ylides required as the dipole element of the cycloaddition were prepared *in situ* from isatin derivatives and α -amino acids, and were reacted with selected compounds **4**, acting as dipolarophiles, under focused microwave irradiation at 100 °C in ethanol solution (Scheme 4.1 and Table 4.1). The target dispiro compounds were obtained with full regio- and diastereoselection, generally in good yields. Probably because of steric hindrance, the reaction was more efficient in the case of reactions starting from sarcosine in comparison to those involving the use of proline.



Scheme 4.1

¹⁶⁸ For a review of the use of multicomponent 1,3-dipolar cycloaddition reactions in the synthesis of spiroheterocycles, see: Arumugam, N.; Suresh Kumar, R.; Almansour A. I.; Perumal, S. *Curr. Org. Chem.* **2013**, *17*, 1929-1956.

¹⁶⁹ For a review of methods for the design of multicomponent reactions towards molecular diversity and complexity, see: Ruijter, E.; Scheffelaar, R.; Orri, R. V. A. *Angew. Chem. Int. Ed.* **2011**, *50*, 6234-6246.

¹⁷⁰ For a review of the combination of multicomponent and multi-catalysis cascade reactions, see: Ramachary, D. B.; Jain, S. *Org. Biomol. Chem.* **2011**, *9*, 1277-1300.

Table 4.1. Results obtained in the synthesis of dispiro compounds **5** and **6**

Entry	Cmpd	R ¹	R ²	R ³	R ⁴	R ⁵	Yield (%)
1	5a	<i>n</i> -Bu	Me	H	H	H	50
2	5b	<i>n</i> -Bu	Me	H	Cl	H	56
3	5c	Bn	Me	H	Cl	H	73
4	5d	Bn	Me	H	I	H	52
5	5e	Bn	Me	H	Me	H	55
6	5f	Bn	Me	H	H	H	65
7	5g	Bn	Me	H	H	Bn	75
8	5h	Bn	Me	OMe	H	Bn	68
9	5i	Bn	Me	OMe	H	H	55
10	5j	Bn	Me	OMe	Cl	H	73
11	5k	Bn	Me	OMe	I	H	50
12	5l	Bn	Me	OMe	Me	H	54
13	5m	Bn	Me	Cl	H	H	78
14	5n	Bn	Me	Br	H	H	88
15	6a	<i>n</i> -Bu	Me	H	H	H	42
16	6b	<i>n</i> -Bu	Et	H	H	H	38

The dispiro compounds thus obtained were fully characterized by NMR studies. Thus, a NOESY experiment shows NOE enhancements between the phenyl *o*-proton and the α -amino proton in compound **6b**, suggesting the *endo* structure **I** (see Scheme 4.2 below). Furthermore, the benzylic proton gives a NOE with one of the CH₂ hydrogens, which is compatible only with structure **I**, since in the alternative *exo* structure **II** the benzyl hydrogen and the CH₂ are too distant. The proposed structure was finally confirmed by a single-crystal X-Ray diffraction study of compound **6b**.¹⁷¹ Figure 4.4 shows this X-Ray structure, together with a summary of the NOE effects observed in the NOESY experiment.

¹⁷¹ Deposited at the Cambridge Crystallographic Data Centre with code CCDC 1456952.

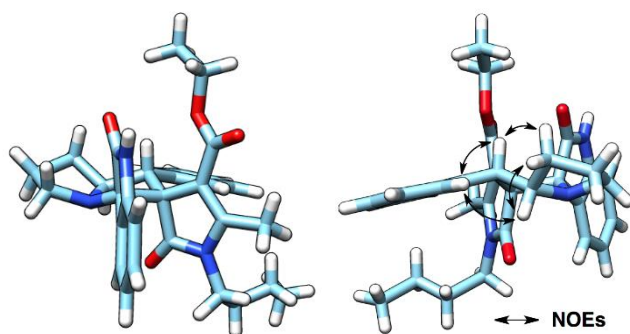
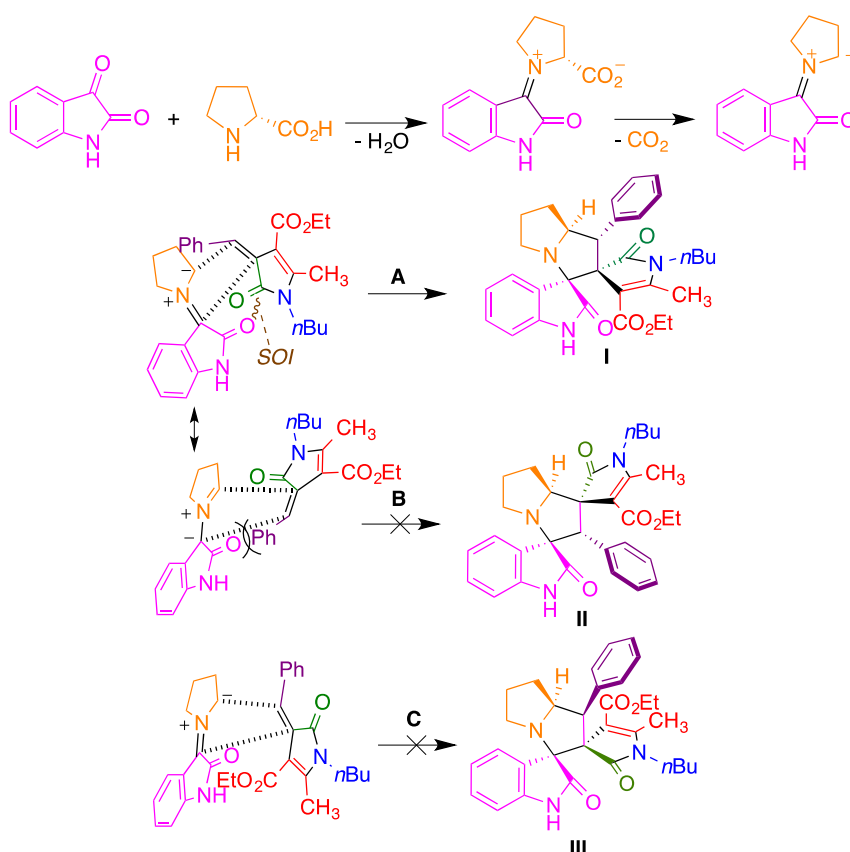


Figure 4.4

A mechanism that explains the regio- and diastereoselective formation of compounds **5** and **6** is given in Scheme 4.2, using **6b** as a representative example. The condensation of proline with isatin, followed by decarboxylation,¹⁷² furnishes a nitrogen ylide, which acts as the 1,3-dipole. In principle, this intermediate would be able to react with the dipolarophile following the alternative pathways A and B, affording regioisomers **I** and **II**, respectively. The exclusive formation of **I** can be explained by the steric clash



Scheme 4.2

¹⁷² For an example of the generation of an azomethine ylide by decarboxylative coupling of an α -amino acid and a ketone, see: Suresh Kumar, R.; Osman, H.; Perumal, S.; Menéndez, J. C.; Ashraf Ali, M.; Ismail R.; Choon, T. S. *Tetrahedron* **2011**, *67*, 3132- 3139.

between the phenyl and carbonyl groups of the reacting species in pathway B. Finally, the preference for the *endo* structure **I** over the *exo* **III** (pathway C), can be due to a favourable secondary orbital interaction (SOI) between the carbonyl groups of the dipolarophile and the dipole in the transition state leading to **I**.¹⁷³

4.4. Pharmacological study of dispirooxindoles **5** and **6**

As in the case of compounds **3**, the pharmacological study of compounds **5** and **6** was carried out by Sheila Abril at the group of Dr. Rafael León (Hospital Universitario de la Princesa and Instituto Teófilo Hernando, Universidad Autónoma de Madrid). So far, only a representative subset of the library (compounds **5h-n** and **6a-b**) has been studied.

4.4.1. SHSY5Y cytotoxicity

Compounds **5** and **6** proved to be safe when studied on neuroblastoma SHSY5Y cells, showing LD₅₀ values above 100 μ M in all cases.

4.4.2. Radical scavenging

The antioxidant activity of our compounds was examined by the DPPH method, but they did not show relevant radical scavenging properties in this assay (Table 4.2).

Table 4.2

Entry	Compound	% Scavenging at 0.1 mM	% Scavenging at 1 mM	IC ₅₀ (μ M)
1	Trolox			11.4 \pm 1.0 (9)
2	Ascorbic acid			16.2 \pm 0.7 (9)
3	Melatonin			1988 \pm 1397 (2)
4	5g	28.9 \pm 8.4	99.1 \pm 0.5	218.6 \pm 38.4(3)
5	5h	7.4 \pm 2.1	5.9 \pm 2.8	-
6	5l	6.4 \pm 8.5	26.6 \pm 4.5	-
7	5n	3.6 \pm 2.2	47.9 \pm 0.1	
8	6a	43.6 \pm 1.1	99.7 \pm 2.3	879.6 \pm 21.1(3)
9	6b	6.4 \pm 4.5	11.2 \pm 3.4	-

¹⁷³ For representative examples of the use of secondary orbital interactions to explain the outcome of related 1,3-dipolar cycloadditions, see: (a) Lakshmi, N. V.; Thirumurugan, P.; Perumal, P. T. *Tetrahedron Lett.* **2010**, *51*, 1064-1068. (b) Arun, Y.; Saranraj, K.; Balachandran, C.; Perumal, P. T. *Eur. J. Med. Chem.* **2014**, *74*, 50-64.

4.4.3. Nrf2 induction in the AREc32 cell line

The Nrf2 induction assay was carried out as described in Chapter 3. The CD values for each compound, *i.e.*, the concentration of compound that doubles the luciferase activity compared to its basal expression, are shown in Table 4.3. Only two of the compounds (**6a** and **5g**) showed a significant ability to induce Nrf2.

Table 4.3

Entry	Compound	CD (μM)
1	5g	30.87 \pm 3.93
2	5h	> 60
3	5l	> 60
4	5n	> 60
5	6a	22.91 \pm 3.32
6	6b	> 60

4.4.4. Acetylcholinesterase inhibition

As for other compound libraries, we also examined the ability of compounds **5** and **6** to inhibit acetylcholinesterase, a well-known target in Alzheimer's disease. Most compounds showed some degree of activity in this assay, with the exception of **5n**, although their potency was low. The IC₅₀ values are summarized in Table 4.4.

Table 4.4

Entry	Compound	IC ₅₀ (μM), <i>EeAChE</i>
1	5g	92.6 \pm 10.4 (2)
2	5h	71.7 \pm 19.6 (5)
3	5l	>100 (2)
4	5n	68.1 (1)
5	6a	71.5 \pm 14.4 (5)
6	6b	73.8 \pm 18.4 (5)

4.4.5. Neuroprotection in a rotenone/oligomycin A oxidative stress model

The rotenone-oligomycin combination generates an intracellular model of oxidative stress by inhibiting complexes **I** and **V** of the mitochondrial electron transport chain, respectively. All our compounds showed an excellent activity in this assay, since all of

them provided a higher protection than the well-known neuroprotective agent melatonin. Compounds **5h**, **5n** and **6b** are particularly noteworthy in this regard (Table 4.5 and Figure 4.5).

Table 4.5^a

Entry	Compound	% Survival \pm SEM at 1 μ M	% Neuroprotection \pm SEM at 1 μ M	Statistical significance
1	Basal	100		
2	R/O (30/10 μ M)	43.27 \pm 1.97		###
3	Melatonin	78.14 \pm 5.70	61.41 \pm 8.75	***
4	5g	88.79 \pm 6.61	80.79 \pm 11.29	***
5	5h	93.31 \pm 11.13	89.42 \pm 20.02	***
6	5l	82.84 \pm 4.04	69.56 \pm 6.57	***
7	5n	96.38 \pm 8.07	92.80 \pm 15.14	***
8	6a	89.12 \pm 7.84	81.51 \pm 13.09	***
9	6b	91.35 \pm 6.14	84.46 \pm 10.95	***

^a Data are expressed as mean \pm SEM of three experiments by triplicate. One way ANOVA Newman Keuls post test ### p < 0.001; compared to basal. * p < 0.05, ** p < 0.01; *** p < 0.001; compared to toxic.

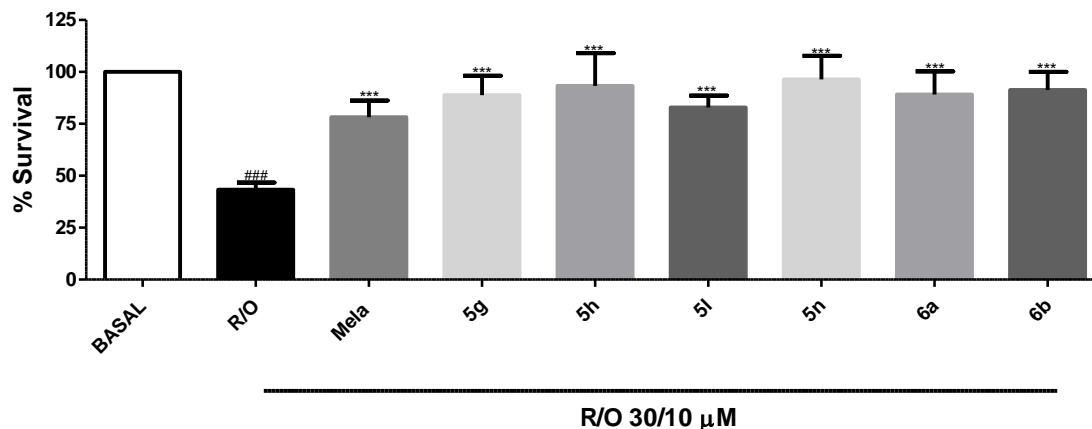


Figure 4.5. Neuroprotective effect of compounds **5g-n** and **6a-b** (1 μ M) against toxicity elicited by the combination of rotenone (30 μ M) and oligomycin A (10 μ M) in SH-SY5Y cells.

4.4.6. Neuroprotection against tau hyperphosphorylation induced by okadaic acid

Finally, we also examined the protective effect of our compounds in SH-SY5Y cell line treated with okadaic acid. This compound inhibits protein phosphatase 2A and thereby induces tau hyperphosphorylation, which is known to be an important feature in Alzheimer's and Parkinson's disease, and also in a number of degenerative diseases known as tauopathies. The results obtained in this model are summarized in Table 4.6 and Figure 4.6, and again show good to excellent neuroprotection for all compounds, three of which (**6a**, **5g** and **5n**) are more active than melatonin.

Table 4.6^a

Entry	Compound	% Survival ± SEM at 1 μM	% Neuroprotection ± SEM at 1 μM	Statistical significance
1	Basal	100		
2	Okadaic acid (20 nM)	60.32 ± 5.48		###
3	Melatonin	85.48 ± 7.77	67.70 ± 13.95	**
4	5g	90.67 ± 7.02	81.64 ± 16.63	***
5	5h	80.47 ± 7.60	51.17 ± 15.71	*
6	5l	82.49 ± 4.09	56.01 ± 8.17	***
7	5n	87.20 ± 4.79	70.49 ± 10.53	***
8	6a	91.15 ± 5.33	81.91 ± 10.07	***
9	6b	74.93 ± 8.43	40.42 ± 16.04	

^a Data are expressed as mean ± SEM of three experiments by triplicate. One way ANOVA Newman Keuls post test ### p < 0.001; compared to basal. * p < 0.05, ** p < 0.01; *** p < 0.001; compared to toxic.

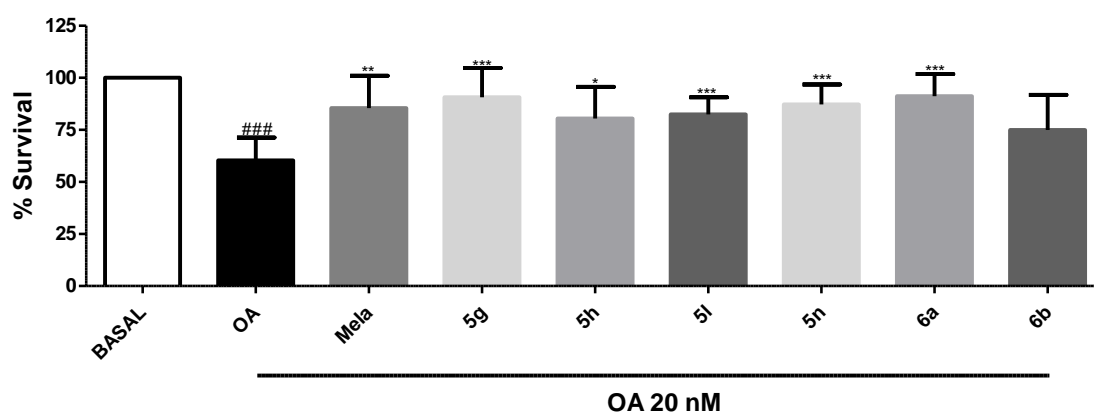


Figure 4.6. Neuroprotective effect of compounds **5g-n** and **6a-b** (1 μM) against toxicity elicited by the okadaic acid (20 nM) in SH-SY5Y cells.

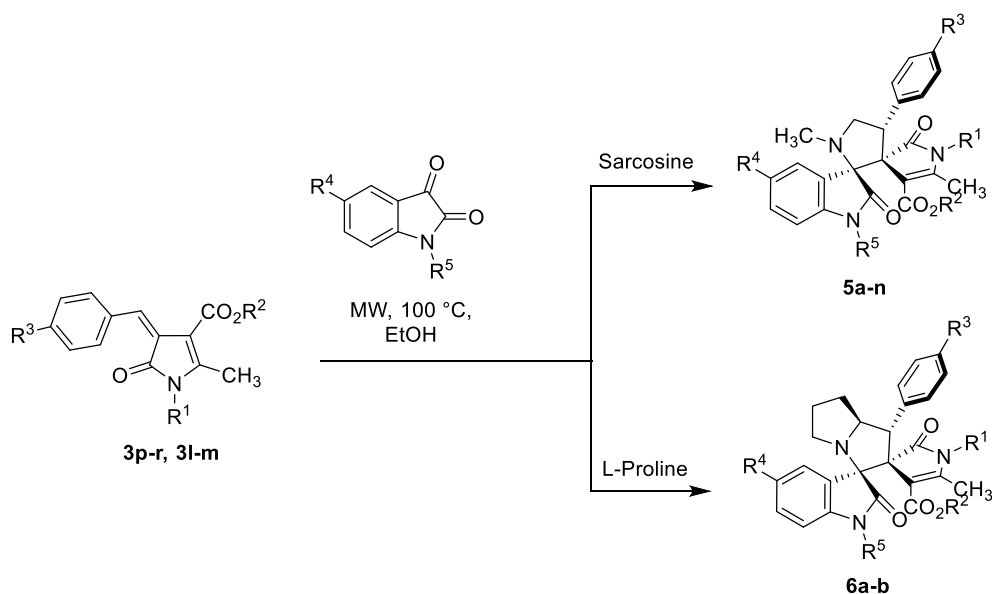
In conclusion, compounds **5h-n** and **6a-b** display highly promising neuroprotective properties. **5n**, in particular, has shown excellent neuroprotection in both cellular models tested, and is a suitable candidate for further development. The mechanism of the neuroprotective effect is not completely clear and its unravelment will require further studies. However, it is significant that the two compounds with the highest Nrf2 induction ability also showed the highest neuroprotection against an insult caused by the phosphatase inhibitor okadaic acid, which is connected to the activity of GSK3 β via the control of phosphorylation levels.

4.5. Experimental section

General experimental details

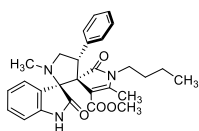
All reagents and solvents were of commercial quality and were used as received. Reactions were monitored by thin layer chromatography on aluminium plates coated with silica gel and fluorescent indicator. Microwave-assisted reactions were performed on a CEM Discover focused microwave reactor. Separations by flash chromatography were performed using a Combiflash Teledyne automated flash chromatograph or on conventional silica gel columns. Melting points were measured with a Kofler-type heating platine microscope from Reichert, 723 model, and are uncorrected. Infrared spectra were recorded with an Agilent Cary630 FTIR spectrophotometer with a diamond ATR accessory for solid and liquid samples, requiring no sample preparation; wavenumbers are given in cm^{-1} . NMR spectroscopic data were obtained using spectrometers maintained by the CAI de Resonancia Magnética, UCM, operating at 250, 300, 400 and 700 MHz for ^1H NMR and, 63, 100 and 176 MHz for ^{13}C NMR; chemical shifts are given in (δ) parts per million and coupling constants (J) in hertz. Elemental analyses were determined by the CAI de Microanálisis, Universidad Complutense, using a Leco CHNS-932 combustion microanalyzer. The enantiomeric excess analysis has been conducted in a HPLC Agilent 1220 Infinity LC with a chiral column ULTRON ES.

4.5.1. General procedure for the synthesis of dispirooxindoles 5 and 6



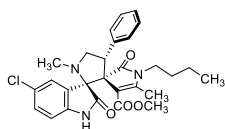
The suitable isatine (1.5 eq.) and the appropriate amino acid (1.5 eq.) were placed in a microwave reaction vial. Then, the corresponding 4-arylmethylen-2-pyrrolin-5-one (1 eq.) suspended in ethanol (2 mL) was added and irradiated at 100 °C for 1h. After the reaction completion, the mixture was cooled at room temperature and a precipitate was formed. The solid compound was filtered and washed twice with cold ethanol. No further purification was needed.

Methyl (3*S,3'*R**,4'*R**)-1''-butyl-1',5''-dimethyl-2,2''-dioxo-4'-phenyl-1'',2''-dihydrodispiro[indoline-3,2'-pyrrolidine-3',3''-pyrrole]-4''-carboxylate (5a)**



Prepared from pyrrolinone **3p** (1 mmol), sarcosine (1.5 mmol) and isatine (1.5 mmol); pale brown solid (237 mg, 50%): **mp** 215-218 °C; $^1\text{H NMR}$ (250 MHz, CDCl_3) δ 7.90 (br s, 1H), 7.44-7.29 (m, 2H), 7.29-7.03 (m, 5H), 6.86 (td, $J = 7.7, 0.9$ Hz, 1H), 6.74 (d, $J = 7.7$ Hz, 1H), 5.34 (dd, $J = 10.1, 8.7$ Hz, 1H), 4.24 (t, $J = 8.7$ Hz, 1H), 3.78 (s, 3H), 3.65 (dd, $J = 10.1, 8.7$ Hz, 1H), 3.34-3.13 (m, 1H), 3.02-2.78 (m, 1H), 2.34 (s, 3H), 1.96 (s, 3H), 1.17-0.94 (m, 2H), 0.94-0.79 (m, 2H), 0.79-0.62 (m, 3H); $^{13}\text{C NMR}$ (63 MHz, CDCl_3) δ 178.1, 175.2, 165.6, 156.0, 142.5, 137.7, 129.7, 129.3 (2C), 128.3 (2C), 127.1, 126.0, 122.4, 110.2, 103.6, 78.2, 68.2, 56.2, 51.2, 43.5, 39.7, 36.3, 30.9, 20.0, 14.1, 12.8; **IR** (neat, cm^{-1}): 3140, 1725, 1702, 1688, 1602, 1208; **elemental analysis** (%) calcd. for $\text{C}_{28}\text{H}_{31}\text{N}_3\text{O}_4$: C 71.02, H 6.60, N 8.87; found: C 70.84, H 6.54, N 8.85.

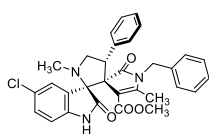
Methyl (3*S,3'*R**,4'*R**)-1''-butyl-5-chloro-1',5''-dimethyl-2,2''-dioxo-4'-phenyl-1'',2''-dihydrodispiro[indoline-3,2'-pyrrolidine-3',3''-pyrrole]-4''-carboxylate (5b)**



Prepared from pyrrolinone **3p** (1 mmol), sarcosine (1.5 mmol) and 5-chloroisatine (1.5 mmol); pale brown solid (284 mg,

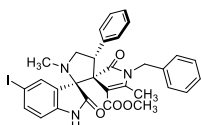
56%): **mp** 102-104 °C; $^1\text{H NMR}$ (250 MHz, CDCl_3) δ 8.55 (br s, 1H), 7.35 (dd, J = 7.9, 1.4 Hz, 2H), 7.29-7.05 (m, 5H), 6.74 (d, J = 8.3 Hz, 1H), 5.34 (dd, J = 9.9, 8.7 Hz, 1H), 4.22 (t, J = 8.7 Hz, 1H), 3.73 (s, 3H), 3.69-3.56 (m, 1H), 3.23-2.98 (m, 2H), 2.34 (s, 3H), 1.99 (s, 3H), 1.29-1.07 (m, 1H), 1.07-0.83 (m, 3H), 0.78 (t, J = 6.4 Hz, 3H); $^{13}\text{C NMR}$ (63 MHz, CDCl_3) δ 179.5, 176.3, 166.8, 157.4, 142.5, 138.7, 131.0, 130.6 (2C), 129.6 (2C), 129.2, 129.2, 128.5, 127.7, 112.7, 104.6, 79.5, 69.6, 57.5, 52.5, 44.9, 41.2, 37.6, 32.4, 21.4, 15.3, 14.3; **IR** (neat, cm^{-1}): 3238, 1717, 1689, 1613, 1210, 1175; **elemental analysis (%) calcd. for $\text{C}_{28}\text{H}_{30}\text{ClN}_3\text{O}_4$** : C 66.20, H 5.95, N 8.27; found: C 66.02, H 5.71, N 8.21.

Methyl (3S*,3'R*,4'R*)-1''-benzyl-5-chloro-1',5''-dimethyl-2,2''-dioxo-4'-phenyl-1'',2''-dihydrodispiro[indoline-3,2'-pyrrolidine-3',3''-pyrrole]-4''-carboxylate (5c)

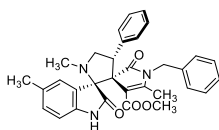


Prepared from pyrrolinone **3I** (1 mmol), sarcosine (1.5 mmol) and 5-chloroisatine (1.5 mmol); beige solid (396 mg, 73%): **mp** 166-169 °C; $^1\text{H NMR}$ (250 MHz, CDCl_3) δ 8.06 (br s, 1H), 7.49-7.34 (m, 2H), 7.28-6.89 (m, 8H), 6.67 (d, J = 8.3 Hz, 1H), 6.23 (d, J = 7.0 Hz, 2H), 5.37 (dd, J = 10.0, 8.5 Hz, 1H), 4.81 (d, J = 16.3 Hz, 1H), 4.24 (t, J = 8.5 Hz, 1H), 3.88 (d, J = 16.3 Hz, 1H), 3.77-3.51 (m, 4H), 2.30 (s, 3H), 1.72 (s, 3H); $^{13}\text{C NMR}$ (63 MHz, CDCl_3) δ 177.7, 175.0, 165.4, 156.1, 141.0, 137.3, 136.1, 129.9, 129.6 (2C), 129.1 (2C), 128.6 (2C), 128.2, 127.9, 127.5, 127.4, 126.2 (2C), 111.3, 103.7, 78.4, 77.6, 68.8, 56.0, 51.3, 43.5, 43.0, 36.3, 13.2; **IR** (neat, cm^{-1}): 3224, 1721, 1692, 1617, 1255, 1181; **elemental analysis (%) calcd. for $\text{C}_{31}\text{H}_{28}\text{ClN}_3\text{O}_4$** : C 68.69, H 5.21, N 7.75%; found C 68.75, H 5.10, N 7.67.

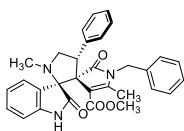
Methyl (3S*,3'R*,4'R*)-1''-benzyl-5-iodo-1',5''-dimethyl-2,2''-dioxo-4'-phenyl-1'',2''-dihydrodispiro[indoline-3,2'-pyrrolidine-3',3''-pyrrole]-4''-carboxylate (5d)



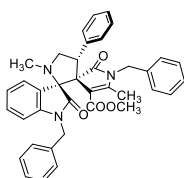
Prepared from pyrrolinone **3I** (1 mmol), sarcosine (1.5 mmol) and 5-iodoisatine (1.5 mmol); beige solid (329 mg, 52%): **mp** 140-143 °C; $^1\text{H NMR}$ (250 MHz, CDCl_3) δ 7.70-7.61 (m, 2H), 7.55 (dd, J = 8.2, 1.8 Hz, 1H), 7.52-7.43 (m, 2H), 7.36-7.27 (m, 3H), 7.19-7.00 (m, 3H), 6.61 (d, J = 8.2 Hz, 1H), 6.32 (d, J = 6.9 Hz, 2H), 5.44 (dd, J = 10.1, 8.5 Hz, 1H), 4.96 (d, J = 16.3 Hz, 1H), 4.34 (t, J = 8.5 Hz, 1H), 3.95 (d, J = 16.3 Hz, 1H), 3.80 (s, 3H), 3.72 (app. t, J = 9.6 Hz, 1H), 2.42 (s, 3H), 1.82 (s, 3H); $^{13}\text{C NMR}$ (63 MHz, CDCl_3) δ 175.0, 165.3, 156.3, 142.0, 138.7, 138.7, 136.1, 134.7, 129.6 (2C), 129.2 (2C), 128.7 (2C), 127.5, 127.4, 126.2 (2C), 112.3, 103.6, 85.1, 78.1, 77.6, 68.8, 56.1, 51.4, 43.4, 43.0, 36.5, 31.4, 13.2; **IR** (neat, cm^{-1}): 3222, 1719, 1688, 1607, 1177; **elemental analysis (%) calcd. for $\text{C}_{31}\text{H}_{28}\text{IN}_3\text{O}_4$** : C 58.78, H 4.46, N 6.63; found C 58.67, H 4.39, N 6.71.

Methyl (3S*,3'R*,4'R*)-1''-benzyl-1',5,5''-trimethyl-2,2''-dioxo-4'-phenyl-1'',2''-dihydrodispiro[indoline-3,2'-pyrrolidine-3',3''-pyrrole]-4''-carboxylate (5e)

Prepared from pyrrolinone **3I** (1 mmol), sarcosine (1.5 mmol) and 5-methylisatine (1.5 mmol); beige solid (287 mg, 55%): **mp** 217 °C; $^1\text{H NMR}$ (250 MHz, CDCl_3) δ 7.78 (br s, 1H), 7.61-7.42 (m, 2H), 7.31-7.29 (m, 3H), 7.20-6.93 (m, 5H), 6.70 (d, $J = 7.8$ Hz, 1H), 6.30 (d, $J = 7.3$ Hz, 2H), 5.48 (app. t, $J = 8.9$ Hz, 1H), 4.86 (d, $J = 16.3$ Hz, 1H), 4.33 (app. t, $J = 8.9$ Hz, 1H), 3.96 (d, $J = 16.3$ Hz, 1H), 3.81 (s, 3H), 3.72 (app. t, $J = 9.6$ Hz, 1H), 2.40 (s, 3H), 2.26 (s, 3H), 1.80 (s, 3H); $^{13}\text{C NMR}$ (63 MHz, CDCl_3) δ 177.9, 175.2, 165.5, 155.7, 140.0, 137.7, 136.3, 132.1, 130.1, 129.7 (2C), 129.1 (2C), 128.6 (2C), 127.5, 127.2, 126.5, 126.1 (2C), 126.0, 110.0, 104.1, 68.7, 56.1, 51.3, 43.5, 42.8, 36.4, 31.4, 21.5, 13.2; **IR** (neat, cm^{-1}): 3155, 1705, 1682, 1616, 1216, 1190; **elemental analysis (%) calcd. for $\text{C}_{32}\text{H}_{31}\text{N}_3\text{O}_4$** : C 73.68, H 5.99, N 8.06; found: C 73.54, H 6.01, N 8.18.

Methyl (3S*,3'R*,4'R*)-1''-benzyl-1',5''-dimethyl-2,2''-dioxo-4'-phenyl-1'',2''-dihydrodispiro[indoline-3,2'-pyrrolidine-3',3''-pyrrole]-4''-carboxylate (5f)

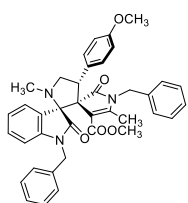
Prepared from pyrrolinone **3I** (1 mmol), sarcosine (1.5 mmol) and isatine (1.5 mmol); white solid (330 mg, 65%): **mp** 200-203 °C; $^1\text{H NMR}$ (250 MHz, CDCl_3) δ 7.74 (br s, 1H), 7.52 (s, 2H), 7.41-6.97 (m, 8H), 6.91 (t, $J = 7.6$ Hz, 1H), 6.79 (d, $J = 7.6$ Hz, 1H), 6.31 (d, $J = 7.3$ Hz, 2H), 5.48 (app. t, $J = 9.0$ Hz, 1H), 4.91 (d, $J = 16.3$ Hz, 1H), 4.34 (app. t, $J = 8.4$ Hz, 1H), 3.91 (d, $J = 16.3$ Hz, 1H), 3.82 (s, 3H), 3.73 (app. t, $J = 9.6$ Hz, 1H), 2.40 (s, 3H), 1.81 (s, 3H); $^{13}\text{C NMR}$ (63 MHz, CDCl_3) δ 175.1, 165.5, 155.9, 142.4, 137.7, 136.3, 129.9, 129.7 (2C), 129.0 (2C), 128.6 (2C), 127.5, 127.2, 126.3 (2C), 125.9, 125.8, 122.6, 110.2, 104.0, 78.4, 77.6, 68.7, 56.0, 51.3, 43.4, 43.0, 36.3, 13.1; **IR** (neat, cm^{-1}): 3139, 1708, 1684, 1614, 1252, 1218; **elemental analysis (%) calcd. for $\text{C}_{31}\text{H}_{29}\text{N}_3\text{O}_5$** : C 73.35, H 5.76, N 8.28; found: C 73.13, H 5.60, N 8.14.

Methyl (3S*,3'R*,4'R*)-1,1''-dibenzyl-1',5''-dimethyl-2,2''-dioxo-4'-phenyl-1'',2''-dihydrodispiro[indoline-3,2'-pyrrolidine-3',3''-pyrrole]-4''-carboxylate (5g)

Prepared from pyrrolinone **3I** (1 mmol), sarcosine (1.5 mmol) and 1-benzylisatine (1.5 mmol); light yellow solid (448 mg, 75%): **mp** 113-115 °C; $^1\text{H NMR}$ (250 MHz, CDCl_3) δ 7.53-7.54 (m, 2H), 7.39-7.25 (m, 9H), 7.17-7.02 (m, 4H), 6.89 (t, $J = 7.4$ Hz, 1H), 6.58 (d, $J = 7.7$ Hz, 1H), 6.31 (d, $J = 7.2$ Hz, 2H), 5.56 (dd, $J = 10.0, 8.4$ Hz, 1H), 5.10 (d, $J = 15.8$ Hz, 1H), 4.92 (d, $J = 16.3$ Hz, 1H), 4.58 (d, $J = 15.8$ Hz, 1H), 4.37 (t, $J = 8.4$ Hz, 1H), 3.90 (d, $J = 16.3$ Hz, 1H), 3.84-3.68 (m, 4H), 2.40 (s, 3H), 1.79 (s, 3H); $^{13}\text{C NMR}$ (63 MHz, CDCl_3) δ 175.7, 175.2, 165.3, 155.3, 144.3, 137.8, 136.3, 136.1, 129.8, 129.7 (2C), 129.2 (2C), 129.0 (2C), 128.6 (2C), 127.9, 127.6 (2C), 127.5, 127.2, 126.3, 125.4, 125.2, 122.6, 109.7, 104.2, 78.4, 68.9, 56.2, 51.3, 44.0, 43.5, 43.0, 36.4, 13.1; **IR** (neat, cm^{-1}): 1709, 1688, 1260, 1210; **elemental**

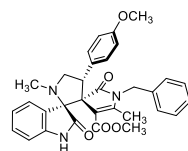
analysis (%) calcd. for C₃₈H₃₅N₃O₄: C 76.36, H 5.90, N 7.03; found: C 76.23, H 5.81, N 7.16.

Methyl (3*S,3*R**,4*R**)-1,1''-dibenzyl-4'-(4-methoxyphenyl)-1',5''-dimethyl-2,2''-dioxo-1'',2''-dihydrodispiro[indoline-3,2'-pyrrolidine-3',3''-pyrrole]-4''-carboxylate (5h)**



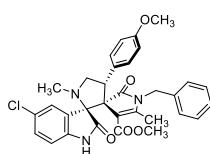
Prepared from pyrrolinone **3m** (1 mmol), sarcosine (1.5 mmol) and 1-benzylisatine (1.5 mmol); light yellow solid (427 mg, 68%): **mp** 198-200 °C; ¹H NMR (250 MHz, CDCl₃) δ 7.37 (d, *J* = 8.7 Hz, 2H), 7.30-7.11 (m, 6H), 7.11-6.87 (m, 4H), 6.85-6.68 (m, 3H), 6.48 (d, *J* = 7.7 Hz, 1H), 6.21 (d, *J* = 7.2 Hz, 2H), 5.41 (dd, *J* = 10.2, 8.4 Hz, 1H), 5.00 (d, *J* = 15.8 Hz, 1H), 4.84 (d, *J* = 16.4 Hz, 1H), 4.48 (d, *J* = 15.8 Hz, 1H), 4.21 (t, *J* = 8.4 Hz, 1H), 3.81 (d, *J* = 16.4 Hz, 1H), 3.74 (s, 3H), 3.71-3.57 (m, 4H), 2.29 (s, 3H), 1.69 (s, 3H); ¹³C NMR (63 MHz, CDCl₃) δ 175.7, 175.3, 165.3, 158.9, 155.2, 144.3, 136.3, 136.1, 130.8 (2C), 129.8, 129.6, 129.2 (2C), 128.9 (2C), 127.9, 127.6 (2C), 127.5, 126.3 (2C), 125.4, 125.3, 122.6, 113.9 (2C), 109.7, 104.2, 78.3, 77.6, 69.0, 56.4, 55.5, 51.3, 44.0, 42.9, 36.4, 13.0; IR (neat, cm⁻¹): 1713, 1685, 1605, 1243, 1225; elemental analysis (%) calcd. for C₃₉H₃₇N₃O₅: C 74.62, H 5.94, N 6.69; found C 74.33, H 6.02, N 6.81.

Methyl (3*S,3*R**,4*R**)-1''-benzyl-4'-(4-methoxyphenyl)-1',5''-dimethyl-2,2''-dioxo-1'',2''-dihydrodispiro[indoline-3,2'-pyrrolidine-3',3''-pyrrole]-4''-carboxylate (5i)**



Prepared from pyrrolinone **3m** (1 mmol), sarcosine (1.5 mmol) and isatine (1.5 mmol); beige solid (296 mg, 55%): **mp** 212-214 °C; ¹H NMR (250 MHz, CDCl₃): δ 7.57 (br s, 1H), 7.44 (d, *J* = 8.7 Hz, 2H), 7.33-6.97 (m, 5H), 6.98-6.68 (m, 4H), 6.31 (d, *J* = 7.2 Hz, 2H), 5.43 (dd, *J* = 10.2, 8.7 Hz, 1H), 4.93 (d, *J* = 16.3 Hz, 1H), 4.29 (t, *J* = 8.7 Hz, 1H), 3.92 (d, *J* = 16.3 Hz, 1H), 3.83 (s, 3H), 3.82 (s, 3H), 3.70 (dd, *J* = 10.2, 8.7 Hz, 1H), 2.39 (s, 3H), 1.81 (s, 3H); ¹³C NMR (63 MHz, CDCl₃) δ 177.9, 175.4, 165.7, 159.1, 155.9, 142.5, 136.4, 130.9 (2C), 130.0, 129.6, 129.1 (2C), 127.7, 126.5 (2C), 126.0, 122.8, 114.1, 110.3 (2C), 104.2, 78.5, 77.8, 69.0, 56.4, 55.7, 51.4, 43.1, 43.0, 36.5, 13.3; IR (neat, cm⁻¹): 3140, 1721, 1702, 1685, 1611, 1245, 1212; elemental analysis (%) calcd. for C₃₂H₃₁N₃O₅: C 71.49, H 5.81, N 7.82; found: C 71.36, H 5.57, N 7.88.

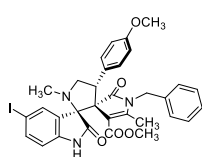
Methyl (3*S,3*R**,4*R**)-1''-benzyl-5-chloro-4'-(4-methoxyphenyl)-1',5''-dimethyl-2,2''-dioxo-1'',2''-dihydrodispiro[indoline-3,2'-pyrrolidine-3',3''-pyrrole]-4''-carboxylate (5j)**



Prepared from pyrrolinone **3m** (1 mmol), sarcosine (1.5 mmol) and 5-chloroisatine (1.5 mmol); light yellow solid (418 mg, 73%): **mp** 181-185 °C; ¹H NMR (250 MHz, CDCl₃) δ 8.04 (br s, 1H), 7.42 (d, *J* = 8.8 Hz, 2H), 7.33 (d, *J* = 2.0 Hz, 1H), 7.23-7.01 (m, 4H), 6.84 (d, *J* = 8.8 Hz, 2H), 6.76 (d, *J* = 8.3 Hz, 1H), 6.31 (d,

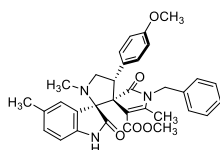
$J = 7.1$ Hz, 2H), 5.41 (dd, $J = 10.0, 8.6$ Hz, 1H), 4.94 (d, $J = 16.3$ Hz, 1H), 4.28 (app. t, $J = 8.6$ Hz, 1H), 3.99 (d, $J = 16.4$ Hz, 1H), 3.84 (s, 3H), 3.78 (s, 3H), 3.68 (dd, $J = 10.0, 9.2$ Hz, 1H), 2.39 (s, 3H), 1.82 (s, 3H); ^{13}C NMR (63 MHz, CDCl_3) δ 177.7, 175.1, 165.4, 159.0, 156.0, 141.0, 136.1, 130.7 (2C), 129.8, 129.1, 129.0 (2C), 128.2, 128.0, 127.6, 126.2, 126.2 (2C), 114.0 (2C), 111.3, 103.7, 78.3, 68.9, 56.2, 55.5, 51.4, 42.9, 36.3, 31.4, 13.2; IR (neat, cm^{-1}): 3199, 1721, 1688, 1605, 1245, 1207. **elemental analysis (%) calcd. for $\text{C}_{32}\text{H}_{30}\text{ClN}_3\text{O}_5$:** C 67.19, H 5.29, N 7.35; found: C 67.02, H 5.34, N 7.30.

Methyl (3S*,3'R*,4'R*)-1''-benzyl-5-iodo-4'-(4-methoxyphenyl)-1',5''-dimethyl-2,2''-dioxo-1'',2''-dihydrodispiro[indoline-3,2'-pyrrolidine-3',3''-pyrrole]-4''-carboxylate (5k)



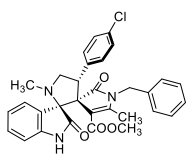
Prepared from pyrrolinone **3m** (1 mmol), sarcosine (1.5 mmol) and 5-iodoisatine (1.5 mmol); pale brown solid (331 mg, 50%): **mp** 141-143 °C; ^1H NMR (250 MHz, CDCl_3) δ 8.35 (br s, 1H), 7.42 (d, $J = 1.8$ Hz, 1H), 7.32 (dd, $J = 8.2, 1.8$ Hz, 1H), 7.21 (d, $J = 8.8$ Hz, 2H), 7.00-6.80 (m, 3H), 6.63 (d, $J = 8.8$ Hz, 2H), 6.44 (d, $J = 8.2$ Hz, 1H), 6.10 (d, $J = 7.0$ Hz, 2H), 5.21 (dd, $J = 10.0, 8.6$ Hz, 1H), 4.77 (d, $J = 16.4$ Hz, 1H), 4.07 (app. t, $J = 8.6$ Hz, 1H), 3.76 (d, $J = 16.4$ Hz, 1H), 3.63 (s, 3H), 3.54 (s, 3H), 3.48 (dd, $J = 10.0, 9.1$ Hz, 1H), 2.18 (s, 3H), 1.61 (s, 3H); ^{13}C NMR (63 MHz, CDCl_3) δ 177.5, 175.2, 165.4, 159.0, 156.1, 142.3, 138.6, 136.1, 134.5, 130.7 (2C), 129.1, 129.0 (2C), 128.5, 127.6, 126.2 (2C), 113.9 (2C), 112.6, 103.6, 85.1, 78.2, 68.9, 56.3, 55.6, 51.4, 42.8, 42.8, 36.4, 13.3; IR (neat, cm^{-1}): 3164, 1714, 1694, 1671, 1245, 1176; **elemental analysis (%) calcd. for $\text{C}_{32}\text{H}_{30}\text{IN}_3\text{O}_5$:** C 57.93, H 4.56, N 6.33; found: C 57.75, H 4.42, N 6.46.

Methyl (3S*,3'R*,4'R*)-1''-benzyl-4'-(4-methoxyphenyl)-1',5,5''-trimethyl-2,2''-dioxo-1'',2''-dihydrodispiro[indoline-3,2'-pyrrolidine-3',3''-pyrrole]-4''-carboxylate (5l)



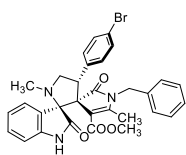
Prepared from pyrrolinone **3m** (1 mmol), sarcosine (1.5 mmol) and 5-methylisatine (1.5 mmol); light yellow solid (298 mg, 54%): **mp** 213-215 °C; ^1H NMR (250 MHz, CDCl_3) δ 7.41 (br s, 1H), 7.34 (d, $J = 8.7$ Hz, 2H), 7.10-6.85 (m, 5H), 6.79-6.68 (m, 2H), 6.57 (d, $J = 7.9$ Hz, 1H), 6.22 (d, $J = 7.1$ Hz, 2H), 5.32 (dd, $J = 10.3, 8.6$ Hz, 1H), 4.78 (d, $J = 16.3$ Hz, 1H), 4.18 (t, $J = 8.6$ Hz, 1H), 3.88 (d, $J = 16.3$ Hz, 1H), 3.74 (s, 3H), 3.72 (s, 3H), 3.59 (dd, $J = 10.3, 8.6$ Hz, 1H), 2.29 (s, 3H), 2.16 (s, 3H), 1.70 (s, 3H); ^{13}C NMR (63 MHz, CDCl_3) δ 177.7, 175.3, 165.5, 158.9, 155.6, 139.8, 136.3, 132.1, 130.7 (2C), 130.1, 129.5, 128.9 (2C), 127.5, 126.6, 126.2 (2C), 113.9 (2C), 109.8, 104.1, 78.3, 77.6, 68.8, 56.3, 55.5, 51.3, 42.9, 42.8, 36.3, 21.5, 13.1; IR (neat, cm^{-1}) 3162.5, 1706.6, 1687.8, 1616.8, 1247.0, 1217.0; **elemental analysis (%) calcd. for $\text{C}_{33}\text{H}_{33}\text{N}_3\text{O}_5$:** C 71.85, H 6.03, N 7.62; found: C 71.91, H 5.97, N 7.58.

Methyl (3*S,3'*R**,4'*R**)-1''-benzyl-4'-(4-chlorophenyl)-1',5''-dimethyl-2,2''-dioxo-1'',2''-dihydrodispiro[indoline-3,2'-pyrrolidine-3',3''-pyrrole]-4''-carboxylate (5m)**



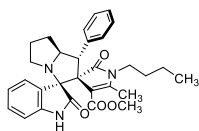
Prepared from pyrrolinone **3n** (1 mmol), sarcosine (1.5 mmol) and isatine (1.5 mmol); white solid (423 mg, 78%): **mp** 118-120 °C; $^1\text{H NMR}$ (250 MHz, CDCl_3) δ 7.45 (d, $J = 8.5$ Hz, 2H), 7.37 (br s, 1H), 7.29-7.03 (m, 7H), 6.92 (td, $J = 7.6, 0.6$ Hz, 1H), 6.78 (d, $J = 7.6$ Hz, 1H), 6.39-6.20 (m, 2H), 5.45 (dd, $J = 10.1, 8.3$ Hz, 1H), 4.93 (d, $J = 16.3$ Hz, 1H), 4.28 (t, $J = 8.3$ Hz, 1H), 3.90 (d, $J = 16.3$ Hz, 1H), 3.83 (s, 3H), 3.79-3.66 (m, 1H), 2.40 (s, 3H), 1.82 (s, 3H); $^{13}\text{C NMR}$ (63 MHz, CDCl_3) δ 176.6, 174.1, 164.3, 154.9, 141.3, 135.2, 135.1, 132.1, 130.1 (2C), 129.0, 128.1 (2C), 127.7 (2C), 126.8, 125.2 (2C), 124.7, 121.7, 109.3, 102.7, 77.4, 67.6, 55.0, 50.4, 42.0, 41.8, 35.2, 30.4, 12.1; IR (neat, cm^{-1}) 3142, 1724, 1705, 1686, 1615, 1286, 1209; elemental analysis (%) calcd. for $\text{C}_{31}\text{H}_{28}\text{ClN}_3\text{O}_4$: C 68.69, H 5.21, N 7.75; found: C 68.57, H 5.07, N 7.81.

Methyl (3*S,3'*R**,4'*R**)-1''-benzyl-4'-(4-bromophenyl)-1',5''-dimethyl-2,2''-dioxo-1'',2''-dihydrodispiro[indoline-3,2'-pyrrolidine-3',3''-pyrrole]-4''-carboxylate (5n)**



Prepared from pyrrolinone **3r** (1 mmol), sarcosine (1.5 mmol) and isatine (1.5 mmol); pale brown solid (516 mg, 88%): **mp** 222 °C; $^1\text{H NMR}$ (250 MHz, $d_6\text{-DMSO}$) δ 10.34 (br s, 1H), 7.50 (d, $J = 8.6$ Hz, 2H), 7.33 (d, $J = 8.6$ Hz, 2H), 7.24-7.00 (m, 5H), 6.86 (td, $J = 7.6, 0.9$ Hz, 1H), 6.74 (d, $J = 7.6$ Hz, 1H), 6.32 (d, $J = 6.8$ Hz, 2H), 5.32 (dd, $J = 10.1, 8.2$ Hz, 1H), 4.72 (d, $J = 16.6$ Hz, 1H), 4.25 – 3.95 (m, 2H), 3.70 (s, 3H), 3.57-3.46 (m, 1H), 2.15 (s, 3H), 1.71 (s, 3H); $^{13}\text{C NMR}$ (63 MHz, $d_6\text{-DMSO}$) δ 176.6, 174.4, 164.5, 154.5, 143.7, 137.1, 136.6, 131.4 (2C), 131.3 (2C), 129.9, 128.6 (2C), 127.3, 125.9 (2C), 125.1, 124.8, 121.6, 120.5, 110.0, 103.2, 77.5, 67.7, 51.2, 42.0, 41.9, 35.5, 31.1, 12.5; IR (neat, cm^{-1}): 3141, 1724, 1704, 1686, 1614, 1285, 1208; elemental analysis (%) calcd. for $\text{C}_{31}\text{H}_{28}\text{BrN}_3\text{O}_4$: C 63.49, H 4.81, N 7.1; found: C 63.62, H 4.77, N 7.05.

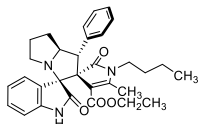
Methyl (1'*R,2'*R**,3*S**,7*a*'*S*)-1''-butyl-5''-methyl-2,2''-dioxo-1'-phenyl-1'',2'',5',6',7',7*a*'-hexahydro-1'*H*-dispiro[indoline-3,3'-pyrrolizine-2',3''-pyrrole]-4''-carboxylate (6a)**



Prepared from pyrrolinone **3p** (1 mmol), proline (1.5 mmol) and isatine (1.5 mmol); light yellow solid (210 mg, 42%): **mp** 156-158 °C; $^1\text{H NMR}$ (250 MHz, CDCl_3) δ 7.81 (br s, 1H), 7.46 (d, $J = 6.5$ Hz, 2H), 7.38 (d, $J = 7.5$ Hz, 1H), 7.28-7.09 (m, 4H), 6.90 (t, $J = 7.5$ Hz, 1H), 6.71 (d, $J = 7.7$ Hz, 1H), 4.91 (s, 2H), 3.81 (s, 3H), 3.34-3.16 (m, 1H), 3.11-2.95 (m, 1H), 2.88 (t, $J = 7.1$ Hz, 1H), 2.81-2.64 (m, 1H), 2.31-2.00 (m, 4H), 1.94 (s, 3H), 1.22-1.05 (m, 2H), 1.04-0.88 (m, 2H), 0.80 (t, $J = 6.9$ Hz, 3H); $^{13}\text{C NMR}$ (63 MHz, CDCl_3) δ 178.7, 175.8, 165.8, 154.8, 141.4, 137.8, 129.4 (2C), 129.3, 128.4 (2C), 127.1, 126.0, 122.5, 109.8, 104.2, 77.3, 73.2, 68.7, 51.2, 49.7, 47.9, 39.8,

32.4, 31.0, 30.5, 20.1, 14.1, 12.7; IR (neat, cm^{-1}): 3138, 1707, 1687, 1615, 1254, 1205; elemental analysis (%) calcd. for $\text{C}_{30}\text{H}_{33}\text{N}_3\text{O}_4$: C 72.12, H 6.66, N 8.41; found: C 71.98, H 6.55, N 8.46.

Ethyl (1'R*,2'R*,3S*,7a'S)-1''-butyl-5''-methyl-2,2''-dioxo-1'-phenyl-1'',2'',5',6',7',7a'-hexahydro-1'H-dispiro[indoline-3,3'-pyrrolizine-2',3''-pyrrole]-4''-carboxylate (6b)



Prepared from pyrrolinone **3q** (1 mmol), proline (1.5 mmol) and isatine (1.5 mmol); light yellow solid (195 mg, 38%): mp 155-157 °C; $^1\text{H NMR}$ (250 MHz, CDCl_3) δ 7.58 (br s, 1H), 7.46 (d, $J = 6.9$ Hz, 2H), 7.35 (d, $J = 7.5$ Hz, 1H), 7.28-7.00 (m, 4H), 6.87 (t, $J = 7.7$ Hz, 1H), 6.66 (d, $J = 7.7$ Hz, 1H), 4.91 (s, 1H), 4.99-4.77 (m, 2H), 4.32 (m, 1H), 4.16 (m, 1H), 3.29-3.13 (m, 1H), 3.06-2.91 (m, 1H), 2.85 (t, $J = 7.5$ Hz, 1H), 2.70 (dd, $J = 16.4, 7.9$ Hz, 1H), 2.26-1.96 (m, 4H), 1.91 (s, 3H), 1.39 (t, $J = 7.1$ Hz, 3H), 1.18-1.01 (m, 2H), 1.01-0.83 (m, 2H), 0.76 (t, $J = 6.6$ Hz, 3H); $^{13}\text{C NMR}$ (63 MHz, CDCl_3) δ 178.6, 175.8, 165.4, 154.5, 141.4, 137.8, 129.4 (2C), 128.4 (2C), 128.0, 127.1, 126.0, 122.5, 109.8, 104.2, 77.3, 73.3, 68.7, 60.6, 49.7, 47.8, 39.8, 32.4, 31.0, 30.5, 30.1, 20.1, 14.6, 14.1, 12.6; IR (neat, cm^{-1}): 3190, 1708, 1681, 1612, 1249, 1203; elemental analysis (%) calcd. for $\text{C}_{31}\text{H}_{35}\text{N}_3\text{O}_4$: C 72.49, H 6.87, N 8.18; found: C 72.33, H 6.90, N 7.97.

**CHAPTER 5. MELATONIN/2,5,8-
QUINOLINETRIONE HYBRIDS**

5.1. Biological importance of quinones

Quinone moieties, in particular 1,2- and 1,4-quinones, are present in several molecules involved in physiological processes and can be found in natural products with a broad activity spectrum.

An example of a 1,4-benzoquinone with a remarkable relevance in physiological processes is coenzyme Q10 (CoQ), or ubiquinone 10, which takes part in oxidative phosphorylation process involved in cell energy production. Also, Q10 participates in single electron transfer reactions inside cells. Recent research on Q10 coenzyme shows its potential neuroprotective effect in Alzheimer's disease, since it is able to prevent β -amyloid-induced neural stem cell death.¹⁷⁴ These neuroprotective effects have been ascribed, at least in part, to Nrf2 induction due to the presence of electrophilic Michael acceptors in the quinone moiety.¹⁷⁵ Furthermore, low CoQ10 levels have been correlated with a greater risk of dementia in a Japanese general population.¹⁷⁶

Besides Q10, other quinones have attracted attention in the field of medicinal chemistry (Figure 5.1). An example is the 1,4-naphthoquinone-tryptophan hybrid, with a protein aggregation inhibitory activity.¹⁷⁷ Memoquine is another example of a successful

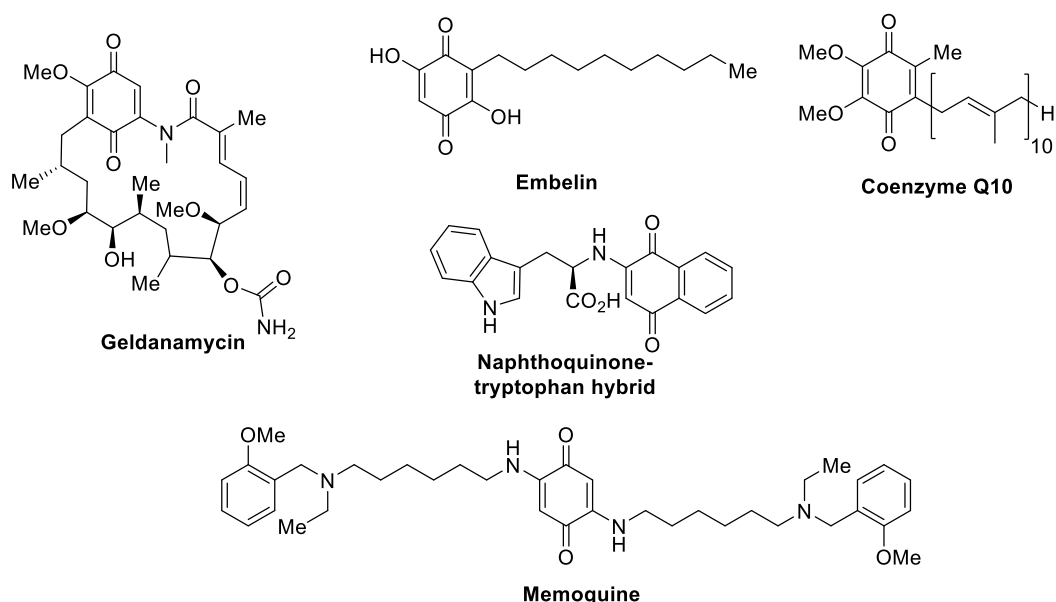


Figure 5.1

¹⁷⁴ Ko, S.H.; Choi, H.; Park, H.-H.; Lee, K.-Y.; Lee, Y.-J.; Kim, S. H. *Alzheimers Dement.* **2010**, *6*, S209.

¹⁷⁵ Magesh, S.; Chen, Y.; Hu, L. *Med. Res. Rev.* **2012**, *32*, 687-726.

¹⁷⁶ Momiyama, Y. *Atherosclerosis* **2014**, *237*, 433-434.

¹⁷⁷ Krishna Kumar, V. G.; Paul, A.; Gazit, E.; Segal, D. *Sci. Rep.* **2018**, *8*, 71.

compound developed against neurodegenerative diseases.¹⁷⁸ It shows a broad spectrum of activities, including ROS scavenging and inhibition of amyloid- β aggregation, beta-secretase 1 activity (BACE-1) and acetylcholinesterase. The antioxidant properties of memoquine were evaluated by direct ROS scavenging and *via* its prior transformation into its hydroquinone derivative by the NAD(P)H/quinone oxidoreductase 1 (NQO1). The hydroquinone may scavenge ROS to afford again the memoquine, which is able to re-start the redox cycle. It is important to note that NQO1 is overexpressed in hippocampal neurons in AD patients. Furthermore, memoquine inhibits AChE and BACE-1 at nanomolar concentrations, thus being able to improve cholinergic neuronal survival and decrease in tau hyperphosphorylation. All these pharmacological activities and its ability to cross the blood-brain barrier explain its ability to afford improvement memory in several animal models (Figure 5.2).

Memoquine was one of the first examples that suggested that the multitarget approach could be a successful strategy to treat multifactorial neurodegenerative diseases, while also highlighting the importance of quinones in medicinal chemistry.

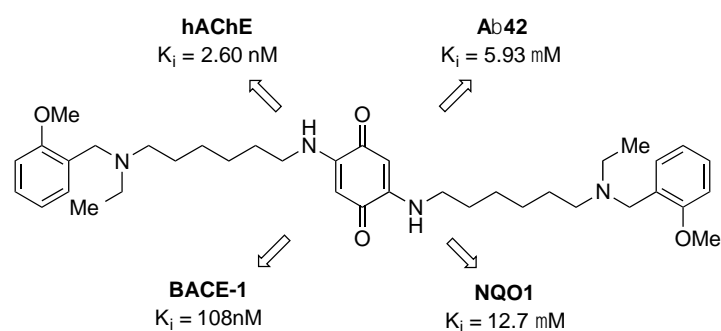


Figure 5.2

5.2. Design of quinone-melatonin based multitarget ligands

5-Methoxytryptamine and its N-acetylated derivative (melatonin) are produced in the pineal gland and their physiological role is the control of wake-sleep cycles. Furthermore, melatonin is a well-known antioxidant acting as a ROS scavenger, and its

¹⁷⁸ For a review, see: Bolognesi, M. L.; Cavalli, A.; Melchiorre, C. *Neurotherapeutics* **2009**, *6*, 152-162.

role in the induction of cytoprotective biochemical pathways is well documented.^{179, 180, 181}

On this basis, we designed the tryptamine-quinolinetrione hybrids I. In the first place, this hybrid structure contains a vinyllogous melatonin structure shown in. The quinolinone heterocyclic core possesses two electrophilic positions, presumably able to induce the Keap1-Nrf2-ARE pathway,¹⁸² and a 1,4-quinone that should be reduced by NQO1 to afford a hydroquinone-derivative with an improved antioxidant activity. This Keap1-Nrf2-ARE pathway activation induce the synthesis of phase I antioxidant enzymes like NQO1, among others. This increase in NQO1, combined with the reduction of quinone to an antioxidant hydroquinone for NQO1, is expected to induce a redox cycle with a very potent antioxidant effect (Figure 5.3).

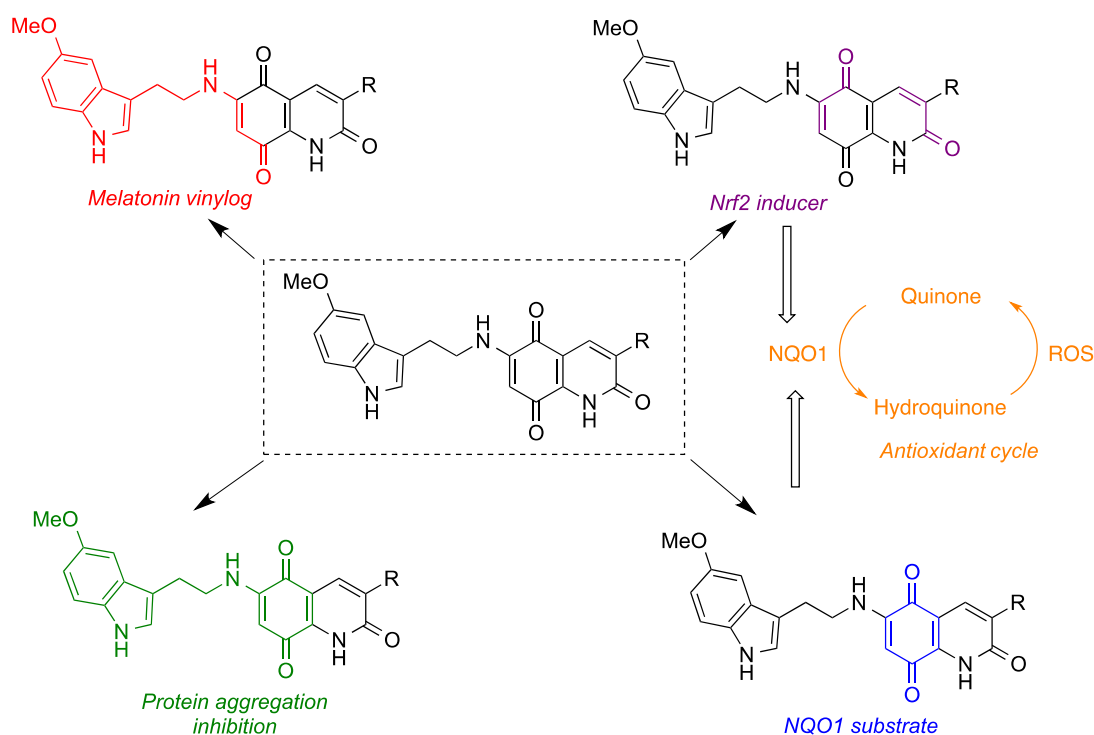


Figure 5.3

¹⁷⁹ Tan, D.-X.; Manchester, L. C.; Terron, M. P.; Flores, L. J.; Reiter, R. J. *J. Pineal Res.* **2007**, *42*, 28–42.

¹⁸⁰ Johns, J. R.; Platts, J. A. *Org. Biomol. Chem.* **2014**, *12*, 7820–7827.

¹⁸¹ Reiter, R. J.; Acuña-Castroviejo, D.; Tan, D. X.; Burkhardt, S. *Ann. N. Y. Acad. Sci.* **2001**, *939*, 200-215.

¹⁸² For an example of Nrf2 activation by a 2-quinolinetrione derivative, see: Hur, W.; Sun, Z.; Jiang, T.; Mason, D. E.; Peters, E. C.; Zhang, D. D.; Luesch, H.; Schultz, P. G.; Gray, N. S. *Chem. Biol.* **2010**, *17*, 537-547.

In order to obtain additional data towards a more meaningful structure-activity relationship, alternative linking points between quinone and tryptamine cores were also considered (Figure 5.4).

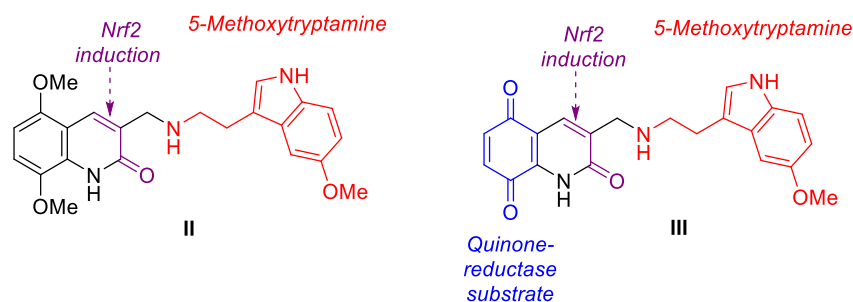


Figure 5.4

Electrophilic compounds such as quinones **III** can induce toxic effects by alkylation of biomolecules in a non-specific way.¹⁸³ It is relevant to point out that the starting quinones selected to obtain these hybrids and structurally related compounds were previously synthesized in our group and showed a good safety profile and low cytotoxicity.

5.3. Synthesis of tryptamine-quinolinetriene hybrids

5.3.1 Synthesis of 3-alkyl- and 3-formyl-5,8-dimethoxyquinolin-2-ones¹⁸⁴

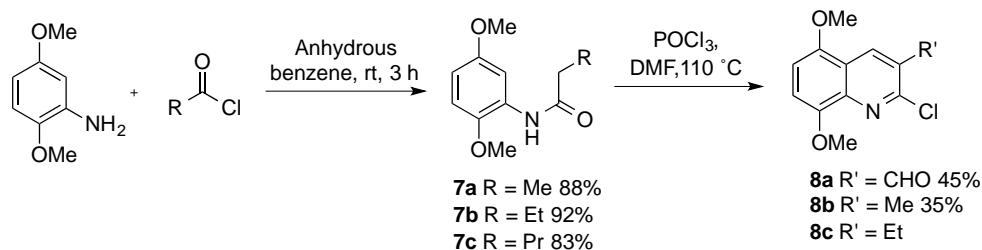
Anilides **7a-c** were synthesized in good yields by acylation of 2,5-dimethoxyaniline with the suitable acyl chloride, after purification by crystallization. The Meth-Cohn method was then employed to achieve the synthesis of 2,5-dimethoxyquinolines bearing alkyl or carboxaldehyde groups in its C-3 position. In this method, the starting amides were treated with the Vilsmeier-Haack reagent, obtained *in situ* from DMF and POCl₃. Afterwards, the suitable 2,5-dimethoxyanilide **7a-c** was added to give the 2-chloquinoline derivatives **8a-c** (Scheme 5.1).

The usual purification of compound **8a** by silica gel chromatography led to extensive decomposition. To improve the purification process, the silica gel was deactivated by stirring with a 0.1 M aqueous oxalic acid solution, filtration and oven drying. The use of

¹⁸³ Zheng, H.; Fridkin, M.; Youdim, M. *Perspect. Med. Chem.* **2015**, *7*, 1-8.

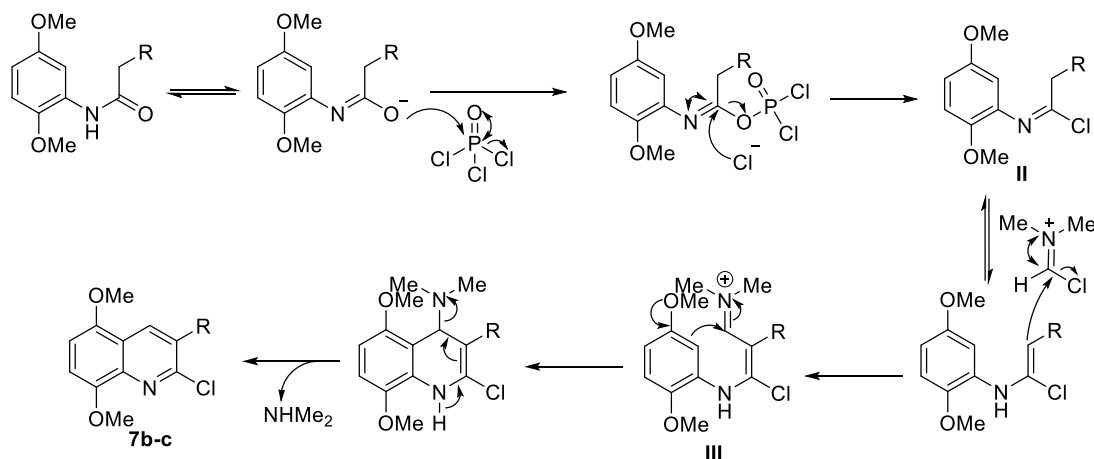
¹⁸⁴ A method from our group was used: Alonso, M. A.; Blanco, M. M.; Avendaño, C.; Menéndez, J. C. *Heterocycles* **1993**, *36*, 2315-2325.

this oxalic acid pre-treated silica gel led to improved results and increased the isolated yield of **2a** from 29% to 45%. Compound **8c** was sufficiently pure to be used in the next step without further purification.



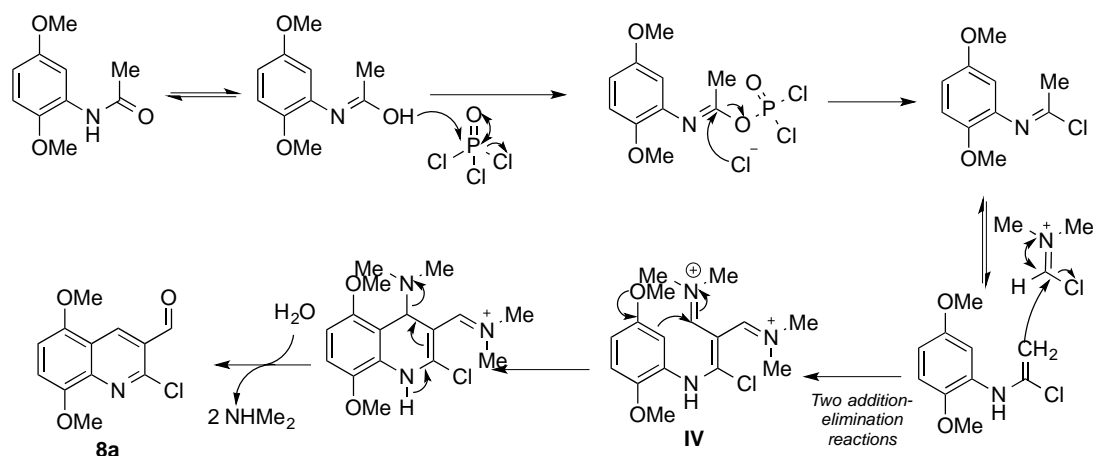
Scheme 5.1

The mechanism of the reaction starts with the formation of the Vilsmeier-Haack reagent from DMF and POCl_3 *via* intermediate **I**. Then, the same reaction takes place on the amide of compound **1** to yield the chloroimine intermediate **II**, which tautomerizes to an enamine and attacks the Vilsmeier reagent furnishing intermediate **III**. Finally, an electrophilic aromatic substitution (EAS) and a subsequent dimethylamine elimination affords compounds **8b-c** (Scheme 5.2).



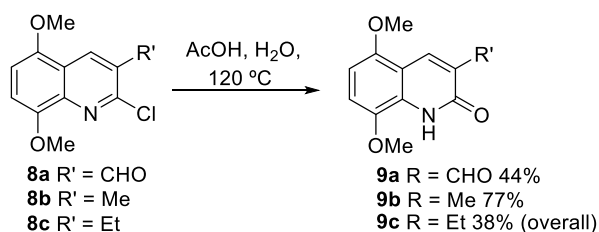
Scheme 5.2

This same procedure affords the 3-carboxaldehyde compound **8a** when compound **7a** was the starting material. In this case, two consecutive addition-elimination reactions of enamine **IV** to the Vilsmeier reagent afford intermediate **V**. Then, an electrophilic aromatic substitution (EAS) followed by dimethylamine elimination affords the 2-chloroquinoline substituted with a carboxaldehyde group in position 3 (compound **8a**), arising from hydrolysis of the iminium function during aqueous workup (Scheme 5.3).



Scheme 5.3

2-Chloroquinolines **8a-c** were finally treated with aqueous AcOH, affording the 5,8-dimethoxy-2(1*H*)-quinolinones **9a-c** in variable yields, after purification by silica gel chromatography (Scheme 5.4).

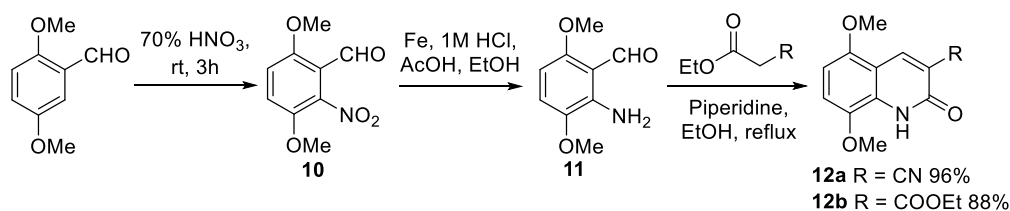


Scheme 5.4

5.3.2. Synthesis of 5,8-dimethoxyquinolin-2-ones bearing electron-withdrawing groups at C-3¹⁸⁵

The synthesis of bearing electron-withdrawing groups at C-3 was based on the use of the Friedländer quinoline synthesis. The *o*-aminobenzaldehyde **11**, a suitable starting material for this purpose, was obtained from the corresponding benzaldehyde derivative by nitration and subsequent reduction with Fe/HCl. Treatment of **11** with several acetate esters bearing electron-withdrawing substituents in a refluxing mixture of ethanol and piperidine afforded good yields of compounds **12a,b** that precipitated from the reaction mixture, allowing their purification by simple filtration (Scheme 5.5).

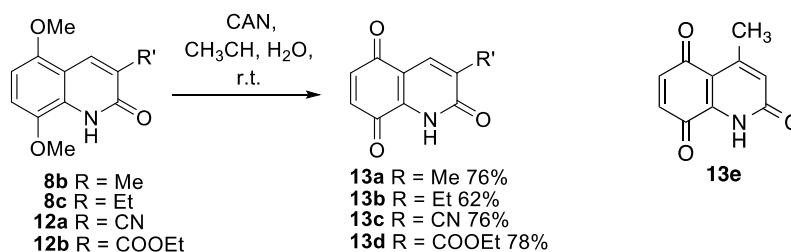
¹⁸⁵ A method from our group was used: Blanco, M. M.; Cabezas, N.; Avendaño, C.; Menéndez, J. C. *Heterocycles* **1993**, *36*, 1387-1398.



Scheme 5.5

5.3.3. Synthesis of 2,5,8-quinolinetriones

Finally, the 5,8-dimethoxyquinolines **8** and **12** were transformed into the corresponding quinones **13a-d** by oxidative demethylation with ceric ammonium nitrate (CAN) in a CH₃CN/H₂O mixture, followed by silica gel chromatography. The 4-methylquinone **13e**, which was available in our laboratory,¹⁸⁶ was also examined as a control (Scheme 5.6).

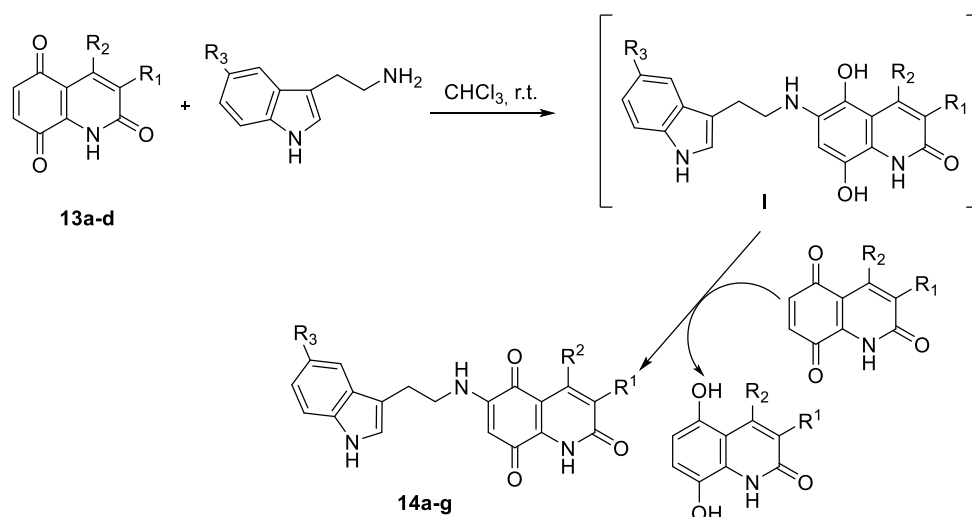


Scheme 5.6

5.3.4. Coupling of tryptamines and 2,5,8-quinolinetriones

The target hybrid compounds (**14**) were synthesized from the suitable quinolinetriones **13** and tryptamine derivatives by a aza-Michael addition/oxidation sequence (Scheme 5.7), generally in modest yields. (Table 5.1). The reaction can be proposed to involve an initial aza-Michael addition of the tryptamine derivative onto the most electrophilic position of the quinone at C-6 (see below), to furnish hydroquinone **I**. This intermediate is readily oxidized by a second molecule of the starting quinone, yielding the observed final product. The hydroquinone derived from compounds **13**, although not isolated, could be observed by TLC.

¹⁸⁶ Alonso, M. A.; López-Alvarado, P.; Avendaño, C.; Menéndez, J. C. *Tetrahedron*, **2003**, *59*, 2821-2830



Scheme 5.7

Table 5.1

Compound	R ¹	R ²	R ³	Yield (%)
14a	H	Me	H	24
14b	CN	H	H	62
14c	COOEt	H	H	32
14d	CN	H	OMe	43
14e	Me	H	H	56
14f	Et	H	H	47
14g	H	Me	OMe	47

The 1,4-addition was completely regioselective in favour of position 6, which is more electrophilic than C-7 due to its conjugation to a more electrophilic carbonyl group, owing to its conjugation to a lactam group that is electron-releasing at its nitrogen and electron-withdrawing at its carbonyl.¹⁸⁷ This reasoning was supported by a computational study that showed that C-6 has a higher Mulliken charge than C-7 in compound **13a** (Figure 5.5).

¹⁸⁷ For precedent of this complete regioselectivity in the addition of amines to 2,5,8-quinolinetrienes, see: Pascual-Alfonso, E.; Avendaño, C.; Menéndez, J. C. *Synlett* **2000**, 2000, 205-208.

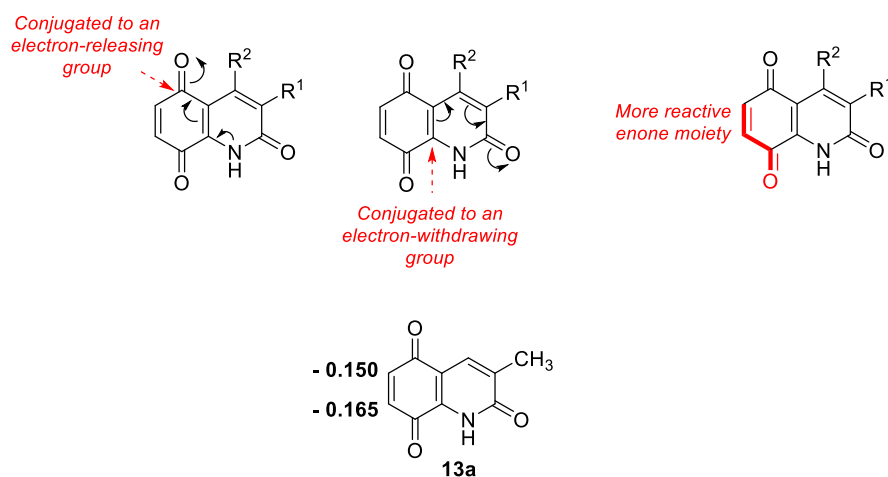
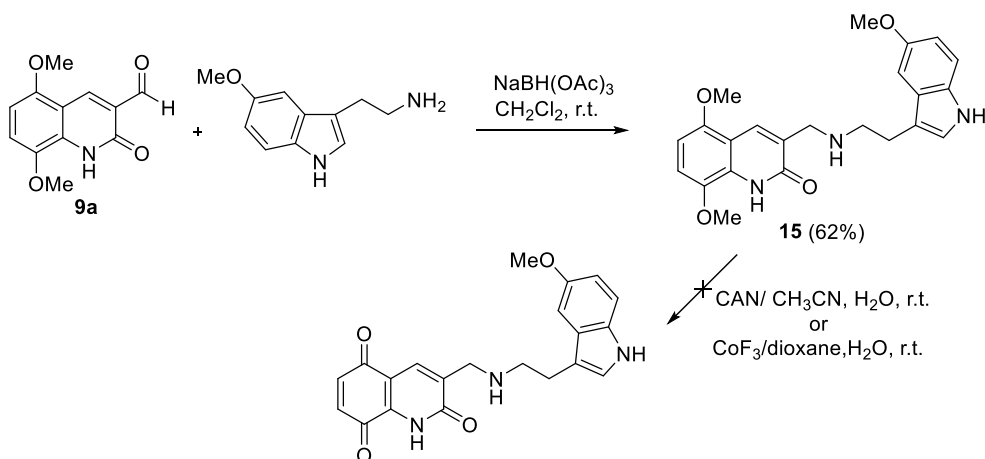


Figure 5.5

After the synthesis of compounds **14a-g**, another linking mode between tryptamine and the 2,5,8-quinolinetriene framework was studied. The synthesis of compound **15** was readily accomplished by a reductive amination of **9a** and 5-methoxytryptamine in the presence of sodium triacetoxyborohydride. Unfortunately, the attempted oxidative demethylation with CAN afforded a complex mixture, and a milder alternative such as cobalt trifluoride¹⁸⁸ gave a similar result (Scheme 5.8).



Scheme 5.8

The pharmacological study of compounds **14** is in progress in the group of Dr. Pilar Gómez-Serranillos, at the School of Pharmacy in Universidad Complutense. Preliminary data show a very potent antioxidant activity in the ORAC assay.

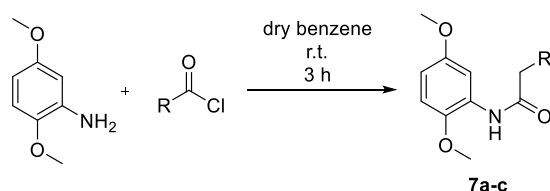
¹⁸⁸ (a) Tomatsu, A.; Takemura, S.; Hashimoto, K.; Nakata, M. *Synlett* **1999**, 1474–1476. (b) Pascual-Alfonso, E.; Avendaño, C.; Menéndez, J. C. *Tetrahedron Lett.* **2003**, *44*, 6003–6005.

5.4. Experimental section

General experimental details

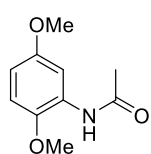
All reagents and solvents were of commercial quality and were used as received. Reactions were monitored by thin layer chromatography on aluminium plates coated with silica gel and fluorescent indicator. Microwave-assisted reactions were performed on a CEM Discover focused microwave reactor. Separations by flash chromatography were performed using a Combiflash Teledyne automated flash chromatograph or on conventional silica gel columns. Melting points were measured with a Kofler-type heating platine microscope from Reichert, 723 model, and are uncorrected. Infrared spectra were recorded with an Agilent Cary630 FTIR spectrophotometer with a diamond ATR accessory for solid and liquid samples, requiring no sample preparation; wavenumbers are given in cm^{-1} . NMR spectroscopic data were obtained using spectrometers maintained by the CAI de Resonancia Magnética, UCM, operating at 250, 300, 400 and 700 MHz for ^1H NMR and, 63, 100 and 176 MHz for ^{13}C NMR; chemical shifts are given in (δ) parts per million and coupling constants (J) in hertz. Elemental analyses were determined by the CAI de Microanálisis, Universidad Complutense, using a Leco CHNS-932 combustion microanalyzer. The enantiomeric excess analysis has been conducted in a HPLC Agilent 1220 Infinity LC with a chiral column ULTRON ES.

5.4.1. Synthesis of N-(2,5-dimethoxyphenyl)anilides 7

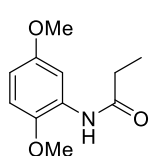


To a solution of 2,5-dimethoxyaniline (33 mmol, 1 eq.) in anhydrous toluene (50 mL) at 0 °C and under argon atmosphere was added the suitable acyl chloride (1.2 eq) and the mixture was stirred at room temperature for 3 h. Then, a 25% (w/v) sodium carbonate solution was added and both phases were separated. The aqueous phase was washed with CHCl_3 (3 x 50 mL). The combined organic layers were dried over anhydrous sodium sulphate, filtered and the solvent was removed under reduce pressure. The residue was crystallized from petroleum ether.

N-(2,5-Dimethoxyphenyl)acetamide (7a)

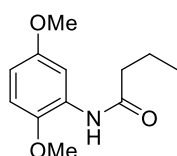


Beige solid (5.3 g, 88%); **mp**: 90 °C; ^1H RMN (250 MHz, CDCl_3) δ 8.10 (d, J = 3.0 Hz, 1H), 7.78 (s, 1H), 6.78 (d, J = 8.9 Hz, 1H), 6.56 (dd, J = 8.9, 3.0 Hz, 1H), 3.84 (s, 3H), 3.78 (s, 3H), 2.20 (s, 3H); ^{13}C RMN (63 MHz, CDCl_3) δ 168.4, 153.9, 141.9, 124.7, 110.7, 108.4, 106.1, 56.3, 55.9, 25.1; IR (neat, cm^{-1}): 3250, 1663, 1219; **elemental analysis (%) calcd. for $\text{C}_{10}\text{H}_{13}\text{NO}_3$** : C 61.53, H 6.71, N 7.18; found: C 61.52, H 6.59, N 7.26.

***N*-(2,5-Dimethoxyphenyl)propionamide (7b)**

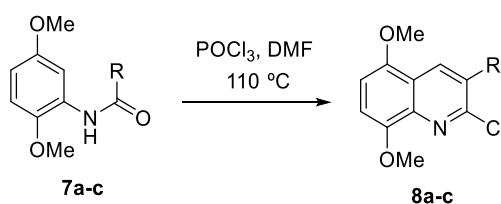
Brown solid (6.3 g, 92%); **mp**: 69-70 °C; **¹H RMN (250 MHz, CDCl₃)** δ 8.14 (d, *J* = 3.0 Hz, 1H), 7.80 (s, 1H), 6.76 (d, *J* = 8.9 Hz, 1H), 6.54 (dd, *J* = 8.9, 3.0 Hz, 1H), 3.81 (s, 3H), 3.76 (s, 3H), 2.41 (q, *J* = 7.5 Hz, 2H), 1.23 (t, *J* = 7.5 Hz, 3H); **¹³C RMN (63 MHz, CDCl₃)** δ 172.0, 153.9, 141.9, 128.4, 110.6, 108.4, 105.8, 56.2, 55.8, 25.1, 31.1, 9.7; **IR** (neat, cm⁻¹): 3245, 1656, 1217;

elemental analysis (%) calcd. for C₁₁H₁₅NO₃: C 63.14, H 7.23, N 6.69; found: C 63.11, H 7.07, N 6.83.

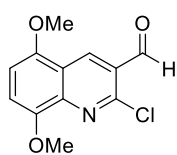
***N*-(2,5-Dimethoxyphenyl)butyramide (7c)**

Brown solid (6.0 g, 83%); **mp**: 40 °C; **¹H RMN (250 MHz, CDCl₃)** δ 8.15 (d, *J* = 2.9 Hz, 1H), 7.78 (s, 1H), 6.78 (d, *J* = 8.9 Hz, 1H), 6.55 (dd, *J* = 8.9, 3.0 Hz, 1H), 3.83 (s, 3H), 3.77 (s, 3H), 2.37 (t, *J* = 7.4 Hz, 2H), 1.80 – 1.71 (m, 2H), 1.00 (t, *J* = 7.4 Hz, 3H); **¹³C RMN (63 MHz, CDCl₃)** δ 171.3, 153.9, 141.9, 128.5, 110.7, 108.5, 105.8, 56.3, 55.9, 40.1, 19.1, 13.9; **IR**

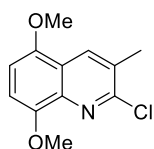
(neat, cm⁻¹): 3236, 1655, 1211; **elemental analysis (%) calcd. for C₁₂H₁₇NO₃**: C 64.55, H 7.67, N 6.27; found: C 64.22, H 7.46, N 6.51.

5.4.2. Synthesis of 2-chloro-5,8-dimethoxyquinolines 8

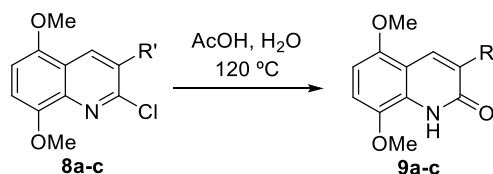
Phosphorous oxychloride (7 eq.) was added dropwise to DMF (3 eq.) at 0 °C under argon atmosphere and stirred for 30 min. Then the suitable anilide **7** (1 eq.) was added and the reaction was heated at 110 °C for 2 h. On completion of the reaction, the mixture was poured on ice, basified with 1M ammonium hydroxide solution, and extracted with CHCl₃ (3 x 50mL). The combined organic layers were dried over anhydrous sodium sulphate, filtered and the solvent was removed. The residue was purified by column chromatography on silica gel previously treated with a 0.1 M oxalic acid solution, eluting with a gradient from 4:1 to 1:1 hexane-ethyl acetate mixture.

2-Chloro-5,8-dimethoxyquinoline-3-carbaldehyde (8a)

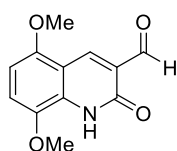
Prepared from anilide **7a** (2.6 mmol); yellow solid (287 mg, 45%); **mp**: 155-156 °C; **¹H RMN (250 MHz, CDCl₃)** δ 10.54 (s, 1H), 9.11 (s, 1H), 7.12 (d, *J* = 8.6 Hz, 1H), 6.81 (d, *J* = 8.6 Hz, 1H), 4.03 (s, 3H), 3.97 (s, 3H); **¹³C RMN (63 MHz, CDCl₃)** δ 189.4, 150.2, 148.4, 141.2, 136.1, 125.9, 120.2, 112.3, 105.3, 56.5, 56.1; **IR** (neat, cm⁻¹): 1688, 1263; **elemental analysis (%) calcd. for C₁₂H₁₀ClNO₃**: C 58.77, H 4.55, N 5.27, found: C 58.39, H 4.24, N 5.75.

2-Chloro-3-methyl-5,8-dimethoxyquinoline (8b)

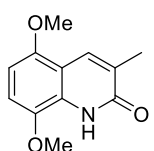
Prepared from anilide **7b** (2.4 mmol); beige solid (201 mg, 35%); **mp**: 108 °C; **¹H RMN (250 MHz, CDCl₃)** δ 8.33 (q, *J* = 0.9 Hz, 1H), 6.88 (d, *J* = 8.5 Hz, 1H), 6.72 (d, *J* = 8.5 Hz, 1H), 3.99 (s, 3H), 3.93 (s, 3H), 2.52 (d, *J* = 0.8 Hz, 3H); **¹³C RMN (63 MHz, CDCl₃)** δ 151.9, 148.6, 148.2, 138.7, 133.1, 130.1, 121.0, 107.2, 104.3, 56.1, 55.9, 20.3; **IR** (neat, cm⁻¹): 1262; **elemental analysis (%) calcd. for C₁₂H₁₂ClNO₂**: C 60.64, H 5.09, N 5.89; found: C 60.55, H 5.05, N 6.11.

5.4.3. Synthesis of 5,8-dimethoxy-2(1H)-quinolinones 9

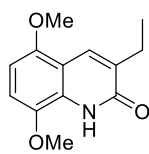
A solution of suitable 2-chloroquinoline (1 eq.) in acetic acid (26 eq.) and water (3 eq.) was refluxed for 3 h. On completion of the reaction, the mixture was poured into ice, basified until pH = 10-11 with 25% ammonium hydroxide solution, and extracted with CHCl₃ (3 x 50 mL). The combined organic layers were dried over anhydrous sodium sulphate, filtered and the solvent was removed in vacuum. The residue was purified by column chromatography on silica gel previously treated with a 0.1 M oxalic acid solution, eluting with a gradient from 4:1 to 1:1 hexane-ethyl acetate mixture.

5,8-Dimethoxy-2-oxo-1,2-dihydroquinoline-3-carbaldehyde (9a)

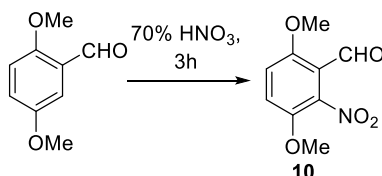
Prepared from chloroquinoline **8a** (1.1 mmol); yellow solid (112 mg, 44%); **mp**: desc. 231 °C; **¹H RMN (250 MHz, CDCl₃)** δ 10.41 (s, 1H), 9.32 (br s, 1H), 8.82 (s, 1H), 6.99 (d, *J* = 8.7 Hz, 1H), 6.50 (d, *J* = 8.8 Hz, 1H), 3.94 (s, 3H), 3.91 (s, 3H); **¹³C RMN (63 MHz, CDCl₃)** δ 189.6, 161.5, 152.0, 139.5, 138.6, 131.8, 125.0, 114.1, 110.6, 101.8, 56.5, 56.0; **IR** (neat, cm⁻¹): 3009, 2843, 1685, 1645, 1264; **elemental analysis (%) calcd. for C₁₂H₁₁NO₄**: C 63.15, H 5.30, N 5.67; found: C 62.54, H 5.43, N 5.38.

5,8-Dimethoxy-3-methylquinolin-2(1H)-one (9b)

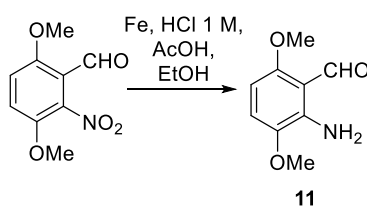
Prepared from chloroquinoline **8b** (0.8 mmol); beige solid (133 mg, 77%); **mp**: 158-159 °C; **¹H RMN (250 MHz, MeOD)** δ 8.00 (q, *J* = 1.2 Hz, 1H), 6.95 (d, *J* = 8.7 Hz, 1H), 6.60 (d, *J* = 8.7 Hz, 1H), 3.92 (s, 3H), 3.88 (s, 3H), 2.18 (d, *J* = 1.2 Hz, 3H); **¹³C RMN (63 MHz, MeOD)** δ 164.8, 150.4, 141.4, 133.6, 129.8, 129.5, 112.6, 110.8, 102.8, 56.6, 56.3, 17.1; **IR** (neat, cm⁻¹): 2987, 1638, 1244; **elemental analysis (%) calcd. for C₁₂H₁₃NO₃**: C 65.74, H 5.98, N 5.39, found: C 65.20, H 5.89, N 6.41.

5,8-Dimethoxy-3-ethylquinolin-2(1H)-one (9c)

Prepared from chloroquinoline **8c** (2 mmol); orange solid (175 mg, 38%); **mp**: 154-155 °C; $^1\text{H NMR}$ (250 MHz, CDCl_3) δ 9.24 (s, 1H), 7.89 (t, $J = 1.2$ Hz, 1H), 6.76 (d, $J = 8.7$ Hz, 1H), 6.44 (d, $J = 8.7$ Hz, 1H), 3.87 (s, 3H), 3.86 (s, 3H), 2.64 (qd, $J = 7.4, 1.2$ Hz, 2H), 1.25 (t, $J = 7.4$ Hz, 3H); $^{13}\text{C NMR}$ (63 MHz, CDCl_3) δ 162.3, 149.4, 139.6, 135.2, 130.0, 128.4, 111.3, 109.1, 101.1, 56.2, 55.8, 23.6, 12.8; **IR** (neat, cm^{-1}): 3128, 2836, 1639, 1237; **elemental analysis (%) calcd. for $\text{C}_{13}\text{H}_{15}\text{NO}_3$** : C 66.94, H 6.48, N 6.00, found: C 66.50, H 6.45, N 6.07.

5.4.4. Preparation of 3,6-dimethoxy-2-nitrobenzaldehyde 10

2,5-Dimethoxybenzaldehyde (5 g, 30 mmol) was dissolved in ethyl ether (50 ml) and glacial acetic acid (50 ml) mixture, and 70 % nitric acid (13.5 ml) was added dropwise. The reaction was stirred at room temperature overnight. Then, the solvent was removed and the residue was dissolved in ethyl ether (100 ml) and washed with water (3 x 25 ml). The organic layer was dried over Na_2SO_4 , filtered and the solvent was removed. The residue was chromatographed on silica gel, eluting with a 3:2 hexane-ethyl ether mixture to yield 3.63 g (60 %) of **10**. $^1\text{H NMR}$ (250 MHz, CDCl_3) δ 10.38 (s, 1H), 7.31 (d, $J = 9.5$ Hz, 1H), 7.14 (d, $J = 9.3$ Hz, 1H), 3.97 (s, 3H), 3.89 (s, 3H). NMR data are identical to those found in the literature.¹⁸⁹

5.4.5. Preparation of 2-amino-3,6-dimethoxybenzaldehyde 11

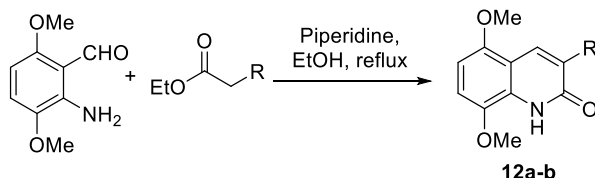
To a solution of **10** (2 g, 9.5 mmol) in EtOH (40 mL) and AcOH (10 mL) was slowly added iron powder (2.1 g). The reaction was cooled to 0 °C, treated with 1M HCl solution (10 mL) and was heated to reflux for 2 h. Then, it was allowed to cool to room temperature and the mixture was filtered through a Celite pad and the filtrate concentrated. The resulting oil was dissolved in EtOAc (100 mL) and basified to pH 8 with a 1M NaOH solution. The organic layer was separated and washed with saturated aqueous NaHCO_3 solution (2 x 30 mL) and brine (30 mL). The organic layer was dried

¹⁸⁹ Blanco, M. M.; Avendaño, C.; Cabezas, N.; Menéndez, J. C. *Synth. Commun.* **1993**, *23*, 1351-1356.

over Na_2SO_4 , filtered and the solvent was removed to provide 1.5 g (87%) of 2-aminobenzaldehyde **11**.

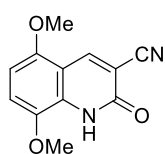
$^1\text{H NMR}$ (250 MHz, CDCl_3) δ 10.39 (s, 1H), 6.75 (d, $J = 8.6$ Hz, 1H), 5.97 (d, $J = 8.6$ Hz, 1H), 3.80 (s, 6H). NMR data are identical to those found in the literature.¹⁹⁰

5.4.6. Friedländer synthesis of 5,8-dimethoxyquinolin-2(1H)-one derivatives **12**



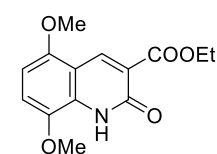
2-Amino-3,6-dimethoxybenzaldehyde (2 eq) and piperidine (1 eq) was dissolved in ethanol (xx mL). Then, the suitable ester was added and the mixture was refluxed and monitored by TLC until the *o*-aminobenzaldehyde was completely consumed. The mixture was cooled to room temperature and the formed precipitate was filtered and washed with a small amount of cold ethanol.

5,8-Dimethoxy-2-oxo-1,2-dihydroquinoline-3-carbonitrile (**12a**)



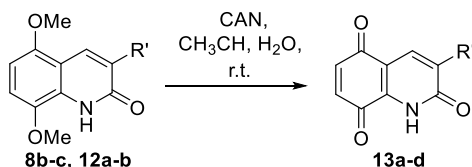
Prepared from 2-amino-3,6-dimethoxybenzaldehyde (4 mmol); yellow solid (880 mg, 96%); $^1\text{H NMR}$ (250 MHz, $d_6\text{-DMSO}$) δ 11.75 (br s, 1H), 8.67 (d, $J = 0.4$ Hz, 1H), 7.26 (d, $J = 8.8$ Hz, 1H), 6.73 (d, $J = 8.8$ Hz, 1H), 3.87 (s, 3H), 3.84 (s, 3H). NMR data are identical to those found in the literature.¹⁹⁰

Ethyl 5,8-dimethoxy-2-oxo-1,2-dihydroquinoline-3-carboxylate (**12b**)



Prepared from 2-amino-3,6-dimethoxybenzaldehyde (4 mmol); yellow solid (980 mg, 88%); $^1\text{H NMR}$ (250 MHz, CDCl_3) δ 8.72 (s, 2H), 8.66 (s, 2H), 7.10 (d, $J = 8.0$ Hz, 1H), 6.69 (d, $J = 8.0$ Hz, 1H), 4.43 (q, $J = 7.1$ Hz, 2H), 3.60 (s, 6H), 1.41 (t, $J = 7.1$ Hz, 3H). NMR data are identical to those found in the literature.¹⁹⁰

5.4.7. Synthesis of 2,5,8(1H)-quinolinetrienes **13**

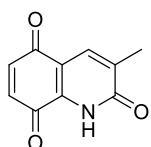


Cerium ammonium nitrate (2.2 eq.) was added portionwise to a suspension of the suitable 5,8-dimethoxy-2(1H)-quinolinone (1 eq.) in acetonitrile-water (5-2 mL per mol). The orange solution was stirred at room temperature for 1 h and then diluted

¹⁹⁰ Blanco, M.M.; Avendaño, C.; Cabezas, N.; Menéndez, J. C. *Heterocycles*, **1993**, *36*, 1387-1398.

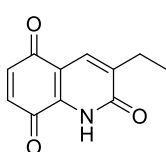
with water and extracted with CHCl_3 (3 x 50 mL). The combined organic layers were dried over sodium sulphate, filtered and the solvent was removed under vacuum.

3-Methylquinoline-2,5,8(1H)-trione (13a)



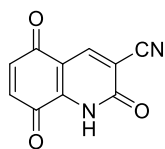
Prepared from quinolinone **8b** (0.5 mmol); orange solid (98mg, 76%); **mp**: 207 °C; $^1\text{H NMR}$ (250 MHz, CDCl_3) δ 9.78 (br s, 1H), 7.78 (q, $J = 1.1$ Hz, 1H), 6.90 (d, $J = 10.4$ Hz, 1H), 6.85 (d, $J = 10.4$ Hz, 1H), 2.27 (d, $J = 1.1$ Hz, 3H); $^{13}\text{C NMR}$ (63 MHz, CDCl_3) δ 182.6, 179.6, 162.0, 138.4, 138.2, 135.6, 134.8, 132.0, 115.2, 17.5; **IR** (neat, cm^{-1}): 2920, 1637.

3-Ethylquinoline-2,5,8(1H)-trione (13b)



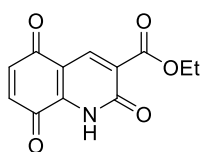
Prepared from quinolinone **8c** (0.7 mmol); orange solid (78 mg, 62%); **mp**: 165-167 °C; $^1\text{H NMR}$ (250 MHz, CDCl_3) δ 9.58 (br s, 1H), 7.76 (t, $J = 1.2$ Hz, 1H), 6.90 (d, $J = 10.4$ Hz, 1H), 6.86 (d, $J = 10.4$ Hz, 1H), 2.67 (qd, $J = 7.4, 1.2$ Hz, 2H), 1.26 (t, $J = 7.4$ Hz, 3H); $^{13}\text{C NMR}$ (63 MHz, CDCl_3) δ 182.71, 179.6, 161.6, 143.8, 138.3, 135.4, 134.8, 130.1, 115.2, 24.0, 12.1; **IR** (neat, cm^{-1}): 2919, 1635; **elemental analysis (%) calcd. for $\text{C}_{11}\text{H}_9\text{NO}_3$** : C 65.02, H 4.46, N 6.89, found: C 64.56, H 4.42, N 6.73.

2,5,8-Trioxo-1,2,5,8-tetrahydroquinoline-3-carbonitrile (13c)



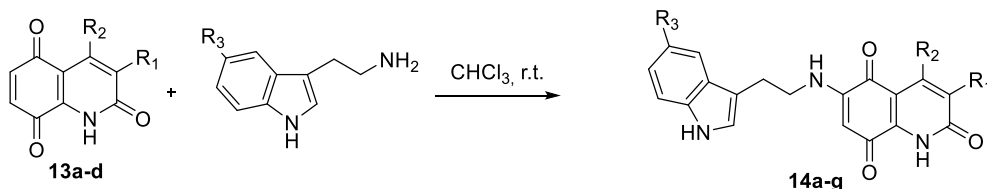
Prepared from quinolinone **12a** (0.5 mmol); orange solid (76 mg, 76%); $^1\text{H NMR}$ (250 MHz, d_6 -acetone) δ 11.68 (br s, 1H), 8.54 (s, 1H), 7.14 (d, $J = 10.4$ Hz, 1H), 7.06 (d, $J = 10.4$ Hz, 1H). NMR data are identical to those found in the literature.¹⁹⁰

Ethyl 2,5,8-trioxo-1,2,5,8-tetrahydroquinoline-3-carboxylate (13d)



Prepared from quinolinone **12b** (0.5 mmol); orange solid (96 mg, 78%); $^1\text{H NMR}$ (250 MHz, CDCl_3) δ 9.63 (s, 1H), 8.66 (s, 2H), 7.00 (d, $J = 1.0$ Hz, 2H), 4.43 (q, $J = 7.1$ Hz, 2H), 1.41 (t, $J = 7.1$ Hz, 3H). NMR data are identical to those found in the literature.¹⁹⁰

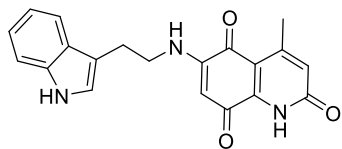
5.4.8. Synthesis of tryptamine-quinone hybrids 14



The suitable quinone **13** (0.22 mmol, 1.2 eq.) was dissolved in CHCl_3 (5 mL) and then tryptamine (1.0 eq) was added portionwise. The mixture was vigorously stirred for 1 h and the reaction was monitored by TLC. When tryptamine was no longer detected, the solvent was removed under vacuum and the residue was chromatographed on silica

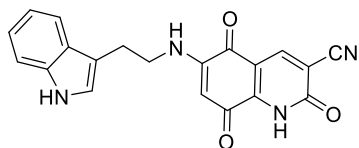
gel using a 90:10:1 CH₂Cl₂:MeOH: Et₃N mixture as eluent. The residue was recrystallized from CHCl₃-hexane to give the desired compound.

4-Methyl-6-[(2-(1H-indol-3-yl)ethyl)amino]quinoline-2,5,8(1H)-trione (14a)



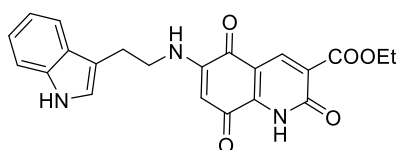
Prepared from tryptamine (0.85 mmol); red solid (45 mg, 24%); **mp**: >250 °C; **¹H NMR (500 MHz, *d*₆-DMSO)** δ 11.30 (s, 1H), 10.87 (s, 1H), 8.00 (t, *J* = 5.8 Hz, 1H), 7.56 (d, *J* = 7.8 Hz, 1H), 7.34 (d, *J* = 7.8 Hz, 1H), 7.25 (s, 1H), 7.07 (t, *J* = 7.5 Hz, 1H), 6.99 (t, *J* = 7.5 Hz, 1H), 6.36 (s, 1H), 5.61 (s, 1H), 3.50 (q, *J* = 7.3 Hz, 2H), 3.01 (t, *J* = 7.3 Hz, 2H), 2.45 (app. s, 3H); **¹³C NMR (126 MHz, *d*₆-DMSO)** δ 179.07, 160.48, 150.35, 149.45, 143.16, 136.22, 127.07, 126.39, 123.15, 122.81, 121.01, 118.33, 118.18, 111.42, 110.93, 110.80, 94.51, 42.84, 23.31, 21.66; **IR** (neat, cm⁻¹): 3301, 3276, 1651, 1618, 1568, 1460, 1369, 1278, 740; **HRMS (MALDI-TOF)**: found *m/z* 370.1168 [M+Na]⁺, calcd. for C₂₀H₁₇N₃O₃Na 370.1174.

6-[(2-(1H-Indol-3-yl)ethyl)amino]-2,5,8-trioxo-1,2,5,8-tetrahydroquinoline-3-carbonitrile (14b)

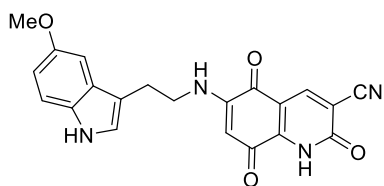


Prepared from 5-methoxytryptamine (0.3 mmol); purple solid (40 mg, 62%); **mp**: >250 °C; **¹H NMR (250 MHz, *d*₆-DMSO)** δ 12.82 (s, 1H), 10.91 (s, 1H), 8.53 (s, 1H), 8.26 (t, *J* = 5.9 Hz, 1H), 7.58 (d, *J* = 7.8 Hz, 1H), 7.36 (d, *J* = 7.8 Hz, 1H), 7.27 (d, *J* = 2.0 Hz, 1H), 7.09 (t, *J* = 7.8 Hz, 1H), 7.01 (t, *J* = 7.8 Hz, 1H), 5.76 (s, 1H), 3.53 (q, *J* = 7.0 Hz, 2H), 3.03 (t, *J* = 7.0 Hz, 2H); **¹³C NMR (63 MHz, *d*₆-DMSO)** δ 177.5, 174.5, 160.4, 149.2, 146.2, 144.4, 136.6, 127.4, 123.6, 121.4, 118.7, 118.5, 115.9, 111.8, 111.6, 111.3, 106.3, 97.5, 43.3, 23.7; **IR** (neat, cm⁻¹): 3353, 3228, 2343, 1665, 1578, 1560, 1461, 1255, 741; **HRMS (MALDI-TOF)**: found *m/z* 359.1135 [M+1]⁺, calcd. for C₂₀H₁₅N₄O₃ 359.1144.

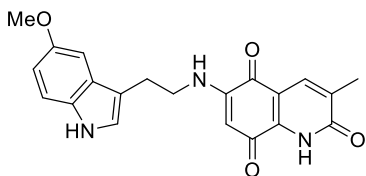
Ethyl 6-[(2-(1H-indol-3-yl)ethyl)amino]-2,5,8-trioxo-1,2,5,8-tetrahydroquinoline-3-carboxylate (14c)



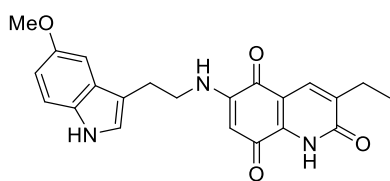
Prepared from tryptamine (0.85 mmol); purple solid (66 mg, 32%); **mp**: >250 °C; **¹H NMR (250 MHz, *d*₆-DMSO)** δ 12.20 (br s, 1H), 10.91 (br s, 1H), 8.31 (s, 1H), 8.12 (t, *J* = 5.0 Hz, 1H), 7.58 (d, *J* = 7.8 Hz, 1H), 7.36 (d, *J* = 7.8 Hz, 1H), 7.28 (s, 1H), 7.09 (t, *J* = 7.8 Hz, 1H), 7.01 (t, *J* = 7.8 Hz, 1H), 5.70 (s, 1H), 4.26 (q, *J* = 7.1 Hz, 2H), 3.52 (q, *J* = 6.8 Hz, 2H), 3.03 (t, *J* = 6.8 Hz, 2H), 1.30 (t, *J* = 7.1 Hz, 3H); **¹³C NMR (63 MHz, *d*₆-DMSO)** δ 177.6, 164.6, 154.0, 149.3, 139.8, 138.8, 136.3, 127.1, 123.2, 121.8, 121.1, 118.4, 118.3, 111.5, 111.0, 110.6, 97.1, 60.6, 42.9, 23.4, 14.2. **IR** (neat, cm⁻¹): 3250, 3222, 1720, 1562, 1468, 1256, 1228, 738; **HRMS (MALDI-TOF)**: found *m/z* 406.1404 [M+1]⁺, calcd. for C₂₂H₂₀N₃O₅ 406.1403.

6-[(2-(5-Methoxy-1*H*-indol-3-yl)ethyl)amino]-2,5,8-trioxo-1,2,5,8-tetrahydroquinoline-3-carbonitrile (14d)

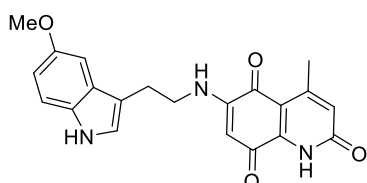
Prepared from 5-methoxytryptamine (0.85 mmol); purple solid (92 mg, 43%); **mp**: >250 °C; **¹H NMR (500 MHz, *d*₆-DMSO)** δ 12.79 (br s, 1H), 10.70 (br s, 1H), 8.53 (s, 1H), 8.24 (t, *J* = 6.0 Hz, 1H), 7.23 (d, *J* = 8.7 Hz, 1H), 7.21 (d, *J* = 2.1 Hz, 1H), 7.05 (d, *J* = 2.1 Hz, 2H), 6.71 (dd, *J* = 8.7, 2.1 Hz, 1H), 3.77 (s, 3H), 3.51 (dd, *J* = 13.8, 7.0 Hz, 2H), 2.98 (t, *J* = 7.0 Hz, 2H); **¹³C NMR (126 MHz, *d*₆-DMSO)** δ 177.5, 174.1, 160.0, 153.4, 149.2, 145.9, 144.4, 131.7, 127.8, 124.2, 115.7, 112.4, 111.5, 111.1, 106.6, 100.4, 97.4, 79.6, 55.7, 43.4, 23.8; **IR (neat, cm⁻¹)**: 3294, 2228, 1656, 1586, 1562, 1316, 1260, 1210, 790; **HRMS (MALDI-TOF)**: found *m/z* 411.1087 [M+Na]⁺, calcd. for C₂₁H₁₆N₄O₄Na 411.1070.

3-Methyl-6-[(2-(5-methoxy-1*H*-indol-3-yl)ethyl)amino]quinolin-2,5,8(1*H*)-trione (14e)

Prepared from 5-methoxytryptamine (0.3 mmol); purple solid (40 mg, 56%); **mp**: desc. at 148 °C; **¹H RMN (250 MHz, *d*₆-DMSO)** δ 11.57 (s, 1H), 10.69 (s, 1H), 8.31 (s, 1H), 7.96 (s, 1H), 7.72 (s, 1H), 7.23-7.19 (m, 2H), 7.04 (s, 1H), 6.70 (d, *J* = 7.1 Hz, 1H), 5.57 (s, 1H), 3.75 (s, 3H), 3.49-3.42 (m, 2H), 2.97 (t, *J* = 7.6 Hz, 2H), 2.06 (s, 3H); **¹³C RMN (63 MHz, *d*₆-DMSO)** δ 178.5, 175.3, 162.3, 153.0, 148.5, 131.3, 127.4, 123.8, 112.1, 111.2, 110.8, 99.9, 95.1, 79.2, 55.3, 42.9, 23.4, 16.5; **IR (neat, cm⁻¹)**: 3326; 3218, 1649, 1624, 1255, 1200; **HRMS (MALDI-TOF)**: found *m/z* 400.1278 [M+Na]⁺, calcd. for C₂₁H₁₉N₃O₄Na 400.1273.

3-Ethyl-6-[(2-(5-methoxy-1*H*-indol-3-yl)ethyl)amino]quinoline-2,5,8(1*H*)-trione (14f)

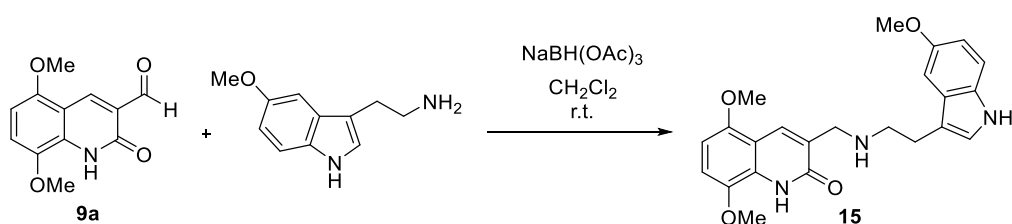
Prepared from 5-methoxytryptamine (0.3 mmol); purple solid (33mg, 47%); **mp**: desc. at 151 °C; **¹H RMN (250 MHz, *d*₆-DMSO)** δ 10.71 (d, *J* = 1.0 Hz, 1H), 7.99 (br s, 1H), 7.64 (s, 1H), 7.22 (d, *J* = 8.8 Hz, 2H), 7.20 (s, 1H), 7.04 (d, *J* = 2.4 Hz, 1H), 6.70 (dd, *J* = 8.8, 2.4 Hz, 1H), 5.58 (s, 1H), 3.75 (s, 3H), 3.51 – 3.42 (m, 2H), 2.97 (t, *J* = 7.2 Hz, 2H), 2.43 (qd, *J* = 7.4 Hz, 1.0 Hz, 2H), 1.11 (t, *J* = 7.4 Hz, 3H); **¹³C RMN (63 MHz, *d*₆-DMSO)** δ 178.6, 175.3, 161.9, 153.1, 148.5, 140.3, 137.7, 131.3, 129.7, 127.5, 123.8, 112.1, 111.2, 110.8, 99.9, 95.2, 55.3, 23.4, 22.9, 12.3; **IR (neat, cm⁻¹)**: 3361, 3035, 1643, 1624, 1254, 1206; **HRMS (MALDI-TOF)**: found *m/z* 392.1606 [M+1]⁺, calcd. for C₂₂H₂₂N₃O₄ 392.1611.

Methyl-6-[(2-(5-methoxy-1*H*-indol-3-yl)ethyl)amino]quinoline-2,5,8(1*H*)-trione (14g)

Prepared from 5-methoxytryptamine (0.85 mmol); purple solid (88 mg, 47%); **mp**: 241 °C; **¹H NMR (250 MHz, *d*₆-DMSO)** δ 11.34 (s, 1H), 10.71 (s, 1H), 8.03 (t, *J* = 5.9 Hz, 1H), 7.23 (d, *J* = 6.3 Hz, 1H), 7.21 (s, 1H), 7.05 (d, *J*

= 2.4 Hz, 1H), 6.72 (dd, $J = 8.8, 2.4$ Hz, 1H), 6.37 (d, $J = 0.9$ Hz, 1H), 5.63 (s, 1H), 3.77 (s, 3H), 3.49 (q, $J = 7.1$ Hz, 2H), 2.98 (t, $J = 7.1$ Hz, 2H), 2.46 (d, $J = 0.9$ Hz, 3H); ^{13}C NMR (63 MHz, d_6 -DMSO) δ 179.5, 174.7, 160.9, 153.4, 150.7, 149.8, 131.7, 130.7, 129.9, 127.8, 124.2, 112.4, 111.5, 111.1, 100.3, 94.9, 79.5, 55.6, 43.3, 23.8, 22.0; IR (neat, cm^{-1}): 3360, 3276, 1653, 1573, 1453, 1372, 1215, 755; HRMS (MALDI-TOF): found m/z 378.1431 [$\text{M}+1$] $^+$, calcd. for $\text{C}_{21}\text{H}_{20}\text{N}_3\text{O}_4$ 378.1454.

5.4.9. Synthesis of 5,8-dimethoxy-3-(((2-(5-methoxy-1H-indol-3-yl)ethyl)amino)-methyl)quinolin-2(1H)-one (15)



Quinoline **9a** (0.4 mmol, 1 eq.) and 5-methoxytryptamine (0.4 mmol, 1 eq.) were dissolved in anhydrous CH_2Cl_2 (10 mL) under argon atmosphere and 4Å molecular sieves were added. The mixture was stirred at room temperature for 1 h. The imine formation was monitored by ^1H -RMN. Then, the reaction was cooled to 0 °C and sodium triacetoxyborohydride (1.3 eq.) was added portionwise and the mixture was stirred at room temperature overnight. When the reaction was finished a saturated Na_2CO_3 solution was added and it was extracted with CH_2Cl_2 (3 x 50 mL). The combined organic layers were dried over anhydrous sodium sulphate, filtered and the solvent was removed to give 105 mg (62%) of the title compound as a white solid.

Mp: 122-124 °C; ^1H NMR (250 MHz, CDCl_3) δ 8.18 (s, 1H), 8.05 (s, 1H), 7.20 (d, $J = 8.8$ Hz, 1H), 7.05 (d, $J = 2.0$ Hz, 1H), 6.94 (d, $J = 2.4$ Hz, 1H), 6.83 (d, $J = 8.7$ Hz, 1H), 6.75 (dd, $J = 8.8, 2.4$ Hz, 1H), 6.48 (d, $J = 8.7$ Hz, 1H), 3.91 (s, 3H), 3.87 (s, 5H), 3.74 (s, 3H), 3.12 – 2.97 (m, 4H); ^{13}C NMR (63 MHz, CDCl_3) δ 161.8, 154.0, 149.8, 139.7, 133.1, 131.6, 128.9, 128.7, 127.6, 123.4, 112.4, 112.4, 112.1, 110.9, 110.1, 101.5, 100.2, 56.3, 55.8, 55.8, 49.5, 48.7, 25.3; IR (neat, cm^{-1}): 3221, 1643, 1617, 1249, 1211; elemental analysis (%) calcd. for $\text{C}_{23}\text{H}_{27}\text{N}_3\text{O}_4$: C 67.46, H 6.65, N 10.26, found: C 67.61, H 6.77, N 10.11.

CHAPTER 6. AZA-CGP-37157/LIPOIC ACID

HYBRIDS

6.1. Calcium homeostasis and neurodegenerative diseases

Calcium plays a central role as a second messenger in all cell types and is related to several biochemical pathways that include motility-related processes involving the cytoskeleton, secretion processes, enzyme phosphorylation/dephosphorylation and cellular death. Calcium is essential in excitable cells, particularly in neurons where it is crucial for synaptic transmission and neuronal plasticity in the neuron environment signalling process.

To maintain a suitable brain function, all these processes and the movement of Ca^{2+} through the plasma membrane, endoplasmic reticulum and mitochondria are coordinated and controlled by a complex network formed by a vast array of Ca^{2+} ion channels, pumps and exchangers, together with G-coupled receptors and Ca^{2+} binding proteins. All these proteins contribute to Ca^{2+} homeostasis and have been described as the “neuronal Ca^{2+} signalling toolkit”.¹⁹¹

6.1.1. Plasma membrane Ca^{2+} flow in neuronal physiology

The Ca^{2+} influx across the cell membrane is operated by Ca^{2+} channels, which are classified into three groups according to their opening mechanism: voltage-gated calcium channels (VGCC), receptor-operated calcium channels (ROCC) and store-operated calcium channels (SOCC).¹⁹²

VGCCs play a central role in neuronal impulse generation and propagation and cellular homeostasis associated to Ca^{2+} entry. These receptors are constituted by five subunits, namely $\alpha 1$, $\alpha 2$, β , γ and δ . They are divided into three families, Cav 1, Cav 2, Cav 3, depending on the $\alpha 1$ pore-forming subunit. Also, VGCCs can be classified into six classes (L, N, P, P, Q, R and T) based on the type of current accomplished. Cav 2 channels are responsible for neurotransmitter release and initiation of synaptic transmission.¹⁹³

ROCC activation was performed by extracellular ligands, usually neurotransmitters, like the most important excitatory neurotransmitter in the brain, L-glutamate. This

¹⁹¹ Brini, M.; Cali, T.; Ottolini, D.; Carafoli, E. *Cell. Mol. Life Sci.*, **2014**, *71*, 2787-2814.

¹⁹² Prakriya, M.; Feske, S.; Gwack, Y.; Srikanth, S.; Rao, A.; Hogan, P. G. *Nature* **2006**, *443*, 230-233.

¹⁹³ Miyashita, T.; Oda, Y.; Horiuchi, J.; Yin, J. C.; Morimoto, T.; Saitoe, M. *Neuron* **2012**, *74*, 887-898.

neurotransmitter can activate two types of ionotropic receptors, namely alpha-amino-3-hydroxy-5-methyl-4-isoxazole propionic acid receptors (AMPA) and *N*-methyl-D-aspartate receptors (NMDAR). Both are formed by 4 different subunits and are primarily permeable to Na⁺, but become permeable to Ca²⁺.

SOCC are opened by the release of Ca²⁺ from endoplasmic reticulum. This store-operated calcium entry was proposed as a mechanism to ensure the refilling of intracellular Ca²⁺ stores and thus contribute to Ca²⁺ homeostasis.¹⁹⁴

After depolarization, the membrane Ca²⁺ gradient should be recovered by the extrusion of Ca²⁺ to the extracellular space or to an intracellular Ca²⁺ reservoir. Ca²⁺ extrusion to the extracellular space is achieved by a plasma membrane Ca²⁺ ATPase (PMCA) and a plasma membrane Na⁺/Ca²⁺ exchanger (NCX_{plasm}). The latter transporter exists in three different isoforms (NCX-1, -2 and -3), which remove calcium from the cytoplasm using the Na⁺ gradient. These three isoforms are widely expressed in neurons and muscles, making it difficult to ascribe a specific function to each exchanger. Nevertheless, the NCX-2 isoform is particularly abundant in neurons, suggesting a pivotal role for this exchanger in neuronal Ca²⁺ homeostasis.

The PMCA pump is a P-type ATPase, which obtains energy from ATP to remove the cytosolic Ca²⁺. PMCA transporters are expressed in four different isoforms (PMCA-1, -2, -3 and -4), specifically distributed in the tissues. The isoforms 2 and 3 are more abundant in neurons and their malfunction has been reported in several neurodegenerative disorders.^{195, 196}

The main membrane proteins involved in calcium transport through the cell membrane are summarized in Figure 6.1.

¹⁹⁴ Putney Jr, J. W. *Cell Calcium* **1986**, 7, 1-12.

¹⁹⁵ Schultz, J. M.; Yang, Y.; Caride, A. J.; Filoteo, A. G.; Penheiter, A. R.; Lagziel, A. Morell, R. J.; Mohiddin S. A.; Fananapazir. L.; Madeo, A. C.; Penniston, J. T.; Griffith A. J. *N. Engl. J. Med.* **2005**, 352, 1557-1564.

¹⁹⁶ Zanni, G.; Calì, T.; Kalscheuer, V. M.; Ottolini, D.; Barresi, S.; Lebrun, N.; Montecchi-Palazzi. L.; Hu, H.; Chelly, J.; Bertini, E.; Brini, M.; Carafoli, E. *Proc. Natl. Acad. Sci. U.S.A.* **2012**, 109, 14514-14519.

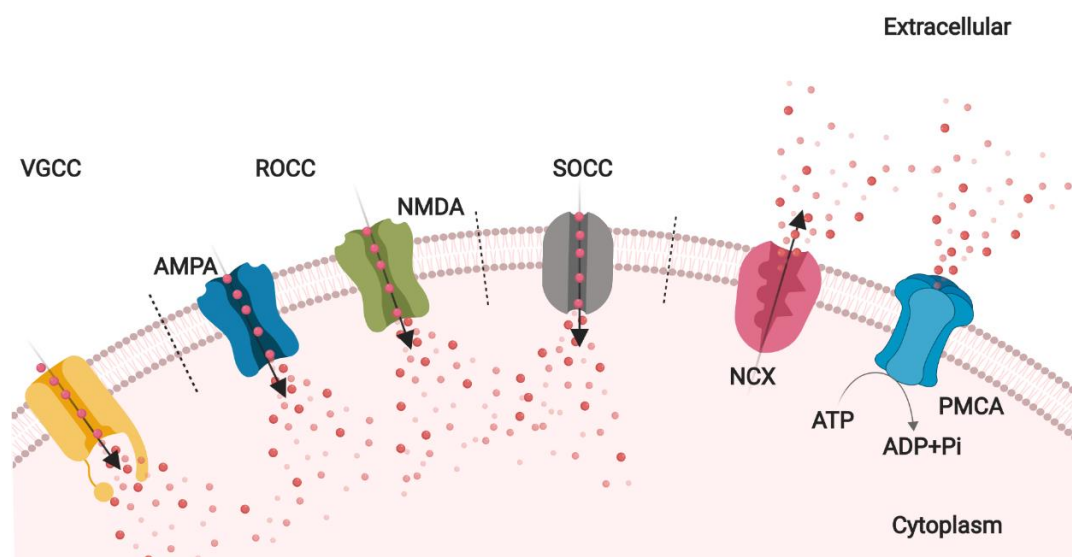


Figure 6.1

6.1.2. Endoplasmic reticulum as a calcium store

Endoplasmic reticulum is the major Ca^{2+} store inside the cell and has an important role in Ca^{2+} homeostasis and several signalling pathways involving Ca^{2+} release to cytoplasm (Figure 6.2). Two receptors take part in the release of calcium from the ER: inositol-1,4,5-tris-phosphate receptors (InsP3Rs), which are widely expressed in all cell types, and ryanodine receptors (RyRs), which are extensively expressed in neurons.

The activation of RyRs is in principle associated to an increase in intracellular calcium level, However these receptors can be triggered by other second messengers like cAMP. Their activation causes a selective increase in intracellular Ca^{2+} concentration.

While the most important activator of InsP3R is Ca^{2+} , intracellular Ca^{2+} can also inhibit these channels, depending on concentration. A low intracellular Ca^{2+} concentration activates the receptor and the channel is opened, and when the Ca^{2+} concentration achieves a high level these channels close.¹⁹⁷

After a massive Ca^{2+} entry in the cell, the neuron can restore the calcium resting levels by ER reuptake. The Ca^{2+} is transported into the ER from cytoplasm by the SERCA pump. SERCA (sarcoendoplasmic reticulum calcium transport ATPase) is a P-type

¹⁹⁷ Taylor, C. W.; Laude, A. J. *Cell Calcium* 32, 2002, 321-334.

ATPase encoded by three different genes, and the alternative splicing generates additional isoforms.¹⁹⁸

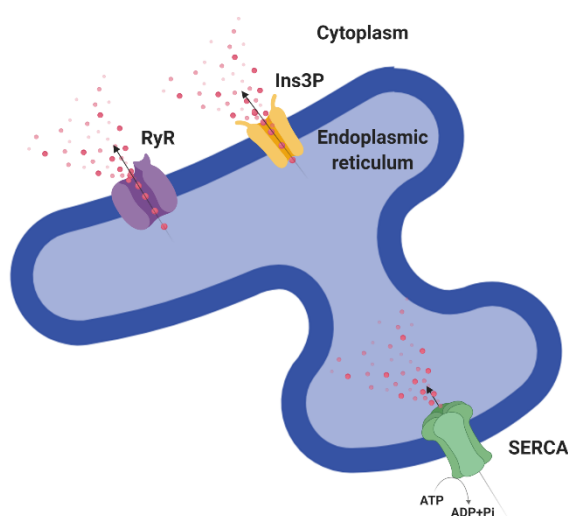


Figure 6.2

6.1.3. Mitochondria and calcium homeostasis

Mitochondria are the second major intracellular Ca^{2+} storage system, together with ER. Mitochondria play a pivotal role in the calcium control and homeostasis, due to their strategic placement close to both ER and plasma membrane Ca^{2+} channels,¹⁹⁹ which enables mitochondria to accumulate in their matrix the Ca^{2+} released either by ER or plasma membrane channels. An increase in the mitochondrial Ca^{2+} concentration causes an improvement in the activity of the Ca^{2+} -dependent NADH dehydrogenases involved in the tricarboxylic acid cycle, and hence an increased ATP biosynthesis.^{200, 201} As discussed in Chapter 1, the Ca^{2+} -gradient maintenance by pumps and exchangers in plasma membrane, endoplasmic reticulum and mitochondria is an ATP-dependent event and can consume 80% of total ATP in neuronal cells.²⁰²

The mitochondrial Ca^{2+} influx is mediated by the mitochondrial calcium uniporter (MCU), using as the driving force the negative electrochemical gradient generated by the mitochondrial respiratory chain. This channel is present in the inner mitochondrial

¹⁹⁸ Brini, M.; Carafoli, E. *Physiol. Rev.* **2009**, *89*, 1341-1378.

¹⁹⁹ Strokin, M.; Reiser, G. *Neurochem. Res.* **2016**, *41*, 1250-1262.

²⁰⁰ McCormack, J. G.; Denton, R. M. *Proc. Nutr. Soc.* **1990**, *49*, 57-75.

²⁰¹ McCormack, J. G.; Halestrap, A. P.; Denton, R. M. *Physiol. Rev.* **1990**, *70*, 391-425.

²⁰² Engl, E.; Attwell, D. J. *Physiol.* **2015**, *593*, 3417-3429.

membrane (IMM). MCU binds regulatory proteins such as the MCU regulator 1 (MCUR1), MCUR2 and the essential MCU regulator (EMRE). MCUR1 has two EF-hand Ca^{2+} domains, i.e., helix-loop-helix motifs able to bind calcium, which participate in the regulation of MCU forming a complex together with MCUR1 and EMRE.²⁰³ The opening of the mitochondrial permeability transition pore (mPTP) is triggered by the accumulated Ca^{2+} reaching a threshold in the mitochondrial matrix or by an increase in the formation of radical species. This pore opening causes a strong membrane depolarization, diminishing ATP production.²⁰⁴ Thus, mPTP opening is suggested to be a first trigger to the activation of cell death mechanisms.^{205, 206}

Ca^{2+} efflux from mitochondria plays a fundamental role in the maintenance of mitochondrial Ca^{2+} homeostasis. The calcium efflux rate is controlled by mNCLX, a $\text{Na}^+/\text{Ca}^{2+}$ exchanger, localized in the inner mitochondrial membrane. The existence of this exchanger was first described in 1974²⁰⁷ and further studies underlined its important roles in heart²⁰⁸, brain²⁰⁹ and pancreas.²¹⁰ Since this transporter also mediates $\text{Li}^+/\text{Ca}^{2+}$ exchange, it is also known as NCLX. mNCLX specific and inducible ablation causes Ca^{2+} overload in cells, an increase in radical formation and mPTP opening.

The main proteins involved in calcium transport through the mitochondrial membrane are summarized in Figure 6.3.

²⁰³ Patron, M.; Checchetto, V.; Raffaello, A.; Teardo, E.; Vecellio Reane, D.; Mantoan, M.; Granatiero, V.; Szabò, I.; De Stefani, D.; Rizzuto, R. *Mol. Cell* **2014**, *53*, 726-737.

²⁰⁴ Stavrovskaya, I. G.; Kristal, B. S. *Free Radic. Biol. Med.* **2005**, *38*, 687-697.

²⁰⁵ Zamzami, N.; Marchetti, P.; Castedo, M.; Hirsch, T.; Susin, S. A.; Mousse, B.; Kroemer, G. *FEBS Lett.* **1996**, *384*, 53-57.

²⁰⁶ Vaseva, A. V.; Marchenko, N. D.; Ji, K.; Tsirka, S. E.; Holzmann, S.; Moll, U. M. *Cell* **2012**, *149*, 1536-1548.

²⁰⁷ Carafoli, E.; Tiozzo, R.; Lugli, G.; Crovetti, F.; Kratzing, C. *J. Mol. Cell. Cardiol.* **1974**, *6*, 361-371.

²⁰⁸ Griffiths, E. J.; Balaska, D.; Cheng, W. H. *BBA. Bioenergetics* **2010**, *1797*, 856-864.

²⁰⁹ Castaldo, P.; Cataldi, M.; Magi, S.; Lariccia, V.; Arcangeli, S.; Amoroso, S. *Prog. Neurobiol.* **2009**, *87*, 58-79.

²¹⁰ Nita, I. I.; Hershinkel, M.; Kantor, C.; Rutter, G. A.; Lewis, E. C.; Sekler, I. *FASEB J.* **2014**, *28*, 3301-3312.

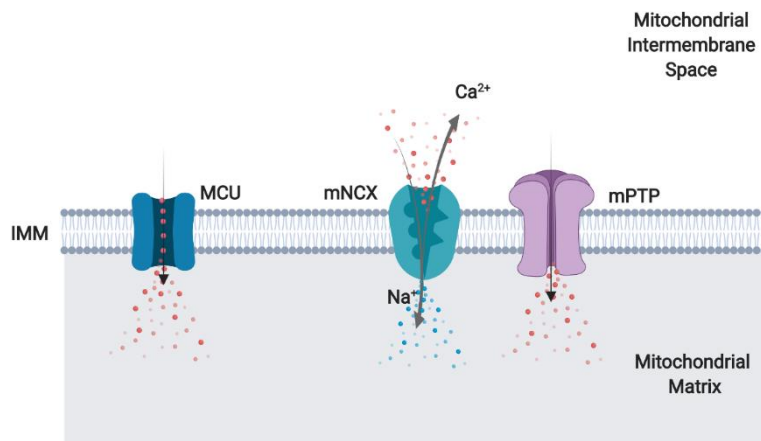


Figure 6.3

6.1.4. Calcium deregulation in neurodegenerative disease

Intracellular calcium deregulation is one of the most striking hallmarks in NDD. Also, the poor control of Ca^{2+} concentrations is connected by a complex biochemical network with other malfunctions, including, among others, oxidative stress, energy impairment and inadequate proteostasis. Parkinson's disease is characterized by the accumulation of α -synuclein aggregates, which cause impairment in plasmatic membrane permeability and lead to an increase in intracellular calcium concentration. In amyotrophic lateral sclerosis (ALS), an abnormally high exposition to glutamate promotes an increment in Ca^{2+} entry through AMPA receptors. The connection between Alzheimer's disease (AD) development and Ca^{2+} deregulation led to the elaboration of the calcium hypothesis in AD. In this hypothesis, the aggregation of the amyloid beta peptide and other amyloidogenic proteins increases cytosolic Ca^{2+} entry through NMDA activation and by plasmatic membrane impairment. The subsequent increase in cytosolic Ca^{2+} entry causes the opening of VGCC, further increasing Ca^{2+} entry. Particularly interesting is the role of CALHM1, which is hypothesized to have a role in the regulation of amyloid metabolism.²¹¹ The cytosolic calcium overload increases the activity of Ca^{2+} -dependent proteases and the aggregation of $\text{A}\beta$. Also, some mutations in proteins related with familiar Alzheimer's disease like presenilin-1

²¹¹ Dreses-Werringloer, U.; Lambert, J. C.; Vingtdeux, V.; Zhao, H.; Vais, H.; Siebert, A.; Jain, A.; Koppel, J.; Rovelet-Lecrux, A.; Hannequin, D.; Pasquier, F.; Galimberti, D.; Scarpini, E.; Mann, D.; Lendon, C.; Campion, D.; Amouyel, P.; Davies, P.; Foskett, J. K.; Campagne, F.; Marambaud, P. *Cell* **2008**, *133*, 1149-1161.

(PS-1) were linked with ER Ca^{2+} release through RyRs and InsP3Rs.^{212, 213} These findings highlight the importance of calcium in the physiological function and in pathogenesis development. Actually, the NMDA antagonists memantine and riluzole have been approved for the treatment of AD and ALS, respectively. However, mitochondrial calcium modifiers are poorly developed for this purpose in spite of the buffering role and the control of calcium concentrations near to the plasma membrane and ER by mitochondria. Only some VGCC blockers have reached clinical trial stage in AD, although their study was discontinued due to cardiovascular side effects.

6.2. mNCX blockers

6.2.1. First mNCX antagonists

The mNCX transporter is a major regulator in the mitochondrial calcium control. Intramitochondrial calcium concentration, in turn, regulates other processes like ATP formation, mPTP activation and radical species formation. However, the neuroprotective role for this transporter in NDDs is still unclear, and selective mNCX ligands (agonist and inhibitors) are needed to understand the role played by this exchanger in NDD and use it as a target towards the design of neuroprotective compounds.

The first blockers described for mNCX were L-type calcium channel blockers, including diltiazem, prenylamine, and verapamil.²¹⁴ The lack of selectivity of these compounds for the various types of calcium channels prevented their use in the pharmacological characterization of the mNCX exchanger. Clonazepam and other benzodiazepines also were described as mNCX inhibitors,²¹⁵ but they were not suitable because the outer mitochondrial membrane contains specific benzodiazepine receptors that interfere with the calcium fluxes promoted by mNCX.²¹⁶

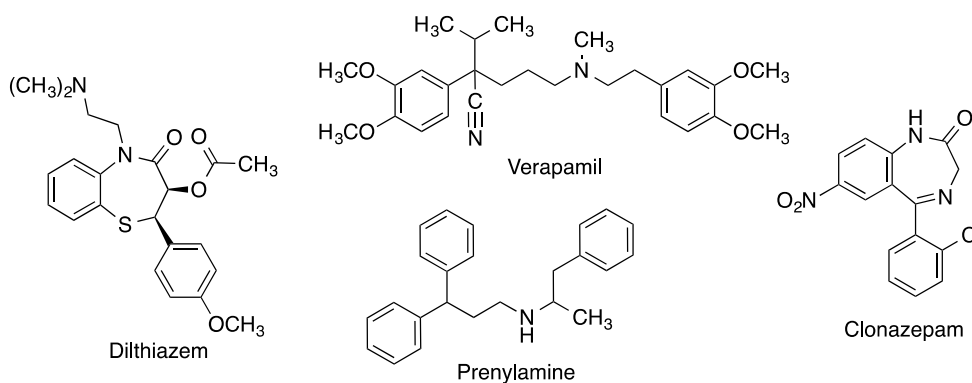
²¹² Stutzmann, G. E.; Smith, I.; Caccamo, A.; Oddo, S.; LaFerla, F. M.; Parker, I. *J. Neurosci.* **2006**, *26*, 5180-5189.

²¹³ Cheung, K. H.; Shineman, D.; Müller, M.; Cárdenas, C.; Mei, L.; Yang, J.; Tomita, T.; Iwatsubo, T.; Lee, V. M.; Foskett, J. K. *Neuron* **2008**, *58*, 871-883.

²¹⁴ Vaghy, P. L.; Johnson, J. D.; Matlib, M. A.; Wang, T.; Schwartz, A. *J. Biol. Chem.* **1982**, *257*, 6000-6002.

²¹⁵ Matlib, M. A.; Schwartz, A. *Life Sci.* **1983**, *32*, 2837-2842.

²¹⁶ O'Rourke, B. *Annu. Rev. Physiol.* **2007**, *69*, 19-49.



6.2.2. CGP-37157, a mNCH inhibitor, as a lead for drug discovery

The benzothiazepine derivative known as CGP-37157 was the first compound reported as a selective mNCX antagonist,²¹⁷ showing a 20-fold more potent mNCX blocking activity than clonazepam or diltiazem. CGP-37157 was therefore regarded as a powerful tool to understand the physiology of mNCX and its role in disease development. CGP-37157 has been shown to be neuroprotective in a number of cellular models. Thus, it provided protection from neuronal death induced by veratridine in both chromaffin cells and rat hippocampal slices,²¹⁸ it also protected rat hippocampal slices against glutamate or ischemia/reperfusion-induced stress,²¹⁹ SH-SY5Y human neuroblastoma cells against 70 mM K⁺ stimulation,²²⁰ and primary cultures of rat cortical neurons against NMDA insults.²²¹ Furthermore, CGP37157 has been shown to extend the lifespan of the nematode *Caenorhabditis elegans*.²²² On the other hand, it failed to protect either chromaffin cells or rat hippocampal slices against the combination of oligomycin A and rotenone, two inhibitors of oxidative phosphorylation that induce mitochondrial stress, as mentioned in chapter 3.^{218b, 219}

²¹⁷ Chiesi, M.; Schwaller, R.; Eichenberger, K. *Biochem. Pharmacol.* **1988**, *37*, 4399-4403.

²¹⁸ (a) Nicolau, S. M.; de Diego, A. M. G.; Cortés, L.; Egea, J.; González, J. C.; Mosquera, M.; López, M. G.; Hernández-Guijo, J. M.; García, A. G. *J. Pharmacol. Exp. Ther.* **2009**, *330*, 844-854. (b) Nicolau, S. M.; Egea, J.; López, M. G.; García, A. G. *Biochem. Biophys. Res. Commun.* **2010**, *400*, 140-144.

²¹⁹ González-Lafuente, L.; Egea, J.; León, R.; Martínez-Sanz, F. J.; Monjas, L.; Pérez, C.; Merino, C.; de Diego, A. M. G.; Rodríguez-Franco, M. I.; García, A. G.; Villarroja, M.; López, M. G.; de los Ríos, C. *ACS Chem. Neurosci.* **2012**, *3*, 519-529.

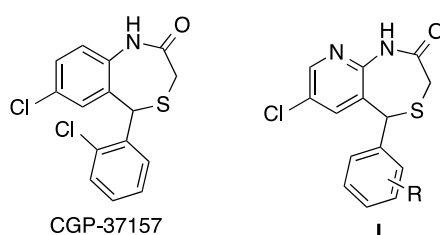
²²⁰ Martínez-Sanz, F. J.; Lajarín-Cuesta, R.; Moreno-Ortega, A. J.; González-Lafuente, L.; Fernández-Morales, J. C.; López-Arribas, R.; Morales, J. C.; López-Arribas, R.; Cano-Abad, M. F.; de los Ríos, C. *ACS Chem. Neurosci.* **2015**, *6*, 1626-1636.

²²¹ Ruiz, A.; Alberdi, E.; Matute, C. *Cell Death Dis.* **2014**, *5*, e1156.

²²² García-Casas, P.; Arias del Val, J.; Álvarez-Illera, P.; Wojnicz, A.; de los Ríos, C.; Fonteriz, R. I.; Montero, M.; Álvarez, J. *Front. Aging Neurosci.* **2019**, *10*, 440.

Although initially considered a selective mNCX blocker, several studies show the ability of CGP-37157 to block additional calcium channels and transporters, including SERCA²²³ and CALHM1.²²⁴ This lack of selectivity questions the outcome of experiments where CGP-37157 was regarded to have selectivity towards mNCX.²²⁵ The pharmacological characterization of CGP-37157 shows additional limitations, including the fact that it has always been tested as a racemic mixture, in spite of being chiral. Enantiopure CGP-37157 may well improve selectivity and potency as described for the case of *D-cis*-diltiazem, which displays a strong enantioselectivity in mNCX blockade.²¹⁴ Another limitation in the pharmacological investigation of CGP-37157 is its poor water solubility, which is due to its high lipophilicity. In an effort to address these problems, several libraries of CGP-37157 analogues have been prepared,^{220, 226} and in particular the pyridothiazepines **I**, where the benzene-fused ring of the parent molecule has been replaced by a pyridine, show an improved water solubility while keeping the neuroprotective properties and having a higher capacity to regulate the mitochondrial Ca²⁺ clearance.²²⁶

Another significant problem posed by CGP-37157 is its short half-life in animal models (0.9 h).²²⁵ The sulfide moiety undergoes rapid oxidative metabolism, leading to the corresponding sulfoxides and sulfones. These metabolites have not been pharmacologically characterized and they may well interfere in the *in vivo* experiments.



²²³ Nerumann, J. T.; Diaz-Sylvester, P. L.; Fleischer, S.; Copello, J. A. *Mol. Pharmacol.* **2011**, *79*, 141-147.

²²⁴ Moreno-Ortega, A. J.; Martínez-Sanz, F. J.; Lajarín-Cuesta, R.; de los Ríos, C.; Cano-Abad, M. F. *Neuropharmacology* **2015**, *95*, 503-510.

²²⁵ Pei, Y.; Lilly, M. J.; Owen, D. J.; D'Souza, L. J.; Tang, X. -Q.; Yu, J.; Nazarbaghi, R.; Hunter, A.; Anderson, C. M.; Glasco, S.; Ede, N. J.; James, I. W.; Maitra, U.; Chandrasekaran, S.; Moos, W. H.; Ghosh, S. S. *J. Org. Chem.* **2003**, *68*, 92-103.

²²⁶ Martínez-Sanz, F.-J.; Lajarín-Cuesta, R.; González-Lafuente, L.; Moreno-Ortega, A. J.; Punzón, E.; Cano-Abad, M. F.; de los Ríos, C. *Eur. J. Med. Chem.* **2016**, *109*, 114-123.

6.3. Enantioselective sulfoxide synthesis and attempted kinetic resolution of the CGP-37157 enantiomers

From the drug discovery perspective, the transformation of the sulfide group in CGP-37157 into a sulfoxide can be a good strategy to improve metabolic stability while simultaneously increasing the water solubility of the parent molecule (see below). Furthermore, it should be possible to carry out the oxidation of sulfide to sulfoxide by enantioselective reactions, and also to use such chemistry to isolate the starting sulfide in enantiomerically pure form *via* a kinetic resolution process. For these reasons, we embarked on a study of the enantioselective oxidation of the sulphur atom in CGP-37157.

6.3.1. Enantioselective synthesis of sulfoxides: Literature precedent

Sulphur is the fifth commonest atom in drug molecules and sulphur-containing drugs have an increasing impact on therapeutic treatments.^{227,228} Sulphur can exist in several forms in organic molecules but the commonest are the sulfide, sulfoxide and sulfone. The oxidation state of sulphur is -2 in sulfides and it is in a sp^3 -hybridization state, presenting two electron pairs. However, when the sulfide is oxidized to sulfoxide, the sp^3 -hybridized sulphur atom only has a single electron pair and may be chiral. The sulphur atom in sulfoxides displays an oxidation state of 0. Finally, the sulfoxide sulphur atom can be oxidized to the S^{2+} state becoming a sulfone, which is again achiral. These oxidation processes are really dynamic in biological media and is carried out by several cytochromes. The oxidation from sulfides to sulfoxides is not an irreversible pathway and enzymes like methionine sulfoxide reductase (Msr) A and B can reduce sulfoxides back to sulfides.

A particularly interesting property of sulfoxides, compared to sulfides and sulfones, is their improved water solubility, due to an increase in the dipole moment and dielectric constant.²²⁹ An example for this solubility improvement is famotidine sulfoxide, that shows a 10.512 mg/mL solubility in water, while that of famotidine itself is 1.565

²²⁷ Scott, K. A.; Njardarson, J. T. *Top. Curr. Chem.* **2018**, 376, 5.

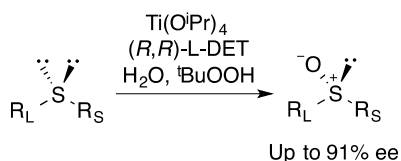
²²⁸ Ilardi, E. A.; Vitaku, E.; Njardarson, J. T. *J. Med. Chem.* **2014**, 57, 2832-2842.

²²⁹ Clark, T.; Murray, J. S.; Lane, P.; Politzer, P. *J. Mol. Model.* **2008**, 14, 689-697.

mg/mL.^{230,231} The other important difference is the chiral nature of sulfoxides, compared with achiral sulfides and sulfones, which is highly relevant to their pharmacokinetic and pharmacodynamic properties.²³² For instance, esomeprazole, the *S*-(-)-enantiomer of omeprazole, is metabolized at a lower rate than *R*-omeprazole. The chirality of sulfoxides and its pharmacological implications has prompted much interest in the development of new synthetic procedures that enable their enantioselective synthesis.

Enantiopure sulfoxides can be synthesised by nucleophilic substitution or by asymmetric oxidation of sulfides. The former strategy involves the use of chiral sulfinates, and is compromised by the fact that only very few sulfinates are readily available. Thus, the most attractive approach to the synthesis of enantiopure sulfoxides is based on asymmetric sulfide oxidations, based on metallic complex-catalysed reactions.

The first method for the enantiopure synthesis of sulfoxides, described almost simultaneously by Kagan and co-workers²³³ and Modena and co-workers,²³⁴ involved the use of a titanium complex similar to the one developed by Sharpless for the epoxidation of allylic alcohols (Scheme 6.1). The main difference was the use of 1 mol equivalent of diethyl tartrate, the source of chirality, in the Kagan method, while Modena described the use of a large excess of this reagent. Both research groups applied their method to the enantioselective synthesis of biologically active compounds.



Scheme 6.1

²³⁰ Moh, J. H.; Choi, Y. H.; Lim, K. M.; Lee, K. -W.; Shin, S. S.; Choi, J. K.; Koh, H. J.; Chung, S. *Bioorg. Med. Chem. Lett.* **2004**, *14*, 1757-1760.

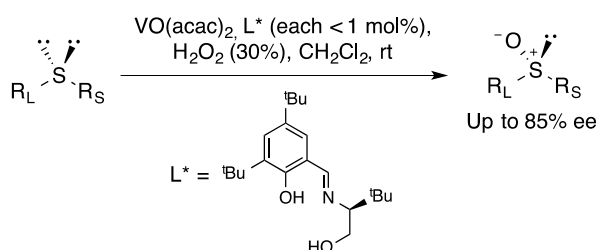
²³¹ Hajnal, K.; Gabriel, H.; Aura, R.; Erzsébet, V.; Blanka, S. S. *Acta. Med. Marisiensis* **2016**, *62*, 102.

²³² Bentley, R. *Chem. Soc. Rev.* **2005**, *34*, 609-624.

²³³ Pitchen, P.; Dunach, E.; Deshmukh, M. N.; Kagan, H. B. *J. Am. Chem. Soc.* **1984**, *106*, 8188-8193.

²³⁴ Di Furia, F.; Modena, G.; Seraglia, R. *Synthesis* **1984**, 325-326.

Bolm and Bienewald developed a new method for asymmetric sulfoxidation²³⁵ based on a vanadium catalyst and using a chiral shift-based ligand derived from a chiral alcohol as the source of chirality, and hydrogen peroxide as the oxidant in a heterogenous reaction system. This method has the advantage over the previous one of requiring only very small amounts of the chiral materials (Scheme 6.2).²³⁶ Other complexes of metals such as titanium, vanadium, iron, manganese, copper, aluminium, zirconium, niobium and molybdenum have been used to catalyse the asymmetric oxidation of sulfides, generally in poor enantioselectivities.



Scheme 6.2

Finally, a combination of peracids with enantiomerically pure oxaziridines, hydroperoxides, or hypervalent iodine-based systems can promote the enantioselective synthesis of sulfoxides. However, these methods have received a limited amount of attention because sulfoxides are obtained in modest enantiopurities and the reagents must be used in near stoichiometric amounts, which reduces the efficiency of the method on a large scale.²³⁶

6.3.2. Studies towards the synthesis of both enantiomers of CGP-37157

This part of the thesis was carried out at the laboratory of Professor James C. Anderson, University College, London, as part of the requirements for the “International Thesis” label.

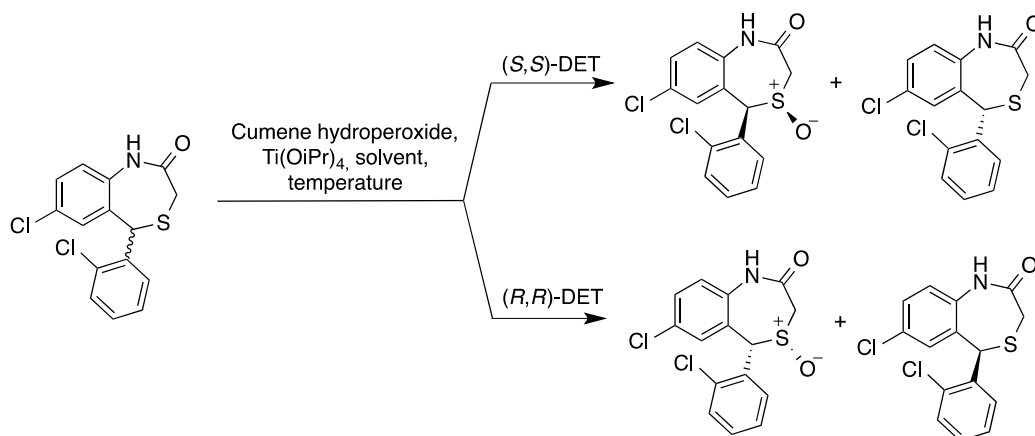
(a) Planning of the sulfide kinetic resolution based on an enantioselective sulfoxidation

According to our initial plan, both enantiomers of the enantiopure benzothiazepine should be accessible through a kinetic resolution process based on the Kagan chiral

²³⁵ Bolm, C.; Bienewald, F. *Angew. Chem. Int. Ed. Engl.* **1996**, *34*, 2640-2642.

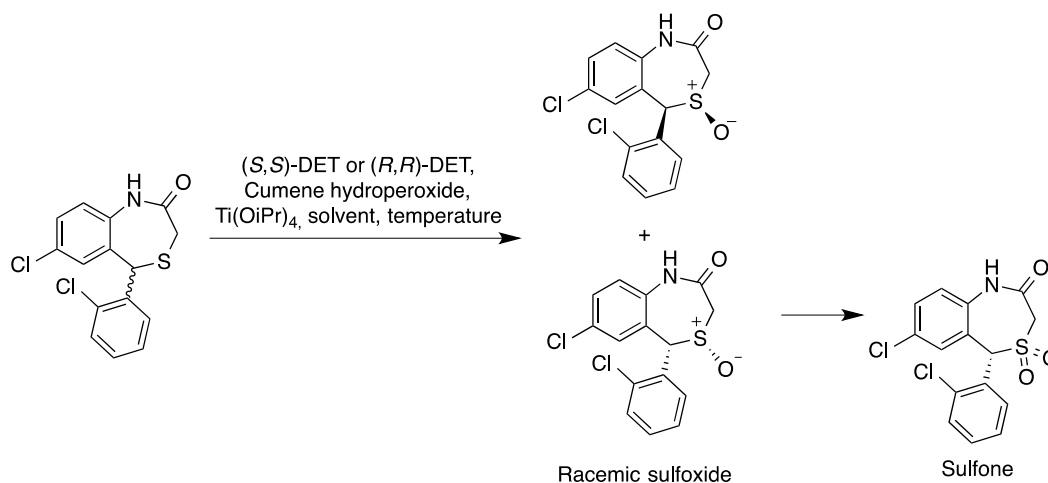
²³⁶ Agranat, I.; Caner, H. *Drug Discov. Today* **1999**, *4*, 313-321.

sulfoxide synthesis.²³⁷ The sulfoxide and unreacted sulfide would be separated by a simple chromatography and a subsequent sulfoxide reduction would provide the enantiopure benzothiazepine. The commercial availability of both enantiomers of the source of chirality, i.e. diethyl tartrate, ought to provide flexibility for the process. (Scheme 6.3).



Scheme 6.3

If the sulfide oxidation would prove not to be amenable to the planned kinetic resolution, an alternative approach would be a kinetic resolution of both diastereomers of the sulfoxide, based on the oxidation of one of them to a sulfone using a similar catalytic system²³⁸ (Scheme 6.4). Then, the sulfoxide and the sulfone could be separated, and the sulfoxide reduced to the enantiopure sulfide.

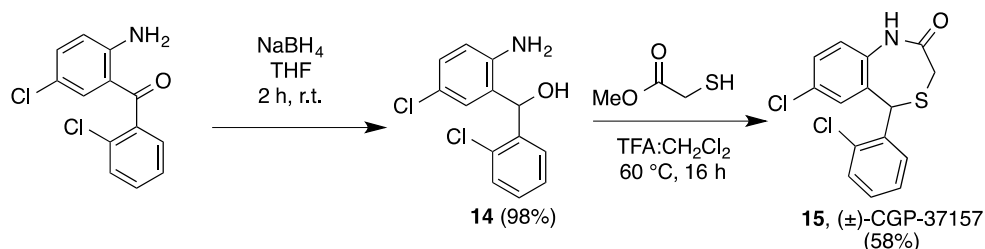


Scheme 6.4

²³⁷ Makino, K.; Yoneda, T.; Ogawa, R.; Kanase, Y.; Tabata, H.; Oshitari, T.; Natsugari, H.; Takahashi, H. *Tetrahedron Lett.* **2017**, *58*, 2885-2888.

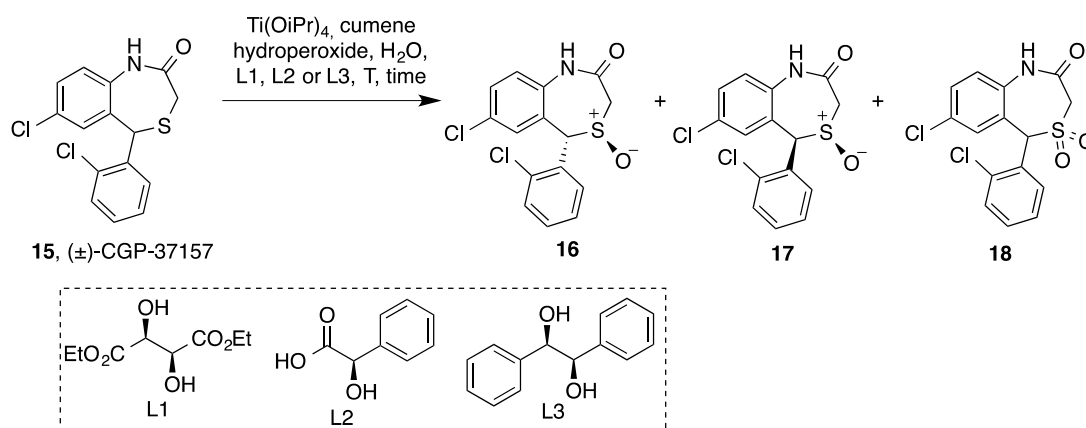
²³⁸ Scettri, A.; Bonadies, F.; Lattanzi, A.; Senatore, A.; Soriente, A. *Tetrahedron: Asymmetry* **1996**, *7*, 657-658.

To begin our study, the synthesis of the racemic benzothiazepine²²⁵ was carried out by reduction of the suitable benzophenone, which is commercially available, to the corresponding diphenylcarbinol, which was then reacted with methyl thioglycate in the presence of trifluoroacetic acid to afford racemic CGP-37157 in good overall yield (Scheme 6.5).



Scheme 6.5

As mentioned above, our planned the next step was a kinetic resolution based on an enantioselective sulfide Kagan-Modena oxidation. Several combinations of solvents, temperature, chiral ligands (diethyl tartrate, L1; mandelic acid, L2; hydrobenzoin, L3) and equivalents of oxidant were tested. Unfortunately, as shown in Scheme 6.6 and Table 6.1, all our attempts to stop the reaction at mid-conversion, which would be ideal for a kinetic resolution, never gave an enantiometric excess of the sulfoxide above 17%. In fact, the best result in terms of enantiomeric excess was only 27% with an 89% of conversion (entry 11). This enantiomeric excess was measured by ¹H-NMR



Scheme 6.6

Table 6.1

Entry	Solvent	Temperature (°C)	Ligand	Mmol eq. peroxide	Time (h)	Conversion (%)	ee of 16 (%)
1	CH ₂ Cl ₂	r.t.	--	1.1	24	0	--
2	CH ₂ Cl ₂	-20	L1	1.1	10	0	--
3	CH ₂ Cl ₂	r.t.	L1	1.1	4	85	9
4	CH ₂ Cl ₂	0	L1	1.1	48	82	22
5	CH ₂ Cl ₂	0	L1	0.8	48	60	17
6	CHCl ₃	0	L1	1.1	48	91	21
7	Toluene	0	L1	1.1	48	48	0
8	CH ₂ Cl ₂	0	L2	1.1	48	0	-
9	CH ₂ Cl ₂	r.t.	L2	1.1	48	90	0
10	CH ₂ Cl ₂	0	L3	1.1	48	0	-
11	CH ₂ Cl ₂	r.t.	L3	1.1	48	89	27

using (*R*)-BINOL as chiral shift reagent. Together with the major *trans* sulfoxide **16**, these experiments afforded small amounts of its *cis* diastereoisomer **17** (dr was about 3:1 for all experiments) and the corresponding sulfone **18**.

The major diastereoisomer of the sulfoxide was characterized by NMR, and its structure was determined to be *trans* on the basis of NOESY spectra, coupled with *ab initio* calculations. Thus, from NOESY experiments, the NOE 1D spectra can be obtained in order to measure the intensity of the NOE effects between the various protons of the molecule. To determine the distances between two nuclei (*r*), a well-known approach was employed based on the NOE effect (*a*), which is inversely proportional to 6th potency of distance.

$$r_{ij} = r_{ref} (a_{ref}/a_{ij})^{1/6}$$

The structure of both diastereoisomers was minimized in Spartan, using Hartree-Fock calculations at the 6-31G** level. Then, starting from a well-established distance such as the one between protons A and B and their NOE intensities, the remaining distances

were calculated using the above formula. The critical distance calculated between protons C and D was 3.6 Å for the minimized *trans*-diastereoisomer, but smaller in the *cis*-diastereoisomer. The other calculated distances were similar for both diastereoisomers (Figure 6.4)

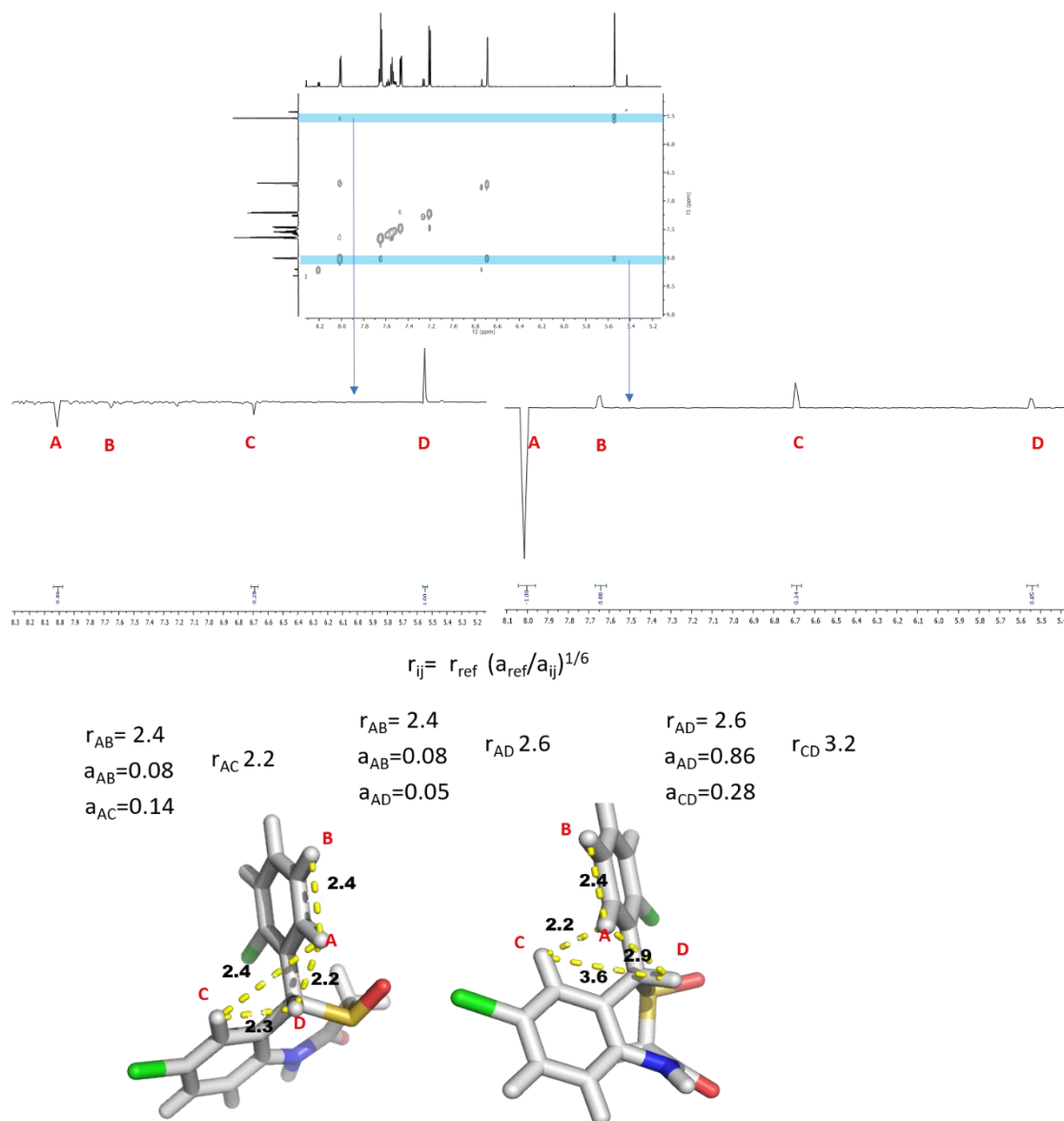
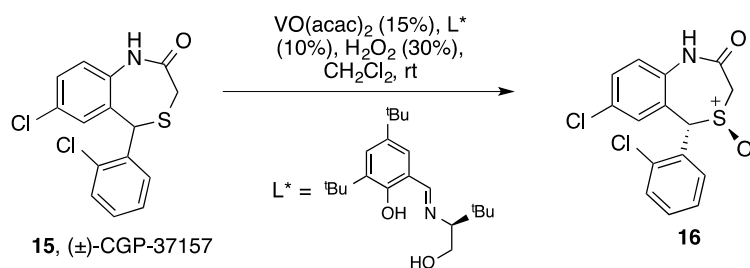


Figure 6.4

In view of the poor results of the kinetic resolution based on the Kagan procedure, the oxidation was attempted based on the Bolm method.²³⁵ In this case, the reaction was carried out in dichloromethane at room temperature, using a higher excess of the vanadium source and the chiral ligand than in the original reference, since no conversion took place otherwise. The reaction was fully diastereoselective and no

over-oxidation to sulfone was observed, but the best enantioselection was 16% ee, for 80% conversion (Scheme 6.6 and Table 6.2).



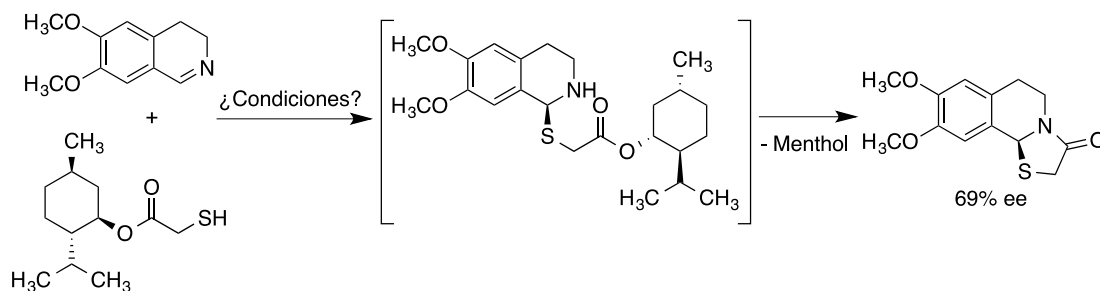
Scheme 6.6

Table 6.2

Entry	Solvent	Temperature (°C)	Time (h)	Conversion (%)	ee (%)
1	CH ₂ Cl ₂	r.t.	48	80	16
2	CH ₂ Cl ₂	0	24	0	-
3	CHCl ₃	r.t.	48	78	0

(b) Attempted resolution based on the use of menthol as an auxiliary

After the lack of success of the kinetic resolution protocols, a diastereoselective nucleophilic attack was attempted using an enantiopure menthyl thioglycate as a chiral auxiliary. This strategy had been previously described for the synthesis of thiazolo[2,3-*a*]isoquinolines (Scheme 6.7), with a moderate stereoselectivity.²³⁹ In this particular case, the menthol auxiliary was released as a consequence of a cyclization step.

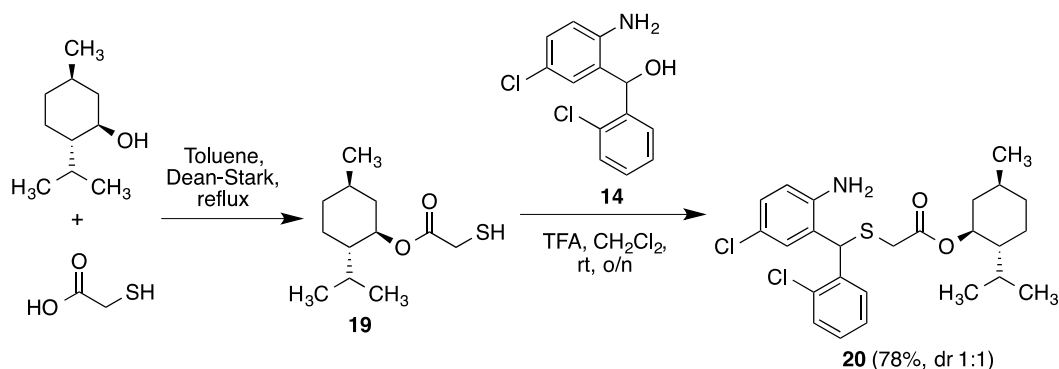


Scheme 6.7

In our case, the cyclization step did not take place and instead we isolated compound **20**, arising from the nucleophilic displacement of the hydroxyl in the starting diphenylcarbynol **14** by the mercapto group in compound **19**, generated by

²³⁹ Rozwadowska, M. D.; Sulima, A.; Gzella, A. *Tetrahedron: Asymmetry* **2002**, *13*, 2329-2333.

esterification of menthol with thioglycolic acid (Scheme 6.8). Not unexpectedly in view of the S_N1 mechanism that can be presumed for this step, no diastereoselectivity was observed. More importantly for our goal, the two diastereoisomers formed due to the presence of the menthol moiety were inseparable by chromatographic techniques.



Scheme 6.8

6.4. Preliminary pharmacological characterization of CGP-37157-derived sulfoxides and sulfones

Some pharmacological studies of compounds **16-18** have been carried out at the group of Dr. Rafael León (Hospital de la Princesa and Instituto Teófilo Hernando, Universidad Autónoma de Madrid), and further characterization is in progress.

6.4.1. Cytotoxicity

The cytotoxicity elicited by **16-18** in the AREc32 cell line was measured as MTT reduction in the presence of increasing concentrations of the compound under assay (24 hours). These studies demonstrated the lower toxicity of these compounds compared with the parent sulfide **15** (CGP-37157) (Figure 6.5).

6.4.2. Nrf2 induction

The Nrf2/ARE pathway constitutes the main mechanism of the phase II antioxidant response and its study is therefore relevant to our purposes. The Nrf2 induction activity of compounds (μM) in the AREc32 cell line is represented in bar graph form, normalized to basal conditions. (Figure 6.6 and Table 6.3). Interestingly, there is a stereoselectivity effect on this activity, since the sulfoxide **16** displays a better Nrf-2

induction compared with parent sulfide CGP-37157, while the other sulfoxide diastereoisomer (**17**) and the sulfone **18** show a similar activity compared with the parent molecule. These findings are relevant for the *in vivo* characterization of CGP-37157, since both the sulfoxide and the sulfone have been characterized as its

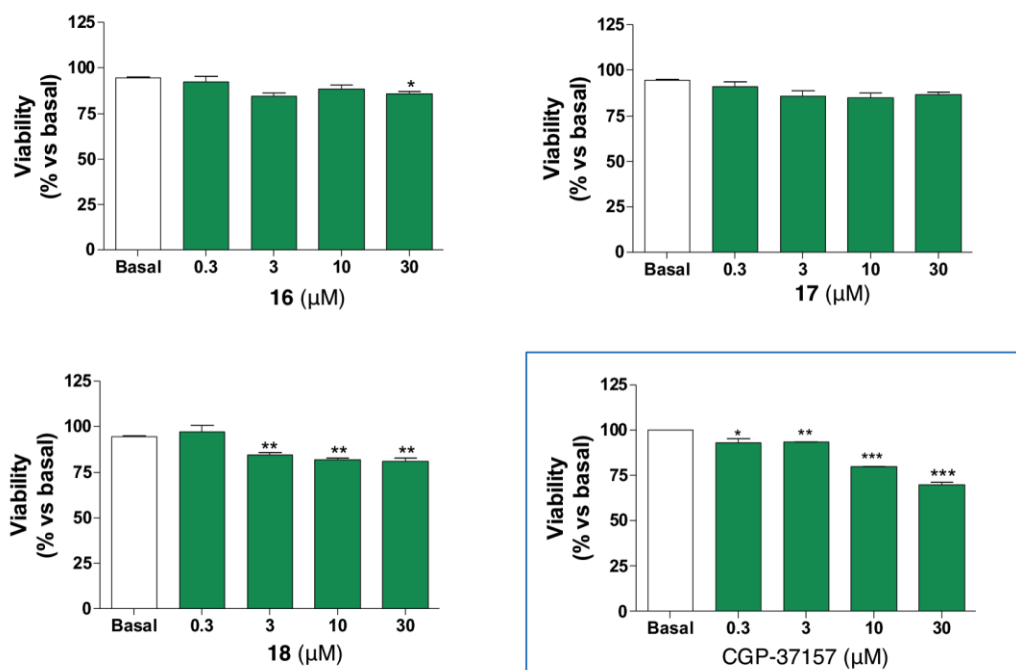


Figure 6.5

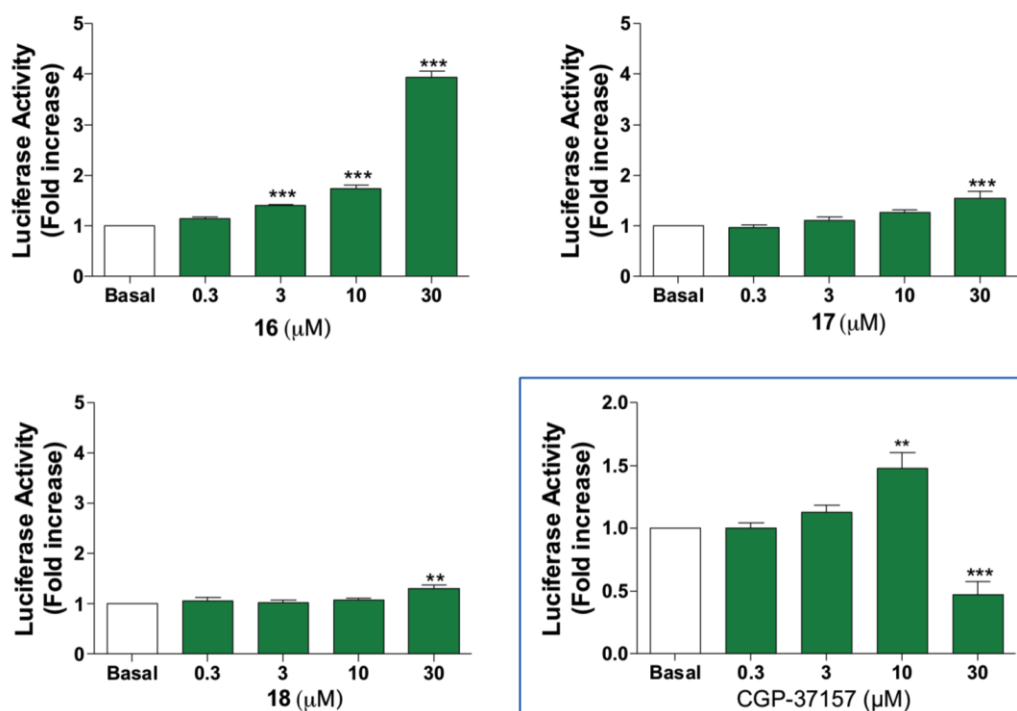


Figure 6.6

Table 6.3

Compound	CD
CGP-37157 (15)	--
16	12.81 ± 0.89
17	>30
18	>30

metabolites. It is interesting to note that in these experiments the reference molecule CGP-37157 was unable to double Nrf2 expression, which decreased at concentrations higher than 10 μ M, probably due to its cytotoxicity.

6.5. Design, synthesis and characterization of a multitarget mitochondrial stabilizer for stroke

Stroke (cerebral ischemia) is one of the commonest causes of morbidity and mortality worldwide.²⁴⁰ However, the Food and Drug Administration (FDA) has only approved the antithrombotic drug alteplase, a recombinant plasminogen activator, for the treatment of ischemic stroke,²⁴¹ while in Japan the radical scavenger edaravone has been in clinical use for several years for the same indication.²⁴² More extensive research is needed in the development of drugs to improve the cognitive decline after a stroke injury, preventing excitotoxicity and avoiding neuronal death. In this context, neuroprotection can be viewed as a useful preventive and therapeutic approach to combat the progression of ischemic damage.

Mitochondrial dysfunction is tightly related to ischemic status²⁴³ and has been proposed as a major cause of cell death in this pathology. Mitochondria, the organelles related with the energy production in the cell, display a broad spectrum of functions,

²⁴⁰ Sarti, C.; Rastenyte, D.; Cepaitis, Z.; Tuomilehto, J. *Stroke* **2000**, *31*, 1588-1601.

²⁴¹ Hacke, W.; Kaste, M.; Bluhmki, E.; Brozman, M.; Dávalos, A.; Guidetti, D.; Larrue, V.; Lees, K. R.; Medeghri, Z.; Machnig, T.; Schneider, D.; von Kummer, R.; Wahlgren, N.; Toni, D.; CASS Investigators. *N. Engl. J. Med.* **2008**, *359*, 1317-1329.

²⁴² Kobayashi, S.; Fukuma, S.; Ikenoue, T.; Fukuhara, S.; Kobayashi, S. *Stroke* **2019**, *50*, 1805–1811.

²⁴³ Russo, E.; Nguyen, H.; Lippert, T.; Tuazon, J.; Borlongan, C. V.; Napoli, E. *Brain Circ.* **2018**, *4*, 84-94.

some of which are related to ischemia including calcium homeostasis,¹⁹¹ reactive oxygen species formation,²⁴⁴ cell cycle control and apoptosis.²⁴⁵

Mitochondria play a pivotal role in calcium homeostasis by the direct storage of vast amounts of Ca²⁺ from the cytoplasm, as discussed in Section 6.1.3. Glucose and oxygen deprivation in ischemia processes leads to an ablation of ATP synthesis and, as a consequence, the ATP-dependent Ca²⁺ extrusion systems from cytosol are unable to fulfil their mission. Furthermore, the cytosolic Ca²⁺ overload causes a massive increase in the release of glutamate,²⁴⁶ an excitatory amino acid that increases the intracellular Ca²⁺ overload by activation of the NMDA receptors. Also, NMDA activation contributes to increase the amount of Na⁺ in the cell, increasing the Ca²⁺ efflux rate by mNCX.²⁴⁷ In this connection, it is relevant to note that CGP-37157, an inhibitor of mNCX²¹⁷ was described as a neuroprotector in several neurodegenerative models, including stroke.²⁴⁸

Radical oxygen species (ROS), including superoxide, hydroxyl radical and peroxide, are produced under physiological conditions in the brain and are involved in several transduction signal pathways.²⁴⁹ The electron transfer chain (ETC) is an important source of electrons in the formation of ROS from the oxygen molecule.²⁵⁰ Under normal conditions, the antioxidant cellular machinery balances ROS production.²⁵¹ After the occlusion of a blood vessel, an increase in ROS formation is observed. Moreover, a second peak in ROS production takes place upon reintroduction of oxygen, causing the highly damaging process known as ischemia/reperfusion injury.²⁵² ROS scavengers can be useful for stroke injury reduction, as well as for most neurodegenerative conditions, acting as antioxidants.

²⁴⁴ Rigoulet, M.; Yoboue, E. D.; Devin, A. *Antioxid. Redox Signal.* **2011**, *14*, 459-468.

²⁴⁵ Wang, C.; Youle, R. J. *Annu. Rev. Genet.* **2009**, *43*, 95-118.

²⁴⁶ Hossmann, K. A. *Brain Pathol.* **1994**, *4*, 23-36.

²⁴⁷ Boyman, L.; Williams, G. S.; Khananshvil, D.; Sekler, I.; Lederer, W. J. *J. Mol. Cell. Cardiol.* **2013**, *59*, 205-213.

²⁴⁸ Martínez-Sánchez, M.; Striggow, F.; Schröder, U. H.; Kahlert, S.; Reymann, K. G.; Reiser, G. *Neuroscience* **2004**, *128*, 729-740.

²⁴⁹ Lei, H.; Kazlauskas, A. *Mol. Cell. Biol.* **2014**, *34*, 110-122.

²⁵⁰ Cino, M.; Del Maestro, R. F. *Arch. Biochem. Biophys.* **1989**, *269*, 623-638.

²⁵¹ Greenlund, L. J.; Deckwerth, T. L.; Johnson Jr, E.M. *Neuron* **1995**, *14*, 303-315.

²⁵² Abe, K.; Tonomura, M.; Ito, M.; Takai, N.; Imamoto, N.; Rokugawa, T.; Momosaki, S.; Fukumoto, K.; Morimoto, K.; Inoue, O. *EJNMMI Res.* **2015**, *5*, 37.

The most relevant processes to be targeted in stroke are Ca^{2+} overload, ROS production and glial activation, but drugs aiming at only one of them have proved inefficient so far, probably due to the complexity of the pathological cascade of events. In this context, we envisioned to combine in a single molecule the ability of CGP-37157 to block the mNCC transporter with the properties of lipoic acid (LA), a well-known antioxidant that displays an important effect as neuroprotector.^{253, 254} LA (as its *R* enantiomer) is also an essential cofactor of the mitochondrial α -ketoacid dehydrogenases, playing a critical role in energy metabolism.

The way to carry out the combination of these two chemical entities needs to be carefully designed to prevent the loss of activity of any of the pharmacophores. There is only one prior study of structure-activity relationships in the CGP-37157 molecule, summarized in Figure 6.7,²²⁵ which has some limitations due to the method used to estimate mNCC inhibition. Nevertheless, this precedent shows that, while some features such as the free NH group, need to be conserved, the sulphur atom is not crucial, and can be replaced by nitrogen, thus providing a potential point of attachment for a spacer chain. In particular, the N-(2-hydroxyethyl) derivative **19** showed an activity only slightly inferior to the reference compound CGP-37157 and was regarded a good starting point for the design of our hybrid compound.

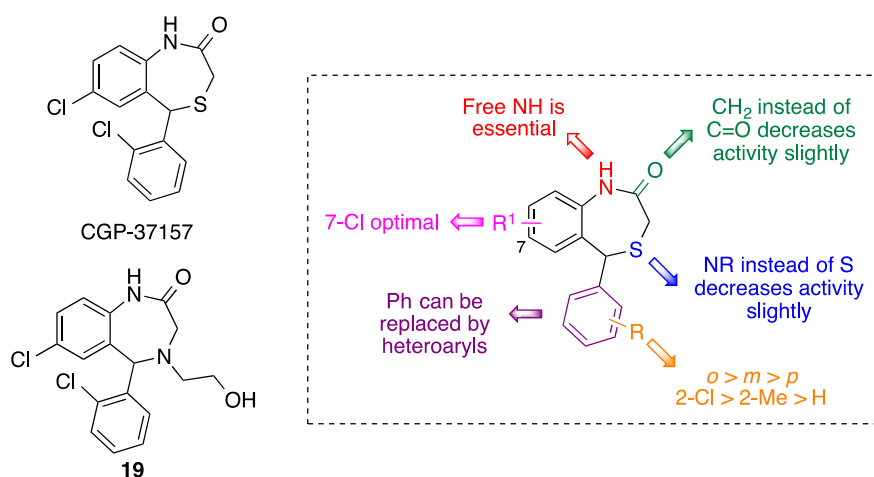


Figure 6.7

²⁵³ Molz, P.; Schröder, N. *Front. Pharmacol.* **2017**, *8*, 849.

²⁵⁴ Moura, F. A.; de Andrade, K. Q.; dos Santos, J. C.; Goulart, M. O. *Curr. Top. Med. Chem.* **2015**, *15*, 458-483.

On the other hand, some ester derivatives of LA have been shown to maintain its antioxidant activity. Hence, we decided to synthesize ester **20** as a multi-target hybrid structure with a potentially promising pharmacological profile in stroke (Figure 6.8).

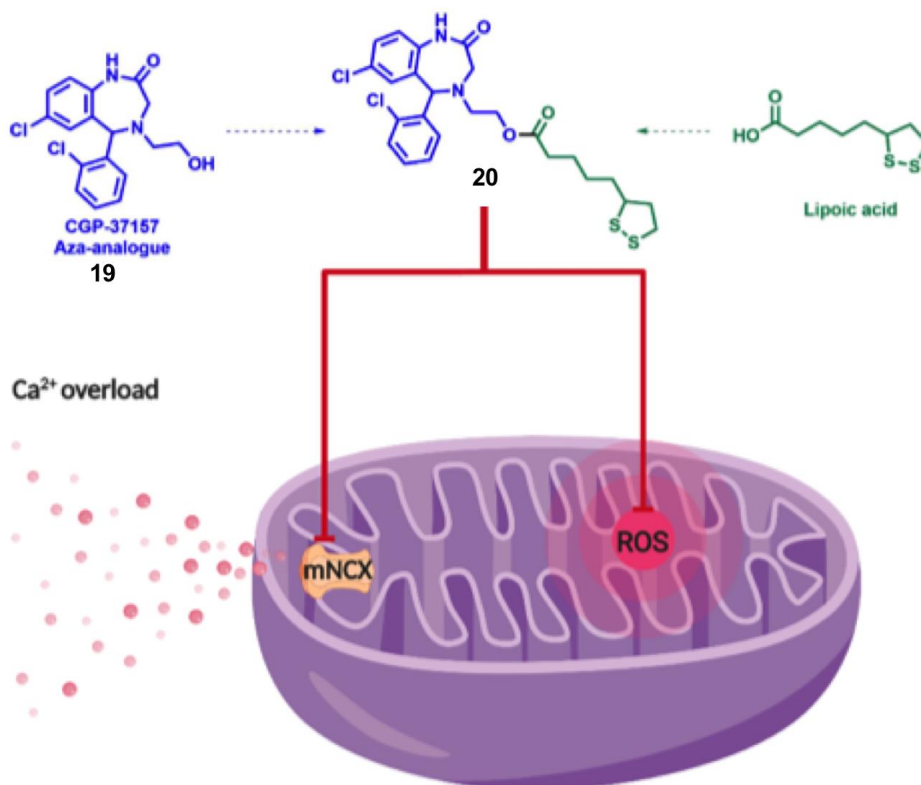


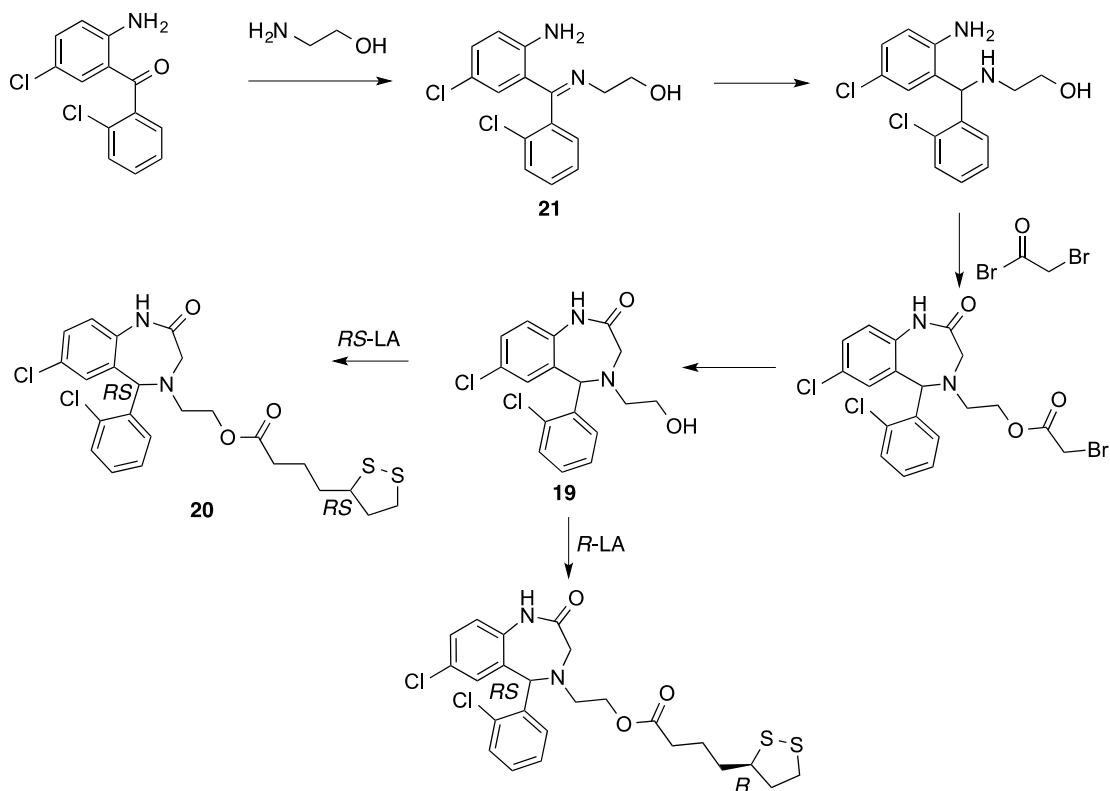
Figure 6.8

6.6. Synthesis of an aza-CGP-37157-lipoic acid hybrid

Since our target compound **20** bears two stereocenters, in principle all possible enantiomers of this structure should be studied. However, before embarking on such a demanding synthetic project, we decided to start by examining the pharmacological profile of lipoic acid esters prepared from the racemic benzothiazepine, which was obtained in a previous PhD thesis in the group.²⁵⁵ In brief, the commercially available (2-amino-5-chlorophenyl) (2-chlorophenyl) ketone and hydroxyethylamine were combined in a sealed tube to yield the corresponding imine **21**. This intermediate was reduced to obtain the corresponding diamine, whose acylation with bromobenzyl bromide followed by hydrolysis yielded the racemic benzothiazepine **19**. Finally, the target hybrid compound **20** was obtained by coupling the racemic **19** and lipoic acid,

²⁵⁵ Tenti, G. Ph. D. Thesis, Universidad Complutense, 2015.

which was employed both in racemic form and as its *R* enantiomer (Scheme 6.9). The pharmacological evaluation of both compounds revealed an interesting neuroprotective profile, which differed in both diastereoisomer mixtures, and these findings prompted us to start work on the synthesis of all possible enantiomers of the structure in pure form, which is the subject of the present Section.

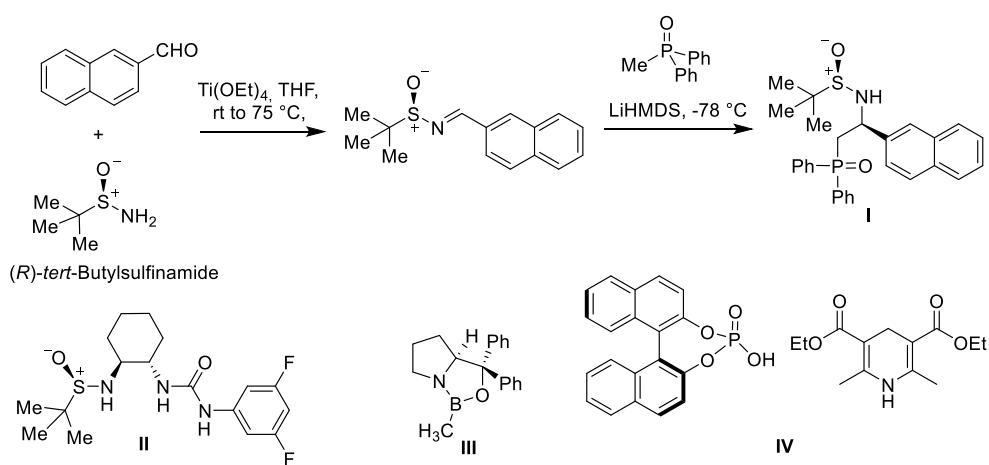


Scheme 6.9

Our first approach to the synthesis of enantiopure benzodiazepines was focused on the development of a procedure for the enantioselective reduction of imine **21**, using several catalytic systems previously described in the literature. The first of these catalysts (**I**)²⁵⁶ was prepared by formation of an imine from (*R*)-*tert*-butylsulfonamide (Ellman's sulfonamide) and naphthalene-2-carbaldehyde, followed by diastereoselective addition of a phosphorous ylide to its C=N bond (Scheme 6.10). The bifunctional catalyst **II**, also derived from Ellman's sulfonamide but containing an additional chiral urea fragment, was also assayed. The well-known Corey–Bakshi–Shibata (CBS) catalyst **III** is very adequate for the asymmetric reduction of ketones but

²⁵⁶ Chelouan, A.; Recio, R.; Borrego, L. G.; Álvarez, E.; Khiar, N.; Fernández, I. *Org. Lett.* **2016**, *18*, 3258-3261.

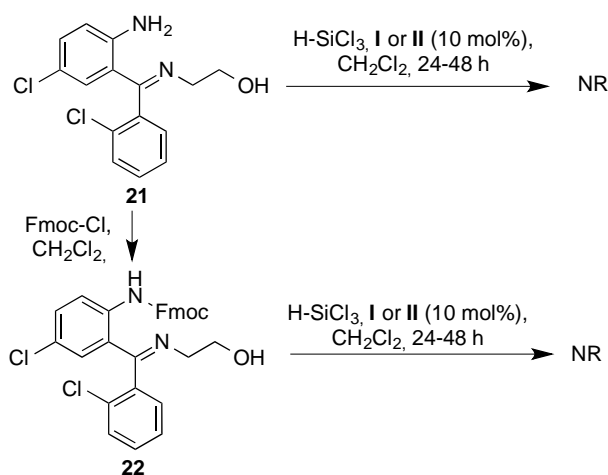
it normally gives poor results for the case of imines due to their rapid *Z-E* equilibration. In this particular case, however, we reasoned that an intramolecular hydrogen bond would maintain **21** as the *Z* isomer and that therefore the CBS reagent stood a chance to give the desired result. Finally, a combination of the chiral phosphoric acid **IV** and a Hantzsch dihydropyridine as a hydride donor²⁵⁷ was also assayed. In order to potentially enhance enantioselection by increasing steric hindrance in one of the sides of the C=N double bond while blocking its nucleophilic amino group, we also prepared compound **22**, the Fmoc derivative of **21**.



Scheme 6.10

Unfortunately, all the attempts to perform the reduction of imines **21** and **22** by silyl hydride donor in the presence of catalysts **I** and **II** failed, which can be due to the low reactivity of our imine associated to its doubly aromatic nature and the presence of bulky groups around the imine (Scheme 6.11). The CBS reagent **III** achieved the reduction but without enantioselectivity, and the combination of **IV** with the Hantzsch dihydropyridine also failed to reduce the imine.

²⁵⁷ Nugent, T. C.; El-Shazly, M. *Adv. Synth. Catal.* **2010**, 352, 753–819.



Scheme 6.11

Following the failure of the imine reduction by enantioselective catalysis, we decided to resort to the use of above-mentioned Ellman's sulfinamide, this time as a chiral auxiliary. As in the example shown in Scheme 6.10, this compound can react with aldehydes in the presence of Lewis acids to yield the corresponding imines, where the sulfinamide moiety efficiently directs the stereoselective reduction of the C=N bond. Finally, the auxiliary can be removed by acid hydrolysis. This route to a single enantiomer of the target 4-(2-hydroxyethyl)-4-aza-CGP37157 was successful, and is summarized in Scheme 6.12. Sulfinylimine **23** was prepared from the commercially available 2-aminobenzophenone previously employed for the racemic synthesis and commercial (*R*)-*tert*-butylsulfinamide in the presence of titanium tetraethoxide, and was isolated exclusively as a *Z* isomer. Reduction of the sulfinylimine function to give compound **24** was assayed with different reagents, as summarized in Table 6.4. The best results corresponded to the use of DIBAL or lithium tri(*tert*-butoxy)aluminium hydride, the latter of which afforded **24** in quantitative yield, as a single diastereomer. The reducing agent presumably generates a six-membered transition state shown in Figure 6.9, placing the bulkier groups in equatorial positions and allowing a fully diastereo controlled intramolecular hydride transfer to the C=N bond.

Table 6.4

Entry	Reagent	Yield	dr
1	NaBH ₄	quant.	71:29
2	L-selectride	0	--
3	DIBAL	quant.	100:0
4	(<i>t</i> -BuO) ₃ LiAlH	quant.	100:0

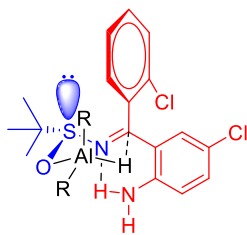


Figure 6.9

The sulfonamide function was then cleaved by acid hydrolysis with 1M aqueous HCl to give the diamine **25** in 85% yield as the *S*-enantiomer. For the introduction of the 2-hydroxyethyl chain, this compound was treated with a solution of ethylene oxide in THF, in the presence of indium trichloride as a Lewis acid and under microwave irradiation,²⁵⁸ affording **26** in a moderate 39% yield because of the unavoidable formation of a disubstituted product. The diazepinone ring was generated in 56% yield by one-pot acylation/intramolecular alkylation of compound **26** with bromoacetyl bromide in the presence of diethylamine, a transformation that was accompanied by acylation of the hydroxyl group to give compound **27**. Finally, the basic hydrolysis of this side chain afforded the 4-(2-hydroxyethyl)-4-aza derivative of CGP37157 **28** in quantitative yield. This compound was then esterified with (*R*)-lipoic acid via activation of the carboxy group in the presence of a diimide (EDCI) and 4-dimethylaminopyridine (DMAP) to furnish the hybrid molecule **29**.

Since both the Ellman sulfonamide and lipoic acid are commercially available as both enantiomers, the synthetic route summarized above was be easily adapted to achieve the preparation in pure form of the four possible enantiomers of our target structure (compounds **29-32**).

²⁵⁸ The reaction failed under non-catalyzed conditions and in the presence of HCl.

6.7. Preliminary pharmacological studies

6.7.1. Cytotoxicity

The effect of these compounds on cell viability was studied on the AREc32 cell line measured as MTT reduction. A low cytotoxicity was observed for all compounds, which were better in this regard than CGP-37157 in all cases (Figure 6.10 for the enantiomeric aza-CGP-37157 analogues compared with the reference compound and Figure 6.11 for the four enantiomers of the aza-CGP-37157/lipoic acid hybrid compounds).

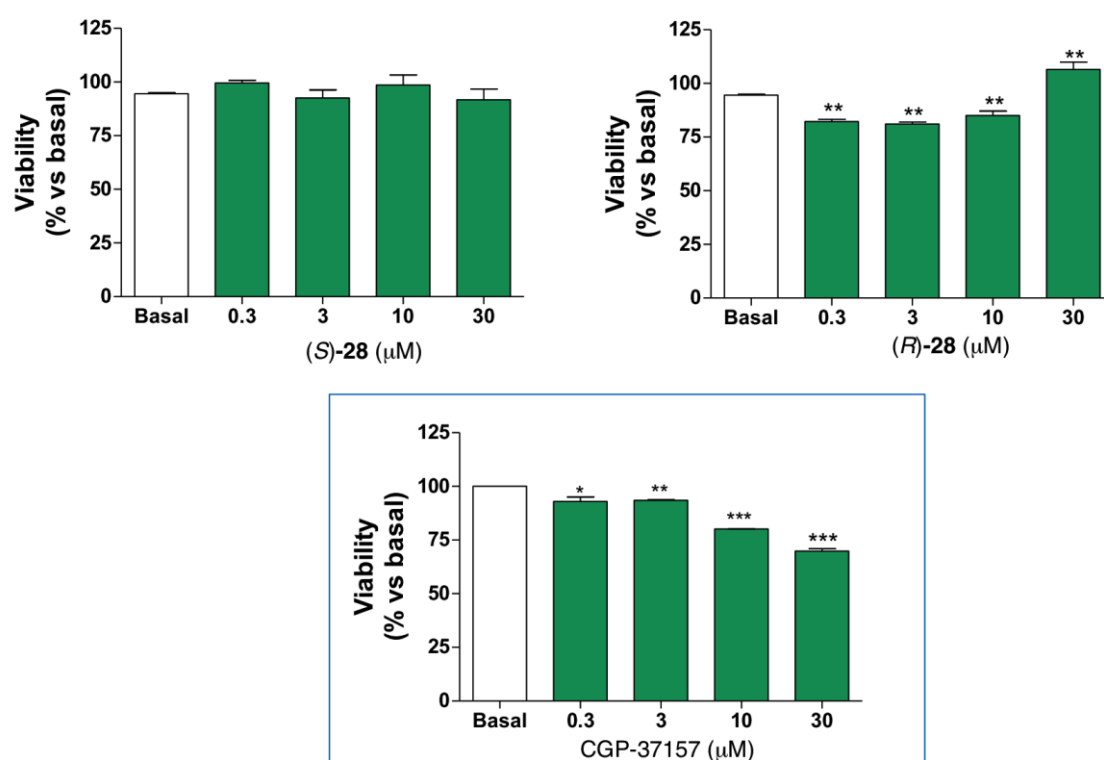


Figure 6.10

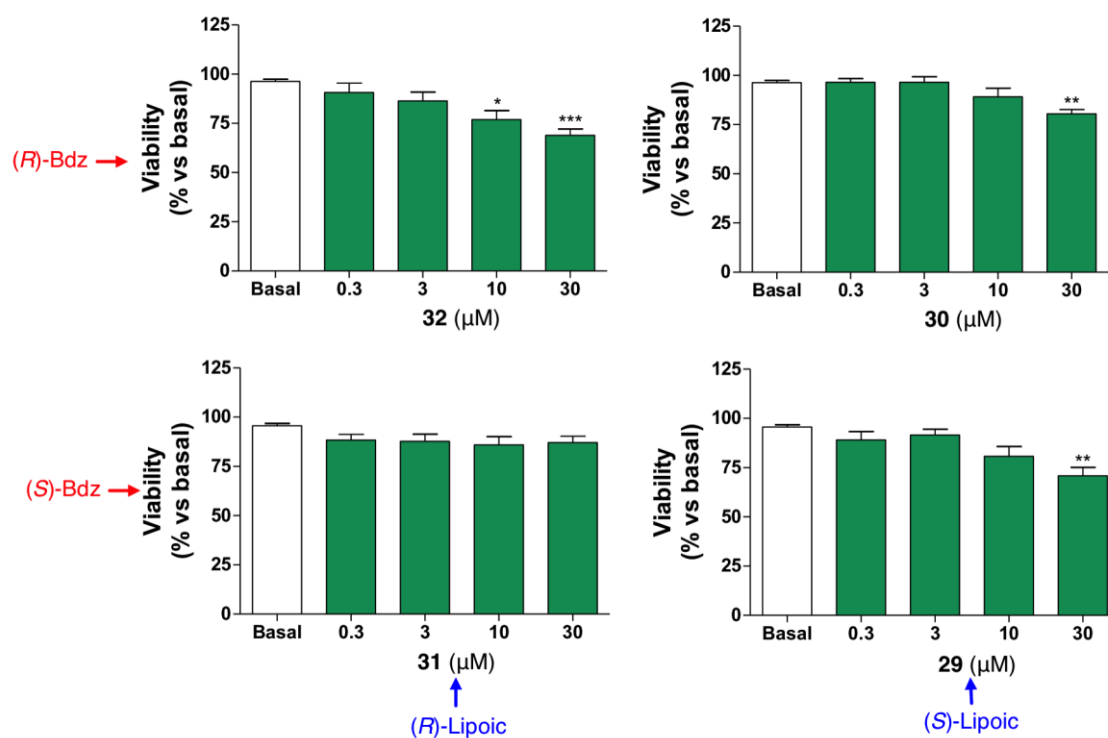


Figure 6.11

The alcohol (*R*)-**28** and its (*S*)-enantiomer were both potent Nrf-2 inducers compared with CGP-37157, with a slight enantiospecificity in favour of the former (Figure 6.12).

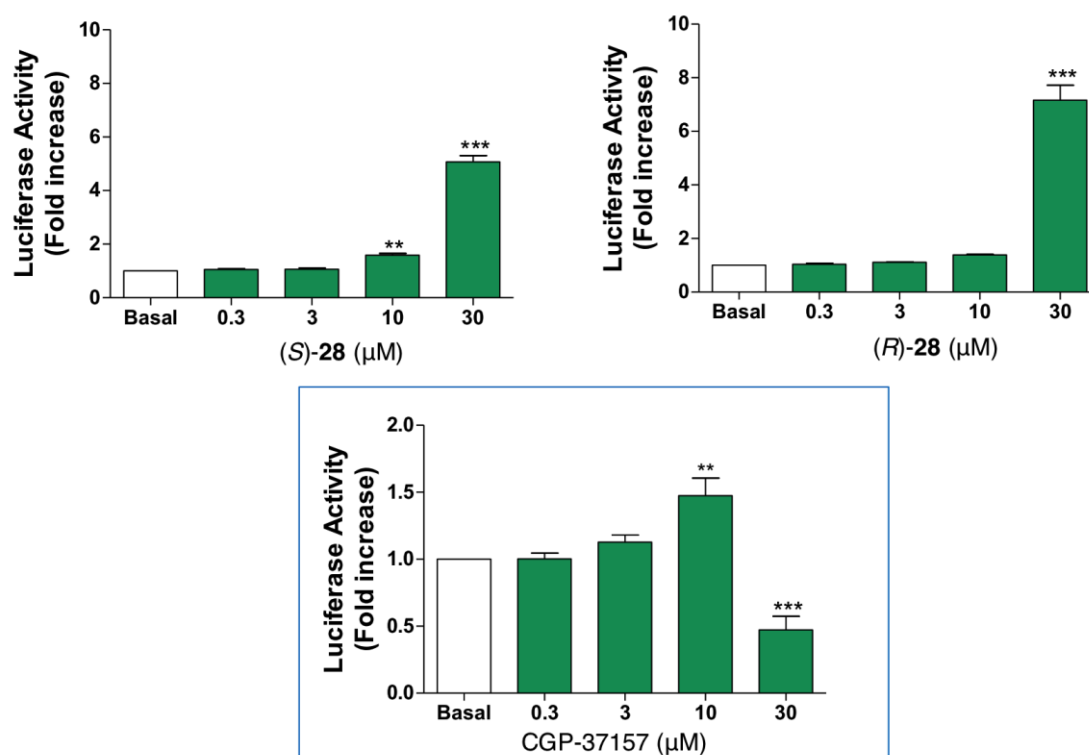


Figure 6.12

The enantiopure **32** doubled the activity of its diastereomer **30** as an Nrf-2 inducer, showing that the configuration of the lipoic acid fragment (*R* vs. *S*) has some importance in terms of this property. On the other hand, **29** and **31**, having an *R* configuration at the dibenzoazepine stereocenter, were inactive (Figure 6.13).

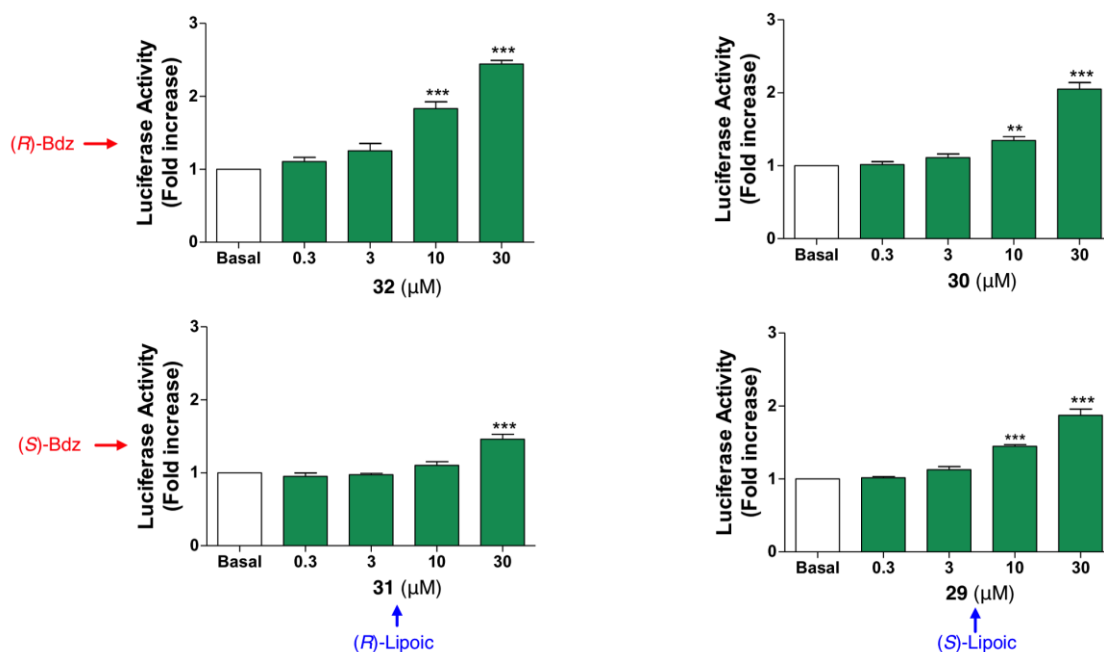


Figure 6.13

The CD values (*i.e.* the concentrations required to double the expression of Nrf2) for all these compounds are compared in Table 6.5.

Table 6.5

Entry	Compound	CD
1	(<i>S</i>)- 28	14.39 ± 0.17
2	(<i>R</i>)- 28	11.77 ± 0.51
3	29	>30
4	30	26.52 ± 1.29
5	31	>30
6	32	11.91 ± 1.32
7	(<i>S</i>)-LA	>600
8	(<i>R</i>)-LA	>600
9	(±)-LA	>600

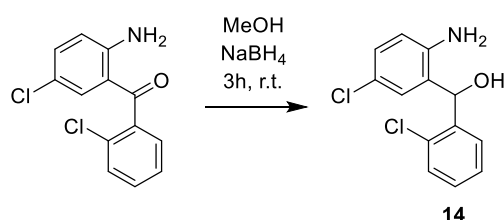
6.8. Experimental section

General experimental details

All reagents and solvents were of commercial quality and were used as received. Reactions were monitored by thin layer chromatography on aluminium plates coated with silica gel and fluorescent indicator. Microwave-assisted reactions were performed on a CEM Discover focused microwave reactor. Separations by flash chromatography were performed using a Combiflash Teledyne automated flash chromatograph or on conventional silica gel columns. Melting points were measured with a Kofler-type heating platine microscope from Reichert, 723 model, and are uncorrected. Infrared spectra were recorded with an Agilent Cary630 FTIR spectrophotometer with a diamond ATR accessory for solid and liquid samples, requiring no sample preparation; wavenumbers are given in cm^{-1} . NMR spectroscopic data were obtained using spectrometers maintained by the CAI de Resonancia Magnética, UCM, operating at 250, 300, 400 and 700 MHz for ^1H NMR and, 63, 100 and 176 MHz for ^{13}C NMR; chemical shifts are given in (δ) parts per million and coupling constants (J) in hertz. Elemental analyses were determined by the CAI de Microanálisis, Universidad Complutense, using a Leco CHNS-932 combustion microanalyzer. The enantiomeric excess analysis has been conducted in a HPLC Agilent 1220 Infinity LC with a chiral column ULTRON ES.

6.8.1. Synthesis of CGP-37157

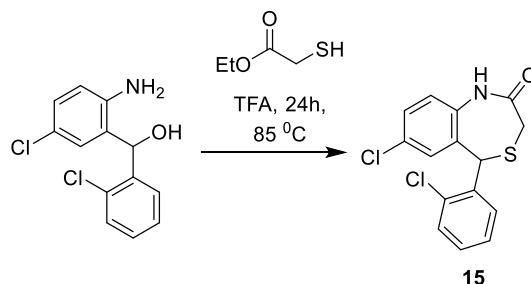
(2-Amino-5-chlorophenyl)(2-chlorophenyl)carbinol (**14**)



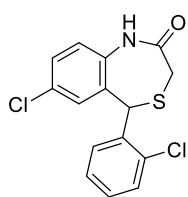
2-Amino-2',5-dichlorobenzophenone (1 g, 3.76 mmol) was dissolved in methanol (20mL), sodium borohydride (780 mg) was added and the mixture was stirred at room temperature for 3 hours. Water (20 ml) was added to the reaction mixture, extracted with ethyl acetate (3 x 60 mL) and washed with brine (20 mL). The combined organic layers were dried over anhydrous sodium sulfate and the solvent was removed *in vacuo* to give 987 mg (98%) of the title compound.

^1H NMR (400 MHz, CDCl_3) δ 7.48 – 7.43 (m, 1H), 7.42 – 7.37 (m, 1H), 7.32 – 7.22 (m, 2H), 7.06 (dd, $J = 8.5, 2.5$ Hz, 1H), 6.86 (d, $J = 2.5$ Hz, 1H), 6.61 (d, $J = 8.5$ Hz, 1H), 6.12 (s, 1H), 4.05 (br s, 2H), 3.00 (br s, 1H).²⁵⁹

²⁵⁹ Nakafuji K.; Muneuchi, A. *Jpn. Kokai Tokkyo Koho* JP Patent No. 2006032275 A 20060202.

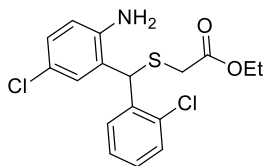
7-Chloro-5-(2-chlorophenyl)-1,5-dihydrobenzo[e][1,4]thiazepin-2(3H)-one (15)

Carbinol **14** (1.0 mmol) was mixed with methyl thioglycolate (6 eq) and TFA (2 mL) and the reaction was stirred at 85 °C for 24 h. Then, the solution was diluted with CH₂Cl₂ (80 mL) and washed with 1.0 M aqueous NaOH solution (20 mL) and brine (20 mL). The organic layer was dried over sodium sulfate and the solvent concentrated under vacuum. The residue was purified by column chromatography on silica gel using a 4:1 hexane-ethyl acetate mixture as eluent to give 190 mg (58%) of the desired benzothiazepine as a white solid. The corresponding thioether was also isolated as a minor component from the crude products (71 mg, 19%).

7-Chloro-5-(2-chlorophenyl)-1,5-dihydrobenzo[e][1,4]thiazepin-2(3H)-one (15)

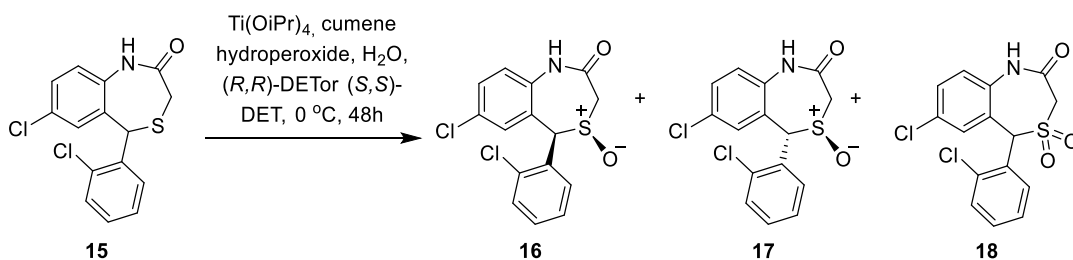
Mp 116 °C; ¹H NMR (700 MHz, CDCl₃) δ 7.82 (dd, *J* = 8.0, 1.6 Hz, 1H), 7.73 (s, 1H), 7.47 – 7.39 (m, 2H), 7.39 – 7.31 (m, 1H), 7.27 (dd, *J* = 8.1, 2.6 Hz, 1H), 7.06 (d, *J* = 8.4 Hz, 1H), 6.71 (d, *J* = 2.3 Hz, 1H), 6.15 (s, 1H), 3.33 (d, *J* = 12.3 Hz, 1H), 3.03 (dd, *J* = 12.3, 1.8 Hz, 1H); ¹³C NMR (176 MHz, CDCl₃) δ 169.8, 135.7, 135.0, 134.3, 134.1, 133.5, 131.0, 130.5, 129.9, 128.9, 128.2, 127.4, 125.3, 43.7, 31.5; **IR (neat, cm⁻¹):**

elemental analysis (%) calcd. for C₁₅H₁₁Cl₂NOS: C 55.57, H 3.42, N 4.32, S 9.89; found: C 55.41, H 3.56, N 4.27, S 9.77.

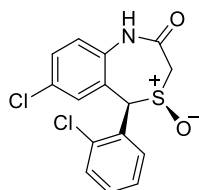
Ethyl 2-(((2-amino-5-chlorophenyl)(2-chlorophenyl)methyl)thio)acetate

Pale yellow solid; **mp:** 94 °C; ¹H NMR (700 MHz, CDCl₃) δ 7.93 (d, *J* = 7.6 Hz, 1H), 7.43 – 7.35 (m, 2H), 7.29 (td, *J* = 7.7, 1.4 Hz, 1H), 7.02 (dd, *J* = 8.5, 2.4 Hz, 1H), 6.76 (d, *J* = 2.4 Hz, 1H), 6.65 (d, *J* = 8.5 Hz, 1H), 5.79 (s, 1H), 4.41 (s, 2H), 4.19 (q, *J* = 7.1 Hz, 2H), 3.18 (d, *J* = 16.1 Hz, 1H), 3.11 (d, *J* = 16.1 Hz, 1H), 1.28 (t, *J* = 7.1 Hz, 3H); ¹³C NMR (176 MHz, CDCl₃) δ 170.7, 143.9, 135.8, 134.9, 130.6, 130.2, 129.3, 128.7, 128.2, 127.4, 124.7, 123.1, 117.7, 62.0, 46.2, 33.9, 14.3; **IR (neat, cm⁻¹):** **elemental analysis (%) calcd. for C₁₇H₁₇Cl₂NO₂S:** C 55.14, H 4.63, N 3.78, S 8.66; found: C 54.98, H 4.21, N 3.90, S 8.99.

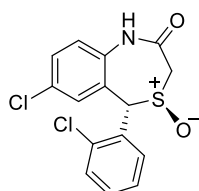
6.8.2. Asymmetric oxidation of CGP-37157



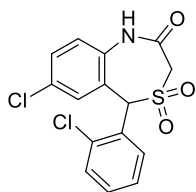
$\text{Ti(O-}i\text{-Pr)}_4$ (149 μL , 0.5 mmol) and (R,R) -DET or (S,S) -DET (171 mL, 1 mmol) were dissolved in CH_2Cl_2 (3 mL) at room temperature under nitrogen atmosphere. H_2O (0.5 mmol) was introduced through a septum via a microsyringe. After 15 min, a solution of benzothiazepine **15** (172 mg, 0.5 mmol) in CH_2Cl_2 (2 mL) was added. The solution was cooled to $0\text{ }^\circ\text{C}$, and 0.55 mmol of a cumene hydroperoxide solution in CH_2Cl_2 (1 mL) are then introduced. The reaction was monitored by TLC. After 48h, water (10 mol equiv) was added dropwise by a microsyringe to the solution. A strong stirring was maintained for 30 min. The white gel obtained was filtered and thoroughly washed with CH_2Cl_2 . The filtrate was kept in the presence of NaOH (10 min) and then separated. The organic layer was dried over Na_2SO_4 and the solvent removed under reduced pressure to give the crude product. Chromatography on silica gel using a 1:1 AcOEt-hexane mixture as eluent gave 20 mg (13%) of cis-sulfoxide **16**, 71 mg (41%) of trans-sulfoxide **17**, 22 mg (12%) of sulfone **18**, and 27 mg of the starting material **15**.

cis-7-Chloro-5-(2-chlorophenyl)-1,5-dihydrobenzo[e][1,4]thiazepin-2(3H)-one 4-oxide (16)

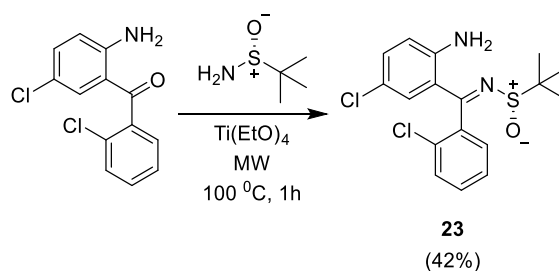
White solid; mp 133°C ; $^1\text{H NMR}$ (250 MHz, d_6 -DMSO) δ 10.34 (br s, 1H), 8.29 – 8.05 (m, 1H), 7.63 – 7.46 (m, 4H), 7.26 (d, $J = 8.5$ Hz, 1H), 6.73 (d, $J = 2.4$ Hz, 1H), 5.44 (s, 1H), 4.26 (d, $J = 11.8$ Hz, 1H), 3.06 (d, $J = 11.8$ Hz, 1H); $^{13}\text{C NMR}$ (63 MHz, d_6 -DMSO) δ 164.7, 137.2, 133.4, 132.8, 130.7, 130.4, 130.3, 129.7, 129.2, 129.1, 127.9, 125.9, 59.7, 57.8.; IR (neat, cm^{-1}): 2913, 1680, 1025; HRMS (ESI): found m/z 361.9791 [$\text{M}+\text{Na}^+$] $^+$, calcd for [$\text{C}_{15}\text{H}_{11}\text{Cl}_2\text{NO}_3\text{S}+\text{Na}^+$] 361.9785.

trans-7-Chloro-5-(2-chlorophenyl)-1,5-dihydrobenzo[e][1,4]thiazepin-2(3H)-one 4-oxide (17)

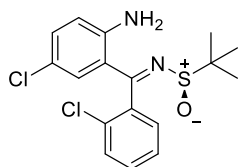
White solid; mp $141\text{--}143^\circ\text{C}$ $^1\text{H NMR}$ (700 MHz, d_6 -DMSO) δ 10.58 (br s, 1H), 8.06 (dd, $J = 7.6, 1.2$ Hz, 1H), 7.72 – 7.67 (m, 2H), 7.61 – 7.58 (m, 1H), 7.51 (dd, $J = 8.5, 2.4$ Hz, 1H), 7.26 (d, $J = 8.5$ Hz, 1H), 6.74 (d, $J = 2.2$ Hz, 1H), 5.59 (s, 1H), 3.87 (d, $J = 13.9$ Hz, 1H), 3.62 (d, $J = 13.9$ Hz, 1H); $^{13}\text{C NMR}$ (176 MHz, d_6 -DMSO) δ 169.8, 142.9, 139.7, 136.6, 136.4, 136.1, 135.8, 135.0, 134.9, 133.5, 133.2, 131.0, 73.5, 57.9; IR (neat, cm^{-1}): 2924, 1665, 1044; HRMS (ESI): found m/z 361.9771 [$\text{M}+\text{Na}^+$] $^+$, calcd for [$\text{C}_{15}\text{H}_{11}\text{Cl}_2\text{NO}_3\text{S}+\text{Na}^+$] 361.9785.

7-Chloro-5-(2-chlorophenyl)-1,5-dihydrobenzo[e][1,4]thiazepin-2(3H)-one 4,4-dioxide (18).

$^1\text{H NMR}$ (400 MHz, d_6 -DMSO) δ 10.94 (br s, 1H), 8.26 – 8.23 (m 1H), 7.71 – 7.57 (m, 4H), 7.34 (d, $J = 8.6$ Hz, 1H), 7.06 (d, $J = 2.3$ Hz, 1H), 5.94 (s, 1H), 4.44 (d, $J = 13.6$ Hz, 1H), 4.25 (d, $J = 13.6$ Hz, 1H).; **IR** (neat, cm^{-1}): 2926, 2409, 1686, 1132, 1113, 1036; **HRMS (ESI)**: found m/z 355.9911 $[\text{M}+\text{H}^+]^+$, calcd for $[\text{C}_{15}\text{H}_{11}\text{Cl}_2\text{NO}_3\text{S}+\text{H}^+]$ 355.9909.

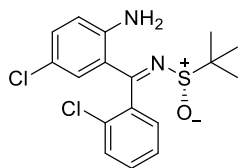
6.8.3. Diastereoselective synthesis of CGP-37157 aza-analogue**Synthesis of sulfinilimine 23**

2-Amino-2',5-dichlorobenzophenone (1.0 g, 8 mmol), (*R,S*)-*tert*-butanesulfinamide (1.0 eq) and neat $\text{Ti}(\text{OEt})_4$ (4.0 eq) were placed in microwaves tube at 100 °C for 1h under argon atmosphere. Then, the reaction was cooled to ambient temperature, a mixture of water and ethyl acetate was added and resulting slurry was filtered through a plug of Celite. The filter cake was washed with ethyl acetate. The organic layer from the filtrate was washed with brine, dried over anhydrous Na_2SO_4 , and the solvent was removed *in vacuo*. The residue was purified by column chromatography on silica gel using as eluent a 6:4 *n*-hexane-ethyl acetate mixture to afford 1240 mg (42%) of **23** as a yellow solid.

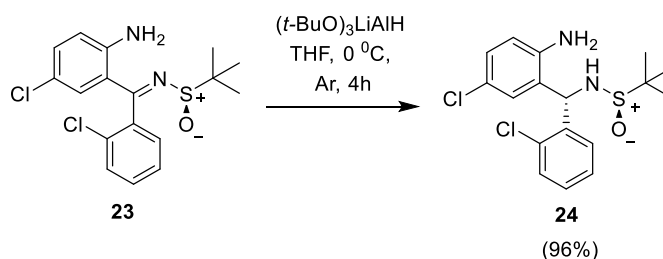
(*R,Z*)-N-((2-Amino-5-chlorophenyl)(2-chlorophenyl)methylene)-2-methylpropane-2-sulfinamide (*R-23*)

Mp: 138-139 °C; $[\alpha]_D^{25} = -40.00$ ($c = 1.00$ mg/mL, CHCl_3); $^1\text{H NMR}$ (250 MHz, CDCl_3) δ 7.61 – 7.32 (m, 4H), 7.24 – 7.11 (m, 1H), 6.76 (d, $J = 2.3$ Hz, 1H), 6.73 (d, $J = 8.9$ Hz, 1H), 5.90 (br s, 2H), 1.30 (s, 9H); $^{13}\text{C NMR}$ (63 MHz, CDCl_3) δ 149.3, 135.5, 133.9, 132.4, 131.0, 130.9, 130.8, 129.9, 129.7, 127.1, 120.6, 118.6, 117.4, 55.4, 22.4;

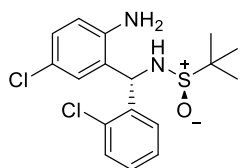
IR (neat, cm^{-1}): 3373, 3273, 1516, 1237, 1053; **elemental analysis (%) calcd. for $\text{C}_{17}\text{H}_{18}\text{Cl}_2\text{N}_2\text{OS}$** : C 55.29, H 4.91, N 7.59, S 8.68; found: C 55.06, H 4.97, N 7.71, S 8.82.

(S,Z)-N-((2-Amino-5-chlorophenyl)(2-chlorophenyl)methylene)-2-methylpropane-2-sulfinamide (S-23)

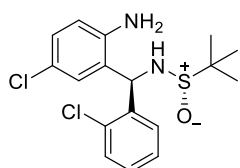
$[\alpha]_D^{25} = +43.00$ ($c = 1.09$ mg/mL, CHCl_3); $^1\text{H NMR}$ (250 MHz, CDCl_3) δ 7.61 – 7.32 (m, 4H), 7.24 – 7.11 (m, 1H), 6.76 (d, $J = 2.3$ Hz, 1H), 6.73 (d, $J = 8.9$ Hz, 1H), 5.90 (br s, 2H), 1.30 (s, 9H);

Diastereoselective reduction of sulfinylimine 23

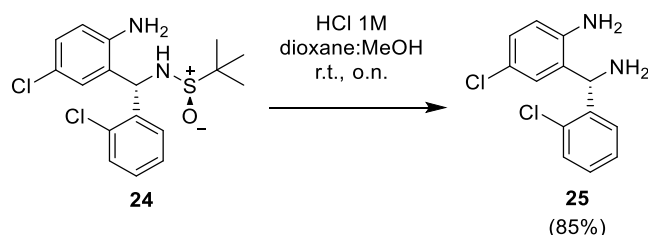
Sulfinylimine **23** (4.33 mmol) was dissolved in anhydrous THF (10 mL/mmol of **23**) and cooled to 0 °C under argon atmosphere. Lithium tri-*tert*-butoxyaluminum hydride (1.0 M solution in THF, 4.0 eq) was added dropwise, and the resulting solution was stirred and warmed to room temperature for 4 h. The reaction was monitored by TLC and after the imine consumption the reaction was diluted with EtOAc (60 mL). The mixture was cooled to 0 °C and water (20 mL) was added and the layers were separated. The organic phase was washed with brine, dried over anhydrous Na_2SO_4 , and concentrated to dryness to give 692 mg (96%) of compound **24** as a single diastereomer, without the need of further purification.

(R)-N-[(S)-(2-Amino-5-chlorophenyl)(2-chlorophenyl)methyl]-2-methylpropane-2-sulfinamide (R,S-24)

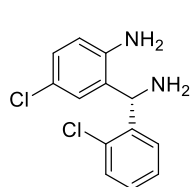
Pale yellow solid; mp: 165 °C; $^1\text{H NMR}$ (250 MHz, CDCl_3) δ 7.72 (dd, $J = 7.9, 1.7$ Hz, 1H), 7.43 – 7.27 (m, 3H), 7.06 (dd, $J = 8.5, 2.4$ Hz, 1H), 6.68 (d, $J = 8.5$ Hz, 1H), 6.46 (d, $J = 2.4$ Hz, 1H), 5.88 (d, $J = 2.1$ Hz, 1H), 4.28 (br s, 2H), 3.53 (d, $J = 2.1$ Hz, 1H), 1.27 (s, 9H); $^{13}\text{C NMR}$ (63 MHz, CDCl_3) δ 143.4, 137.8, 133.7, 130.2, 129.4, 129.4, 129.2, 127.8, 126.9, 125.7, 122.4, 118.1, 56.1, 54.2, 22.7; IR (neat, cm^{-1}): 3358, 3290, 1632, 1486, 1054; elemental analysis (%) calcd. for $\text{C}_{17}\text{H}_{20}\text{Cl}_2\text{N}_2\text{OS}$: C 54.99, H 5.43, N 7.54, S 8.63; found: C 55.57, H 5.67, N 7.30, S 8.77.

(S)-N-[(R)-(2-Amino-5-chlorophenyl)(2-chlorophenyl)methyl]-2-methylpropane-2-sulfinamide(S,R-24)

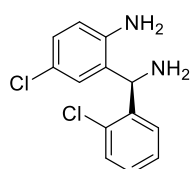
$^1\text{H NMR}$ (250 MHz, CDCl_3) δ 7.80 – 7.63 (m, 1H), 7.43 – 7.21 (m, 1H), 7.01 (dd, $J = 8.5, 2.4$ Hz, 1H), 6.65 (d, $J = 8.5$ Hz, 1H), 6.45 (d, $J = 2.4$ Hz, 1H), 5.87 (d, $J = 2.4$ Hz, 1H), 4.60 (br s, 2H), 3.64 (d, $J = 2.5$ Hz, 1H), 1.25 (s, 9H).

Cleavage of the *N*-*tert*-butylsulfinyl chiral auxiliary

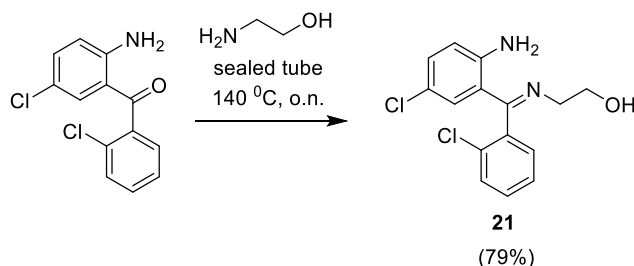
To a solution of acetyl chloride (4.0 equiv) in a 1:1 mixture of 1,4-dioxane and MeOH (20 mL) was added compound **24** (2.69 mmol) and the mixture was stirred at room temperature for 3 h. Then, the reaction was concentrated *in vacuo* to dryness and the residue was dissolved in water (20 mL), basified to pH 8 with concentrated aqueous NH_4OH solution and extracted with EtOAc (3 x 40 mL). The combined organic layers were dried over anhydrous Na_2SO_4 and the solvent was removed under reduced pressure to afford 610 mg (85%) of the pure diamine **25** as a colourless oil.

(S)-2-[Amino(2-chlorophenyl)methyl]-4-chloroaniline (**S**-25)

$[\alpha]_D^{25} = +36.00$ ($c = 1.00$ mg/mL, CHCl_3); $^1\text{H NMR}$ (250 MHz, CDCl_3) δ 7.39 (app dt, $J = 7.1, 2.4$ Hz, 2H), 7.26 (m, 2H), 7.04 (dd, $J = 8.4, 2.4$ Hz, 1H), 6.94 (d, $J = 2.4$ Hz, 1H), 6.59 (d, $J = 8.4$ Hz, 1H), 5.50 (s, 1H), 3.01 (br s, 4H); $^{13}\text{C NMR}$ (63 MHz, CDCl_3) δ 144.1, 140.6, 133.5, 129.9, 128.9, 128.7, 128.5, 128.0, 127.6, 127.4, 122.8, 117.5, 53.5; IR (neat, cm^{-1}): 3302, 2970, 1484, 1033; elemental analysis (%) calcd. for $\text{C}_{13}\text{H}_{12}\text{Cl}_2\text{N}_2$: C 58.45, H 4.53, N 10.49; found: C 58.28, H 4.39, N 10.79.

(R)-2-(Amino(2-chlorophenyl)methyl)-4-chloroaniline (**R**-25)

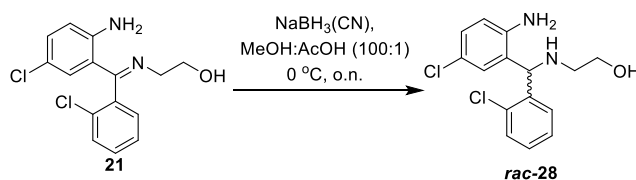
$[\alpha]_D^{25} = -36.00$ ($c = 1.00$ mg/mL, CHCl_3); $^1\text{H NMR}$ (250 MHz, CDCl_3) δ ; 7.40 (app dt, $J = 7.1, 2.4$ Hz, 2H), 7.27 (pd, $J = 7.3, 3.5$ Hz, 2H), 7.04 (dd, $J = 8.4, 2.4$ Hz, 1H), 6.94 (d, $J = 2.4$ Hz, 1H), 6.59 (d, $J = 8.4$ Hz, 1H), 5.50 (s, 1H), 4.37 (br s, 2H).

Synthesis of 2-[[[(2-amino-5-chlorophenyl)(2-chlorophenyl)methylene]amino]ethanol **21**

In a sealed tube 2-amino-2',5-dichlorobenzophenone (5 mmol) and ethanolamine (60 mmol) were stirred at 140 °C overnight. The mixture was cooled to room temperature and diluted with CH₂Cl₂ (60 mL). The organic layer was washed with water (3 x 20 mL), dried over anhydrous sodium sulfate and the solvent was removed under vacuum. The residue was purified by flash chromatography on silica gel eluting with a 3:1 hexane-ethyl acetate mixture to give compound **21** (1220 mg, 79%) as a yellow solid.

Mp: 125 °C; **¹H NMR (250 MHz, CDCl₃)** δ 7.55 – 7.46 (m, 1H), 7.45 – 7.32 (m, 2H), 7.13 – 7.02 (m, 2H), 6.73 (br s, 2H), 6.66 (d, *J* = 1.1 Hz, 1H), 6.64 (d, *J* = 4.9 Hz, 1H), 4.02 – 3.77 (m, 2H), 3.47 – 3.19 (m, 2H), 1.99 (br s, 1H); **¹³C NMR (63 MHz, CDCl₃)** δ 169.7, 147.8, 135.5, 131.5, 131.3, 130.9, 130.3, 130.1, 129.0, 127.5, 120.3, 119.5, 118.0, 63.2, 55.8; **IR (neat, cm⁻¹):** 3213, 1612, 1054; **elemental analysis (%) calcd. for C₁₅H₁₄Cl₂N₂O:** C 58.27, H 4.56, N 9.06; found: C 58.71, H 4.57, N 8.89.

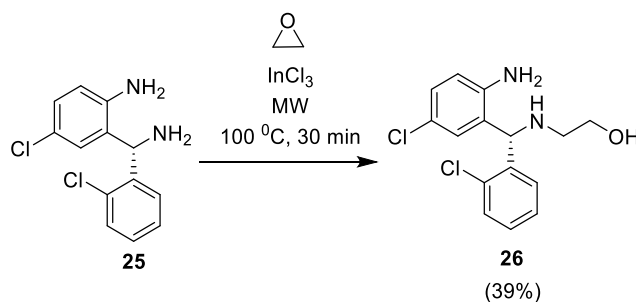
Synthesis of (±)-2-(((2-amino-5-chlorophenyl)(2-chlorophenyl)methyl)amino)ethanol **28**



To a stirred solution of **21** (7.0 mmol) in a 100:1 MeOH/AcOH mixture (70 mL), cooled in an ice bath, NaBH₃(CN) (35.0 mmol) was added. The mixture was stirred overnight and then, water (30 mL) was cautiously added and the reaction was warmed to room temperature. The mixture was extracted with CH₂Cl₂ (2 x 100 mL). The combined organic layers were dried over anhydrous magnesium sulfate, and concentrated under vacuum to give compound **rac-28** in quantitative yield as a light yellow solid.

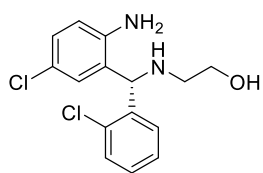
Mp 95 °C; **¹H NMR (250 MHz, CDCl₃)** δ 7.45 – 7.33 (m, 2H), 7.33 – 7.17 (m, 2H), 7.04 (dd, *J* = 8.4, 2.5 Hz, 1H), 6.98 (d, *J* = 2.5 Hz, 1H), 6.60 (d, *J* = 8.4 Hz, 1H), 5.26 (s, 1H), 3.73 (t, *J* = 5.1 Hz, 2H), 2.91 – 2.68 (m, 2H); **¹³C NMR (63 MHz, CDCl₃)** δ 144.5, 138.1, 134.0, 130.1, 129.4, 129.0, 128.6, 128.2, 127.5, 127.0, 123.0, 117.8, 61.9, 60.6, 49.8; **IR (neat, cm⁻¹):** 3234, 2925, 2848, 1485, 1468, 1034; **elemental analysis (%) calcd. for C₁₅H₁₆Cl₂N₂O:** C 57.89, H 5.18, N 9.00; found: C 55.10, H 4.91, N 8.35.

(*R*)-2-(((2-Amino-5-chlorophenyl)(2-chlorophenyl)methyl)amino)ethan-1-ol (**R-26**)



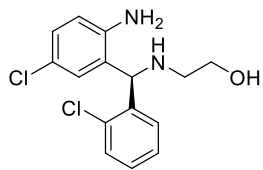
To a solution of diamine **25** (490 mg, 1.8 mmol) in dioxane (1 mL) placed in a microwaves tube was added a 2.5-3.3 M THF ethylene oxide solution (2.5 mL) and indium trichloride (0.18 mmol). The mixture was irradiated at 100 °C for 1 h under argon atmosphere. Then, the reaction was cooled to room temperature, diluted with ethyl acetate (30 mL) and washed with saturated sodium carbonate solution (10 mL) and water (10 mL). The organic layer was dried over anhydrous Na₂SO₄ and solvent was removed under reduced pressure. The residue was purified by column chromatography on silica gel using as eluent a 6:4 *n*-hexane-ethyl acetate mixture to afford 220 mg (39%) of the desired compound.

(S)-2-(((2-Amino-5-chlorophenyl)(2-chlorophenyl)methyl)amino)ethan-1-ol (S-26)



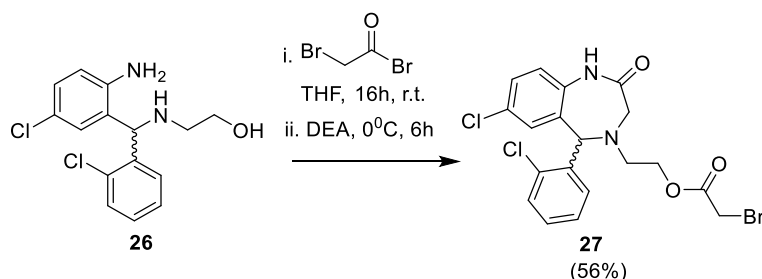
$[\alpha]_D^{25} = + 81.00$ (c = 0.9 mg/mL, CHCl₃) ee 93% The enantiomers were separated by HPLC (ULTRON ES OVM Chiral Analytical Reverse Phase, 5 μm, 4.6 mm x 150 L, buffer H₂PO₄ 20 mM pH 5.9/ MeOH 80:20, flow 1.0 mL/min, retention time 4.560 min (major), 5.210 min (minor); ¹H NMR (250 MHz, CDCl₃) δ 7.44 – 7.33 (m, 2H), 7.32 – 7.18 (m, 2H), 7.03 (dd, *J* = 8.4, 2.5 Hz, 1H), 6.97 (d, *J* = 2.4 Hz, 1H), 6.60 (d, *J* = 8.4 Hz, 1H), 5.25 (s, 1H), 3.72 (t, *J* = 5.1 Hz, 2H), 2.90 – 2.65 (m, 2H).

(R)-2-(((2-amino-5-chlorophenyl)(2-chlorophenyl)methyl)amino)ethan-1-ol (R-26)



$[\alpha]_D^{25} = - 78.00$ (c = 1.00 mg/mL, CHCl₃) ee 95% The enantiomers were separated by HPLC (ULTRON ES OVM Chiral Analytical Reverse Phase, 5 μm, 4.6 mm x 150 L, buffer H₂PO₄ 20 mM pH 5.9/ MeOH 80:20, flow 1.0 mL/min, retention time 4.603 min (minor), 5.023 min (major); ¹H NMR (250 MHz, CDCl₃) δ 7.44 – 7.33 (m, 2H), 7.31 – 7.18 (m, 2H), 7.03 (dd, *J* = 8.4, 2.5 Hz, 1H), 6.96 (d, *J* = 2.5 Hz, 1H), 6.59 (d, *J* = 8.4 Hz, 1H), 5.25 (s, 1H), 3.74 – 3.70 (dd, *J* = 4.8, 1.0 Hz, 1H), 3.69 (d, *J* = 4.8 Hz, 1H), 2.88 – 2.64 (m, 2H).

Synthesis of 2-(7-chloro-5-(2-chlorophenyl)-2-oxo-2,3,4,5-tetrahydro-1H-benzo[e][1,4]diazepin-4-yl)ethyl 2-bromoacetate



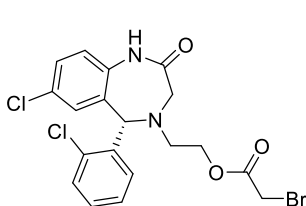
To a stirred solution of compound **26** (420 mg, 1.35 mmol) in CH₂Cl₂ (15 mL) at 0 °C was added bromoacetyl bromide (305 mL, 3.5 mmol). The stirring was continued at 0 °C for 1 hour and then at room temperature for 16 hours. DIEA (3.5 mL, 20 mmol) was added, and the reaction was stirred at 50 °C for 5 h. The mixture was cooled to room temperature, diluted with CH₂Cl₂ (30 mL) and washed with water (20 mL). The organic

layer was dried over anhydrous Na_2SO_4 and concentrated to dryness. The crude product was purified by column chromatography on silica gel eluting with a gradient from hexane to 6:4 hexane-ethyl acetate to give 1.9 g (59%) of compound **27** as a white solid.

2-(7-Chloro-5-(2-chlorophenyl)-2-oxo-2,3,4,5-tetrahydro-1H-benzo[e][1,4]diazepin-4-yl)ethyl 2-bromoacetate

Mp: 148-149 °C; **$^1\text{H NMR}$ (250 MHz, CDCl_3)** δ 8.28 (br s, 1H), 7.66 – 7.57 (m, 1H), 7.44 – 7.32 (m, 3H), 7.25 (dd, $J = 8.4, 2.2$ Hz, 2H), 6.99 (d, $J = 8.4$ Hz, 1H), 6.61 (d, $J = 2.2$ Hz, 1H), 5.29 (s, 1H), 4.41 (ddd, $J = 11.8, 7.9, 4.3$ Hz, 1H), 4.21 (dt, $J = 11.8, 4.8$ Hz, 1H), 3.86 (s, 2H), 3.56 (d, $J = 15.5$ Hz, 1H), 3.45 (dd, $J = 15.5, 1.2$ Hz, 1H), 3.06 (dt, $J = 14.2, 4.3$ Hz, 1H), 2.98 – 2.80 (ddd, $J = 14.2, 7.9, 4.8$ Hz, 1H); **$^{13}\text{C NMR}$ (63 MHz, CDCl_3)** δ 171.4, 167.2, 136.9, 136.6, 134.6, 132.7, 130.9, 130.8, 130.4, 130.3, 129.7, 129.1, 127.3, 122.2, 65.0, 63.9, 52.8, 52.0, 25.9; **IR (neat, cm^{-1}):** 2956, 1735, 1666, 905; **elemental analysis (%) calcd. for $\text{C}_{19}\text{H}_{17}\text{BrCl}_2\text{N}_2\text{O}_3$:** C 48.33, H 3.63, N 5.93; found: C 48.18, H 3.52, N 5.82.

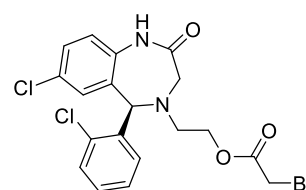
(S)-2-(7-Chloro-5-(2-chlorophenyl)-2-oxo-1,2,3,5-tetrahydro-4H-benzo[e][1,4]diazepin-4-yl)ethyl 2-bromoacetate (S-27)



$^1\text{H NMR}$ (250 MHz, CDCl_3) δ 8.49 (br s, 1H), 7.68 – 7.61 (m, 1H), 7.50 – 7.33 (m, 3H), 7.26 (dd, $J = 8.5, 2.2$ Hz, 1H), 7.02 (d, $J = 8.5$ Hz, 1H), 6.63 (d, $J = 2.2$ Hz, 1H), 5.31 (s, 1H), 4.43 (ddd, $J = 11.7, 7.9, 4.3$ Hz, 1H), 4.24 (dt, $J = 11.7, 4.9$ Hz, 1H), 3.88 (s, 2H), 3.58 (d, $J = 15.5$ Hz, 1H), 3.48 (dd, $J = 15.5, 1.3$ Hz, 1H), 3.09 (dt, $J = 14.2, 4.3$ Hz, 1H), 2.92 (ddd, $J = 14.2, 7.9, 4.9$ Hz,

1H).

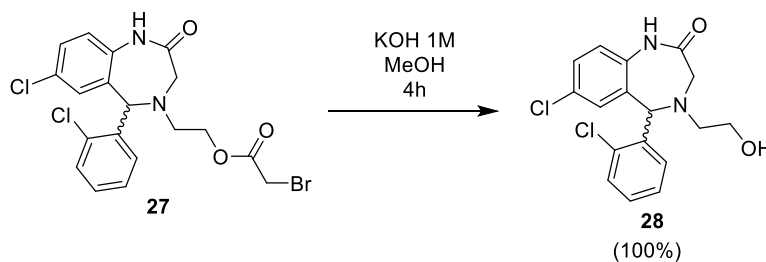
(R)-2-(7-Chloro-5-(2-chlorophenyl)-2-oxo-1,2,3,5-tetrahydro-4H-benzo[e][1,4]diazepin-4-yl)ethyl 2-bromoacetate (R-27)



$^1\text{H NMR}$ (250 MHz, CDCl_3) δ 8.90 (s, 1H), 7.66 – 7.59 (m, 1H), 7.47 – 7.33 (m, 3H), 7.26 (d, $J = 2.3$ Hz, 1H), 7.05 (d, $J = 8.5$ Hz, 1H), 6.64 (d, $J = 2.2$ Hz, 1H), 5.32 (s, 1H), 4.44 (ddd, $J = 11.8, 7.9, 4.4$ Hz, 1H), 4.24 (dt, $J = 11.8, 4.9$ Hz, 1H), 3.88 (s, 2H), 3.59 (d, $J = 15.5$ Hz, 1H), 3.49 (dd, $J = 15.5, 1.1$ Hz, 1H), 3.09

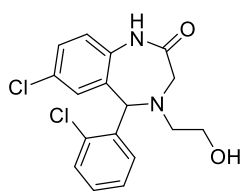
(dt, $J = 14.2, 4.4$ Hz, 1H), 3.02 – 2.86 (ddd, $J = 14.2, 7.9, 4.9$ Hz, 1H).

Synthesis of 7-chloro-5-(2-chlorophenyl)-4-(2-hydroxyethyl)-4,5-dihydro-1H-benzo[e][1,4]diazepin-2(3H)-one



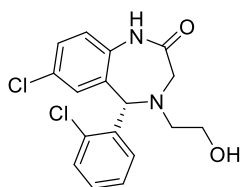
Compound **27** (1 mmol) was dissolved in methanol and a 10% KOH methanol solution (10 mL) was added. The reaction was monitored by TLC and additional 10% KOH methanol solution was added until the starting material was no longer detected. Then, the reaction was diluted with water (20 mL), neutralized with 2M HCl solution and extracted with CHCl_3 (3 x 40 mL). The combined organic layers were dried over sodium sulphate, filtered and the solvent was removed *in vacuo*. No further purification was needed.

rac-7-Chloro-5-(2-chlorophenyl)-4-(2-hydroxyethyl)-4,5-dihydro-1H-benzo[e][1,4]diazepin-2(3H)-one (**19**)



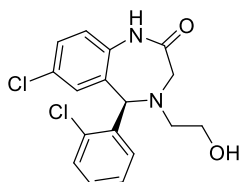
Mp: 163 °C; $^1\text{H NMR}$ (250 MHz, CDCl_3) δ 8.48 (s, 1H), 7.48 – 7.42 (m, 1H), 7.35 – 7.19 (m, 5H), 6.98 (d, $J = 8.5$ Hz, 1H), 6.82 (d, $J = 2.3$ Hz, 1H), 5.39 (s, 1H), 3.85 – 3.57 (m, 2H), 3.52 (s, 2H), 3.02 – 2.80 (m, 2H), 2.50 (br s, 1H); $^{13}\text{C NMR}$ (63 MHz, CDCl_3) δ 173.0, 137.0, 135.8, 134.4, 131.5, 131.1, 130.8, 130.7, 130.1, 129.8, 129.2, 127.4, 121.9, 65.8, 58.8, 55.1, 52.4.; **IR** (neat, cm^{-1}): 3396, 2925, 1676, 1040; **elemental analysis (%) calcd. for $\text{C}_{17}\text{H}_{16}\text{Cl}_2\text{N}_2\text{O}_2$:** C 58.14, H 4.59, N 7.98; found: C 58.46, H 4.72, N 7.74.

(*5S*)-7-Chloro-5-(2-chlorophenyl)-4-(2-hydroxyethyl)-4,5-dihydro-1H-benzo[e][1,4]diazepin-2(3H)-one (**S-28**)



$[\alpha]_D^{25} = +114$ ($c = 1.00$ mg/mL, CHCl_3); ee 93% The enantiomers were separated by HPLC (ULTRON ES OVM Chiral Analytical Reverse Phase, 5 μm , 4.6 mm x 150 L, buffer H_2PO_4 20 mM pH 5.9/ *i*-PrOH80:20, flow 1.0 mL/min, retention time 4.643 min (minor), 5.090 min (major); $^1\text{H NMR}$ (250 MHz, CDCl_3) δ 8.48 (s, 1H), 7.48 – 7.42 (m, 1H), 7.35 – 7.19 (m, 5H), 6.98 (d, $J = 8.5$ Hz, 1H), 6.82 (d, $J = 2.3$ Hz, 1H), 5.39 (s, 1H), 3.85 – 3.57 (m, 2H), 3.52 (s, 2H), 3.02 – 2.80 (m, 2H), 2.50 (br s, 1H).

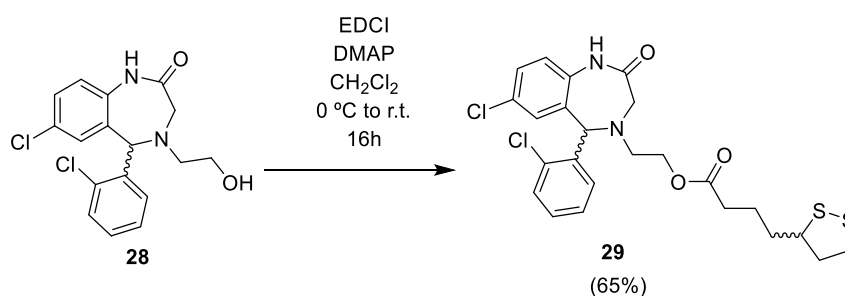
(*5R*)-7-Chloro-5-(2-chlorophenyl)-4-(2-hydroxyethyl)-4,5-dihydro-1H-benzo[e][1,4]diazepin-2(3H)-one (**R-28**)



$[\alpha]_D^{25} = -116.00$ ($c = 1.04$ mg/mL, CHCl_3); ee 97% The enantiomers were separated by HPLC (ULTRON ES OVM Chiral Analytical

Reverse Phase, 5 μ m, 4.6 mm x 150 L, buffer H₂PO₄ 20 mM pH 5.9/ CH₃CN 80:20, flow 1.0 mL/min, retention time 4.427 min (major), 5.457 min (major); ¹H NMR (250 MHz, CDCl₃) δ 8.48 (s, 1H), 7.48 – 7.42 (m, 1H), 7.35 – 7.19 (m, 5H), 6.98 (d, *J* = 8.5 Hz, 1H), 6.82 (d, *J* = 2.3 Hz, 1H), 5.39 (s, 1H), 3.85 – 3.57 (m, 2H), 3.52 (s, 2H), 3.02 – 2.80 (m, 2H), 2.50 (br s, 1H).

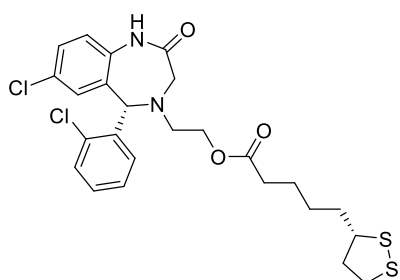
6.8.4. Synthesis of 2-(7-chloro-5-(2-chlorophenyl)-2-oxo-2,3,4,5-tetrahydro-1H-benzo[e][1,4]diazepin-4-yl)ethyl 5-(1,2-dithiolan-3-yl)pentanoate (20)



Compound **28** (50 mg, 0.14 mmol), α -lipoic acid (racemic mixture (\pm), (*R*)-(+)-enantiomer or (*S*)-(-)-enantiomer) (0.17 mmol) and DMAP (0.43 mmol) were dissolved in anhydrous dichloromethane (5 mL) in argon atmosphere. The mixture was cooled at 0 °C and a solution of EDCI (0.17 mmol) in anhydrous dichloromethane (2 mL) was added dropwise. The reaction was kept at room temperature for 16 hours. Then, the reaction was diluted with dichloromethane (30 mL), washed with water (10 mL), dried over anhydrous Na₂SO₄ and the solvent was removed under reduced pressure. The residue was purified by column chromatography in silica gel eluting with a gradient from hexane to 6:4 hexane-ethyl acetate to give 49 mg (65%) of compound **29** as a colourless viscous oil.

¹H NMR (250 MHz, CDCl₃) δ 8.50 (s, 1H), 7.66 – 7.55 (m, 1H), 7.48 – 7.41 (m, 1H), 7.37 (m, 2H), 7.32 – 7.24 (m, 1H), 7.02 (d, *J* = 8.4 Hz, 1H), 6.64 (d, *J* = 1.8 Hz, 1H), 5.33 (s, 1H), 4.40 – 4.25 (m, 1H), 4.25 – 4.10 (m, 1H), 3.68 – 3.42 (m, 3H), 3.29 – 2.98 (m, 3H), 2.97 – 2.80 (m, 1H), 2.57 – 2.41 (m, 1H), 2.36 (t, *J* = 7.2 Hz, 2H), 2.01 – 1.84 (m, 1H), 1.80 – 1.59 (m, 4H), 1.59 – 1.39 (m, 2H); ¹³C NMR (63 MHz, CDCl₃) δ 173.4, 172.0, 137.0, 136.6, 134.6, 132.6, 130.8, 130.6, 130.4, 130.2, 129.6, 129.0, 127.1, 122.2, 65.1, 62.1, 56.4, 53.0, 52.2, 40.3, 38.6, 34.7, 34.1, 28.9, 24.7; IR (neat, cm⁻¹): 2927, 1728, 1665, 1483, 1034; elemental analysis (%) calcd. for C₂₄H₂₆Cl₂N₂O₃S₂: C 54.85, H 4.99, N 5.33, S 11.89; found: C 55.47, H 5.08, N 5.16, S 11.75.

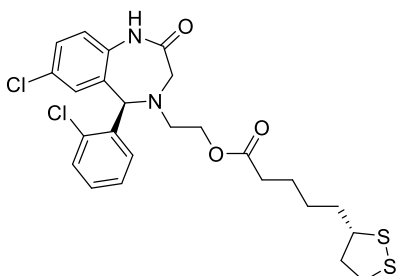
2-((*S*)-7-Chloro-5-(2-chlorophenyl)-2-oxo-1,2,3,5-tetrahydro-4H-benzo[e][1,4]diazepin-4-yl)ethyl 5-((*S*)-1,2-dithiolan-3-yl)pentanoate (29)



$[\alpha]_D^{25}$ = + 165.00 (c = 1.00 mg/mL, CHCl₃); ¹H NMR (300 MHz, CDCl₃) δ 8.71 (s, 1H), 7.62 – 7.52 (m, 1H), 7.44 – 7.38 (m, 1H), 7.35 – 7.29 (m, 2H), 7.24 (dd, *J* = 8.5, 2.2 Hz, 1H), 7.00 (d, *J* = 8.5 Hz, 1H), 6.61 (d, *J* = 2.2 Hz, 1H), 5.30 (s, 1H), 4.34 – 4.23 (m, 1H), 4.20 – 4.05 (m, 1H), 3.61 – 3.42 (m, 4H), 3.22 – 2.97 (m, 3H), 2.95 – 2.79

(m, 1H), 2.53 – 2.38 (m, 1H), 2.32 (t, $J = 7.3$ Hz, 2H), 1.97 – 1.80 (m, 1H), 1.74 – 1.58 (m, 4H), 1.52 – 1.39 (m, 2H).

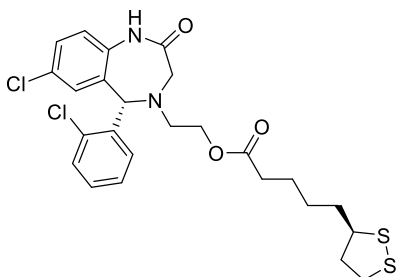
2-((*R*)-7-Chloro-5-(2-chlorophenyl)-2-oxo-1,2,3,5-tetrahydro-4*H*-benzo[*e*][1,4]diazepin-4-yl)ethyl 5-((*S*)-1,2-dithiolan-3-yl)pentanoate (30)



$[\alpha]_D^{25} = +140.00$ ($c = 1.00$ mg/mL, CHCl_3); $^1\text{H NMR}$ (300 MHz, CDCl_3) δ 8.30 (br s, 1H), 7.63 – 7.54 (m, 1H), 7.44 – 7.39 (m, 1H), 7.38 – 7.27 (m, 2H), 7.24 (dd, $J = 8.4$, 2.2 Hz, 1H), 6.97 (d, $J = 8.4$ Hz, 1H), 6.61 (d, $J = 2.2$ Hz, 1H), 5.30 (s, 1H), 4.35 – 4.21 (m, 1H), 4.21 – 4.09 (m, 1H), 3.61 – 3.39 (m, 3H), 3.22 – 2.96 (m, 3H), 2.94 – 2.78 (m, 1H), 2.51 – 2.39 (m, 1H), 2.32 (td, $J = 7.3$, 1.6 Hz, 2H), 1.96 – 1.83 (m, 1H), 1.72 – 1.58 (m, 4H), 1.52

– 1.38 (m, 2H).

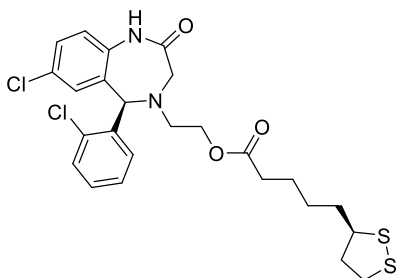
2-((*S*)-7-Chloro-5-(2-chlorophenyl)-2-oxo-1,2,3,5-tetrahydro-4*H*-benzo[*e*][1,4]diazepin-4-yl)ethyl 5-((*R*)-1,2-dithiolan-3-yl)pentanoate (31)



$[\alpha]_D^{25} = -138.00$ ($c = 0.9$ mg/mL, CHCl_3) $^1\text{H NMR}$ (300 MHz, CDCl_3) δ 8.31 (br s, 1H), 7.56 – 7.47 (m, 1H), 7.38 – 7.31 (m, 1H), 7.31 – 7.22 (m, 2H), 7.17 (dd, $J = 8.5$, 2.2 Hz, 1H), 6.91 (d, $J = 8.5$ Hz, 1H), 6.55 (d, $J = 2.2$ Hz, 1H), 5.23 (s, 1H), 4.30 – 4.14 (m, 1H), 4.14 – 4.00 (m, 1H), 3.55 – 3.32 (m, 3H), 3.16 – 2.88 (m, 3H), 2.87 – 2.67 (m, 1H), 2.47 – 2.31 (m, 1H), 2.25 (t, $J = 7.3$ Hz, 2H), 1.93 – 1.74 (m, 1H), 1.66 – 1.53 (m, 4H), 1.48 –

1.29 (m, 2H).

2-((*R*)-7-Chloro-5-(2-chlorophenyl)-2-oxo-1,2,3,5-tetrahydro-4*H*-benzo[*e*][1,4]diazepin-4-yl)ethyl 5-((*R*)-1,2-dithiolan-3-yl)pentanoate (32)



$[\alpha]_D^{25} = -160.00$ ($c = 1.00$ mg/mL, CHCl_3); $^1\text{H NMR}$ (300 MHz, CDCl_3) δ 8.41 (br s, 1H), 7.62 – 7.51 (m, 1H), 7.45 – 7.38 (m, 1H), 7.37 – 7.27 (m, 2H), 7.24 (dd, $J = 8.5$, 2.2 Hz, 1H), 6.98 (d, $J = 8.5$ Hz, 1H), 6.61 (d, $J = 2.2$ Hz, 1H), 5.30 (s, 1H), 4.35 – 4.22 (m, 1H), 4.21 – 4.09 (m, 1H), 3.61 – 3.40 (m, 3H), 3.23 – 2.96 (m, 3H), 2.93 – 2.78 (m, 1H), 2.52 – 2.38 (m, 1H), 2.32 (td, $J = 7.3$, 1.5 Hz, 2H), 1.97 – 1.82 (m, 1H), 1.73 – 1.57 (m, 4H), 1.54

– 1.38 (m, 2H).

**CHAPTER 7. CARBOHYDRATE HETEROCYCLIC
HYBRIDS AS GALECTIN MODULATORS**

7.1. Galectins: structure, function and location.

7.1.1. Introduction to galectins

Lectins are a large group of specific carbohydrate-binding molecules that take part in several molecular and cellular recognition processes like promoting the migration of immune cells through the endothelium, activation or inhibition of T or B cells, cytokine secretion and signalling, recognition of pathogen-associated patterns of glycan-containing molecules like lipopolysaccharide (LPS), among others.²⁶⁰

Galectins are a subset of lectins defined by a common carbohydrate recognition domain (CRD). The CRD motif has a β -sheet sandwich structure conformed by two antiparallel β -sheet layers (Figure 7.1). This structure contains a pocket in which carbohydrates can be recognized. The term galectin was proposed in 1994,²⁶¹ because the short carbohydrate ligand for most galectins contains lactosamine, *i.e.* galactose and *N*-acetylglucosamine bound by a β -linkage. In mammals there are 15 different subtypes of galectins and are widespread localized in cytoplasm, nucleus, extracellular matrix. Although they lack enzymatic activity, galectins are involved in cell cycle regulation, immune response and apoptosis. Hence, galectins are attractive targets for the development of selective modulators.

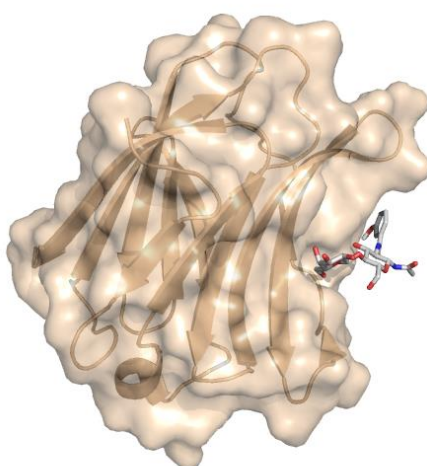


Figure 7.1: Structure of galectin-3. PDB: 5NF9

²⁶⁰ Thiemann, S.; Baum, L. G. *Annu. Rev. Immun.* **2016**, *34*, 243-264.

²⁶¹ Barondes, S. H.; Castronovo, V.; Cooper, D. N. W.; Cummings, R. D.; Drickamer, K.; Felzi, T.; Gitt, M. A.; Hirabayashi, J.; Hughes, C.; Kasai, K. -I.; Leffler, H.; Liu, F. -T.; Lotan, R.; Mercurio, A. M.; Monsigny, M.; Pillai, S.; Poirer, F.; Raz, A.; Rigby, P. W. J.; Rini, J. M.; Wang, J. L. *Cell* **1994**, *76*, 597-598.

In mammals, galectins are classified into three subfamilies, namely prototype, chimera and tandem-repeat according to their structure. The prototype subfamily is formed by galectins-1, -2, -5, -7, -10, -11, -13, -14 and -15 and is characterized by the formation of homodimers non-covalently joined by the back of CDR.

Galectin-4, -6, -8, -9 and -12 form the tandem-repeat or bivalent subset. These galectins are formed by two different CDR moieties linked by a flexible peptide. These galectins can show linkers with varied lengths,²⁶² caused by alternative splicing of linker-encoding RNA.²⁶³

The chimera type is a subset of galectins formed by galectin-3 in mammals. This galectin has the CRD in C-terminal and can dimerize in this point.²⁶⁴ However, the N-terminal domain is responsible for the multimerization of chimera-type galectins resulting in a pentamer.²⁶⁵ This multimerization process allows galectin-3 to bind multivalent glycan ligands in a surface (Figure 7.2).²⁶⁶

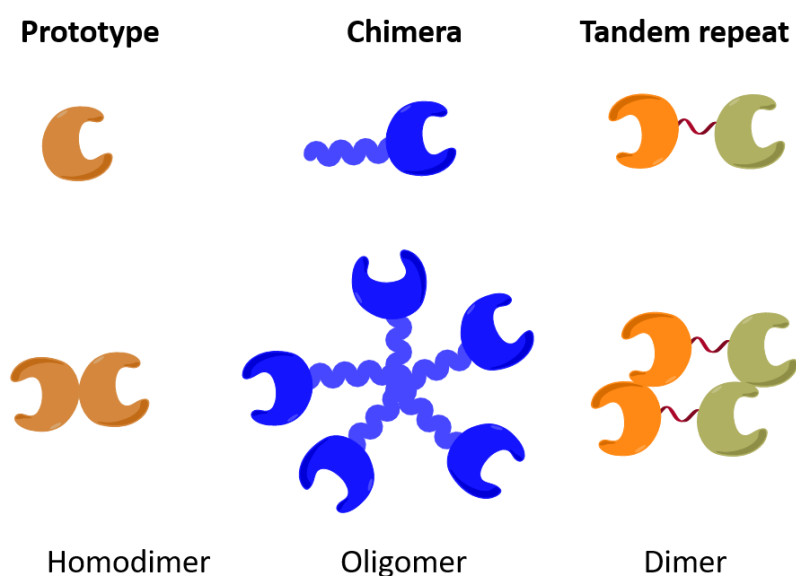


Figure 7.2

²⁶² Sato, M.; Nishi, N.; Shoji, H.; Seki, M.; Hashidate, T.; Hirabayashi, J.; Kasai, K. -I.; Hata, Y.; Suzuki, S.; Hirashimata, M.; Nakamura, T. *Glycobiology* **2002**, *12*, 191-197.

²⁶³ Spitzenberger, F.; Graessler, J.; Schroeder, H. E. *Biochimie* **2001**, *83*, 851-862.

²⁶⁴ Yang, R. Y.; Hill, P. N.; Hsu, D. K.; Liu, F. T. *Biochemistry* **1998**, *37*, 4086-4092.

²⁶⁵ Lepur, A.; Salomonsson, E.; Nilsson, U. J.; Leffler, H. *J. Biol. Chem.* **2012**, *287*, 21751-21756.

²⁶⁶ Ahmad, N.; Gabius, H. J.; André, S.; Kaltner, H.; Sabesan, S.; Roy, R.; Bingcan, L.; Macaluso, F.; Brewer, C. F. *J. Biol. Chem.* **2004**, *279*, 10841-10847.

The galectins can be found in the cytosol, participate in protein-protein interactions and take part in several intracellular events. For example, galectin-3 regulates apoptosis and autophagy.^{267, 268} Also, galectins -3 and -1 can moved to the nucleus and stabilize protein-DNA interactions, promoting transcription.²⁶⁹ However, the best-known and studied role for galectins is the binding to cell surface glycolipids and glycoprotein receptors. Galectins are synthesized in cytoplasm by free ribosomes,²⁷⁰ and are not able to be exported by the endoplasmic reticulum-Golgi secretory pathway.²⁷¹ These galectins are secreted by a non-classical pathway by accumulation in the cytosolic side of the plasma membrane and secreted by exosomes or formation of vesicles. Also, some evidences shown the ability of these molecules to directly translocate through membranes by a poorly understood mechanism.^{272, 273}

7.1.2. Role of Gal-3 in neuroinflammation

The role of galectin-3 in neuroinflammation remains controversial. Their role in the CNS remains poorly known and both neuroprotective or neuroinflammatory roles were reported by different studies.

Some recent evidences seem to point to a deleterious role of galectin 3 in brain injury and degeneration. In acute brain inflammation, an increased release of galectin-3 was described.²⁷⁴ Also, binding and subsequent activation of TLR4 was described, rising the proinflammatory microglia M1 phenotype. Thus, galectin-3 has a role in ischemic environment and contributes to the long-term proinflammatory response.

On the other hand, galectin-3 induces a neuroprotective effect *via* crosslinking of growth factor receptors (GFRs) by oligomerized galectin-3, avoiding their removal from

²⁶⁷ Yu, F.; Finley, R. L.; Raz, A.; Kim, H. R. C. *J. Biol. Chem.* **2002**, *277*, 15819-15827.

²⁶⁸ Shi, Y.; He, B.; Kuchenbecker, K. M.; You, L.; Xu, Z.; Mikami, I.; Yagui-Beltran, A.; Genevieve, C.; Yu-Chin, L.; Okamoto, J.; Bravo, D. T. *Int. J. Cancer* **2007**, *121*, 1175-1181.

²⁶⁹ Patterson, R. J.; Wang, W.; Wang, J. L. *Glycoconj. J.* **2002**, *19*, 499-506.

²⁷⁰ Rabinovich, G. A.; Rubinstein, N.; Fainboim, L. *J. Leukoc. Biol.* **2002**, *71*, 741-752.

²⁷¹ Cooper, D. N.; Barondes, S. H. *J. Cell Biol.* **1990**, *110*, 1681-1691.

²⁷² Nickel, W. *Eur. J. Biochem.* **2003**, *270*, 2109-2119.

²⁷³ Cho, M.; Cummings, R. D. *J. Biol. Chem.* **1995**, *270*, 5207-5212.

²⁷⁴ Burguillos, M. A.; Svensson, M.; Schulte, T.; Boza-Serrano, A.; García-Quintanilla, A.; Kavanagh, E.; Santiago, M.; Viceconte, N.; Oliva-Martin, M. J.; Osman, A. M.; Salomonsson, E.; Amar, L.; Persson, A.; Blomgren, K.; Achour, A.; Englund, E.; Leffler, H.; Venero, J. L.; Joseph, B.; Deierborg, T. *Cell Reports* **2015**, *10*, 1626-1638.

the cell surface by endocytosis and leading to an improvement in GF signalling.^{275, 276} Galectin 3 can also induce alternative microglia activation by CD98 binding.²⁷⁷ As discussed in the introduction, microglia activation is a hallmark in NDDs and brain injuries like stroke.

Furthermore, Boza-Serrano and co-workers²⁷⁸ noted overexpression of galectin-3 in a 5xFAD AD mouse model, defined by 5 linked AD mutations. These mice display a decrease both in load and size of β -amyloid plaques. Also, galectin-3 downregulation in this mouse model leads to a change in size and morphology of dystrophic neurites, which recover the irregular morphology. Besides, the downregulation in galectin-3 promotes an important decrease in microglial cells in the neighbourhood of β A plaques. All these biological relevant alterations may be due to the binding of galectin-3 to TREM2 (triggering receptor expressed on myeloid cells 2), which is tightly related to AD progression. Both galectin-3 and TREM2 colocalize in the β A plaques of AD samples.

7.1.3. Galectin-3 modulators

As described above, the roles of galectin-3 in neurodegenerative disease and ischemia are unclear. However, there is much evidence for an important microglial phenotype tuning by galectin-3. For this reason, the design of new selective modulators of the function of galectin-3 in the neuroprotective phenotype in microglia offers a pathway for a better understanding of these pathologies and can be regarded as an innovative target in NDD.

²⁷⁵ Lalancette-Hébert, M.; Swarup, V.; Beaulieu, J. M.; Bohacek, I.; Abdelhamid, E.; Weng, Y. C.; Sato, S.; Kriz, J. J. *Neurosci.* **2012**, *32*, 10383–10395.

²⁷⁶ Partridge, E. A.; Le Roy, C.; Di Guglielmo, G. M.; Pawling, J.; Cheung, P.; Granovsky, M.; Nabi, I.R.; Wrana, J. L.; Dennis, J. W. *Science* **2004**, *306*, 120-124.

²⁷⁷ MacKinnon, A. C.; Farnworth, S. L.; Hodkinson, P. S.; Henderson, N. C.; Atkinson, K. M.; Leffler, H.; Nilsson, U. J.; Haslett, C.; Forbes, S. J.; Sethi, T. J. *Immunol.* **2008**, *180*, 2650-2658.

²⁷⁸ Boza-Serrano Ruiz, A.; Sánchez-Varo, R.; García-Revilla, J.; Jiménez-Ferrer Y. Y.; Paulus, A.; Wennström, M.; Vilalta, A.; Allendorf, D.; Dávila, J. C.; Stegmayr, J.; Jiménez, S.; Roca-Ceballos M. A.; Navarro-Garrido, V.; Swanberg, M.; Hsieh, C. L.; Real, L. M.; Englund, E.; Linse, S.; Leffler, H.; Nilsson, U. J.; Brown, G. C.; Gutiérrez, A.; Vitorica, J.; Venero, J. L. *Acta Neuropathol.* **2019**, *138*, 251-273.

7.2. Design of selective galectin-3 modulators²⁷⁹

The design was carried out *via* a fragment-based approach, by virtual screening of different drug-like fragments in the Maybridge database in several galectins, choosing the fragments with the best scores and proper orientation and conformation to bind the position 3 of OMe-Lac in their binding site. Then, from the 106 fragments that fulfil the conditions previously described, the heterocycle-disaccharide hybrid was built. Finally, the 106 structures were docked in galectins-1, -3 and 9. The lowest scoring energy lactose-like configuration was chosen. Also, commercial ability and synthetic accessibility criteria were applied (Figure 7.3).

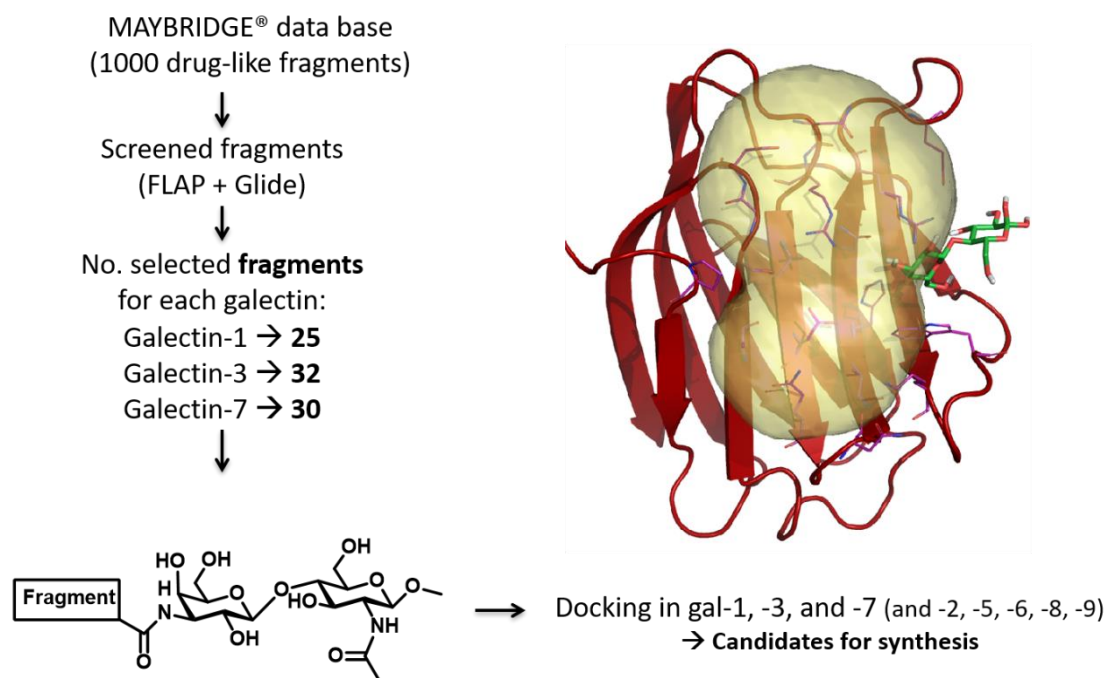


Figure 7.3

The compounds that were finally chosen as synthetic targets are shown in Figure 7.4.

²⁷⁹ The design briefly summarized in this Section was carried out by the group led by Dr. Sonsoles Martín Santamaría at CIB-CSIC and is described here to complete the background of this chapter.

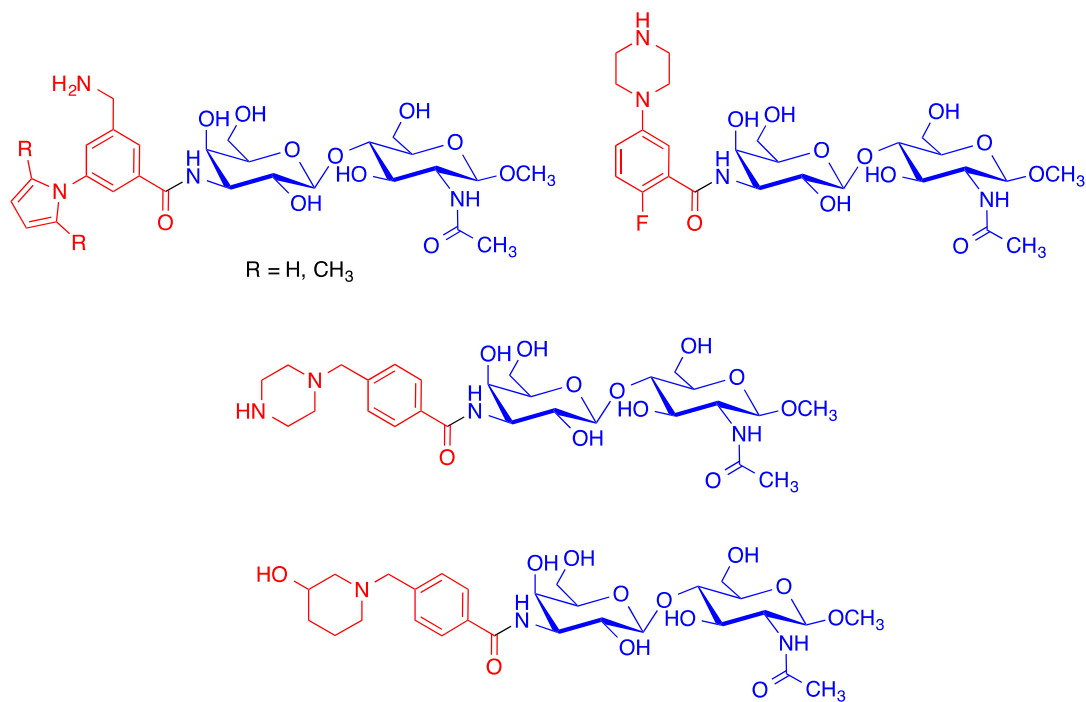
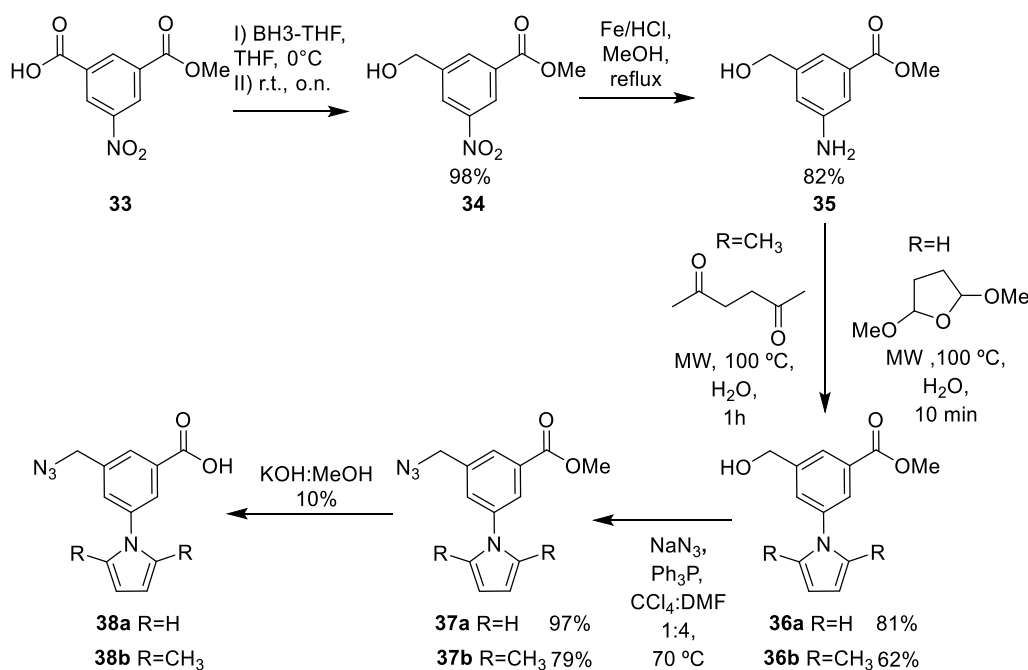


Figure 7.4

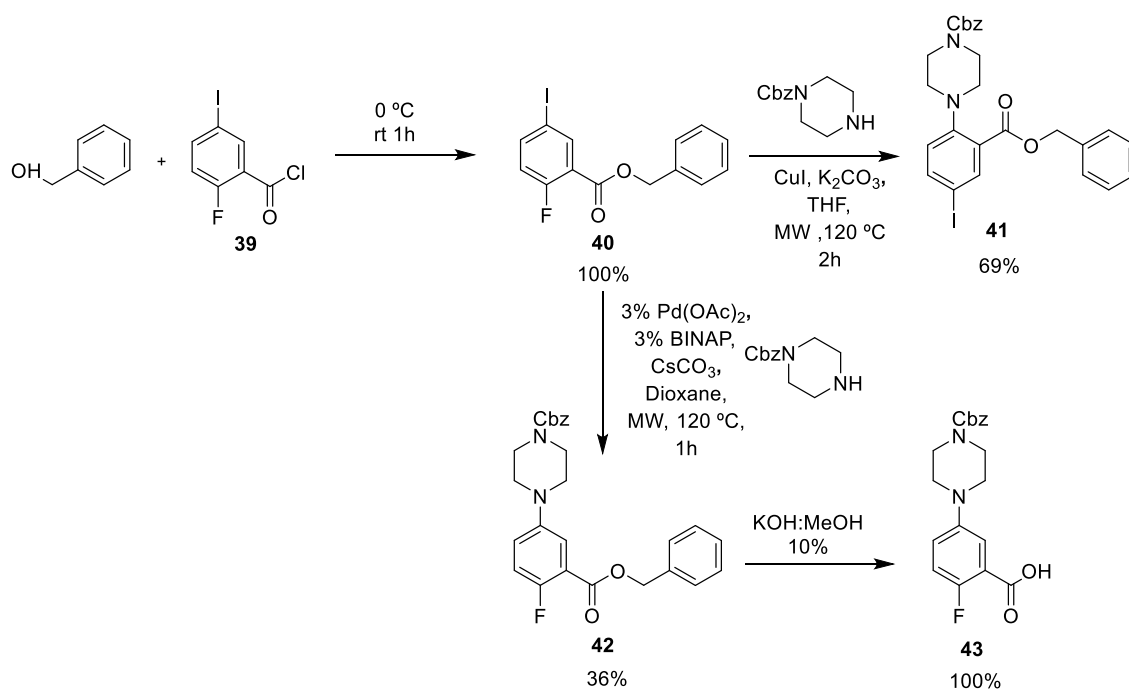
7.3. Synthesis of heterocyclic-OMe-Lac derivatives as galectin ligands

Scheme 7.1 shows the synthetic pathway employed to obtain the benzoic acid derivative **36** from the commercially available material **33**. The first step was a chemoselective reduction of the carboxylic acid to alcohol, followed by nitro group reduction with iron in aqueous hydrochloric acid to afford compound **35** in quantitative overall yield for both steps and without the need for purification. The construction of the pyrrole ring was out by a microwave-assisted Clauson-Kaas reaction to obtain compound **36a** (R = H) in 81% yield and by Paal-Knorr reaction, again under microwave irradiation, to yield compound **36b** (R = Me) in 62% yield. Then the alcohol functions from **36** were transformed into azides **37**, under Mitsunobu conditions, and the ester was finally hydrolysed with methanolic potassium hydroxide to give the acids **38**. The azide groups were expected to be reduced to the desired amines in the hydrogenation process required at a later stage to remove the benzyl ether used as protection of the lactose hydroxyls (see below).



Scheme 7.1

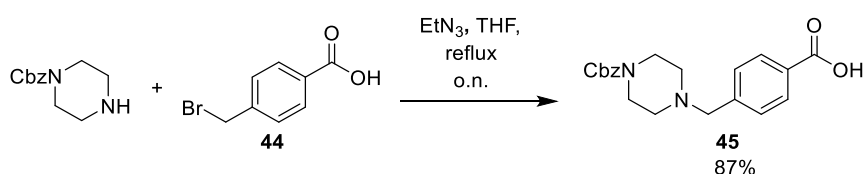
Compound **43** was synthesized from the commercially available benzoyl chloride derivative **39** by the route shown in Scheme 7.2. The first step was the synthesis of the benzyl ester **40**, which was achieved in quantitative yield by treatment with benzyl alcohol. Then the first attempt to obtain the compound **42** was carried out under Ullman coupling conditions. However, compound **41** from aromatic nucleophilic



Scheme 7.2

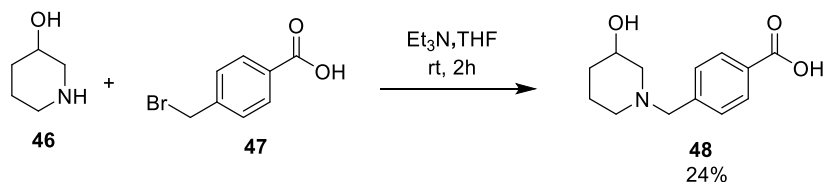
substitution was obtained instead of the desired product. In order to obtain the suitable fluorinated compound **42**, another coupling reaction was required, and a palladium-catalyzed coupling Buchwald reaction in the presence of BINAP gave the best results with a 36% yield. In the final step the benzyl ester moiety from **42** was hydrolyzed, affording compound **43**.

Compound **45** was synthesized from 4-(bromomethyl)benzoic acid **44** and monoprotected Cbz-piperazine by nucleophilic substitution (Scheme 7.3). The Cbz protecting group was expected to be removed at a later stage by catalytic palladium hydrogenation, along with the lactose O-benzyl protecting groups.



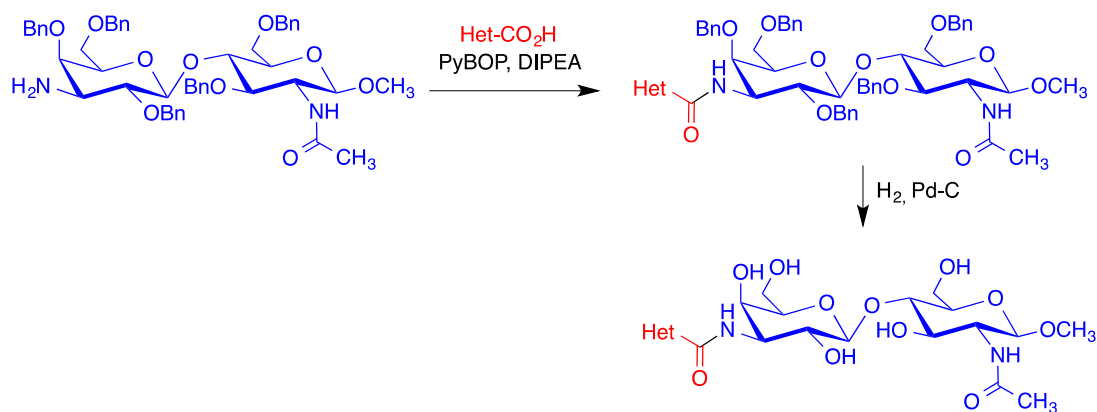
Scheme 7.3

Similarly, compound **48** was synthesized by S_N2 substitution starting from commercially available **47** and 3-hydroxypiperidine **46**, albeit in modest yield (Scheme 7.4).



Scheme 7.4

The last stages of the synthesis are being carried out at the group of Professor Stefan Oscarson at Centre for Synthesis and Chemical Biology, University College Dublin, according to the two-step route summarized in Scheme 7.5.



Scheme 7.5

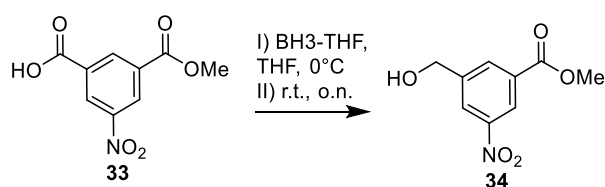
7.4. Experimental section

General experimental details

All reagents and solvents were of commercial quality and were used as received. Reactions were monitored by thin layer chromatography on aluminium plates coated with silica gel and fluorescent indicator. Microwave-assisted reactions were performed on a CEM Discover focused microwave reactor. Separations by flash chromatography were performed using a Combiflash Teledyne automated flash chromatograph or on conventional silica gel columns. Melting points were measured with a Kofler-type heating platine microscope from Reichert, 723 model, and are uncorrected. Infrared spectra were recorded with an Agilent Cary630 FTIR spectrophotometer with a diamond ATR accessory for solid and liquid samples, requiring no sample preparation; wavenumbers are given in cm^{-1} . NMR spectroscopic data were obtained using spectrometers maintained by the CAI de Resonancia Magnética, UCM, operating at 250, 300, 400 and 700 MHz for ^1H NMR and, 63, 100 and 176 MHz for ^{13}C NMR; chemical shifts are given in (δ) parts per million and coupling constants (J) in hertz. Elemental analyses were determined by the CAI de Microanálisis, Universidad Complutense, using a Leco CHNS-932 combustion microanalyzer. The enantiomeric excess analysis has been conducted in a HPLC Agilent 1220 Infinity LC with a chiral column ULTRON ES.

7.4.1. Synthesis of fragment 38

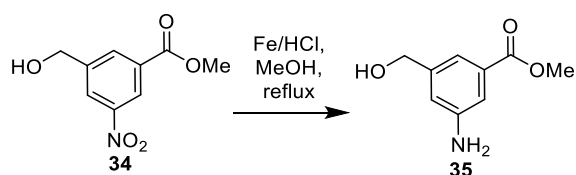
Methyl 3-(hydroxymethyl)-5-nitrobenzoate (34)



A solution of 3-(methoxycarbonyl)-5-nitrobenzoic acid (1.0 g, 4.5 mmol) in THF (30 mL) was cooled to 0°C. Then, a 1 M borane tetrahydrofuran complex solution (8.9 mL, 8.9 mmol) was cautiously added over 15 min and the reaction mixture was stirred at room temperature overnight. The excess of borane was quenched with methanol (5 mL) at 0°C and concentrated *in vacuo*. The solid residue was dissolved in ethyl acetate (60 mL), washed with saturated aqueous sodium carbonate solution (2 × 30 mL), then brine (30 mL), and dried over sodium sulphate. The solvent was removed under reduced pressure to afford 1.83 g (98%) of the title compound as a white solid, which was used in the next step without further purification.

Mp: 78-79 °C; **¹H NMR (250 MHz, CDCl₃)** δ 8.68 (s, 1H), 8.40 (s, 1H), 8.30 (s, 1H), 4.86 (s, 2H), 3.98 (s, 3H), 3.09 (br s, 1H); **¹³C NMR (63 MHz, CDCl₃)** δ 165.5, 148.7, 144.2, 133.5, 132.1, 125.6, 123.7, 63.8, 53.3; **IR (neat, cm⁻¹):** 3485, 1708, 1522, 1349, 1294; **HRMS (ESI):** found m/z 210.0408 [M]⁺, calcd. for C₉H₈NO₅ 210.040.

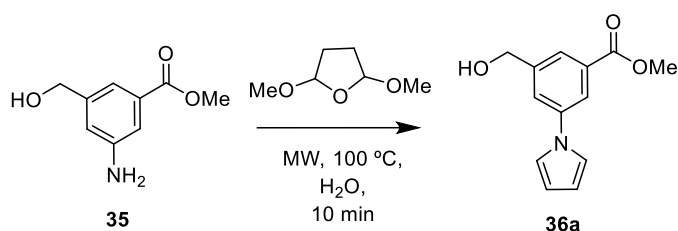
Methyl 3-amino-5-(hydroxymethyl)benzoate (35)



Compound **34** (1.76 g, 8.4 mmol) was dissolved in methanol (30 mL) and a 1M HCl solution was added (10 mL) and then, Fe powder (14 g, 25 mmol). The mixture was refluxed for 4 h. Then, the reaction was diluted with ethyl acetate (50 mL) and was washed with saturated sodium carbonate solution (3 x 20 mL). The organic layer was dried over sodium sulphate, filtered, and the solvent was removed under reduce pressure to give 1.25 g (82%) of a pale yellow solid, that was used in the next step without further purification.

Mp: 96-97 °C; **¹H NMR (250 MHz, d₆-DMSO)** δ 7.14 – 7.03 (m, 2H), 6.78 (s, 1H), 5.35 (s, 2H), 5.16 (t, *J* = 5.8 Hz, 1H), 4.41 (d, *J* = 5.7 Hz, 2H), 3.80 (s, 3H); **¹³C NMR (63 MHz, d₆-DMSO)** δ 167.7, 149.7, 144.6, 130.8, 117.1, 115.4, 113.5, 63.5, 52.6; **IR (neat, cm⁻¹):** 3338, 1703, 1604, 1437, 1243, 1017; **HRMS (ESI):** found m/z 204.0631 [M]⁺, calcd. for C₉H₁₁NNaO₃ 204.0636.

Methyl 3-(hydroxymethyl)-5-(1H-pyrrol-1-yl)benzoate (36a)

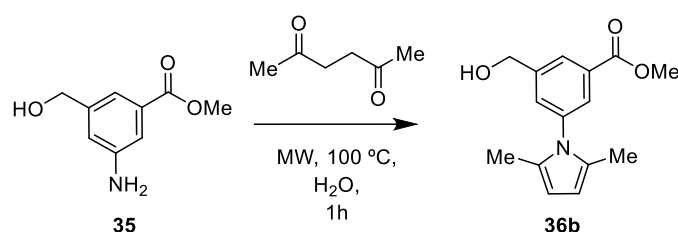


Compound **35** (1 mmol) was placed in a microwave tube and 2,5-dimethoxytetrahydrofuran (2 mmol) was added. The mixture was irradiated at 100 °C for 10 min and monitored by TLC. The mixture was diluted with CHCl₃ (20 mL) and

washed with water (2 × 10 mL), dried over sodium sulphate, filtered, and the solvent was removed under reduced pressure. The crude product was purified by flash chromatography on silica gel using a 1:4 ethyl acetate-petroleum ether mixture as eluent, affording 188 mg (81%) of the expected compound as a white solid.

Mp: 84-85 °C; **¹H NMR (250 MHz, CDCl₃)** δ 7.94 (s, 1H), 7.85 (s, 1H), 7.60 (s, 1H), 7.18 – 7.10 (m, 2H), 6.42 – 6.33 (m, 2H), 4.77 (s, 2H), 3.94 (s, 3H), 2.70 (br s, 1H); **¹³C NMR (63 MHz, CDCl₃)** δ 167.1, 143.8, 141.8, 132.5, 125.3, 123.3, 121.0, 120.0, 111.8, 65.2, 53.2; **IR (neat, cm⁻¹):** 3247, 1710, 1599, 1487, 1434, 1351, 1260; **HRMS (ESI):** found m/z 230.0823 [M]⁺, calcd. for C₁₃H₁₂NO₃ 230.0813.

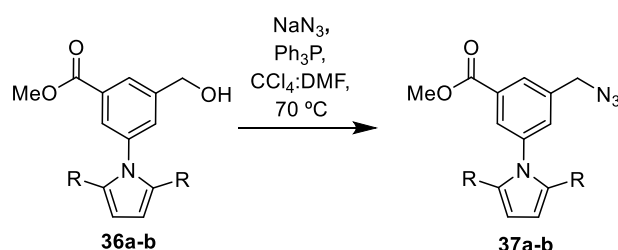
Methyl 3-(2,5-dimethyl-1H-pyrrol-1-yl)-5-(hydroxymethyl)benzoate (36b)



Compound **35** (1 mmol) was placed in a microwave tube and 2,5-hexanedione (2 mmol) was added. The mixture was irradiated at 100 °C for 1 h and monitored by TLC. The mixture was diluted with CHCl₃ (20 mL) and washed with water (2 × 10 mL), dried over sodium sulphate, filtered, and the solvent was removed under reduced pressure. The crude product was purified by flash chromatography on silica gel using a 1:4 ethyl acetate-petroleum ether mixture as eluent, affording 136 mg (62%) of the expected compound as a colourless oil.

¹H NMR (250 MHz, CDCl₃) δ 8.10 (s, 1H), 7.84 (s, 1H), 7.47 (s, 1H), 5.93 (s, 2H), 4.83 (s, 2H), 3.95 (s, 3H), 2.42 (s, 1H), 2.05 (s, 6H); **¹³C NMR (63 MHz, CDCl₃)** δ 166.8, 143.2, 139.9, 131.8, 131.2, 129.1, 128.7, 127.3, 106.6, 64.5, 52.9, 13.5; **IR (neat, cm⁻¹):** 3239, 1702, 1610, 1481, 1434, 1338, 12656; **HRMS (ESI):** found m/z 258.1123 [M]⁺, calcd. for C₁₅H₁₆NO₃ 258.1136.

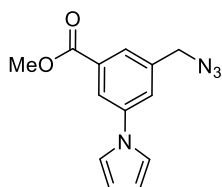
Synthesis of methyl 3-(azidomethyl)-5-(1H-pyrrol-1-yl)benzoate derivatives 37



The suitable alcohol **36a-b** (2 mmol), sodium azide (2.4 mmol), and triphenylphosphine (2.4 mmol) were placed in a round bottom flask and dissolved in DMF (8 mL). Then, CCl₄ was added dropwise and the reaction was stirred at 70 °C for 2 h. The mixture was diluted with water (30 mL) and extracted with diethyl ether (2 × 20 mL). The combined

organic layers were dried over sodium sulphate, filtered, and the solvent was removed *in vacuo*. The residue was purified by flash chromatography on silica gel using a 1:4 ethyl acetate-hexane mixture as eluent.

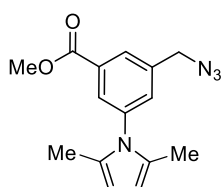
Methyl 3-(azidomethyl)-5-(1H-pyrrol-1-yl)benzoate (37a)



Colourless oil (512 mg, 97%); $^1\text{H NMR}$ (250 MHz, CDCl_3) δ 8.19 – 7.99 (m, 1H), 7.94 – 7.84 (m, 1H), 7.60 – 7.49 (m, 1H), 7.22 – 7.09 (m, 2H), 6.43 – 6.40 (m, 2H), 4.49 (s, 2H), 3.99 (s, 3H); $^{13}\text{C NMR}$ (63 MHz, CDCl_3) δ 166.5, 141.8, 138.2, 132.7, 126.3, 124.1, 121.3, 119.7, 111.8, 54.6, 53.1; IR (neat, cm^{-1}): 2094, 1718, 1602, 1490, 1433, 1355, 1255, 1195, 1070; HRMS (ESI): found m/z 279.0860

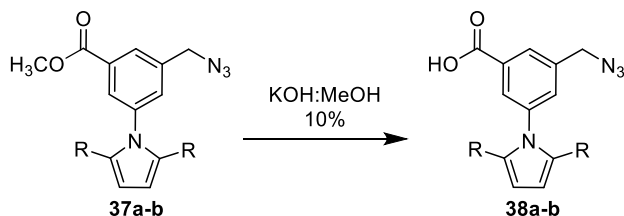
$[\text{M}]^+$, calcd. for $\text{C}_{13}\text{H}_{12}\text{N}_4\text{NaO}_2$ 279.0853.

Methyl 3-(azidomethyl)-5-(2,5-dimethyl-1H-pyrrol-1-yl)benzoate (37b)



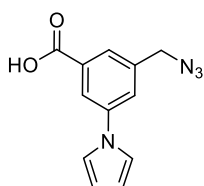
Yellow oil (224 mg, 79%); $^1\text{H NMR}$ (250 MHz, CDCl_3) δ 8.11 – 8.04 (m, 1H), 7.92 (t, $J = 1.6$ Hz, 1H), 7.47 – 7.39 (m, 1H), 5.96 (s, 2H), 4.51 (s, 2H), 3.98 (s, 3H), 2.07 (s, 6H); $^{13}\text{C NMR}$ (63 MHz, CDCl_3) δ 166.3, 140.2, 137.6, 132.4, 132.3, 129.5, 129.1, 128.7, 106.8, 54.3, 53.0, 13.5; IR (neat, cm^{-1}): 2920, 1721, 1434, 1397, 1221; HRMS (ESI): found m/z 285.1369 $[\text{M}]^+$, calcd. for $\text{C}_{15}\text{H}_{17}\text{N}_4\text{O}_2$ 285.1346.

Synthesis of 3-(azidomethyl)-5-(1H-pyrrol-1-yl)benzoic acid derivatives 38



The suitable ester **37a-b** (0.5 mmol) was dissolved in methanol and a 10% KOH methanol solution (5 mL) was added. The reaction was monitored by TLC and additional 10% KOH methanol solution was added until the starting material was no longer detected. Then, the reaction was diluted with water (10 mL), neutralized with 2M HCl solution and extracted with CHCl_3 (3 x 20 mL). The combined organic layers were dried over sodium sulphate, filtered and the solvent was removed *in vacuo*. No further purification was needed.

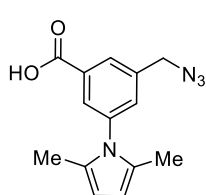
3-(Azidomethyl)-5-(1H-pyrrol-1-yl)benzoic acid (38a)



Pale brown solid (quant.); mp: 113–114 °C; $^1\text{H NMR}$ (250 MHz, CDCl_3) δ 10.04 (s, 1H), 8.16 – 8.12 (m, 1H), 7.96 (s, 1H), 7.64 (s, 1H), 7.20 (t, $J = 2.2$ Hz, 2H), 6.44 (t, $J = 2.2$ Hz, 2H), 4.53 (s, 2H); $^{13}\text{C NMR}$ (63 MHz, CDCl_3) δ 171.5, 141.8, 138.4, 131.7, 126.7, 124.9, 121.8, 119.6, 111.9, 54.4; IR (neat, cm^{-1}): 2842, 2095, 1693, 1596, 1488, 1280; HRMS

(ESI): found m/z 241.0719 $[M]^+$, calcd. for $C_{12}H_9N_4O_2$ 241.0731.

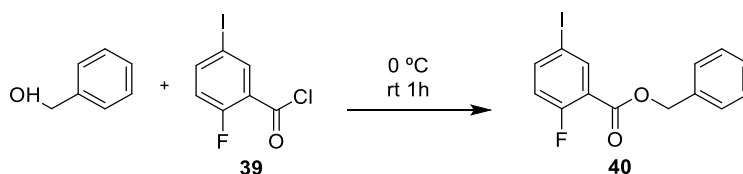
3-(Azidomethyl)-5-(2,5-dimethyl-1H-pyrrol-1-yl)benzoic acid (38b)



Brown solid (quant.); mp: 108-109 °C; 1H NMR (250 MHz, $CDCl_3$) δ 10.60 (s, 1H), 8.16 (s, 1H), 8.01 (t, $J = 1.6$ Hz, 1H), 7.51 (t, $J = 1.7$ Hz, 1H), 5.98 (s, 2H), 4.55 (s, 2H), 2.10 (s, 6H); ^{13}C NMR (63 MHz, $CDCl_3$) δ 171.5, 140.4, 137.9, 133.3, 131.4, 130.0, 129.2, 129.1, 107.0, 54.2, 13.5; IR (neat, cm^{-1}): 2918, 2097, 1694, 1461, 1416, 1234; HRMS (ESI): found m/z 269.10232 $[M]^+$, calcd. for $C_{14}H_{13}N_4O_2$ 269.1044.

7.4.2. Synthesis of fragment 43

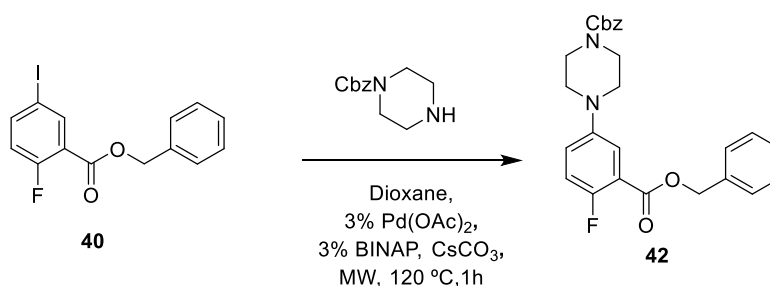
Benzyl 2-fluoro-5-iodobenzoate (40)



To a solution of 2-fluoro-4-iodobenzoyl chloride (0.5 mmol) in anhydrous CH_2Cl_2 (10 mL) cooled at 0 °C, under argon atmosphere, benzyl alcohol was added (1 mmol) and the mixture was stirred at room temperature for 2 h. Then, the reaction was diluted with CH_2Cl_2 (15 mL) and washed with water (2 x 10 mL). The organic layer was dried over sodium sulphate, filtered and the solvent was removed under reduced pressure. The residue was chromatographed on silica gel using a 4:1 hexane-ethyl acetate mixture as eluent, yielding 135 mg (73%) of the desired compound as colourless oil.

1H NMR (250 MHz, $CDCl_3$) δ 8.25 (dd, $J_{H-F} = 6.7$ Hz, $J_{H-H} = 2.4$ Hz, 1H), 7.79 (ddd, $J_{H-H} = 8.7$, 2.4 Hz, $J_{H-F} = 4.4$ Hz, 1H), 7.53 – 7.29 (m, 6H), 6.91 (dd, $J_{H-F} = 10.3$ Hz, $J_{H-H} = 8.7$ Hz, 1H), 5.38 (s, 2H); ^{13}C NMR (63 MHz, $CDCl_3$) δ 163.2 (d, $J = 3.8$ Hz), 162.3 (d, $J = 261.7$ Hz), 143.7 (d, $J = 8.8$ Hz), 141.1, 135.8, 129.1 (2C), 128.9, 128.7 (2C), 121.1 (d, $J = 10.6$ Hz), 119.7 (d, $J = 23.4$ Hz), 87.0, 87.0, 67.8; IR (neat, cm^{-1}): 1718, 1478, 1289, 1269, 1237; HRMS (ESI): found m/z 378.9621 $[M+Na]^+$, calcd. for $C_{14}H_{10}FINaO_2$ 378.9602.

Benzyl 4-(3-((benzyloxy)carbonyl)-4-fluorophenyl)piperazine-1-carboxylate (42)

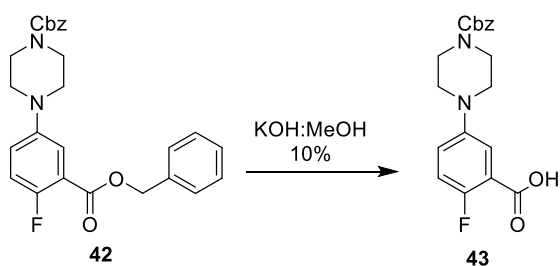


Ethyl 2-fluoro-5-iodobenzoate (0.7 mmol), Cbz-piperazine (0.85 mmol), $CsCO_3$ (0.9 mmol), (\pm)-BINAP (0.02 mmol), $Pd(OAc)_2$ (0.02 mmol) and 1,4-dioxane (3 mL) were

placed in a microwave tube. The mixture was irradiated at 120 °C for 1 h. Then, the reaction was filtered over Celite and the solvent was removed under vacuum. The mixture was purified by flash chromatography on silica gel eluting with a gradient from hexane to 8:1 hexane-ethyl acetate mixture to afford 115 mg (26%) of the title compound as a brown oil.

¹H NMR (250 MHz, CDCl₃) δ 7.54 – 7.32 (m, 11H), 7.14 – 7.04 (m, 2H), 5.42 (s, 2H), 5.21 (s, 2H), 3.76 – 3.64 (m, 4H), 3.20 – 3.04 (m, 4H); **¹³C NMR (63 MHz, CDCl₃)** δ 165.0 (d, *J* = 4.1 Hz), 157.0 (d, *J* = 252.5 Hz), 155.6, 147.9 (d, *J* = 2.7 Hz), 137.0, 136.2, 129.0 (2C), 129.0 (2C), 128.6 (d, *J* = 5.4 Hz), 128.5 (2C), 128.4 (2C), 123.7 (d, *J* = 8.3 Hz), 120.0, 119.0 (d, *J* = 23.7 Hz), 118.0 (d, *J* = 23.7 Hz), 67.8, 67.4, 50.3 (2C), 44.1 (2C); **IR** (neat, cm⁻¹): 1696, 1498, 1421, 1235, 1216; **HRMS (ESI)**: found *m/z* 471.1738 [M+Na]⁺, calcd. for C₂₆H₂₅FN₂NaO₄ 471.1691.

5-[4-((Benzyloxy)carbonyl)piperazin-1-yl]-2-fluorobenzoic acid (**43**)

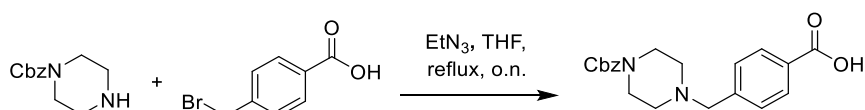


The benzyl ester **42** (0.5 mmol) was dissolved in methanol and a 10% KOH methanol solution (5 mL) was added. The reaction was monitored by TLC and additional 10% KOH methanol solution was added until the starting material was no longer detected. Then, the reaction was diluted with water (10 mL), neutralized with 2M HCl solution and extracted with CHCl₃ (3 x 20 mL). The combined organic layers were dried over sodium sulphate, filtered and the solvent was removed *in vacuo*. No further purification was needed.

Brown oil (quant.); **¹H NMR (250 MHz, CDCl₃)** δ 9.97 (br s, 1H), 7.55 (dd, *J* = 6.0, 2.9 Hz, 1H), 7.47 – 7.32 (m, 4H), 7.22 – 7.05 (m, 2H), 5.21 (s, 2H), 3.81 – 3.59 (m, 4H), 3.28 – 3.02 (m, 4H); **¹³C NMR (63 MHz, CDCl₃)** δ 169.4 (d, *J* = 3.4 Hz), 157.5 (d, *J* = 256.4 Hz), 155.7, 147.8, 136.8, 129.0 (2C), 128.6, 128.5 (2C), 124.7 (d, *J* = 8.2 Hz), 120.4, 118.3 (d, *J* = 11.3 Hz), 118.0 (d, *J* = 2.6 Hz), 67.90, 50.4 (2C), 44.1 (2C); **IR** (neat, cm⁻¹): 1695, 1498, 1429, 1236, 1217; **HRMS (ESI)**: found *m/z* 357.1243 [M]⁺, calcd. for C₁₉H₁₈FN₂O₄ 357.1256.

7.4.3. Synthesis of fragment 45

4-[(4-((Benzyloxy)carbonyl)piperazin-1-yl)methyl]benzoic acid (45)

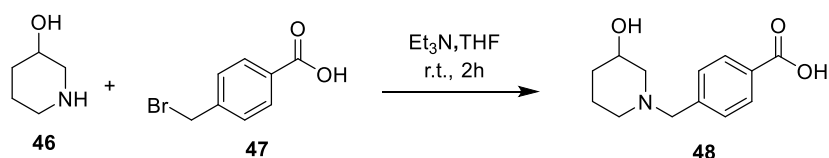


To a solution of Cbz-piperazine (1 mmol) and triethylamine (1.1 mmol) in THF (10 mL) under argon atmosphere was added 4-(bromomethyl)benzoic acid (1 mmol) and the mixture was stirred at reflux overnight. The reaction was cooled to room temperature, and a white precipitate was collected by filtration. The white solid was washed with THF (2 x 10 mL) to afford a white solid (308 mg, 87%).

Mp: 177-178 °C; **¹H NMR (250 MHz, *d*₆-DMSO)** δ 7.91 (d, *J* = 8.2 Hz, 2H), 7.43 (d, *J* = 8.2 Hz, 2H), 7.40 – 7.28 (m, 5H), 5.08 (s, 2H), 3.47 – 3.31 (m, 4H), 2.44 – 2.29 (m, 4H); **¹³C NMR (63 MHz, *d*₆-DMSO)** δ 167.7, 154.7, 143.4, 137.3, 130.3, 129.7, 129.2, 128.8, 128.2, 127.9, 66.5, 61.8, 52.7, 43.8; **IR (neat, cm⁻¹):** 1695, 1446, 1426, 1238; **HRMS (ESI):** found *m/z* 353.1507 [*M*]⁺, calcd. for C₂₀H₂₁N₂O₄ 353.1467.

7.4.4. Synthesis of fragment 48

4-[(3-Hydroxypiperidin-1-yl)methyl]benzoic acid (48)



4-(Bromomethyl)benzoic acid (1 mmol) was added to a solution of 3-hydroxypiperidine (1 mmol) and triethylamine (1.1 mmol) in THF (10 mL) under argon atmosphere and the mixture was stirred at room temperature overnight. The reaction was cooled at room temperature, and a white precipitate was collected by filtration. The white solid was washed with THF (2 x 10 mL) to afford a white solid (55 mg, 24 %).

Mp: 181 °C **¹H NMR (250 MHz, *d*₆-DMSO)** δ 7.90 (d, *J* = 8.1 Hz, 2H), 7.41 (d, *J* = 8.1 Hz, 2H), 4.67 (bs, 1H), 3.65 – 3.36 (m, 3H), 2.85 – 2.71 (m, 1H), 2.71 – 2.55 (m, 1H), 1.97 – 1.54 (m, 4H), 1.54 – 1.31 (m, 1H), 1.17 – 0.95 (m, 1H); **¹³C NMR (63 MHz, *d*₆-DMSO)** δ 167.7, 144.1, 130.0, 129.6, 129.1, 66.4, 62.1, 61.5, 53.4, 33.6, 23.0; **IR (neat, cm⁻¹):** 3313, 1596, 1558, 1371, 1321, 1093; **HRMS (ESI):** found *m/z* 234.1125 [*M*]⁺, calcd. for C₁₃H₁₆NO₃ 234.1136.

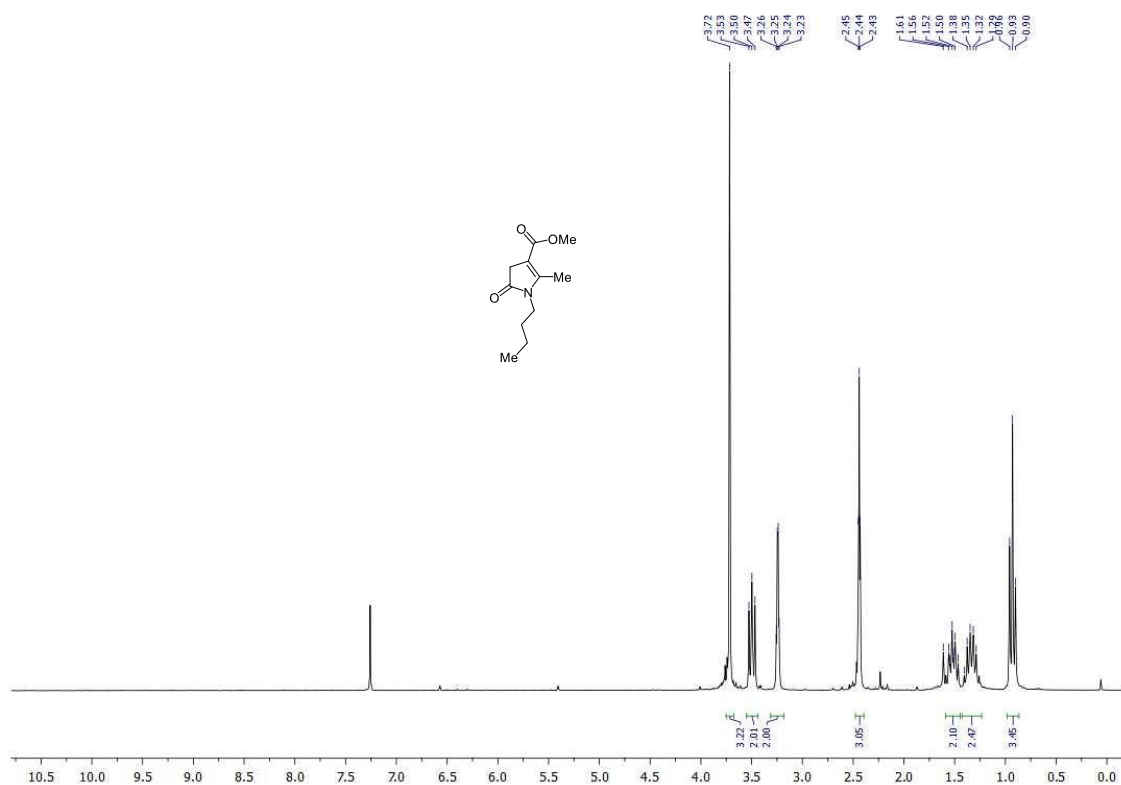
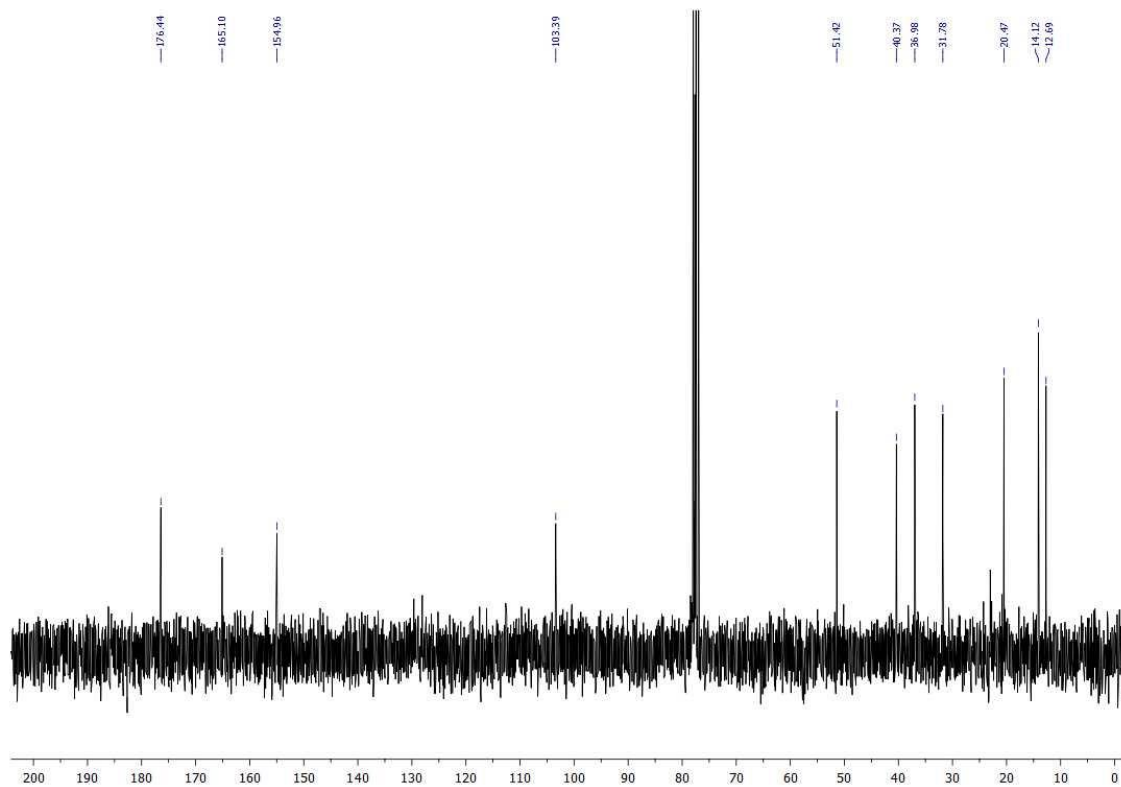
CHAPTER 8. CONCLUSIONS

1. The microwave-assisted, three-component reaction of β -dicarbonyl compounds, α -haloesters and primary amines provides a fully regioselective access to functionalized 2-pyrrolin-5-one derivatives.
2. 4-Arylmethylene-2-pyrrolin-5-ones, which can be viewed as analogues to natural antioxidant cinnamic acid derivatives, are readily accessible by simple Knoevenagel chemistry. They have an interesting pharmacological profile, with generally low toxicity for human neuronal cells and good ability to induce the Nrf2-ARE antioxidant pathway. They also show a good neuroprotective activity against oxidative stress generated by blockade of the mitochondrial electron transport chain of SH-SY5Y neuroblastoma cells with rotenone-oligomycin. They are also neuroprotective against damage caused by the hyperphosphorylation induced by the phosphatase inhibitor okadaic acid.
3. The acylation of the C-4 position of 2-pyrrolin-5-one derivatives provides cyclic analogues of curcumin, a natural antioxidant and neuroprotectant. These compounds had also an interesting profile when compared to curcumin, with a lower cytotoxicity, similar or higher radical scavenging activities and a similar activity as inhibitors of the aggregation of the AcPHF6 peptide, a suitable model to study tau protein aggregation inhibition.
4. A 1,3-dipolar cycloaddition-based three-component reaction from α -amino acids and isatin, which generate *in situ* a 1,3-dipole, and 4-arylmethylene-2-pyrrolin-5-ones, acting as the dipolarophile, provides dispiro compounds bearing three adjacent stereocenters with full regio- and diastereoselectivity. These compounds are structurally related to the oxindole alkaloid rynchophylline and were potent neuroprotectors, both in the rotenone-oligomycin and the okadaic acid models.
5. Hybrid compounds containing vinylogous melatonin and 2,5,8-quinolinetriene structural fragments were constructed from the unsubstituted quinones and tryptamine derivatives by a regioselective Michael addition-oxidation process. These compounds have a very potent antioxidant activity.

Chapter 8. Conclusions

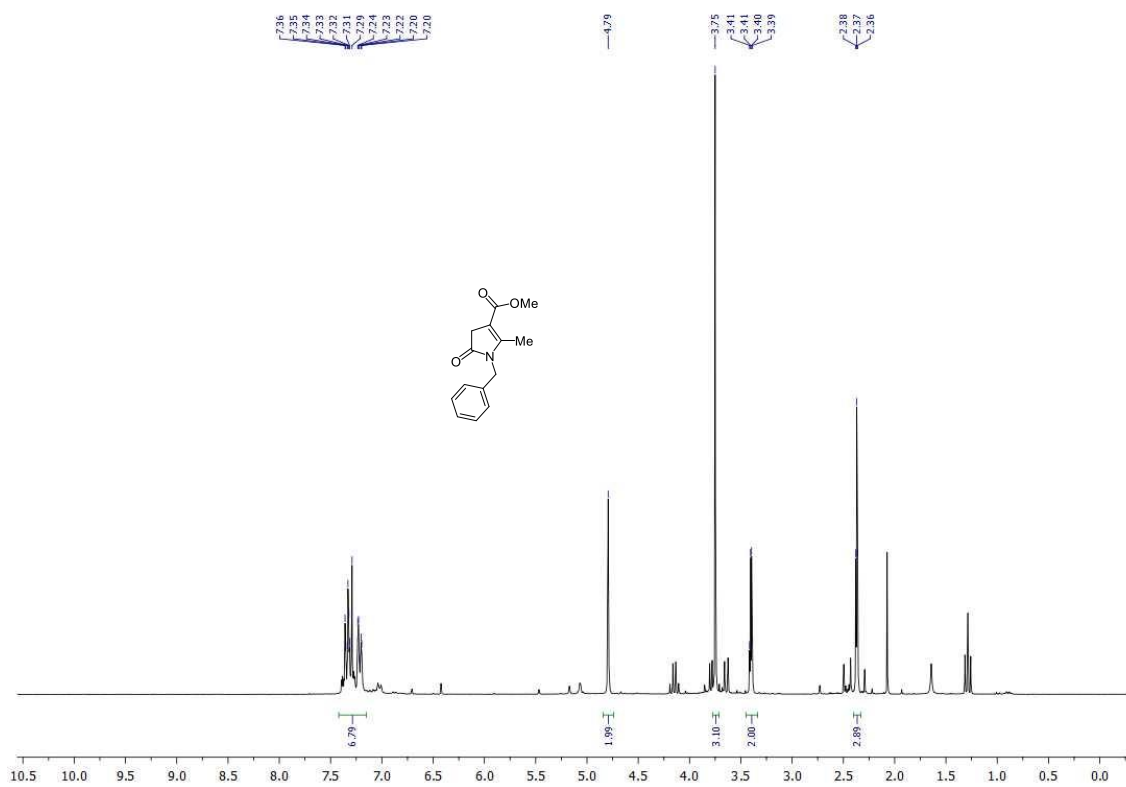
6. The use of Ellman's sulfinamide as a chiral auxiliary allows a fully diastereoselective reduction of a highly hindered diarylimine that corresponds to the aromatic fragment of the mNCX inhibitor CGP-37157. The product of this reaction was transformed in six steps into an aza-CGP-37157-lipoic acid hybrid compound. This chemistry could be extended to the preparation of all possible enantiomers of the hybrid compound. Their pharmacological study has shown the existence of enantiospecificity in the induction of the Nrf2-ARE pathway.
7. Multistep routes, usually based on Pd-catalyzed cross-coupling reactions, have allowed the preparation of four heterocyclic molecules needed for the preparation of the corresponding heterocyclic galactose hybrids, designed as galectin modulators *via* a fragment-based approach.

REPRESENTATIVE SPECTRA

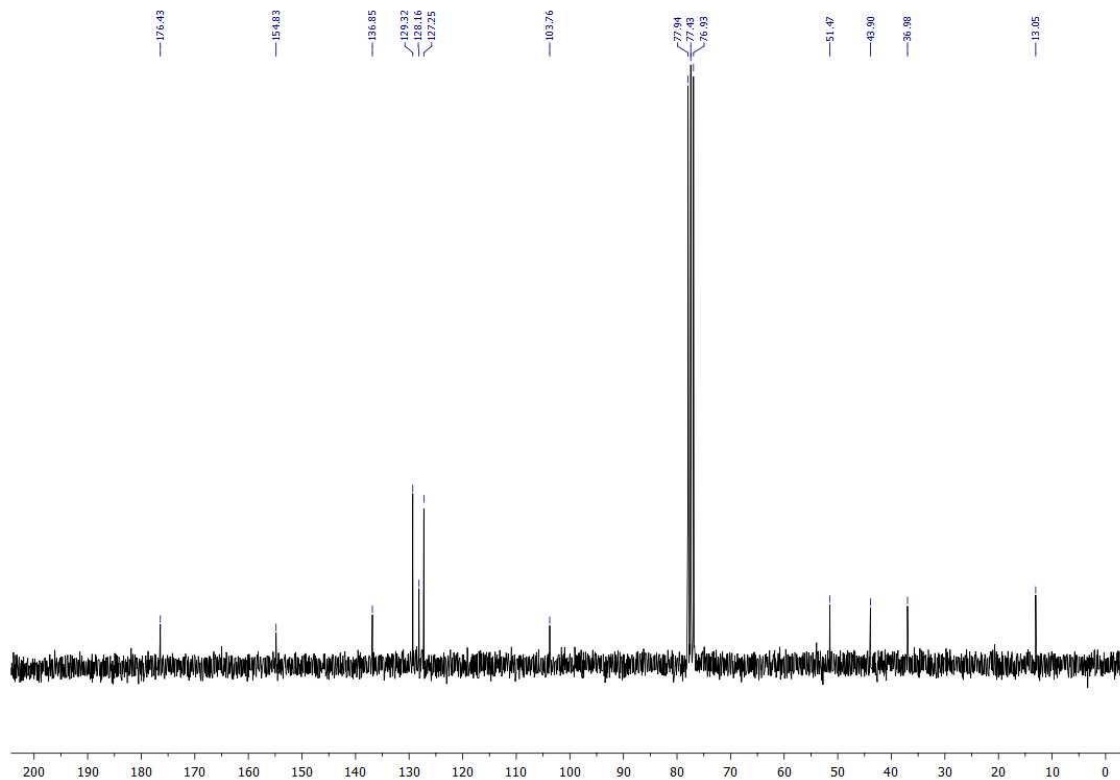
Methyl 1-butyl-2-methyl-5-oxo-4,5-dihydro-1H-pyrrole-3-carboxylate (1b) **$^1\text{H-NMR}$ (250 MHz, CDCl_3)** **$^{13}\text{C-NMR}$ (63 MHz, CDCl_3)**

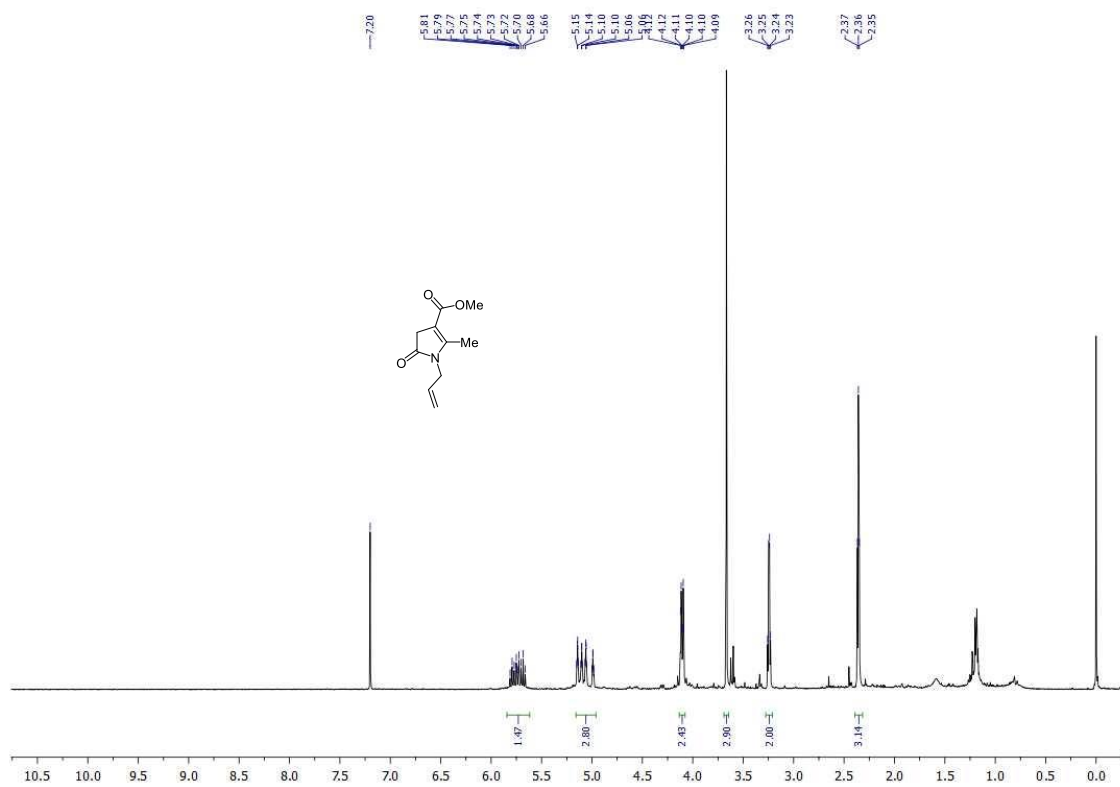
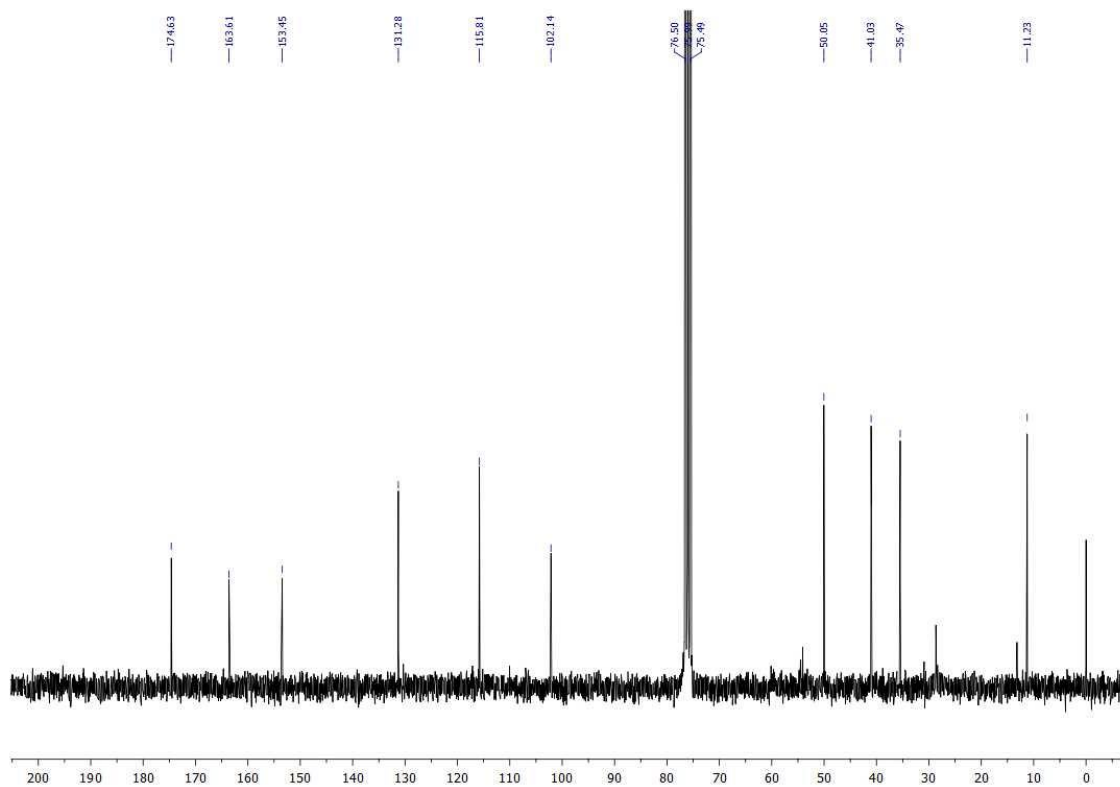
Representative spectra

Methyl 1-benzyl-2-methyl-5-oxo-4,5-dihydro-1H-pyrrole-3-carboxylate (1f)
¹H NMR (250 MHz, CDCl₃)



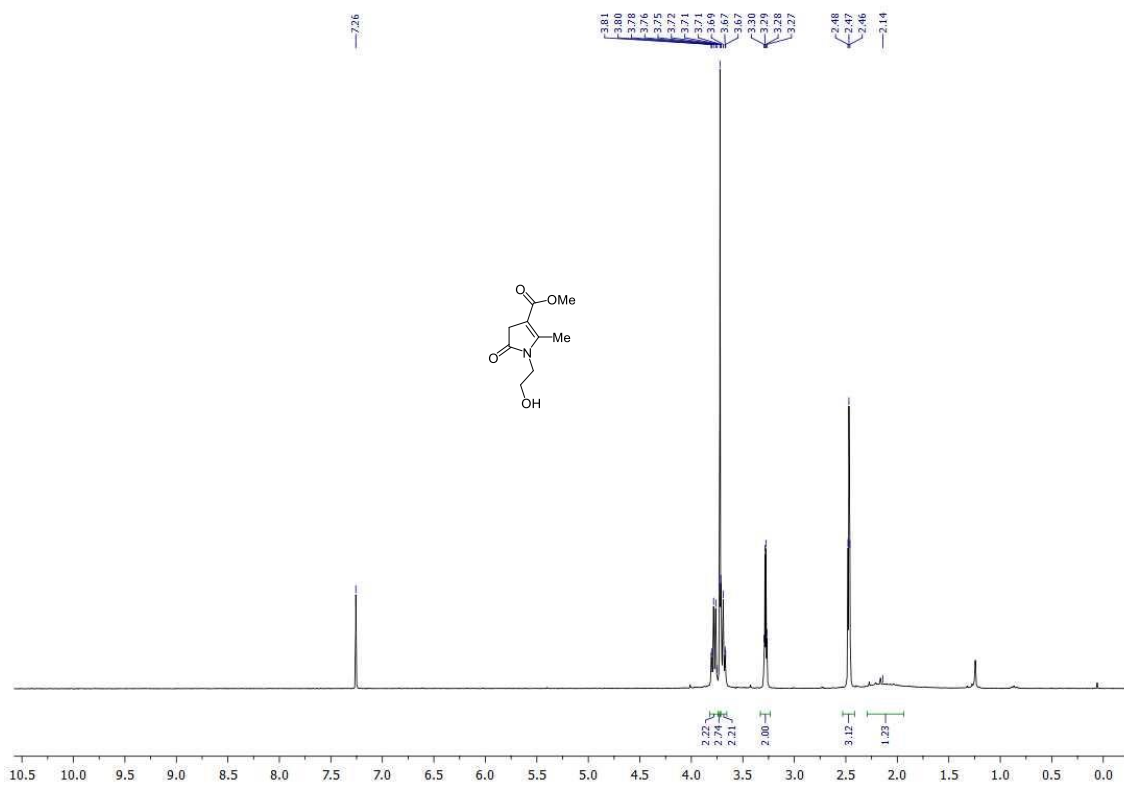
¹³C NMR (63 MHz, CDCl₃)



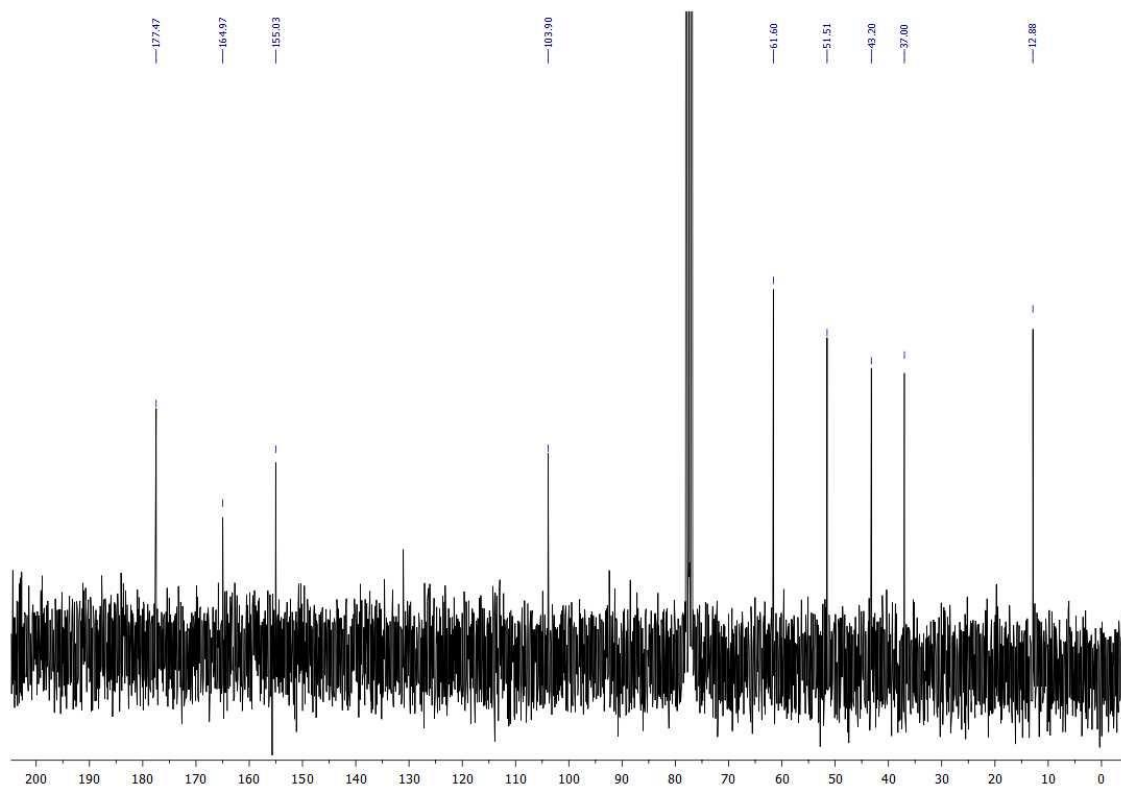
Methyl 1-allyl-2-methyl-5-oxo-4,5-dihydro-1H-pyrrole-3-carboxylate (1j)**¹H NMR (250 MHz, CDCl₃)****¹³C NMR (63 MHz, CDCl₃)**

Representative spectra

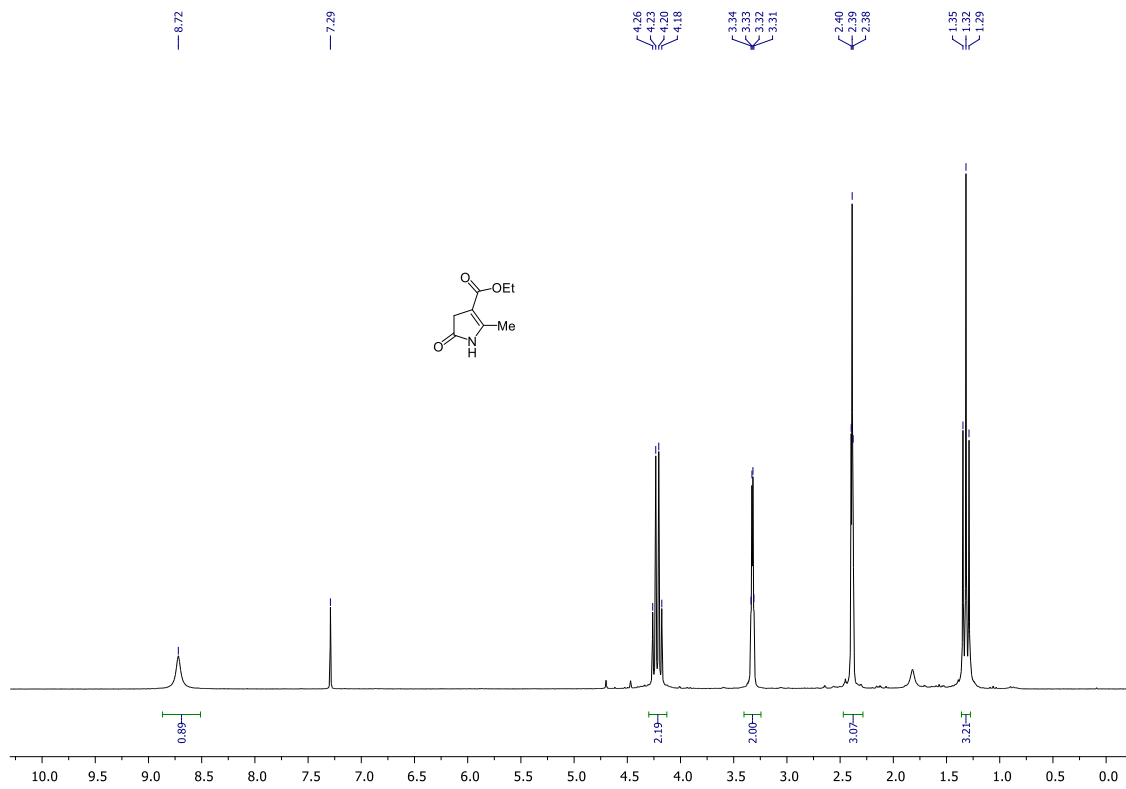
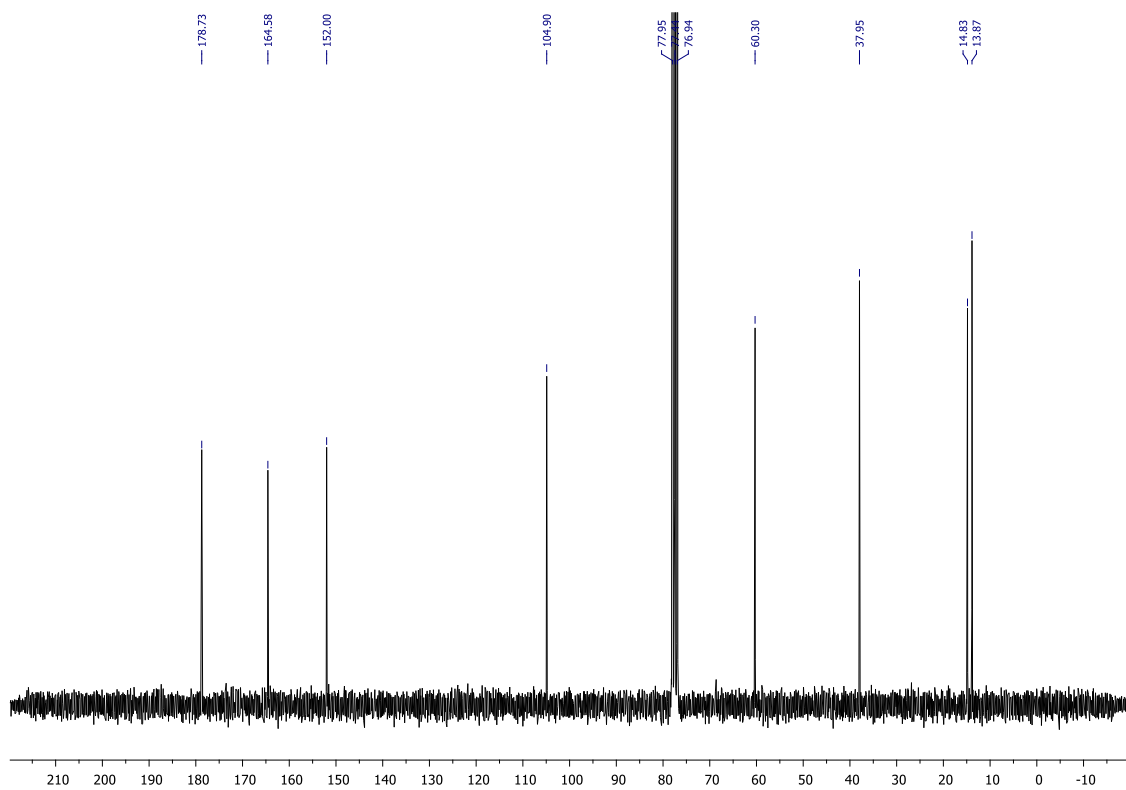
Methyl 1-(2-hydroxyethyl)-2-methyl-5-oxo-4,5-dihydro-1H-pyrrole-3-carboxylate (1k)
¹H NMR (250 MHz, CDCl₃)



¹³C NMR (63 MHz, CDCl₃)



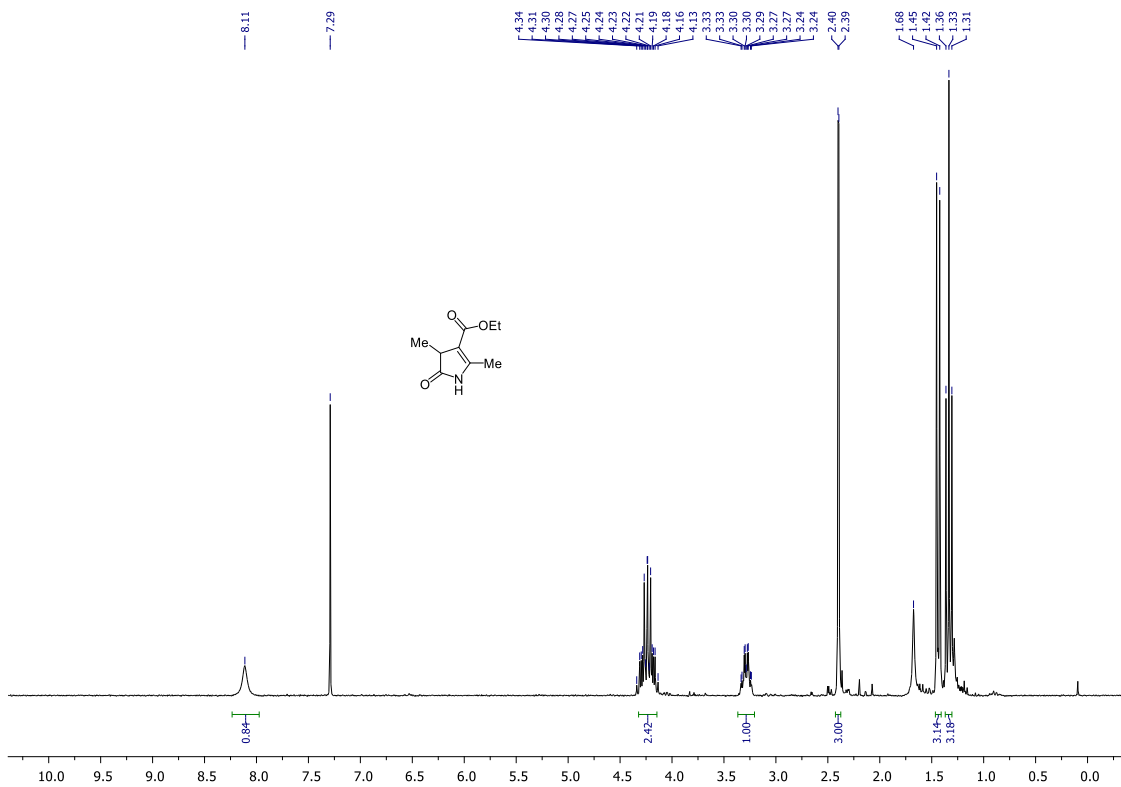
Ethyl 2-methyl-5-oxo-4,5-dihydro-1H-pyrrole-3-carboxylate (1n)

 ^1H NMR (250 MHz, CDCl_3) ^{13}C NMR (63 MHz, CDCl_3)

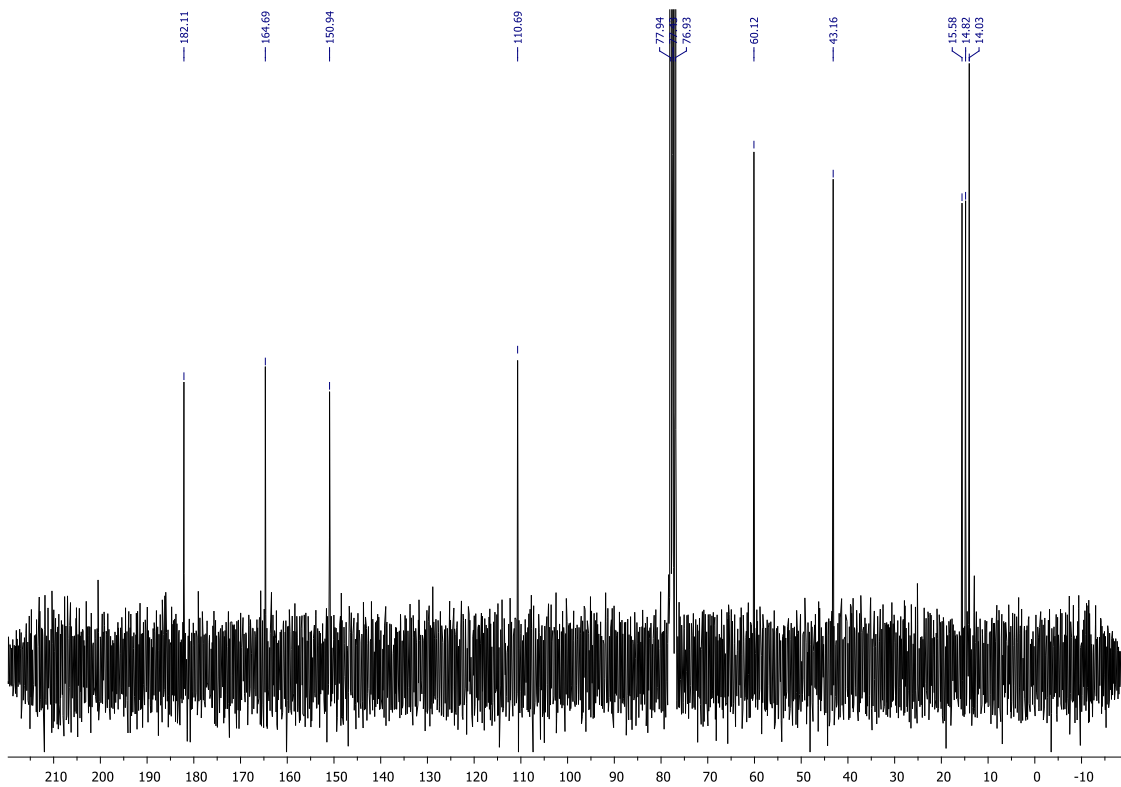
Representative spectra

Ethyl 2,4-dimethyl-5-oxo-4,5-dihydro-1H-pyrrole-3-carboxylate (**1o**)

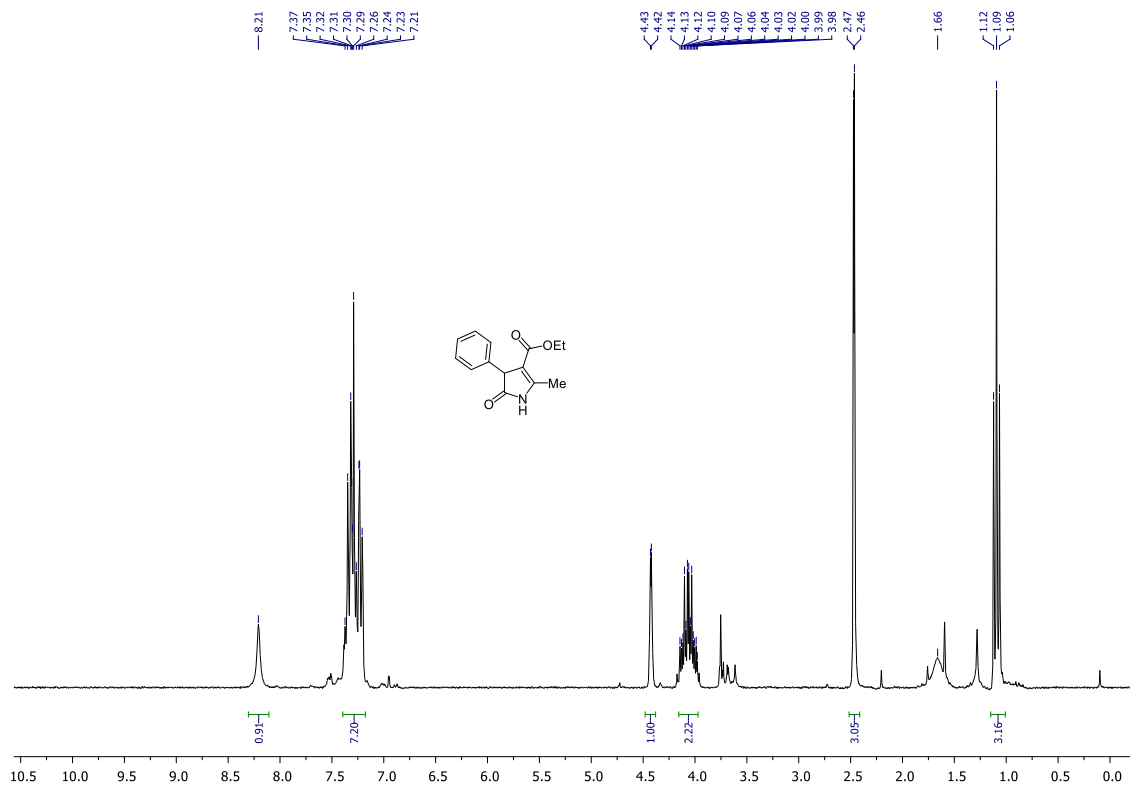
^1H NMR (250 MHz, CDCl_3)



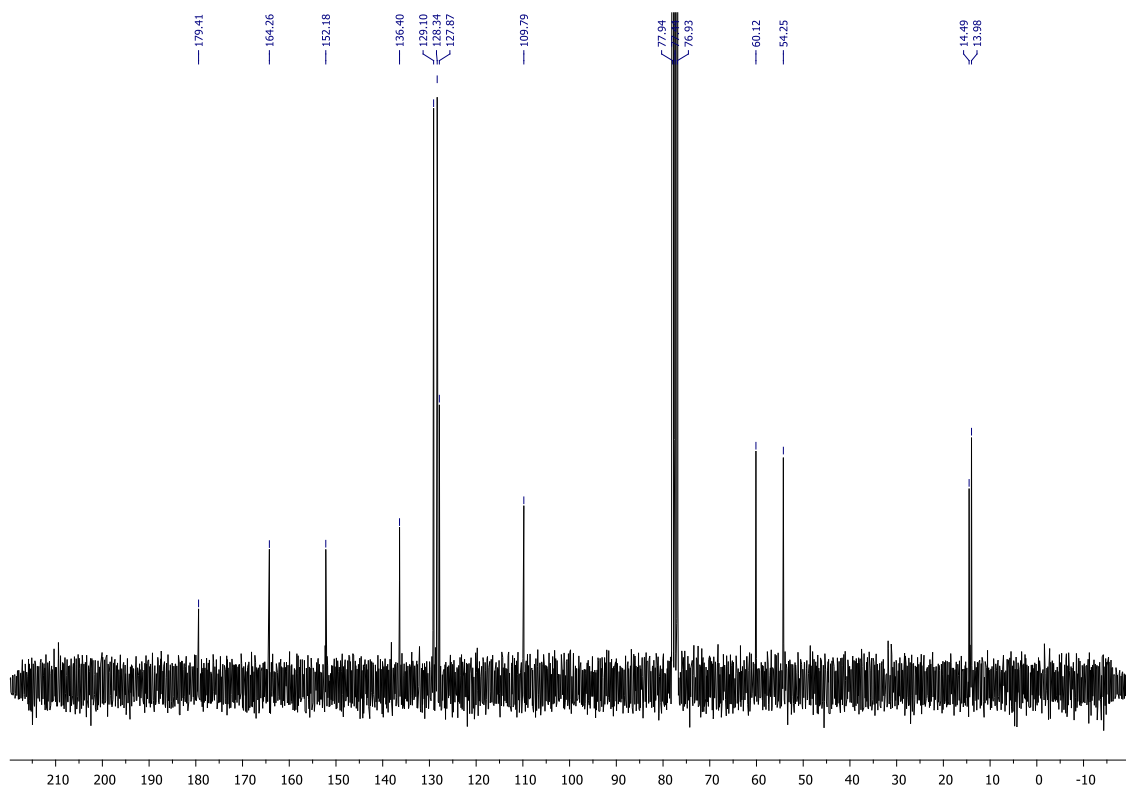
^{13}C NMR (63 MHz, CDCl_3)



Ethyl 2-methyl-5-oxo-4-phenyl-4,5-dihydro-1H-pyrrole-3-carboxylate (1q)
¹H NMR (250 MHz, CDCl₃)



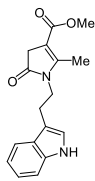
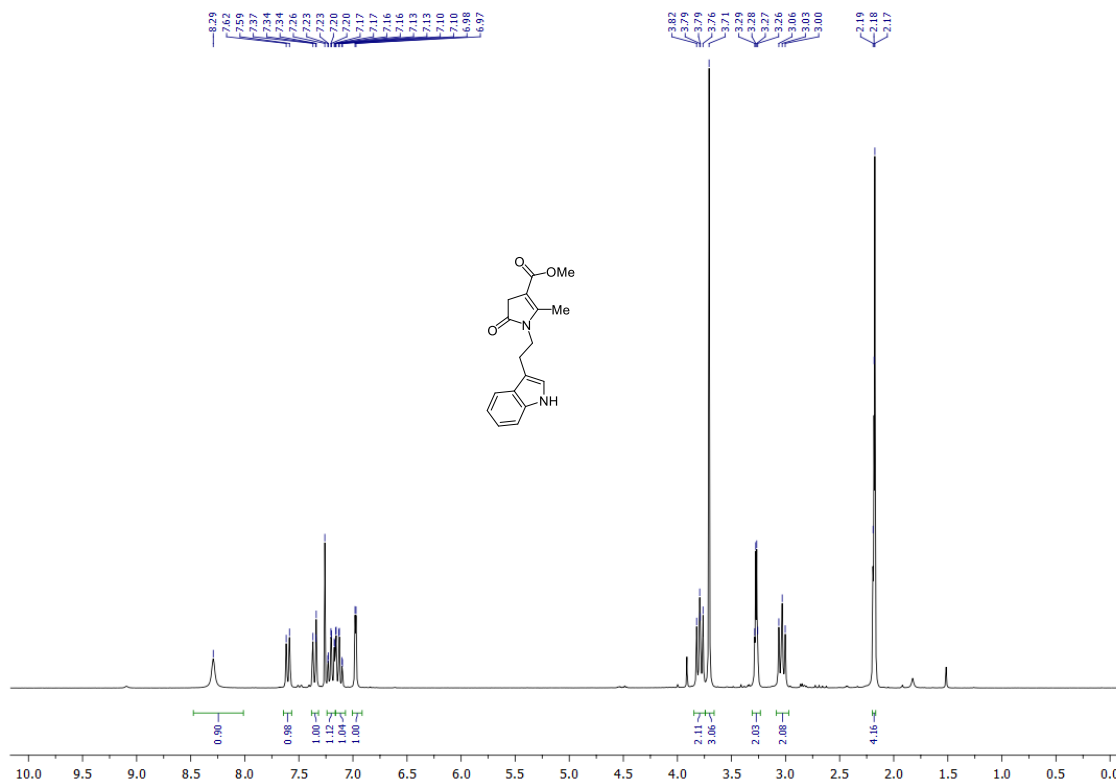
¹³C NMR (63 MHz, CDCl₃)



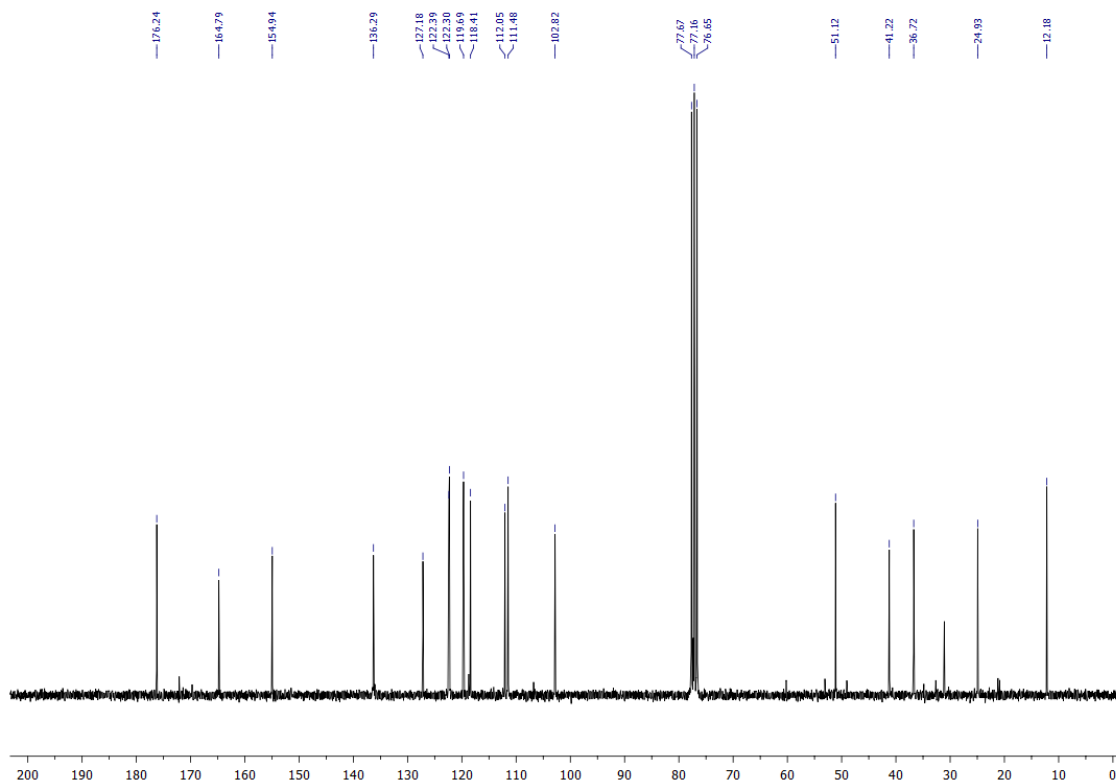
Representative spectra

Methyl 1-(2-(1*H*-indol-3-yl)ethyl)-2-methyl-5-oxo-4,5-dihydro-1*H*-pyrrole-3-carboxylate (1u)

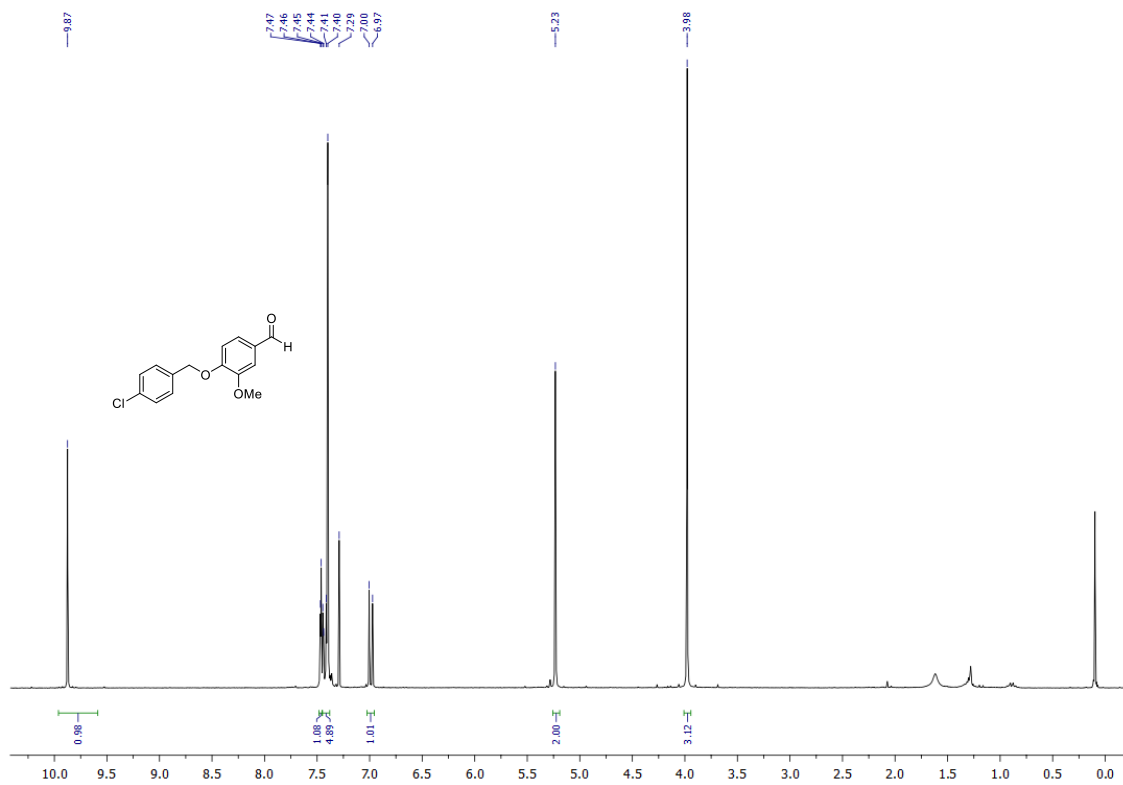
¹H NMR (250 MHz, CDCl₃)



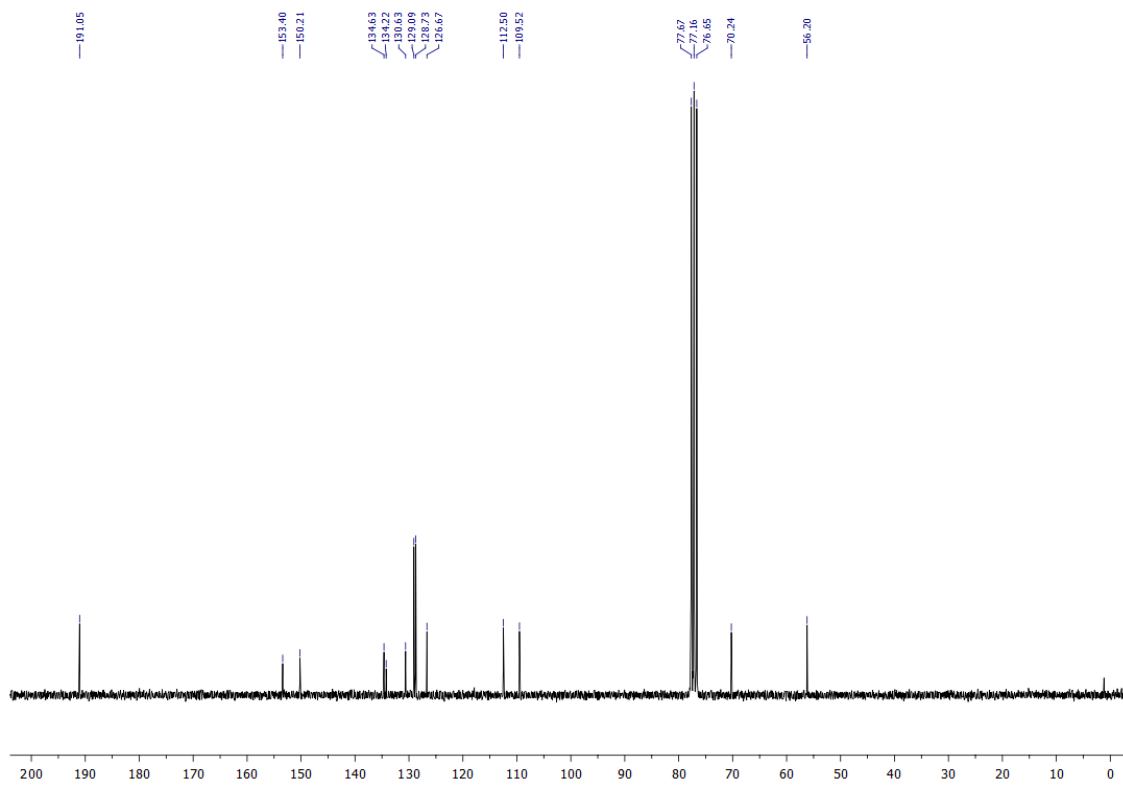
¹³C NMR (63 MHz, CDCl₃)



4-[(4-Chlorobenzyl)oxy]-3-methoxybenzaldehyde (2a)
¹H NMR (250 MHz, CDCl₃)



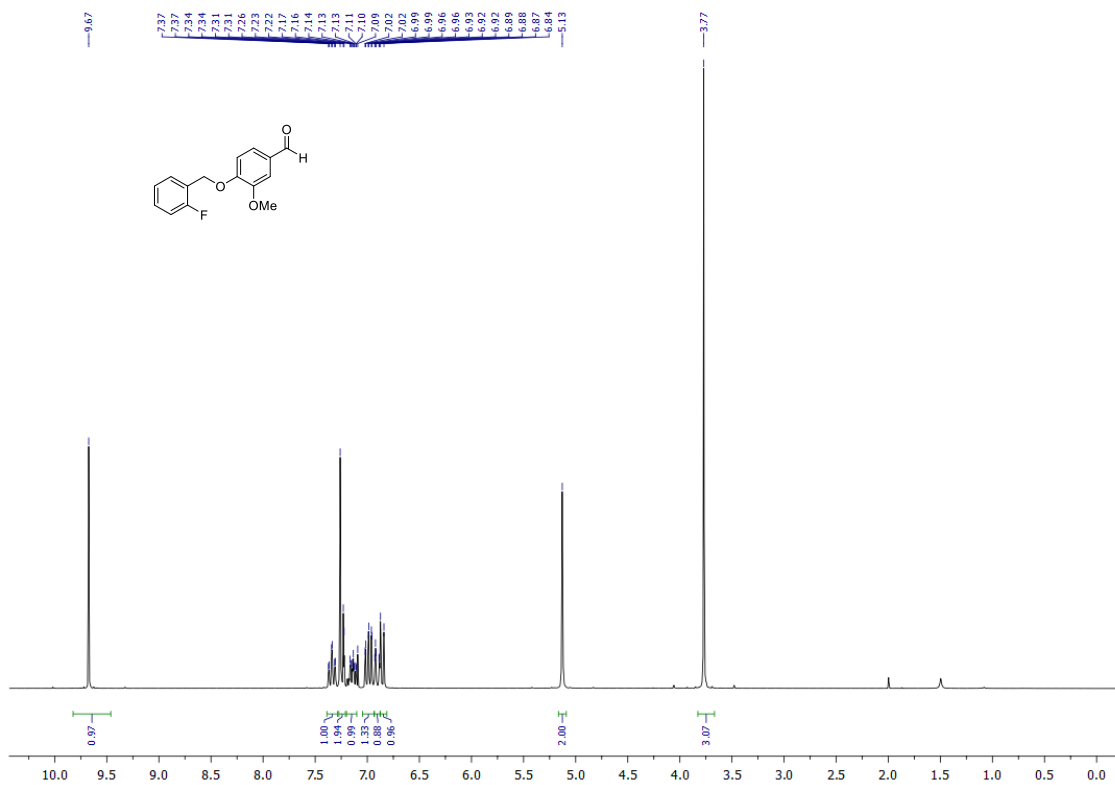
¹³C NMR (63 MHz, CDCl₃)



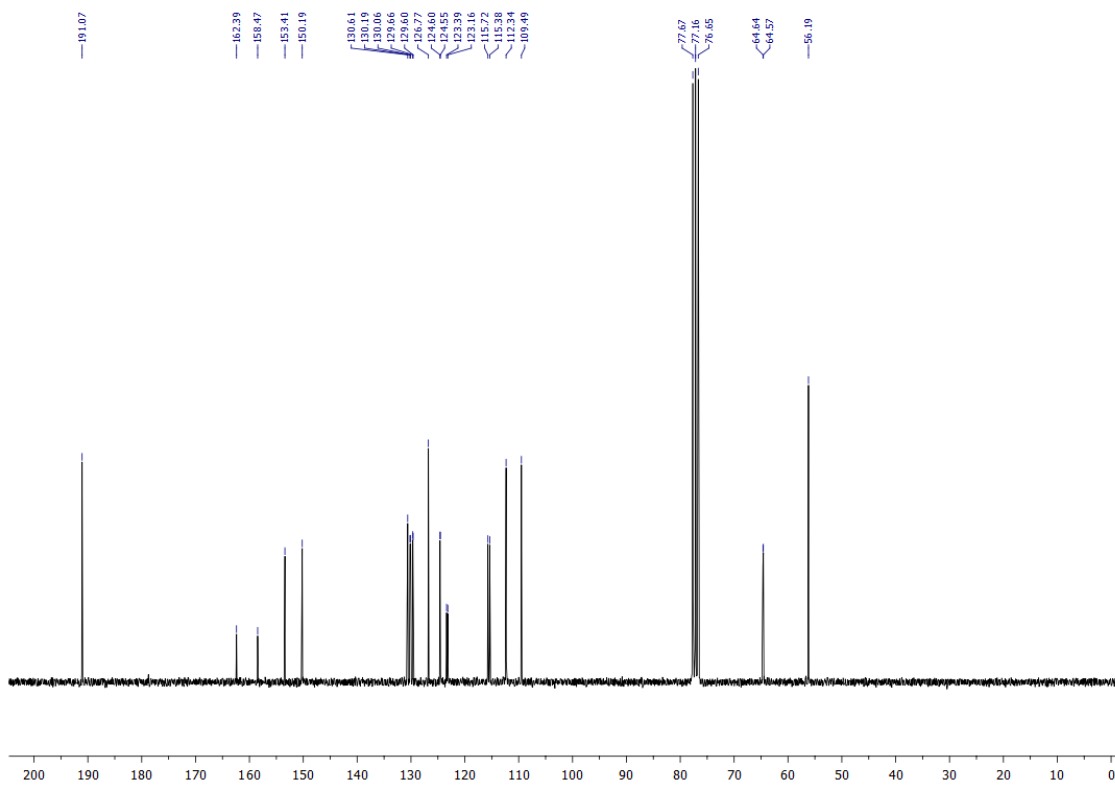
Representative spectra

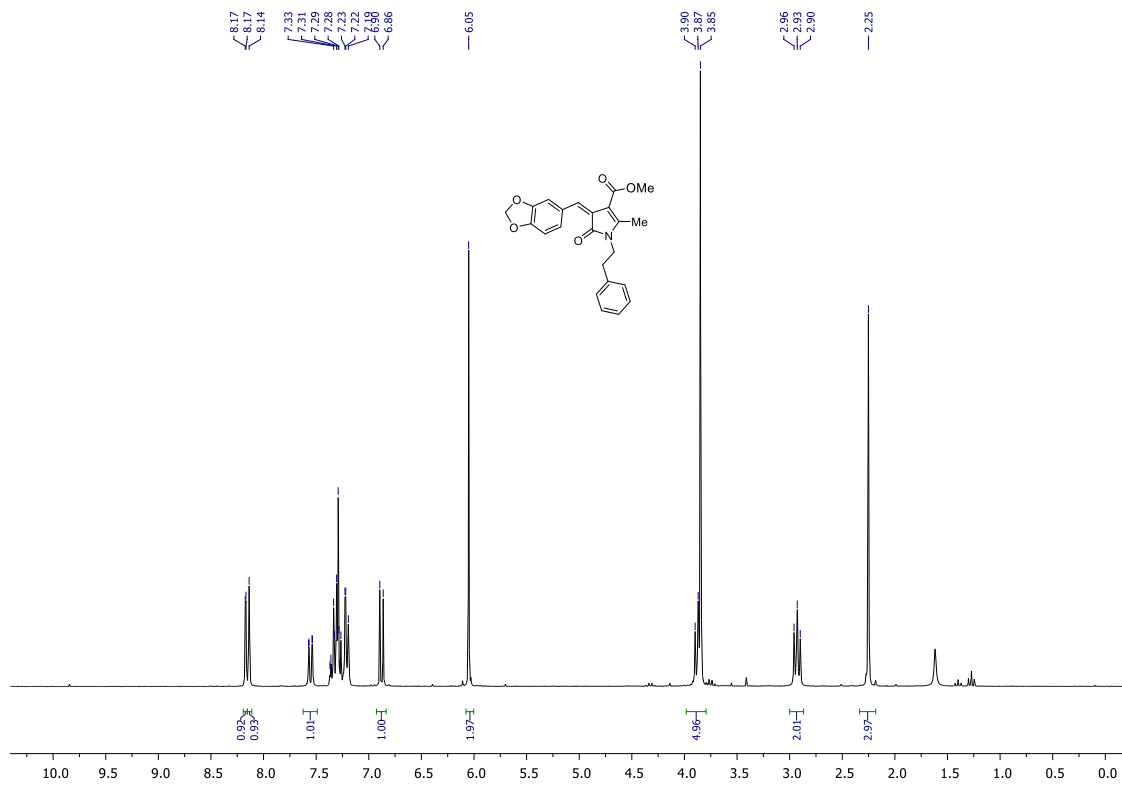
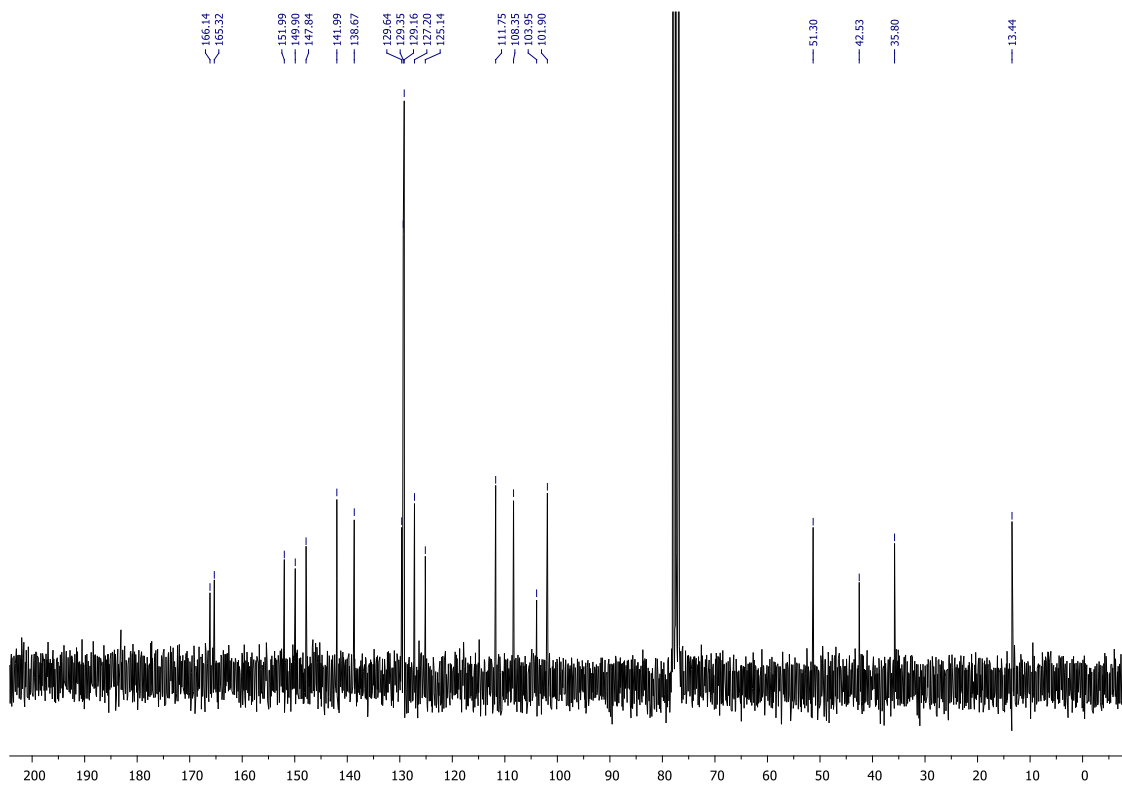
4-[(2-Fluorobenzyl)oxy]-3-methoxybenzaldehyde (2c)

^1H NMR (250 MHz, CDCl_3)



^{13}C NMR (63 MHz, CDCl_3)

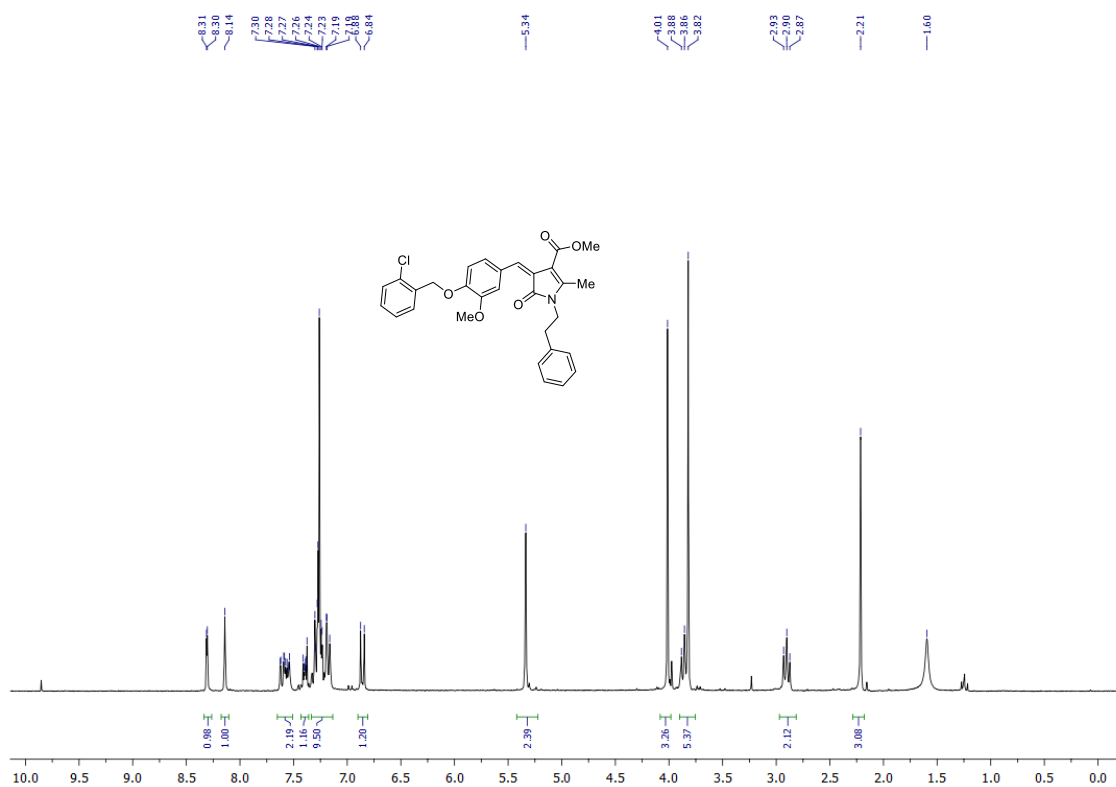


Methyl (Z)-4-benzylidene-2-methyl-5-oxo-1-phenethyl-4,5-dihydro-1H-pyrrole-3-carboxylate (3a)**¹H NMR (250 MHz, CDCl₃)****¹³C NMR (63 MHz, CDCl₃)**

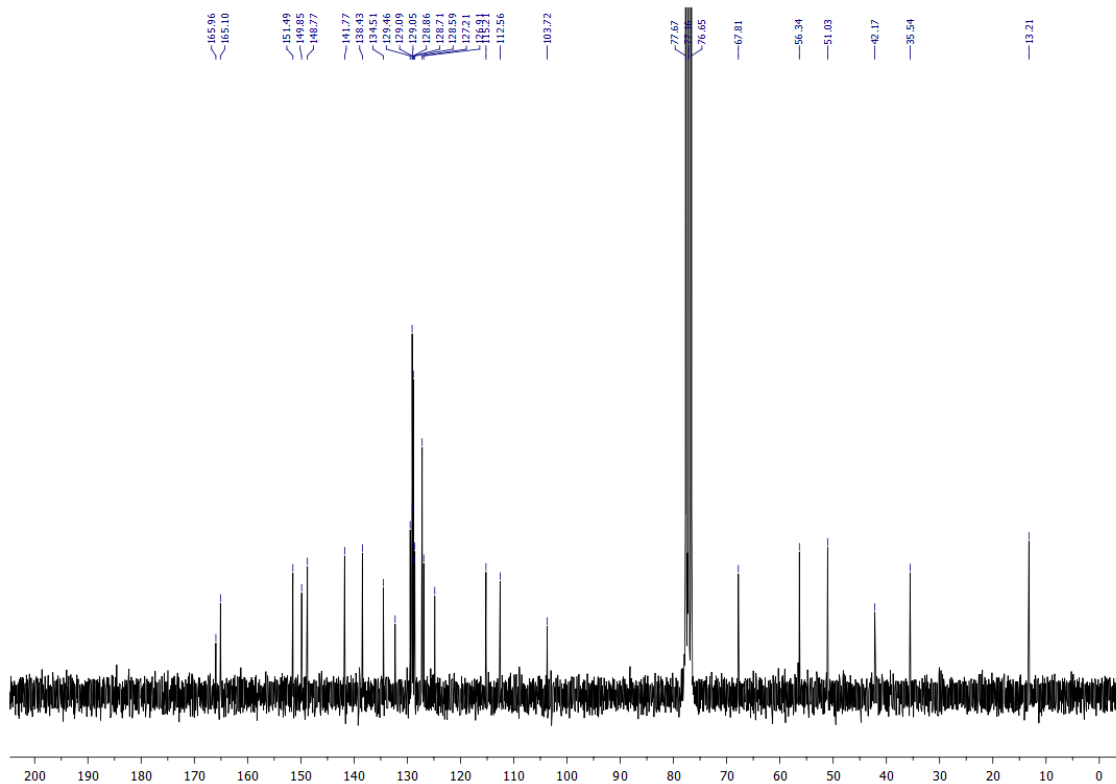
Representative spectra

Methyl (Z)-4-[4-[(2-chlorobenzyl)oxy]-3-methoxybenzylidene]-2-methyl-5-oxo-1-phenethyl-4,5-dihydro-1H-pyrrole-3-carboxylate (3g)

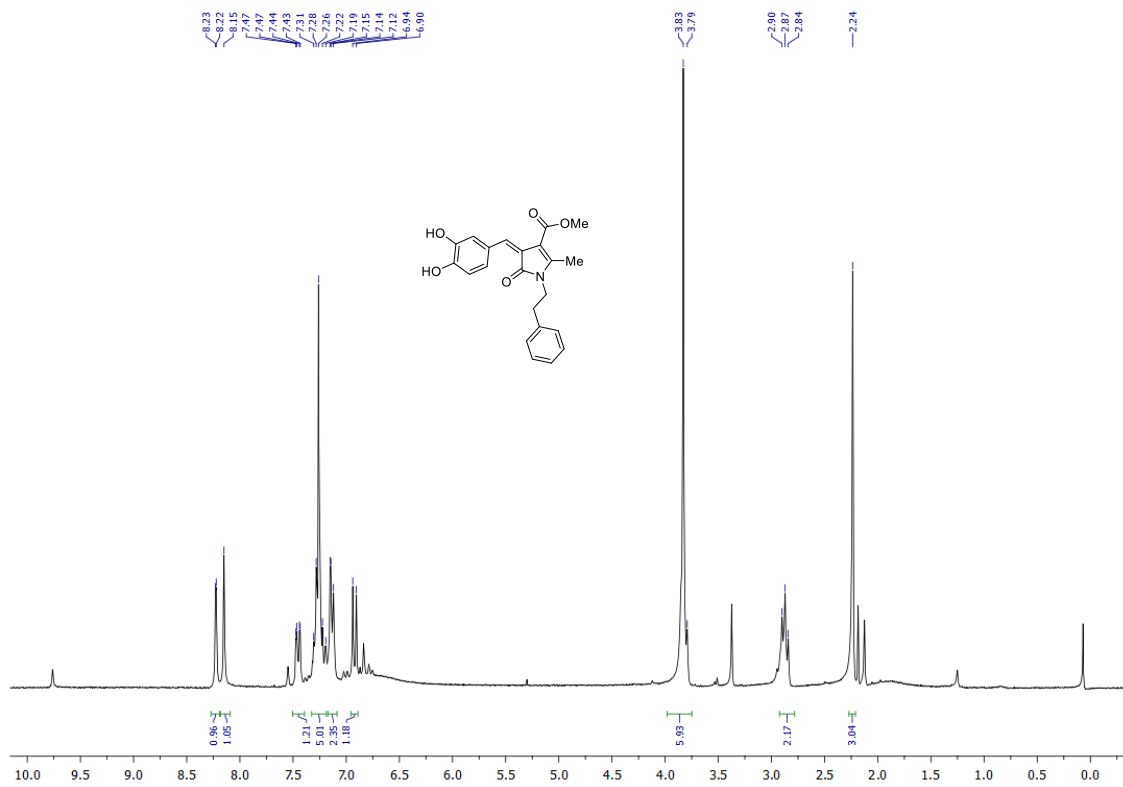
¹H NMR (250 MHz, CDCl₃)



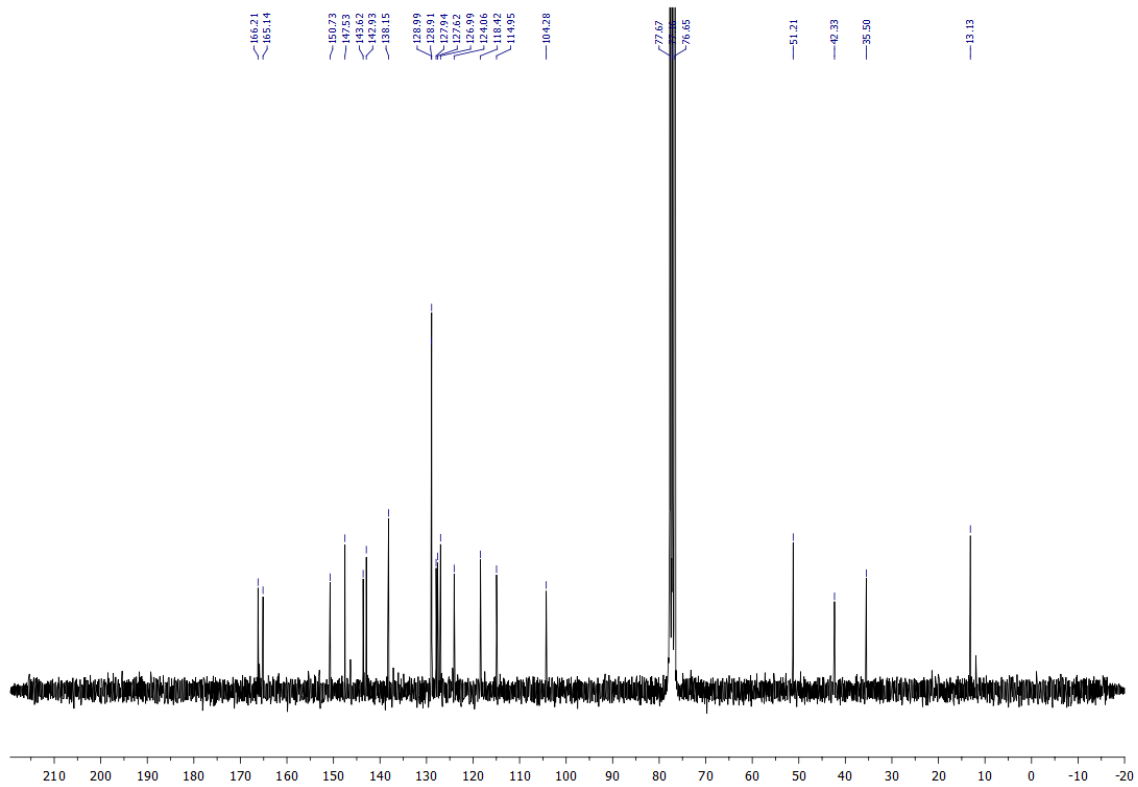
¹³C NMR (63 MHz, CDCl₃)



Methyl (Z)-4-(3,4-dihydroxybenzylidene)-2-methyl-5-oxo-1-phenethyl-4,5-dihydro-1H-pyrrole-3-carboxylate (3i)
¹H NMR (250 MHz, CDCl₃)



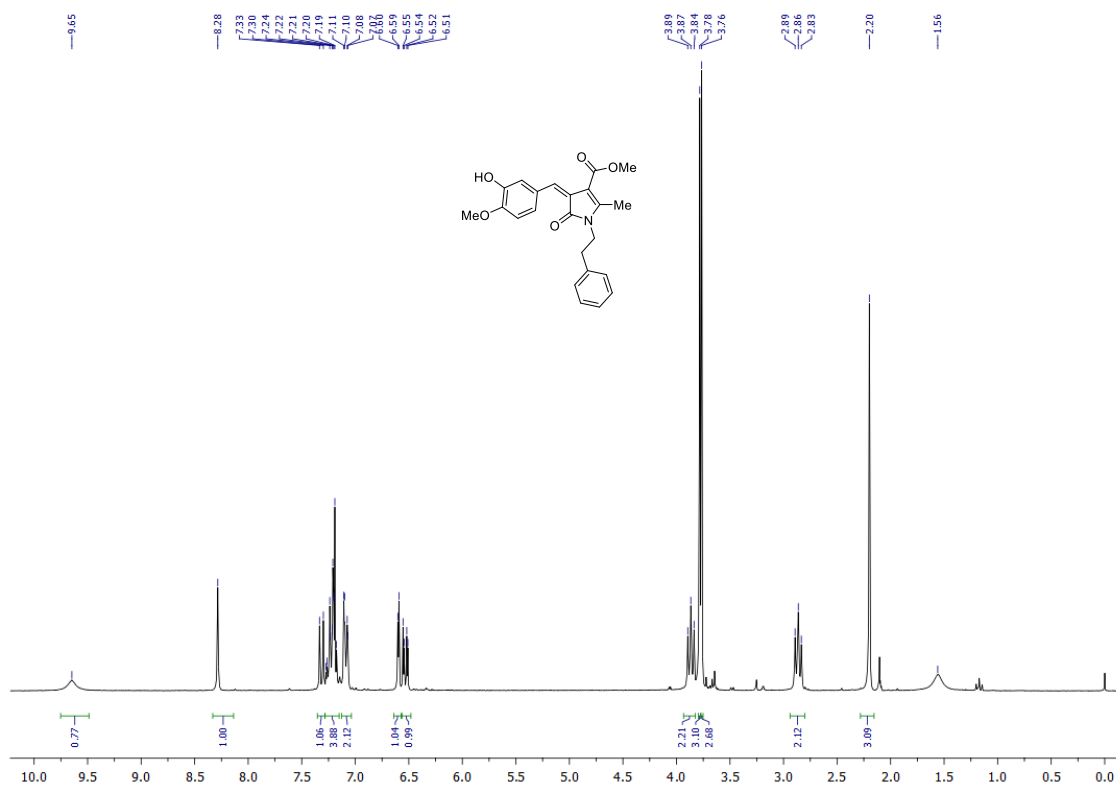
¹³C NMR (63 MHz, CDCl₃)



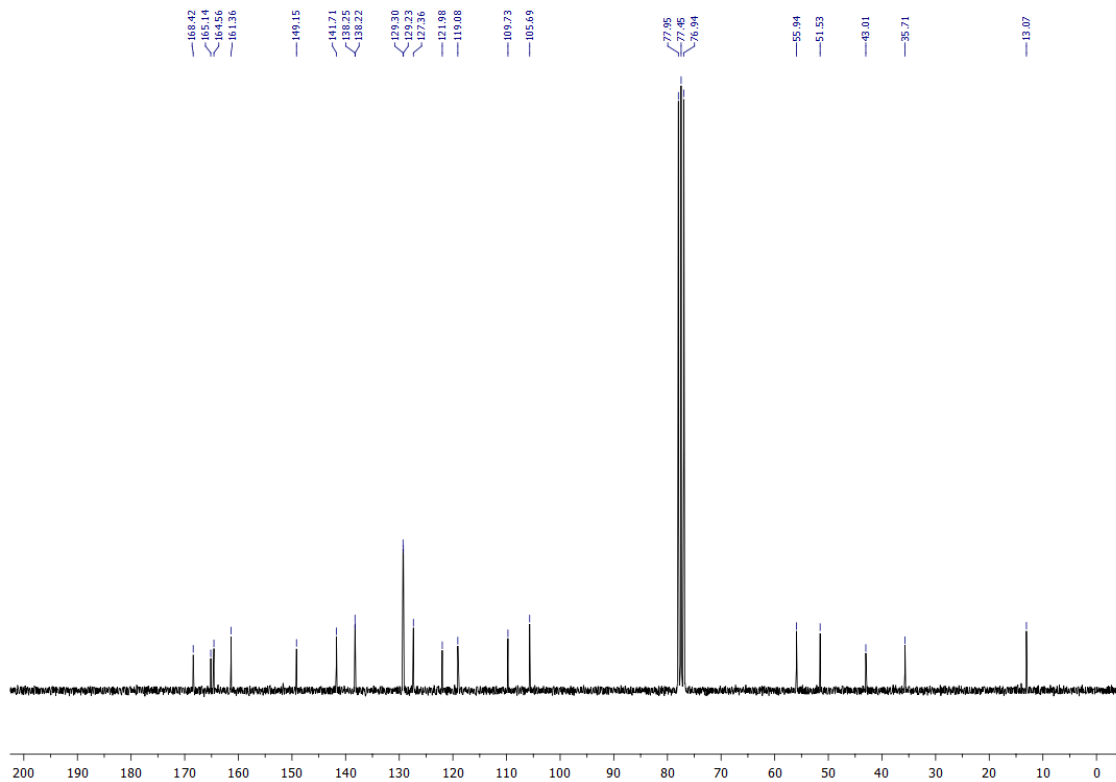
Representative spectra

1H-pyrrole-3-carboxylate (3k)

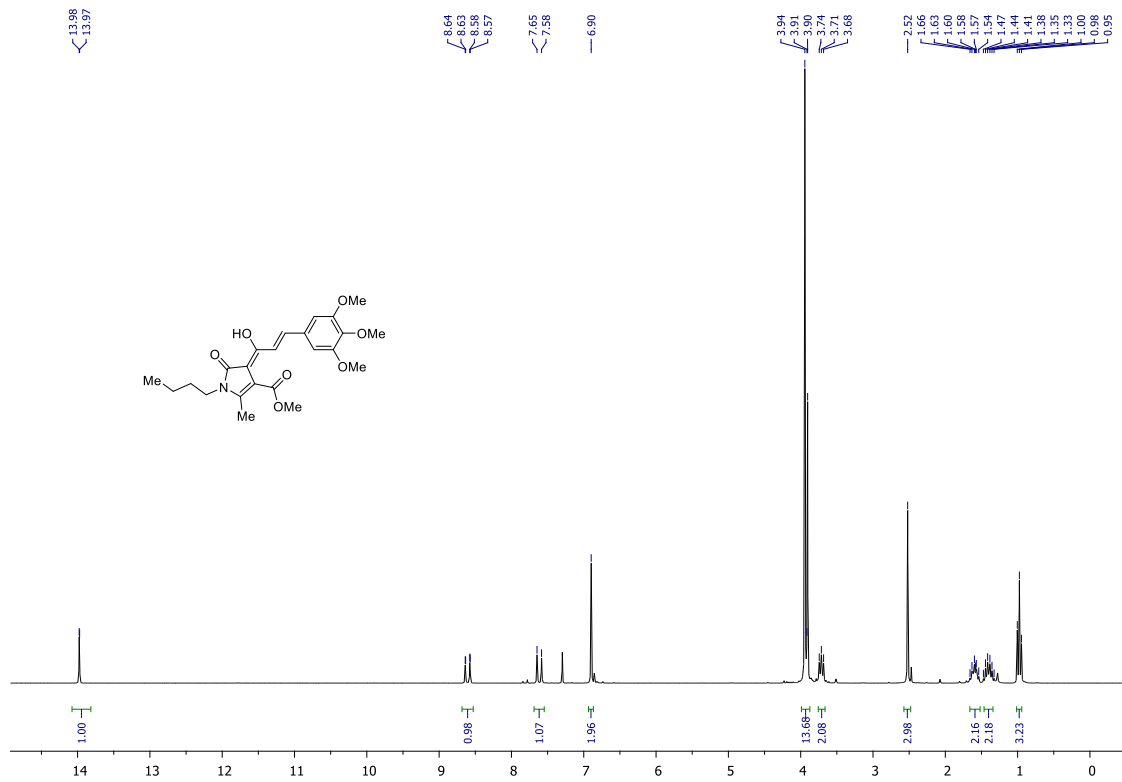
¹H NMR (250 MHz, CDCl₃)



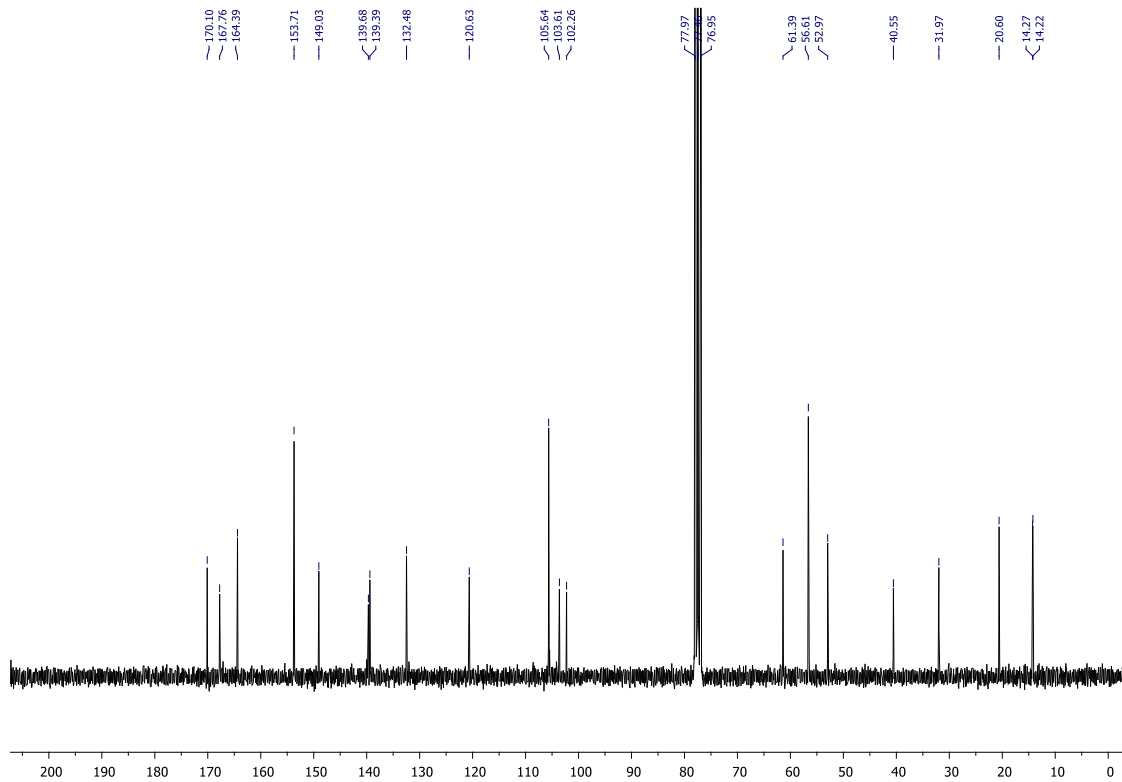
¹³C NMR (63 MHz, CDCl₃)



Methyl (Z)-1-butyl-4-((E)-1-hydroxy-3-(3,4,5-trimethoxyphenyl)allylidene)-2-methyl-5-oxo-4,5-dihydro-1H-pyrrole-3-carboxylate (4b)
¹H NMR (250 MHz, CDCl₃)



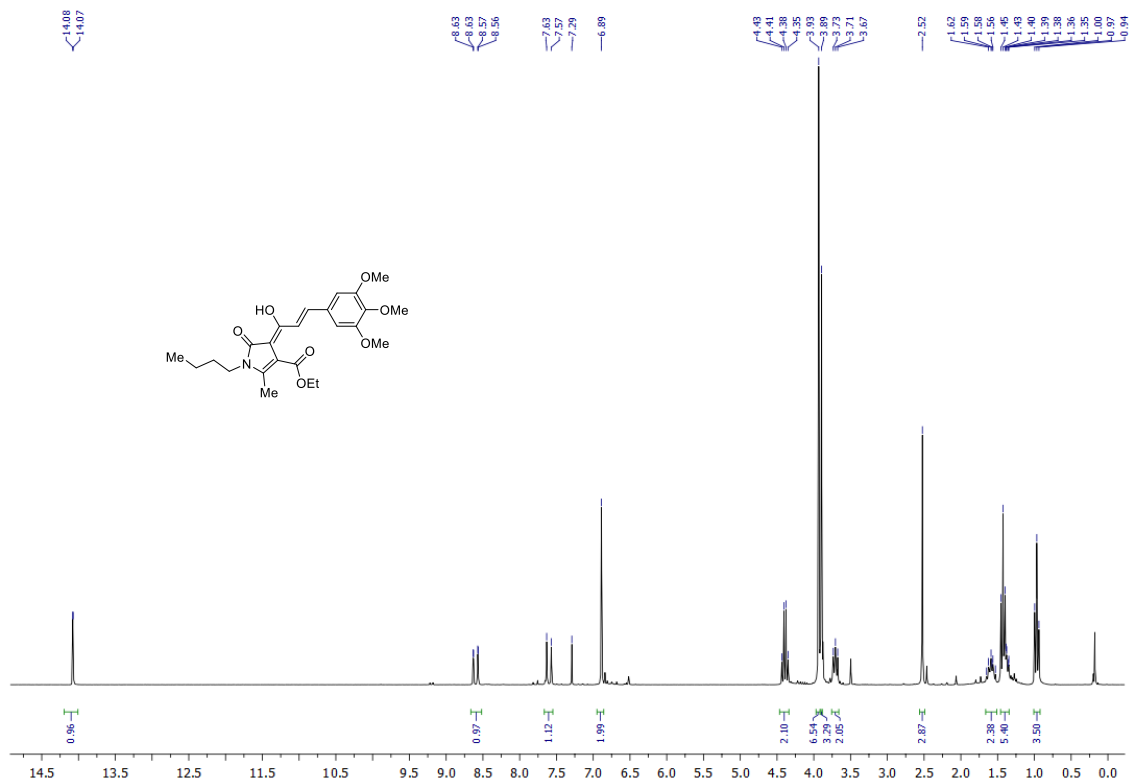
¹³C NMR (63 MHz, CDCl₃)



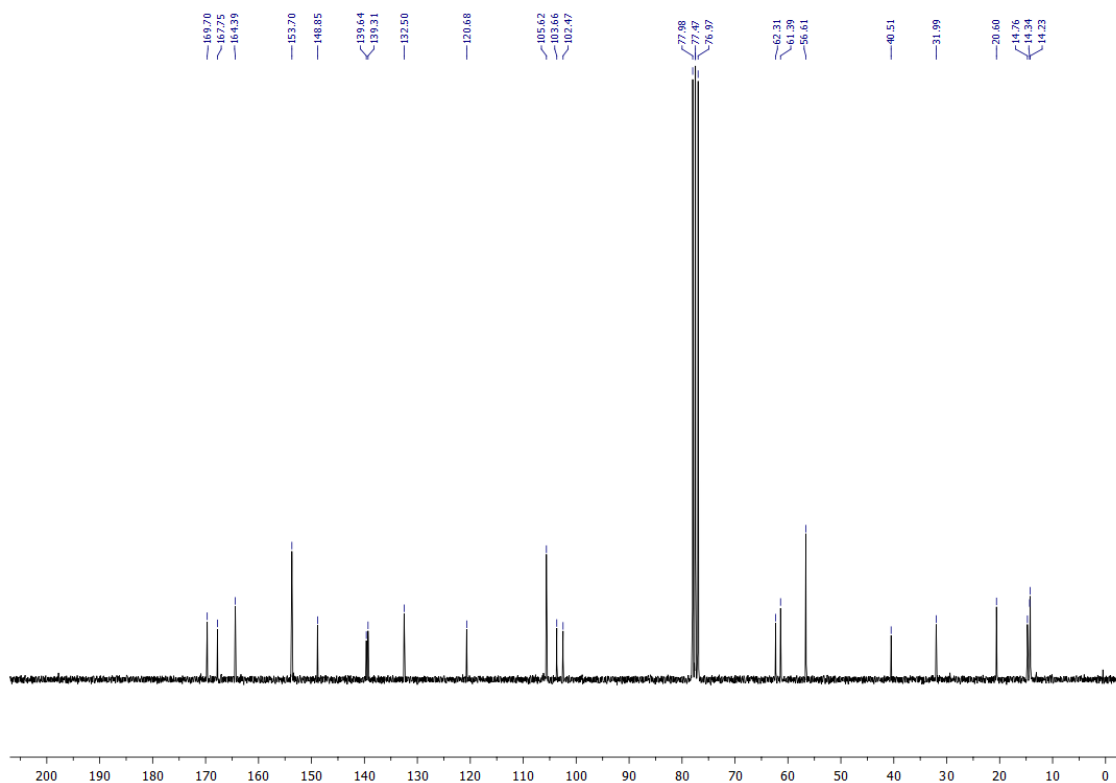
Representative spectra

Ethyl (Z)-1-butyl-4-((E)-1-hydroxy-3-(3,4,5-trimethoxyphenyl)allylidene)-2-methyl-5-oxo-4,5-dihydro-1H-pyrrole-3-carboxylate (4e)

¹H NMR (250 MHz, CDCl₃)

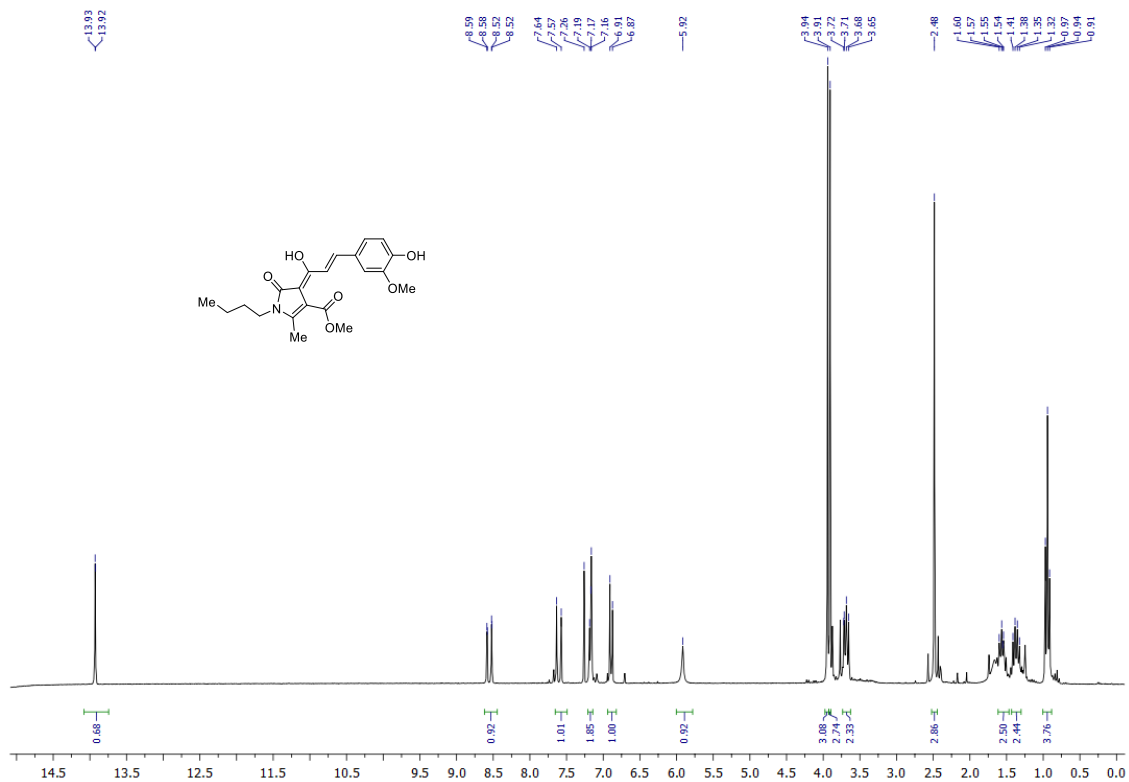


¹³C NMR (63 MHz, CDCl₃)

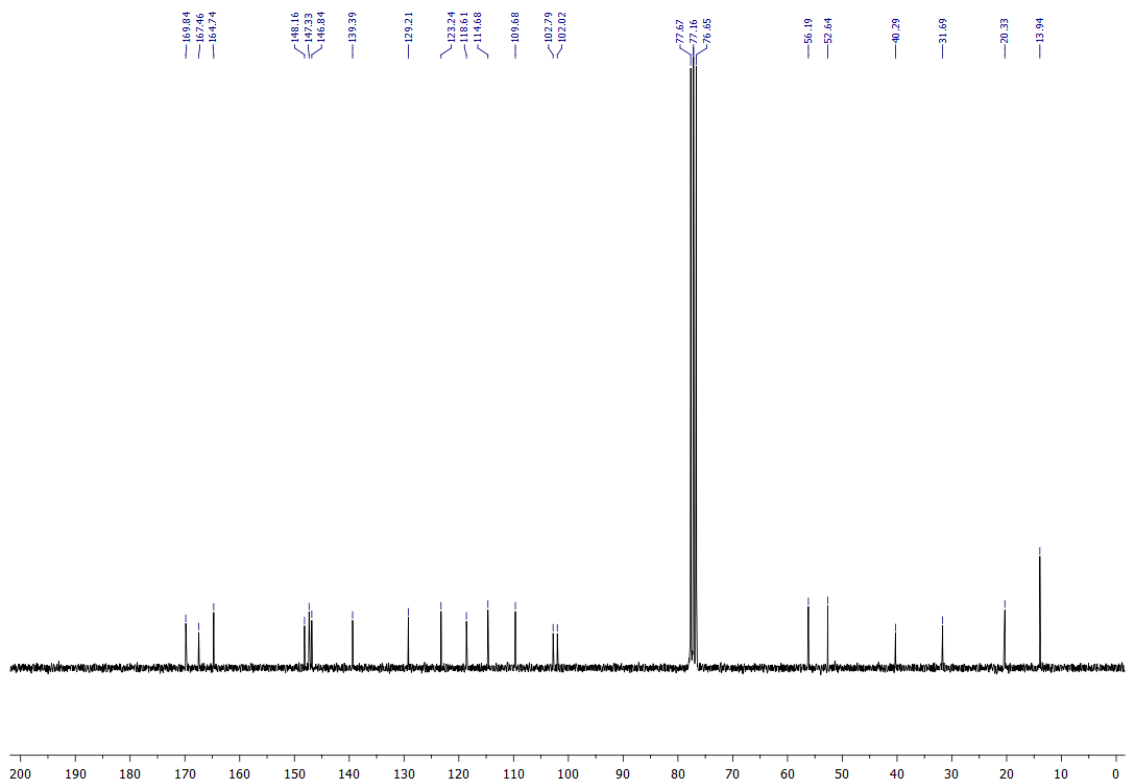


Methyl (Z)-1-butyl-4-((E)-1-hydroxy-3-(4-hydroxy-3-methoxyphenyl)allylidene)-2-methyl-5-oxo-4,5-dihydro-1H-pyrrole-3-carboxylate (4f)

¹H NMR (250 MHz, CDCl₃)

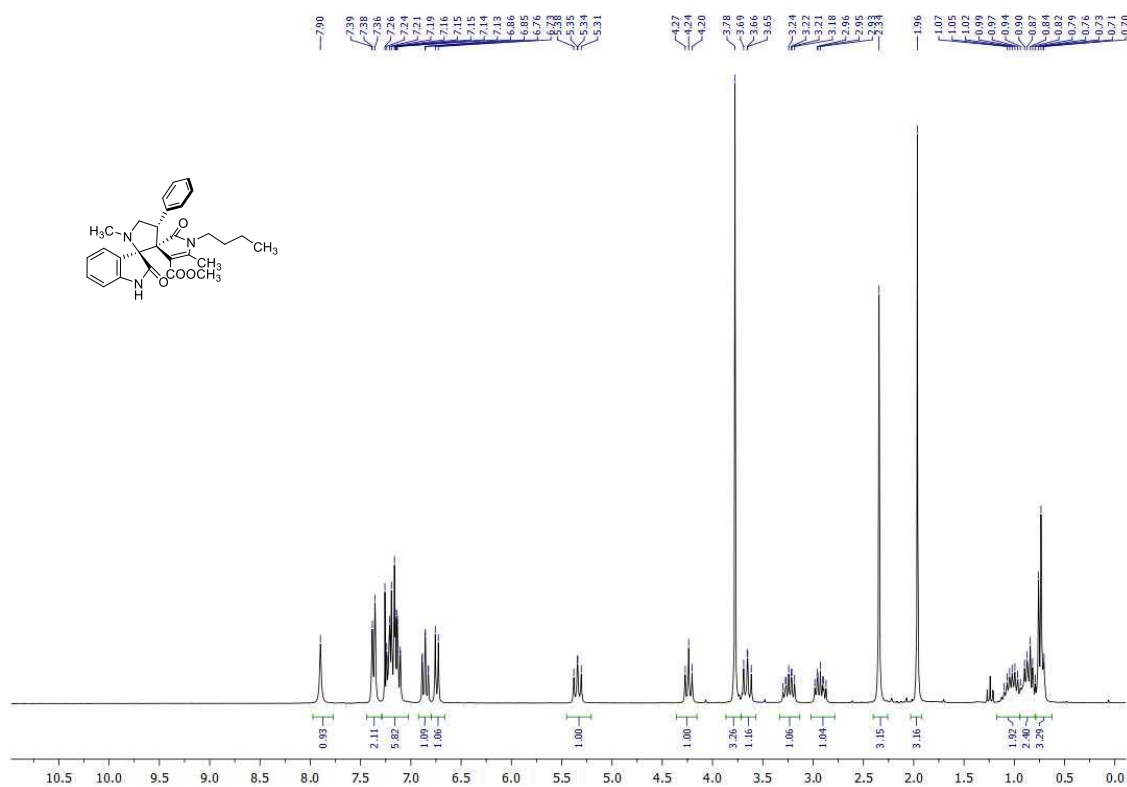


¹³C NMR (63 MHz, CDCl₃)

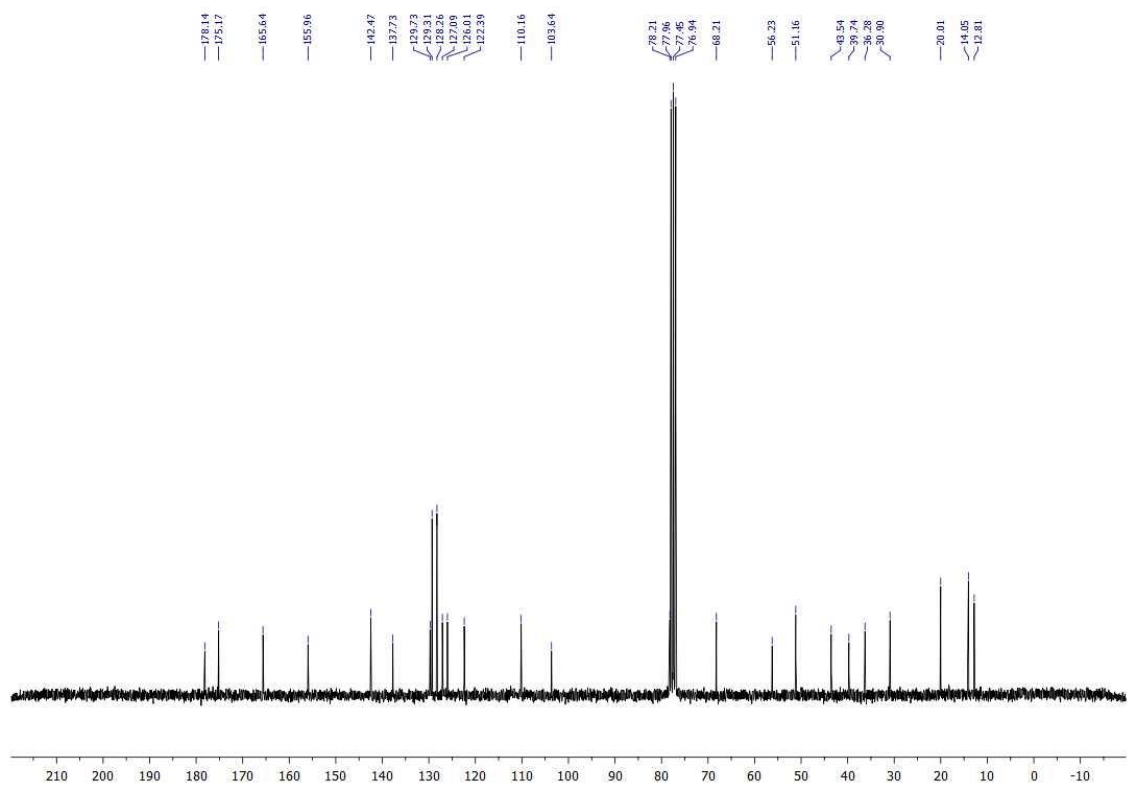


Representative spectra

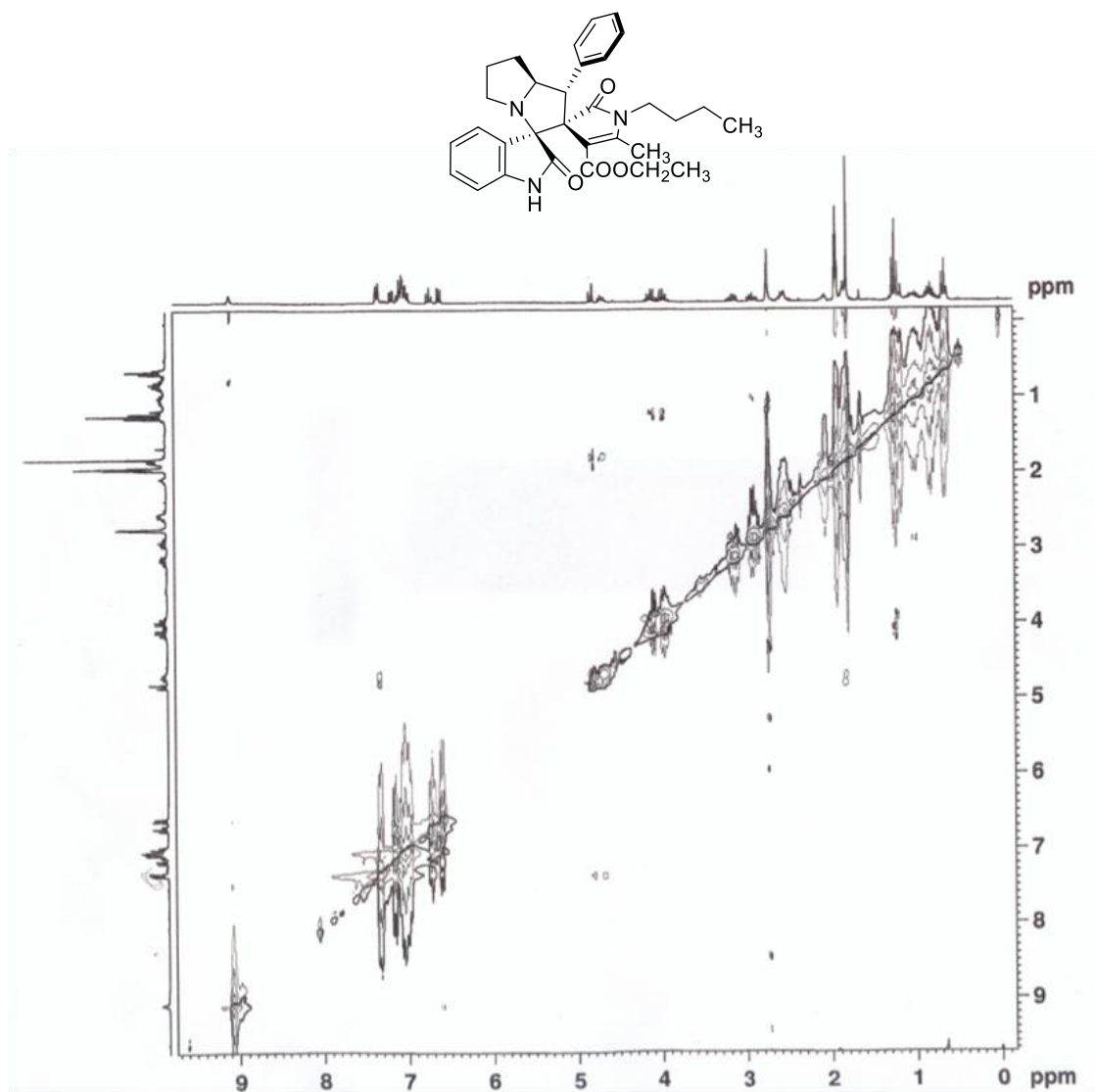
Methyl (3*S,3'*R**,4'*R**)-1'-butyl-1',5''-dimethyl-2,2''-dioxo-4'-phenyl-1'',2''-dihydrodispiro[indoline-3,2'-pyrrolidine-3',3''-pyrrole]-4''-carboxylate (5a)**
¹H NMR (250 MHz, CDCl₃)



¹³C NMR (63 MHz, CDCl₃)



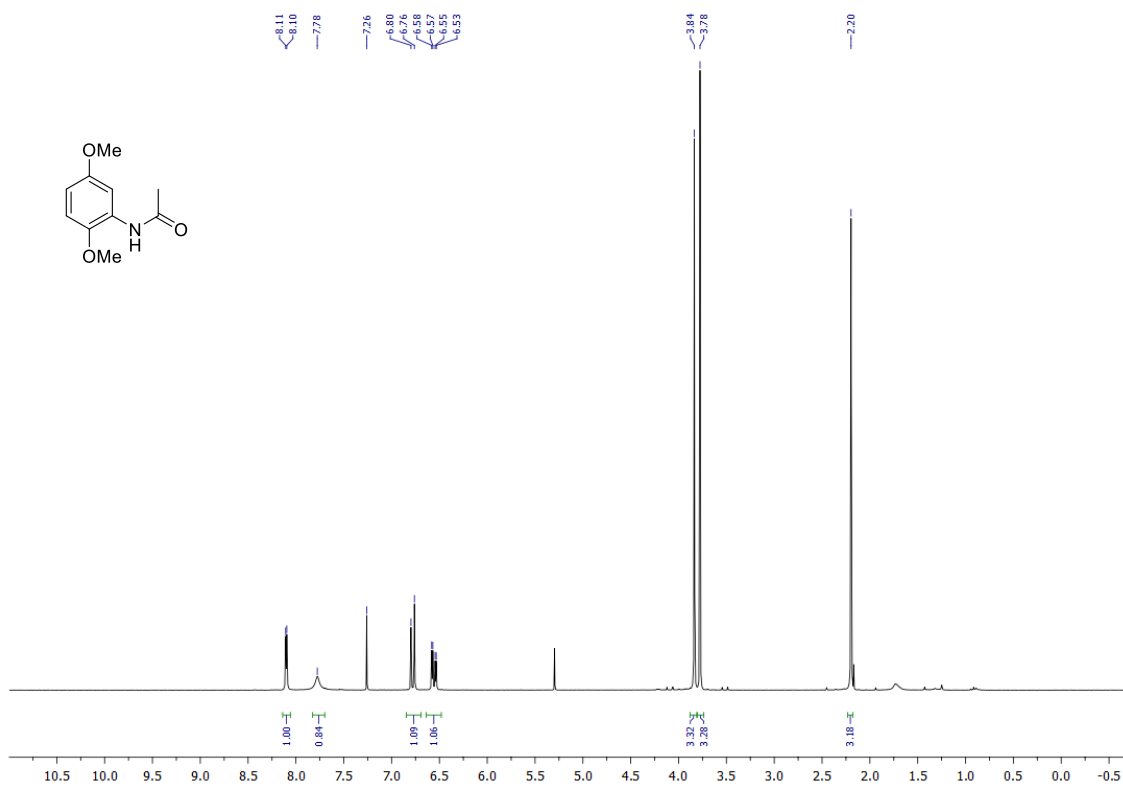
4b NOESY



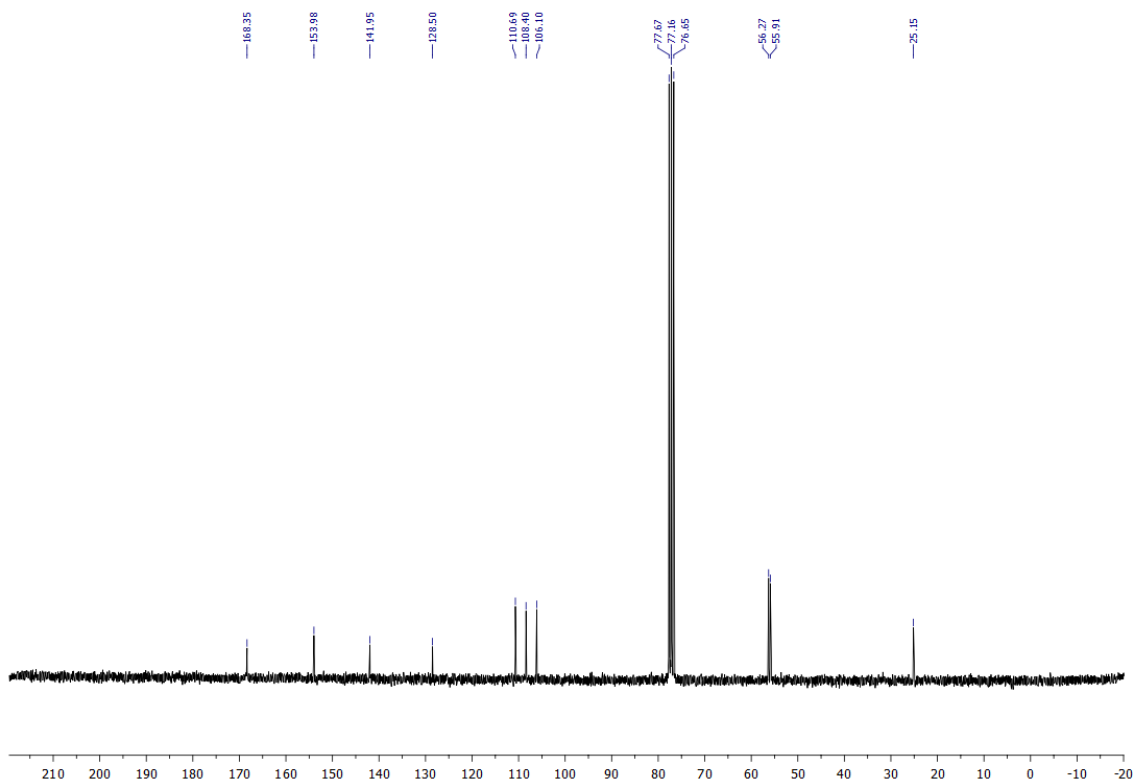
Representative spectra

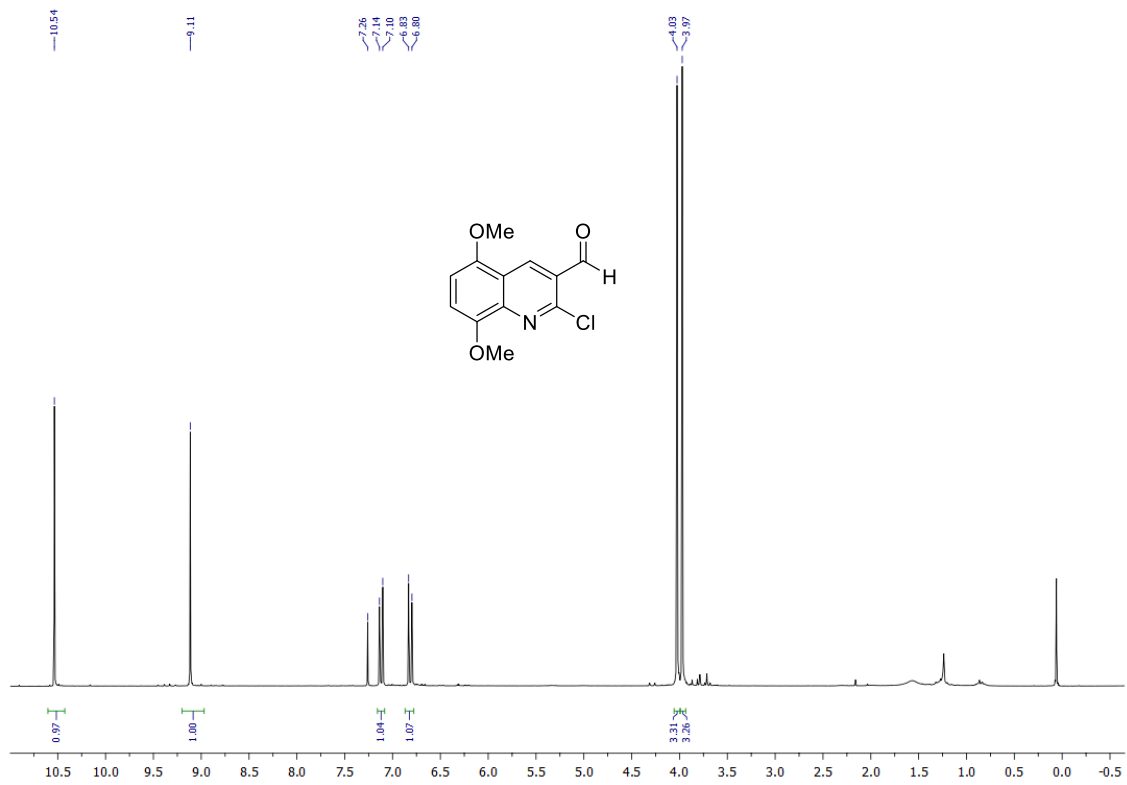
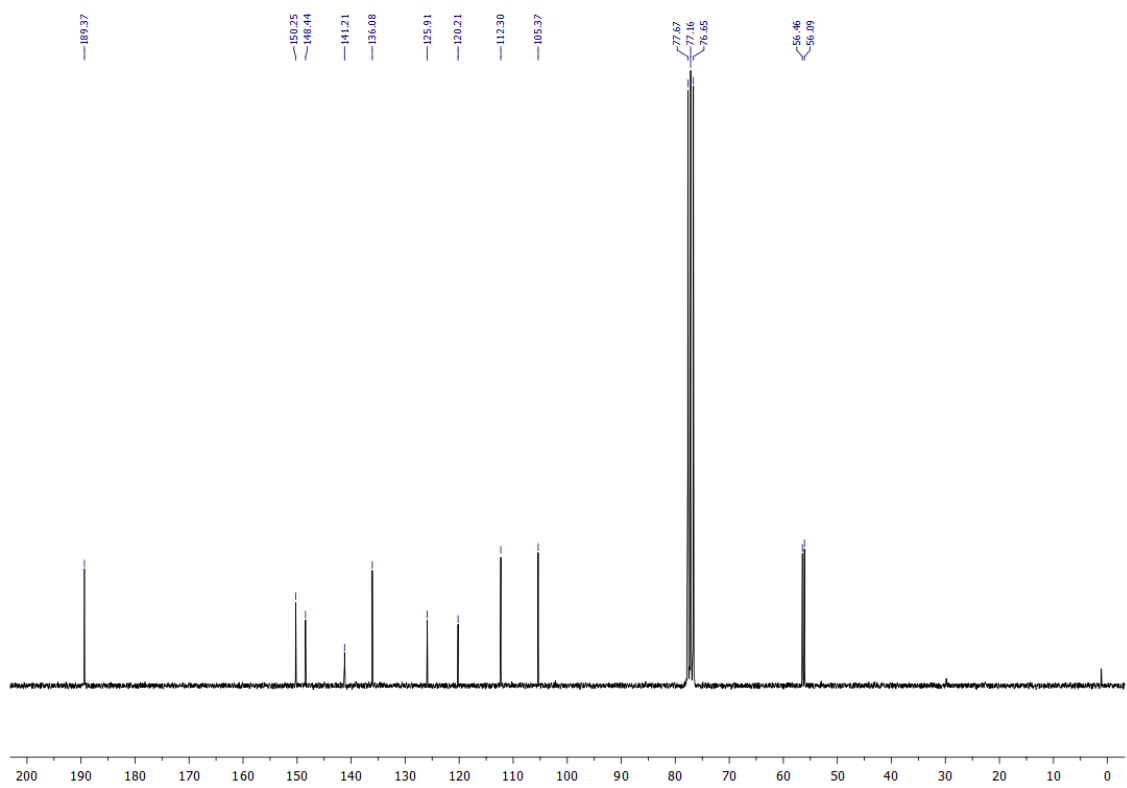
***N*-(2,5-Dimethoxyphenyl)acetamide (7a)**

¹H RMN (250 MHz, CDCl₃)



¹³C RMN (63 MHz, CDCl₃)

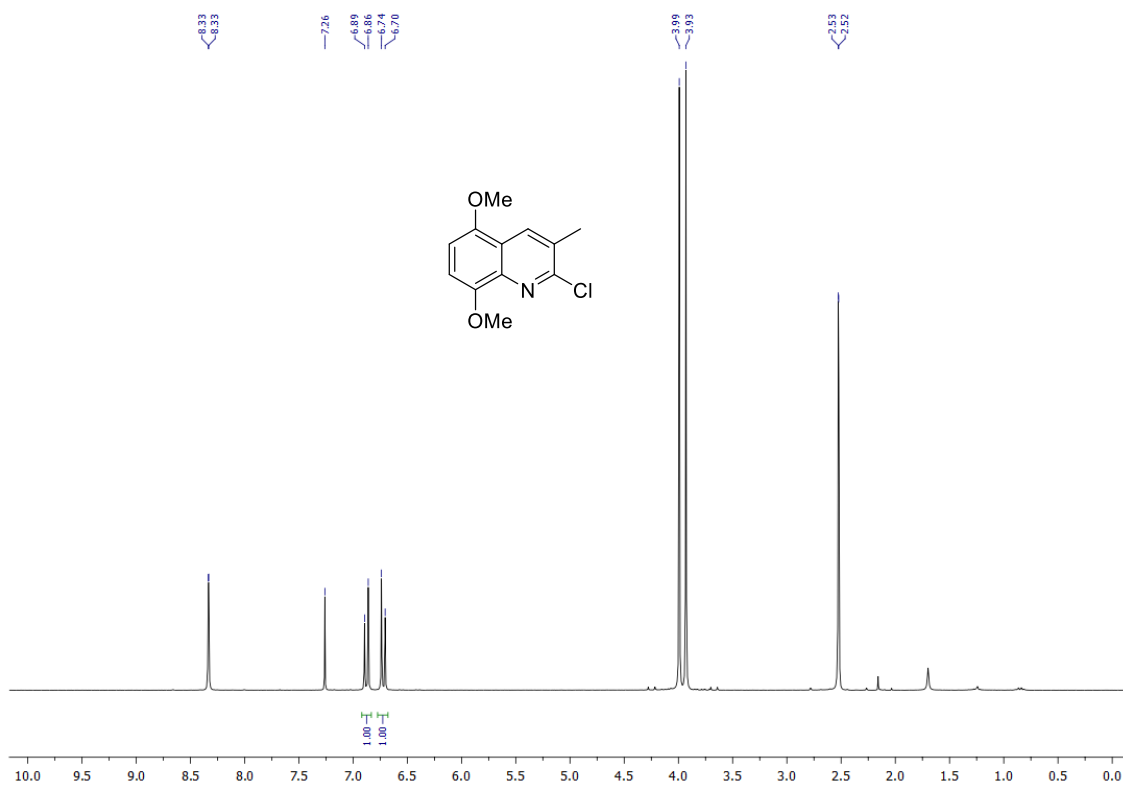


2-Chloro-5,8-dimethoxyquinoline-3-carbaldehyde (8a)**¹H RMN (250 MHz, CDCl₃)****¹³C RMN (63 MHz, CDCl₃)**

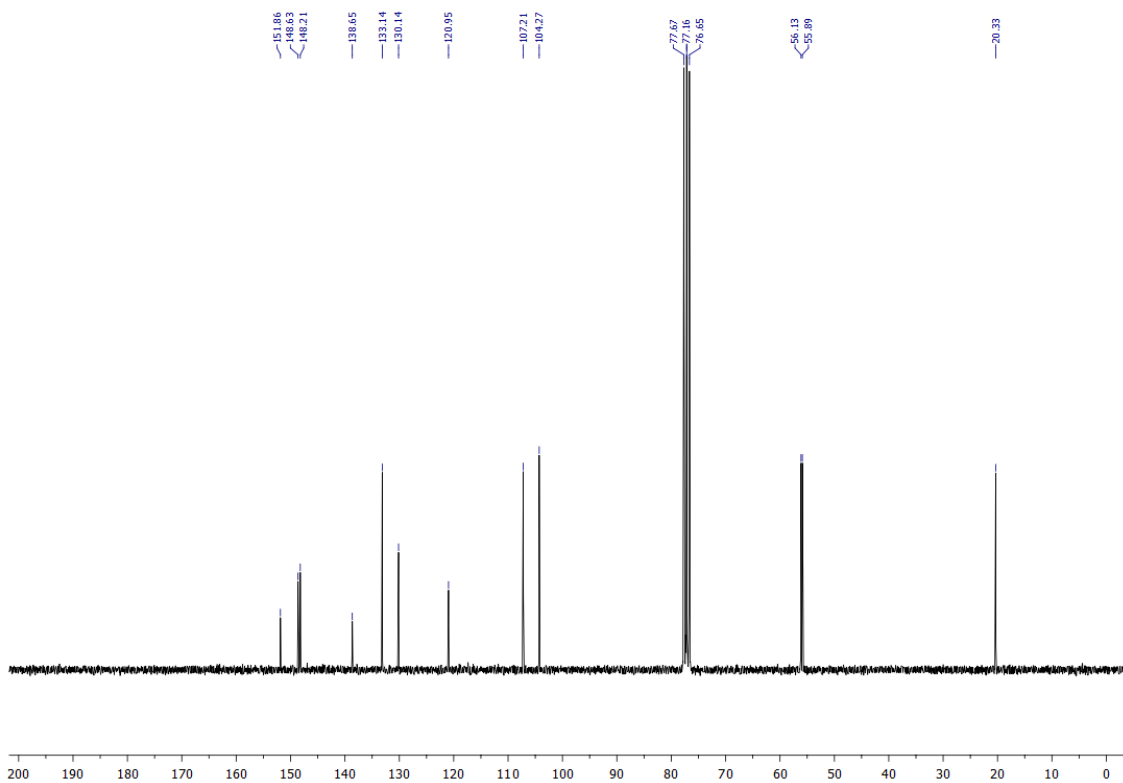
Representative spectra

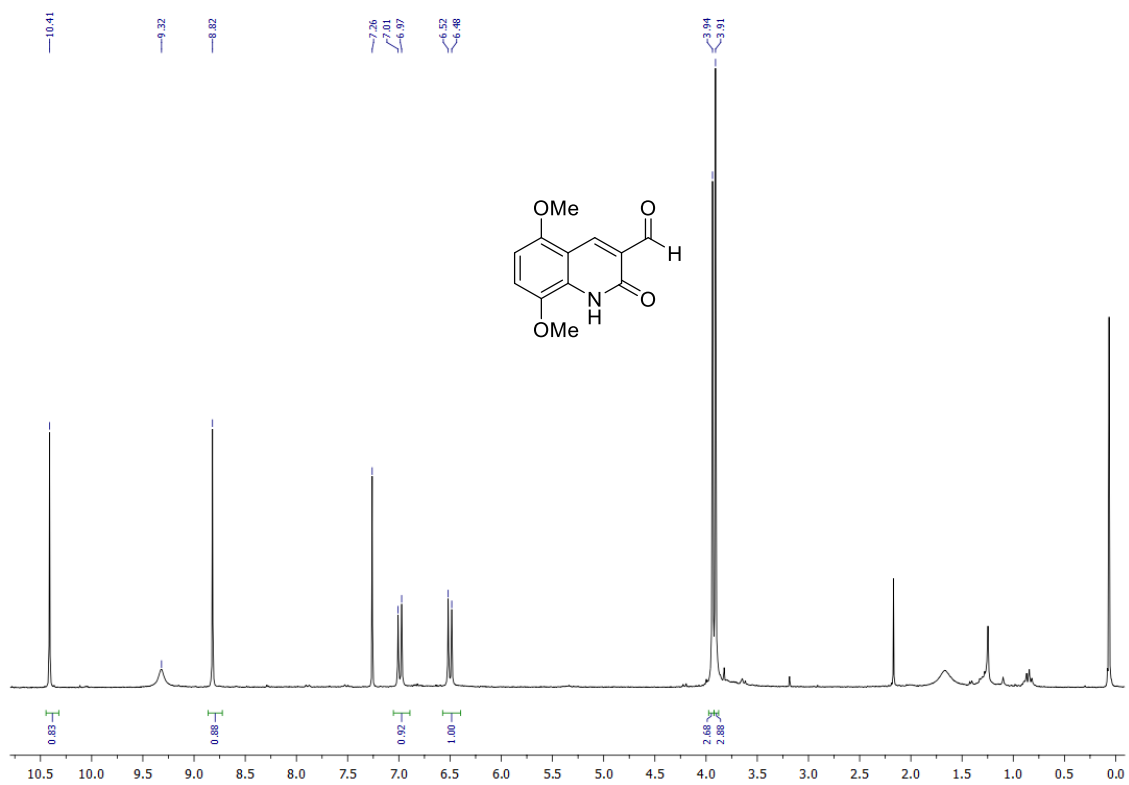
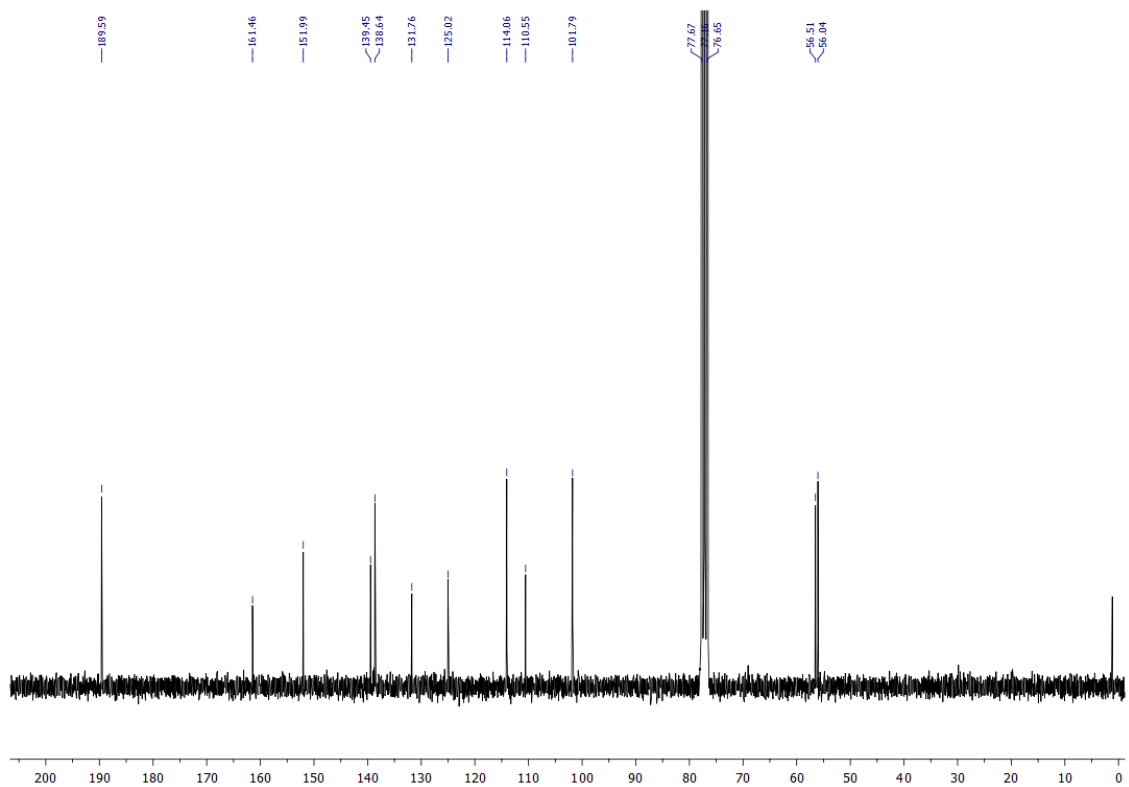
2-Chloro-3-methyl-5,8-dimethoxyquinoline (8b)

^1H RMN (250 MHz, CDCl_3)



^{13}C RMN (63 MHz, CDCl_3)

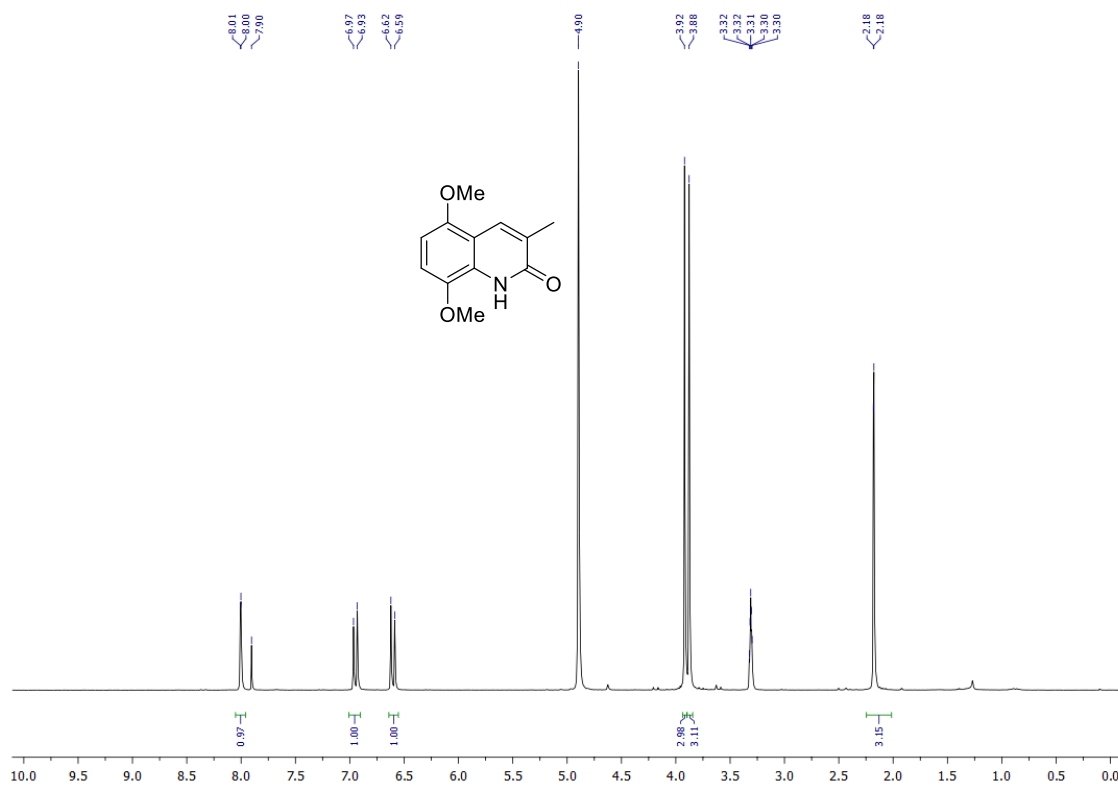


5,8-Dimethoxy-2-oxo-1,2-dihydroquinoline-3-carbaldehyde (9a) **^1H RMN (250 MHz, CDCl_3)** **^{13}C RMN (63 MHz, CDCl_3)**

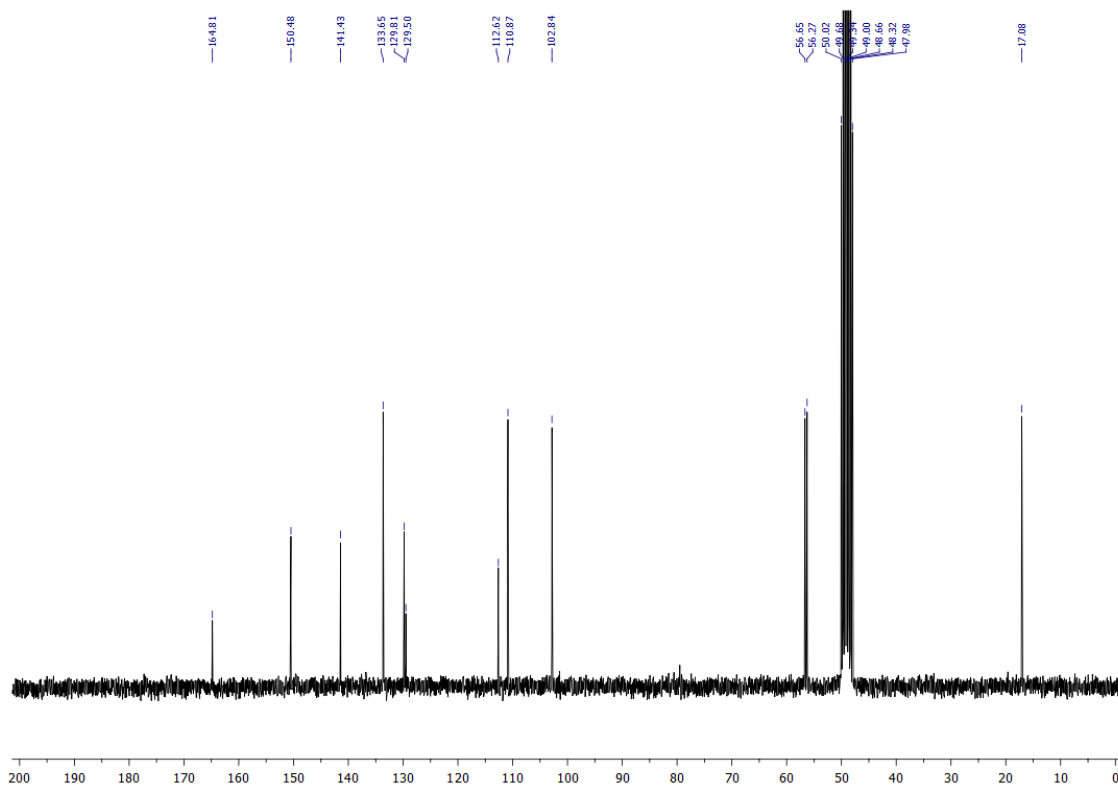
Representative spectra

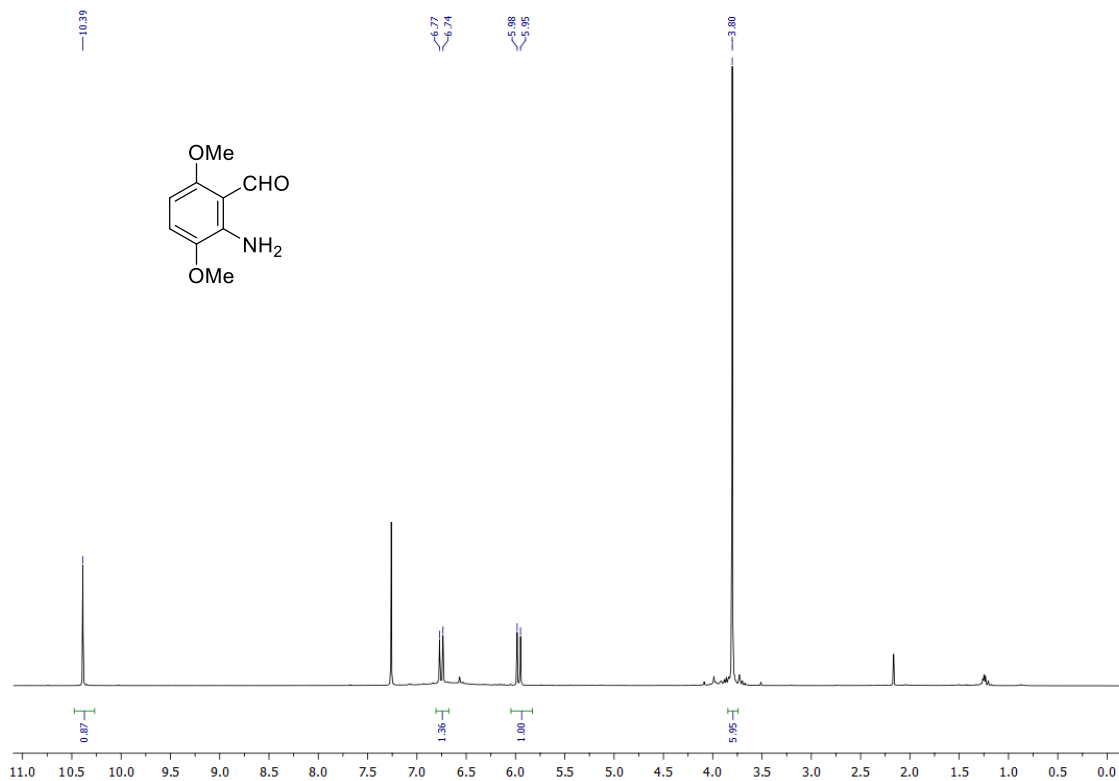
5,8-Dimethoxy-3-methylquinolin-2(1H)-one (9b)

^1H RMN (250 MHz, MeOD)



^{13}C RMN (63 MHz, MeOD)

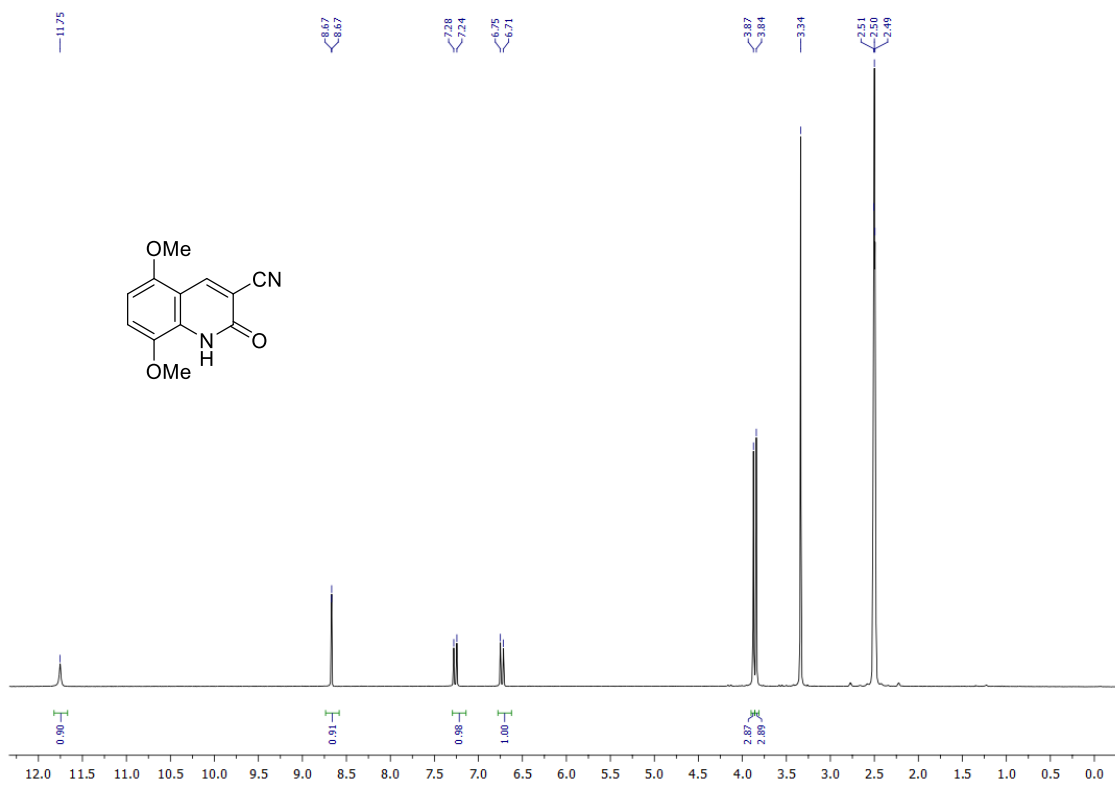


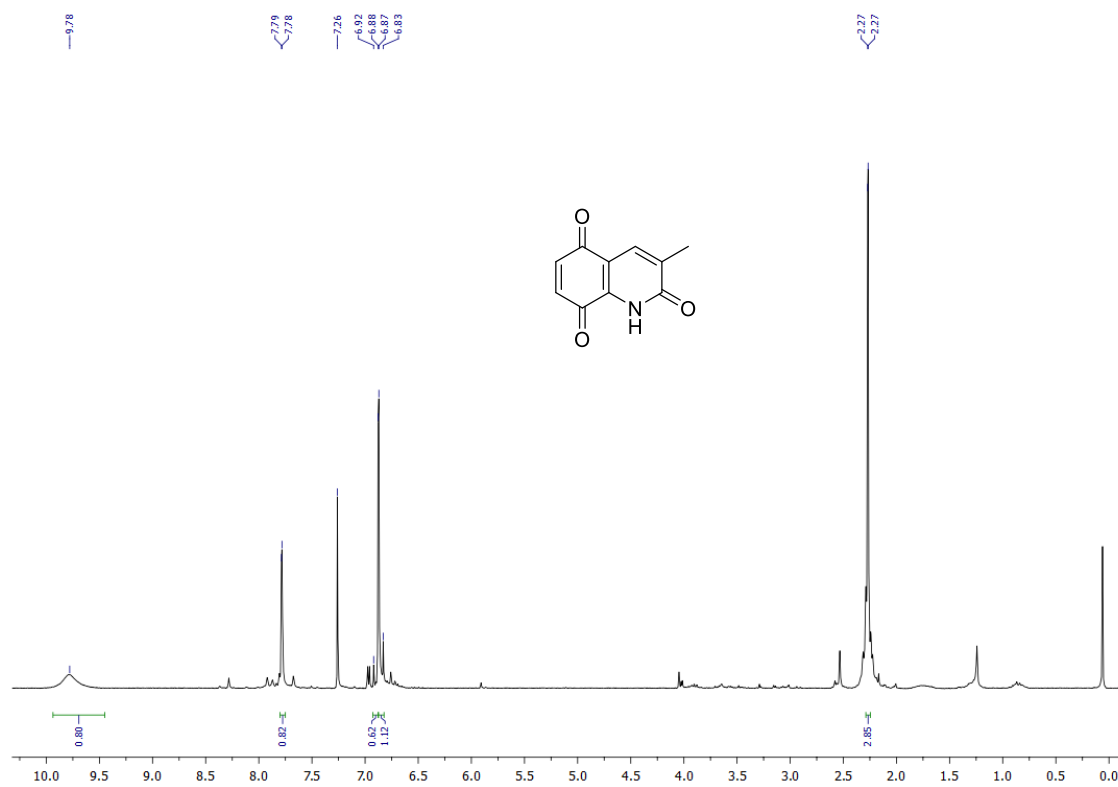
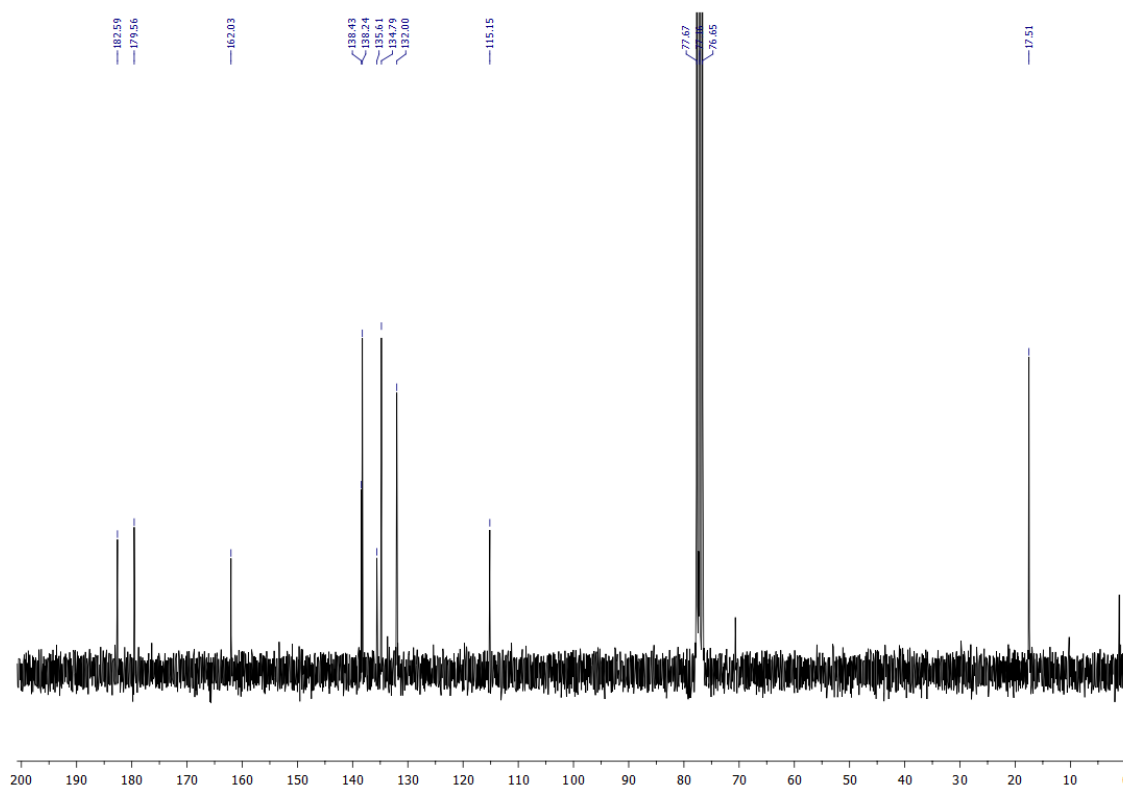
2-Amino-3,6-dimethoxybenzaldehyde (11) **^1H NMR (250 MHz, CDCl_3)**

Representative spectra

5,8-Dimethoxy-2-oxo-1,2-dihydroquinoline-3-carbonitrile (12a)

¹H NMR (250 MHz, *d*₆-DMSO)

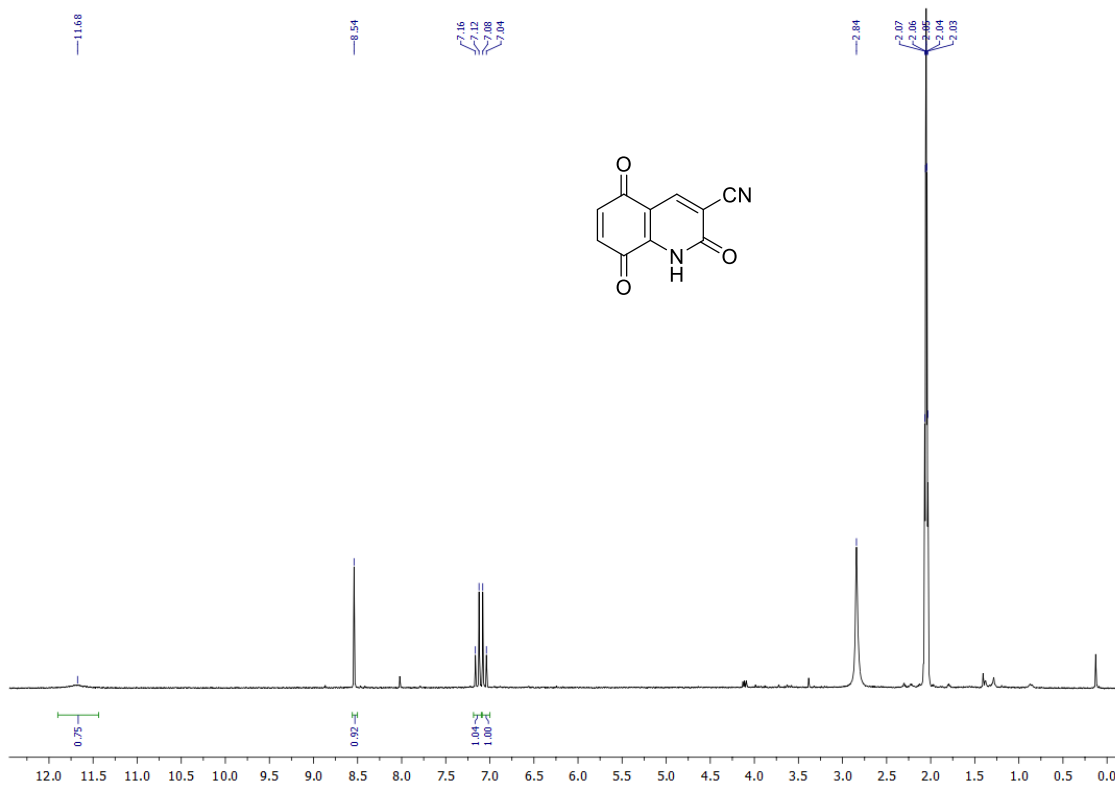


3-Methylquinoline-2,5,8(1H)-trione (13a)
¹H NMR (250 MHz, CDCl₃)**¹³C NMR (63 MHz, CDCl₃)**

Representative spectra

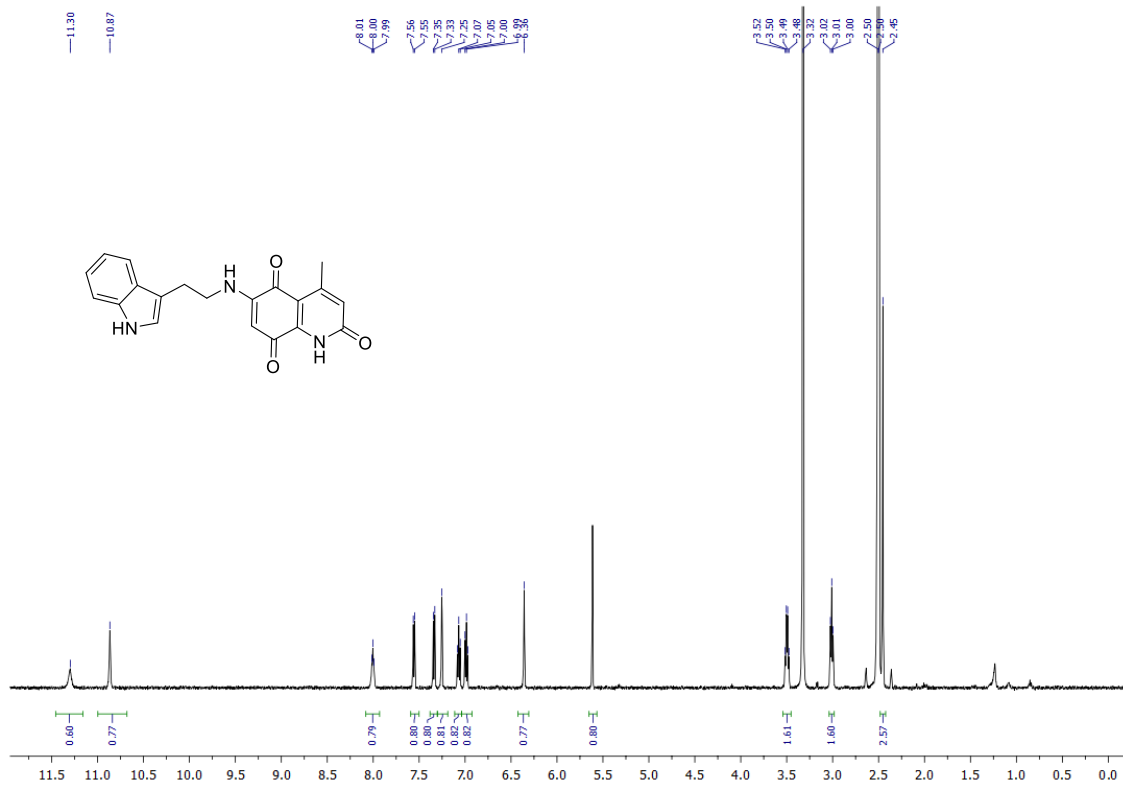
2,5,8-Trioxo-1,2,5,8-tetrahydroquinoline-3-carbonitrile (13c)

¹H NMR (250 MHz, *d*₆-acetone)

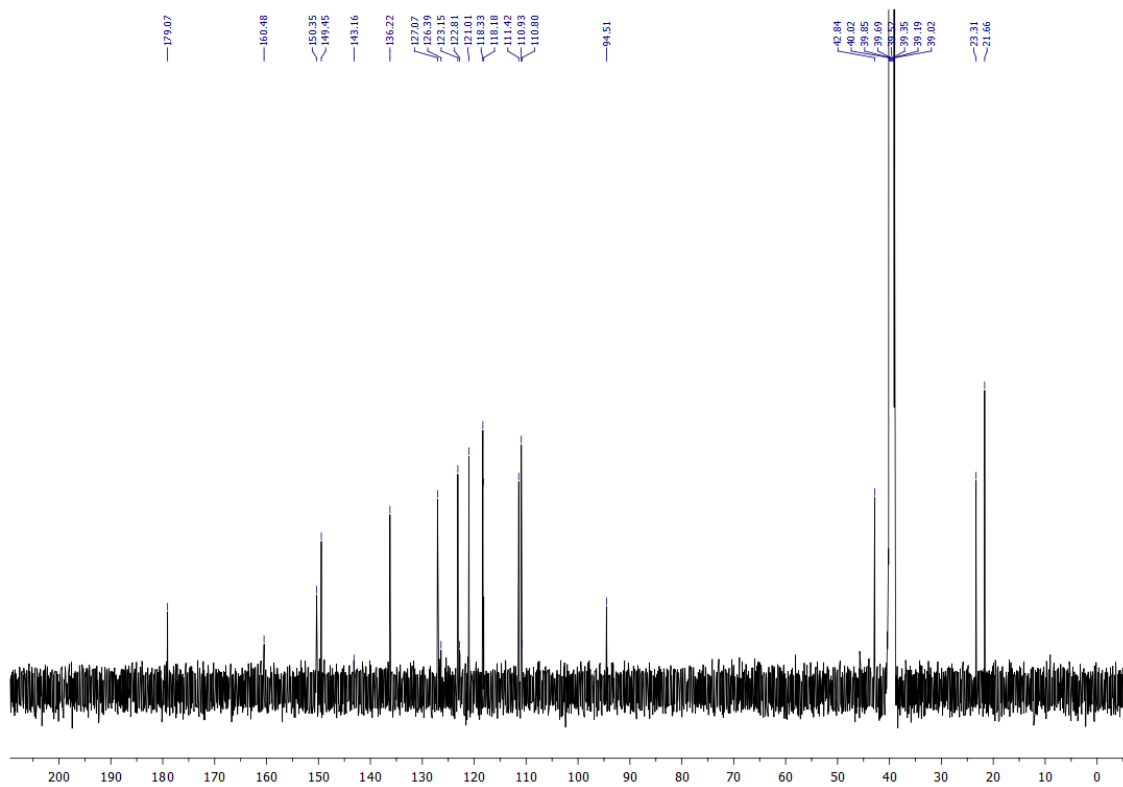


4-Methyl-6-[(2-(1*H*-indol-3-yl)ethyl)amino]quinoline-2,5,8(1*H*)-trione (14a)

¹H NMR (500 MHz, *d*₆-DMSO)



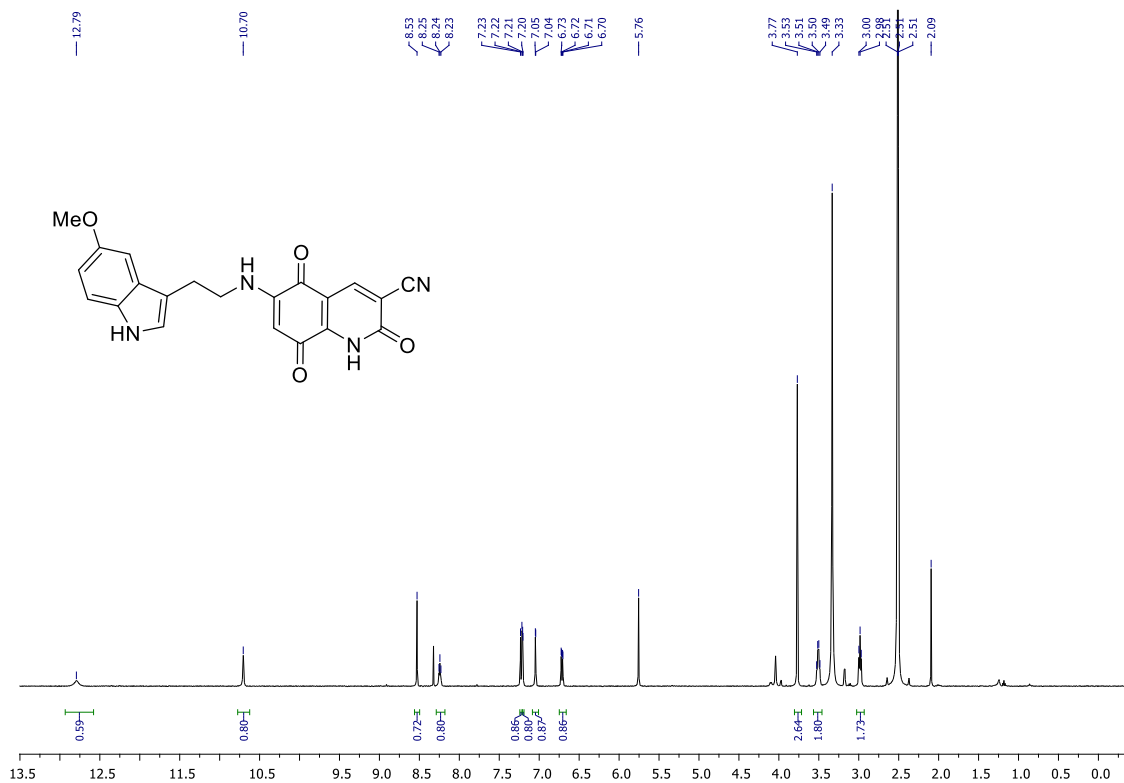
¹³C NMR (126 MHz, *d*₆-DMSO)



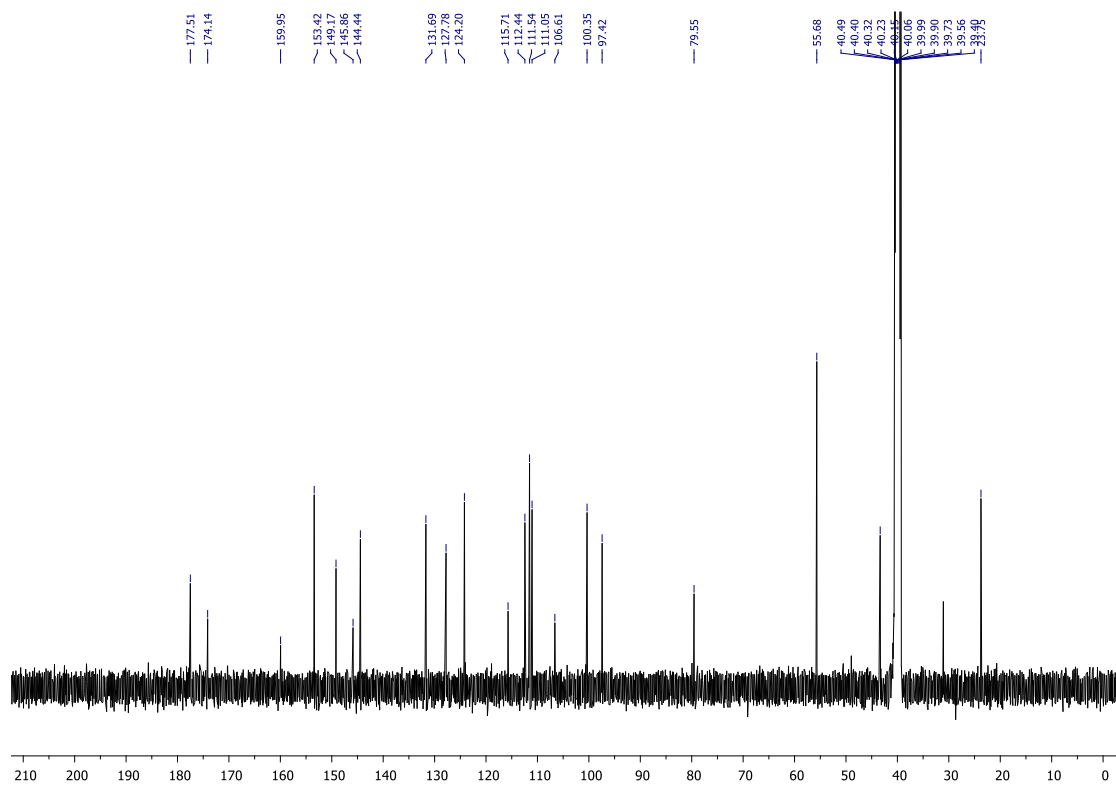
Representative spectra

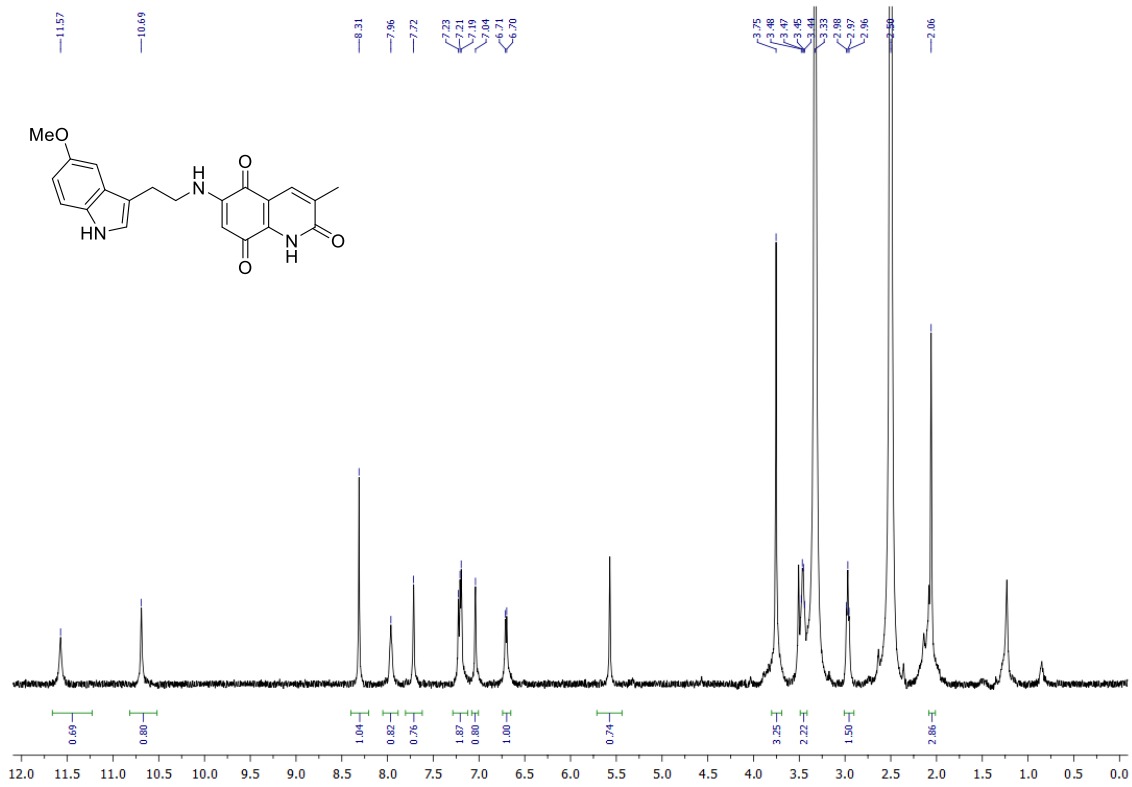
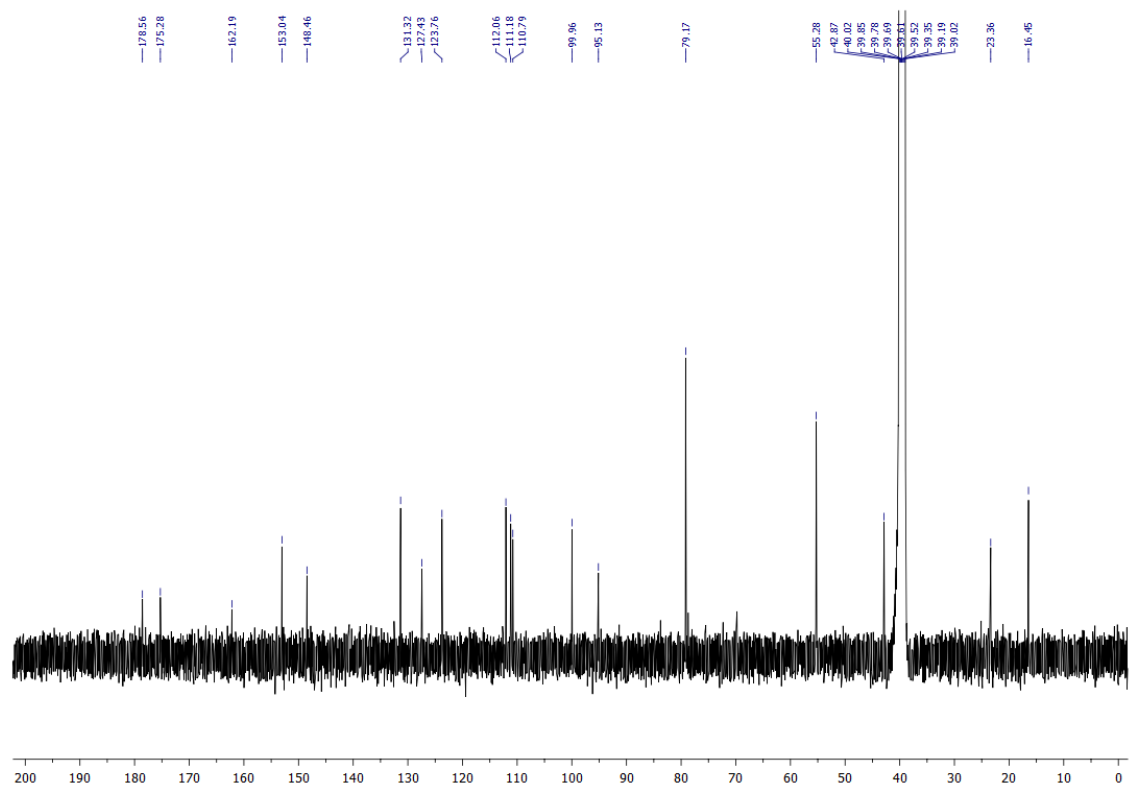
6-[(2-(5-Methoxy-1H-indol-3-yl)ethyl)amino]-2,5,8-trioxo-1,2,5,8-tetrahydroquinoline-3-carbonitrile (14d)

¹H NMR (500 MHz, *d*₆-DMSO)



¹³C NMR (126 MHz, *d*₆-DMSO)

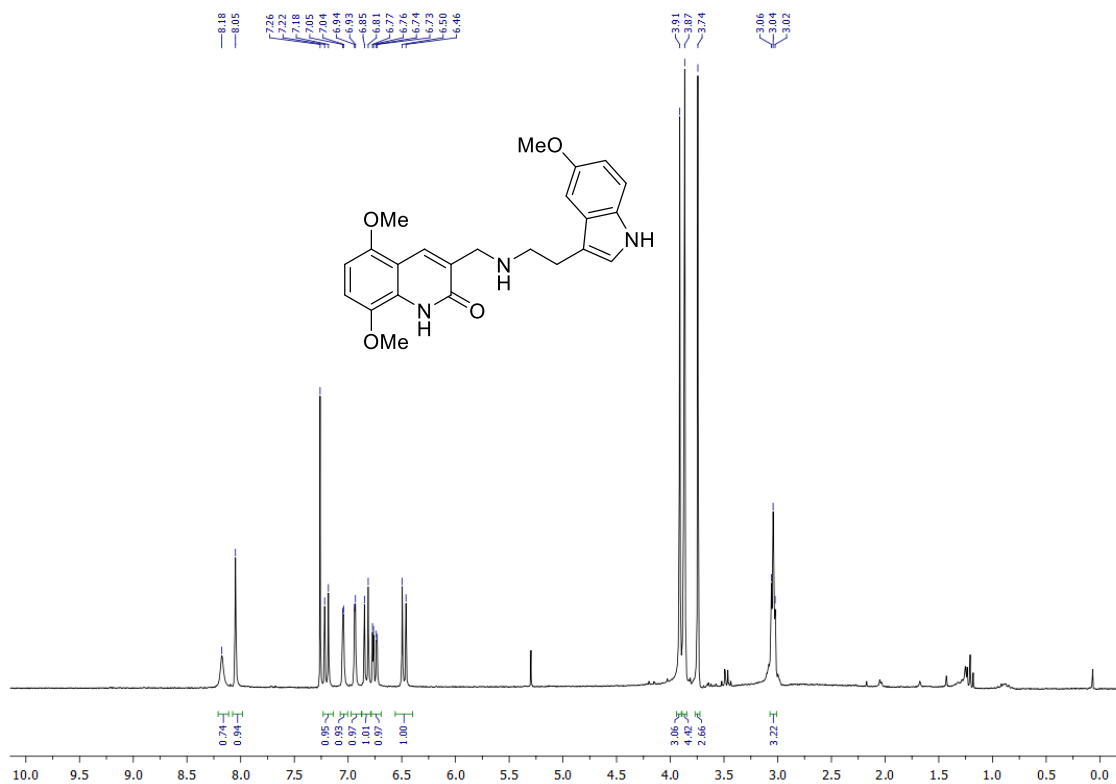


3-Methyl-6-[(2-(5-methoxy-1H-indol-3-yl)ethyl)amino]quinolin-2,5,8(1H)-trione (14e)**¹H RMN (250 MHz, *d*₆-DMSO)****¹³C RMN (63 MHz, *d*₆-DMSO)**

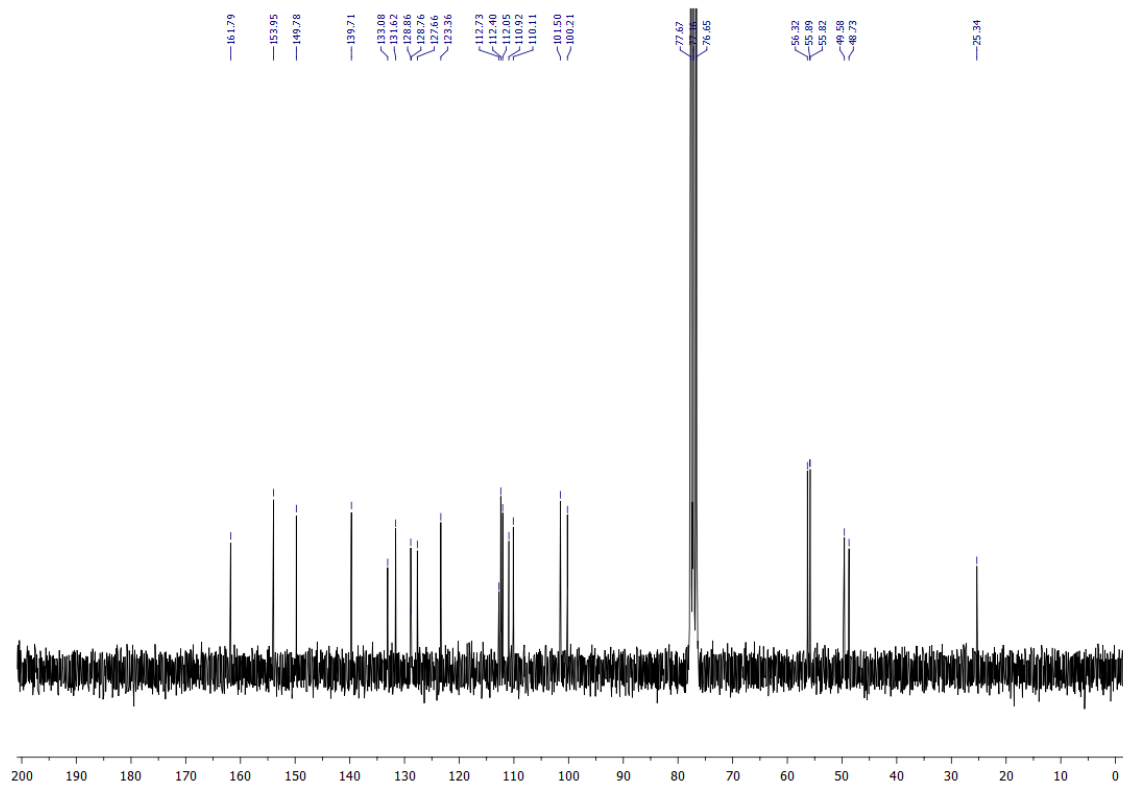
Representative spectra

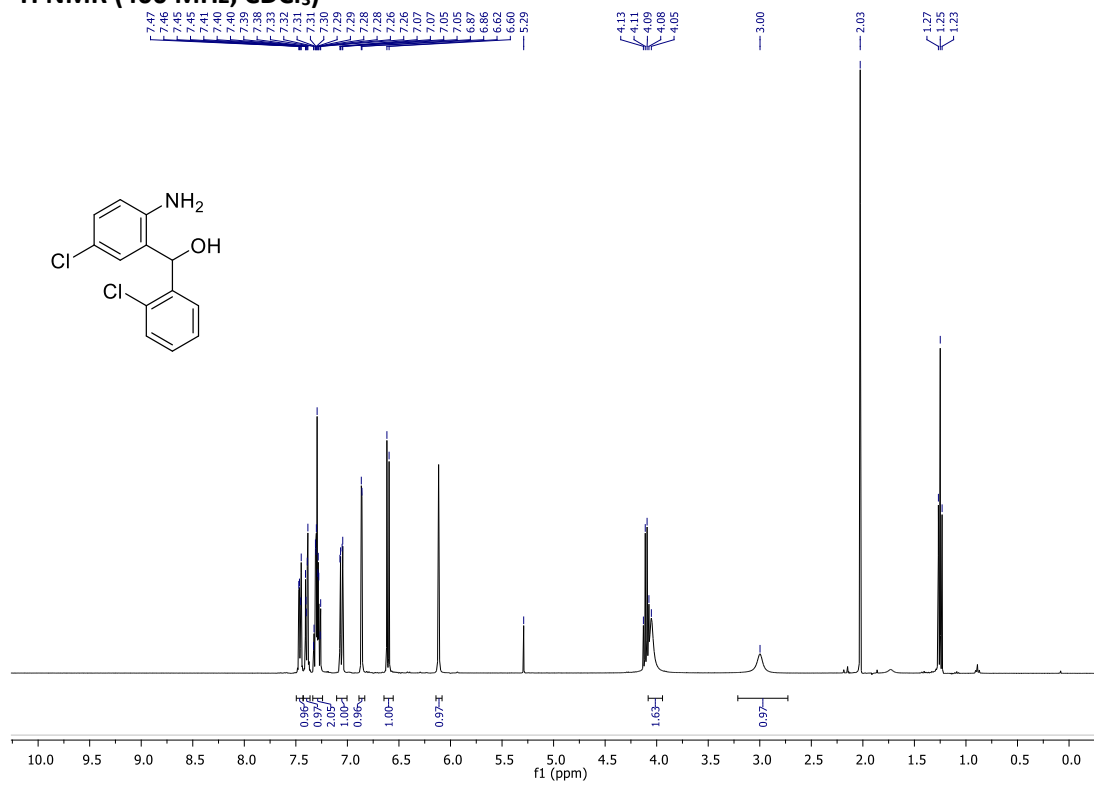
5,8-Dimethoxy-3-(((2-(5-methoxy-1H-indol-3-yl)ethyl)amino)-methyl)quinolin-2(1H)-one (15)

¹H NMR (250 MHz, CDCl₃)



¹³C NMR (63 MHz, CDCl₃)

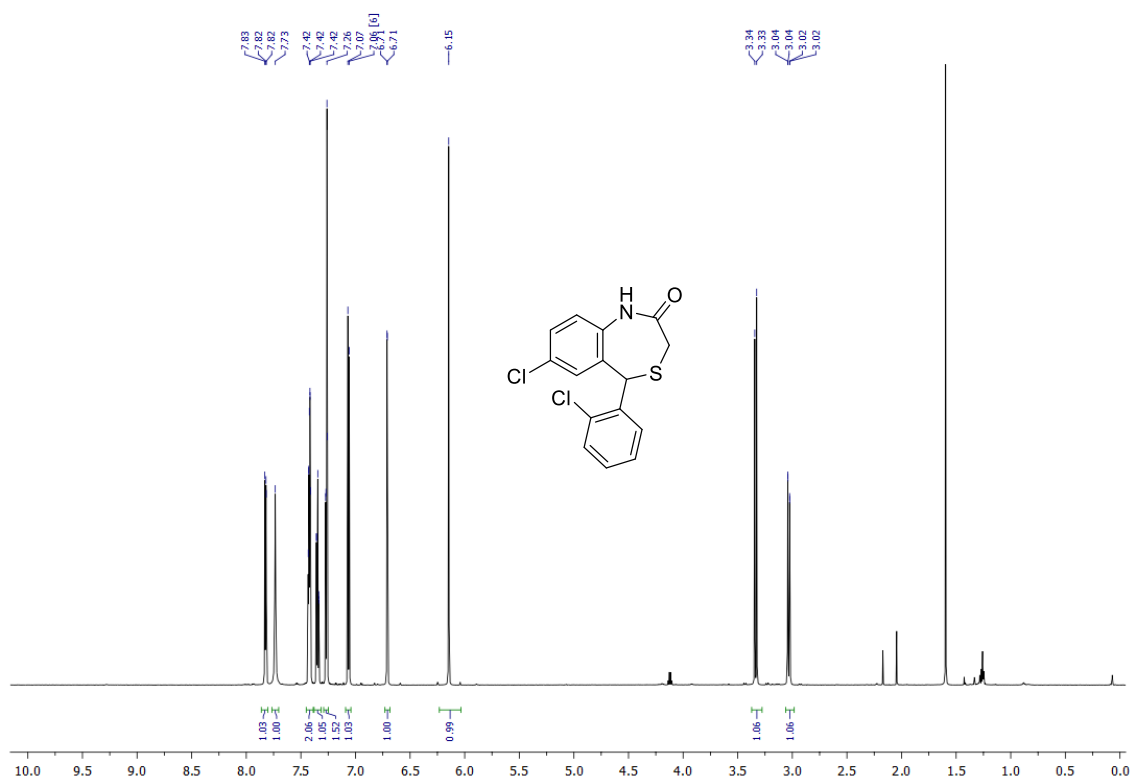


(2-Amino-5-chlorophenyl)(2-chlorophenyl)carbinol (14)**¹H NMR (400 MHz, CDCl₃)**

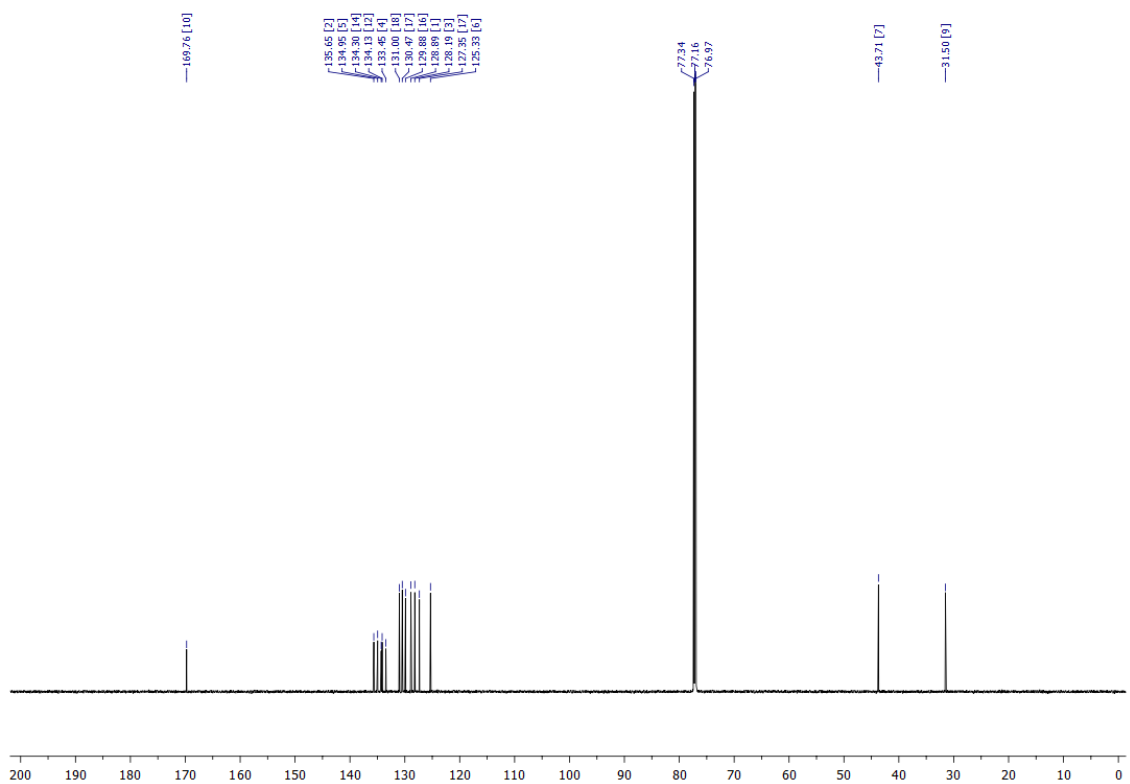
Representative spectra

7-Chloro-5-(2-chlorophenyl)-1,5-dihydrobenzo[e][1,4]thiazepin-2(3H)-one (15)

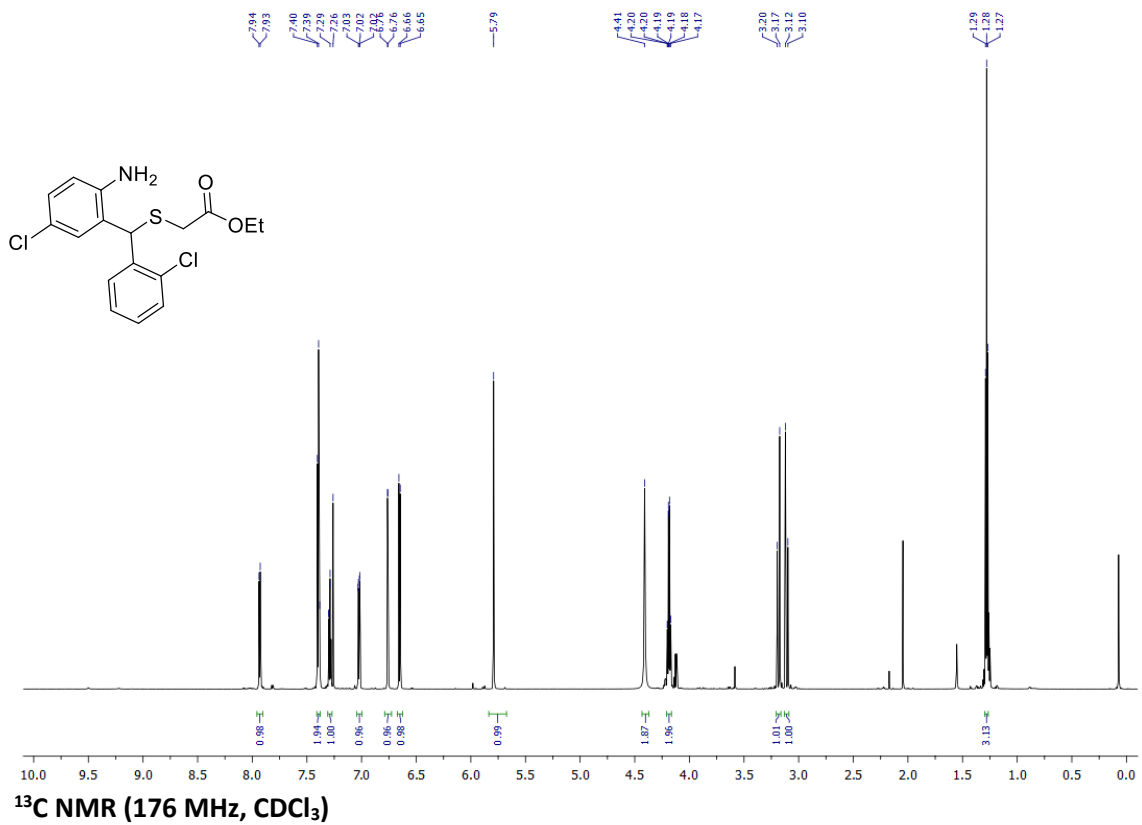
^1H NMR (700 MHz, CDCl_3)



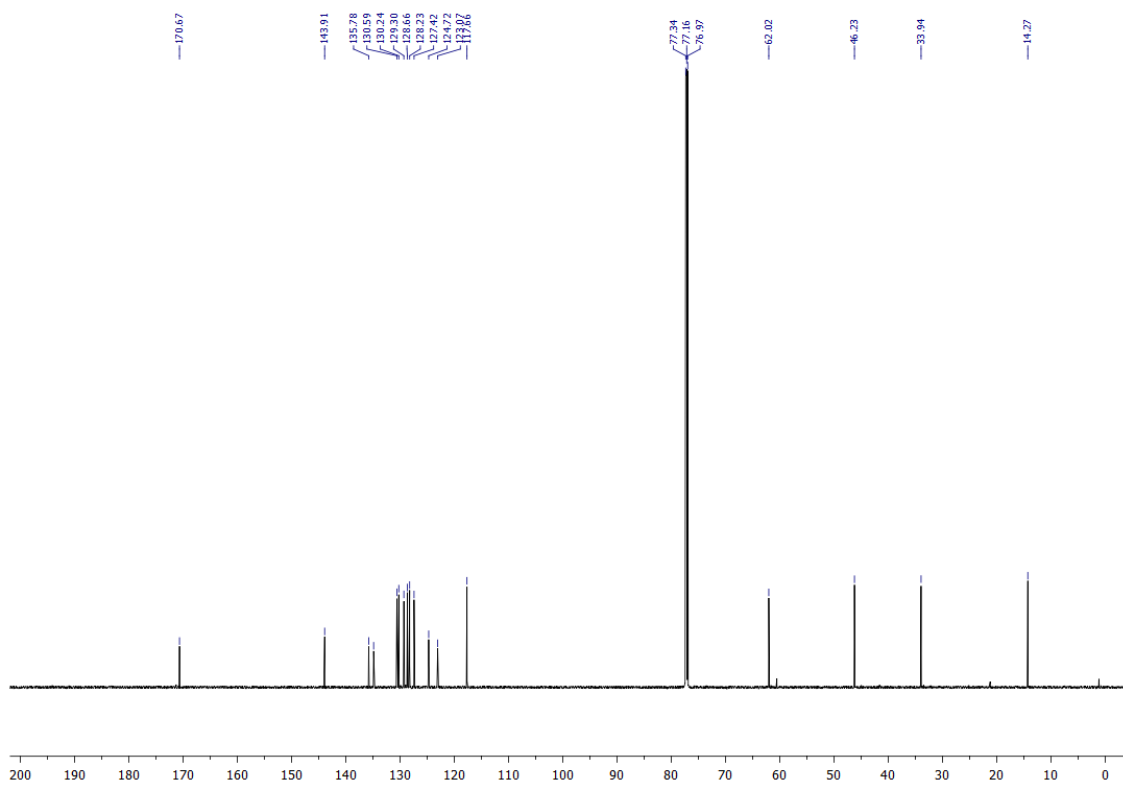
^{13}C NMR (176 MHz, CDCl_3)



Ethyl 2-(((2-amino-5-chlorophenyl)(2-chlorophenyl)methyl)thio)acetate
¹H NMR (700 MHz, CDCl₃)

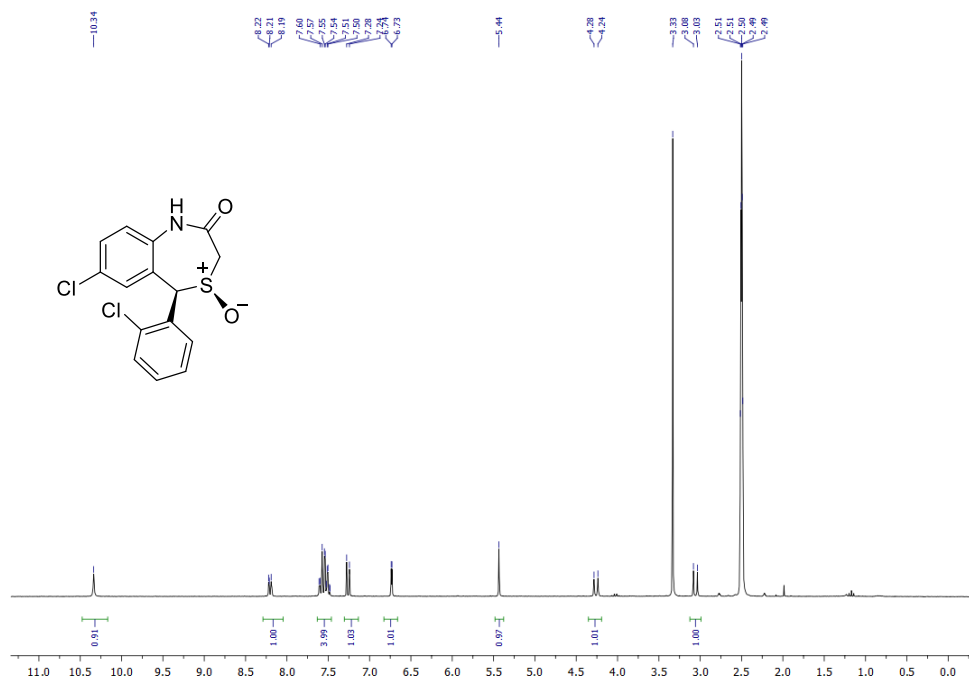


¹³C NMR (176 MHz, CDCl₃)

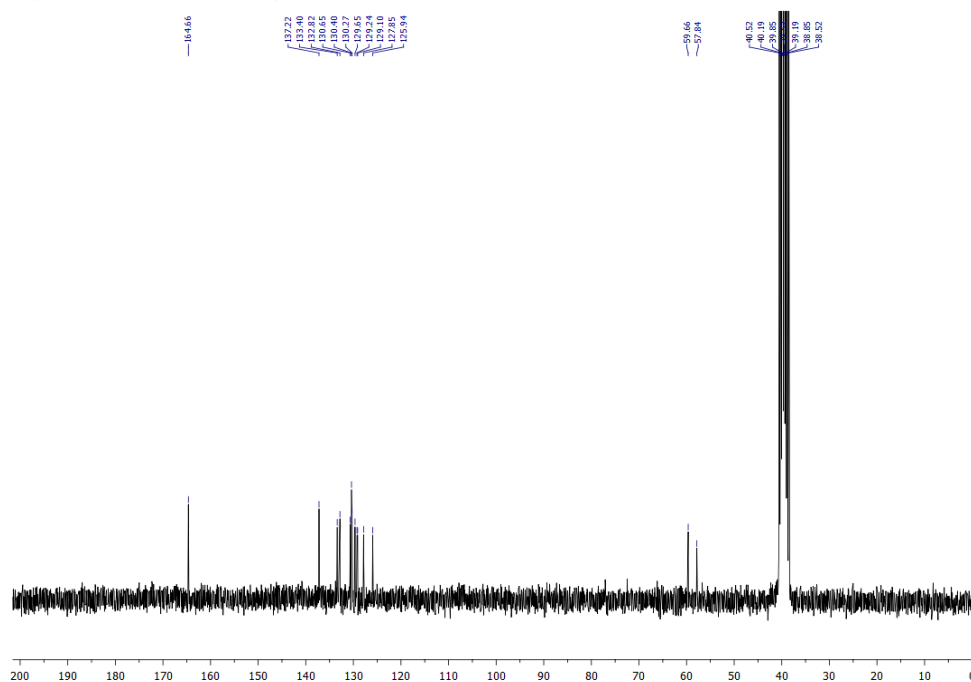


Representative spectra

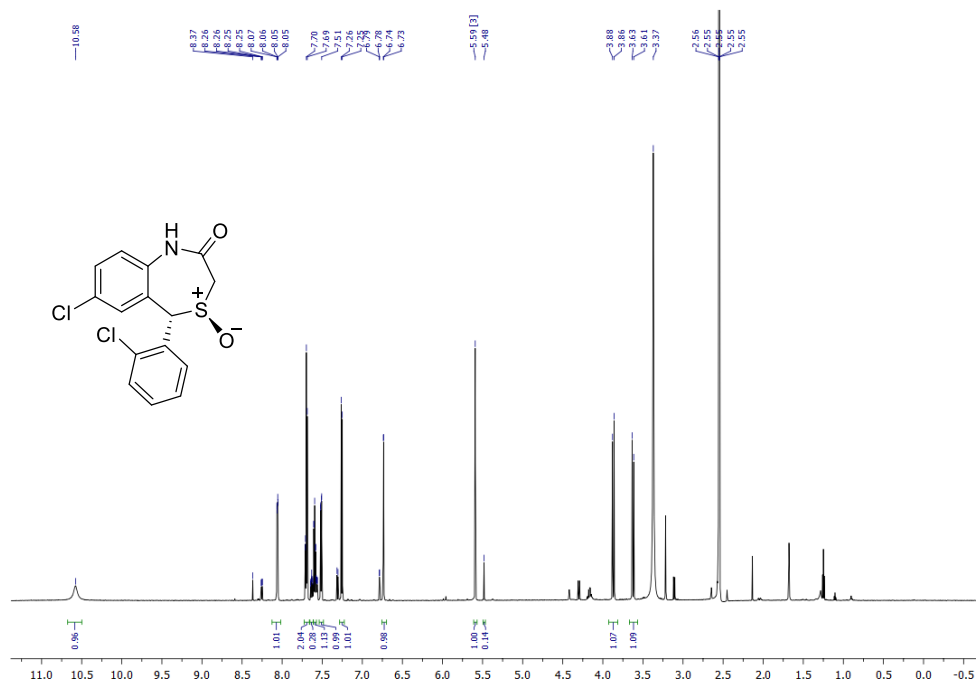
***cis*-7-Chloro-5-(2-chlorophenyl)-1,5-dihydrobenzo[e][1,4]thiazepin-2(3*H*)-one 4-oxide (16)**
¹H NMR (250 MHz, *d*₆-DMSO)



¹H NMR (250 MHz, *d*₆-DMSO)



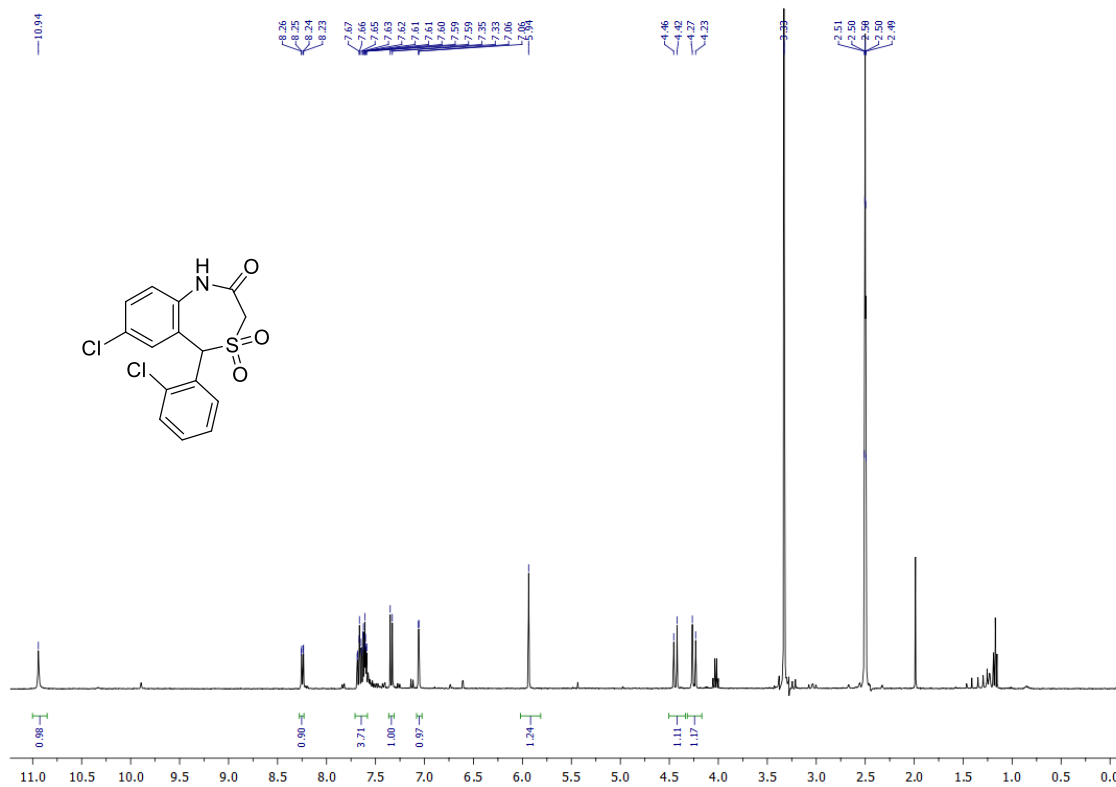
***trans*-7-Chloro-5-(2-chlorophenyl)-1,5-dihydrobenzo[e][1,4]thiazepin-2(3*H*)-one 4-oxide (17)**
¹H NMR (700 MHz, *d*₆-DMSO)



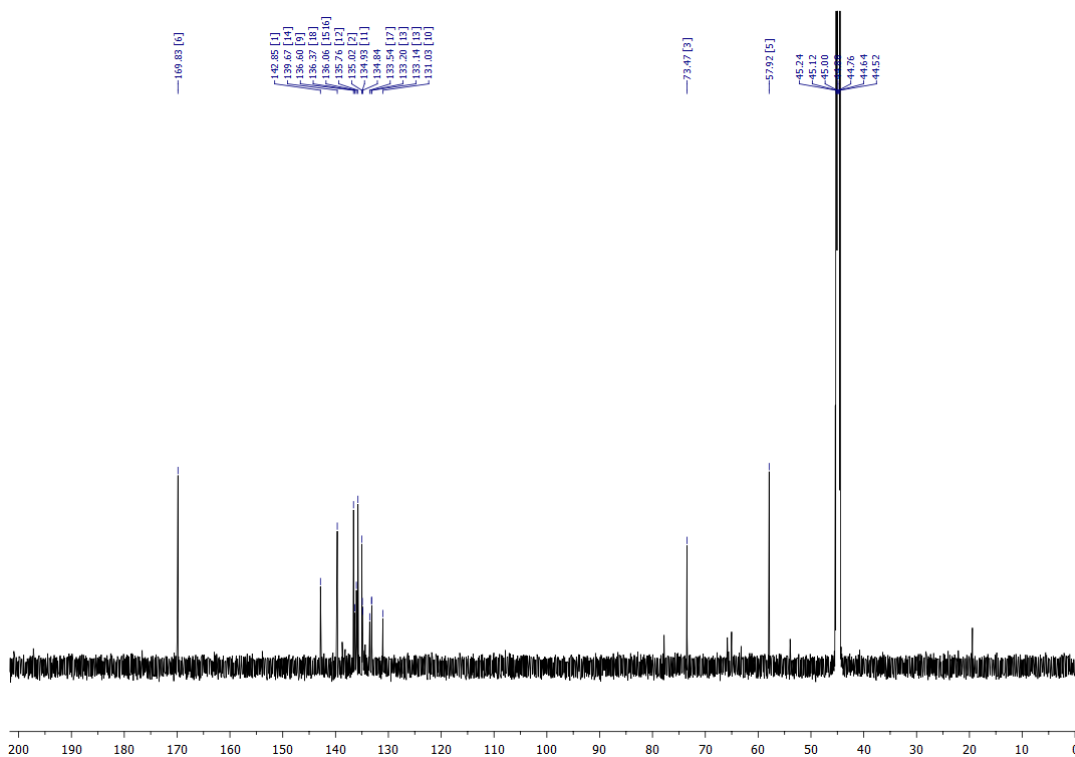
Representative spectra

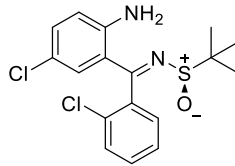
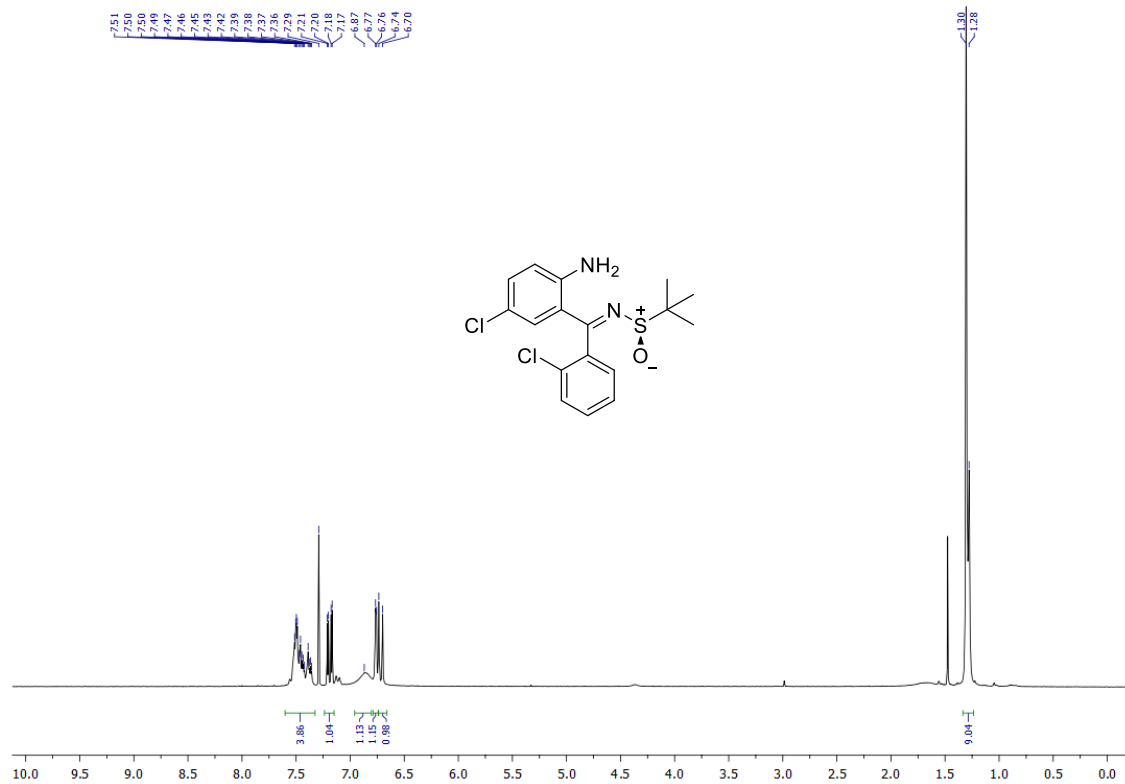
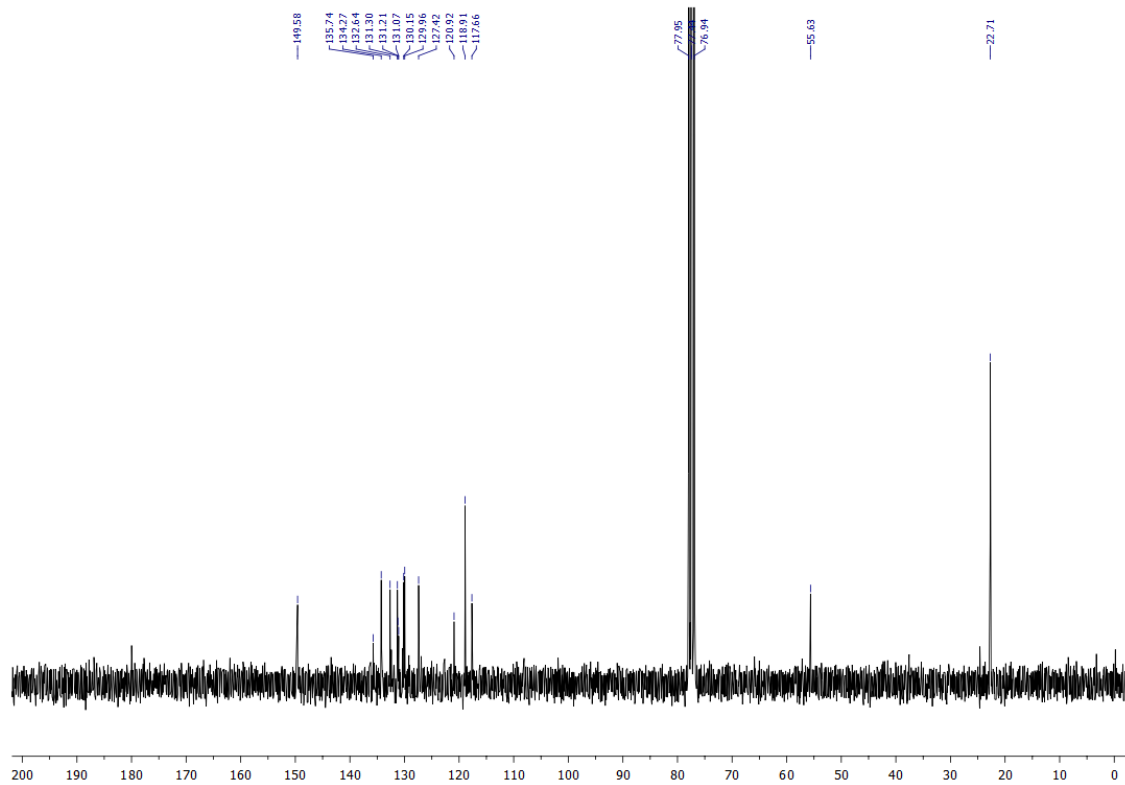
7-Chloro-5-(2-chlorophenyl)-1,5-dihydrobenzo[e][1,4]thiazepin-2(3H)-one 4,4-dioxide (18).

¹H NMR (400 MHz, *d*₆-DMSO)



¹³C NMR (100 MHz, *d*₆-DMSO)

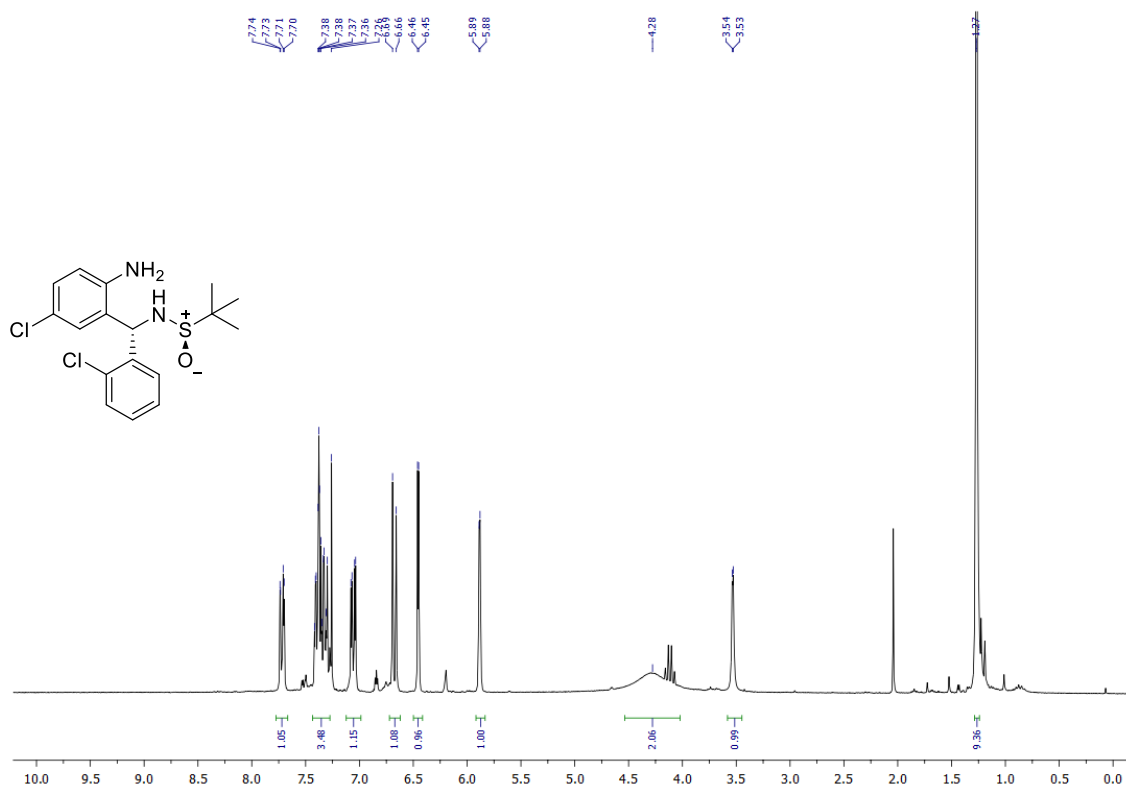


(*R,Z*)-N-((2-Amino-5-chlorophenyl)(2-chlorophenyl)methylene)-2-methylpropane-2-sulfonamide (*R-23*)**¹H NMR (250 MHz, CDCl₃)****¹³C NMR (63 MHz, CDCl₃)**

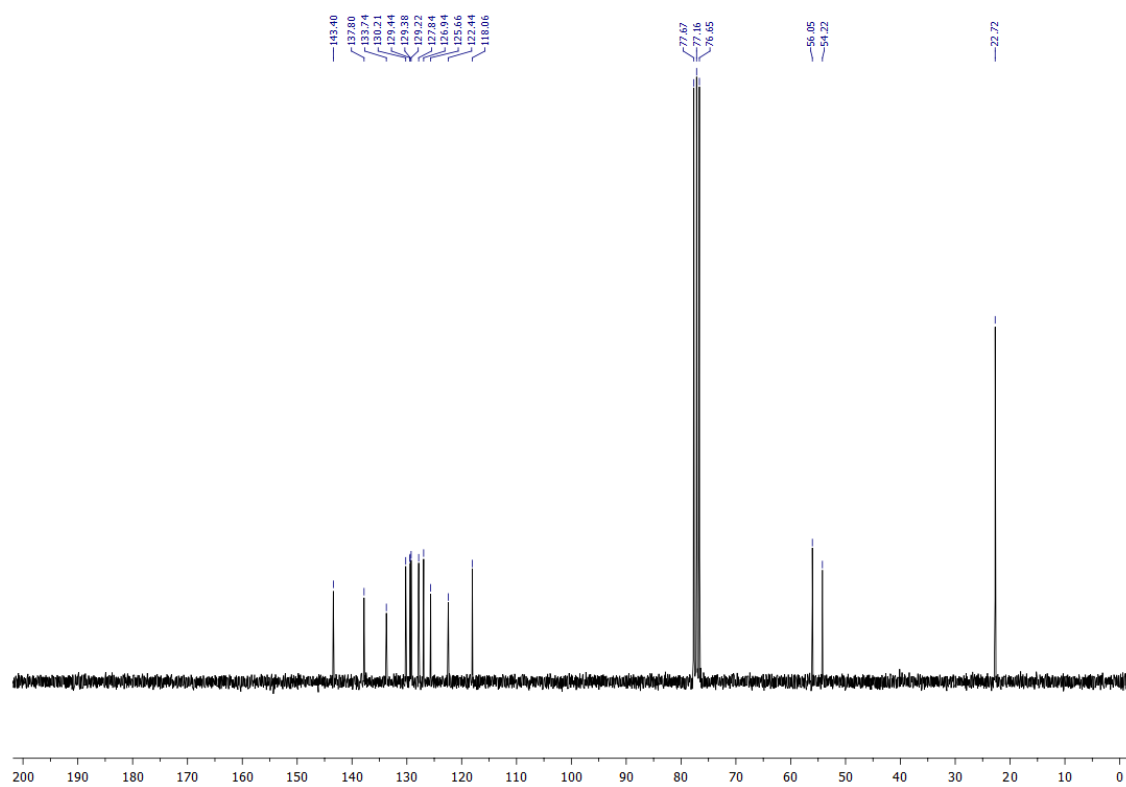
Representative spectra

**(R)-N-[(S)-(2-Amino-5-chlorophenyl)(2-chlorophenyl)methyl]-2-methylpropane-2-sulfonamide
(R,S-24)**

¹H NMR (250 MHz, CDCl₃)

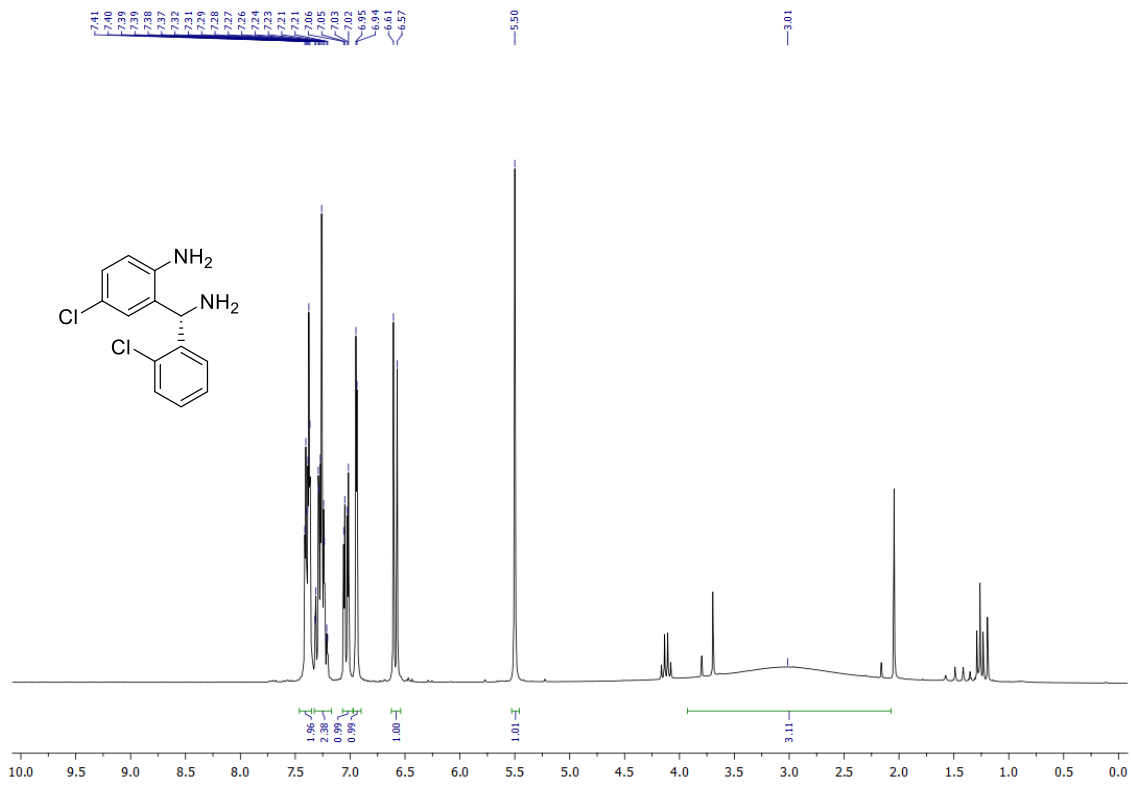


¹³C NMR (63 MHz, CDCl₃)

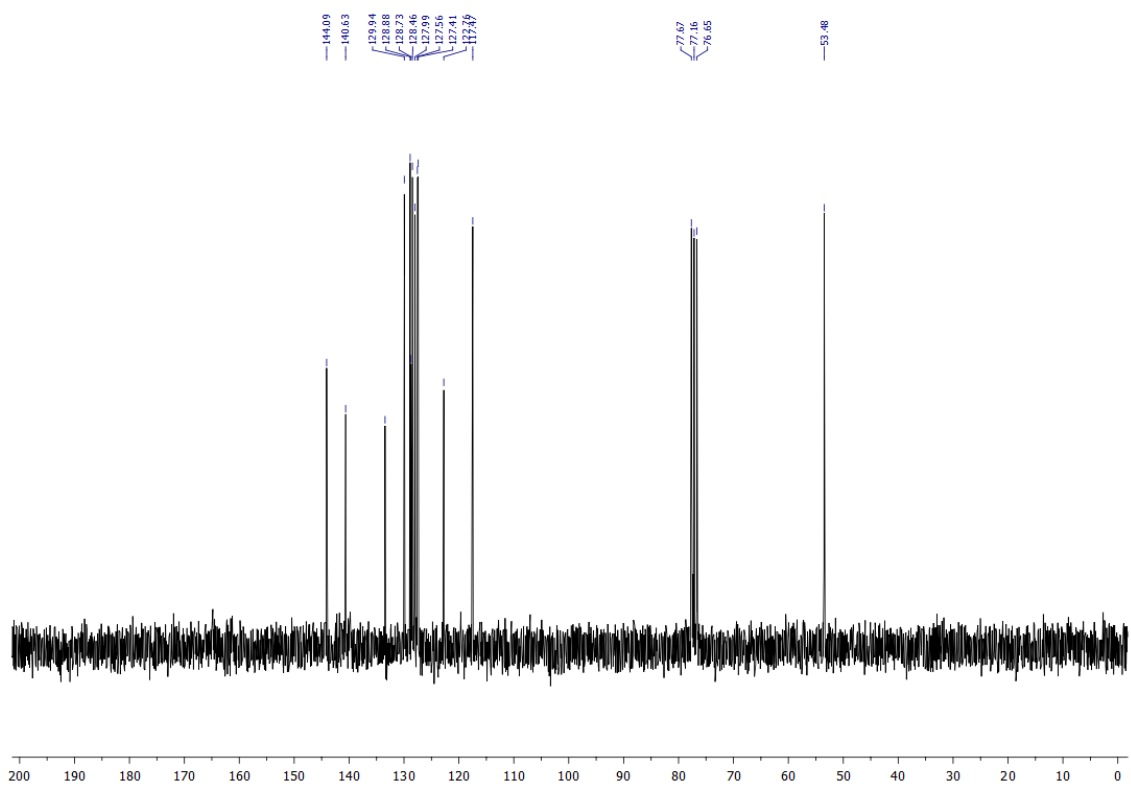


(S)-2-[Amino(2-chlorophenyl)methyl]-4-chloroaniline (S-24)

¹H NMR (250 MHz, CDCl₃)

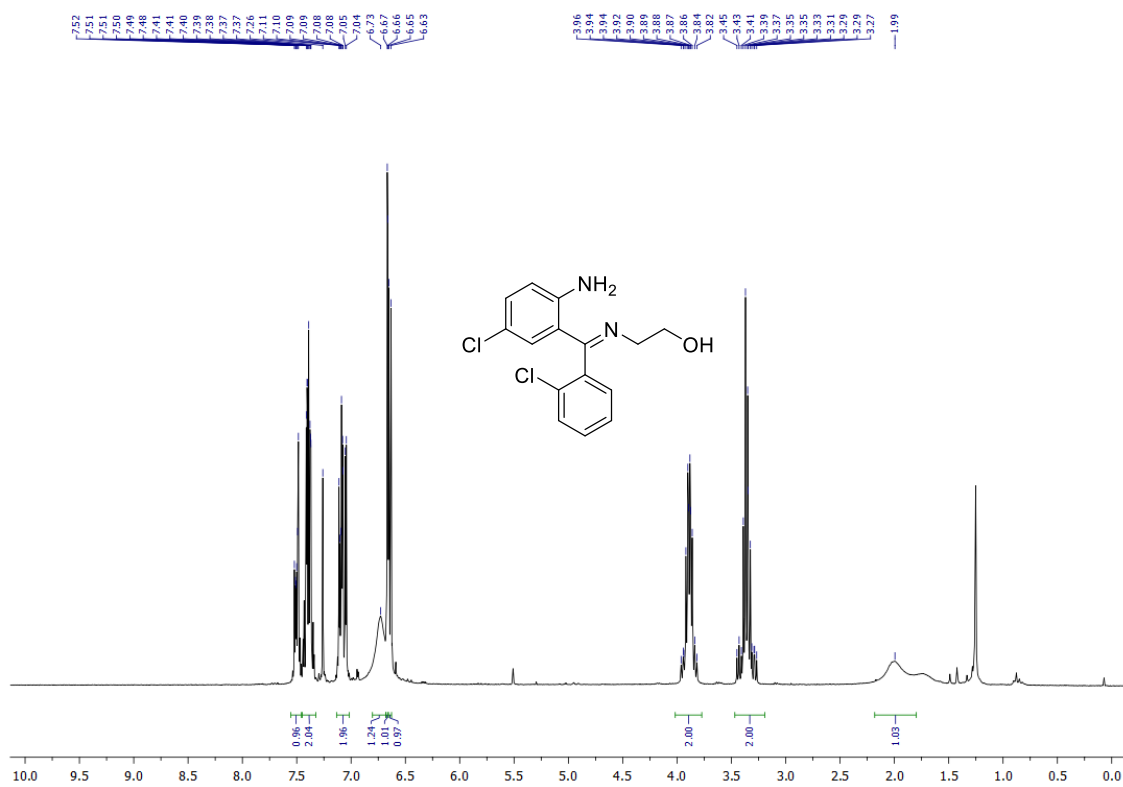


¹³C NMR (63 MHz, CDCl₃)

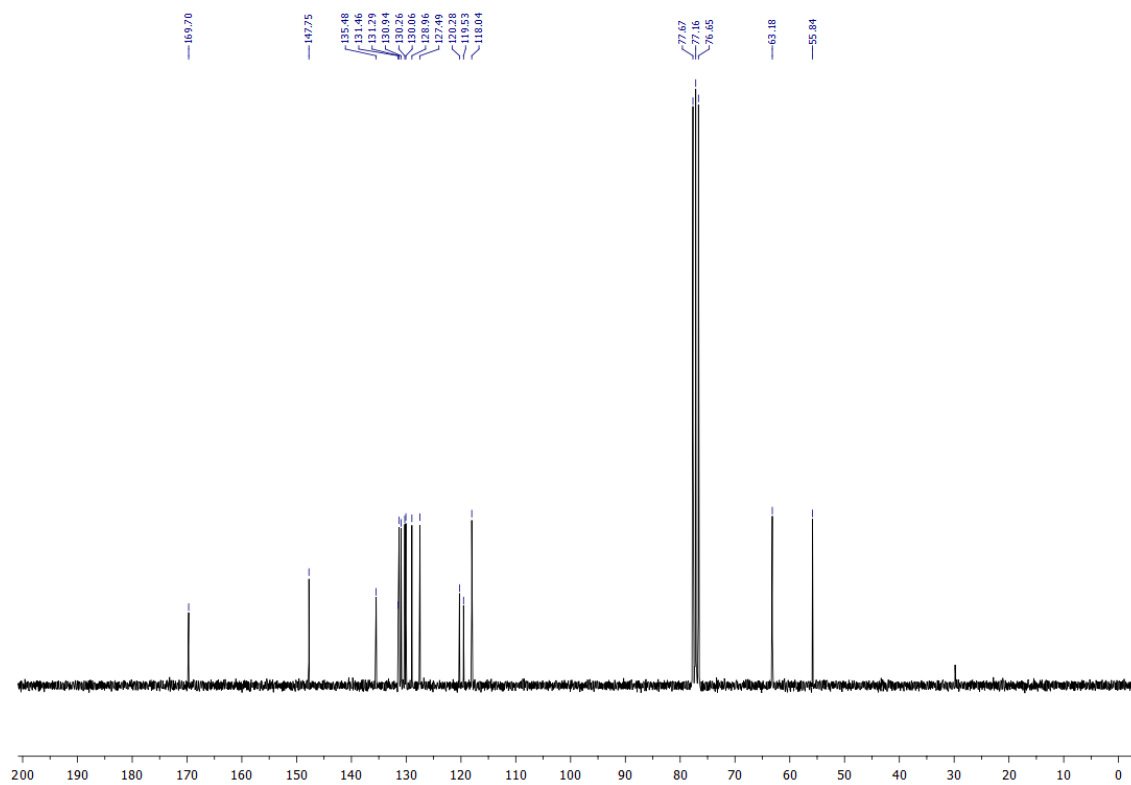


Representative spectra

2-[[2-(2-Amino-5-chlorophenyl)(2-chlorophenyl)methylene]amino]ethanol 21
¹H NMR (250 MHz, CDCl₃)

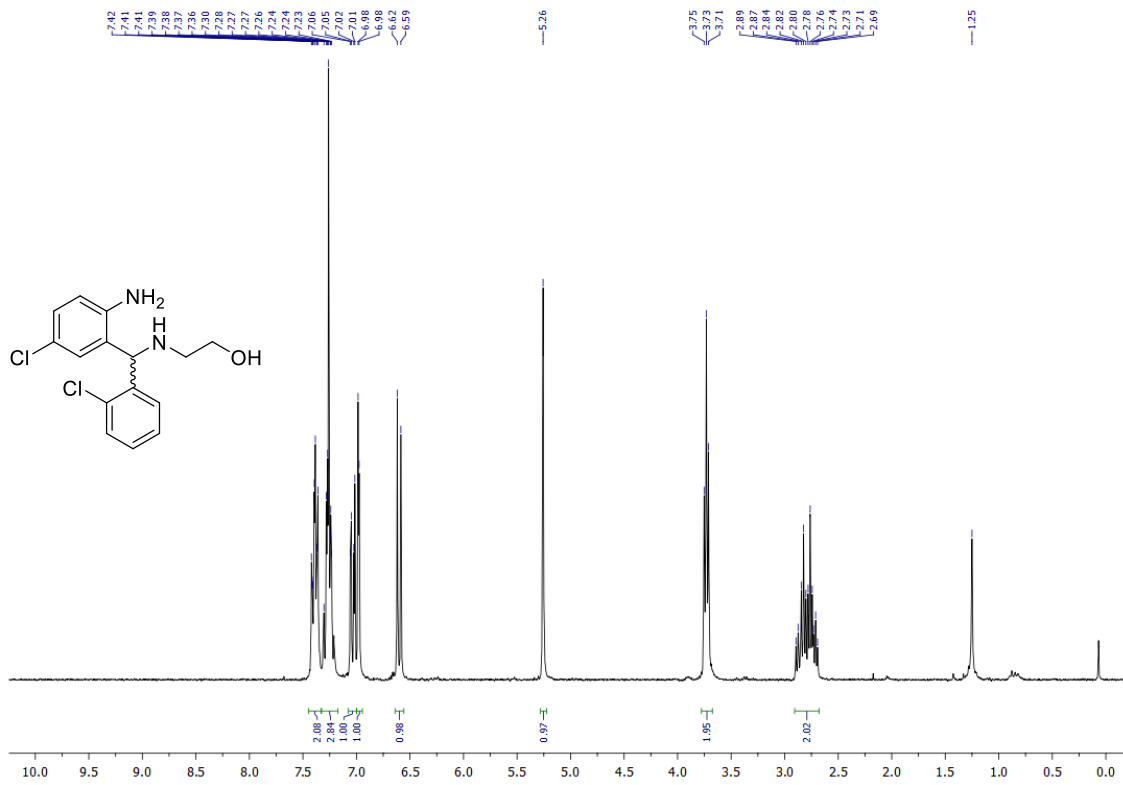


¹³C NMR (63 MHz, CDCl₃)

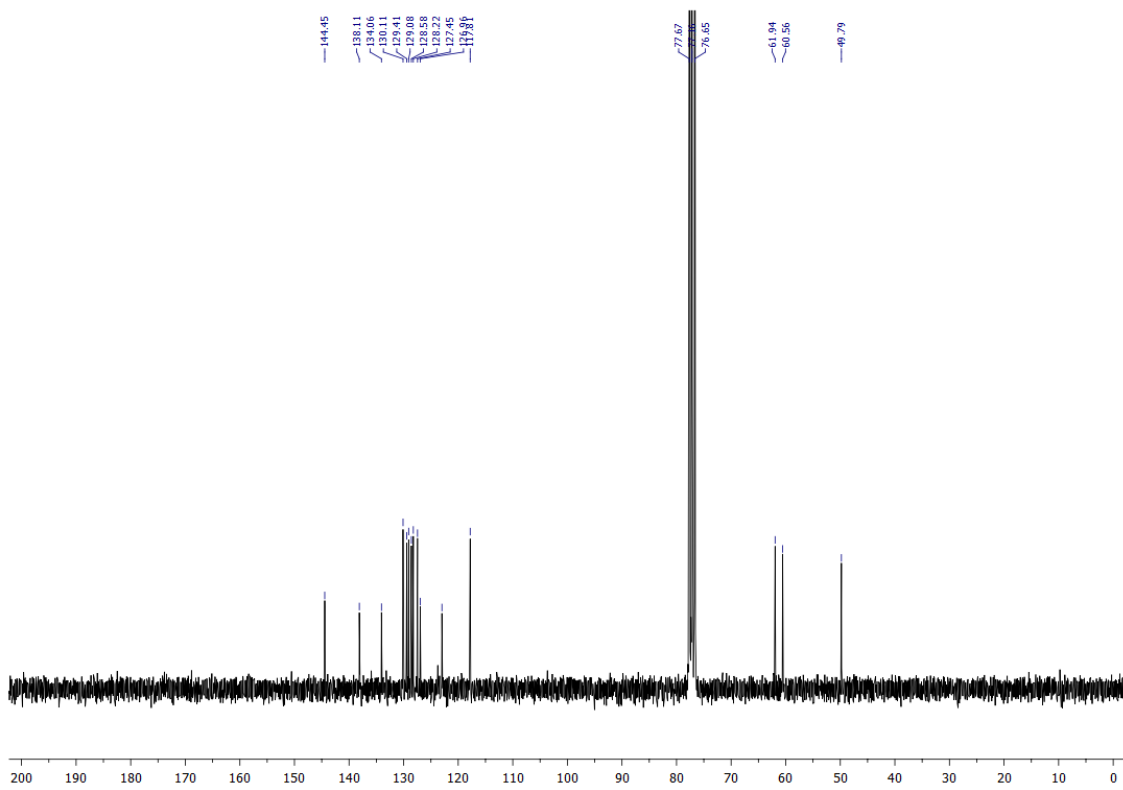


(±)-2-(((2-Amino-5-chlorophenyl)(2-chlorophenyl)methyl)amino)ethanol 28

¹H NMR (250 MHz, CDCl₃)



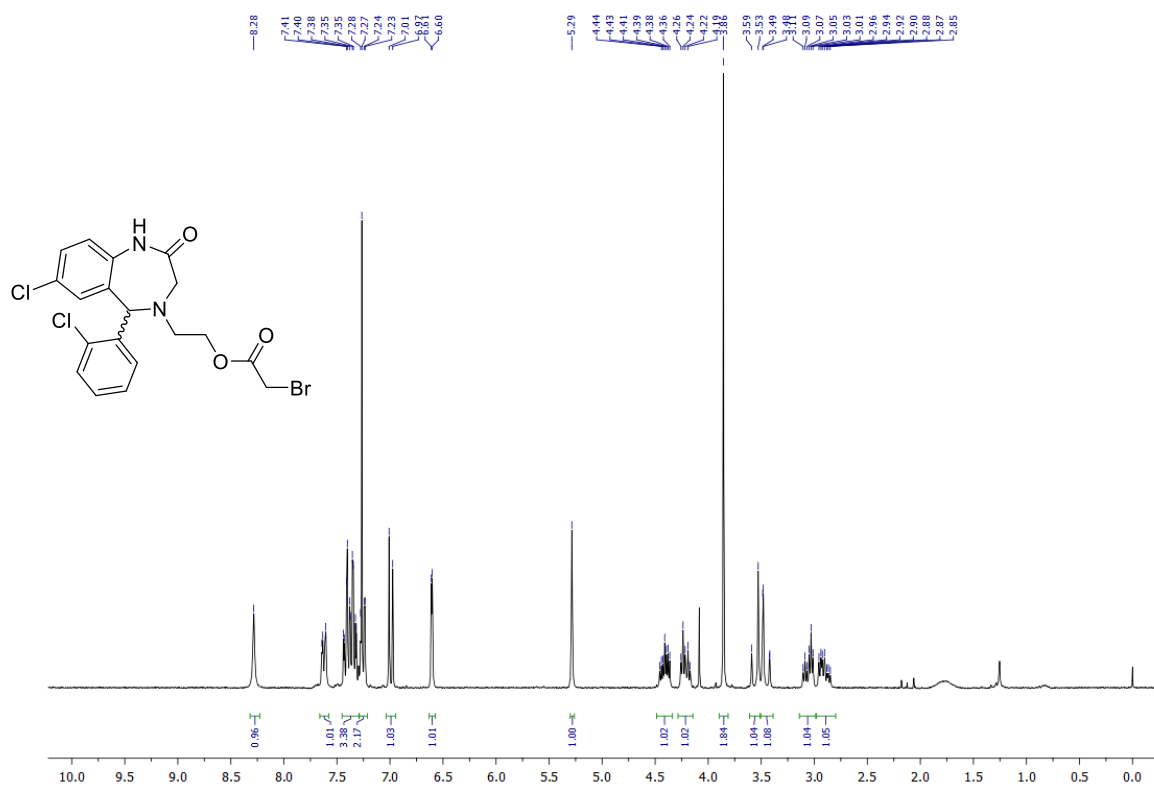
¹³C NMR (63 MHz, CDCl₃)



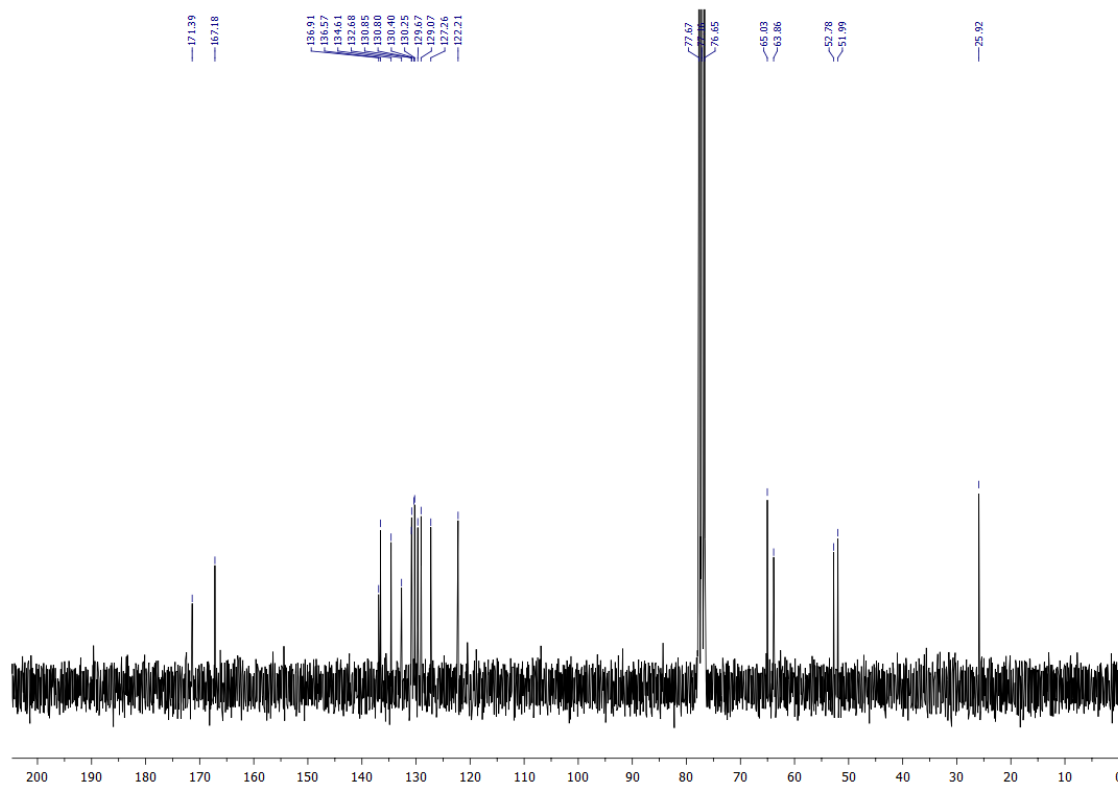
Representative spectra

***rac*-2-(7-Chloro-5-(2-chlorophenyl)-2-oxo-2,3,4,5-tetrahydro-1H-benzo[e][1,4]diazepin-4-yl)ethyl 2-bromoacetate (27)**

¹H NMR (250 MHz, CDCl₃)

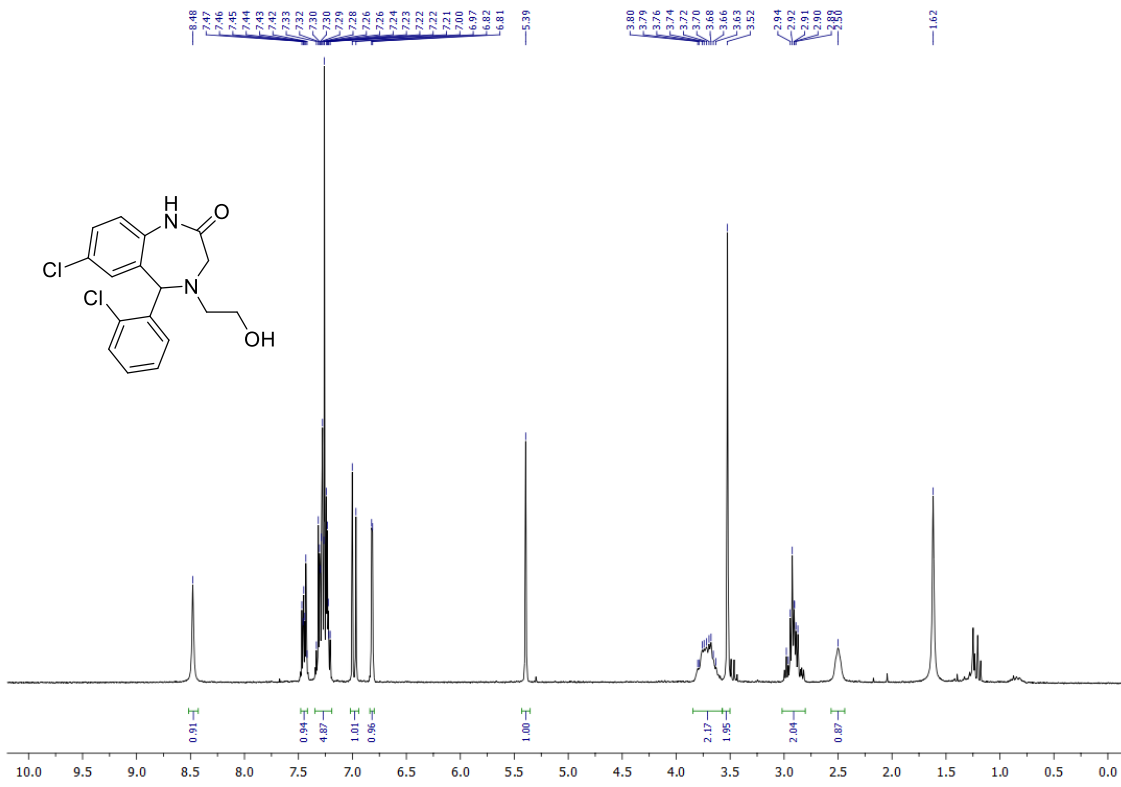


¹³C NMR (63 MHz, CDCl₃)

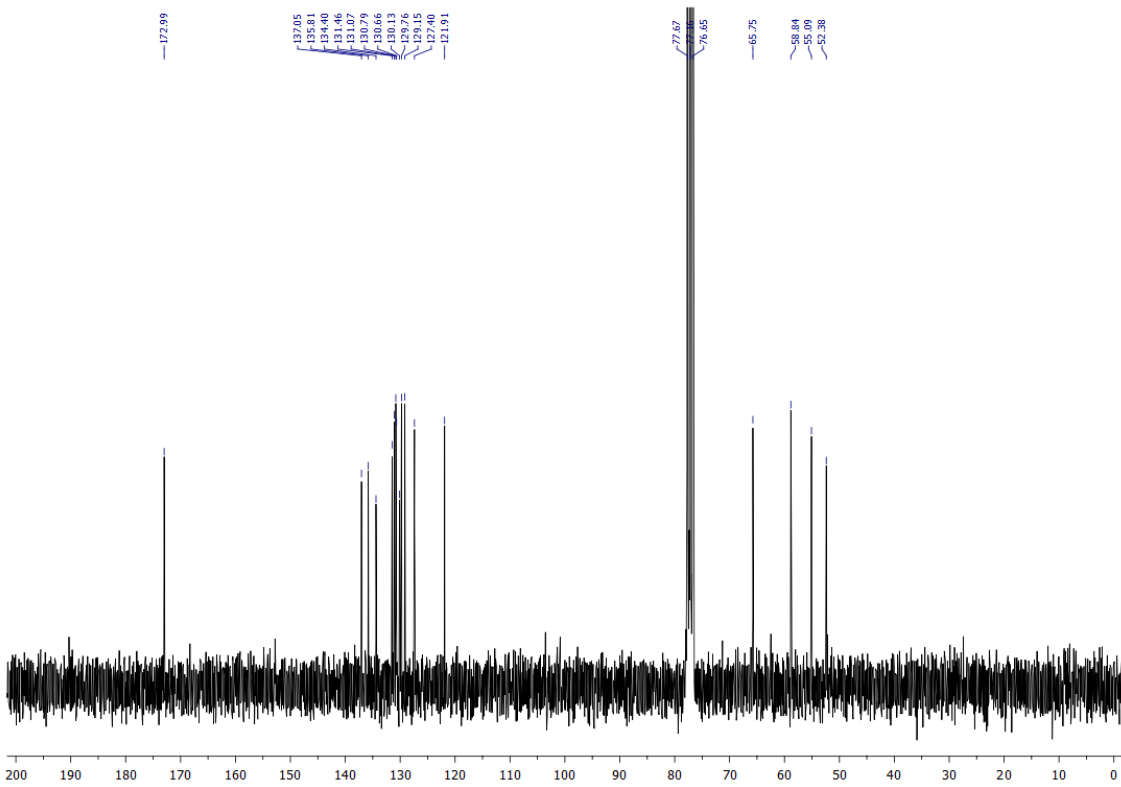


7-Chloro-5-(2-chlorophenyl)-4-(2-hydroxyethyl)-4,5-dihydro-1H-benzo[e][1,4]diazepin-2(3H)-one

¹H NMR (250 MHz, CDCl₃)



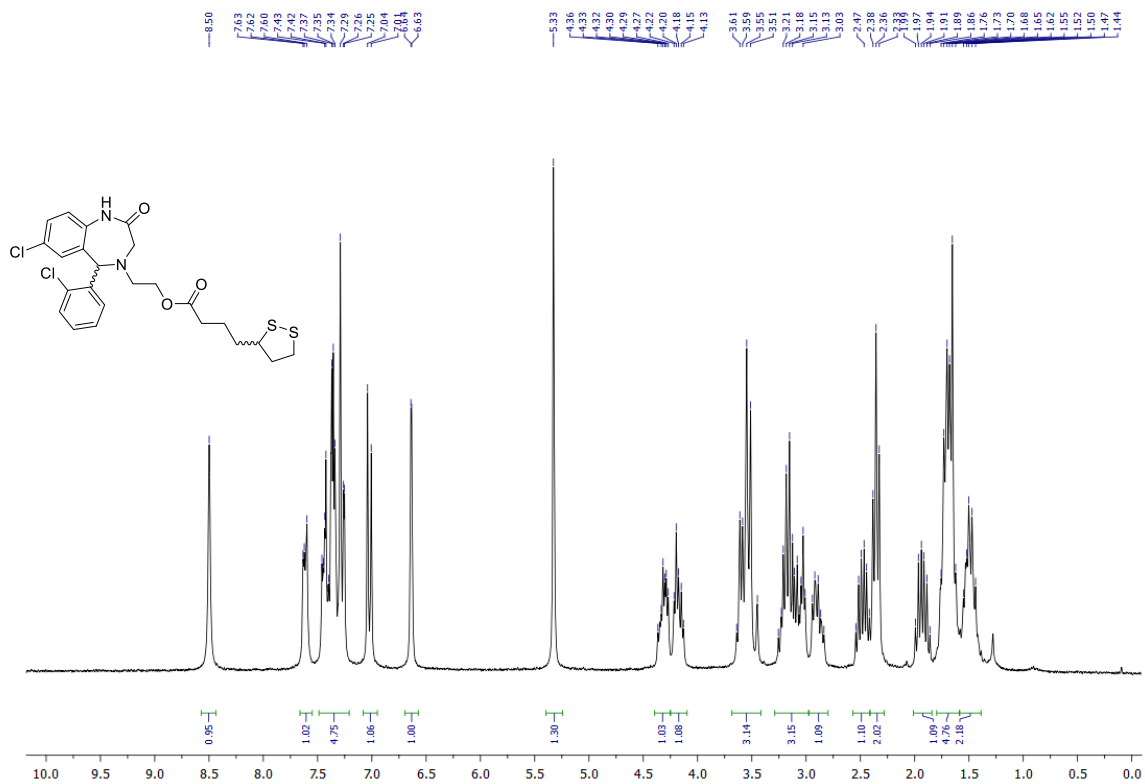
¹³C NMR (63 MHz, CDCl₃)



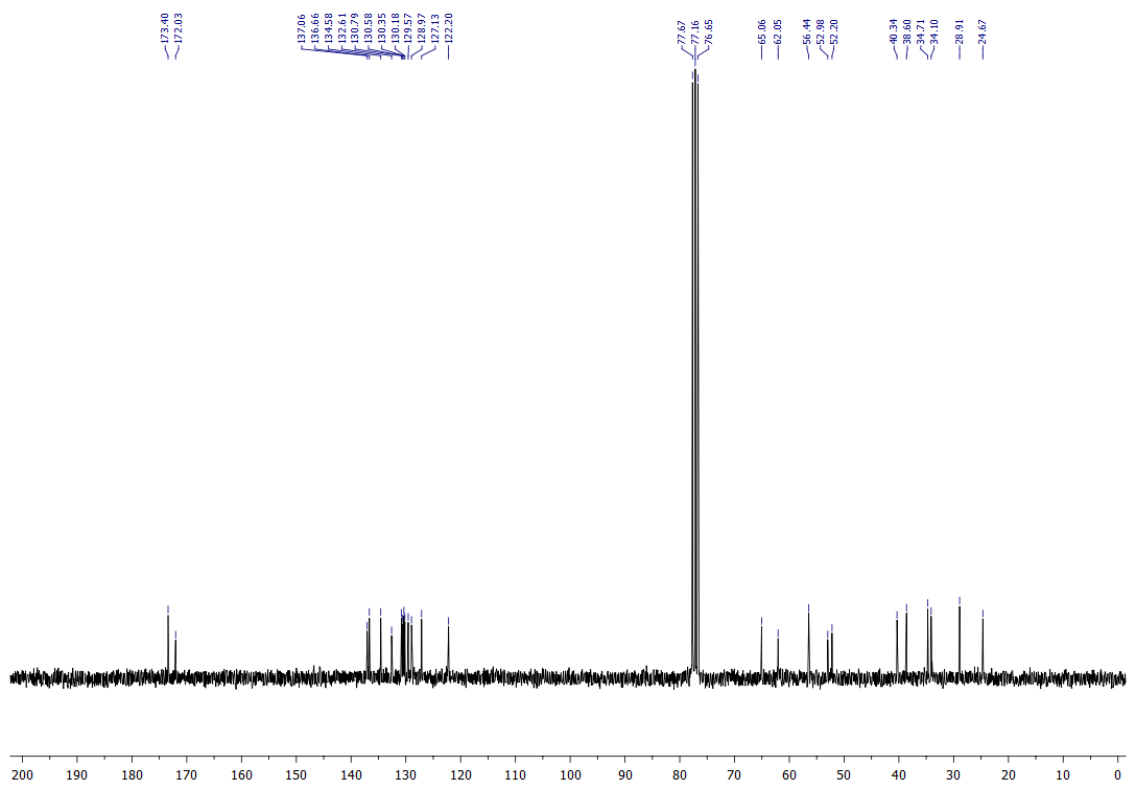
Representative spectra

2-(7-Chloro-5-(2-chlorophenyl)-2-oxo-2,3,4,5-tetrahydro-1H-benzo[e][1,4]diazepin-4-yl)ethyl 5-(1,2-dithiolan-3-yl)pentanoate (20)

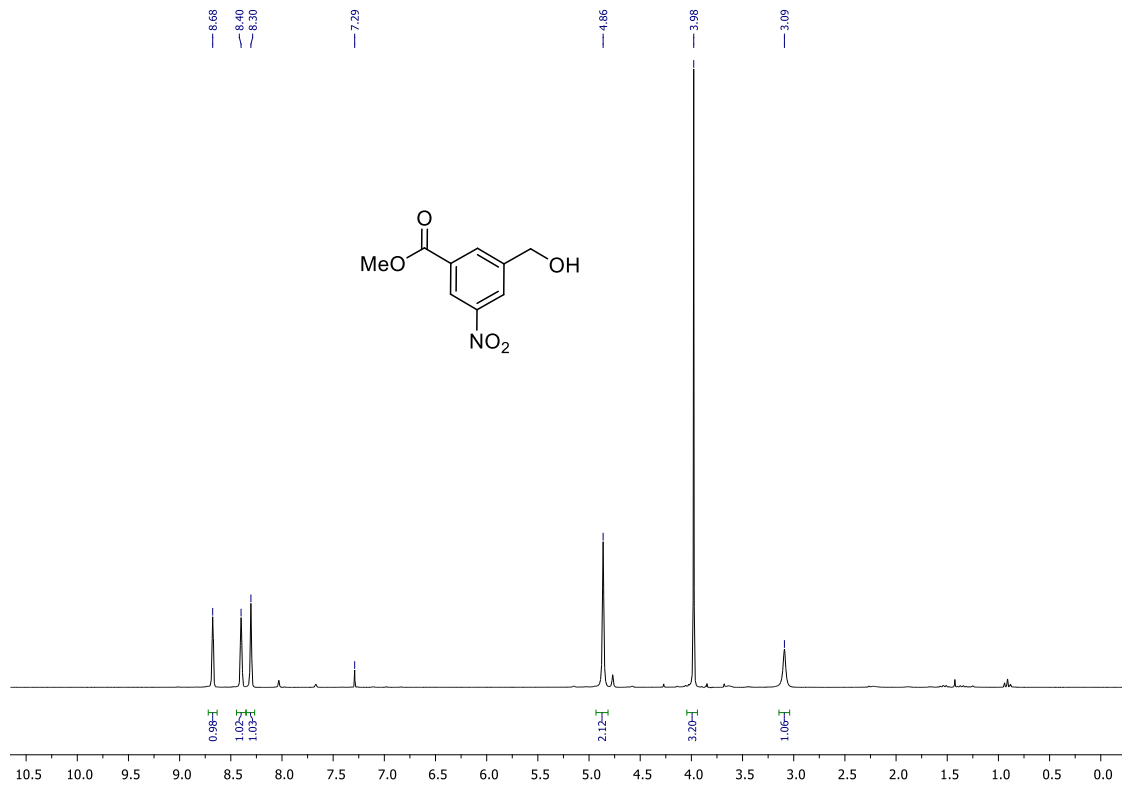
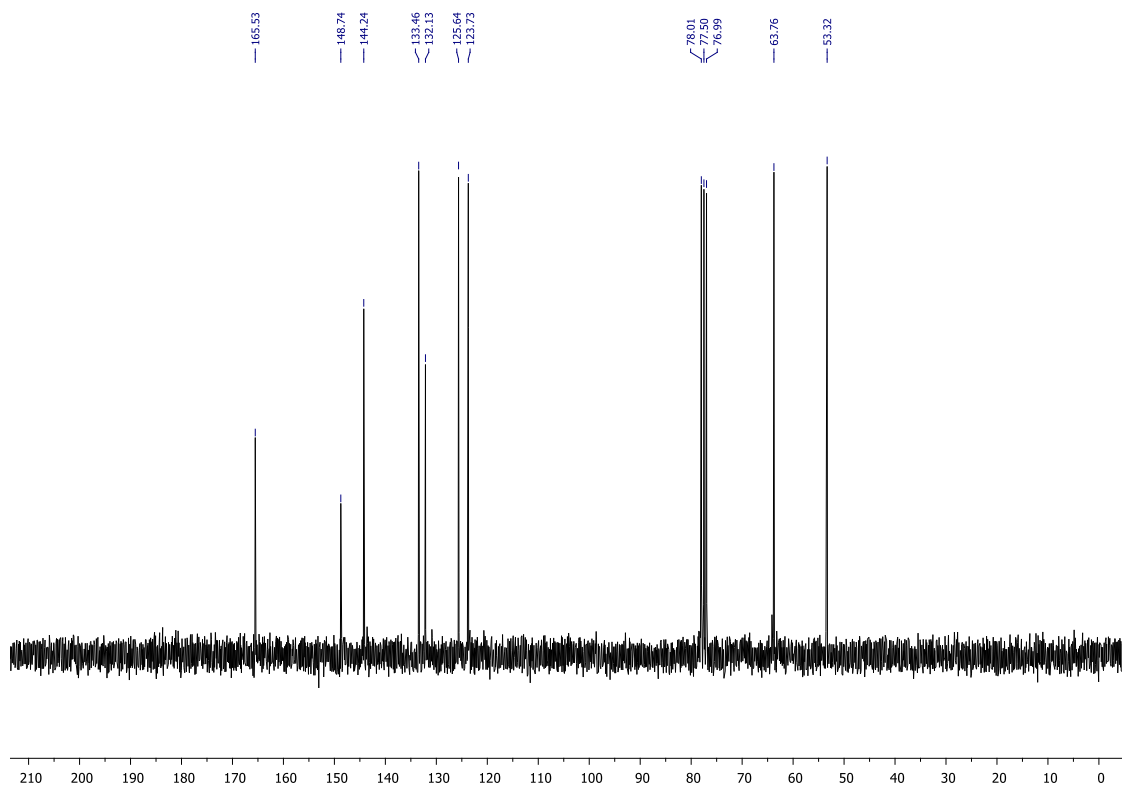
¹H NMR (250 MHz, CDCl₃)



¹³C NMR (63 MHz, CDCl₃)



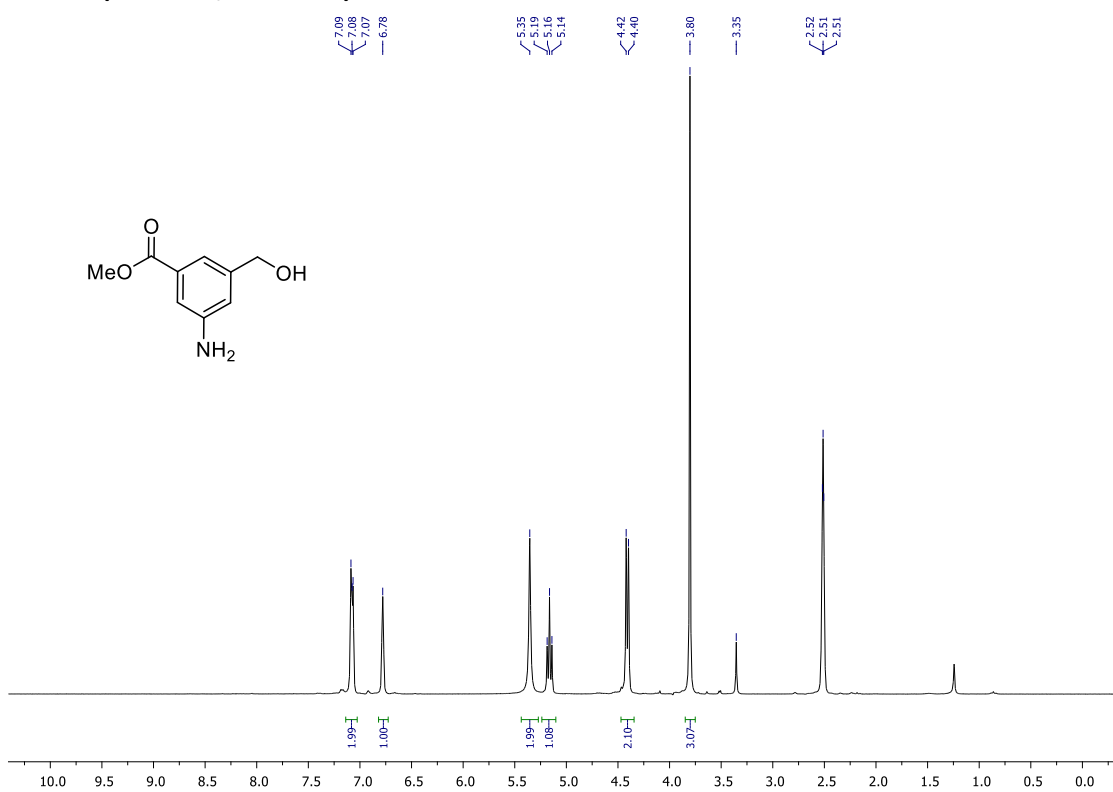
Methyl 3-(hydroxymethyl)-5-nitrobenzoate (34)

 ^1H NMR (250 MHz, CDCl_3) ^{13}C NMR (63 MHz, CDCl_3)

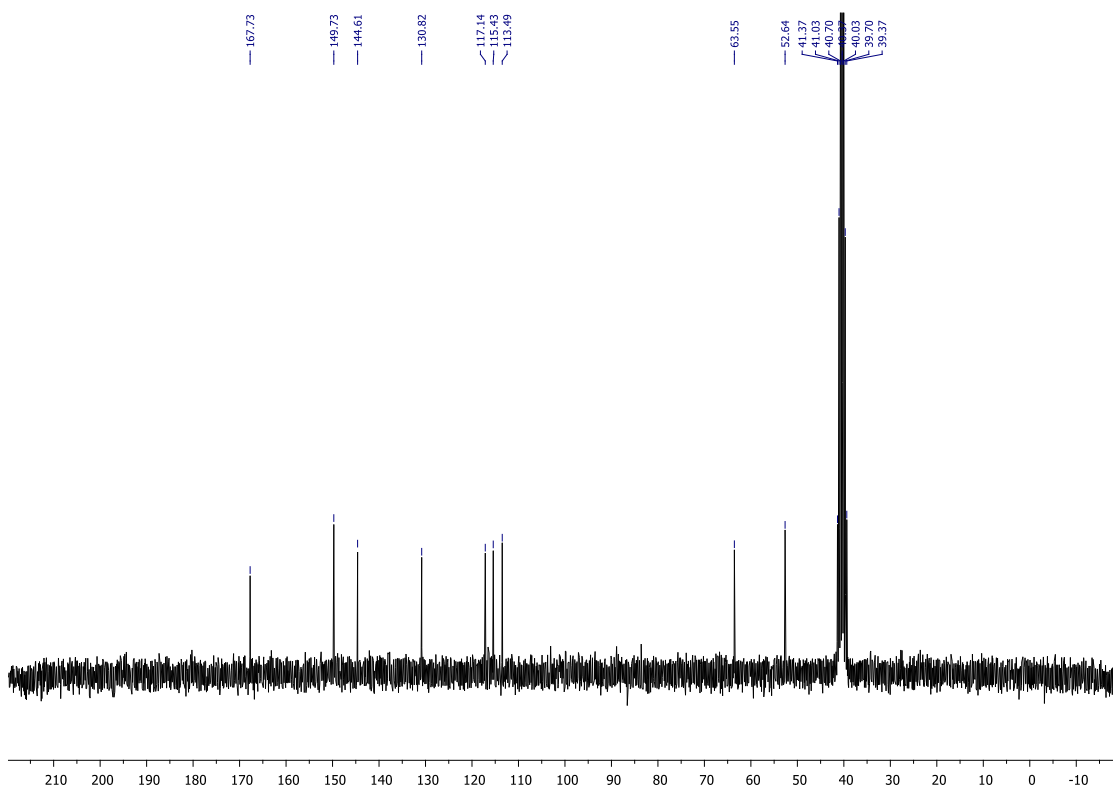
Representative spectra

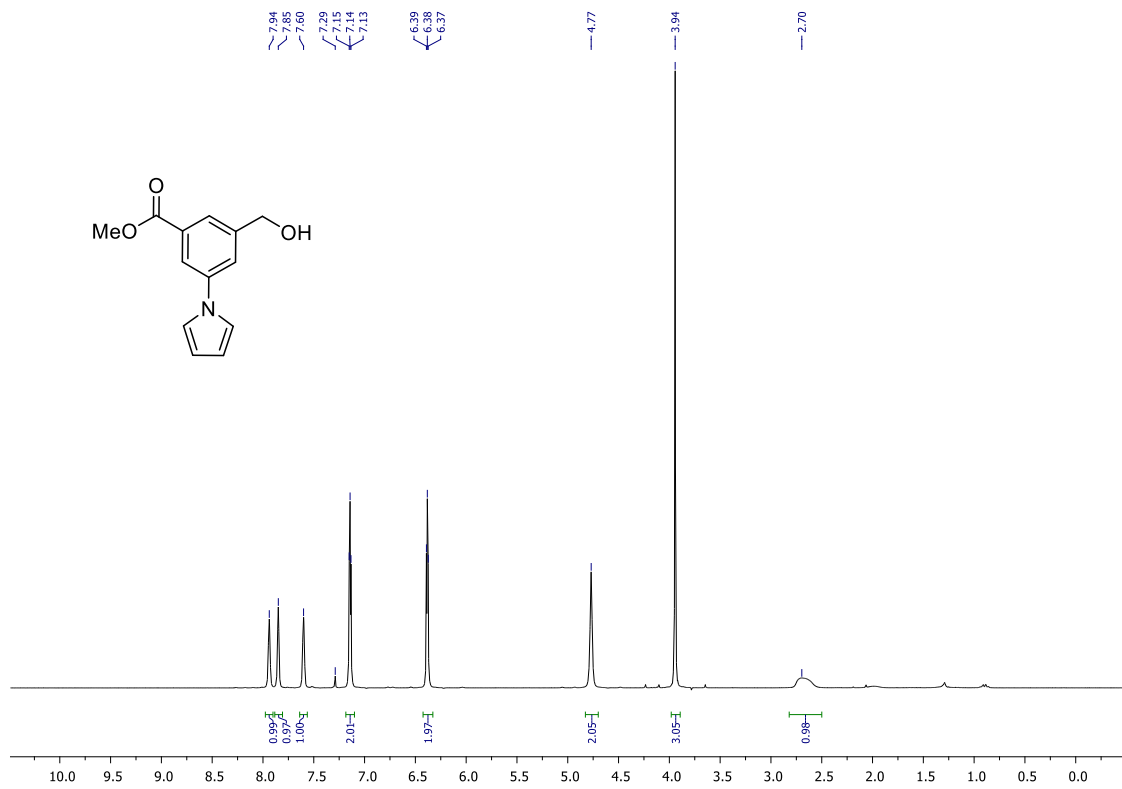
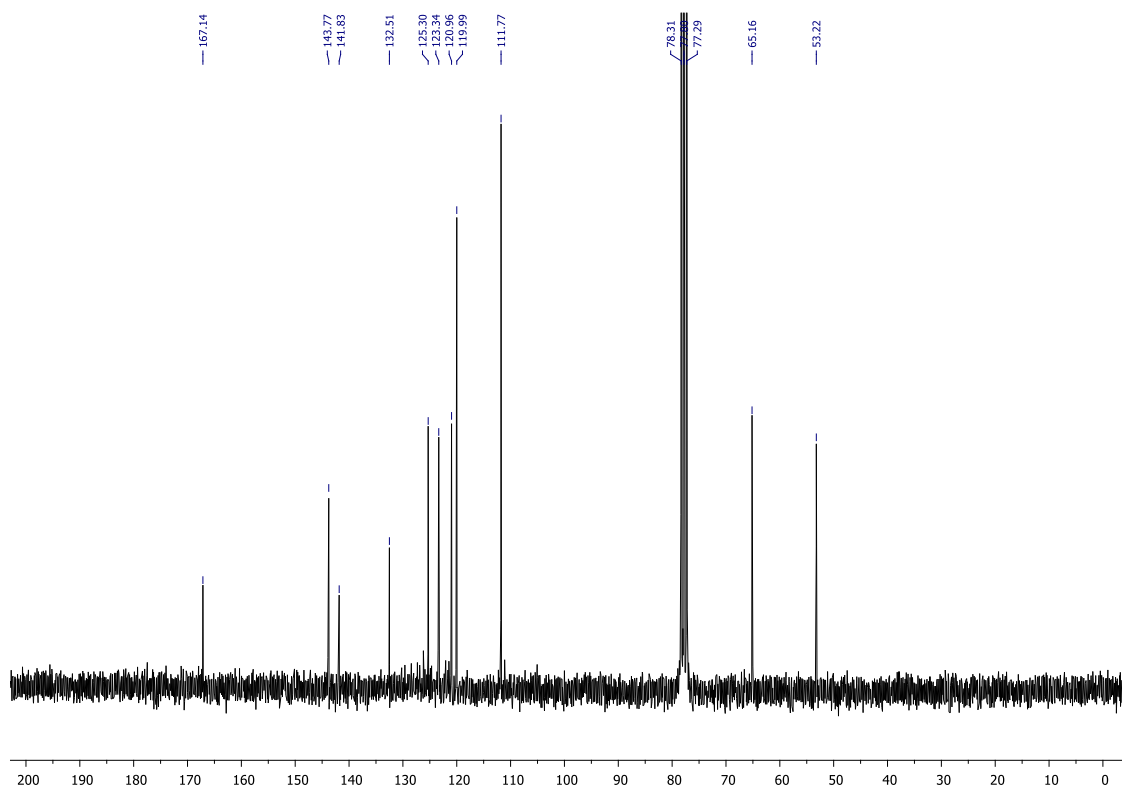
Methyl 3-amino-5-(hydroxymethyl)benzoate (35)

¹H NMR (250 MHz, *d*₆-DMSO)



¹³C NMR (63 MHz, *d*₆-DMSO)

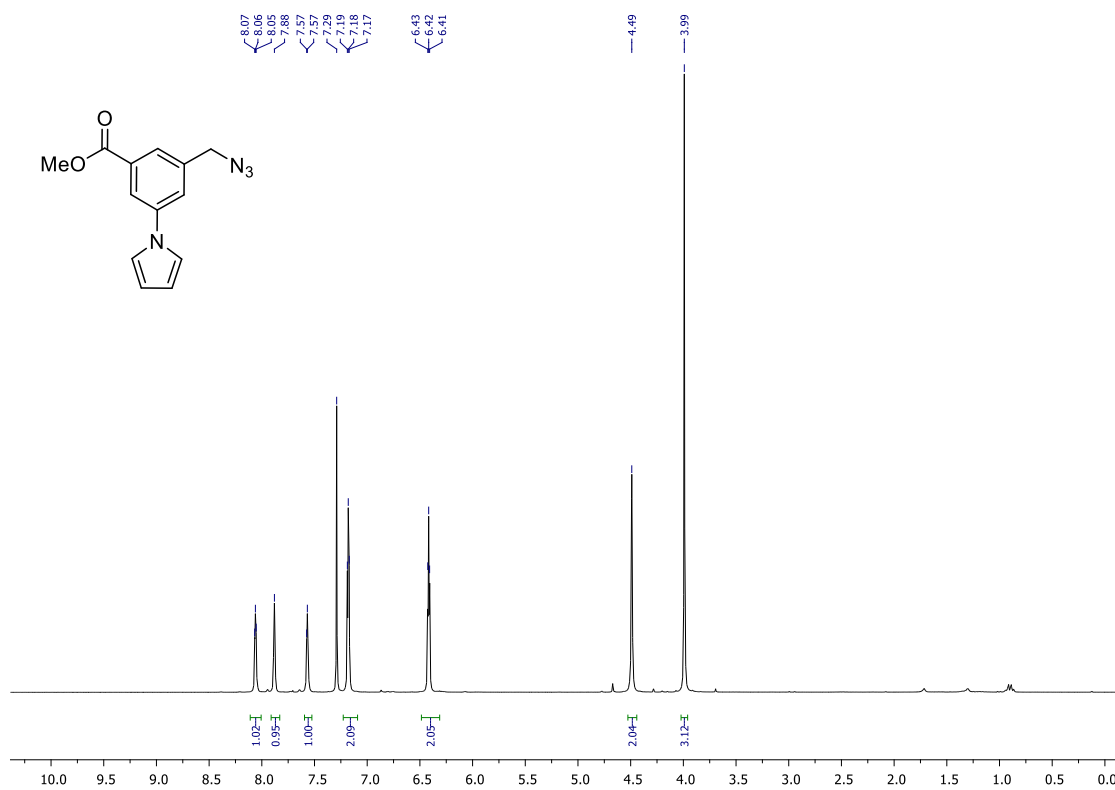


Methyl 3-(hydroxymethyl)-5-(1H-pyrrol-1-yl)benzoate (36a)**¹H NMR (250 MHz, CDCl₃)****¹³C NMR (63 MHz, CDCl₃)**

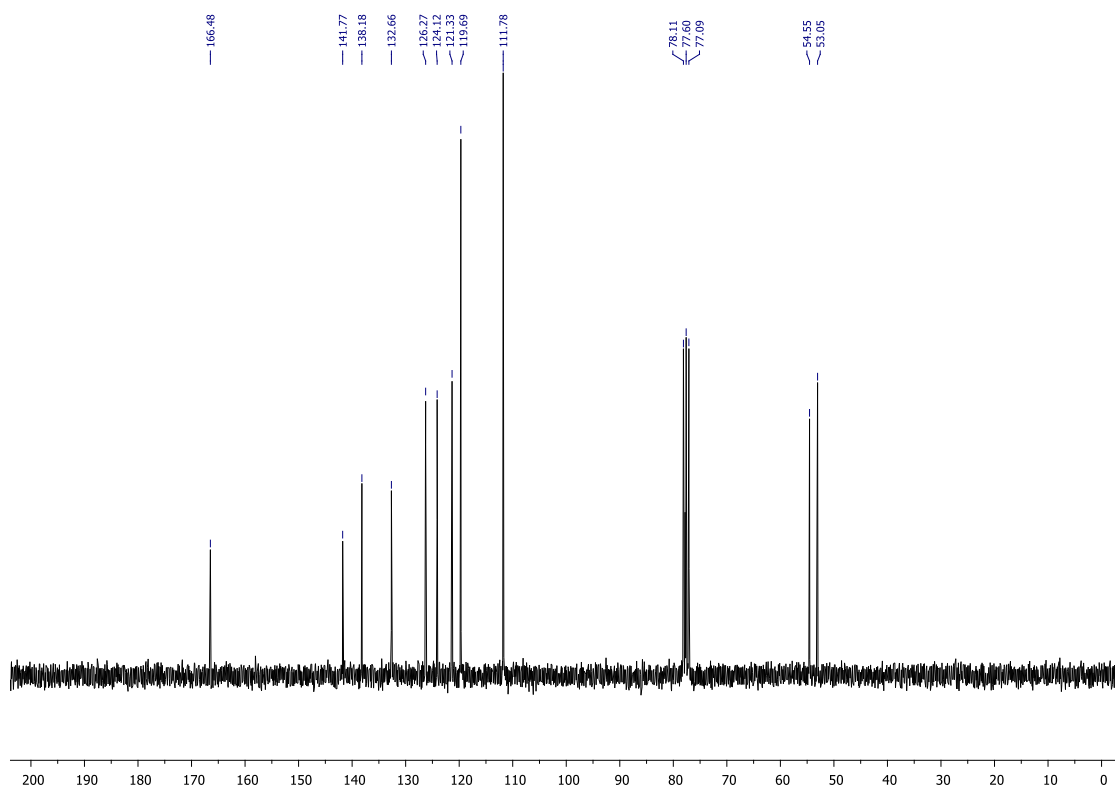
Representative spectra

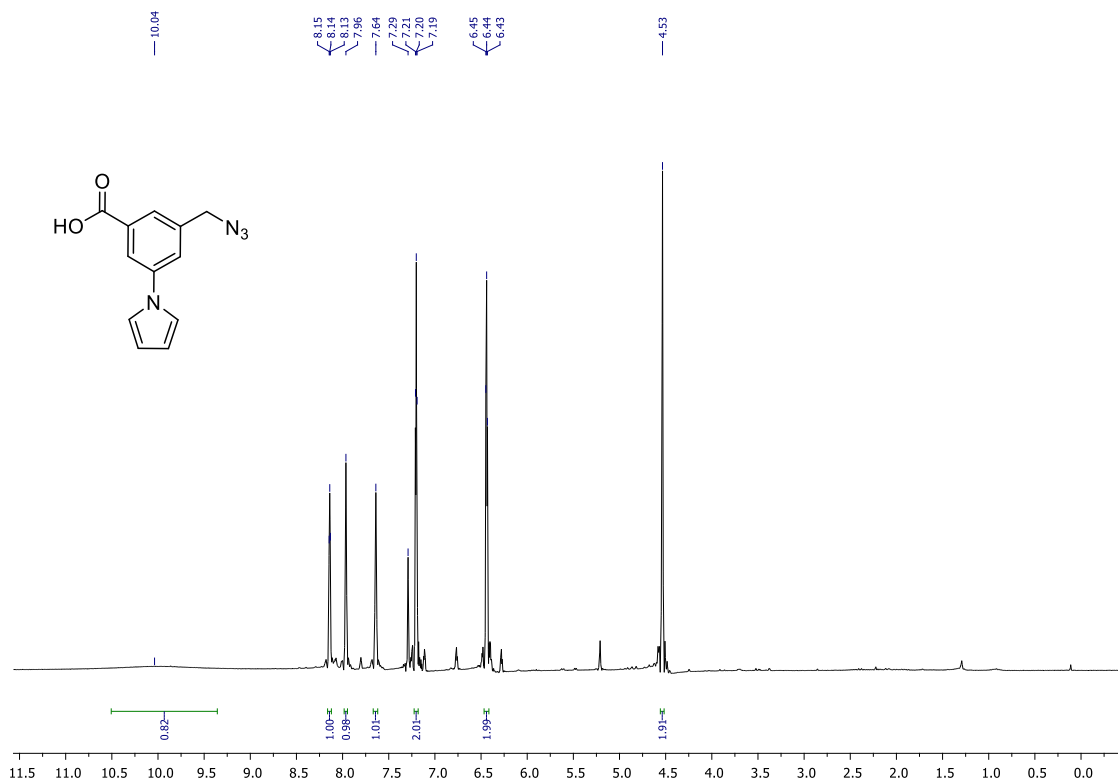
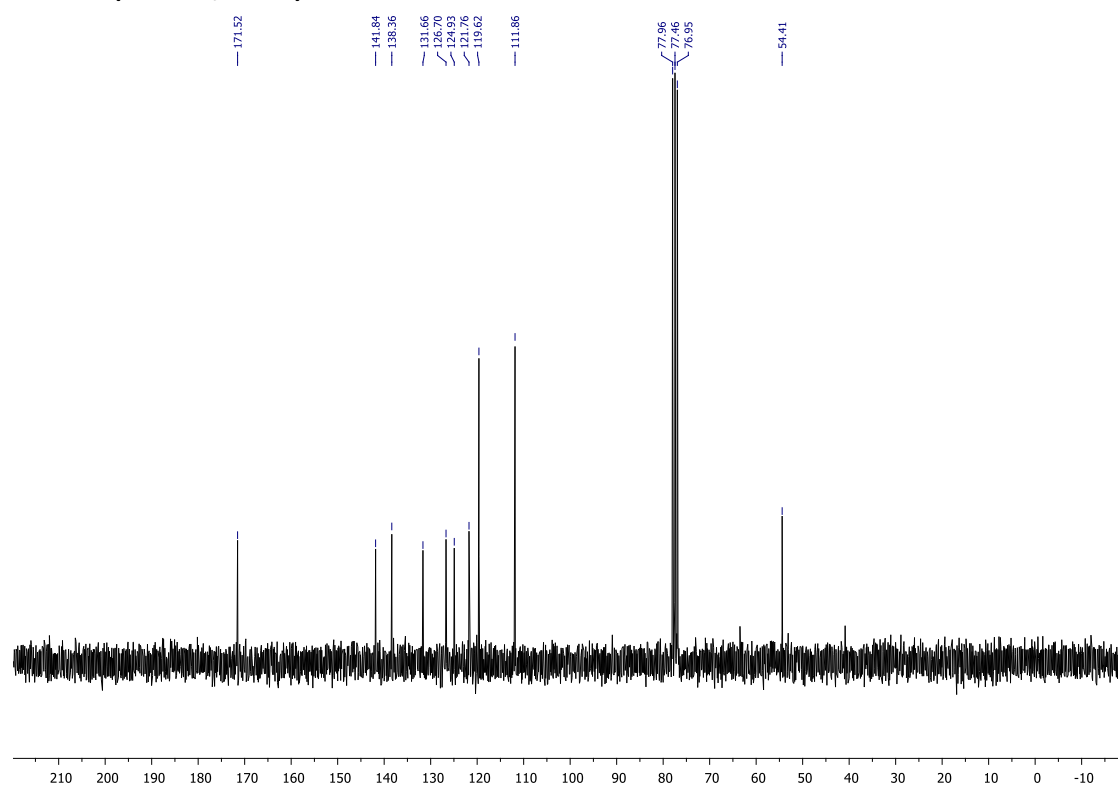
Methyl 3-(azidomethyl)-5-(1H-pyrrol-1-yl)benzoate (37a)

^1H NMR (250 MHz, CDCl_3)



^{13}C NMR (63 MHz, CDCl_3)

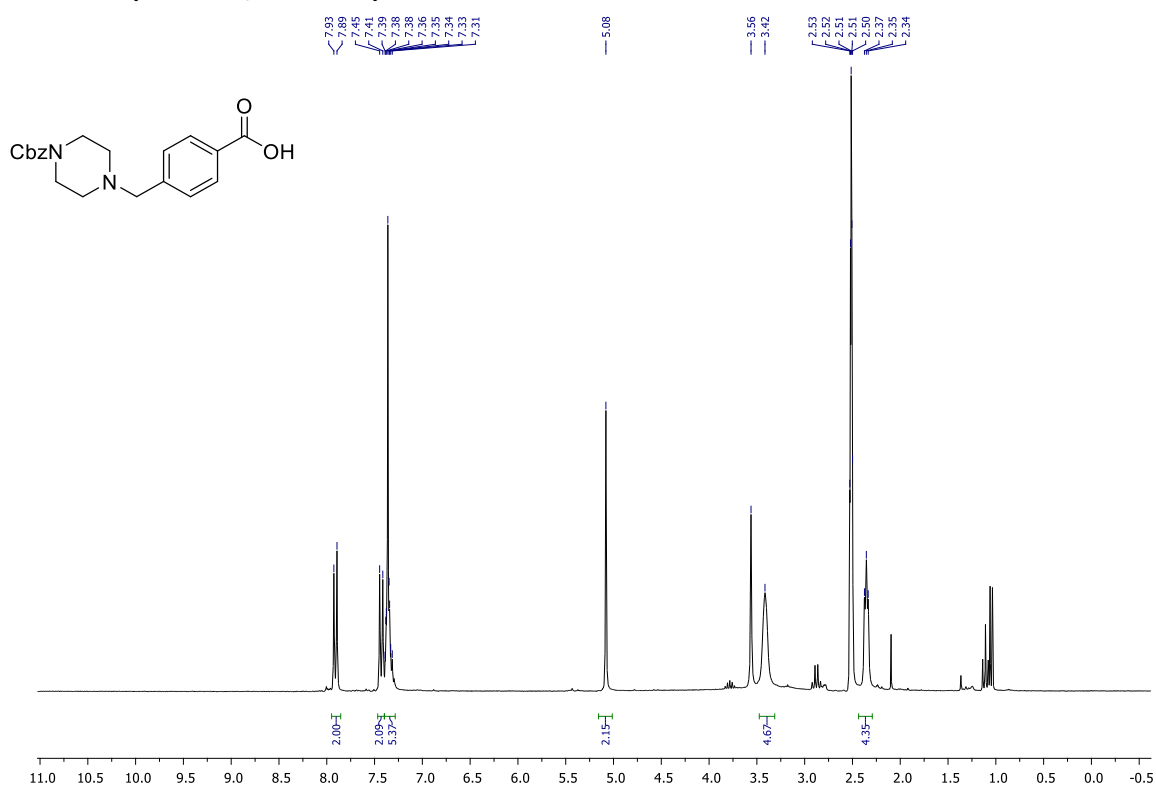


3-(Azidomethyl)-5-(1*H*-pyrrol-1-yl)benzoic acid (38a)**¹H NMR (250 MHz, CDCl₃)****¹³C NMR (63 MHz, CDCl₃)**

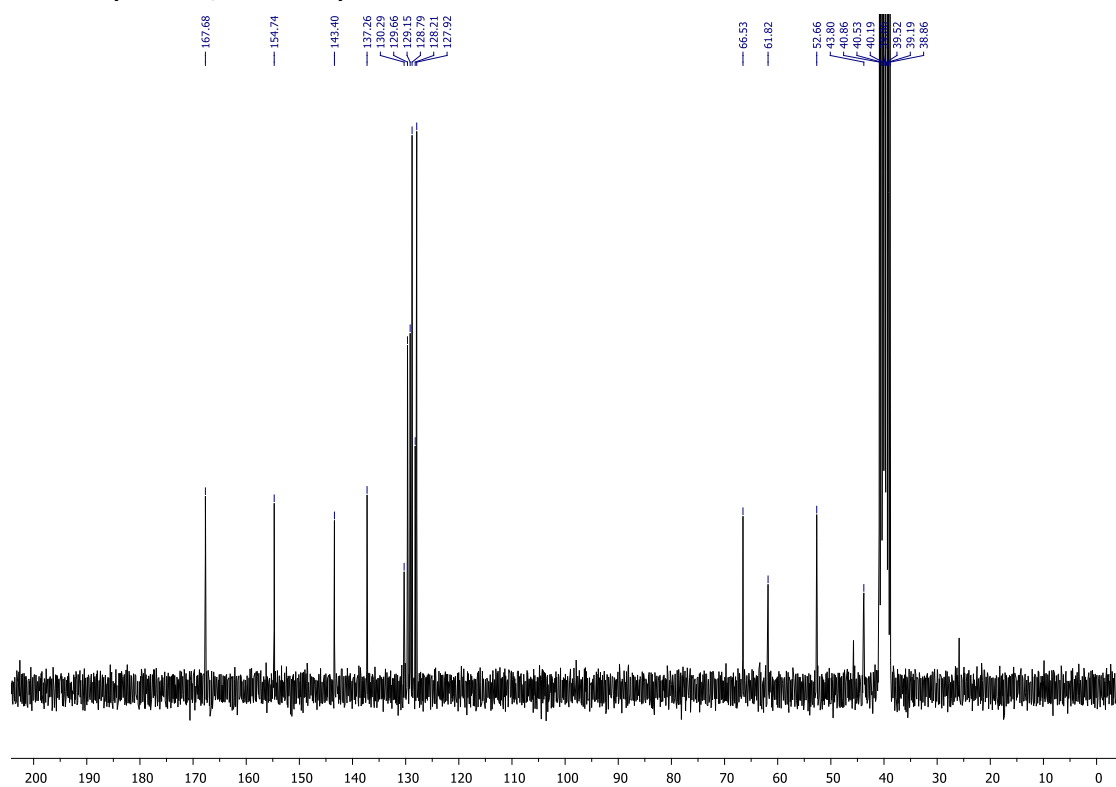
Representative spectra

4-[(4-((Benzyloxy)carbonyl)piperazin-1-yl)methyl]benzoic acid (45)

^1H NMR (250 MHz, d_6 -DMSO)

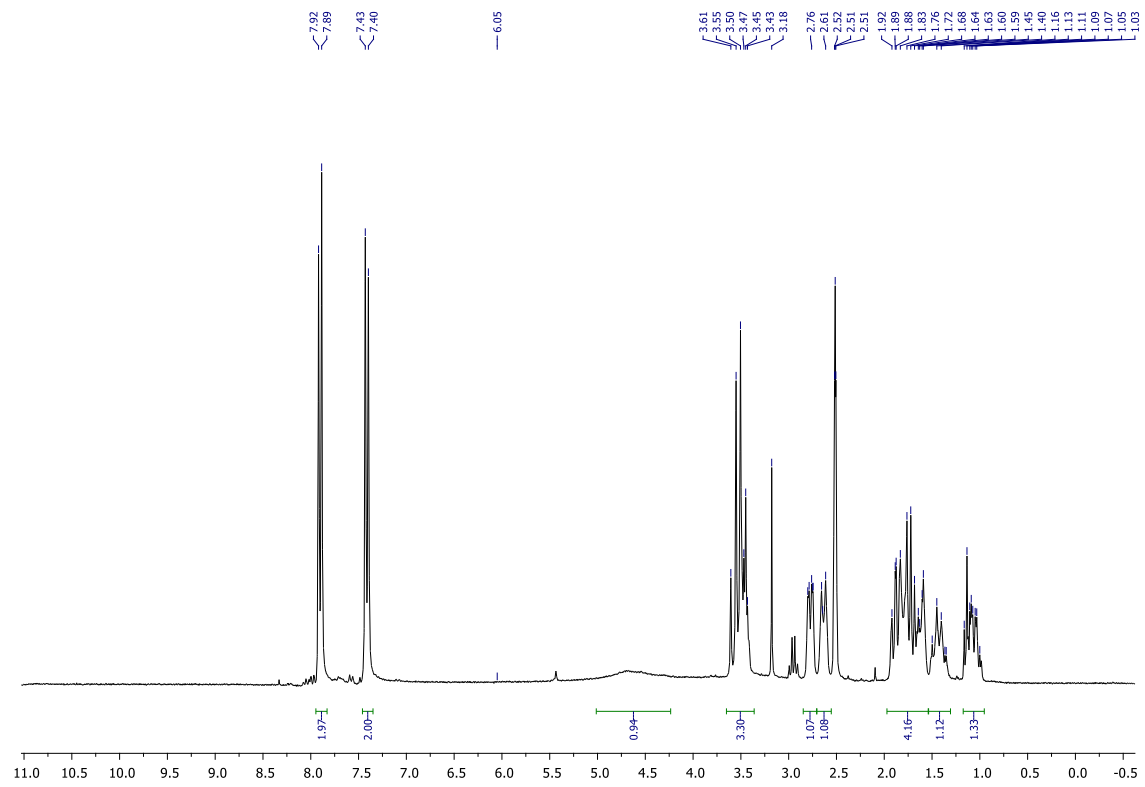


^{13}C NMR (63 MHz, d_6 -DMSO)

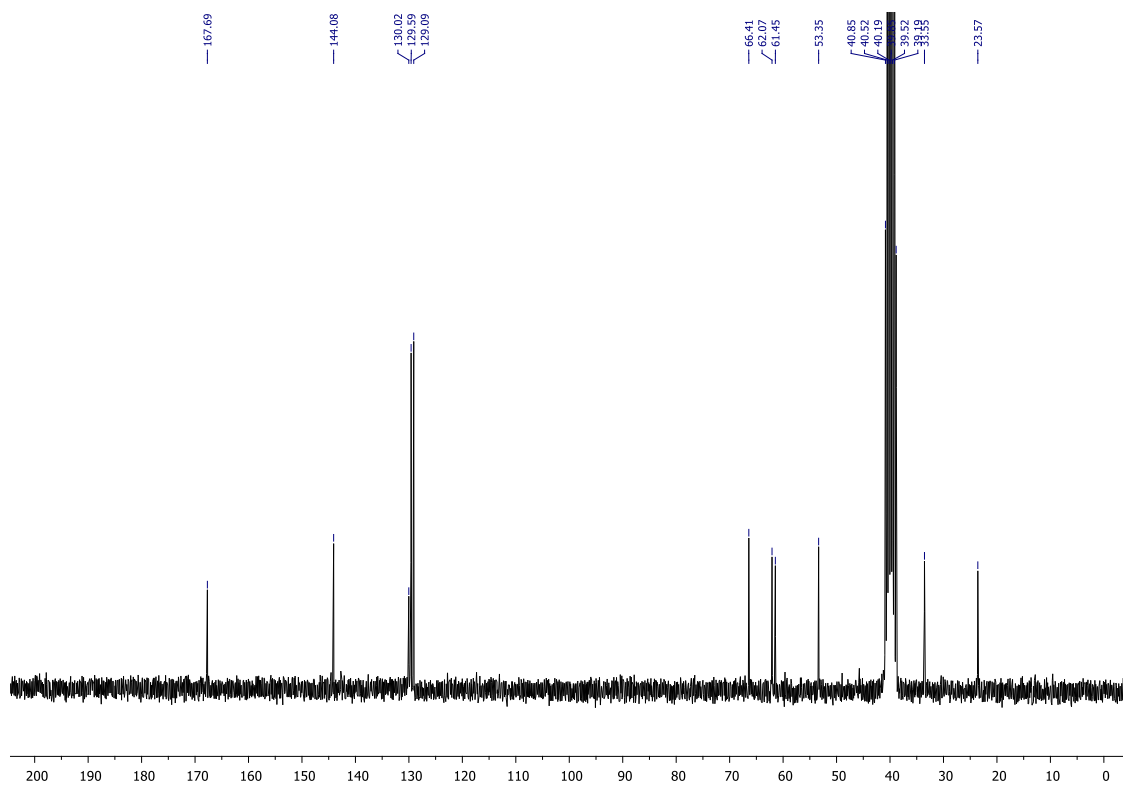


4-[(3-Hydroxypiperidin-1-yl)methyl]benzoic acid (48)

¹H NMR (250 MHz, *d*₆-DMSO)



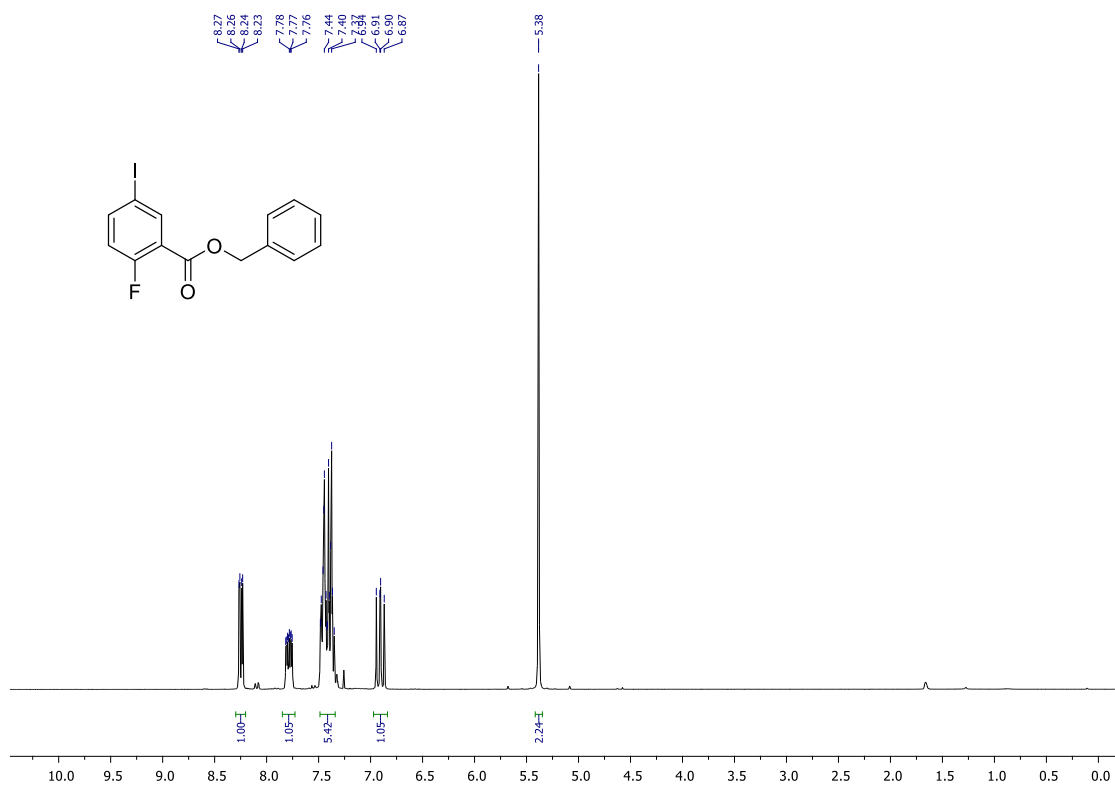
¹³C NMR (63 MHz, *d*₆-DMSO)



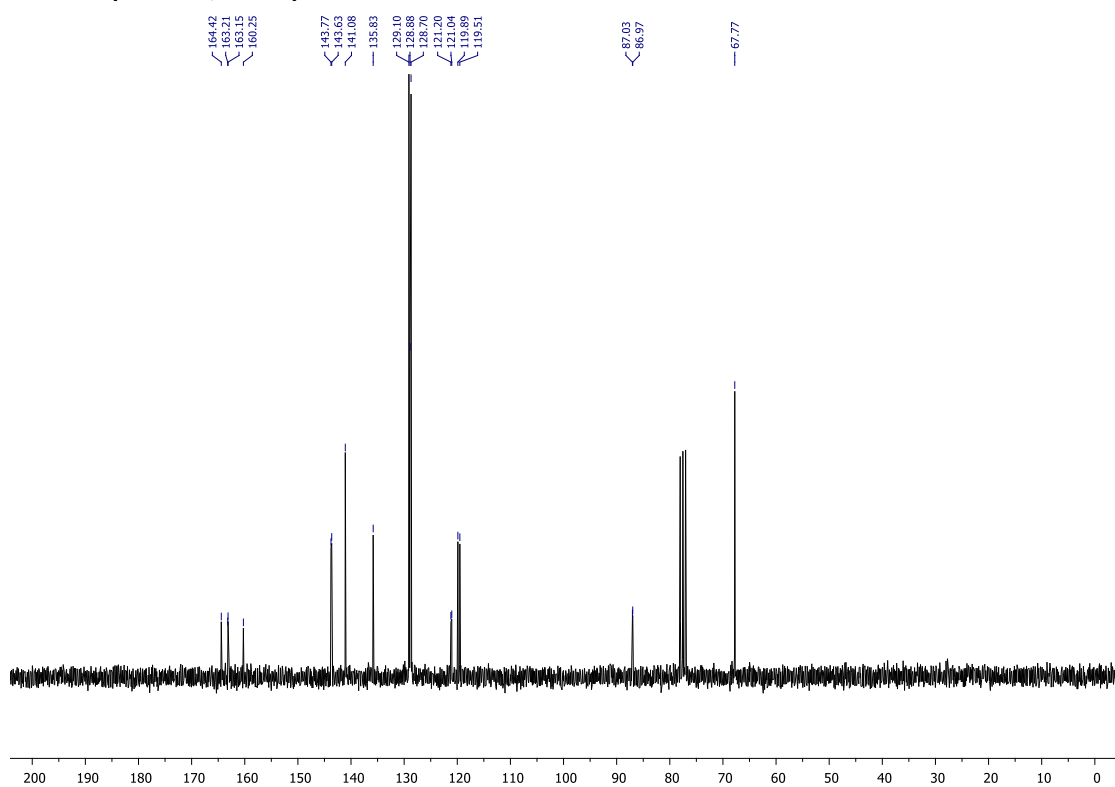
Representative spectra

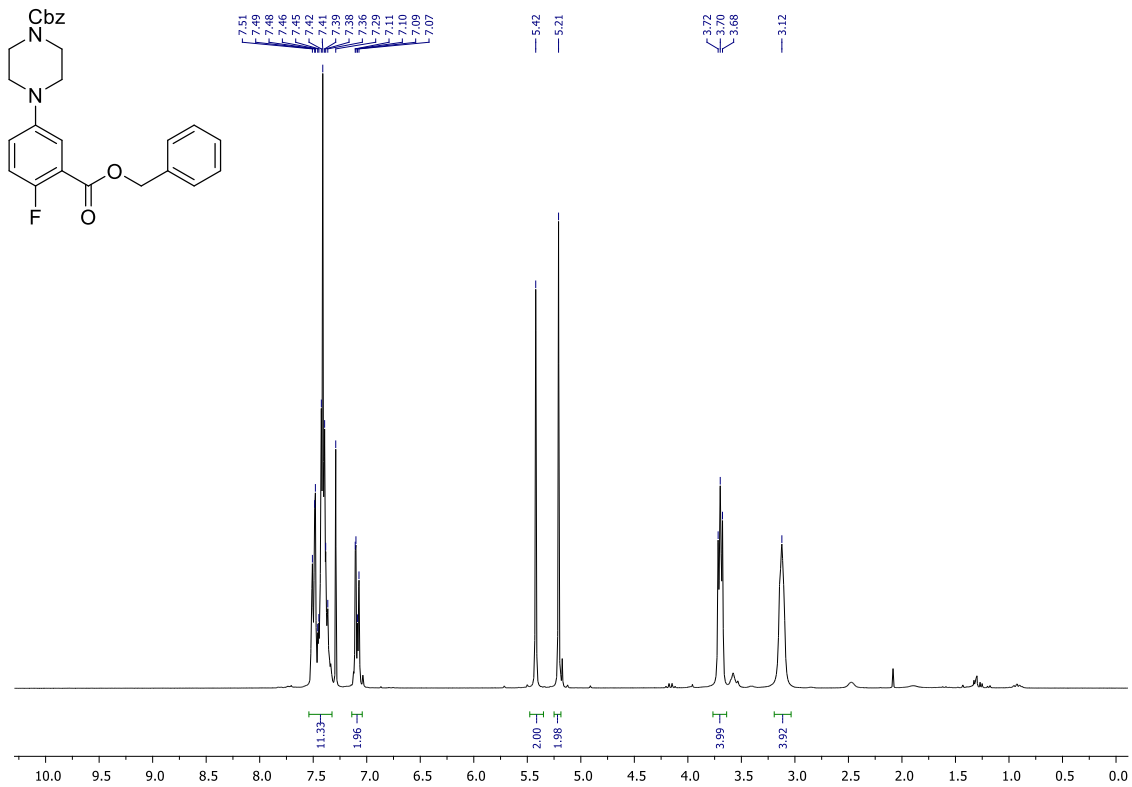
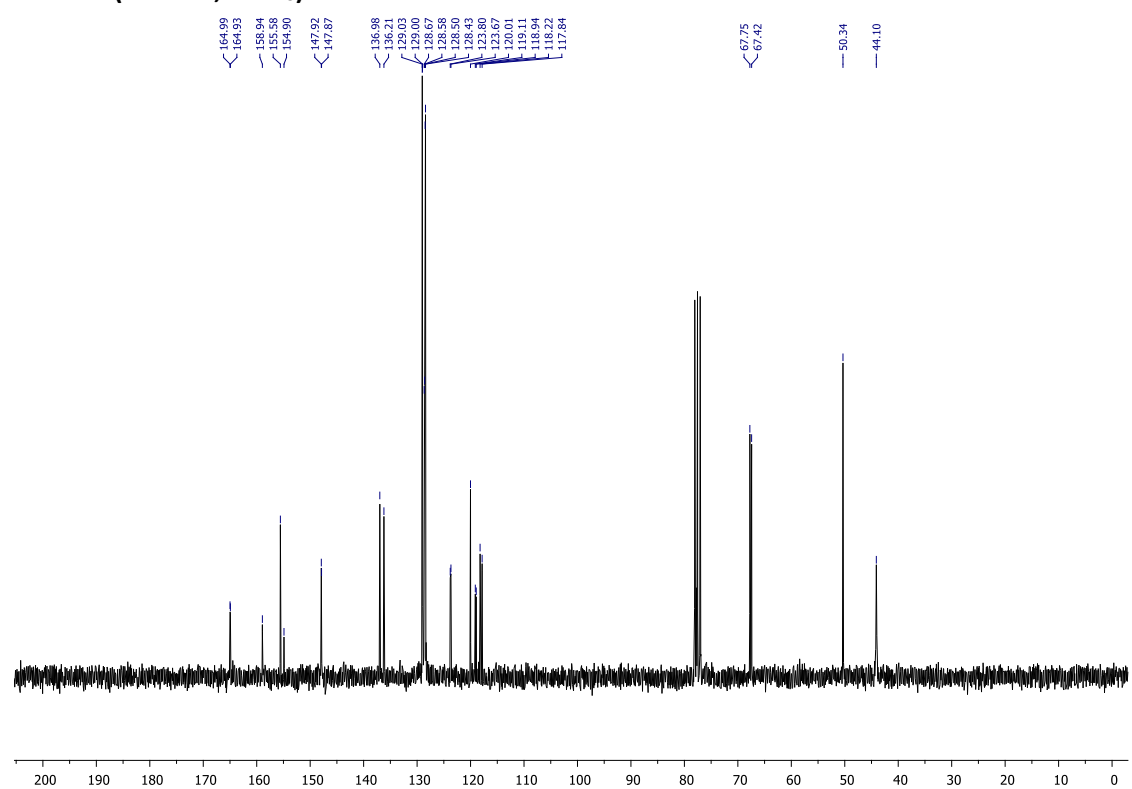
Benzyl 2-fluoro-5-iodobenzoate (40)

¹H NMR (250 MHz, CDCl₃)



¹³C NMR (63 MHz, CDCl₃)

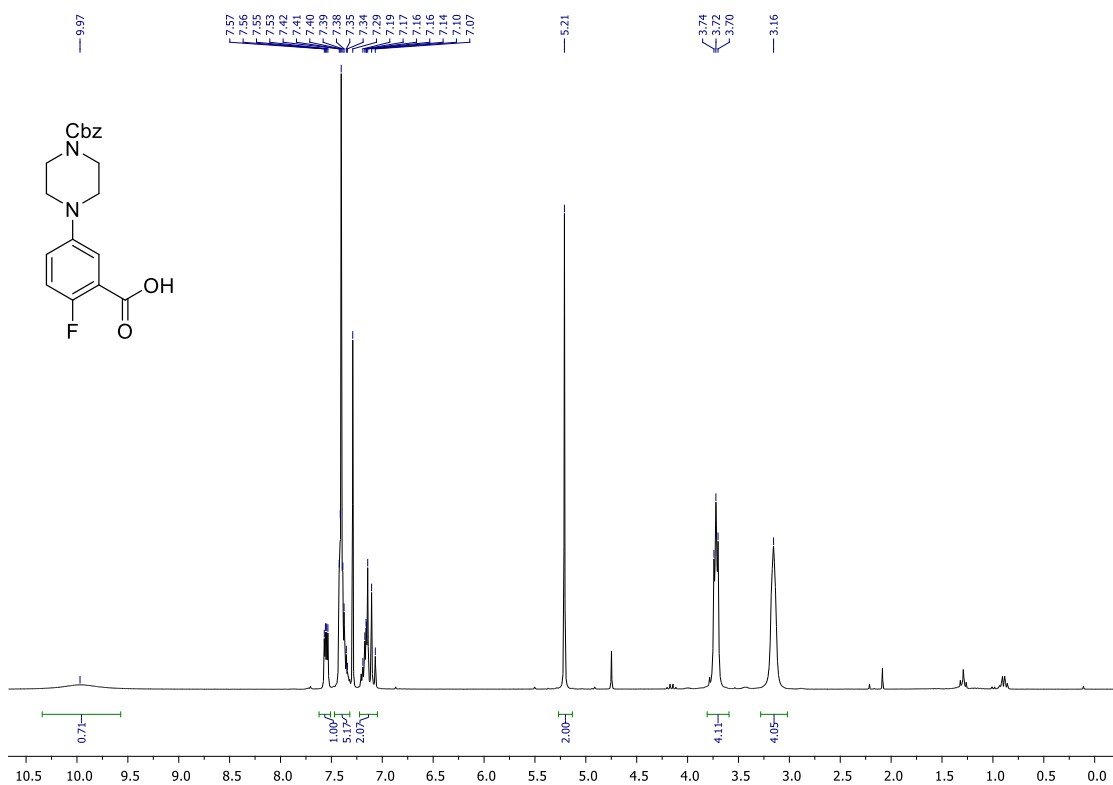


Benzyl 4-(3-((benzyloxy)carbonyl)-4-fluorophenyl)piperazine-1-carboxylate (42)**¹H NMR (250 MHz, CDCl₃)****¹³C NMR (63 MHz, CDCl₃)**

Representative spectra

5-[4-((Benzyloxy)carbonyl)piperazin-1-yl]-2-fluorobenzoic acid (43)

¹H NMR (250 MHz, CDCl₃)



¹³C NMR (63 MHz, CDCl₃)

